ELLIPTICAL POLARIMETRY OF ELEVEN LUMINOUS LATE-TYPE VARIABLES

Bruce D. Holenstein

A DISSERTATION

in

ASTRONOMY AND ASTROPHYSICS

Presented to the Faculties of the University of Pennsylvania in partial fulfillment of the requirements for the degree of Doctor of Philosophy.

1991

Robert H. Koch
Supervisor of Dissertation

Robert H. Koch
Graduate Group Chairperson

ACKNOWLEDGMENTS

This thesis would have been impossible were it not for the support and assistance received from many people. I owe society and my friends and family more than I can express.

My wife, Denise, has put up with a husband that was not always there for her when she needed help. She supported my efforts by making our home work by raising two children and yet working full-time.

Dr. Robert H. Koch, my advisor, instilled into me a deep respect for the astronomical profession. Dr. Koch was both a mentor and a role model.

I received numerous technical assistance from Dr. William Blitzstein, Dr. Raymond Pfeiffer, Richard J. Mitchell and Dr. Nicholas M. Elias. In particular, Dr. Blitzstein and Dr. Pfeiffer served on my thesis examination committee. Also, Dr. Blitzstein helped me with developing astronomical equipment. Mr. Mitchell helped me with running the astronomical equipment (especially in the early morning). Dr. Elias, while getting his degree, rekindled my drive to finish my own degree.

I remember with fondness the stimulating discussions I had and many interesting things I learned over the years with my colleagues Robert Nemiroff, Jeffrey Goldstein, Mike Corcoran, Christ Ftaclas, Paul Wiita, Victor Mighnes, Jeffrey Bowen, and Richard Clarke.

I was fortunate in my later graduate student years to have an employer, Compucon Services Corporation, that was flexible enough to allow me to devote time to research. Paul Holenstein, my brother and partner, assisted me by having a different perspective on business matters. Victor Berutti asisted me by answering computing questions.

My parents raised me in a stimulating environment. They sacrificed their own comfort and financial security to enable me to attend Blair Academy and Bucknell University.

The developers of the *SIMBAD* astronomical software deserve thanks. This software helped find over 5000 citations to the eleven program

objects.

Dr. Janet Mattei, the Director of the *AAVSO*, kindly supplied visual light curves for ten of the program objects. She also provided photoelectric data for four of the program objects.

Support was gratefully received in my last year from a Zaccheus Daniel fellowship.

Undoubtedly, some people are not mentioned above that should have been mentioned. To them and to all the others in my life that made a difference I express my sincere thanks.

"If light is man's most useful tool, polarized light is the quintessence of utility." W. A. Shurcliff

ABSTRACT

ELLIPTICAL POLARIMETRY OF
ELEVEN LUMINOUS LATE-TYPE VARIABLES

Bruce D. Holenstein
Robert H. Koch

Instrumentation has been developed to measure the normalized V Stokes vector coincident with the Q and U Stokes vectors of the filtered radiation field from a celestial source. The hybrid method developed to calibrate the system used null-polarization standards for the system offset and linear polarization standards along with a quarter-wave-plate-induced rotation on the Poincarè sphere for the system gain.

An observing program was completed that concentrated upon eleven Luminous Late-Type Variables (LLTVs). The program objects are 119 CE Tau, α Ori, 6 BU Gem, ψ^1 Aur, 72 Leo, V CVn, α Sco, α^1 Her, μ Cep, VV Cep, and β Peg. The data for the program objects show circular polarization behavior that is as rich and as complex as was already known for the linear polarization.

The infrared excesses of the LLTVs were used to place useful limits on the dust shell particle numbers and masses. The calculations were accomplished by using the stellar flux at visible wavelengths to estimate and remove the stellar flux at infrared wavelengths.

A Monte Carlo software model was developed to aid in the explanation of the observations. The model components include contributions from limb darkening, stellar spots, Rayleigh/Thomson scattering in the stellar atmosphere, Mie scattering from multiple particle types in the dust shell, and interstellar birefringence. The output of the software is an ensemble of maps which display the Stokes vectors and relative flux expected when looking at the modelled object from any direction.

It was concluded that the linear polarization for most of the program objects arises from Rayleigh and Thomson scattering in the atmosphere of the objects and from single scattering by small silicate grains in the dust shells. The bulk of the circular polarization arises from three mechanisms: 1) single scattering of light linearly polarized in the stellar atmosphere and subsequently Mie scattered by spherical or irregularly-shaped aligned particles, 2) magneto-emission arising from spots, and 3) interstellar birefringence acting on an intrinsic stellar linear polarization.

TABLE OF CONTENTS

CHAPTER		PAGE
1.	History and Background	1
1.1	Pennsylvania Polarimeter Program	1
1.2	Observing Program	2
1.3	Program Objects	4
1.4	Thesis Objective	9
1.5	Data Presentation	10
2.	The Pennsylvania Elliptical Polarimeter	26
2.1	Overview of the Elliptical Polarimeter	26
2.2	Idealized Theory of Operation for an Elliptical Polarimeter	27
2.3	Variable Integration Lengths	31
2.4	Data Acquisition and Reduction Software	33
2.5	Calibration Technique	36
3.	Morphology of Program Stars Observations	54
3.1	Polarimetric Data	54
3.2	Determination of Interstellar Polarization Vectors	55
3.3	Intrinsic Polarizations	61
3.4	Polarization Spectra	65
3.5	Period and Cycle Length Determinations	66
3.6	*IUE*, *IRAS*, and *AAVSO* Data	68
4.	Elliptical Polarization Sources	151
4.1	Massive Dust Shells	151
4.2	Multi-Parameter Polarization Model	153

TABLE OF CONTENTS (cont.)

CHAPTER		PAGE
4.3	Representative Model Output	163
4.4	Discussion on the Program Objects	168
4.5	Conclusions and Remaining Questions	183
APPENDIX		
A.	PEMP Observing Procedure	210
B.	Derivation of Stationary Errors	214
C.	Data Acquisition and Reduction Software Listings for the Circular Subsystem	216
D.	Journal of Observations for Standard Polarization Sources	230
E.	Journal of Standardized Observations for Program Objects	245
F.	Linear Polarization Observations of Field Stars	269
G.	Circular Polarization Observations of Field Stars	277
H.	Multi-Parameter Polarization Model Software Listings	280
	References	297
	Index	304

TABLES

TABLE		PAGE
1.1	Program Object Parameters	11
1.2	Program Object Variability State	12
2.1	Stellar Polarization Standards	39
2.2	Circular Subsystem Calibration Runs	43
2.3	Standardization Coefficients for the Linear and Circular Subsystems	44
3.1	Interstellar Linear Polarization for Program Objects	70
3.2	Polarization Spectral Indices for Program Objects	71
3.3	*IUE* 0.22μm Feature for Program Objects	76
3.4	Program Object Radiometry	77
4.1	Analysis of Radiometry for Program Objects	187
4.2	Program Object Summary	188

FIGURES

FIGURE		PAGE
1.1	Absolute Magnitude vs. Effective Temperature for Program Objects	13
1.2	Galactic Positions of Program Objects	13
1.3	Observed Linear Stokes Vectors for 119 Tau	13
1.4	Observed Linear Stokes Vectors for α Ori	13
1.5	Observed Linear Stokes Vectors for 6 Gem	13
1.6	Observed Linear Stokes Vectors for ψ^1 Aur	13
1.7	Observed Linear Stokes Vectors for 72 Leo	14
1.8	Observed Linear Stokes Vectors for V CVn	14
1.9	Observed Linear Stokes Vectors for α Sco	14
1.10	Observed Linear Stokes Vectors for μ Cep	14
1.11	Observed Linear Stokes Vectors for VV Cep	14
1.12	Observed Linear Stokes Vectors for β Peg	14
2.1	Schematic of the PEMP System	45
2.2	Reference Linear Polarization Values Versus Natural Polarization Values	45
2.3	Reference Circular Polarization Values Versus Natural Polarization Values	45

FIGURES (cont.)

FIGURE		PAGE
2.4	Stokes Vectors as a Function of JD for the Null Standards	45
2.5	The q Versus u Plots for the Null Standards	45
3.1	Polarization Observations of 119 Tau Field Stars	78
3.2	Polarization Observations of α Ori Field Stars	78
3.3	Polarization Observations of 6 Gem Field Stars	78
3.4	Polarization Observations of ψ^1 Aur Field Stars	78
3.5	Polarization Observations of 72 Leo Field Stars	78
3.6	Polarization Observations of V CVn Field Stars	78
3.7	Polarization Observations of α Sco Field Stars	78
3.8	Polarization Observations of μ Cep Field Stars	79
3.9	Polarization Observations of VV Cep Field Stars	79
3.10	Polarization Observations of β Peg Field Stars	79
3.11	Intrinsic Polarization Observations of 119 Tau	79
3.12	Intrinsic Polarization Observations of α Ori	79
3.13	Intrinsic Polarization Observations of 6 Gem	79

FIGURES (cont.)

FIGURE		PAGE
3.14	Intrinsic Polarization Observations of ψ^1 Aur	79
3.15	Intrinsic Polarization Observations of 72 Leo	80
3.16	Intrinsic Polarization Observations of V CVn	80
3.17	Intrinsic Polarization Observations of α Sco	80
3.18	Intrinsic Polarization Observations of α^1 Her	80
3.19	Intrinsic Polarization Observations of μ Cep	80
3.20	Intrinsic Polarization Observations of VV Cep	80
3.21	Intrinsic Polarization Observations of β Peg	81
3.22	Polarization Spectra for α Ori	81
3.23	Polarization Spectra for 72 Leo	81
3.24	Polarization Spectra for α Sco	81
3.25	Polarization Spectra for α^1 Her	81
3.26	Polarization Spectra for VV Cep	81
3.27	Polarization Spectra for β Peg	81
3.28	Polarization Spectra for 119 Tau, 6 Gem, μ Cep, ψ^1 Aur, and V CVn	82
3.29	Periodograms for α Ori	82
3.30	Periodograms for β Peg	82
3.31	Periodograms for V CVn	82
3.32	Periodograms for μ Cep	82
3.33	Periodograms for VV Cep	82

FIGURES (cont.)

FIGURE		PAGE
3.34	*AAVSO* Visual Light Curves for the Program Objects	83
3.35	*AAVSO* Photoelectric Light Curve for 119 Tau	83
3.36	*AAVSO* Photoelectric Light Curve for α Ori	83
3.37	*AAVSO* Photoelectric Light Curve for α Sco	83
3.38	*AAVSO* Photoelectric Light Curve for μ Cep	83
4.1	Dereddened Multi-bandpass Radiometry	189
4.2	Scattering Geometry	189
4.3	Layers in the Multi-Parameter Polarization Model	189
4.4	Contour Maps for Case 1	189
4.5	Contour Maps for Case 2	190
4.6	Contour Maps for Case 3	190
4.7	Contour Maps for Case 4	190
4.8	Contour Maps for Case 5	191
4.9	Contour Maps for Case 6	191
4.10	Contour Maps for Case 7	191
4.11	Contour Maps for Case 8	191
4.12	Contour Maps for Case 9	192
4.13	α Ori Linear Polarization Data Phased with a 400.0 Day Period	192
4.14	α Ori Linear Polarization Data Phased with an 800.0 Day Period	192

CHAPTER 1. History and Background

1.1 Pennsylvania Polarimeter Program

Extensive polarimetry has been accomplished at the Flower and Cook Observatory over the twenty-two year period from 1969 to 1991 (*cf.* Wolf 1970, Wolf 1972, Pfeiffer 1975, Koch and Pfeiffer 1978, Koch *et al.* 1985, Pfeiffer and Koch 1987, Corcoran 1988, Elias 1990, Koch *et al.* 1992). Currently attached to the 72cm Cassegrain reflector is a photoelastic modulator polarimeter (PEMP). PEMP type systems give superior signal-to-noise ratios for the detection of polarimetric signals (*cf.* Kemp 1969, Stokes, Ekstrom, and Swedlund 1976). In the conventional configuration, PEMP has been used for making measurements of linear polarization in programs investigating interacting and eclipsing binaries (*cf.* Pfeiffer and Koch 1977, Pfeiffer and Koch 1987, Koch *et al.* 1989, Koch *et al* 1992). Linear polarization yields information about the circumstellar and interstellar environments and, in particular, the types of scatterers, their number densities, and their locations. In another configuration, PEMP makes measures of circular polarization which provide information about magnetic fields, birefringence, and scattering in the systemic and interstellar environments. Before November, 1986, the PEMP configuration for circular polarization measurements was mutually exclusive to the configuration for linear polarization measurement: the experimental configurations were non-simultaneous and required some modifications in order to switch between configurations. The configuration change effort, non-simultaneity and the fact that the circular signals are typically two orders of magnitude smaller than measured stellar linear polarizations for non-degenerate stars (Kemp 1970, Stokes *et al.* 1974) resulted in the circular polarization measuring mode rarely being used and was never calibrated. Scanning *The Astrophysical Journal* of the last twenty-five years will convince the reader that other institutions have also focused primarily on linear polarization.

Incoherent light can be completely described in terms of the four

Stokes vectors I, Q, U, and V in intensity scale (Jackson 1975) or q, u, and v in percent. The first vector describes the intensity of the incident radiation. The next two vectors are the components, respectively, of the linear polarization at orientations of 0 degrees and +45 degrees (*i.e.* toward East) with respect to North. The last vector is the circular polarization. Note that phase information is needed for completely describing coherent light (Shurcliff 1966). No stellar visible-wavelength polarimeters have the capability of measuring the complete polarization form for coherent light.

The benefits of collecting circular polarization data in addition to linear polarization data prompted the development of a technique, and the assembly, and calibration of a subsystem in order to enable PEMP to make linear and circular polarization measures simultaneously and in a single experimental configuration. The resulting experimental system thus more than doubles the throughput for making polarization measurements of the three normalized Stokes vectors. Specifically, PEMP now measures and reports the Stokes q and u vectors by the original linear polarization subsystem and the v vector by the new circular polarization subsystem. This experimental setup has been extensively tested and used over the last four years by Holenstein (1987), Holenstein, Koch and Pfeiffer (1988), Elias (1990), Elias and Dorren (1990), and Koch *et al.* (1992).

1.2 Observing Program

An observing program utilizing PEMP for observations of luminous late-type variables (LLTVs) was planned. Magalhães (1988) provides a recent review of the polarization mechanisms in LLTVs. Koch (1992) provides a review of polarized radiation from LLTVs which are components of close binary systems. LLTVs are known to have extended, dusty circumstellar atmospheres (*cf.* Dyck *et al.* 1971, Zellner 1971, Dyck and Simon 1975, Tsuji 1978, Stencel, Pesce, and Bauer 1988, Coyne 1988), and/or stellar patches or spots (Schwarzschild 1975, Hayes 1984, Hebden *et al.*

1986) and are known by previous linear and circular polarization studies (*cf.* Kruszewski, Gehrels and Serkowski 1968, Dyck and Jennings 1971, Shawl 1975a and b, Tinbergen, Greenberg and de Jager 1981, Hayes 1984, Koch and Pfeiffer 1978) to be interesting polarimetrically. One common theme in the LLTV studies is that many different mechanisms are used to explain the same linear and circular polarization observations. Evidence for this confusion will become apparent as the individual program stars are discussed in Section 1.3.

Since systemic circular polarization is typically only a small fraction of the linear polarization for non-degenerate stars, bright objects are desired. In addition to α Ori, which happens to be the apparently brightest cool supergiant in the sky, the present study was limited to ten other bright giants and supergiants. They are 119 CE Tau, 6 BU Gem, ψ^1 Aur, 72 Leo, V CVn, α Sco, α^1 Her, μ Cep, VV Cep, and β Peg. The selection criteria consisted of:

i). late K or M bright giants or supergiants,

ii). $-27° < \delta < +66°$ (declination limits of telescope and polarimeter),

iii). $m_v < +7$.

The customary particulars for the program stars are summarized in Table 1.1. Table 1.2 is a compilation of the variability state for each star. The information contained in both of these tables was largely gathered from references contained in *SIMBAD* (Egret, Wenger and Dubois 1991) and from the *Sky Catalog 2000.0* (Hirshfield and Sinnot 1982). All of the program stars were known to already have been observed polarimetrically before. However, few published circular polarization values existed for any of them. Specifically, nearly 1500 visible-bandpass linear polarization observations were located in the literature for the eleven program objects. In contrast, only twenty-three published circular polarization observations were found for the program objects. Seventeen of them were made by Wolf (1972) working at Flower and Cook Observatory and Kitt Peak National

Observatory. Wolf's instrument did not use the current PEMP design and lacked sufficient sensitivity to detect any circular signals positively. The other six measures are spread over only three stars (Avery *et al.* 1975, Kemp and Wolstencroft 1972). It is obvious that little is known about the intrinsic circular polarization of stars in the upper right-hand corner of the Hertzsprung-Russell diagram.

Figure 1.1 is a combined absolute magnitude *vs.* effective temperature diagram for the program objects. Figure 1.2 is a map of the galactic position of all program objects.

1.3 Program Objects

The eleven stars chosen for the observing program are discussed below in order of increasing right ascension. Observed characteristic polarizations are presented in the normalized Stokes row vector format "[bandpass,q,u,v]" or the normalized azimuthal row format "{bandpass,p,Θ,v}". In all cases, the *p*, *q*, *u*, and *v* vectors are in percent scale and the Θ parameter is in degrees. Underlines (_) hold the place of missing values or unknown effective bandpasses. Other data presentation notation and conventions used in this thesis are discussed in Section 1.5.

(a) 119 CE Tau (M2 Iab-Ib)

This SRc star has a pulsational period of 165 days. Figure 1.3a and b is a compilation of the linear polarization observations of Hiltner (1951), Behr (1959), Dyck (1968), Dyck and Jennings (1971). The polarization is large. A typical value is {B,1.5,167,_}. The position angle cycles by more than 25 degrees. The spotty coverage over these twenty years clearly indicates that a large intrinsic polarization exists. No circular polarization data were found.

(b) α Ori (Betelgeuse, M1-2 Ia-Iab)

α Ori is an SRc variable with a pulsational period of about 420 days (Dupree *et al.* 1987, Smith, Patten, and Goldberg 1989, Smith 1990). The star has a shell of gas and dust which extends out to about 150 stellar radii (*i.e.* about 450 AU). At 2 μm it is the strongest IR emitter in the sky. There are at least four companions. Companion B has a period of 5.781 years.

The compiled linear polarimetry is presented in Figure 1.4a and b. The observers are Hiltner (1951), Behr (1959), Dyck (1968), Dyck and Jennings (1971), Tinbergen, Greenberg and de Jager (1981), Clarke and Schwartz (1984), Hayes (1984), and Le Borgne, Mauron and Leroy (1986). A characteristic Hayes datum is {B,0.41,102,_}. Hayes interpreted the polarization variation to be due to atmospheric effects. On the other hand, Karovska *et al.* (1985) analyzed Hayes' data for periodicity and concluded, along with evidence from speckle interferometry, that α Ori has two companions, one of which reaches periastron within the chromosphere of the supergiant. Hayes' data were entirely in the blue bandpass. Speckle detail from other researchers were interpreted to arise from atmospheric causes (Hebden *et al.* 1986). Further, Doherty (1986) proposed a model using Rayleigh scattering in the photosphere and dust scattering in the circumstellar shell to explain the linear polarization variability. It should be pointed out that attention was focused on M supergiants for this thesis, in part, because of the prospects of settling this matter.

Shafter and Jura (1980) predicted that the circumstellar shell 15" from α Ori would produce circular polarization at the 0.005% level.

(c) 6 BU Gem (M1-2 Ia-Iab)

6 Gem varies too much to classify it as anything other than an Lc: variable. The available linear polarization is presented in Figure 1.5a and b. The sources for the observations are Hiltner (1951), Dyck (1968), Dyck and Jennings (1971), and Wolf (1972). A characteristic Dyck datum is

{B,2.32,175,_}. The observations indicate that some activity is present with a time scale of hundreds of days and a polarization variation amplitude of about 2%. The only circular polarization measurements located for this object are by Wolf and are inconclusive.

(d) ψ^1 Aur (K5-M0 Iab-Ib)

The spectral type of this star varies considerably. The light variations characterize this star as an Lc: variable. Only Behr (1959), Dyck (1968), and Dyck and Jennings (1971) report linear polarization values for this star. These data are presented in Figure 1.6a and b. The Dyck and Jennings value of {R,0.64,163,_} indicates considerable rotation and amplitude change from the Behr value of {_,0.85,3,_}.

(e) 72 Leo (M3 IIb)

72 Leo is considered an Lb: variable. The star has been observed polarimetrically by Dyck and Jennings (1971), Dyck *et al.* (1971) and Jennings and Dyck (1971). The few reported data show that the polarization of 72 Leo varies to a high degree. In the blue-bandpass for example, the variation is from {B,1.50,167,_} to {B,0.33,176,_} over two years. The data are shown in Figure 1.7a and b.

(f) V CVn (M4-6 IIIe)

V CVn is an SRa variable with a 192 day period (Loeser *et al.* 1985); however, Loeser *et al.* (1985) argue that it may be a short period Mira type variable. The long polarization history of this star is displayed in Figure 1.8a and b. The sources for this polarimetry are Shakhovskoi (1964), Serkowski (1966a,b), Kruszewski, Gehrels, and Serkowski (1968), Dyck and Jennings (1971), Dyck, Forbes and Shawl (1971), Shawl (1975b), Wolf (1972), Coyne and Magalhães (1979), Boyle *et al.* (1986), Magalhães, Coyne and Benedetti (1986), and Koch (1987). The polarization is cyclic and shows large excursions in all bandpasses. Serkowski (1966b) reports

that the peak in the linear polarization occurs at minimum light. The peak polarization in the B-bandpass is greater than 6%! The polarization of this star at maximum can actually be seen with a small telescope and a piece of Polaroid filter.

Daniel (1980) developed a Monte Carlo code for the analysis of the polarization of V CVn. His conclusion was consistent with the Shawl (1975a) interpretation that multiple scattering could not be avoided in the explanation of the polarization of this star.

Some inconclusive circular polarimetry was reported by Wolf (1972) and by Avery *et al.* (1975). The Avery datum is [R,_,_,+0.0013(90)].

(g) α Sco (Antares, M1.5 Iab-Ib + B4Ve)

α Sco is an SRc variable with a B4 V companion at 3". The B star is slightly evolved away from the main sequence and is in the center of a vast reflection nebulosity of about 2000AU radius. α Sco shows ultraviolet FeII emission and the 5μm measurements indicate carbon monoxide to be present. There is a 1733 day period in the light. This variation extends in the visual from an apparent magnitude of +0.88 to +1.8. The radial velocity period is 7.5 years (Smith 1990) and is interpreted to be due to pulsation.

Shown in Figure 1.9a and b are the compiled polarization observations of Treanor (1963), Coyne and Wickramasinghe (1969), and Tinbergen, Greenberg and de Jager (1981). The Coyne and Wickramasinghe data are centered about [R,-0.43,+0.52,_]. The Tinbergen data are centered about [R,-0.1,+0.4,_]. Obviously, the polarizing environment changed considerably over eight years.

α Sco was observed by Kemp and Wolstencroft (1972) for circular polarization. Their one datum is [B,_,_,-0.0005(10)]. A small value such as this may tell us that α Sco either produces no circular polarization or was at a null epoch.

(h) α^1 Her (M5 Ib-II)

α^1 Her is an SRc variable with one period between 50 and 130 days superimposed upon a 6 year period. It has a G5 III companion at 4.6". Together they share a common envelope (Deutsch 1955).

Shakhovskoi (1964) measured {_,0.29(11),112,_}. The five-bandpass linear polarization set from Dyck and Jennings (1971) shows a strong rise from near zero in the R-bandpass to {U,0.33(11),95,_}. No published circular polarization data were found for this star.

(i) μ Cep (M2 Iae)

μ Cep is an SRc variable with a 730 day period and shows a large infrared excess. Maximum light is coincident with minimum polarization (Polyakova 1984). The mean light level varies with a period of 13.5 years.

Intrinsic stellar polarization was first proved by the variable polarization of μ Cep (Grigorian 1958). The published linear polarization for this object is shown in Figure 1.10a and b. These data were compiled from Hiltner (1951), Grigorian (1958), Coyne and Gherels (1966), Coyne and Kruszewski (1968), Wolf (1972), Shawl (1975b), Avery *et al.* (1975), Arsenijevic, Kubicela, and Vince (1980), Hayes (1981), Hayes (1982), Coyne and Magalhães (1979), Polyakova (1984), Le Borgne, Mauron, and Leroy (1986), and Le Borgne and Mauron (1989). Hayes (1982) concluded that the rapid polarization changes could only be seated in the lower atmosphere. The problem resulting from this interpretation is that the likely polarization mechanism is scattering from dust grains (Coyne 1988) and these should be destroyed at the temperature of the assigned level.

μ Cep was observed for circular polarization by Wolf (1972) and by Avery *et al.* (1975). The Avery data are [IR,_,_,-0.0057(24)], [R,_,_,-0.0060(18)], [V,_,_,-0.0155(24)], and [B,_,_,-0.0139(35)]. These data imply a strong negative trend towards the short wavelength region. Shafter and Jura (1980) calculated that 15" away from μ Cep there would be

observed circular polarization at the 0.01% level from light scattered in the circumstellar nebula.

(j) VV Cep (M2 Iape + O8 V)

VV Cep is the prototype for a class of long period eclipsing binaries with M supergiant primaries and O or B secondaries (*cf.* Cowley 1969). The orbit for VV Cep is 7430 days. The M supergiant is an SRc variable. The spectra were rich in emission but the V-bandpass light variation is small.

The available linear polarization data are shown in Figure 1.11a and b. The data were compiled from Shakhovskoi (1964), Serkowski and Chojnacki (1969) and Pfeiffer and Koch (1987). Pfeiffer and Koch developed a complex Rayleigh and electron scattering model for the system. The components of their model included an accretion disk around the B star. Rayleigh and/or electron scattering cannot directly produce circular polarization. Thus, circular polarimetry observations provide a useful probe of their model.

(k) β Peg (M2.5 II-III)

β Peg is an Lb variable showing over 0.5 magnitude variation. It shows ultraviolet FeII emission.

The Behr (1959) measure is {_,0.03,93.5,_}. Typical measures seen in the Dyck (1968) linear polarization data are {B,0.17,100,_} and {V,0.12,140,_}. The position angle is known to vary widely. Figure 1.12a and b displays these measures.

1.4 Thesis Objective

New heterochromatic polarimetric linear data would contribute to pinpointing the nature of the polarization sources and the types of scatterers, differentiating between mechanisms, and providing verification or denial for claims of binarity. Further, heterochromatic polarimetric circular data might constrain the dust grain models, indicate the presence of stellar spots, and yield an understanding of the systemic magnetic

fields indicative of spots and degenerate companions. In addition, the program objects taken as a group might yield ensemble characteristics for the upper right corner of the Hertzsprung-Russell diagram.

1.5 Data Presentation

In this thesis, uncertainty is presented in the form of one sigma standard deviation. Numbers are presented using the notation that the standard deviation of the least significant digits of a value is reported in parentheses. For example, the standard deviation of 0.0014 for a reported value +0.0556 is written in the format +0.0556(14). When errors are shown graphically, they are one sigma errors. Any departure from this rule is clearly pointed out. Three dots in a column position in a table indicate that the indicated value is not known or is unavailable. A colon after a reported data value indicates that uncertainty is considered to be large.

Unless otherwise stated, the three numbers inside square or curly braces are polarization row vectors. This format has been described in Section 1.3. The sign convention used in this thesis for the Stokes v vector is defined in Chapter 2.

Table 1.1. Program Object Parameters

HR	Name	DM	HD	RA(2000) (h)(m)(s)	DEC (°)(')(")	--GALACTIC-- LONG (°)	LAT (°)	<V>	<B-V>	<U-B>	<R-I>	SPEC. CLASS.	<Mv>	TRIG. PAR. (")	<RV> (km/s)	d_{sp} (pc)
1845	119 CE Tau	+18° 875	36389	05 32 12.7	+18 35 39	187.18	-08.07	+4.38	+2.07	+2.21	+1.44	M2 Iab-Ib	-4.8	+0.002	+23	320
2061	58 α Ori	+ 7° 1055	39801	05 55 10.3	+07 24 25	199.79	-08.96	+0.50	+1.85	+2.06	+1.28	M1-2 Ia-Iab	-6.5	+0.005	+21SB	150
2197	6 BU Gem	+22° 1220	42543	06 12 19.1	+22 54 30	188.22	+02.19	+6.39	+2.24	+2.48	+1.48	M1-2 Ia-Iab	-6.5	+0.003	+22	1400
2289	46 ψ1 Aur	+49° 1488	44537	06 24 53.8	+49 17 17	165.35	+16.17	+4.91	+1.97	+2.29	+1.07	K5-M0 Iab-Ib	-5.7	+0.007	+5SB	600
4362	72 Leo	+23° 2322	97778	11 15 12.2	+23 05 44	218.10	+67.88	+4.63	+1.66	+1.85	+1.31	M3 IIb	-0.5	+0.010	+16	90
	V CVn	+46° 1862	115898	13 19 27.9	+45 31 38	107.90	+70.77	+7.54	+1.51	+1.16		M4-6 IIIe	-0.4		-3	380
6134	21 α Sco	-26°11359	148478	16 29 24.4	-26 25 55	351.95	+15.06	+0.96	+1.83	+1.34	+1.23	M1.5 Iab-Ib + B4 Ve	-5.0	+0.024	-3SB	100
6406	64 α1 Her	+14° 3207	156014	17 14 38.8	+14 23 25	35.53	+27.82	+3.14	+1.44	+1.01	+2.14	M5 Ib-II +?	-3.5	-0.002	-33V	210
8316	μ Cep	+58° 2316	206936	21 43 30.3	+58 46 48	100.60	+04.32	+4.08	+2.35	+2.42	+1.76	M2 Iae	-7.0	+0.003	+19V	520
8383	VV Cep	+62° 2007	208816	21 56 39.1	+63 37 32	104.92	+07.05	+4.90	+1.75	+0.38	+1.34	M2 Iape + O8 V	-7.0	+0.001	-12V	1500
8775	53 β Peg	+27° 4480	217906	23 03 46.4	+28 04 58	95.74	-29.05	+2.42	+1.67	+1.96	+1.32	M2.5 II-III	-1.4	+0.022	+9V	48

Table 1.2. Program Object Variability State

Name	Variability Type (Note 1)	Max (mag)	Method (Note 2)	Min (mag)	Period (days)	Epoch of Primary (JD)	Duration of rise-time (%)
119 CE Tau	SRc	+6.10	p	+6.50	165	...	...
58 α Ori	SRc	0.42	v	1.30	2070	2410600	...
6 BU Gem	Lc:	6.10	v	7.50	...	...	...
46 ψ1 Aur	Lc:	6.60	p	7.20	...	...	...
72 Leo	Lb:	4.59:	v	4.65:	...	...	...
V CVn	SRa	6.80	v	8.80	191.88	2434930	50.0
21 α Sco	SRc	0.88	V	1.80	1733	2408600	...
64 α1 Her	SRc	3.0	v	4.0	...	...	...
μ Cep	SRc	3.60	v	5.10	730	...	...
VV Cep	EA/GS + SRc	6.65	p	7.46	7430.5	2435931	6.6
53 β Peg	Lb	+2.30	v	+2.80	...	...	...

Note 1. Variability types are defined in Hirshfield and Sinnot (1982).

Note 2. Method types are:

p = photographic

v = visual

V = V bandpass photoelectric

CHAPTER 1. Figure Captions

Figure 1.1. The absolute magnitude vs. effective temperature for the program objects.

Figure 1.2. The galactic positions of the program objects.

Figure 1.3. The observed linear Stokes vectors for 119 Tau from the literature. The ">" sign on the ordinate indicates the V-bandpass interstellar polarization vector determined in Section 3.2. The Hiltner (1951) data [_,+0.92,+0.29,_] and Behr (1959) data [_,+0.88,+0.48,_] are not shown. a) q in percent, b) u in percent.

Figure 1.4. The observed linear Stokes vectors for α Ori from the literature. The ">" sign on the ordinate indicates the V-bandpass interstellar polarization vector determined in Section 3.2. The Behr (1959) data [_,+0.002,+0.060,_] are not shown. a) q in percent, b) u in percent.

Figure 1.5. The observed linear Stokes vectors for 6 Gem from the literature. The ">" sign on the ordinate indicates the V-bandpass interstellar polarization vector determined in Section 3.2. The Hiltner (1951) data [_,+2.05,-0.44,_] are not shown. a) q in percent, b) u in percent.

Figure 1.6. The observed linear Stokes vectors for ψ^1 Aur from the literature. The ">" sign on the ordinate indicates the V-bandpass interstellar polarization vector determined in Section 3.2. a) q in percent, b) u in percent.

Figure 1.7. The observed linear Stokes vectors for 72 Leo from the literature. The ">" sign on the ordinate indicates the V-bandpass interstellar polarization vector determined in Section 3.2. a) q in percent, b) u in percent.

Figure 1.8. The observed linear Stokes vectors for V CVn from the literature. The ">" sign on the ordinate indicates the V-bandpass interstellar polarization vector determined in Section 3.2. a) q in percent, b) u in percent.

Figure 1.9. The observed linear Stokes vectors for α Sco from the literature. The ">" sign on the ordinate indicates the V-bandpass interstellar polarization vector determined in Section 3.2. a) q in percent, b) u in percent.

Figure 1.10. The observed linear Stokes vectors for μ Cep from the literature. The ">" sign on the ordinate indicates the V-bandpass interstellar polarization vector determined in Section 3.2. a) q in percent, b) u in percent.

Figure 1.11. The observed linear Stokes vectors for VV Cep from the literature. The ">" sign on the ordinate indicates the V-bandpass interstellar polarization vector determined in Section 3.2. a) q in percent, b) u in percent.

Figure 1.12. The observed linear Stokes vectors for β Peg from the literature. The ">" sign on the ordinate indicates the V-bandpass interstellar polarization vector determined in Section 3.2. The Behr (1959) data [_,-0.004,-0.032,_] are not shown. a) q in percent, b) u in percent.

Figure 1.1

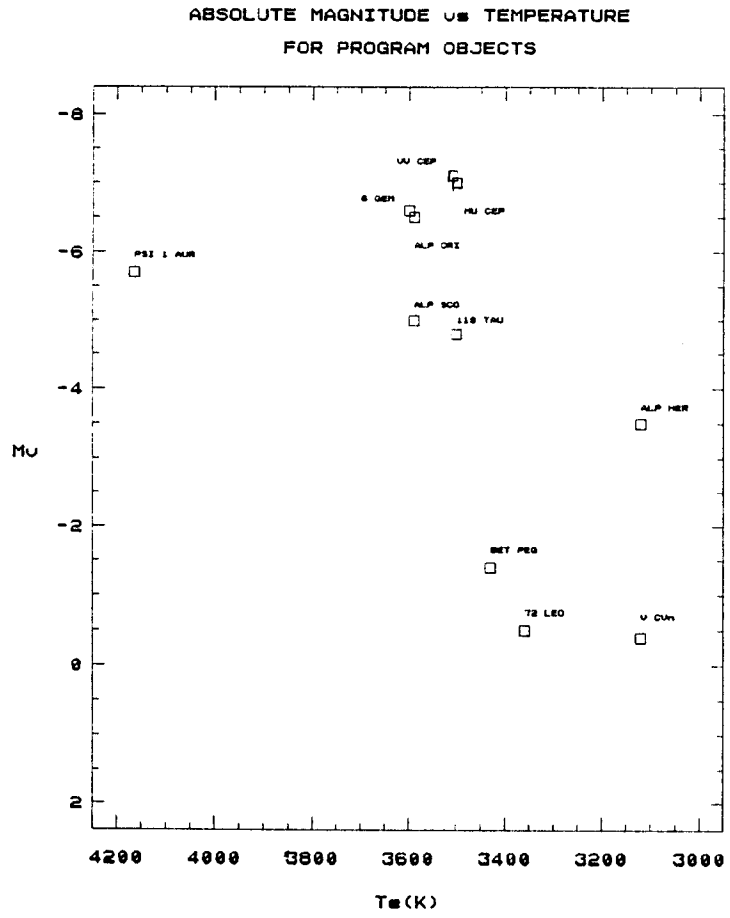

Figure 1.2

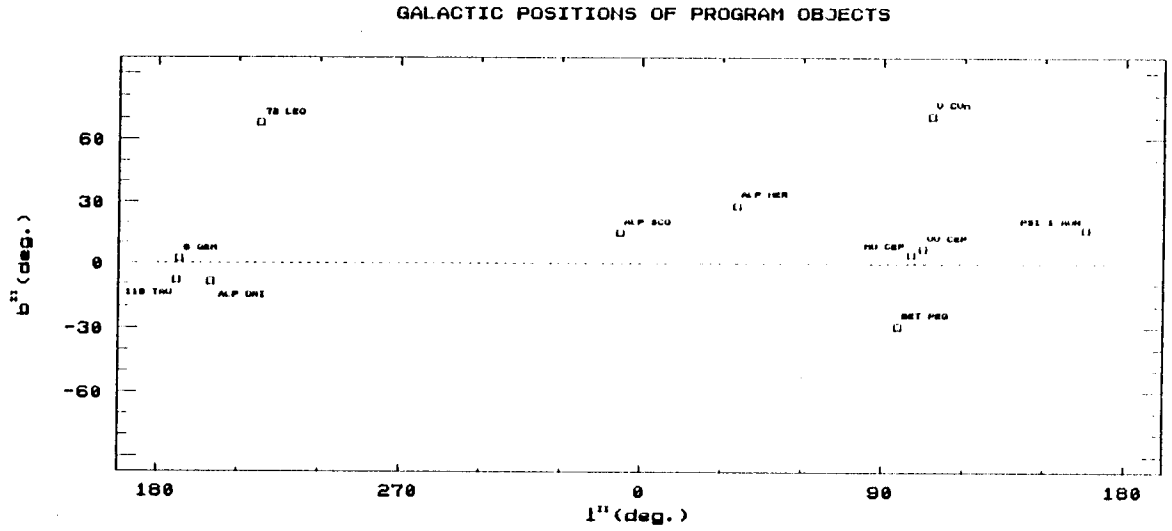

Figure 1.3

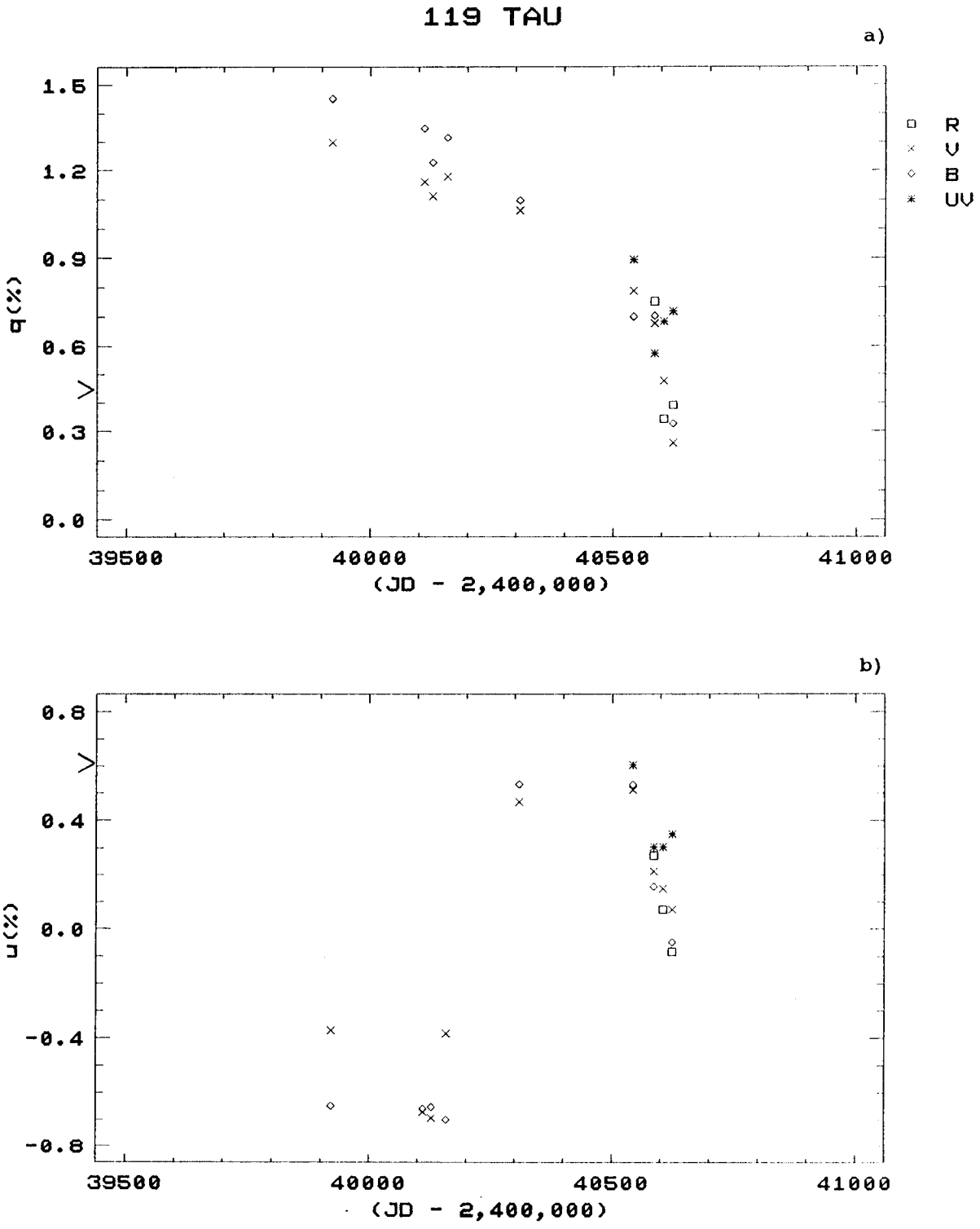
119 TAU
a)
1.5
1.2
0.9
0.6
0.3
0.0
q(%)
R
V
B
UV
39500
40000
40500
41000
(JD - 2,400,000)
b)
0.8
0.4
0.0
-0.4
-0.8
u(%)
39500
40000
40500
41000
(JD - 2,400,000)

Figure 1.4

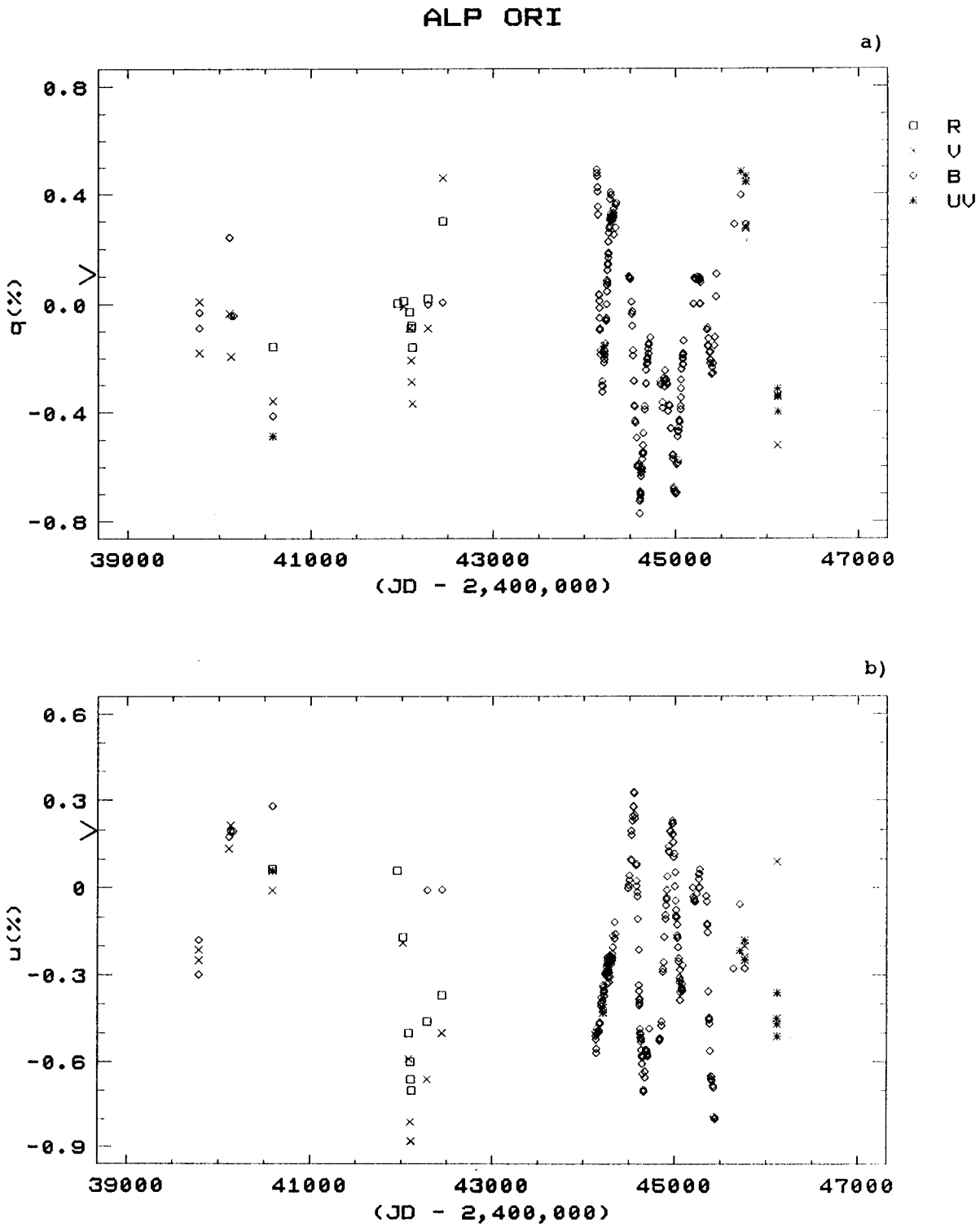
ALP ORI
a)
0.8
0.4
0.0
-0.4
-0.8
q(%)
39000
41000
43000
45000
47000
(JD - 2,400,000)
R
V
B
UV
b)
0.6
0.3
0
-0.3
-0.6
-0.9
u(%)
39000
41000
43000
45000
47000
(JD - 2,400,000)

Figure 1.5

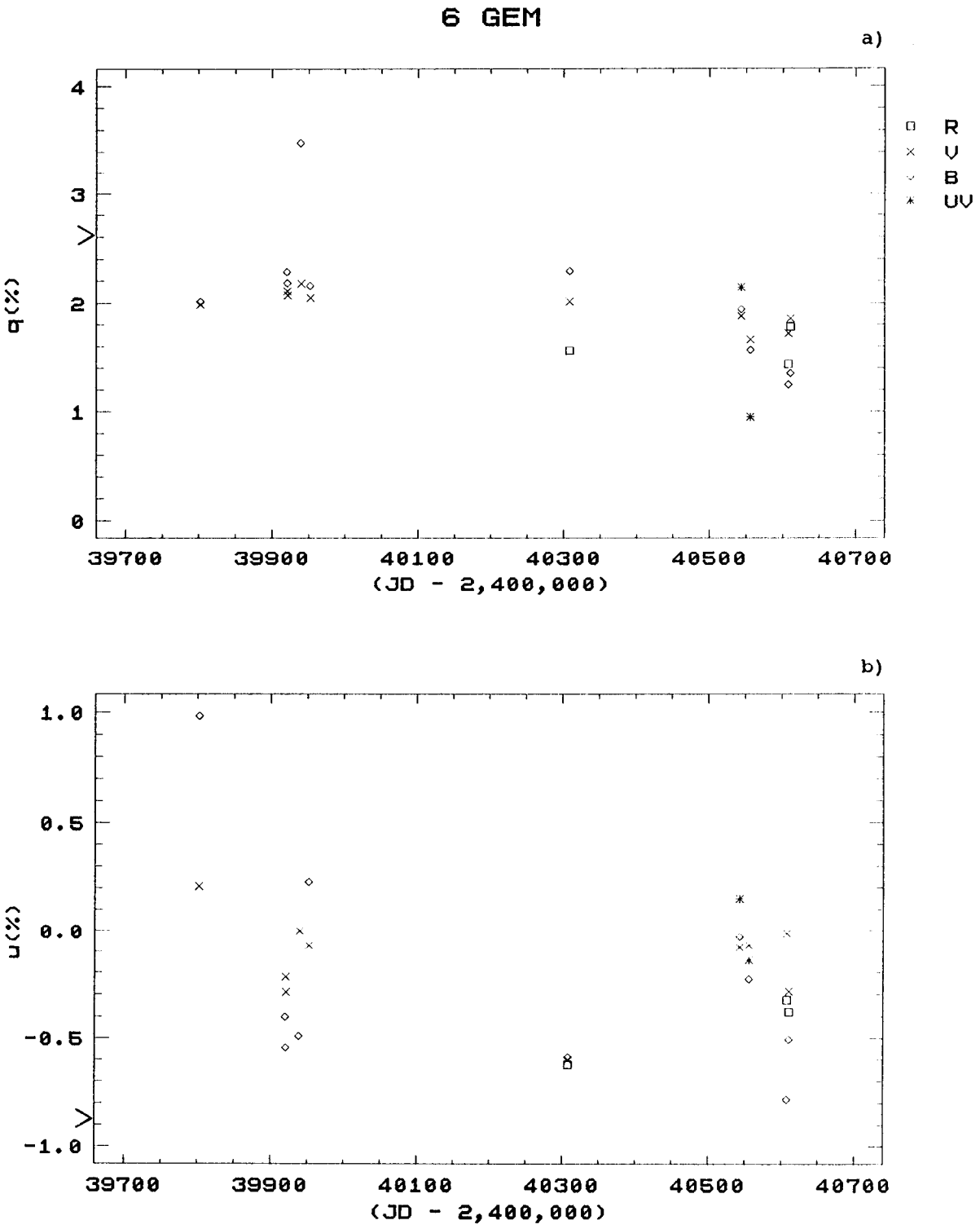
6 GEM
a)
q(%)
4
3
2
1
0
39700
39900
40100
40300
40500
40700
(JD - 2,400,000)
R
V
B
UV
b)
u(%)
1.0
0.5
0.0
-0.5
-1.0
39700
39900
40100
40300
40500
40700
(JD - 2,400,000)

Figure 1.6

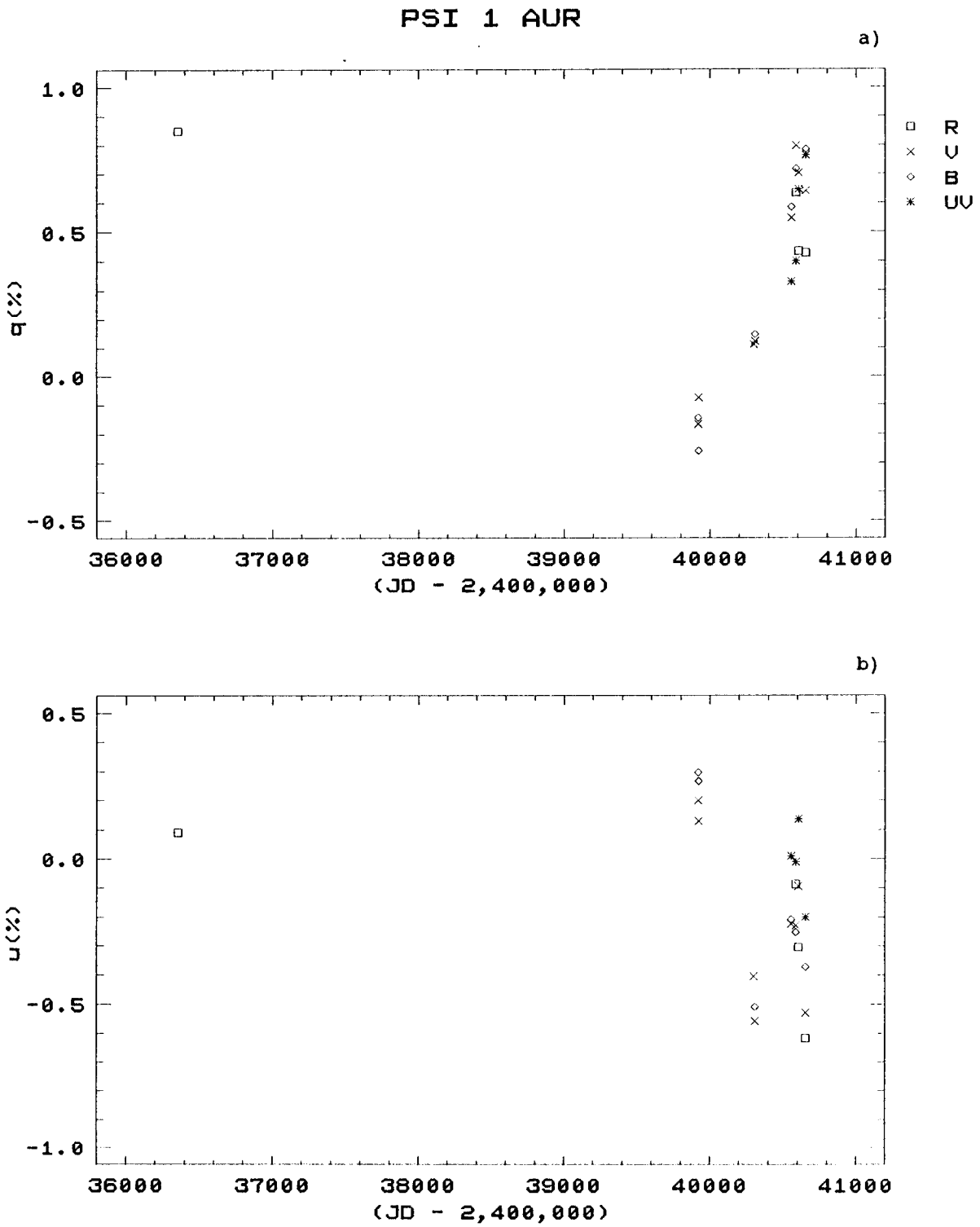
PSI 1 AUR
a)
1.0
0.5
0.0
-0.5
q(%)
36000
37000
38000
39000
40000
41000
(JD - 2,400,000)
R
V
B
UV
b)
0.5
0.0
-0.5
-1.0
u(%)
36000
37000
38000
39000
40000
41000
(JD - 2,400,000)

Figure 1.7

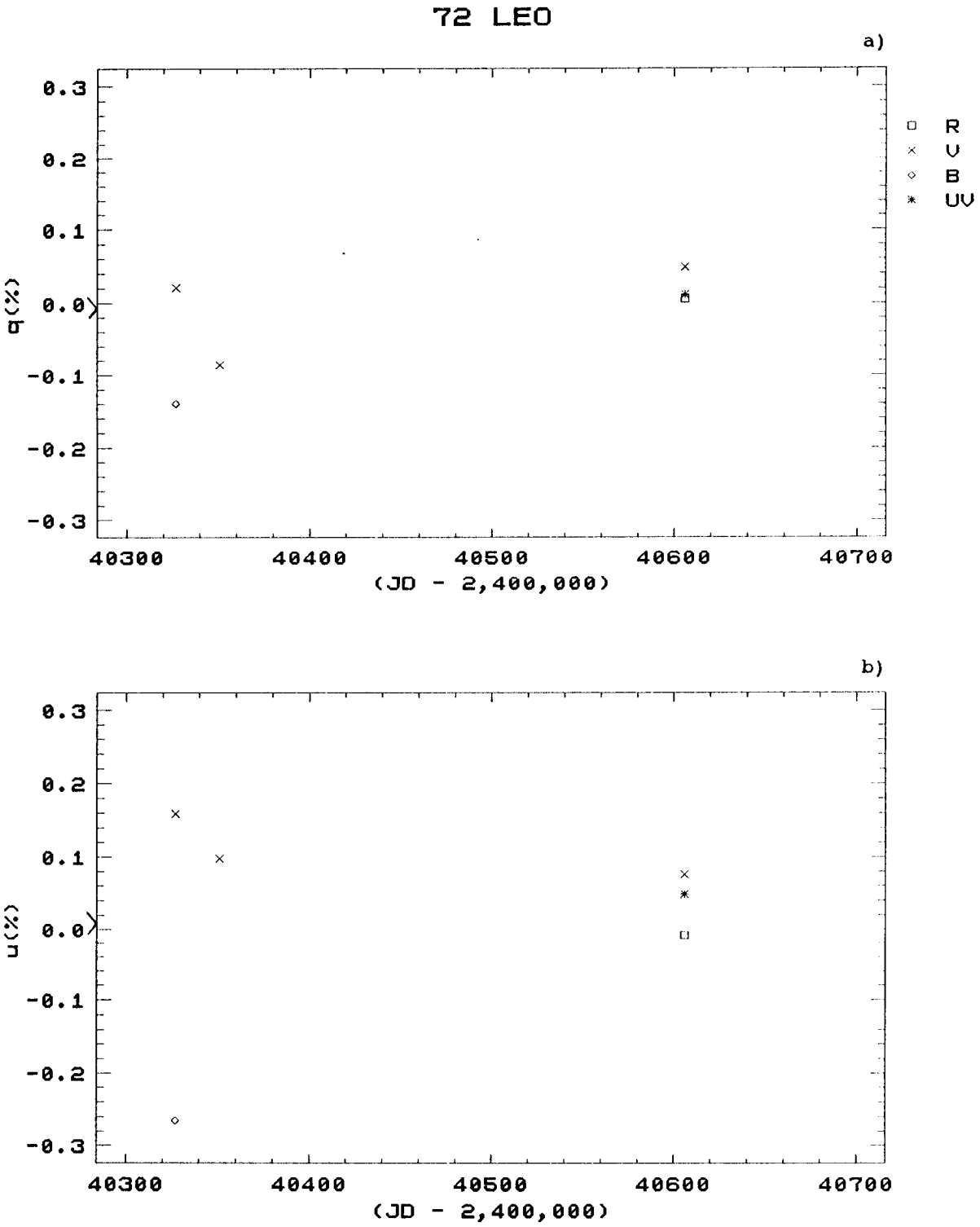
72 LEO
a)
0.3
0.2
0.1
0.0
-0.1
-0.2
-0.3
q(%)
40300
40400
40500
40600
40700
(JD - 2,400,000)
R
V
B
UV
b)
0.3
0.2
0.1
0.0
-0.1
-0.2
-0.3
u(%)
40300
40400
40500
40600
40700
(JD - 2,400,000)

Figure 1.8

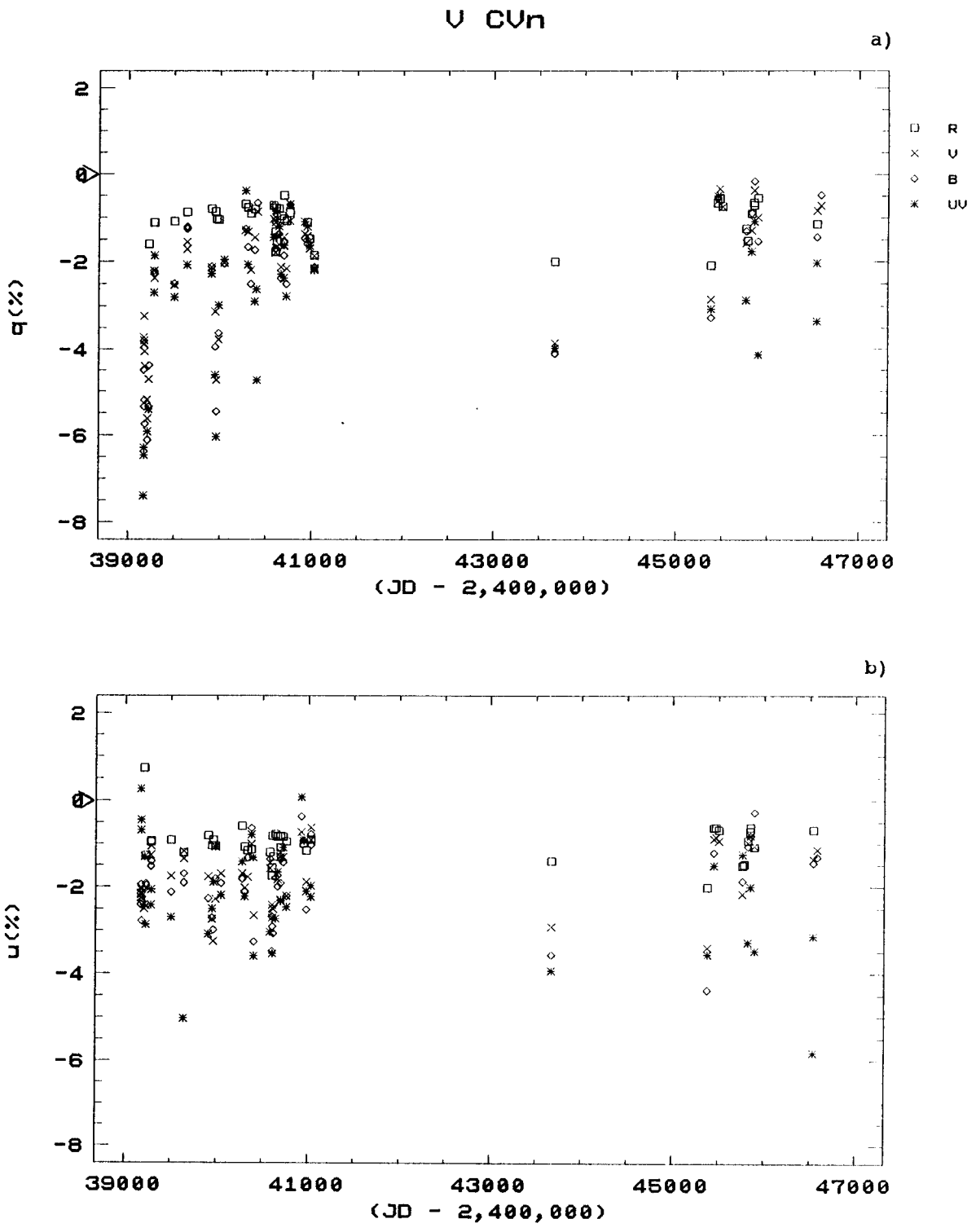
V CVn
a)
q(%)
u(%)
R
V
B
UV
2
0
-2
-4
-6
-8
39000
41000
43000
45000
47000
(JD - 2,400,000)
b)

Figure 1.9

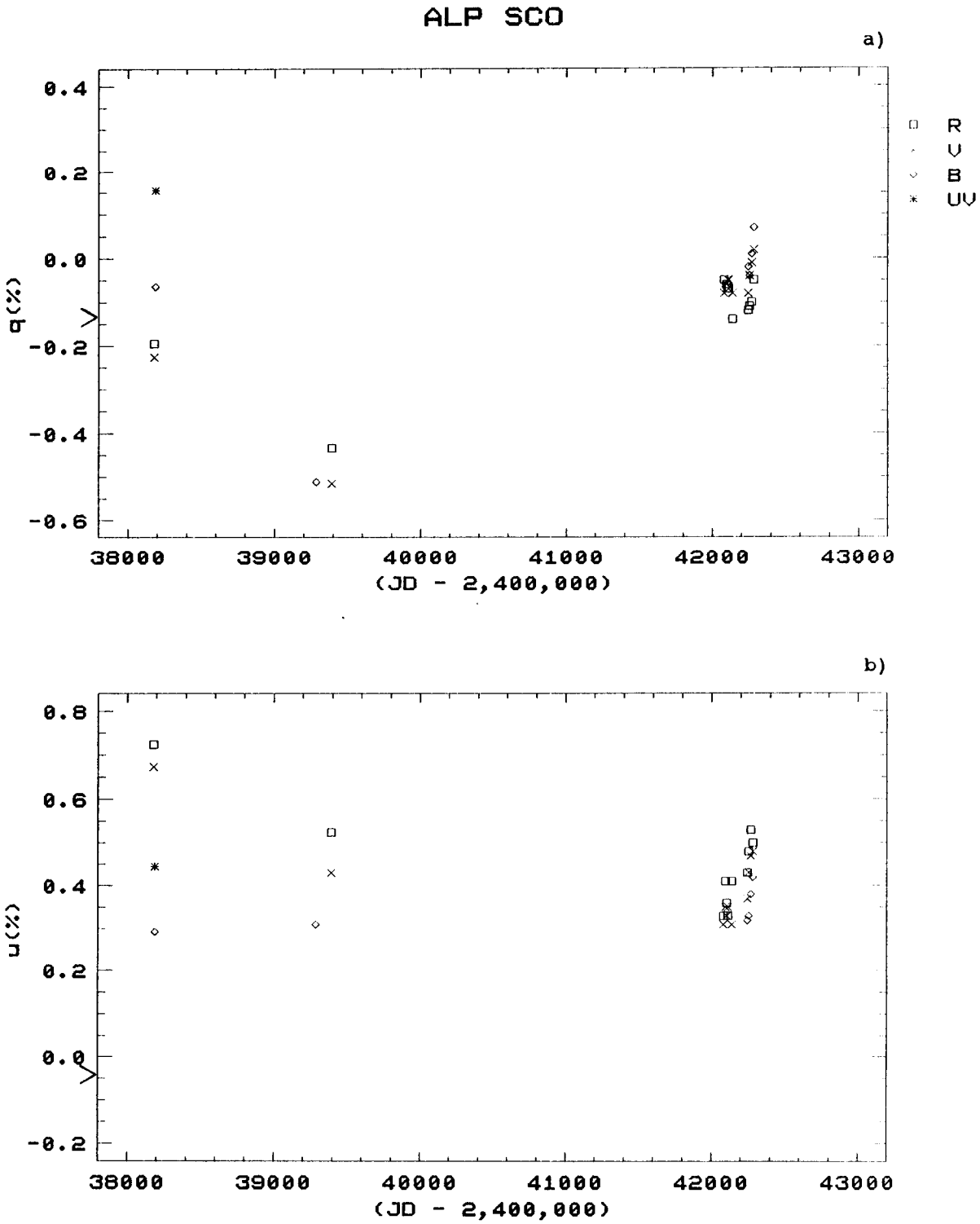
ALP SCO
a)
0.4
0.2
0.0
-0.2
-0.4
-0.6
q(%)
38000
39000
40000
41000
42000
43000
(JD - 2,400,000)
R
V
B
UV
b)
0.8
0.6
0.4
0.2
0.0
-0.2
u(%)
38000
39000
40000
41000
42000
43000
(JD - 2,400,000)

Figure 1.10

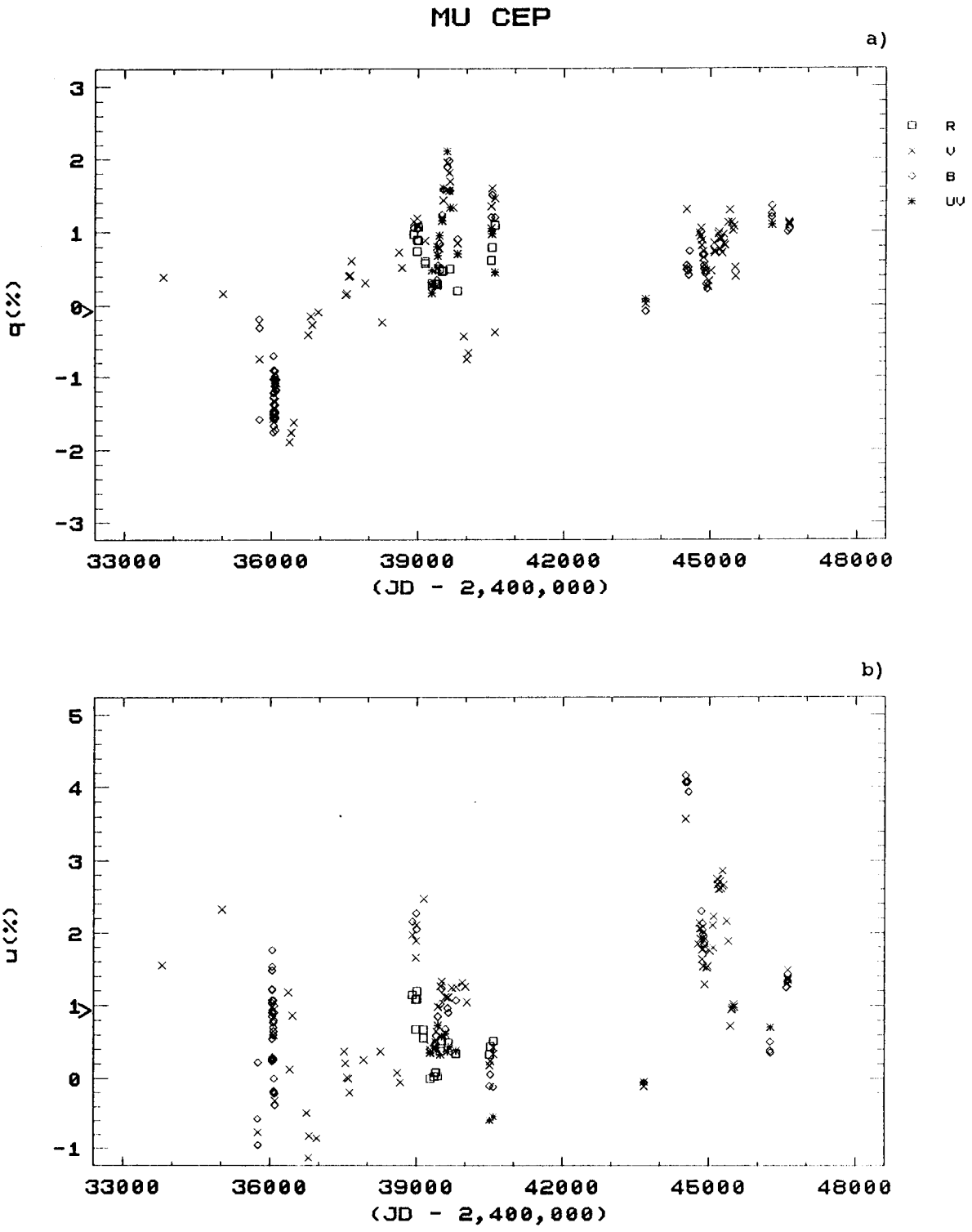
MU CEP
a)
q(%)
3
2
1
0
-1
-2
-3
33000
36000
39000
42000
45000
48000
(JD - 2,400,000)
R
V
B
UV
b)
u(%)
5
4
3
2
1
0
-1
33000
36000
39000
42000
45000
48000
(JD - 2,400,000)

Figure 1.11

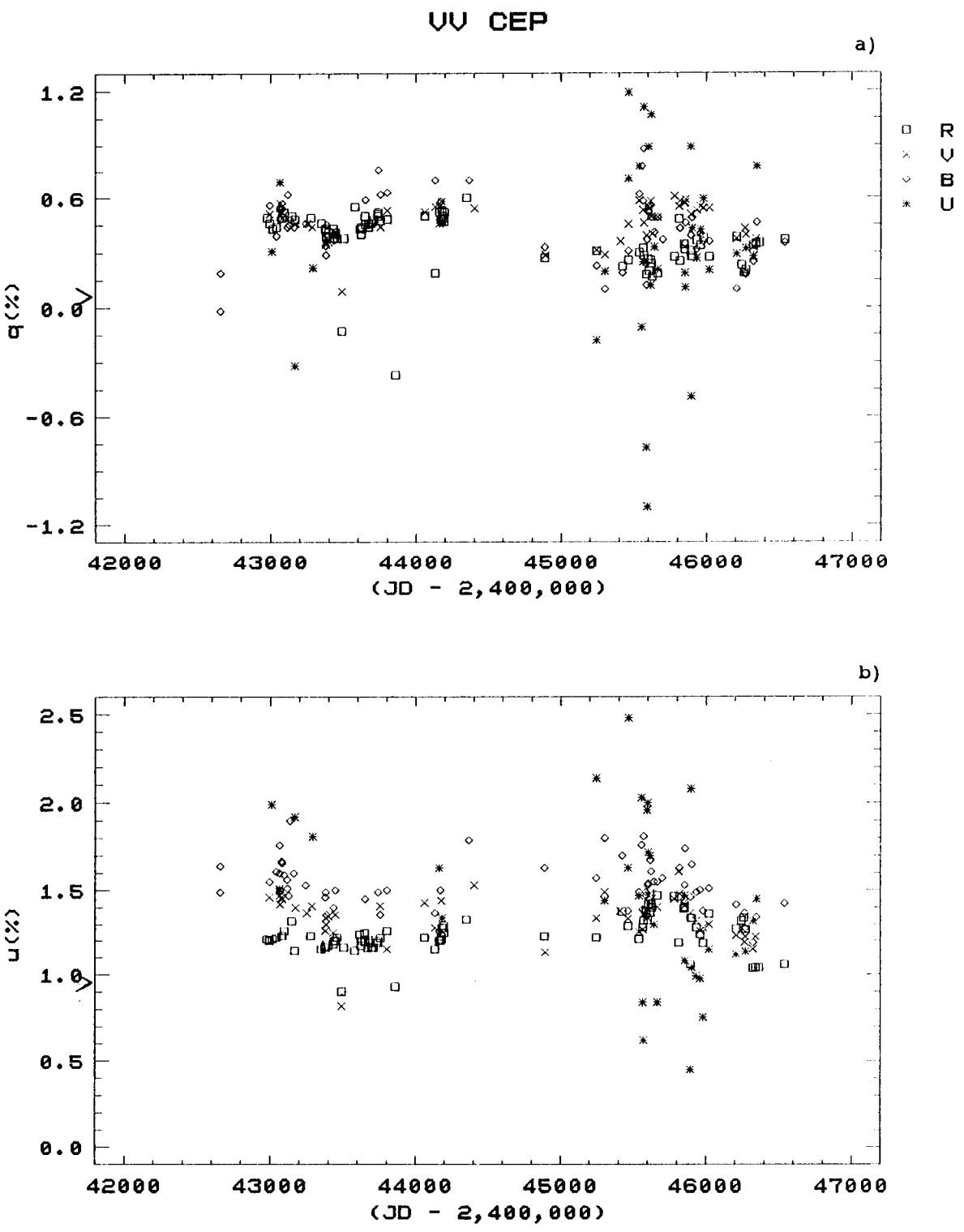
VV CEP
a)
1.2
0.6
0.0
-0.6
-1.2
q(%)
R
V
B
U
42000
43000
44000
45000
46000
47000
(JD - 2,400,000)
b)
2.5
2.0
1.5
1.0
0.5
0.0
u(%)
42000
43000
44000
45000
46000
47000
(JD - 2,400,000)

Figure 1.12

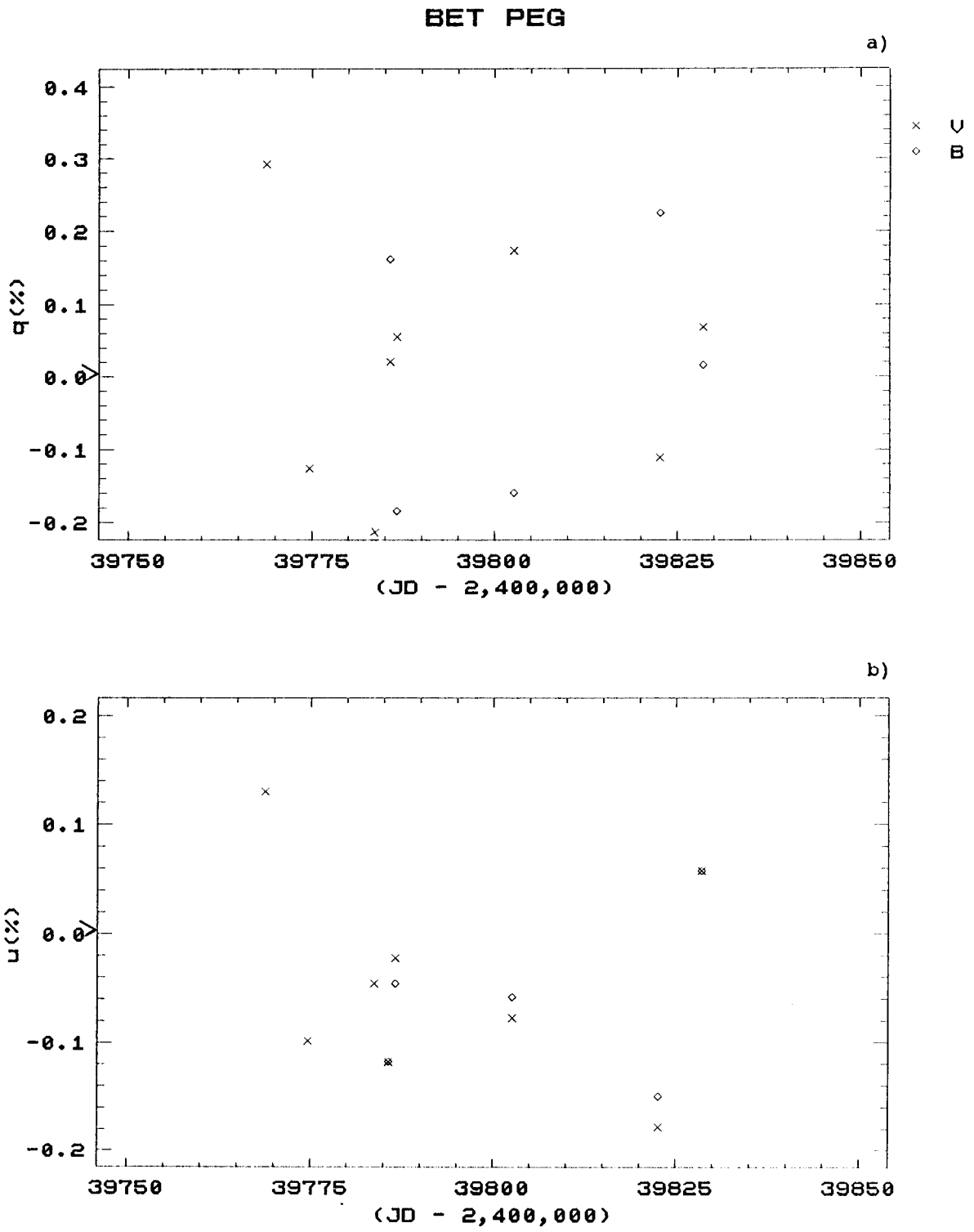
BET PEG
a)
0.4
0.3
0.2
0.1
0.0
-0.1
-0.2
q(%)
V
B
39750
39775
39800
39825
39850
(JD - 2,400,000)
b)
0.2
0.1
0.0
-0.1
-0.2
u(%)
39750
39775
39800
39825
39850
(JD - 2,400,000)

CHAPTER 2. The Pennsylvania Elliptical Polarimeter

2.1 Overview of the Elliptical Polarimeter

The first phase of the dissertation research involved designing and installing a polarimetric subsystem for the 72-cm Cassegrain reflector at the Flower and Cook Observatory so as to double throughput by permitting elliptical polarization measures. This was accomplished by enabling circular polarization measurements to be made simultaneously with linear polarization measurements. The linear polarimetry subsystem has been described by Koch *et al.* (1985), Blitzstein (1987a, b), Corcoran (1988) and Elias (1990). Holenstein (1987) and Elias have briefly described the circular polarimetry subsystem; however, neither author has described the fundamental operation of this subsystem.

Figure 2.1 presents a schematic diagram of PEMP which is updated from the diagram presented by Koch *et al.* Light from the *f*/14.7 telescope optics enters from the top left in this figure. The light passes through a background limiting aperture (1.5, 2.5, or 5.0mm diameter) and is collimated by a Fabry lens before passing through one of the filters mounted in a movable slide. Four filters are available which, in conjunction with the photomultiplier tube, approximate the Johnson B-, V-, and R-bandpasses and generate a natural u-bandpass. Corcoran and Elias present details concerning these filters. After passing through one of the filters, the light impinges upon a Morvue PEM-FS3 photoelastic modulator (PEM) bar. Kemp (1969) provides a good general description of the theory of the PEM. The bar acts as a time-variable, presumably linear, retarder with a fundamental excitation frequency of 50kHz. The light next passes through a Glan-Thompson linear polarizer/analyzer prism before impinging on an RCA 4509 photomultiplier tube. The photomultiplier electrical output is split with one leg going to an FET-input AC amplifier (for the Channel 1 linear and Channel 3 circular subsystems) and the other leg going to a 100ms time-constant operational DC amplifier (for Channel 2). Channels 1

and 3 measure the flux modulation produced by the PEM. Channel 2 measures the average value of the incident flux. The output of the DC amplifier is fed into a voltage controlled oscillator (VCO)/32-bit binary upcounter integrator. Channel 2 provides the normalizing voltage for the linear and circular subsystems. The output of the AC amplifier is connected to both an Ithaco 391A DynaTrack lock-in amplifier run in the $2f$ reference mode (Channel 1) with integration provided by a VCO arrangement analagous to the DC channel and to a Stanford Research Systems SR530 dual channel lock-in amplifier run in the f reference mode (Channel 3) with integration provided through software. Both the linear and the circular subsystems get their reference signals from the 50 kHz excitation reference output provided by the driver unit for the PEM-FS3 photoelastic modulator bar. The linear subsystem is controlled by an IBM-AT and the circular subsystem is controlled by an IBM-XT compatible.

Appendix A gives a detailed listing of the steps which must be taken in order to observe using the elliptical polarimeter.

2.2 Idealized Theory of Operation for an Elliptical Polarimeter

The electrical output of the photomultiplier is proportional to the incident radiant flux from the star as operated upon by the filter, time-variable retarder (PEM), and analyzer. The optical path of the pulse-counting polarimeter used by Stokes, Ekstrom, and Swedlund (1976) is similar to the optical path of the Pennsylvania polarimeter and therefore may be used as a model. The radiant flux, I_d, incident upon the photomultiplier tube detector is proportional to the orientation, Φ, of the fast axis of the PEM with respect to North on the celestial sphere and to time, t, in the following manner (*cf.* Equation 4 of Stokes, Ekstrom, and Swedlund):

$$I_d(\Phi, t) = \tfrac{1}{2}I_T + \tfrac{1}{2}P_I\cos(2\Phi)\cos(2\Psi) + \tfrac{1}{2}\sin(2\Psi) \bullet$$
$$\{(P_I\sin(2\Phi)\cos\alpha + V\sin\alpha)\,[J_o(\beta) + 2\sum_{n=1}^{\infty} J_{2n}(\beta)\cos(2n\omega t)]$$
$$+ (V\cos\alpha - P_I\sin(2\Phi)\sin\alpha)\,[2\sum_{n=0}^{\infty} J_{2n+1}(\beta)\sin((2n+1)\omega t)]\}, \qquad (2.1)$$

where I_T is the flux collected by the telescope incident upon the time-variable retarder, P_1 is the amplitude of the linear polarization flux (and is equal to $\sqrt{Q^2 + U^2}$), Ψ is the angle between the fast axis of the PEM and the pass axis of the analyzer (set and fixed at 45°), α is the residual retardence of the PEM bar (about one degree), J is the Bessel function term indicated by the subscript, β is the amplitude of the PEM retardance modulation, and ω is the fundamental angular frequency corresponding to the 50kHz excitation of the PEM. By convention, β is set to π, which corresponds to $0.5\lambda_{eff}$ for the effective wavelength of the filter's peak transmittance. Equation 2.1 is only approximate since β can correspond precisely to only one wavelength. However, with the use of a bandpass filter, the equation's departure from equality is small as has been verified by measurement. PEM units are preferable to Pockels cells because they have a wide acceptable incidence angle, but they share the Pockels cell limitation of not being achromatic.

The Channel 1 (linear) lock-in amplifier, operating in the 2f mode, picks out the first overtone modulation term from Equation 2.1 and produces a time-averaged VCO output count, $\langle CH_1(\Phi)\rangle$, as follows:

$$\langle CH_1(\Phi)\rangle = K_1\sin(2\Psi)\,(P_I\sin(2\Phi)\cos\alpha + V\sin\alpha)\,J_2(\beta), \qquad (2.2)$$

where K_1 is a constant which depends upon the AC amplifier gain, photomultiplier voltage, integration time, and Channel 1 lock-in gain. For

all channels, constant integrator output offsets are subtracted by software since differential observing between background and star plus background is performed.

Likewise, the Channel 3 (circular) lock-in amplifier, operating in the *f* mode, picks out the fundamental modulation term from Equation 2.1 and produces a time-averaged output voltage, $\langle CH_3(\Phi)\rangle$, as follows:

$$\langle CH_3(\Phi)\rangle = K_3 \sin(2\Psi)\,(V\cos\alpha - P_1 \sin(2\Phi)\sin\alpha)\,J_1(\beta), \qquad (2.3)$$

where K_3 is a constant which depends upon the AC amplifier gain and photomultiplier voltage. Channel 3 integrates through software which results in K_3 not having an integration time dependence.

It should be remarked that the choice of $\beta = \pi$ for all observations is near optimum (optimum is at $\beta = 3.8$) for the linear subsystem since $J_2(\beta)$ in Equation 2.2 is then near its global maximum. However, $J_1(\beta)$ in Equation 2.3 is about 50% lower than its global maximum resulting in an efficiency handicap for the circular subsystem. The choice of keeping β constant was made so as to avoid having to recalibrate the linear subsystem after the circular system was installed.

The DC amplifier has a 100ms time-constant feedback and produces an integrated VCO output count, $\langle CH_2(\Phi)\rangle$, as follows:

$$\begin{aligned}\langle CH_2(\Phi)\rangle = {} & K_2\{(I_T + P_1\cos(2\Phi)\cos(2\Psi) + \\ & \sin(2\Psi)\,[P_1\sin(2\Phi)\cos\alpha + V\sin\alpha]\,J_0(\beta)\}\end{aligned} \qquad (2.4)$$

where K_2 is a constant which depends upon the DC amplifier gain, integration time, and photomultiplier voltage.

The proper correction angle for the phase difference between the

electrical reference of the PEM driver and the electrical output of the FET-input AC amplifier is determined by measuring a bright source of large linear polarization (the "electric vector" (EV) source: an LED and mirror combination built into the optics head yielding $p \approx 82\%$) for Channel 1 and a bright source of circular polarization (EV source plus Polaroid HNCP37 sheet yielding $v \approx 83\%$) for Channel 3. The Channel 1 lock-in amplifier is switched 90° out of phase and is zeroed by the observer. Since the Channel 3 lock-in amplifier is a dual channel device, the phase angle difference, ξ, can be determined through software interrogation of this lock-in amplifier's reference axes.

The standard observing procedure is to make measurements of the star *plus* background and background at nine orientations of the polarimeter head nearly equally spaced 40° apart about the optical axis. A net output is thus produced by the following:

$$\langle NET_n(\Phi) \rangle = \langle CH_n(\Phi) \rangle_{star+background} - F_n \langle CH_n(\Phi) \rangle_{background} , \qquad (2.5)$$

where n equals 1, 2 or 3, and F_n removes all differences between the integration time on the star *plus* background versus the background. F_n is unity for Channel 3 since K_3 does not depend upon the integration length, Π, but it equals $\Pi_{star+background}/\Pi_{background}$ for Channels 1 and 2. The importance of the variable integration lengths procedure for reducing error is described in Section 2.3. An additional step needed for Channel 3 is to project the measured output vector onto a unit vector at an orientation of ξ for proper phasing; this is done in software. For the nine orientations, seven-term truncated Fourier series are fitted (*cf.* Smart 1958) to $\langle NET_1(\Phi) \rangle / \langle NET_2(\Phi) \rangle$ and to $\langle NET_3(\Phi) \rangle$. For the former, the amplitude and orientation of the second order harmonic after multiplication by C_1/C_2 (C_1 and C_2 normalize the VCO counts for one minute integrations to millivolts

for Channel 1 and Channel 2, respectively) give the degree and orientation of the linear polarization, that is, p_l and Θ (transformable to q and u for Cartesian coordinates). For the Channel 3 Fourier terms, the DC (or A) term gives the degree (v) and sign of the circular polarization once normalized by multiplying by $C_3/(C_2<<NET_2>>)$, where C_3 normalizes the A term to millivolts and $<<NET_2>>$ is the average over all angles. Since the IBM-AT controls both Channels 1 and 2, the linear calculations benefit from having the measures at each azimuthal angle normalized for variable observing conditions. However, this produces a non-linearity in the measured polarization. The non-linearity has been removed to first-order by the quadratic correction in the reduction software introduced by Blitzstein (1987b). A more precise removal requires a cubic term. Since the program and standardizing stars all have polarizations below six percent, the linear reduction procedure was not changed. This results in an amplitude error less than one percent of the measured value.

Bleeding of linear polarization into a circular polarization signal and *vice versa* due to a non-zero α are eliminated from the reduced data, since this effect appears in the discarded DC term for the determination of the linear polarization (see Equation 2.2), and in the discarded second overtone terms for the determination of the circular polarization (see Equation 2.3). The calibration process compensates for the gain reduction imposed by α on the assorted Fourier terms.

2.3 Variable Integration Lengths

Differential observing of star *plus* background and background can be shown to remove the background signal from observations better than a technique by which the size of the aperture is varied. Further, it was recognized that differential observing can be optimized by using different integration lengths, $\Pi_{star+background}$ and $\Pi_{background}$, for the star *plus* background and the background, respectively. Longer integrations generally produce higher signal-to-noise ratios. It is the present objective to show

that, because the background signal is not infinite, shorter integration lengths for the background will maximize the signal-to-noise ratio of the desired stellar signal subject to the observing constraint. Consider the following:

$$\Pi_{total} = \Pi_{star+background} + \Pi_{background}\,, \tag{2.6}$$

where Π_{total} is the fixed, total amount of time available for an observation.

From Equation 2.5 the error at each angle is given by:

$$\sigma^2_{\langle NET_n\Phi\rangle} = \sigma^2_{\langle CH_n\Phi\rangle_{star+background}} + F^2\sigma^2_{\langle CH_n\Phi\rangle_{background}}. \tag{2.7}$$

Both subsystems are linear. Therefore, if error in the system is entirely random due, for example, to shot-noise when observing faint stars or scintillation noise when observing bright stars, then:

$$\begin{aligned} \sigma^2_{\langle CH_n\Phi\rangle_{star+background}} &= (S_n + B_n)\,\Pi_{star+background} \\ \sigma^2_{\langle CH_n\Phi\rangle_{background}} &= B_n\Pi_{background}, \end{aligned} \tag{2.8}$$

where S_n and B_n stand for the amplitudes of the signals (arising from I_T, p_l, or v) from the star and the background, respectively. If the stellar signal is used for normalization, then the normalized variance, V_ϵ, is given by:

$$\begin{aligned} V_\epsilon &= \frac{\sigma^2_{\langle NET_n\Phi\rangle}}{S_n^2\Pi^2_{star+background}} \\ &= \frac{S_n + B_n}{S_n^2\Pi_{star+background}} + \frac{B_n}{S_n^2(\Pi_{total} - \Pi_{star+background})}, \end{aligned} \tag{2.9}$$

where F was replaced by the equivalent ratio. Setting the first derivative of V_ϵ with respect to $\Pi_{star+background}$ equal to zero gives for the minimum:

$$\Pi_{star+background} = \frac{\Pi_{total}}{1 + \sqrt{\frac{B_n}{S_n + B_n}}}. \qquad (2.10)$$

This equation shows that, if the background signal is small with respect to the star, little observing time should be spent on the background. However, if the background signal is large with respect to the star then, at most, one half of the observing time should be spent on the background. At Flower and Cook Observatory, knowledge that the assumption of random errors made in Equation 2.8 is not perfect was used to limit most observations on the program stars to 90 second integrations on the star and 30 second integrations on the background. Thus, in comparison with not using variable integration lengths, this procedure enabled the 72cm Cassegrain primary mirror to act as if it had nearly 50% more area. As a final note, observe that Equation 2.10 predicts different integration lengths for the different channels. In cases of conflict, it is recommended that the largest $\Pi_{background}$ should be used.

2.4 Data Acquisition and Reduction Software

The data acquisition and reduction software for the linear subsystem have been described by Blitzstein (1987b) and Corcoran. No changes have been made in this reduction technique except in the error calculation. Corcoran remarked that the calculated errors were not realistic. The primary reason for this is that the number of Fourier coefficients previously used in the data reduction was equal to the number of degrees of freedom, specifically nine angles were measured and nine coefficients were determined. This left no degree of freedom for determination of the error.

Elias argues that, for linear polarimetry on bright stars, only the DC term and second harmonic should be used, and that for faint stars only the second harmonic should be used.

Elias and Blitzstein disagree about a possible third harmonic signal. Blitzstein (1991) reported on a statistical study of a number of observations on the same star and night under identical circumstances. He found that the third and also the fourth harmonic terms for this data set are spurious and purely the result of noise. So far, Blitzstein cannot find a physical justification for the third and fourth angular harmonics in the Pennsylvania polarimeter data. Blitzstein has tried assuming that the PEM is not a linear, but a slightly elliptical, retarder. No fourth harmonics ensued.

Varying the number of terms that are evaluated does not change the amplitude of the desired terms greatly, but the estimated errors are determined more correctly. It is shown in Appendix B that the mean-squared error, $\langle\sigma^2\rangle$, of the desired terms is stationary for random errors from variations in the number of harmonics evaluated as long as excess degrees of freedom remain after the Fourier fitting:

$$\langle\sigma_k^2\rangle - \langle\sigma_{k+1}^2\rangle = 0, \qquad (2.11)$$

where the subscripts are the number of harmonics in the Fourier fit. Thus it is felt that representative errors are calculated by using the DC and the first through third overtones of the Fourier reduction step since two degrees of freedom remain after the Fourier fitting process. This is satisfying since the first harmonic definitely arises, in part, from the star's Ramsden disk moving over the surface of the photomultiplier cathode and the third harmonic may arise due to heterodyning between the first and second harmonics. Omitting the first and/or third harmonics could cause

misrepresentation in the reported errors. Equation 2.11 shows that solving for the first and third terms can only help. It is remarked that more than nine angles should be observed in order to reduce the errors significantly. This same argument applies to the number of harmonics evaluated for the circular subsystem.

Data acquisition and reduction with the circular subsystem will now be described. In accordance with Equation 2.5, from analysis of $\langle NET_3(\Phi)\rangle$ the DC Fourier term, A, is proportional to the object's circular polarization:

$$V = \frac{C_3\, A}{C_2 \langle NET_2 \rangle} \frac{\Pi_{star+background}}{60}, \qquad (2.12)$$

where $\Pi_{star+background}$ is measured in seconds.

The error reported for the circular system, σ_V, is calculated from:

$$\sigma_V = \frac{\Pi_{star+background}}{60} \sqrt{(C_2 \langle NET_2 \rangle)^{-2} \left(A^2 \sigma_{C_3}^2 + C_3^2 \sigma_A^2\right) + \left(\frac{C_3 A}{C_2 \langle NET_2 \rangle}\right)^2 \left(\frac{\sigma_{C_2}^2}{C_2^2} + \frac{\sigma_{\langle NET_2 \rangle}^2}{\langle NET_2 \rangle^2}\right)}, \qquad (2.13)$$

where σ_{C3} is determined from observations of standardized sources of circular polarization (see Section 2.6), σ_A is determined through the Fourier fit to the data in accordance with Equation 2.11, σ_{C2} is determined from the least-squares fit to C_2 calibration data (a value of 0.5% having been adopted), and $\sigma_{\langle\langle NET2\rangle\rangle}$ is determined by $\sqrt{\langle\langle NET_2 \rangle\rangle}$.

Appendix C discusses the program flow and contains listings for the data acquisition and reduction software for Channel 3.

2.5 Calibration Technique

Hybrid methods for calibration of the linear subsystem were developed by Blitzstein (1987b) and Koch (1987) and by the author for the circular subsystem. For both subsystems, the first calibration mode uses near-null and non-null laboratory standards. At Flower and Cook Observatory there are quarter-wave plates and linear and circular polarization sources for use as laboratory standards. The second calibration mode uses null and non-null stellar sources of polarization. Since there are no known standard sources of circular polarization and few consistent linear sources (*cf.* Hsu and Breger 1982, Kemp *et al.* 1987, Bastien *et al.* 1988 and Elias), the present standardization calibration of the q, u, and v normalized Stokes vectors is not ideal. The zero point for both subsystems has been ascertained by known null linear polarization standard stars. It is surmised that null linear sources are also likely to be null circular sources. The standardization of the amplitude of the q and u vectors is based upon measures of non-null stellar sources.

The standardization of the amplitude of the v vector is determined primarily from laboratory standards. A rotation on the Poincaré sphere can be produced by inserting a retarder into the optical axis at the filter slide position (*cf.* Shurcliff 1966). Specifically, the amplitude of the polarization is invariant under rotation:

$$q_i^2 + u_i^2 + v_i^2 = q_f^2 + u_f^2 + v_f^2, \qquad (2.14)$$

where the subscripts i and f denote the initial and final orientations, respectively. Thus, in principle, measuring the linear polarization of a null circular polarization source before and after the insertion of a quarter wave plate enables the determination of the circular polarization and a resulting standardization coefficient. This was accomplished by using the electric vector source and by using non-null, linearly polarized

stellar sources. This technique is not ideal since it depends upon the calibration of the linear subsystem and upon the optical properties of the quarter wave plate. Experience has shown that the available quarter wave plates partially analyze the incident flux by about 0.05% (*cf.* runs number 5 and 7 in Table 2.2). In addition, the electric vector source permits only a V-bandpass calibration.

A resolution of IAU Colloquium 23 defined the rotation of the electric vector for positive circular polarization to be counter-clockwise when the detector faces the star. Care must be given when interpreting data from other researchers since a mix of conventions may be found in the older literature. For example, this sign convention is consistent with Kemp and Wolstencroft (1972), but is the reverse of the sign convention used by Shurcliff (1966) and Wolf (1972). The sign of the Pennsylvania circular data was verified by use of a retarder and Mueller calculus.

Before Channel 3 was constructed, circular polarimetry data were taken by running the Channel 1 Lock-in amplifier in the f mode instead of the $2f$ mode. The Channel 1 amplifier output is then described by Equation 2.3, with, however, a different constant, K. Data taken in this fashion were cross-calibrated to the new system by measuring sources of laboratory circular polarization. The cross-calibration multiplicative factor to transform old circular data to the current system is -3.55±0.07.

Appendix D is the journal of observations for laboratory and stellar polarization standards. Note that the first set of data in this journal is named EV+LAM. These runs correspond to the use of the electric vector source with the quarter wave plate at the indicated angle. The data reported in this journal are not standardized. Section 3.1 contains a detailed discussion of the calculation of the weighted averages given for each source. The customary particulars and the "standard" reference polarization of the stellar polarization standards are given in Table 2.1. The reference polarizations were averaged from the available data given in the cited references. The weighted mean observed (natural) polarizations

measured using the Pennsylvania polarimeter (during the fifth instrumental-mounting period) are also given in this table. The reduced calibration data for the circular subsystem in the V-bandpass are presented in Table 2.2. This table details the rotation of the Poincaré sphere technique for standardization as discussed in Section 2.5. Table 2.3 lists, by filter, the weighted average, b, of each Stokes vector for the null standards. Also in Table 2.3, the slopes, m, derived by regression using data from Tables 2.1 and 2.2 are reported for the Stokes vectors. The regressions were accomplished by combining data for all filters. The canonical equation for use of the standardization coefficients is then:

$$X_{i,stan} = m_i^f X_{i,nat} - b_i^f, \qquad (2.15)$$

where X_i indicates one of the Stokes vectors, f indicates one of the filters, and m and b are found in Table 2.3.

Figures 2.2 and 2.3 are plots of the linear and circular polarization "standard" reference data from Tables 2.1 and 2.2 vs. the observed, natural values. The plotted lines depict the least-squares fit to the data taking into consideration errors in both the natural and standard polarization values. Stability in the system is demonstrated by the plot of the null standards vs. JD depicted in Figure 2.4. The null standards are shown plotted in the q vs. u manner in Figure 2.5. This plot indicates that there is a slight color gradient in the Stokes vectors among the filters.

Table 2.1. Stellar Polarization Standards

Name	HD	RA(2000)DEC (h)(m)(s) (°)(')(")	SPEC. CLASS	V	PRIMARY OBSERVER (Note 1)	POLARIZATION REFERENCES (Note 2)	FIL.	"STANDARD" -----REFERENCE POL.------ <q> (%)	<u> (%)	<v> (%)	NATURAL ------OBSERVED POL.------ <q> (%)	<u> (%)	<v> (%)
ι Per	19373	03 09 03.9 +49 36 49	G0 V	+4.04	RHK	7	R	+0.000(3)	+0.000(4)	+0.000(7)	+0.007(3)	-0.002(4)	-0.006(7)
						7	V	+0.000(3)	+0.000(2)	+0.000(2)	+0.005(3)	+0.000(2)	-0.001(2)
						7	B	+0.000(6)	+0.000(4)	+0.000(7)	+0.011(6)	-0.008(4)	+0.000(7)
	17378	02 49 30.7 +57 05 03	A5 Ia	6.25	BDH	...	R	...	...	...	-2.569(89)	-5.75(12)	+0.053(42)
						6	V	-2.18(...)	-4.11(...)	...	-2.756(35)	-5.830(66)	+0.016(53)
2H CamAB	21291	03 29 04.1 +59 56 25	B9 Ia	4.21	NME	2,12	B	-1.93(5)	-2.58(3)	-0.027(28)	-1.804(21)	-2.557(28)	...
	21389	03 29 54.8 +58 52 44	A0 Ia	4.54	BDH	...	R	...	...	...	-1.563(13)	-2.889(16)	+0.056(4)
						3,4,6	V	-1.59(15)	-3.01(14)	...	-1.628(63)	-3.080(22)	+0.003(7)
						...	B	...	...	...	-1.549(64)	-2.889(15)	+0.016(12)
						...	u	...	...	...	-1.20(12)	-2.47(15)	+0.54(27)
9 Gem	43384	06 16 58.7 +23 44 27	B3 Iab	6.25	NME	9,12	R	+2.708(67)	-0.713(16)	-0.083(44)	+2.678(31)	-0.805(13)	-0.054(82)
						1,3,4,6,9,12	V	+2.762(37)	-0.964(32)	+0.143(83)	+2.810(52)	-0.772(32)	+0.136(27)
10 α CMiAB	61421	07 39 18.1 +05 13 30	F5 IV	+0.38	BDH	7	R	+0.000(0)	+0.000(1)	+0.000(1)	+0.000(0)	+0.004(1)	-0.007(1)
						7	V	+0.000(1)	+0.000(1)	+0.000(1)	+0.002(1)	+0.000(1)	-0.002(1)
						7	B	+0.000(1)	+0.000(2)	+0.000(4)	+0.001(1)	+0.004(2)	-0.005(4)
						7	u	+0.000(2)	+0.000(1)	+0.000(9)	-0.002(2)	+0.003(1)	-0.027(9)

Table 2.1.(cont.) Stellar Polarization Standards

Name	HD	RA(2000)DEC (h)(m)(s) (°)(')(")	SPEC. CLASS	V	PRIMARY OBSERVER (Note 1)	POLARIZATION REFERENCES (Note 2)	FIL.	"STANDARD" -----REFERENCE POL.------ <q> (%)	<u> (%)	<v> (%)	NATURAL ------OBSERVED POL.------ <q> (%)	<u> (%)	<v> (%)
5 β Vir	102870	11 50 41.6 +01 45 53	F8 V	+3.61	NME	7	R	+0.000(3)	+0.000(3)	+0.000(5)	+0.002(3)	+0.007(3)	-0.012(5)
						7	V	+0.000(1)	+0.000(2)	+0.000(1)	-0.003(1)	+0.009(2)	+0.007(1)
						7	B	+0.000(5)	+0.000(2)	+0.000(2)	-0.018(5)	+0.003(2)	+0.045(2)
						7	u	+0.000(38)	+0.000(33)	+0.00(21)	+0.031(38)	+0.029(33)	-0.06(21)
25 ρ BooA	127665	14 31 49.7 +30 22 17	K3 III	3.58	RHK	7	V	+0.000(7)	+0.000(8)	...	-0.009(7)	+0.015(8)	...
16 Ser	139195	15 36 29.5 +10 00 36	K0p	5.26	NME	7	V	+0.000(45)	+0.000(49)	...	-0.018(45)	+0.023(49)	...
25 Ser	140873	15 46 05.5 -01 48 16	B8 III	5.40	NME	11	V	-0.942(14)	+0.123(11)	...	-0.911(7)	+0.072(7)	+0.024(9)
86 μ HerA	161797	17 46 27.3 +27 43 15	G5 IV	3.42	NME	7	R	+0.000(10)	+0.000(13)	+0.000(13)	+0.003(10)	-0.011(13)	-0.045(13)
						7	B	+0.000(4)	+0.000(1)	+0.000(12)	-0.017(4)	+0.009(1)	-0.006(12)
						7	u	+0.000(8)	+0.000(31)	+0.000(16)	-0.003(8)	+0.062(31)	+0.025(16)
3 α LyrA	172167	18 36 56.2 +38 47 01	A0 V	0.03	BDH	7	R	+0.000(1)	+0.000(1)	+0.000(1)	+0.001(1)	+0.004(1)	-0.003(1)
						7	V	+0.000(2)	+0.000(2)	+0.000(1)	+0.002(2)	+0.007(2)	-0.001(1)
						7	B	+0.000(1)	+0.000(1)	+0.000(1)	-0.004(1)	+0.004(1)	-0.002(1)
						7	u	+0.000(4)	+0.000(2)	+0.000(9)	-0.001(4)	+0.006(2)	-0.030(9)
34 σ Sgr	175191	18 55 15.7 -26 17 48	B3 IV-V	+2.02	BDH	7	R	+0.000(0)	+0.000(2)	+0.000(8)	-0.001(0)	-0.027(2)	+0.010(8)
						7	V	+0.000(11)	+0.000(2)	+0.000(7)	-0.002(11)	-0.016(2)	-0.007(7)
						7	B	+0.000(8)	+0.000(9)	+0.000(5)	+0.011(8)	-0.013(9)	-0.007(5)

Table 2.1.(cont.) Stellar Polarization Standards

Name	HD	RA(2000) (h)(m)(s)	DEC (°)(')(")	SPEC. CLASS	V	PRIMARY OBSERVER (Note 1)	POLARIZATION REFERENCES (Note 2)	FIL.	"STANDARD" -----REFERENCE POL.------ <q> (%)	<u> (%)	<v> (%)	NATURAL ------OBSERVED POL.------ <q> (%)	<u> (%)	<v> (%)
53 α AqlA	187642	19 50 46.8	+08 52 06	A7 IV-V	+0.77	BDH	7	R	+0.000(1)	+0.000(1)	+0.000(4)	+0.002(1)	-0.002(1)	-0.009(4)
							7	V	+0.000(2)	+0.000(4)	+0.000(2)	-0.002(2)	+0.004(4)	-0.009(2)
							7	u	+0.000(4)	+0.000(3)	+0.000(2)	+0.006(4)	+0.004(3)	+0.003(2)
53 ε Cyg	197989	20 46 12.5	+33 58 13	K0 III	2.46	BDH	7	R	+0.000(14)	+0.000(11)	+0.000(4)	-0.006(14)	-0.002(11)	-0.020(4)
55 CygA	198478	20 48 56.2	+46 06 51	B3 Ia	4.84	NME	2,3,4,6	V	+2.83(3)	+0.363(85)	+0.007(8)	+2.695(7)	+0.315(51)	-0.050(3)
61 CygB	201092	21 06 55.1	+38 44 32	K7 V	6.03	NME	7	R	+0.000(17)	+0.000(21)	+0.000(20)	+0.011(17)	-0.027(21)	-0.003(20)
	204827	21 28 57.4	+58 44 24	B0 V	7.95	BDH	2,11	R	...	...	-0.054(2)	-2.486(5)	+3.983(72)	-0.31(31)
							4,6,11	V	-2.59(5)	+4.875(85)	...	-2.780(85)	+4.543(56)	-0.059(23)
							11	B	...	...	-0.008(9)	-2.63(14)	+4.703(19)	+0.208(12)
							11	u	...	...	+0.034(12)	-3.30(87)	+7.3(11)	+1.1(37)
12 Peg	207089	21 46 04.2	+22 56 56	K0 Ib	+5.29	NME	11	V	+0.073(8)	+0.548(12)	...	+0.082(13)	+0.548(19)	...

Notes:

1. Primary Observer (Column 7):

NME = N. M. Elias

BDH = B. D. Holenstein

RHK = R. H. Koch

2. Polarization References (Column 8)

1 = Appenzeller (1966)

2 = Avery *et al* (1975)

3 = Behr (1959)

4 = Hall (1958)

5 = Not used

6 = Hiltner (1956)

7 = Koch (1975)

8 = Not used

9 = Stokes *et al* (1974)

10 = Not used

11 = Serkowski, Mathewson, and Ford (1975)

12 = Wolf (1970)

Table 2.2. Circular Subsystem Calibration Runs

V-Bandpass and Quarter-Wave Plate

Run	Source (JD-2440000)	Retarder Orientation(1) (o)	Before <p> (%)	----After Rotation----- q (%)	u (%)	v (%)	Predicted v (%)
		Standardized:	Yes	Yes	Yes	No	Yes
01	119 Tau (6799.725,6799.753)	...	0.602(9)	+0.049(28)	+0.158(41)	+0.680(52)	+0.579(13)
02	α Ori (6823.700,6823.674)	...	0.636(9)	+0.014(5)	-0.214(8)	-0.509(29)	-0.599(12)
03	α Ori (6881.542,6881.590)	...	0.410(5)	+0.046(2)	-0.239(4)	+0.104(6)	+0.330(19)
04	EV (6887.632)	...	78.83(45)	+7.92(75)	-7.62(78)	+74.4(41)	+78.06(49)
05	α Lyr (7709.742,7716.854)	...	0.023(4)	-0.078(70)	+0.015(24)	+0.026(7)	+0.00(23)
06	α Sco (7715.596,7715.574)	...	0.417(11)	+0.044(10)	+0.173(14)	+0.475(39)	+0.377(9)
07	α Her (7716.733,7716.705)	...	0.093(1)	-0.093(6)	-0.060(6)	-0.042(8)	+0.00(2)
08	EV (7793.263)	0	78.83(45)	-13.8(17)	-40.1(25)	-68.2(37)	-66.4(15)
09	EV (7793.276)	40	78.83(45)	-42.8(45)	+44.9(49)	-50.3(28)	-48.6(64)
10	EV (7793.288)	80	78.83(45)	-41.1(43)	-45.5(47)	+50.9(28)	+49.6(60)
11	EV (7793.300)	120	78.83(45)	-14.4(17)	+40.1(24)	+67.7(37)	+66.3(15)
12	EV (7793.314)	160	78.83(45)	-65.2(71)	-31.5(63)	-28.7(16)	-31(19)
13	EV (7793.326)	200	78.83(45)	+4.31(33)	+17.0(5)	-77.0(42)	-76.9(5)
14	EV (7793.340)	240	78.83(45)	-77.1(87)	+0.0(70)	-0.32(7)	-16(99)
15	EV (7793.352)	280	78.83(45)	+5.35(25)	-15.0(4)	+77.3(42)	+77.2(5)
16	EV (7793.365)	320	78.83(45)	-66.9(75)	+29.8(66)	+27.2(15)	+29(22)
17	HD 204827 (7807.756,7807.734)	...	5.57(19)	-3.52(14)	+1.21(11)	-2.73(35)	-4.14(43)
18	EV (7815.673)	280	78.83(45)	+4.92(27)	-15.6(4)	+77.9(44)	+77.13(46)
19	EV (7815.690)	120	78.83(45)	-15.0(18)	+40.2(25)	+68.0(38)	+66.1(15)

Note 1. Retarder Orientation (fast axis) is measured relative to a fixed reference point on the filter slide.

TABLE 2.3

Standardization Coefficients for the Linear and Circular Subsystems

Filter	q		u		v	
	m	b	m	b	m	b
R	+0.977(7)	-0.0000(5)	+1.066(5)	-0.0001(29)	+0.992(4)	-0.0057(14)
V	+0.977(7)	-0.0002(10)	+1.066(5)	+0.0002(26)	+0.992(4)	+0.0004(21)
B	+0.977(7)	-0.0020(20)	+1.066(5)	+0.0055(16)	+0.992(4)	+0.0062(82)
u	+0.977(7)	-0.0005(16)	+1.066(5)	+0.0037(10)	+0.992(4)	+0.0005(47)

CHAPTER 2. Figure Captions

Figure 2.1. Schematic of the PEMP system based upon Koch *et al.* (1985). The linear (Channel 1) and circular (Channel 3) electrical interconnection is illustrated.

Figure 2.2. Regression of "standard" reference linear polarization values versus natural polarization values from Table 2.1. All filters are combined. One sigma errors are shown for each coordinate. The plotted lines depict the weighted least-square fit from Table 2.3. (*a*) Stokes *q*, (*b*) Stokes *u*.

Figure 2.3. Regression of "standard" reference circular polarization values versus natural polarization values from Tables 2.1 and 2.2. The plotted line depicts the least-squares fit from Table 2.3. All filters are combined. The outlying point with a Natural *v* near zero has a very large error.

Figure 2.4. The Stokes vectors as a function of JD for the null standards of Table 2.1. (*a-c*) R-bandpass, (*d-f*) V-bandpass, (*g-i*) B-bandpass, (*j-l*) u-bandpass.

Figure 2.5. The *q* versus *u* plots for the null standards of Table 2.1. (*a*) R-bandpass, (*b*) V-bandpass, (*c*) B-bandpass, (*d*) u-bandpass.

Figure 2.1

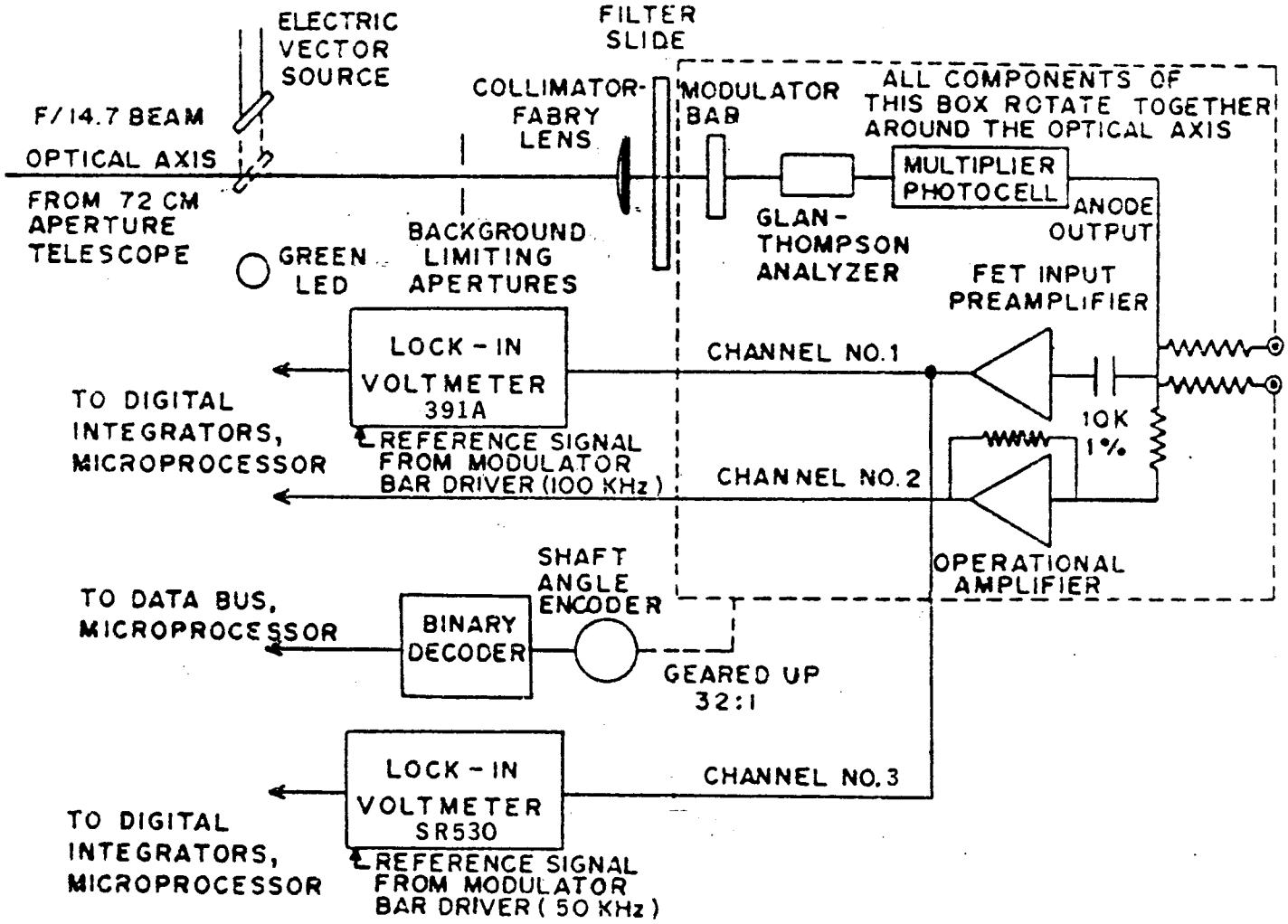
ELECTRIC VECTOR SOURCE
FILTER SLIDE
COLLIMATOR-FABRY LENS
MODULATOR BAB
ALL COMPONENTS OF THIS BOX ROTATE TOGETHER AROUND THE OPTICAL AXIS
F/14.7 BEAM
OPTICAL AXIS
FROM 72 CM APERTURE TELESCOPE
GREEN LED
BACKGROUND LIMITING APERTURES
GLAN-THOMPSON ANALYZER
MULTIPLIER PHOTOCELL
ANODE OUTPUT
FET INPUT PREAMPLIFIER
LOCK-IN VOLTMETER 391A
CHANNEL NO.1
TO DIGITAL INTEGRATORS, MICROPROCESSOR
REFERENCE SIGNAL FROM MODULATOR BAR DRIVER (100 KHz)
10K 1%
CHANNEL NO.2
OPERATIONAL AMPLIFIER
SHAFT ANGLE ENCODER
TO DATA BUS, MICROPROCESSOR
BINARY DECODER
GEARED UP 32:1
LOCK-IN VOLTMETER SR530
CHANNEL NO.3
TO DIGITAL INTEGRATORS, MICROPROCESSOR
REFERENCE SIGNAL FROM MODULATOR BAR DRIVER (50 KHz)

Figure 2.2

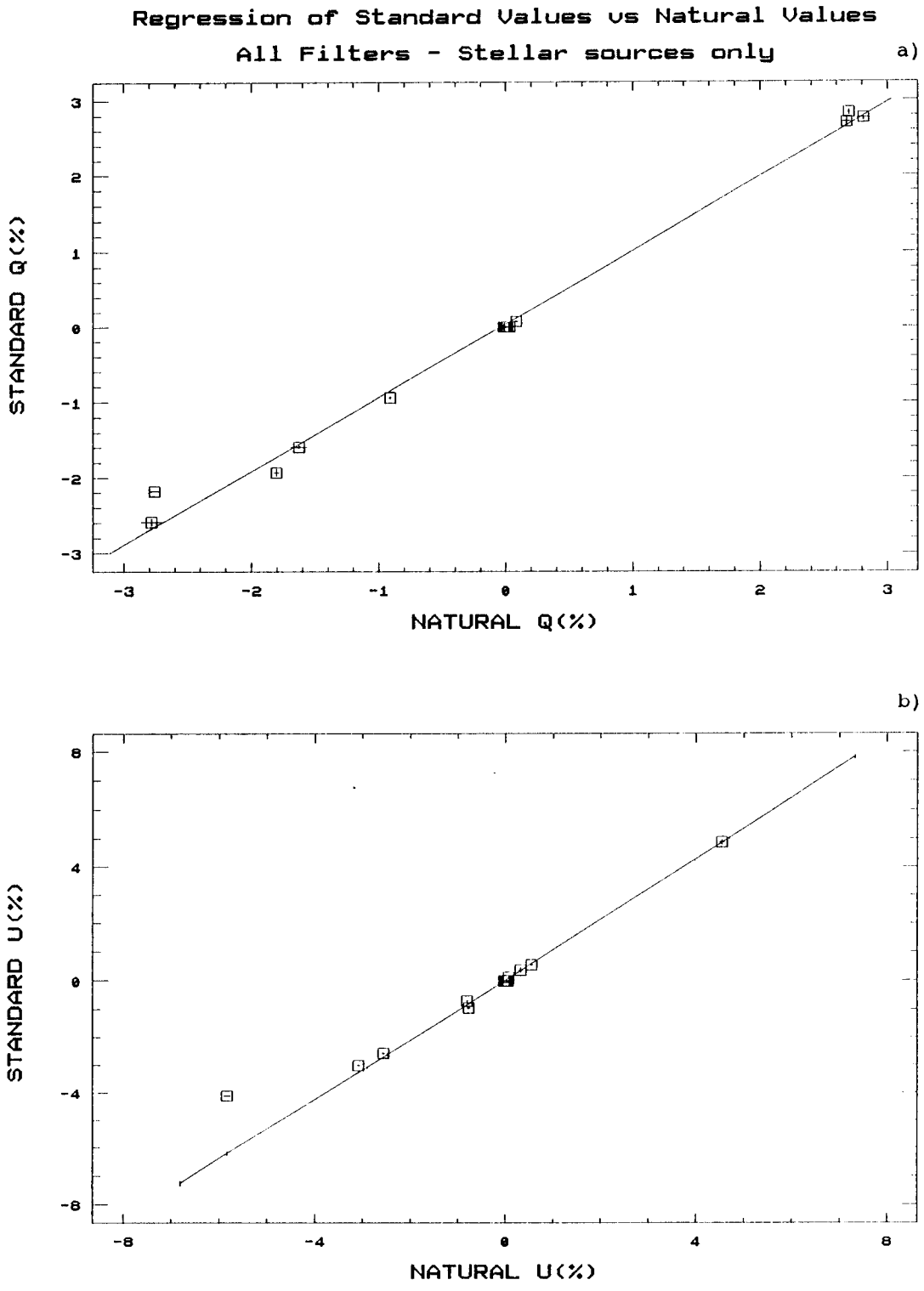
Regression of Standard Values vs Natural Values
All Filters - Stellar sources only
a)
STANDARD Q(%)
NATURAL Q(%)
b)
STANDARD U(%)
NATURAL U(%)

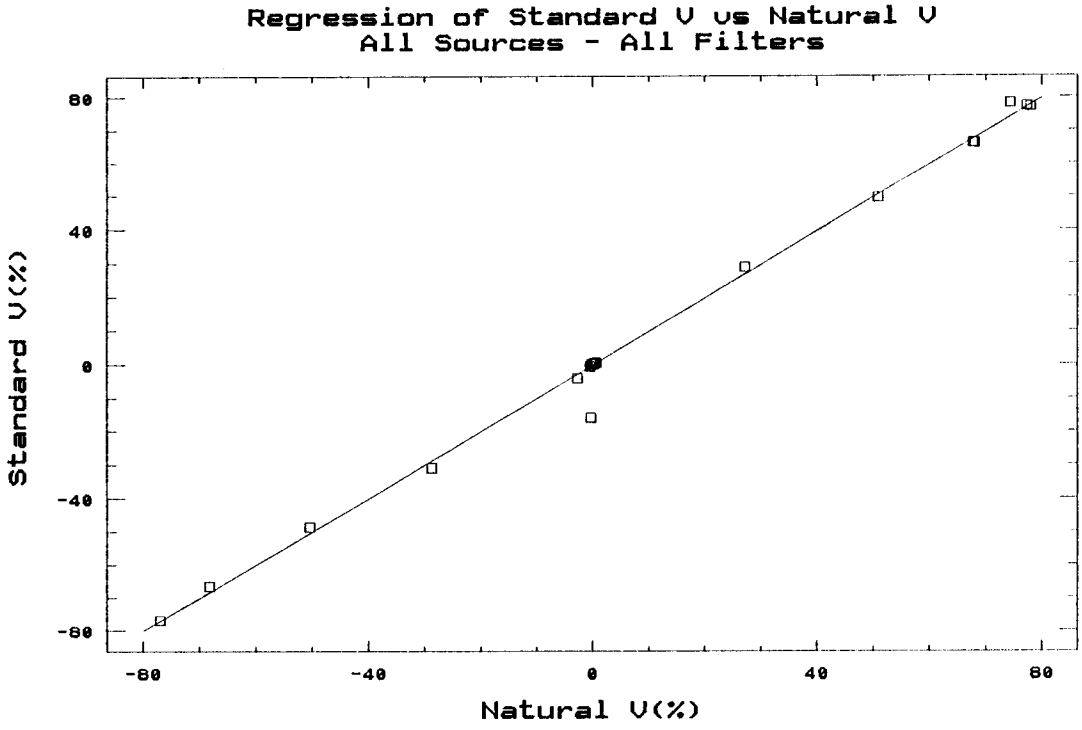
Regression of Standard V vs Natural V
All Sources - All Filters
Standard V(%)
Natural V(%)
80
40
0
-40
-80
-80
-40
0
40
80

Figure 2.3

Figure 2.4

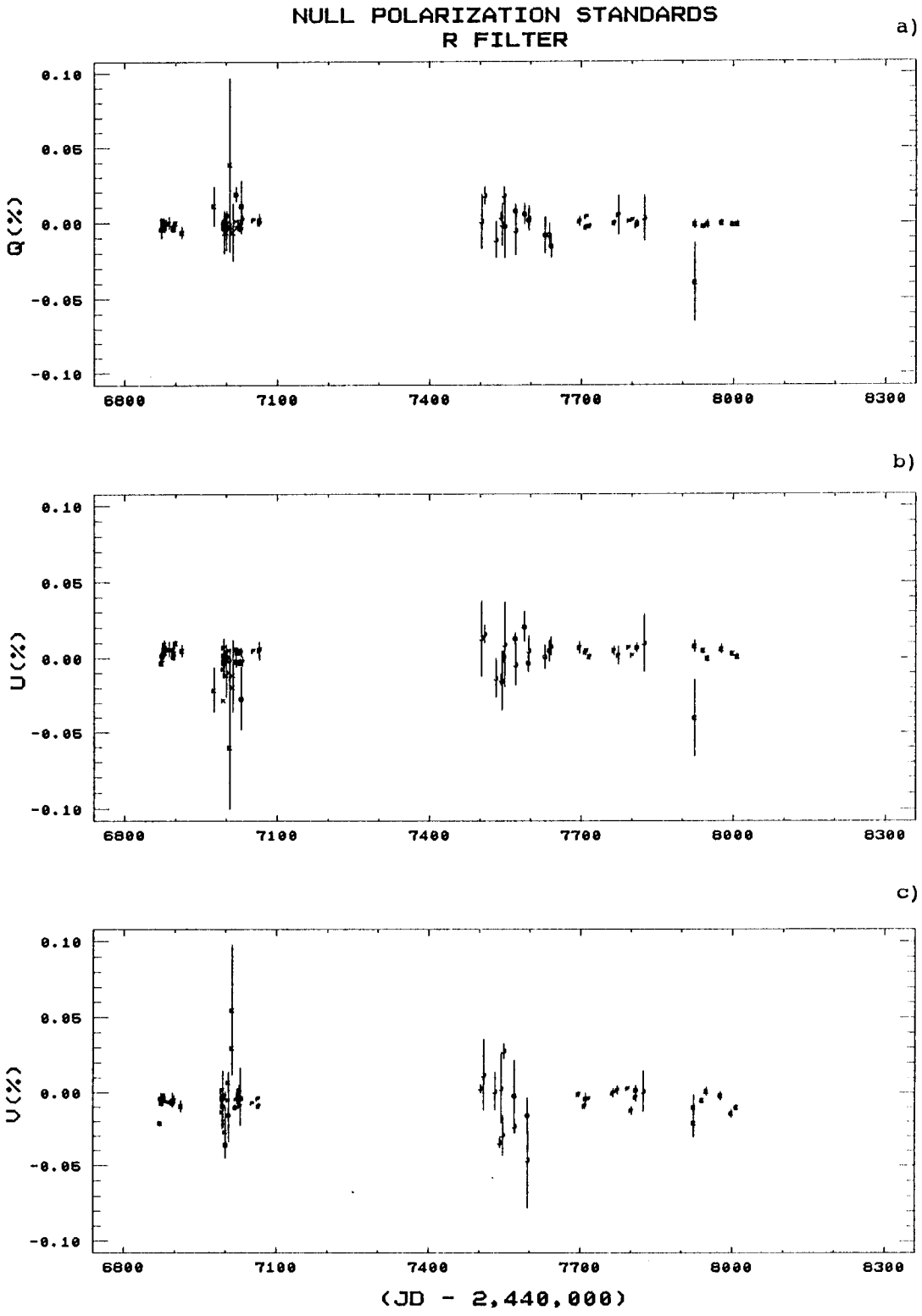
NULL POLARIZATION STANDARDS
R FILTER
a)
Q(%)
b)
U(%)
c)
U(%)
0.10
0.05
0.00
-0.05
-0.10
6800
7100
7400
7700
8000
8300
(JD - 2,440,000)

Figure 2.4 (cont.)

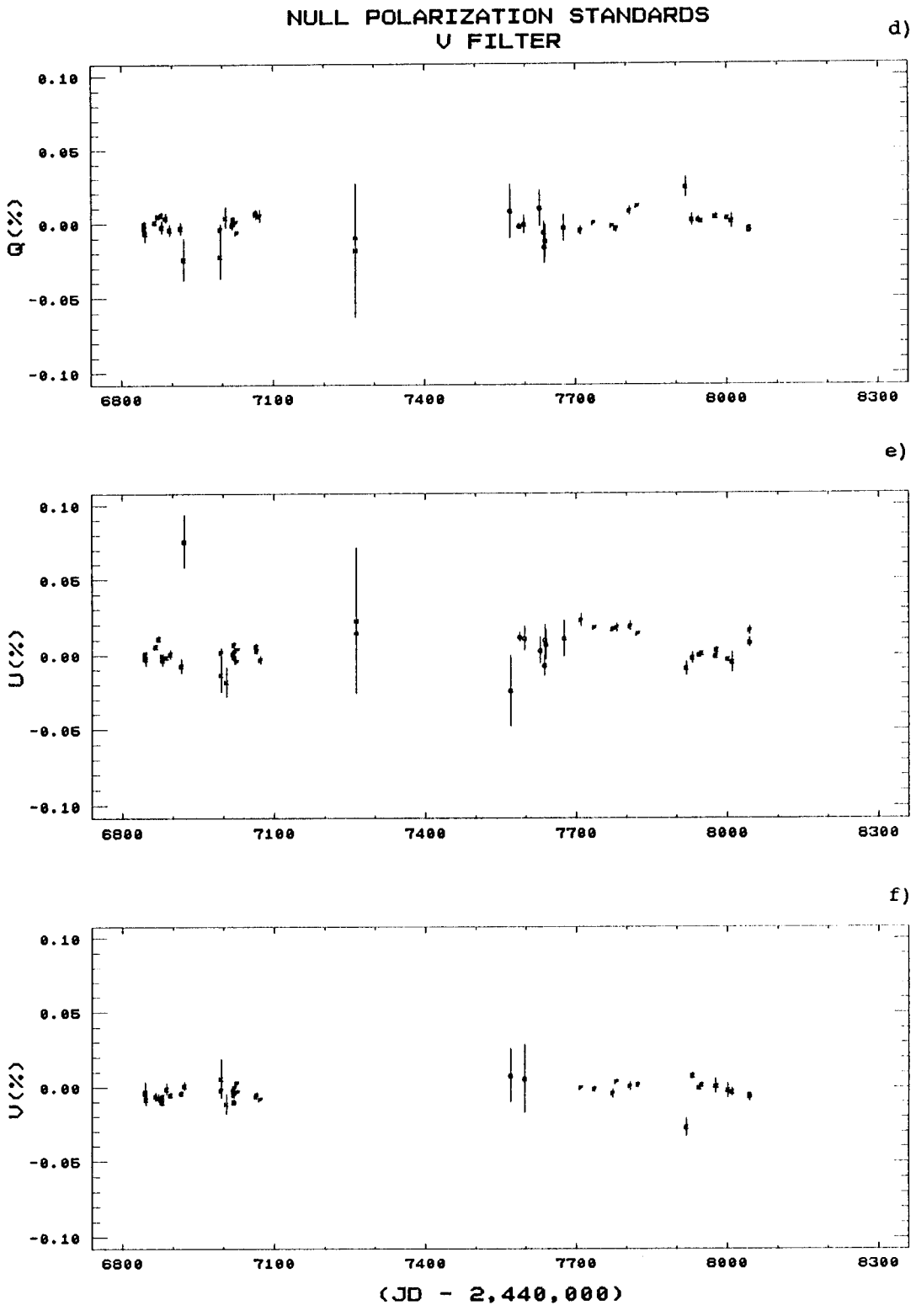

Figure 2.4 (cont.)

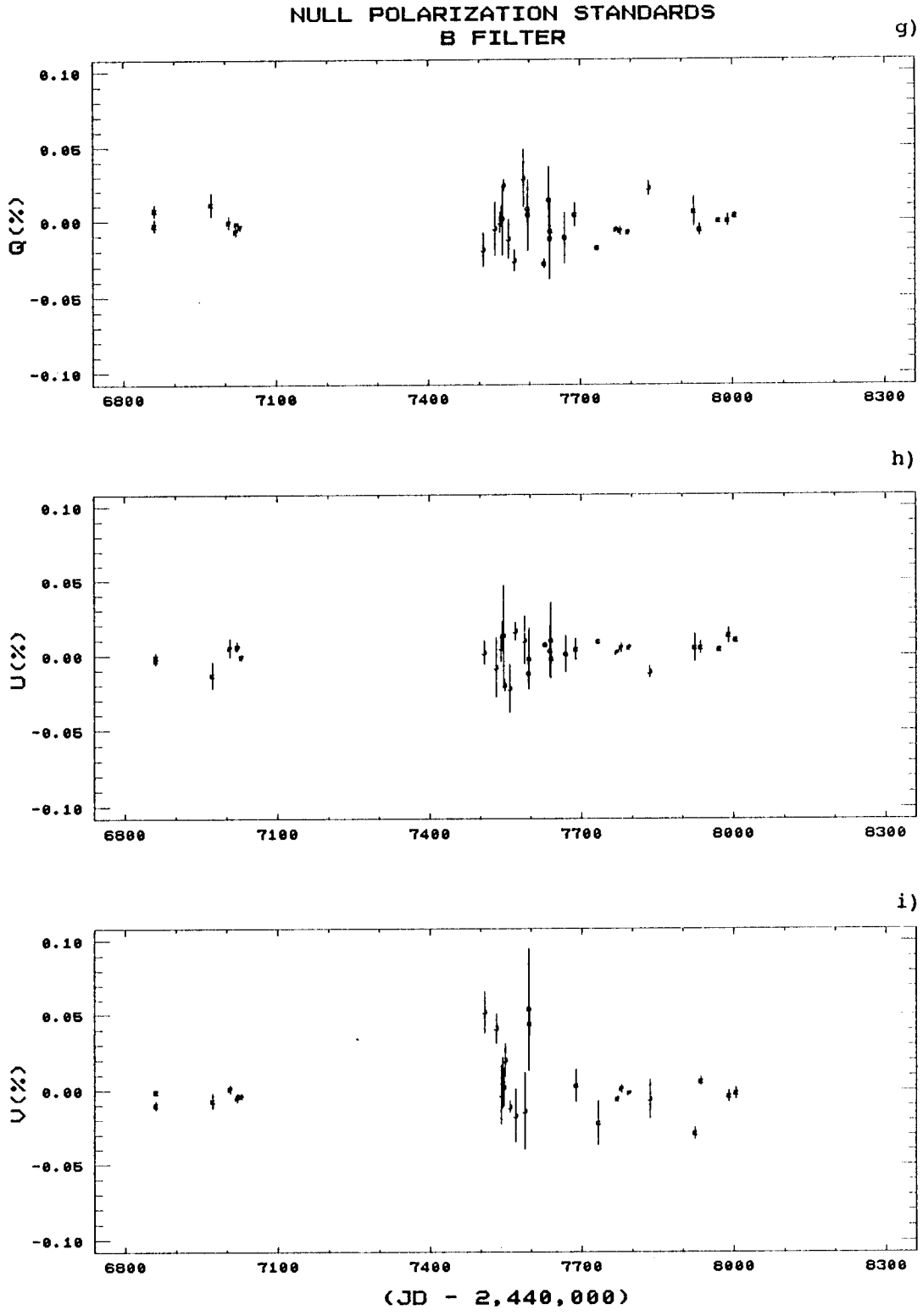

Figure 2.4 (cont.)

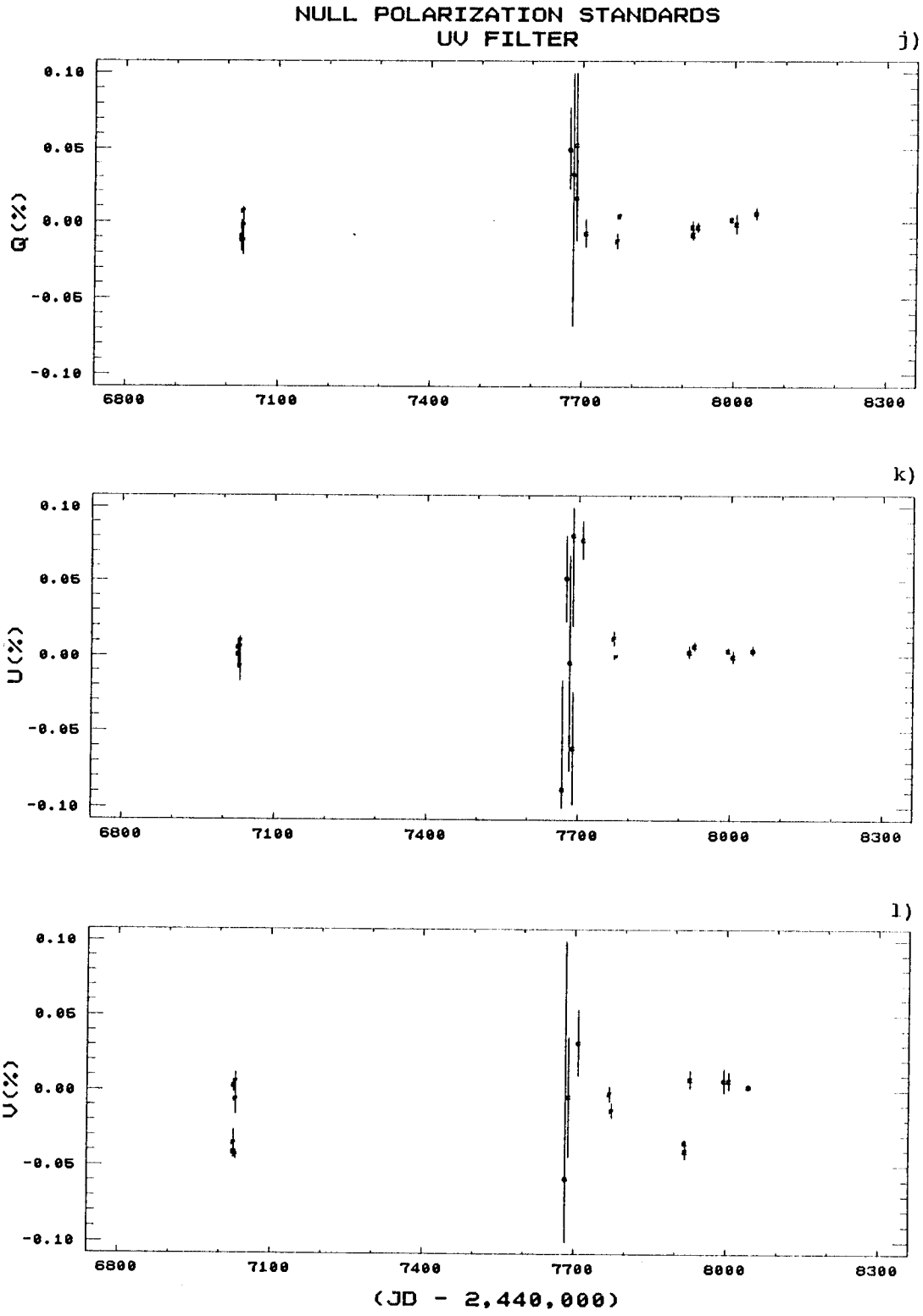

Figure 2.5

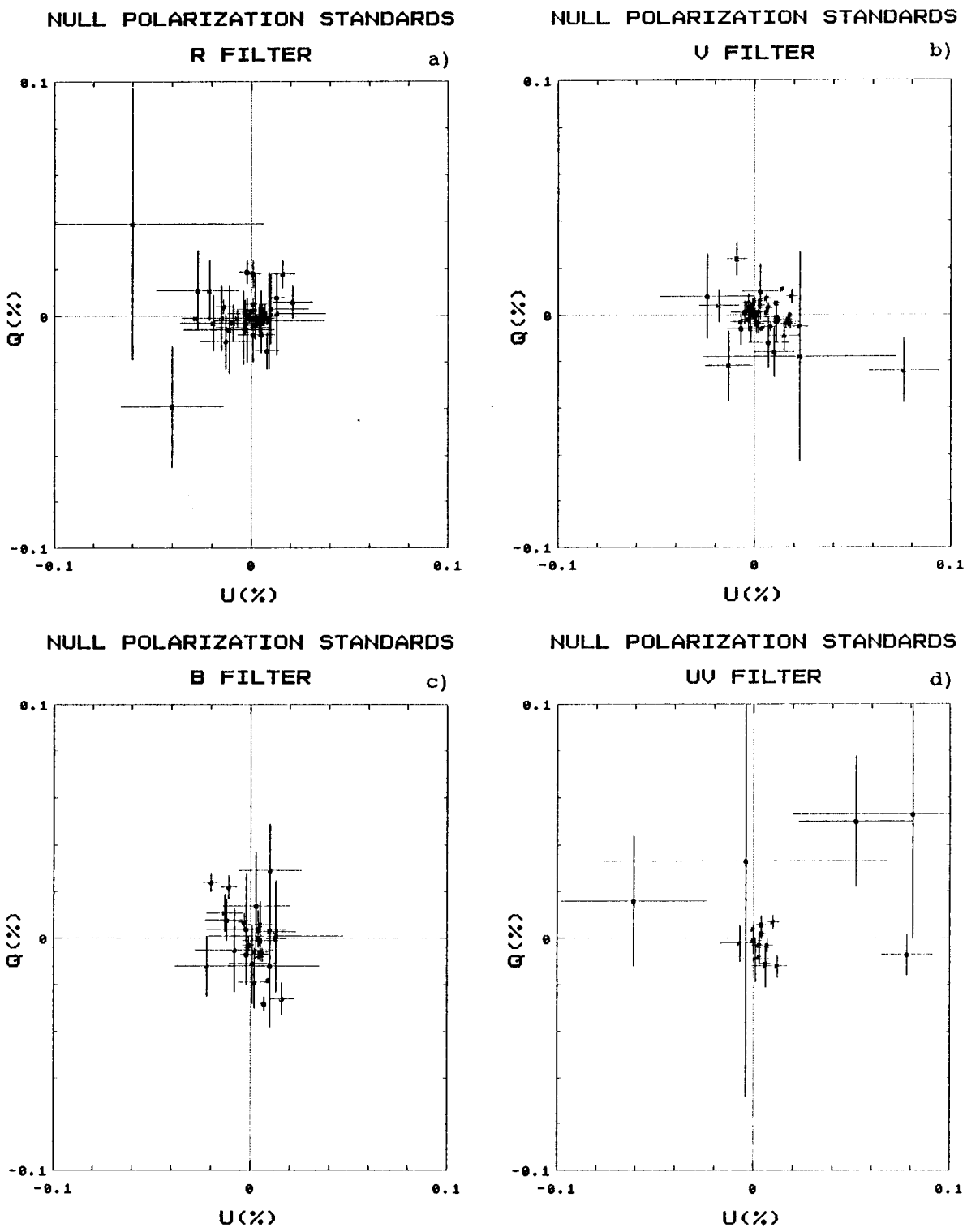
NULL POLARIZATION STANDARDS
R FILTER
a)
NULL POLARIZATION STANDARDS
V FILTER
b)
NULL POLARIZATION STANDARDS
B FILTER
c)
NULL POLARIZATION STANDARDS
UV FILTER
d)
Q(%)
U(%)
0.1
0
-0.1

CHAPTER 3. Morphology of Program Stars Observations

3.1 Polarimetric Data

More than four hundred elliptical polarization measures were made on the eleven program stars over the three and one-half year period between Winter 1986 and Spring 1990. The data are concentrated in the R- and V-bandpasses but also contain numerous measures in the B- and u-bandpasses. The journal of standardized polarimetric data for the program stars is presented in Appendix E. The reported one sigma errors in the polarization values in this table were updated from the calculated natural values by inclusion of the propagated errors from the standardization coefficients in Table 2.3. The weighted average and weighted error were calculated for each Stokes polarization vector by the formulae:

$$\langle X \rangle = \frac{\sum_{i=1}^{n} \frac{X_i}{\sigma_i^2}}{\sum_{i=1}^{n} \frac{1}{\sigma_i^2}},$$

$$\langle \sigma_X \rangle = \sqrt{\frac{\sum_{i=1}^{n} \frac{(X_i - \langle X \rangle)^2}{\sigma_i^2}}{(n-1) \sum_{i=1}^{n} \frac{1}{\sigma_i^2}}}, \qquad (3.1)$$

where X represents one of the Stokes vectors, and n is the number of data points in the bandpass under consideration. The weighted averages for the linear polarization polar coordinates were calculated from the weighted Stokes q and u values and the respective errors.

3.2 Determination of Interstellar Polarization Vectors

The interstellar and intrinsic Stokes polarization vectors add so as to produce the standardized, observed polarization vector as follows:

$$X_{observed} = X_{intrinsic} + X_{interstellar}, \tag{3.2}$$

where X represents one of the Stokes vectors. In order to understand the mechanisms responsible for the intrinsic stellar polarizations the interstellar components must be subtracted from the observed values.

The first step in the determination of the interstellar components for a program star is to map the observed polarization of the (projected) neighboring "field" stars as a function of distance. After the map is completed, the galactic neighborhood is considered in relation to the program object's distance and observed polarization. This technique was used and is described by Pfeiffer (1975), Corcoran (1988), Koch *et al.* (1989) and Elias (1990) for the linear polarimetry conducted by these observers. Elias attempted to use this technique for his circular polarimetry. However, only minimal published circular polarimetry existed for his galactic fields and his efforts were not successful.

Published data for program field stars which have been observed polarimetrically are tabulated in Appendix F for linear polarimetric observations and in Appendix G for circular polarimetric observations. The notes which follow both appendices list the polarization catalog sources. In Appendix F, a star was defined as being a field star if it is located within five degrees of the program star and is not itself a known variable star. Five degrees was chosen as a compromise limit in order to get enough stars from the published catalogs for a reasonable statistical sample and yet limit the field to make it uniform with respect to galactic structures such as dust clouds. Three exceptions were made to the five degree limit. Due to a plethora of catalog data and to galactic location, the field stars

for VV Cep and μ Cep were required to be within only three degrees. The field for the other object, α Her, was doubled to ten degrees due to the dearth of published data since it is located between the Sagittarius and Orion-Cygnus spiral arms. The a) and b) subplots of Figures 3.1 through 3.10 detail the observed linear polarizations of field stars as a function of distance. The c) subplot in each figure is a map of the galactic coordinates of the field stars. No plots are shown for α Her since polarimetry and distance data for only two field stars were found.

The field stars in Appendix F are mainly early stars somewhat reddened. Since the published linear data for the field stars are predominantly unfiltered or through blue-green filters, the effective bandpass of the data in Appendix F is considered to be centered at about 4200Å. Knowledge of the wavelength, λ_{max}, at which the maximum interstellar linear polarization, p_{max}, occurs yields the linear polarization spectra according to following empirical relationship derived by Serkowski, Mathewson and Ford (1975):

$$\frac{p(\lambda)}{p_{max}} = e^{[K \ln^2(\frac{\lambda_{max}}{\lambda})]} , \qquad (3.3)$$

where K is a constant they found to be equal to -1.15. Wilking, Lebofsky, and Rieke (1982) subsequently found that K is a function of λ_{max} as follows:

$$K = +0.10 - 1.86\lambda_{max} . \qquad (3.4)$$

This correction is not large for the program field stars. Figure 6 of Serkowski, Mathewson and Ford provides a map of λ_{max} as a function of galactic position. This map and the data in their Tables 3 and 5 were consulted for the λ_{max} values reported in Table 3.1.

The circular data for field stars reported in Appendix G refer to

only seven of the eleven program stars despite increasing the search for published circular data to stars within fifteen degrees of the program stars. The d) and e) subplots, provided if appropriate for Figures 3.1 through 3.10, show the circular data in a sense analogous to the a), b), and c) linear subplots. The data for α Ori and for V CVn are not graphed since the data are sparse and have large reported errors. The published programs from which the data were taken indicated the effective bandpasses for the observations. The bandpass information is reported both in the appendix and on the plots.

Also shown on the a), b), and d) subplots of Figures 3.1 through 3.10 are curves which indicate the best fit to the polarization data in the vicinity of the program star. The best fit to the linear polarization was accomplished by translating the data to the orthogonal q and u coordinate system so as to avoid the circular statistics problems involved with using the polar coordinates. Special considerations made for the program stars follow.

The line-of-sight to 119 Tau grazes the lower part of the Orion-Cygnus arm. Fortunately, there is a reasonable number of field stars from which a linear model may be fitted as is depicted in Figure 3.1a and b. The electric vector clearly rotates after clearing the arm at about 500pc; however, the electric vector is adequately fitted by considering stars only out to this distance. The large errors in the circular data presented in Figure 3.1d do not yield a conclusive interstellar value.

Light traveling from α Ori passes through a moderately thick section of the Orion-Cygnus arm. The Milky Way field is, however, uncluttered in the vicinity of the star. Figure 3.2a shows the gradual rise in polarization in the direction of the star out to a distance of 175pc. This rise in polarization was modelled by a linear fit in polarization percentage. No rotation of the polarization vector is apparent from Figure 3.2b. It should be noted that the interstellar value adopted by Clarke and Schwartz (1984) is zero. Clarke and Schwartz apparently did not take into

consideration the individual distances to the field stars in their average. The reported observational error in the circular polarimetry of the field stars for α Ori prevents the determination of the interstellar circular polarization.

The large distance to 6 Gem places the star near the inner edge of the Perseus arm. Most of the induced polarization is produced by the light passing through the Orion-Cygnus arm. Therefore, the stars between 800pc and the position of 6 Gem at 1400pc, as shown on Figure 3.3a, may be modelled with a flat line. This premise is further strengthened by the lack of rotation of the polarization vector as seen in Figure 3.3b. The only complication is due to the proximity of 7 η Gem (HD 42995: M3 III). This star has a reflection nebulae that is uncomfortably close to 6 Gem. The circular polarimetry depicted in Figure 3.3d has large errors and is not conclusive.

Most of the Milky Way is avoided by light traveling from ψ^1 Aur. However, Figure 3.4a shows the relatively steep rise in polarization experienced out to 600pc where ψ^1 Aur is located. This is fitted with a linear model. No convincing rotation of the polarization vector is evident from Figure 3.4b. No circular field star data were located.

72 Leo is close to Sun and is located in an uncluttered area of the sky. Despite the small number of linear measures of field stars, the indicated fits on Figure 3.5a and b are adequate since the amplitude of polarization is tiny. No circular field star data were found.

The case of V CVn is difficult since only one field star was located near the distance to this star. The galactic location of this star implies that light along a chord out to only about 80pc is influenced by the Orion-Cygnus arm. Once free of the arm, the polarization and position angle should remain flat as happens in the case of 6 Gem. This levelling off is modelled as indicated in Figure 3.6a and b. The polarization in this direction is not large and therefore the uncertainty in the interstellar value is reasonable. The one circular polarimetry field star datum has a

large error and is not useful.

The field surrounding α Sco is a terribly cluttered section of the Milky Way. There are numerous bright and dark nebulae in the vicinity of this star as well as the self-created reflection nebulosity. Additionally, relatively few stars have been observed polarimetrically in the area. Figure 3.7a and b illustrates a dilemma in the gross mismatch between the observed polarization of α Sco at 0.4% in the B-bandpass and the majority group of field stars which range in value between 1.5% and 3%. The two stars at about 250pc which have polarizations comparable to that of α Sco also happen to be in directions closer to α Sco than the other highly polarized stars. The decision as to which group to use was not determined by consideration of the orientation of the electric vector. Both groups of stars have electric vector orientations which are not close to that of α Sco itself. The higher polarization stars were reluctantly rejected since they would completely change the intrinsic polarization vector of α Sco. The resulting linear model is depicted on Figure 3.7a and b.

Figure 3.7d illustrates that the circular data for α Sco field stars are actually more complete than are the linear data. The circular polarimetry on the field stars is of high quality. Two linear fits are presented: one for the B-bandpass and one for the R-bandpass. The R- and B-bandpass fits intersect at about 200pc. The point of intersection is at a circular amplitude near to zero. Holenstein (1991) explained this effect as arising from birefringence of interstellar grains. The net retardance of the electric vector of incident polarized light increases with distance.

α Her is located in a direction between the Sagittarius and the Orion-Cygnus galactic arms. Only two field stars were found with published linear polarization values. This happens despite the fact that the field was increased to ten degrees. HD 152614 at 99pc has a measured polarization of 0.05%. However, HD 158148 at 190pc has a measured polarization of 0.37%. Since α Her is relatively close at 210 pc, has a small observed polarization, and is in a clear field, it is presumed that

the interstellar linear polarization is 0.00(n)% where n is of the order of five or six.

The linear polarization of the field stars for μ Cep is nicely fitted by a linear model as illustrated in Figure 3.8a. The electric vector also shows no rotation as shown in Figure 3.8b. The star is in a cluttered area of the Milky Way and borders a bright diffuse nebula. The circular field star data illustrated in Figure 3.8d show an increase in circular polarization past 500pc in the R-bandpass before turning over by 1200pc.

VV Cep is located in the direction of a dense region of the Orion-Cygnus arm. However, the distance to VV Cep locates the star on the far side of this arm. Due to this reason, the interstellar polarization is modelled by a flat line after 800pc as depicted in Figure 3.9a and b. The interstellar polarization vector for VV Cep which was determined by Pfeiffer and Koch (1987) is {B,0.81,24,_}. The field star sample size used in the present study is larger. Therefore, the present determination is retained. The interstellar circular polarization is shown in Figure 3.8d and e.

Shown on Figure 3.10a and b are the tidy fits to the linear polarimetry of field stars for β Peg. β Peg lies in a clear section of the sky. No circular data for field stars were located.

Overall, the uncertainties in the interstellar polarization parameters are high due to three reasons. First, the number of stars observed polarimetrically is not large enough to give a useful sample in all areas of the sky. Second, the identification of stars which are not intrinsically polarized is not precise. Third, the galactic dust environment is often not uniform in the neighborhood of the program objects. For these reasons, the error for the interstellar polarization determination was not added in quadrature to the error for the standardized observed polarization of Appendix E for subsequent analysis. Table 3.1 contains the computed interstellar linear Stokes polarization vectors for the program stars.

The large uncertainties in the interstellar circular polarization values have usually prevented the intrinsic circular stellar polarization from being determined. The only exception is α Sco. The interstellar circular R-bandpass polarization at its distance is +0.012%. Likewise, the interstellar circular B-bandpass polarization is -0.015%. In order to treat all of the program objects in a uniform manner, only the linear data described in the next section have had the interstellar components removed. The interstellar circular polarizations are not removed for any program objects. Special consideration is given to α Sco in later sections.

3.3 Intrinsic Polarizations

The intrinsic linear polarization vectors derived by use of Equation 3.2 on the data reported in Appendix E for the eleven program stars are plotted in Figures 3.11 through 3.21 as a function of heliocentric Julian Day number (HJD). The subplots of these figures display the q, u, p_l, and θ intrinsic polarization vectors in each bandpass. The v polarization vector subplots have not had the interstellar polarization removed, as explained in Section 3.2. The last four subplots display the intrinsic Stokes q *vs.* u plots in the bandpasses used.

All eleven of the program objects show non-zero intrinsic linear and observed circular polarizations. This might be expected since they are similiar in spectral type and evolution and all have extended atmospheres that contain dust. They differ from another in the amplitude and time-varying nature of their polarization forms. Not all stars were observed with the same coverage. Nevertheless, it is apparent that certain stars show cyclical and possibly periodic polarization variations. For some stars, as detailed in Chapter 1, the variations of the linear polarization were already known. However, nothing was known of the activity of the circular polarization form.

(a) 119 Tau

It is apparent from Figure 3.11a that the R-bandpass q Stokes vector of 119 Tau shifted from the value of about +0.2% for the group of data near JD 2,446,800 to the value of +0.5% for the group near JD 2,447,900. On a shorter time scale it is apparent that the star shows a fast drop in R- and V-bandpass polarization in the first group of data. The position angle, as shown in Figure 3.11e, shifted ten degrees over this interval. This result is consistent with the large shifts in the polarization vectors shown in Figure 1.3a and b. The circular polarimetry shown in Figure 3.11c is noisy, but is near zero and nearly flat. Figure 3.11f shows that the data for all bandpasses fall in the $+q$, $-u$ quarter plane.

(b) α Ori

Significant linear polarizations are evident from all of the subplots of Figure 3.12. Most of the data for all bandpasses fell predominantly in the $-u$ half plane. After JD 2,447,000, some measures were seen to lie in the $+u$ half plane. Figure 3.12f, l, and r shows that the measures form "petals" that are smooth except near the point of intersection where the measures taken at the end of a season do not fall back smoothly upon the measures taken at the start of a season. These data are consistent with the blue data taken by Hayes (1984) during the 1980-1984 observing seasons (see Figure 1.4a and b). The sense and direction of generation of the figure are counterclockwise and are familiar since half of Hayes' (1984) measures show this sense of circulation. The amplitude of the excursion in the R-bandpass is about 0.5%, which amounts to about half of that found in the blue bandpass.

The circular polarization data, taken during the first observing season, are statistically significant. One surmises that the variability is cyclical and probably not periodic. This distinction is addressed in Chapter 4. The circular polarization is not coupled to the linear polarization in any direct fashion. Thus, the circular signal probably may

not arise from the source and mechanism causing the linear signal. The variability with time of the circular signal is not symmetrical about the origin of the *v* Stokes vector.

(c) 6 Gem

Figure 3.13a and b shows that significant changes occurred in the 6 Gem system over the observing period not unlike the changes seen in Figure 1.5a and b. The linear polarimetry data for 6 Gem fall predominantly into the $-q$, $+u$ quarter planes as seen on Figure 3.13f. Five of the six R-bandpass circular polarization values are negative.

(d) ψ^1 Aur

The linear polarimetry for ψ^1 Aur lies in the $-q$, $-u$ quarter plane as seen in Figure 3.14f. Figure 3.14b shows a large increase in the *u* vector over the observing period. This change is consistent with the variations seen in Figure 1.6a and b. A large amount of variation exists in the circular polarization. Figure 3.14c shows that the circular polarization in the R-bandpass dropped from the +0.08 range to near zero over a few weeks.

(e) 72 Leo

72 Leo shows variations in the *q* and *u* Stokes vectors on a level of 0.05% for the R- and V-bandpasses. The *u* vector is somewhat more constrained. However, there is a distinct rise and fall of the *u* polarization values for the R-bandpass as seen in Figure 3.15b. Figure 3.15c clearly shows that the *v* Stokes vector changed sign over an interval of 100 days.

(f) V CVn

Over the short interval monitored, V CVn shows variations in all bandpasses which are consistent with Figure 1.8a and b. V CVn shows a

distinct rise in the q vector over the observing period as seen in Figure 3.16g and m for the V- and B- bandpasses. The V-bandpass p vector is seen to fall markedly in Figure 3.16j. No distinctive trend exists for the v Stokes vector.

(g) α Sco

Systematic polarization swings occur in all bandpasses for α Sco. Figure 3.16a shows a trend not unlike that seen for α Ori. Figure 3.17f shows that the polarization tends to be tightly clustered near the $+u$ axis in a fashion consistent with the polarimetry shown in Figure 1.9a and b. The circular polarimetry seen in Figure 3.17c shows some variability with a short time scale. The group of data centered around JD 2,447,700 is characteristically different for all Stokes vectors when compared to the group of data taken earlier.

(h) α^1 Her

The data presented in Figure 3.18a and b show a cyclical trend similar to that seen for α Ori. It is apparent from Figure 3.18d and e that both the p and θ vectors show variations. The R-bandpass circular data show a peak at about JD 2,446,975 and then a steep fall. The R-bandpass data after JD 2,447,700 show a noisy rise towards positive values. The V-bandpass data shown in Figure 3.18i show a remarkable change in the system. Around JD 2,447,000 the system started producing circular polarizations on the order of -0.08%. This occurred during a local maximum in the q vector.

(i) μ Cep

The subplots of Figure 3.19 for μ Cep show a profound shift in all bandpasses in the u Stokes vector between the group of data at JD 2,447,000 and the group of data near JD 2,447,800. Also, both the q and u vectors show cyclical trends. These trends are consistent with the polarimetry

shown in Figure 1.10a and b. The v Stokes vector, however, varied widely and does not clearly show cyclical behavior.

(j) VV Cep

The subplots of Figure 3.20 show that VV Cep shows a large degree of intrinsic linear polarization. There is evidenced some organized polarization movement in the R- and V-bandpasses consistent with the Pfeiffer and Koch (1987) results as shown in Figure 1.11a and b. The short time frame of the present data precludes conclusions about periodicity. There appear to be some cyclical trends in the circular data. Figure 3.20c shows a noisy rise in the group of data centered about JD 2,447,000.

(k) β Peg

The β Peg linear polarimetry shows some low amplitude polarization changes which may be semi-regular or periodic. Figure 3.21a and b shows the gyrations in the q and u vectors. Figure 3.21c clearly shows that the circular polarization was at a local peak near JD 2,447,050 and at JD 2,447,800.

Figure 3.20h for VV Cep and Figure 3.21h for β Peg show a striking similarity. Both stars show a "fanning" in the u vector.

3.4 Polarization Spectra

The intrinsic linear and observed circular polarization spectra are plotted in Figures 3.22 through 3.28 for the program objects. Linear polarization spectral indices, ν, are calculated by a least-squares minimization to the following formula:

$$\frac{p_\lambda}{\langle p \rangle} = \alpha \left[\frac{\lambda}{\langle \lambda \rangle} \right]^\nu , \qquad (3.5)$$

where α and ν are the free parameters fitted, λ is the effective filter

bandpass discussed in Chapter 2, $\langle p \rangle$ and $\langle \lambda \rangle$ are averages over the filters used for observing the object on a particular night. In cases where a bandpass was repeated on a particular night, the average value of the polarization in the bandpass was used when calculating $\langle p \rangle$. The indices for the program objects are presented in Table 3.2. Nights when the u-bandpass was observed in addition to the other three bandpasses are presented with and without the u-bandpass.

Polarization spectral indices give indications of the mechanisms producing the intrinsic polarization since ν is zero for Thomson scattering, approximately -4 for Rayleigh scattering, and typically between -1 and -3 for Mie scattering. Multiple scattering and Hydrogen reabsorption can, however, confuse the above indications.

Most of the stars show R/V/B-bandpass spectral indices between -0.5 and -3.0. A notable exception is α Sco which shows a small positive index. Also, α Ori shows indices of both signs. The R/V/B/u-bandpass spectral indices of 72 Leo, 6 Gem, and β Peg are all between -10 and -15.

The azimuth of the electric vector, θ, is nearly flat within its error for most of the program objects. Two exceptions are α Sco and VV Cep. Both of these stars show ten or more degrees of rotation from the R- to the u-bandpass.

The amplitude of the v Stokes vector generally increases towards the short wavelength region for most program objects. Further, the preponderance of short wavelength data is negative. α^1 Her shows two distinct groups of v Stokes spectra. The first group is nearly flat, while the second group has a signal which is weak in the R- and B-bandpasses and strong in the V- and u-bandpasses.

3.5 Period and Cycle Length Determinations

Stellingwerf's (1978) Phase Dispersion Minimization (PDM) technique was carried out on the program object data. The PDM technique works by assuming a trial frequency and then calculating the relative scatter of the

phased data. The strength of this technique lies in the insensitivity to the waveform shape. The output of the PDM process is the Theta, Θ, parameter:

$$\Theta = \frac{s^2}{\sigma^2} , \tag{3.6}$$

where σ^2 is the overall variance in the data set, and the variable s^2 is defined by the following:

$$s^2 = \frac{\sum (n_j - 1)\, s_j^2}{\sum n_j - M} , \tag{3.7}$$

where M is the number of overlapping bins over which the phased data are split, n_j is the number of data points in bin j, and s_j is the variance of the data in bin j. The number of data bins may be varied. Further, the data bins may overlap in phase. Stellingwerf found that the detection sensitivity of the PDM technique for different bin quantities and overlap degenerates above 50 data points. In the following analysis, ten bins with no overlap were used unless otherwise noted.

Stellingwerf's equation 13 is used as follows for the signal-to-noise ratio, ϵ, of a detected period:

$$\epsilon = \left[\frac{1 - \Theta}{\Theta - \left(\frac{\chi}{N_b} \right)^2} \right]^{1/2} , \tag{3.8}$$

where χ is a parameter empirically determined to equal +1.7 for a sine wave, and N_b is the total number of non-overlapping bins: $N_b < M$.

False periods arise due to under-sampling in the data. The Nyquist criterion was followed for the minimum period detectable. In general, no period shorter than two days is valid since the minimum sampling period is about one day. Also, no period which is longer than the duration of the data set under consideration is discernible. In order to gauge the presence of false period determinations between the minimum and maximum intervals expressed above, the standard deviation of the number of points in each bin was calculated. Sampling problems are easily seen since aliasing causes this statistic to be large.

All available data, including data from the literature, were reduced as a group. Secondly, only data from certain observing periods were reduced. The periodograms were scrutinized for aliasing. In general, periodograms for stars which had less than 35 data points in a bandpass could not be used and were rejected for this reason. Plots of Θ versus trial periods for the remaining program objects are presented in Figures 3.29 through 3.33.

All of the periodograms show large amounts of noise. Figure 3.29d shows two wide dips at 400 and 800 days for α Ori in the B-bandpass. Figure 3.29e shows a dip near 400 days. The ϵ parameter is less than two for all periods thus making their identification tentative. Figure 3.31c and d shows dips near 1150 days in the B-bandpass for μ Cep. The ϵ parameter is less than two thus making this period tentative.

3.6 *IUE*, *IRAS*, and *AAVSO* Data

Public domain echelle long wavelength spectra (LWP and LWR) made by the *International Ultraviolet Explorer (IUE)* were gathered on the program objects. The *IUE* Spectral Image Processing System (IUESIPS) was used to examine the spectra in the range from 0.20μm to 0.24μm. The presence or

absence of the 0.22μm spectral feature in the spectra is reported in Table 3.3.

Infrared Astronomical Satellite (IRAS) radiometry on the program objects from the *IRAS* Point Source Catalog (1985) is reported in Table 3.4. Also reported in this table are UBVRIJK "photometry" from Johnson *et al.* (1966) and Lee (1970) which were converted to Janskys ($10^{-26}W/m^2/Hz$) using the absolute calibrations of Johnson (1965). Plots of the *IRAS* and UBVRIJK radiometry are shown in Figure 4.1.

Mattei (1991) supplied *American Association of Variable Star Observers (AAVSO)* visual light curves for all of the program objects except 72 Leo. The latest five year portions of the light curves are presented in Figure 3.34. Mattei also supplied V-bandpass photoelectric measures for 119 Tau, α Ori, α Sco, and μ Cep. These measures are presented in Figures 3.35 through 3.38 along with the p and θ archival plus new polarization data measures. It is seen in Figure 3.36 for α Ori that epochs of maximum light coincide with epochs of local minimums in the linear polarization amplitude.

Table 3.1

Interstellar Linear Polarization for Program Objects

Name	--Galactic-- LONG (o)	LAT (o)	Lambda Max. (micron)	Interstellar Polarization (%) R q	R u	V q	V u	B q	B u	U q	U u
119 CE Tau	187.18	-08.07	0.58	+0.45(26)	+0.61(26)	+0.45(26)	+0.62(26)	+0.41(20)	+0.56(20)	+0.37(26)	+0.51(26)
58 α Ori	199.79	-08.96	0.58	+0.12(5)	+0.21(5)	+0.12(5)	+0.20(5)	+0.11(3)	+0.18(3)	+0.10(5)	+0.16(5)
6 BU Gem	188.22	+02.19	0.54	+2.51(38)	-0.82(38)	+2.62(38)	-0.86(38)	+2.47(12)	-0.81(12)	+2.32(38)	-0.76(38)
46 ψ1 Aur	165.35	+16.17	0.51	+1.26(40)	+0.51(40)	+1.34(40)	+0.54(40)	+1.30(27)	+0.52(27)	+1.24(40)	+0.50(40)
72 Leo	218.10	+67.88	0.57	-0.005(3)	+0.007(3)	-0.005(3)	+0.007(3)	-0.005(2)	+0.006(2)	-0.004(3)	+0.006(3)
V CVn	107.90	+70.77	0.57	+0.000(21)	+0.011(21)	+0.000(21)	+0.011(21)	+0.000(20)	+0.010(20)	+0.000(21)	+0.009(21)
21 α Sco	351.95	+15.06	0.57	-0.13(6)	-0.04(6)	-0.14(6)	-0.04(6)	-0.12(5)	-0.04(5)	-0.12(6)	+0.04(6)
64 α1 Her	35.53	+27.82	0.57	+0.00(6)	+0.00(6)	+0.00(6)	+0.00(6)	+0.00(6)	+0.00(6)	+0.00(6)	+0.00(6)
μ Cep	100.60	+04.32	0.55	-0.07(13)	+0.93(13)	-0.08(13)	+0.96(13)	-0.07(12)	+0.90(12)	-0.07(13)	+0.84(13)
VV Cep	104.92	+07.05	0.51	+0.06(26)	+0.90(26)	+0.06(26)	+0.96(26)	+0.06(19)	+0.93(19)	+0.06(26)	+0.89(26)
53 β Peg	95.74	-29.05	0.52	+0.005(15)	+0.003(15)	+0.005(15)	+0.003(15)	+0.005(15)	+0.003(15)	+0.005(15)	+0.003(15)

Table 3.2

Polarization Spectral Indices for Program Objects

Interstellar Polarization Removed

Name	(HJD-2,400,000) (Note 1)	Bandpasses Compiled	p linear <p>	α	υ
119 CE Tau	40586	R/V/B/U	0.42	1.00(13)	+0.40(55)
		R/V/B	0.47	0.994(4)	-0.25(2)
	40624	R/V/B/U	0.56	1.01(10)	+0.72(41)
		R/V/B	0.63	1.00(6)	+0.25(29)
	46786	R/V/B/U	0.69	0.96(18)	-0.84(81)
		R/V/B	0.58	1.00(6)	+0.31(30)
58 α Ori	42282	R/V/B	0.59	1.00(38)	+1.4(21)
	42447	R/V/B	0.53	1.00(36)	+1.4(19)
	44212/44213	R/V/B/U	0.59	0.98(3)	-0.44(15)
		R/V/B	0.56	0.99(5)	-0.42(28)
	46770	R/V/B/U	0.200	1.00(5)	+1.01(21)
		R/V/B	0.222	1.01(3)	+0.79(19)
	46777	R/V/B/U	0.395	0.98(6)	-0.48(29)
		R/V/B	0.365	1.00(4)	-0.10(19)
	46780	R/V/B/U	0.322	1.01(14)	+0.56(61)
		R/V/B	0.367	1.00(2)	-0.14(10)
	46799	R/V/B/U	0.383	1.01(24)	+0.7(11)
		R/V/B	0.466	0.99(4)	-0.39(22)
	46823	R/V/B	0.660	0.98(4)	-0.64(19)
	46844	R/V/B/U	0.678	1.00(14)	+0.12(61)
		R/V/B	0.741	0.98(6)	-0.55(32)
	46846	R/V/B/U	0.964	0.88(18)	-1.7(8)
		R/V/B	0.746	0.98(7)	-0.57(34)
	46860	R/V/B	0.570	1.00(24)	+0.8(13)
	46865	R/V/B/U	0.673	0.99(6)	-0.17(29)
		R/V/B	0.684	0.99(6)	-0.46(30)
	47824	R/V/B	0.455	0.96(6)	-1.4(3)
6 BU Gem	40308	R/V/B	0.64	0.95(8)	+2.34(49)
	40607	R/V/B	1.22	1.00(1)	-0.07(7)
	40610	R/V/B	0.99	0.98(1)	-0.68(8)

Table 3.2 (cont.)

Polarization Spectral Indices for Program Objects

Interstellar Polarization Removed

Name	(HJD-2,400,000) (Note 1)	Bandpasses Compiled	p linear <p>	α	υ
6 Gem (cont.)	46778	R/V/B/U	2.56	0.08(14)	-12.9(59)
		R/V/B	0.32	0.92(23)	-2.5(13)
46 ψ1 Aur	40587	R/V/B/U	0.94	0.99(1)	-0.21(5)
		R/V/B	0.92	1.00(1)	-0.23(8)
	40654	R/V/B/U	1.14	1.00(3)	+0.79(14)
		R/V/B	1.24	1.00(2)	+0.64(13)
	46777	R/V	1.15	1.00(...)	-0.21(...)
	46842	R/V	1.18	1.00(...)	-0.25(...)
72 Leo	46878	R/V/B/U	0.13	0.03(7)	-15.2(68)
		R/V/B	0.05	0.99(15)	-0.27(78)
	46912	R/V/B	0.06	1.00(6)	+0.65(33)
	46916	R/V/B	0.06	0.97(9)	-0.95(46)
	46922	R/V/B	0.07	0.85(6)	-2.55(31)
	46924	R/V/B/U	0.14	0.05(7)	-14.0(53)
		R/V/B	0.05	0.97(38)	-0.9(19)
	46932	R/V/B/U	0.16	0.06(14)	-13.2(74)
		R/V/B	0.05	1.00(61)	+0.0(32)
V CVn	39910	R/V/B/U	2.72	0.91(11)	-1.54(51)
		R/V/B	2.34	0.94(20)	-1.6(10)
	39951	R/V/B/U	3.89	0.92(14)	-1.53(67)
		R/V/B	3.44	0.92(24)	-1.8(12)
	39966	R/V/B/U	4.93	0.92(20)	-1.46(91)
		R/V/B	4.46	0.91(32)	-1.9(16)
	39988	R/V/B/U	3.28	0.97(22)	-0.70(10)
		R/V/B	3.32	0.95(30)	-1.3(15)
	40277	R/V/B/U	1.68	0.98(21)	-0.58(93)
		R/V/B	1.75	0.95(21)	-1.14(11)
	40727	R/V/B/U	2.45	0.95(9)	-1.06(39)
		R/V/B	2.27	0.95(13)	-1.32(65)

Table 3.2 (cont.)

Polarization Spectral Indices for Program Objects

Interstellar Polarization Removed

Name	(HJD-2,400,000) (Note 1)	Bandpasses Compiled	p linear <p>	α	υ
V CVn (cont.)	43673	R/V/B/U	4.59	0.95(10)	-1.09(45)
		R/V/B	4.25	0.95(15)	-1.37(75)
	45382	R/V/B/U	4.38	0.97(9)	-0.77(41)
		R/V/B	4.25	0.95(6)	-1.24(32)
	46956	V/B	2.09	0.89(...)	-0.81(...)
	46957	R/V	1.54	0.98(...)	-1.47(...)
	46971/46972	R/V/B	1.63	0.96(7)	-1.17(36)
21 α Sco	38180/38189	R/V/B/U	0.56	0.99(11)	+1.23(46)
		R/V/B	0.61	0.99(15)	+1.43(83)
	42246	R/V/B	0.42	1.004(9)	+0.49(5)
	42253	R/V/B	0.46	1.00(3)	+0.66(17)
	42268	R/V/B	0.51	1.00(2)	+0.55(10)
	42282	R/V/B	0.53	1.00(2)	+0.20(10)
	46994/46995	R/V/B	0.50	1.00(1)	+0.14(5)
	46999/47000	R/V/B	0.47	1.00(2)	+0.43(12)
	47005/47006	R/V/B	0.49	1.004(1)	+0.401(5)
64 α1 Her	40654	R/V/B	0.073	0.78(42)	-2.8(24)
	46922	R/V/B	0.16	0.88(4)	-2.22(22)
	46932	R/V/B/U	0.15	0.88(11)	-1.81(52)
		R/V/B	0.12	0.96(3)	-1.09(13)
	46999/47000	R/V/B	0.16	0.93(4)	-1.59(19)
	47005	R/V/B	0.17	0.912(1)	-1.813(4)
	47006/47012	R/V/B	0.16	0.93(2)	-1.61(8)
	47020/47021	R/V/B	0.11	0.98(1)	-1.37(7)
	47022/47023	R/V/B/U	0.14	0.92(2)	-1.44(9)
		R/V/B	0.12	0.93(3)	-1.51(14)
	47027	R/V/B	0.13	0.95(1)	-1.28(6)
	47028/47031	R/V/B/U	0.14	0.85(20)	-2.04(96)
		R/V/B	0.11	0.98(1)	-0.66(8)

Table 3.2 (cont.)

Polarization Spectral Indices for Program Objects

Interstellar Polarization Removed

Name	(HJD-2,400,000) (Note 1)	Bandpasses Compiled	p linear <p>	p linear α	p linear υ
μ Cep	38912	R/V/B	1.47	0.97(8)	-0.85(39)
	39289	R/V/B/U	0.76	1.00(9)	+0.69(43)
		R/V/B	0.77	0.99(8)	+1.22(45)
	39443	R/V/B/U	0.98	1.00(6)	+0.02(27)
		R/V/B	0.97	1.00(8)	+0.22(44)
	39809	R/V/B/U	0.88	0.98(10)	-0.63(44)
		R/V/B	0.87	0.97(11)	-1.03(55)
	40583	R/V/B	1.54	0.99(5)	-0.52(26)
	43673	R/V/B/U	0.98	1.00(4)	+0.05(19)
		R/V/B	1.00	1.00(5)	-0.10(28)
	47772	R/V/B/U	1.81	0.99(12)	-0.34(52)
		R/V/B	1.85	0.97(11)	-0.86(54)
VV Cep	42995	R/V/B	0.66	0.97(4)	-0.94(20)
	43381	R/V/B	0.51	0.98(4)	-0.67(19)
	45245	R/V/B/U	0.70	0.80(18)	-2.49(92)
		R/V/B	0.51	0.96(5)	-1.14(26)
	45665	R/V/B/U	0.53	1.01(28)	+0.7(12)
		R/V/B	0.65	0.98(3)	-0.58(15)
	45894	R/V/B/U	0.62	0.90(12)	-1.60(55)
		R/V/B	0.51	0.96(18)	-1.21(89)
	45933	R/V/B/U	0.48	1.01(21)	+0.51(90)
		R/V/B	0.57	1.01(9)	-0.47(21)
	45978	R/V/B/U	0.52	0.99(6)	-0.27(29)
		R/V/B	0.51	0.99(11)	-0.29(55)
	46993/46994	R/V/B/U	0.50	0.98(3)	-0.45(15)
		R/V/B	0.47	0.99(5)	-0.34(24)
	47018/47020	R/V/B	0.47	0.99(1)	-0.56(7)
	47773	R/V/B/U	0.56	1.00(19)	+0.02(85)
		R/V/B	0.62	0.97(30)	-1.00(15)

Table 3.2 (cont.)

Polarization Spectral Indices for Program Objects

Interstellar Polarization Removed

Name	(HJD-2,400,000) (Note 1)	Bandpasses Compiled	p linear <p>	α	υ
53 β Peg	46799	R/V/B/U	0.019	0.13(14)	-10.2(37)
		R/V/B	0.009	0.90(30)	-1.9(16)
	47764	R/V/B/U	0.098	0.09(14)	-12.7(56)
		R/V/B	0.013	0.99(22)	-0.2(12)
	47822/47826	R/V/B	0.03	0.94(23)	-1.5(12)

Note 1. Absence of a printed HJD indicates that the indices were compiled for the preceding HJD using different filters in the regression.

Table 3.3. *IUE* 0.22μm Feature for Program Objects

Name	IUE Spectra	0.22μ Feature
119 CE Tau	LWR 8951	Not detected
58 α Ori	LWP 5234	Weak dip
6 BU Gem	...	...
46 ψ1 Aur	LWR 10272	Not detected
72 Leo	LWR 11848	Not detected
V CVn	LWP 5318	Not detected
21 α Sco	LWR 5146	Strong dip
64 α1 Her	LWR 5089	Emission ?
μ Cep	LWR 5149	Weak dip
VV Cep	LWR 12538	Strong dip
53 β Peg	LWR 10803	Not detected

Table 3.4. Program Object Radiometry

			Flux Density (Jy)											
	Name	IRAS Point Source ID	Bandpass: Center λ(μ):	U 0.36	B 0.44	V 0.55	R 0.70	I 0.90	J 1.25	K 2.20	L 3.40	12 12	25 25	60 60	100 100
119	CE Tau	05292+1833		0.664	12.1	70.6	287	866	1330	1440	989	145.07	46.44	7.05	5.38
58	α Ori	05524+0723		33.9	539	2640	9010	23600	26300	25300	18300	4681.93	1737.71	298.77	95.90
6	BU Gem	06092+2255		0.0676	1.57	10.6	45.6	144	227	256	175	78.20	47.59	10.50	3.62
46	ψ1 Aur	06210+4918		0.542	9.54	48.0	138	298	441	398	258	44.06	19.32	4.06	2.04
72	Leo	...		1.04	13.5	53.6	178	480	631	630	376	...	...	...	...
	V CVn	13172+4547		0.622	1.07	3.67	...	...	...	...	...	132.16	64.05	5.52	1.43
21	α Sco	16262-2619		43.9	353	1650	5430	13600	20100	20500	12800	3197.53	689.95	115.50	31.88
64	α1 Her	17123+1426		112	27.5	59.8	1240	7210	14200	16000	9540	1515.09	428.44	83.80	24.99
	μ Cep	21419+5832		0.527	11.9	81.8	447	1830	2860	2880	2130	1295.57	607.74	127.04	49.90
	VV Cep	21552+6323		2.43	7.86	32.9	130	400	655	697	465	70.28	21.54	3.66	27.08
53	β Peg	23013+2748		7.48	97.1	381	1280	3450	4610	4780	2910	387.33	97.62	15.57	3.74

CHAPTER 3. Figure Captions

Figure 3.1. Polarization observations of 119 Tau field stars. The caret indicates the adopted distance to 119 Tau from Table 1.1. The plotted lines indicate the interstellar polarization fit described in the text. (*a*) *p vs.* distance. (*b*) θ *vs* distance. (*c*) map of galactic positions of the stars plotted in (*a*) and (*b*). The star indicates the position of 119 Tau. The horizontal lines indicate the amplitude of the polarization using the key displayed on the plot. The diamonds indicate stars which are closer than 119 Tau. (*d*) *v vs.* distance. Some program stars have a plot labeled (*e*) which is a galactic map for *v* as the (*c*) plot is for *p*.

Figure 3.2. Polarization observations of α Ori field stars. (*a-c*) see the caption to Figure 3.1 for explanations.

Figure 3.3. Polarization observations of 6 Gem field stars. (*a-e*) see the caption to Figure 3.1 for explanations.

Figure 3.4. Polarization observations of ψ^1 Aur field stars. (*a-c*) see the caption to Figure 3.1 for explanations.

Figure 3.5. Polarization observations of 72 Leo field stars. (*a-c*) see the caption to Figure 3.1 for explanations.

Figure 3.6. Polarization observations of V CVn field stars. (*a-c*) see the caption to Figure 3.1 for explanations.

Figure 3.7. Polarization observations of α Sco field stars. (*a-e*) see the caption to Figure 3.1 for explanations.

Figure 3.8. Polarization observations of μ Cep field stars. (*a-e*) see the caption to Figure 3.1 for explanations.

Figure 3.9. Polarization observations of VV Cep field stars. (*a-c*) see the caption to Figure 3.1 for explanations. Note that VV Cep and μ Cep share common (*d*) and (*e*) plots.

Figure 3.10. Polarization observations of β Peg field stars. (*a-e*) see the caption to Figure 3.1 for explanations.

Figure 3.11. The R-, V-, and B-bandpass intrinsic polarization observations of 119 Tau measured during this program. The interstellar vectors defined in Table 3.1 have been removed from Appendix E data. The 119 Tau u-bandpass datum fell off scale and is not shown. (*a*) *q vs.* JD. (*b*) *u vs.* JD. (*c*) *v vs.* JD. (*d*) *p vs.* JD. (*e*) θ *vs. u*. (*f*) *q vs. u*.

Figure 3.12. The R-, V-, B-, and u-bandpass intrinsic polarization observations of α Ori measured during this program. See the caption to Figure 3.11 for explanations. (*a-f*) R-bandpass. (*g-l*) V-bandpass. (*m-r*) B-bandpass. (*s-x*) U-bandpass.

Figure 3.13. The R-, V-, and B-bandpass intrinsic polarization observations of 6 Gem measured during this program. See the caption to Figure 3.11 for explanations. (*a-f*) R-, V-, and B-bandpasses.

Figure 3.14. The R- and V-bandpass intrinsic polarization observations of ψ^1 Aur measured during this program. See the caption to Figure 3.11 for explanations. (*a-f*) R- and V-bandpasses.

Figure 3.15. The R-, V-, B-, and u-bandpass intrinsic polarization observations of 72 Leo measured during this program. See the caption to Figure 3.11 for explanations. (*a-f*) R-bandpass. (*g-l*) V-bandpass. (*m-r*) B- and U-bandpasses.

Figure 3.16. The R-, V-, and B-bandpass intrinsic polarization observations of V CVn measured during this program. See the caption to Figure 3.11 for explanations. (*a-f*) R-bandpass. (*g-l*) V-bandpass. (*m-r*) B-bandpass.

Figure 3.17. The R-, V-, and B-bandpass intrinsic polarization observations of α Sco measured during this program. See the caption to Figure 3.11 for explanations. (*a-f*) R-bandpass. (*g-l*) V-bandpass. (*m-r*) B-bandpass.

Figure 3.18. The R-, V-, B-, and u-bandpass intrinsic polarization observations of α^1 Her measured during this program. See the caption to Figure 3.11 for explanations. (*a-f*) R-bandpass. (*g-l*) V-bandpass. (*m-r*) B-bandpass. (*s*-x) u-bandpass.

Figure 3.19. The R-, V-, B-, and u-bandpass intrinsic polarization observations of μ Cep measured during this program. See the caption to Figure 3.11 for explanations. (*a-f*) R-bandpass. (*g-l*) V-, B-, and u-bandpasses.

Figure 3.20. The R-, V-, B-, and u-bandpass intrinsic polarization observations of VV Cep measured during this program. See the caption to Figure 3.11 for explanations. (*a-f*) R-bandpass. (*g-l*) V-bandpass. (*m-r*) B-bandpass. (*s-x*) u-bandpass.

Figure 3.21. The R-, V-, B-, and u-bandpass intrinsic polarization observations of β Peg measured during this program. See the caption to Figure 3.11 for explanations. One R-bandpass datum (JD-2,446,993) fell off scale and is not shown. (*a-f*) R-bandpass. (*g-l*) V-bandpass. (*m-r*) B- and u-bandpasses.

Figure 3.22. The polarization spectra for α Ori. The legend indicates the observing dates in the format (JD-2,440,000). (*a*) *p vs.* $1/\lambda$. (*b*) θ *vs.* $1/\lambda$. (*c*) *v vs.* $1/\lambda$.

Figure 3.23. The polarization spectra for 72 Leo. The legend indicates the observing dates in the format (JD-2,440,000). (*a*) *p vs.* $1/\lambda$. (*b*) θ *vs.* $1/\lambda$. (*c*) *v vs.* $1/\lambda$.

Figure 3.24. The polarization spectra for α Sco. The legend indicates the observing dates in the format (JD-2,440,000). (*a*) *p vs.* $1/\lambda$. (*b*) θ *vs.* $1/\lambda$. (*c*) *v vs.* $1/\lambda$.

Figure 3.25. The polarization spectra for α^1 Her. The legend indicates the observing dates in the format (JD-2,440,000). (*a*) *p vs.* $1/\lambda$. (*b*) θ *vs.* $1/\lambda$. (*c*) *v vs.* $1/\lambda$.

Figure 3.26. The polarization spectra for VV Cep. The legend indicates the observing dates in the format (JD-2,440,000). (*a*) *p vs.* $1/\lambda$. (*b*) θ *vs.* $1/\lambda$. (*c*) *v vs.* $1/\lambda$.

Figure 3.27. The polarization spectra for β Peg. The legend indicates the observing dates in the format (JD-2,440,000). (*a*) *p vs.* $1/\lambda$. (*b*) θ *vs.* $1/\lambda$. (*c*) *v vs.* $1/\lambda$.

Figure 3.28. The polarization spectra for 119 Tau, 6 Gem, μ Cep, ψ^1 Aur, and V CVn. The legend indicates the observing dates in the format (JD-2,440,000). (*a*) *p vs.* $1/\lambda$. (*b*) θ *vs.* $1/\lambda$. (*c*) *v vs.* $1/\lambda$.

Figure 3.29. The periodograms for α Ori. (*a*) R-bandpass *p vs.* trial period. (*b*) R-bandpass θ *vs.* trial period. (*c*) R-bandpass *v vs.* trial period for the first season of data only. Note the 100 day period. (*d*) B-bandpass *p vs.* trial period. Note the possible 400 and 800 day periods. (*e*) B-bandpass θ *vs.* trial period. The possible 400 day period suggests the 800 day period in the *p* data is an overtone.

Figure 3.30. The periodograms for β Peg. (*a*) R-bandpass *p vs.* trial period. (*b*) R-bandpass θ *vs.* trial period.

Figure 3.31. The periodograms for V CVn. (*a*) R-bandpass *p vs.* trial period. (*b*) R-bandpass θ *vs.* trial period. (*c*) V-bandpass *p vs.* trial period. (*d*) V-bandpass θ *vs.* trial period. (*e*) B-bandpass *p vs.* trial period. (*f*) B-bandpass θ *vs.* trial period.

Figure 3.32. The periodograms for μ Cep. (*a*) V-bandpass *p vs.* trial period. (*b*) V-bandpass θ *vs.* trial period. (*c*) B-bandpass *p vs.* trial period. (*d*) B-bandpass θ *vs.* trial period. Note the possible period near 1200 days in the B-bandpass.

Figure 3.33. The periodograms for VV Cep. (*a*) R-bandpass *p vs.* trial period. (*b*) R-bandpass θ *vs.* trial period. (*c*) V-bandpass *p vs.* trial period. (*d*) V-bandpass θ *vs.* trial period. (*e*) B-bandpass *p vs.* trial period. (*f*) B-bandpass θ *vs.* trial period.

Figure 3.34. *AAVSO* visual light curves for the program objects. (*a*) 119 Tau. (*b*) α Ori. (*c*) 6 Gem. (*d*) ψ^1 Aur. (*e*) V CVn. (*f*) α Sco. (*g*) α^1 Her. (*h*) μ Cep. (*i*) VV Cep. (*j*) β Peg.

Figure 3.35. *AAVSO* photoelectric light curve for 119 Tau along with the recent archival plus new polarization data. The apparent magnitude of 119 Tau minus the apparent magnitude of the comparison star (SAO 94573, 6.86V) is reported as the *del mag* quantity. (*a*) *p vs.* JD. (*b*) θ *vs.* JD. (*c*) *del mag vs.* JD.

Figure 3.36. *AAVSO* photoelectric light curve for α Ori along with the recent archival plus new polarization data. The apparent magnitude of α Ori minus the apparent magnitude of the comparison star (SAO 112958, 4.09V) is reported as the *del mag* quantity. (*a*) *p vs.* JD. (*b*) θ *vs.* JD. (*c*) *del mag vs.* JD. Note that the epochs of maximum light coincide with epochs of local minimums in the linear polarization amplitude.

Figure 3.37. *AAVSO* photoelectric light curve for α Sco along with the recent archival plus new polarization data. The apparent magnitude of α Sco minus the apparent magnitude of the comparison star (SAO 184437, 6.2V) is reported as the *del mag* quantity. (*a*) *p vs.* JD. (*b*) θ *vs.* JD. (*c*) *del mag vs.* JD.

Figure 3.38. *AAVSO* photoelectric light curve for μ Cep along with the recent archival plus new polarization data. The apparent magnitude of μ Cep minus the apparent magnitude of the comparison star (SAO 33683, 6.06V) is reported as the *del mag* quantity. (*a*) *p vs.* JD. (*b*) θ *vs.* JD. (*c*) *del mag vs.* JD.

Figure 3.1

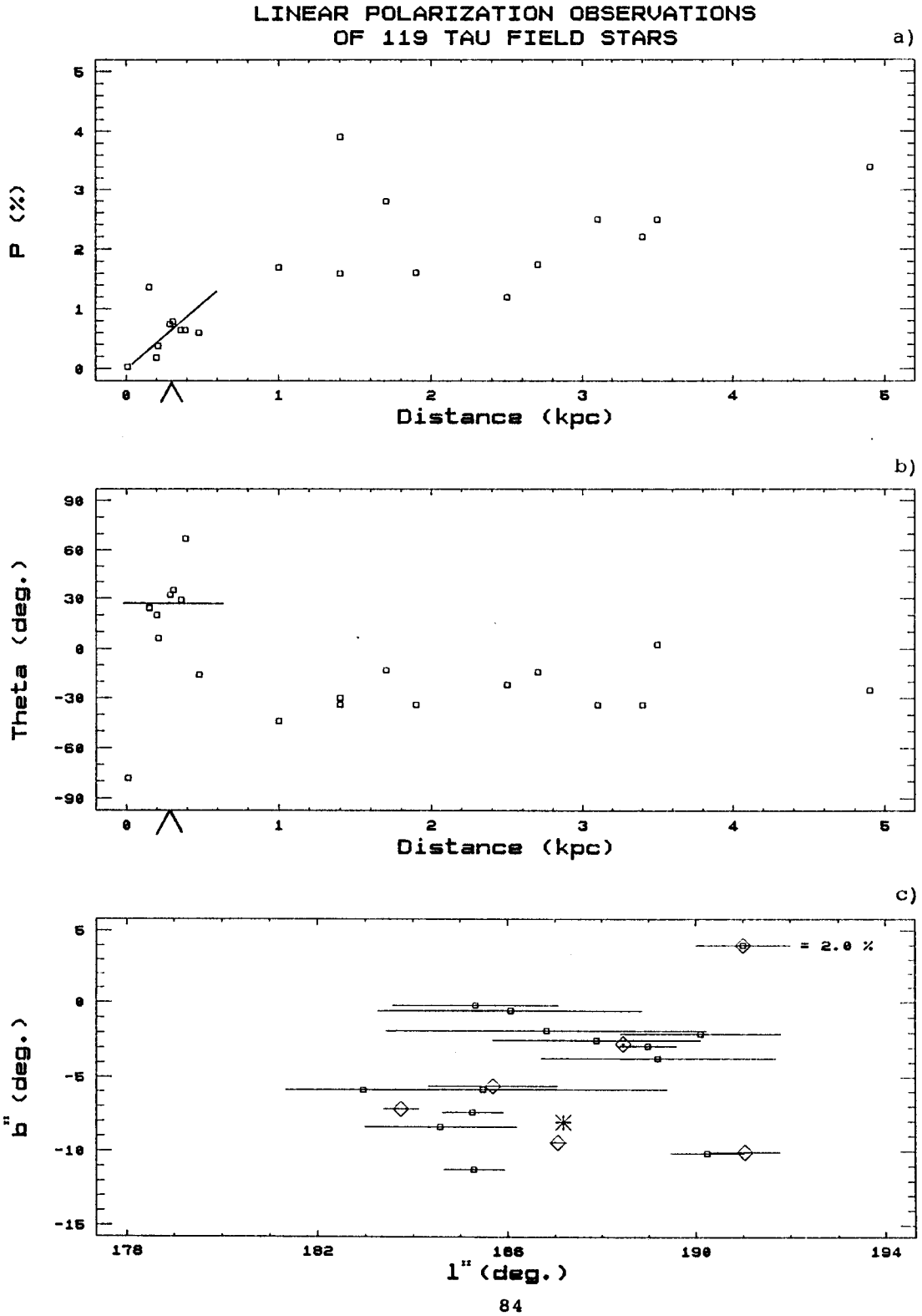
LINEAR POLARIZATION OBSERVATIONS
OF 119 TAU FIELD STARS
a)
P (%)
Distance (kpc)
b)
Theta (deg.)
Distance (kpc)
c)
= 2.0 %
b" (deg.)
l" (deg.)

Figure 3.1 (cont.)

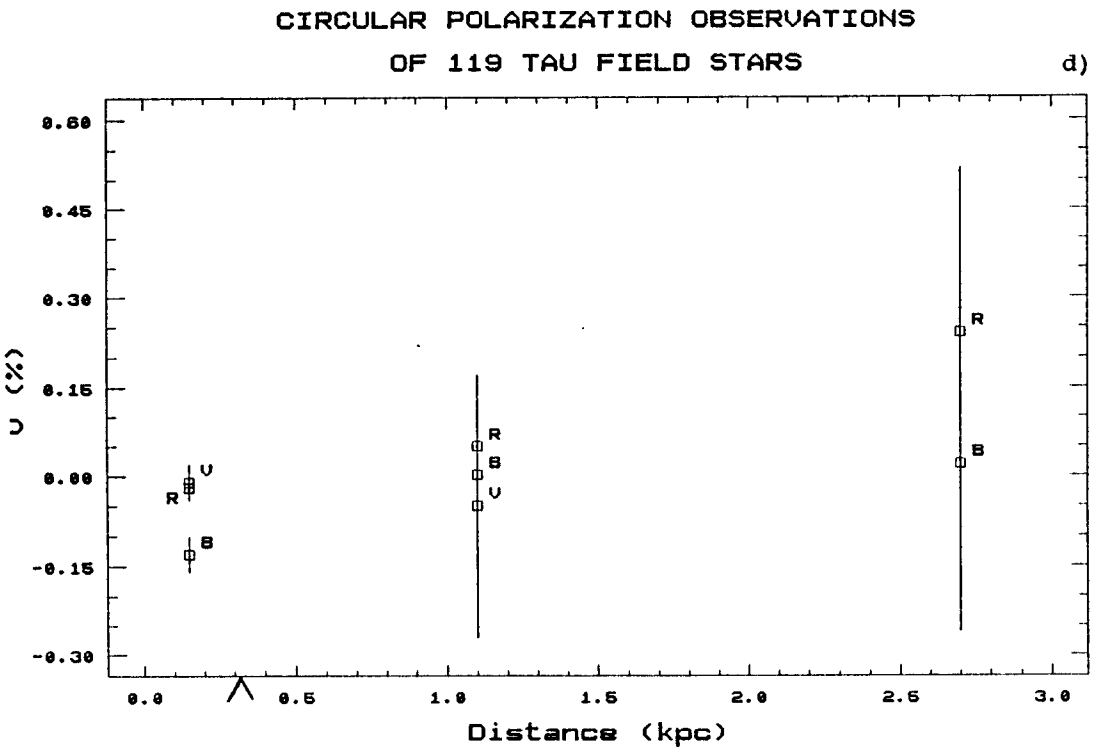

Figure 3.2

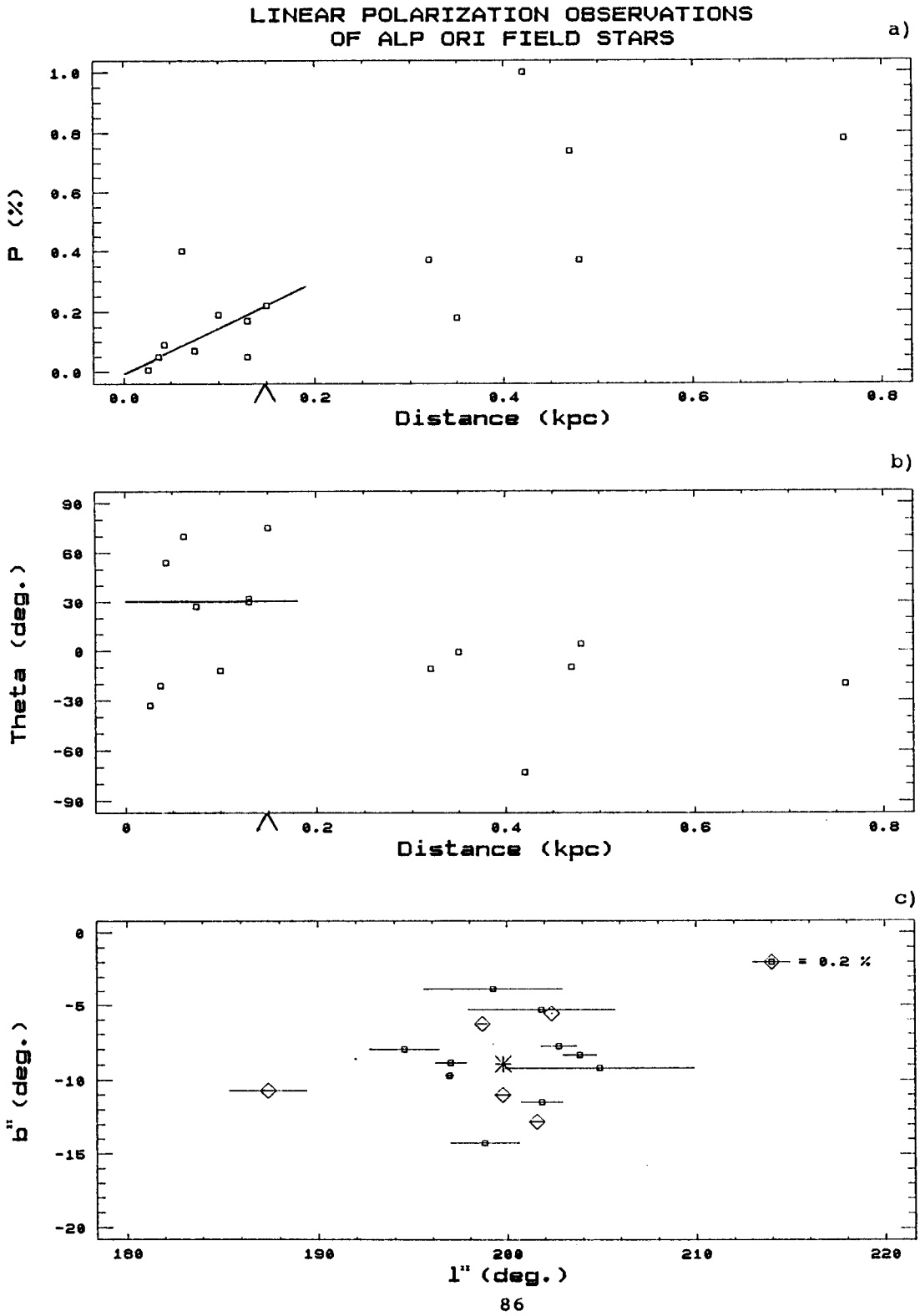
LINEAR POLARIZATION OBSERVATIONS
OF ALP ORI FIELD STARS
a)
P (%)
1.0
0.8
0.6
0.4
0.2
0.0
0.0
0.2
0.4
0.6
0.8
Distance (kpc)
b)
Theta (deg.)
90
60
30
0
-30
-60
-90
0
0.2
0.4
0.6
0.8
Distance (kpc)
c)
= 0.2 %
b" (deg.)
0
-5
-10
-15
-20
180
190
200
210
220
l" (deg.)

Figure 3.3

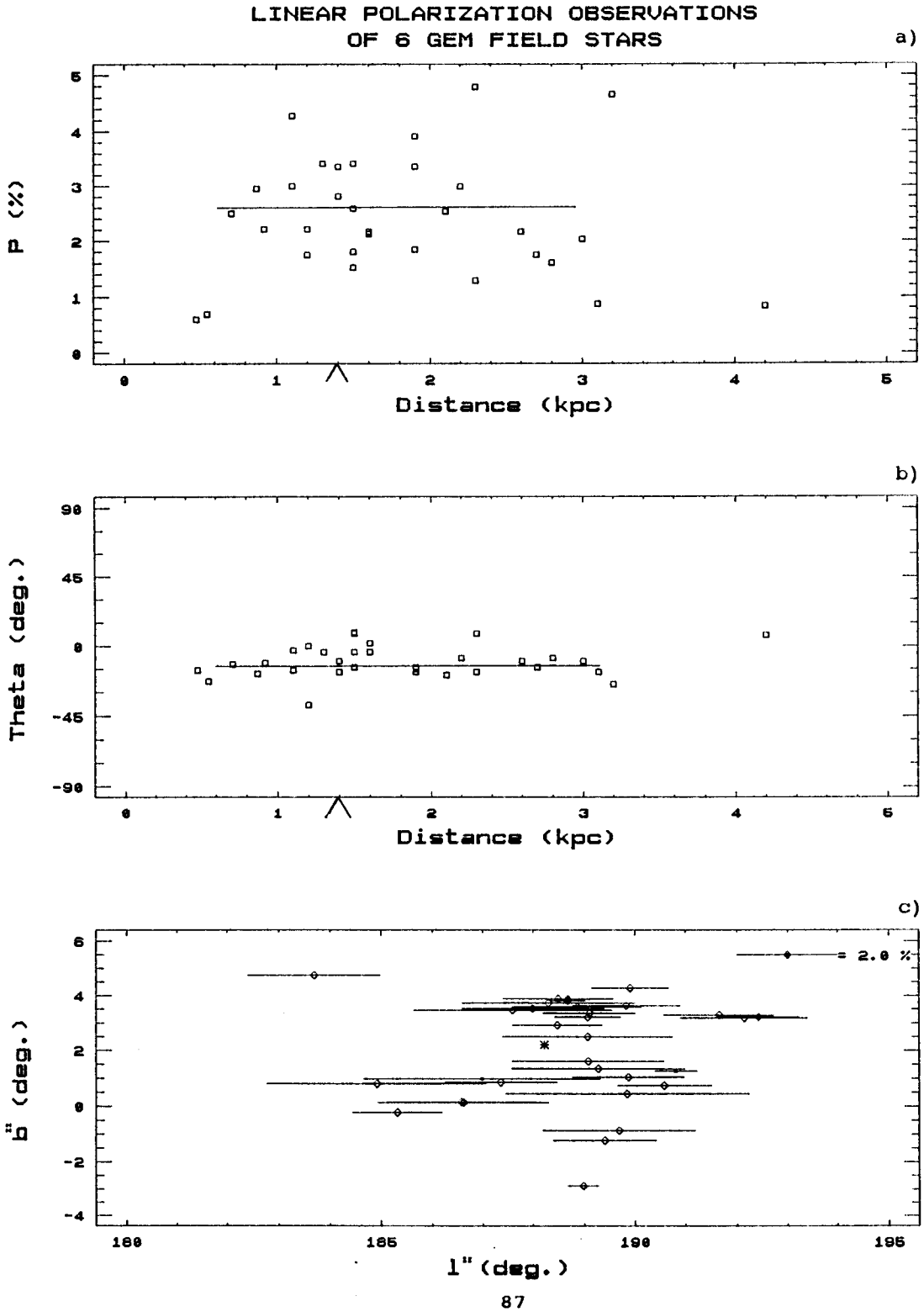
LINEAR POLARIZATION OBSERVATIONS
OF 6 GEM FIELD STARS
a)
P (%)
Distance (kpc)
b)
Theta (deg.)
Distance (kpc)
c)
= 2.0 %
b" (deg.)
l" (deg.)

Figure 3.3 (cont.)

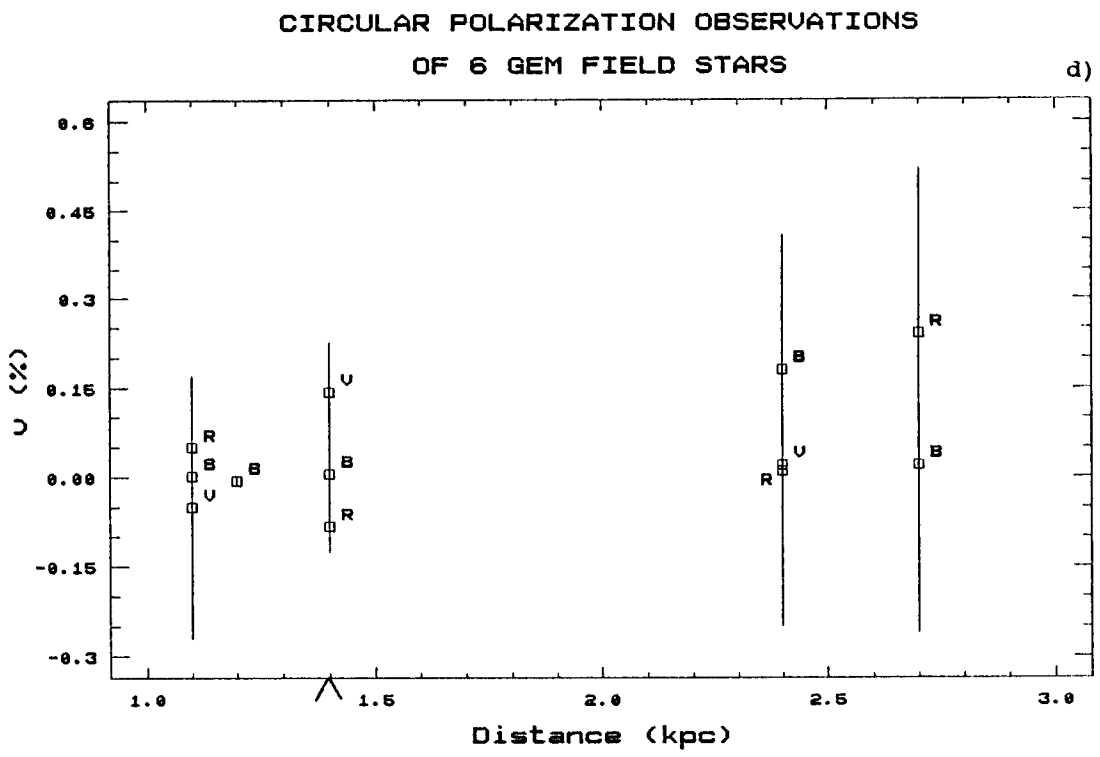

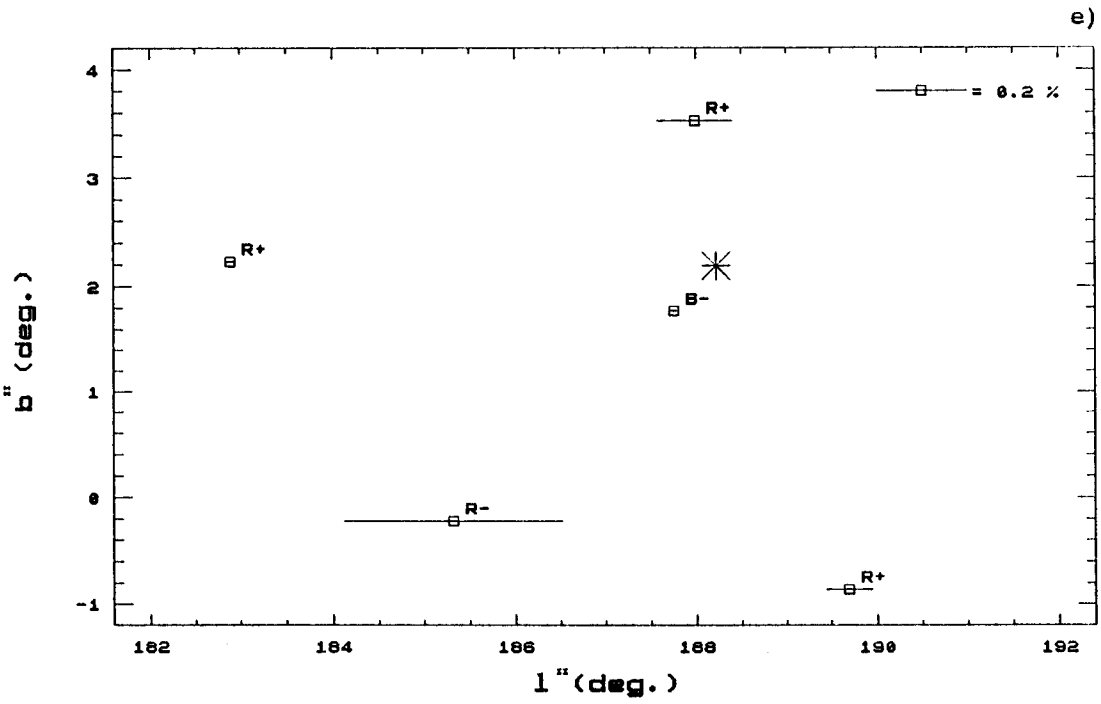

Figure 3.4

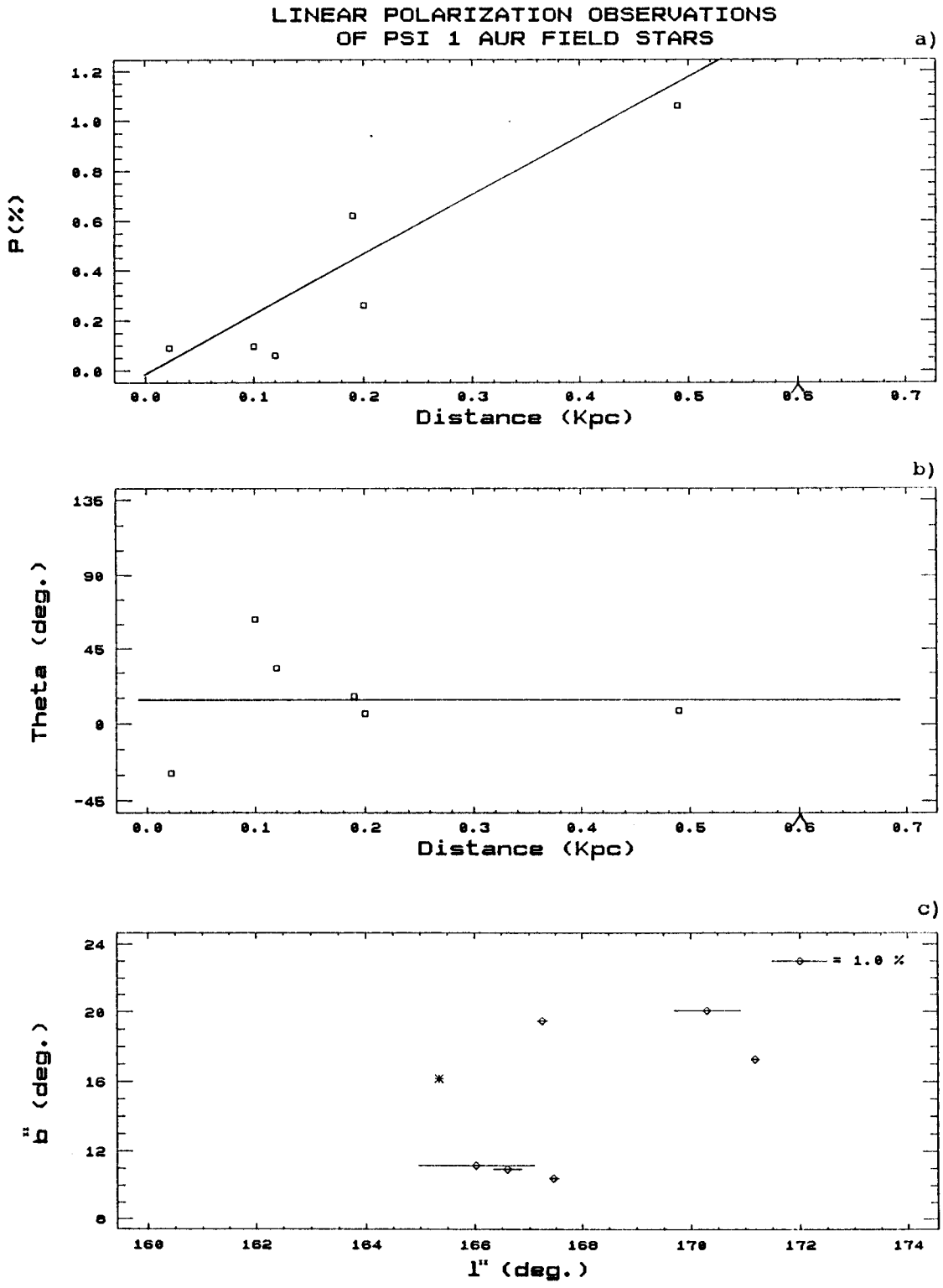
LINEAR POLARIZATION OBSERVATIONS
OF PSI 1 AUR FIELD STARS
a)
P(%)
1.2
1.0
0.8
0.6
0.4
0.2
0.0
0.0
0.1
0.2
0.3
0.4
0.5
0.6
0.7
Distance (Kpc)
b)
Theta (deg.)
135
90
45
0
-45
0.0
0.1
0.2
0.3
0.4
0.5
0.6
0.7
Distance (Kpc)
c)
= 1.0 %
b" (deg.)
24
20
16
12
8
160
162
164
166
168
170
172
174
l" (deg.)

Figure 3.5

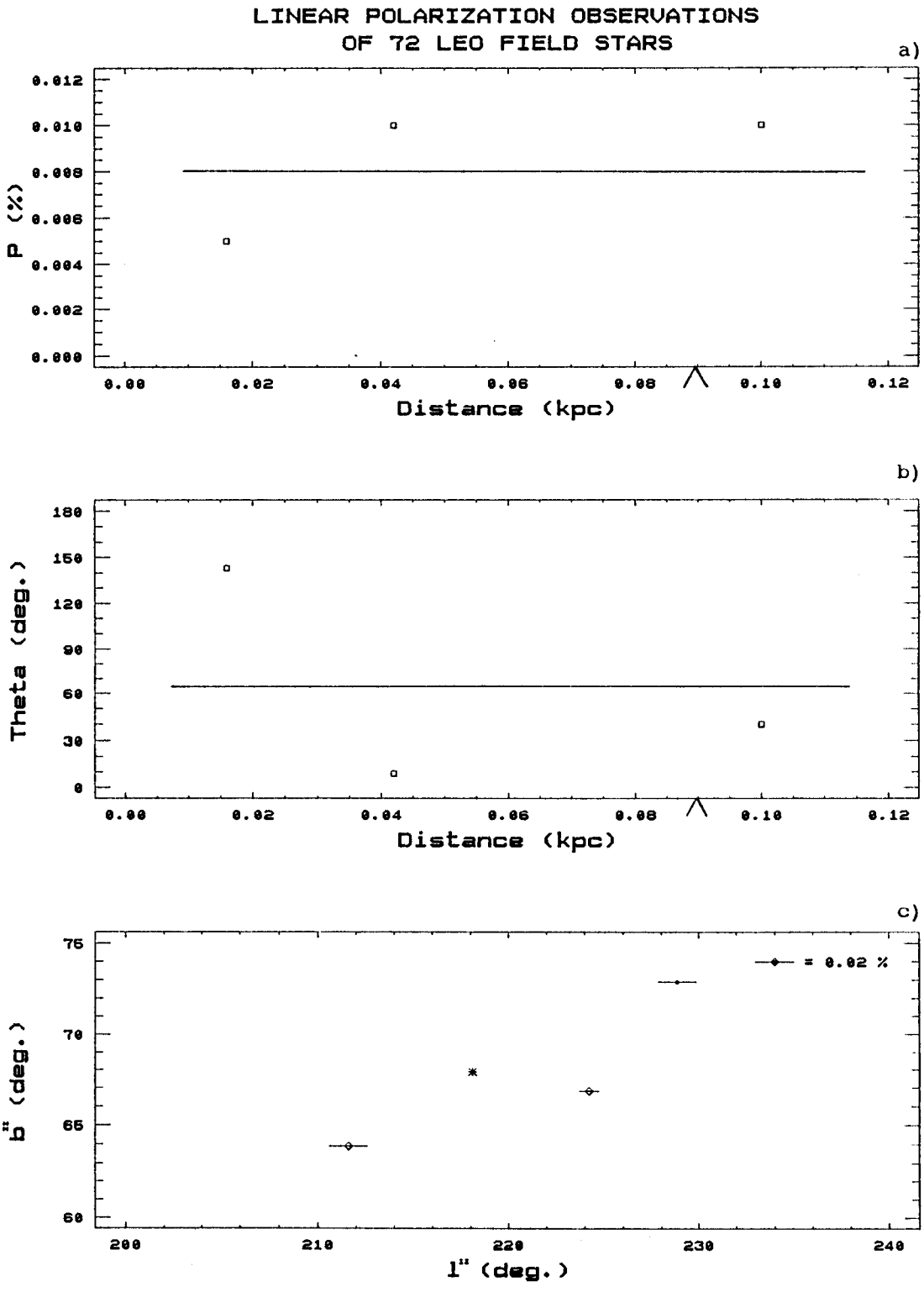
LINEAR POLARIZATION OBSERVATIONS
OF 72 LEO FIELD STARS
a)
P (%)
0.012
0.010
0.008
0.006
0.004
0.002
0.000
0.00
0.02
0.04
0.06
0.08
0.10
0.12
Distance (kpc)
b)
Theta (deg.)
180
150
120
90
60
30
0
0.00
0.02
0.04
0.06
0.08
0.10
0.12
Distance (kpc)
c)
= 0.02 %
75
70
65
60
200
210
220
230
240
l" (deg.)

Figure 3.6

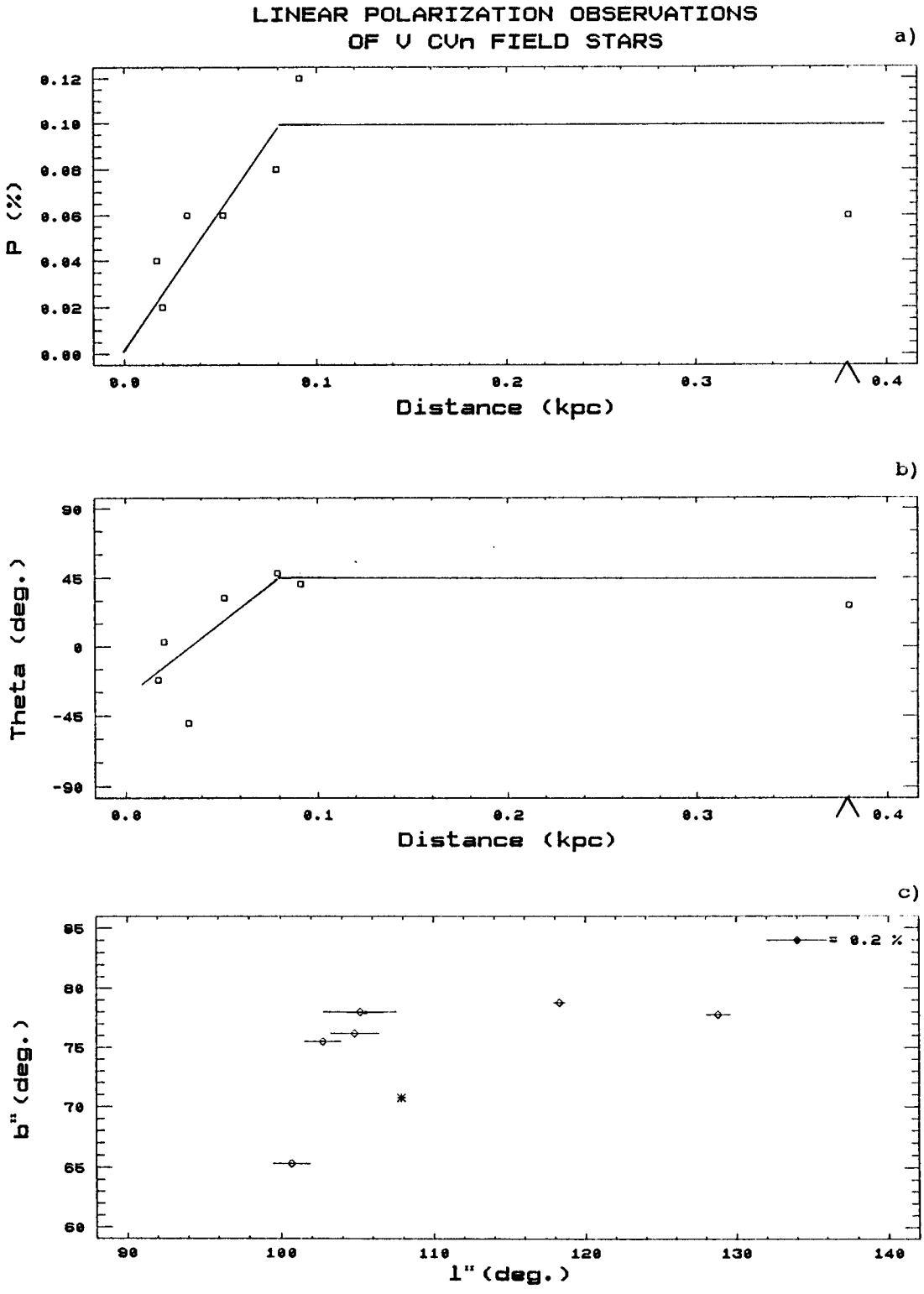
LINEAR POLARIZATION OBSERVATIONS
OF V CVn FIELD STARS
a)
P (%)
0.12
0.10
0.08
0.06
0.04
0.02
0.00
0.0
0.1
0.2
0.3
0.4
Distance (kpc)
b)
Theta (deg.)
90
45
0
-45
-90
0.0
0.1
0.2
0.3
0.4
Distance (kpc)
c)
= 0.2 %
b" (deg.)
85
80
75
70
65
60
90
100
110
120
130
140
l" (deg.)

Figure 3.7

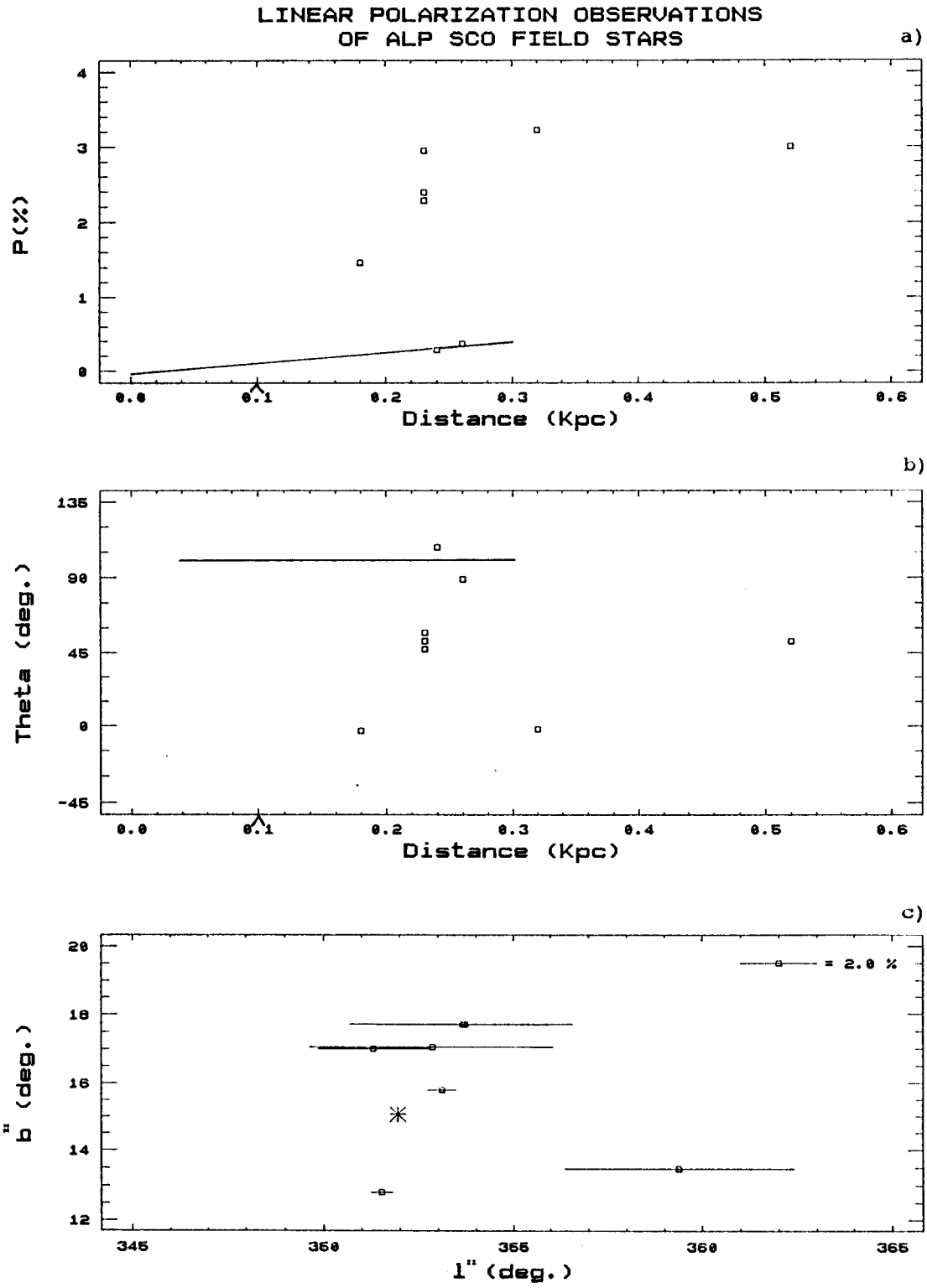
LINEAR POLARIZATION OBSERVATIONS
OF ALP SCO FIELD STARS
a)
P(%)
Distance (Kpc)
b)
Theta (deg.)
Distance (Kpc)
c)
= 2.0 %
b" (deg.)
l" (deg.)

Figure 3.7 (cont.)

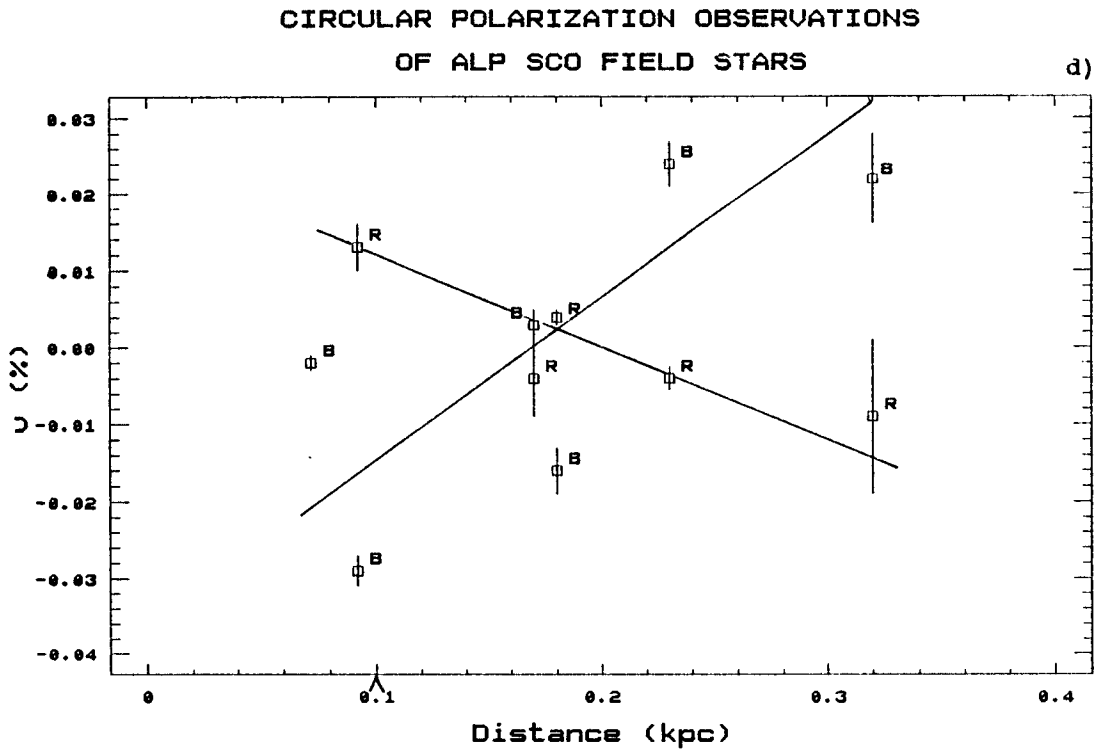

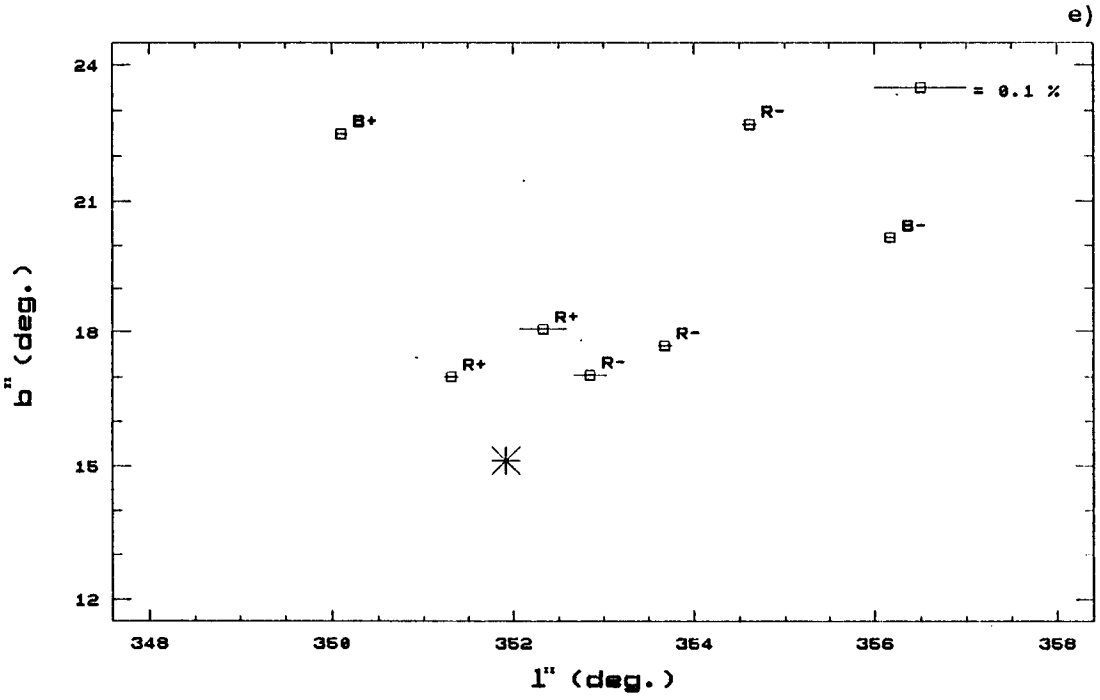

Figure 3.8

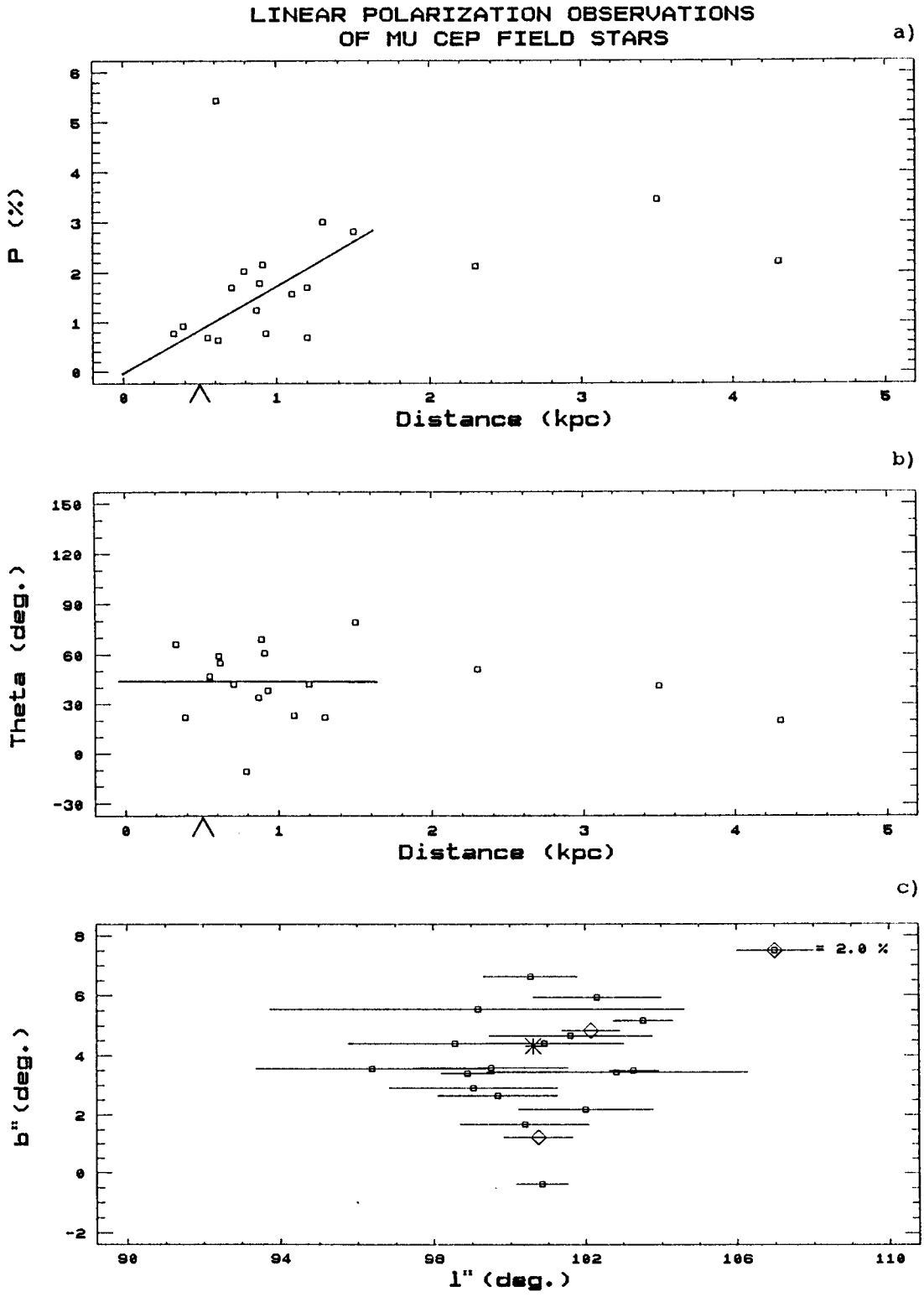
LINEAR POLARIZATION OBSERVATIONS
OF MU CEP FIELD STARS
a)
P (%)
Distance (kpc)
b)
Theta (deg.)
Distance (kpc)
c)
= 2.0 %
b" (deg.)
l" (deg.)

Figure 3.8 (cont.)

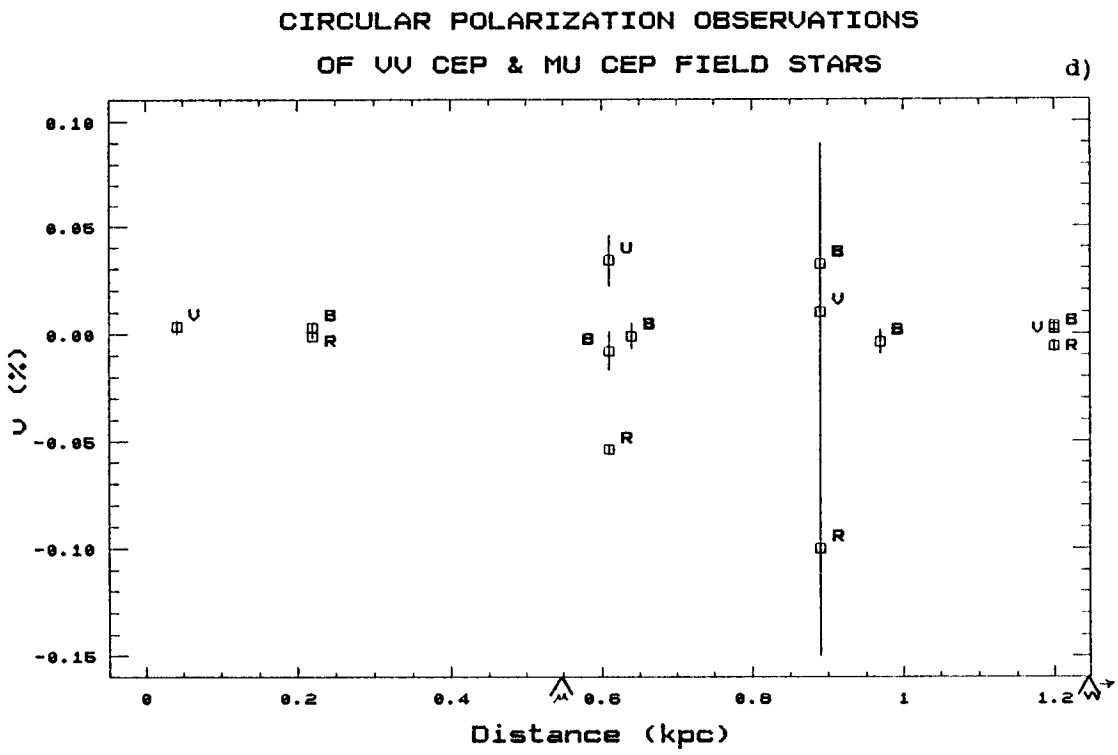

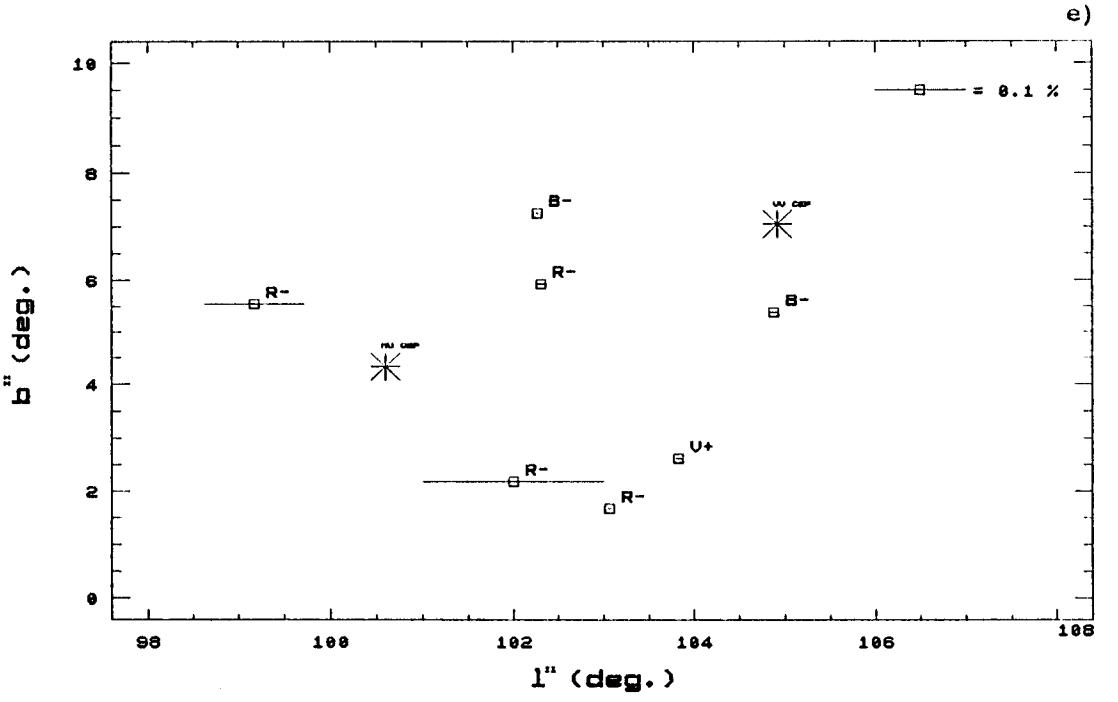

Figure 3.9

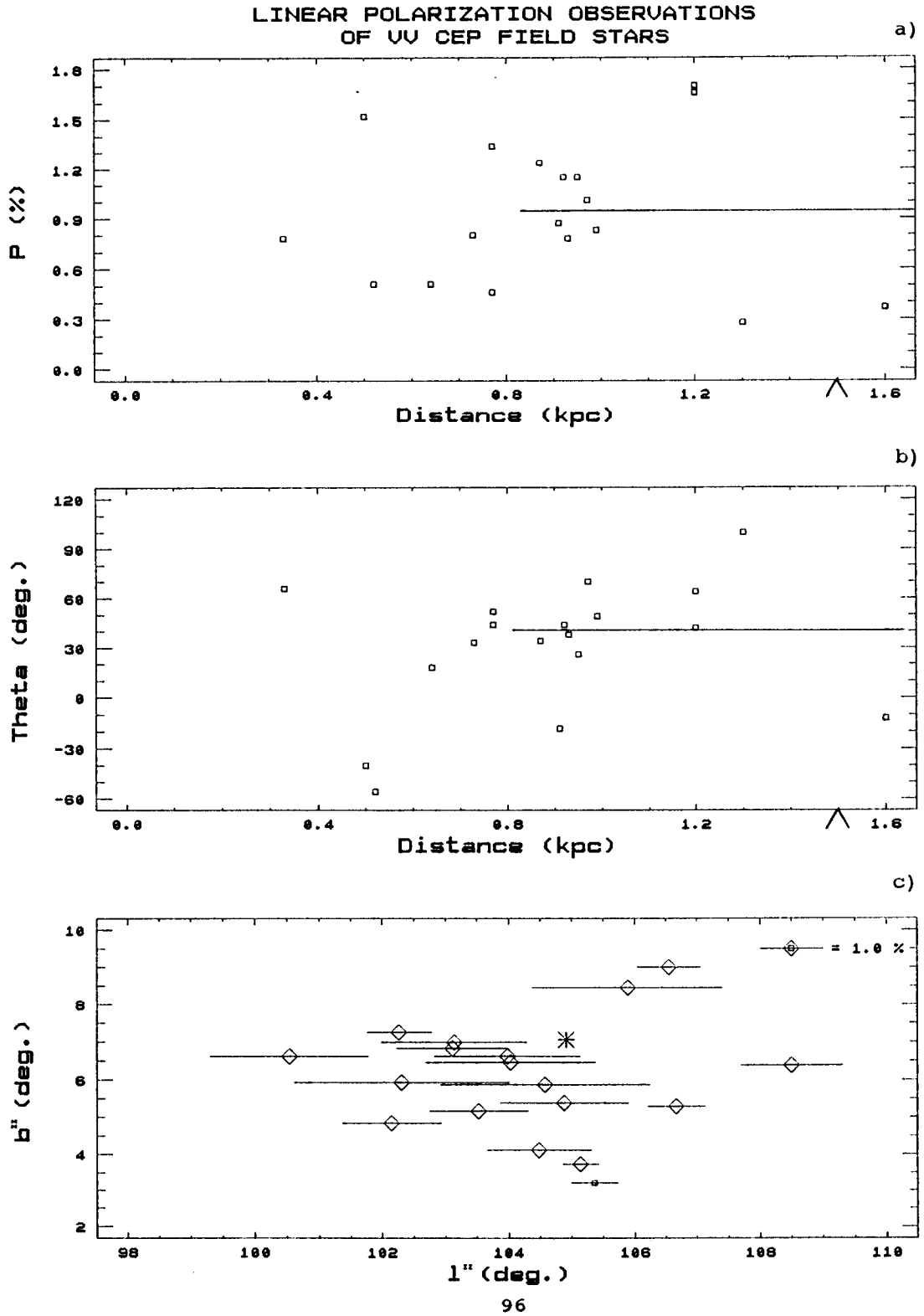
LINEAR POLARIZATION OBSERVATIONS
OF VV CEP FIELD STARS
a)
P (%)
1.8
1.5
1.2
0.9
0.6
0.3
0.0
0.0
0.4
0.8
1.2
1.6
Distance (kpc)
b)
Theta (deg.)
120
90
60
30
0
-30
-60
0.0
0.4
0.8
1.2
1.6
Distance (kpc)
c)
= 1.0 %
b" (deg.)
10
8
6
4
2
98
100
102
104
106
108
110
l" (deg.)

Figure 3.10

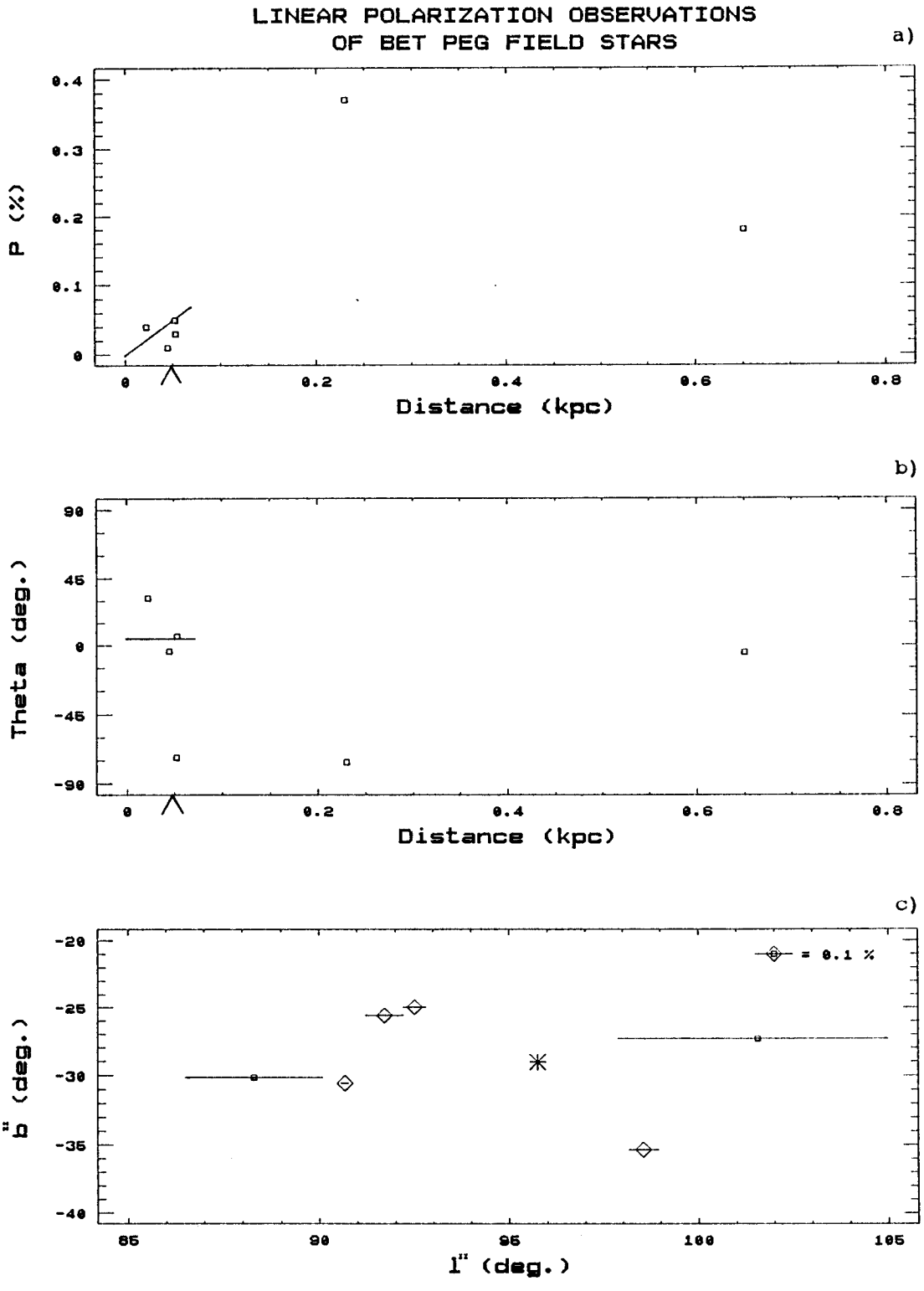
LINEAR POLARIZATION OBSERVATIONS
OF BET PEG FIELD STARS
a)
P (%)
0.4
0.3
0.2
0.1
0
0
0.2
0.4
0.6
0.8
Distance (kpc)
b)
Theta (deg.)
90
45
0
-45
-90
0
0.2
0.4
0.6
0.8
Distance (kpc)
c)
= 0.1 %
b" (deg.)
-20
-25
-30
-35
-40
85
90
95
100
105
l" (deg.)

Figure 3.11

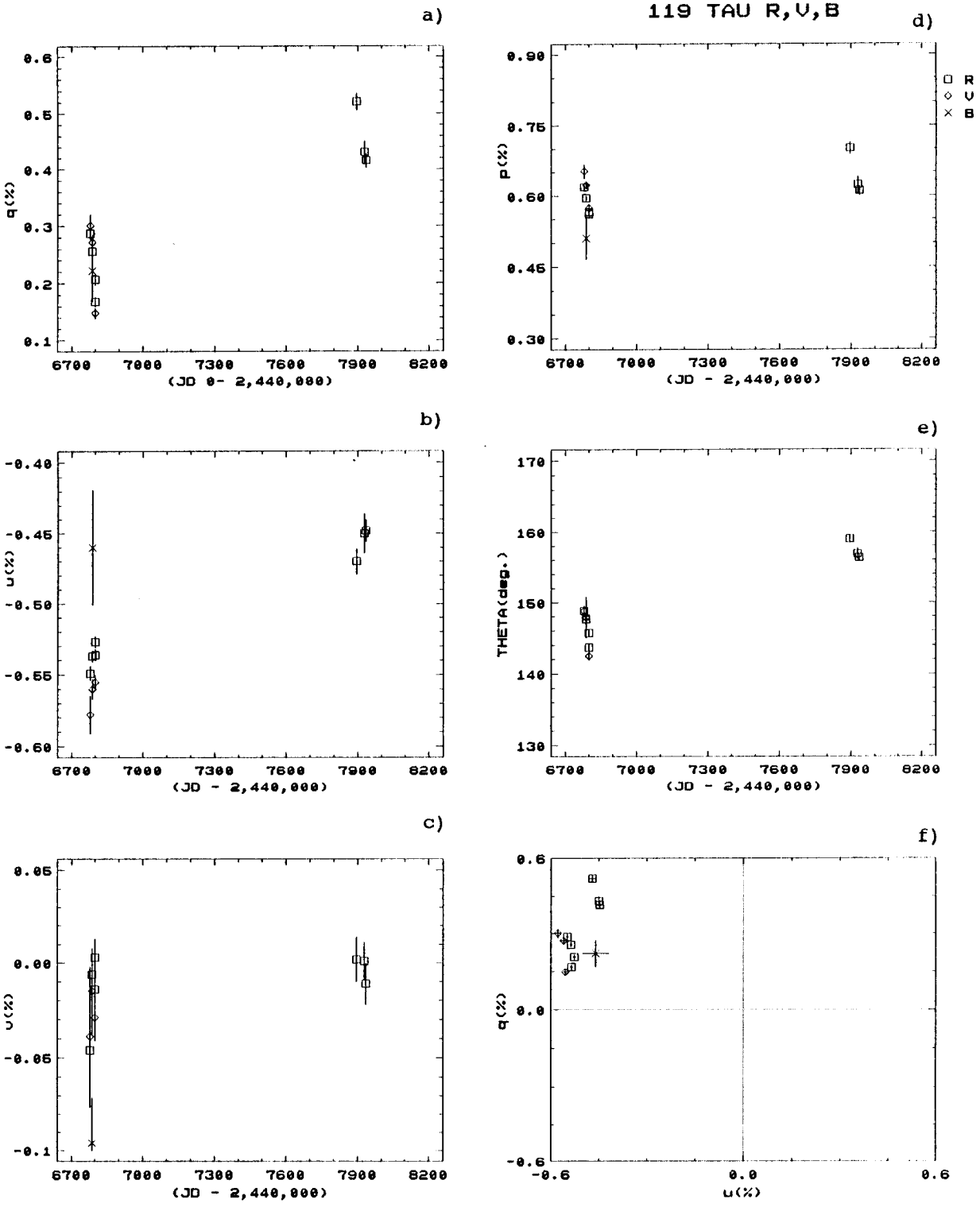

Figure 3.12

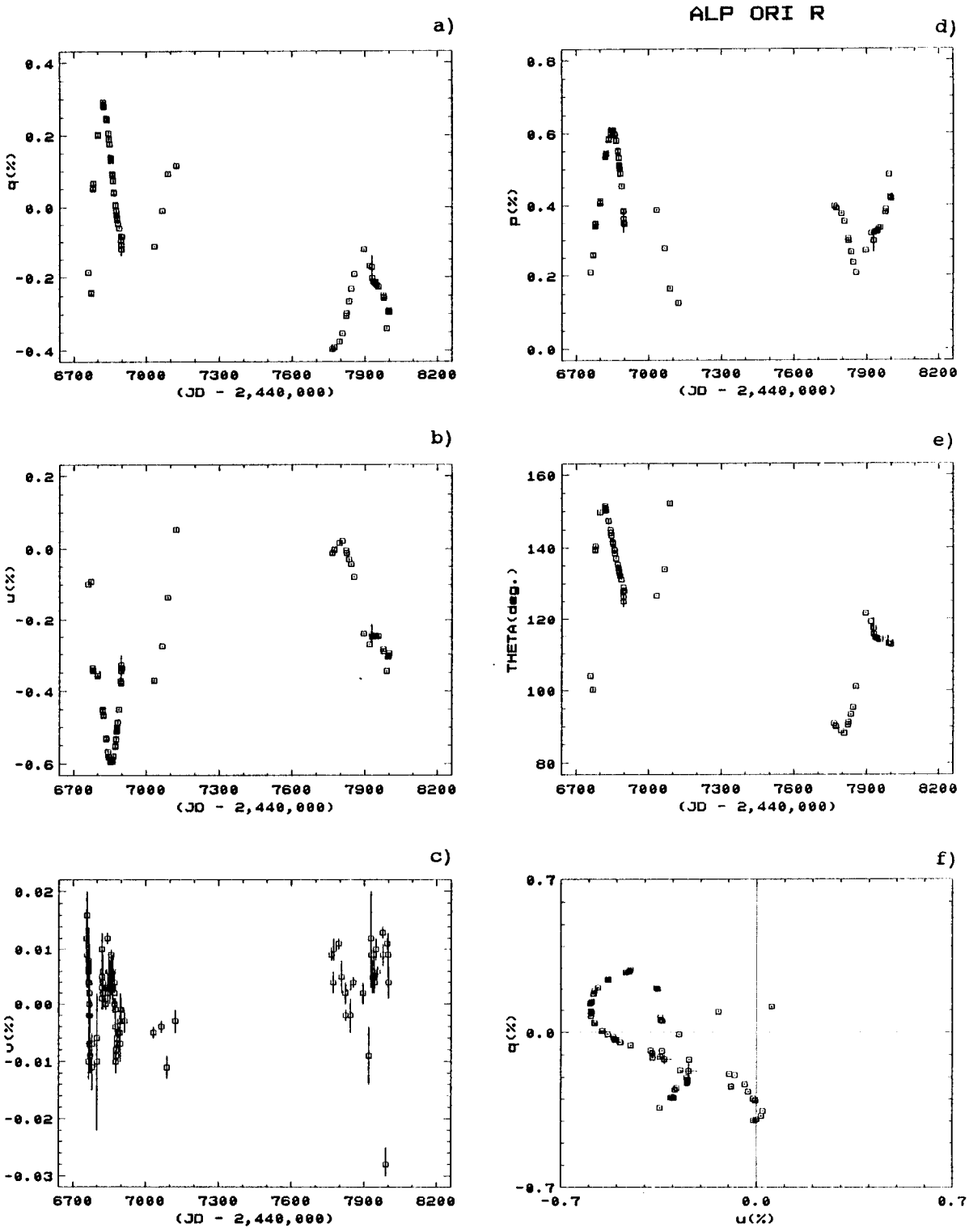
ALP ORI R
a)
b)
c)
d)
e)
f)
q(%)
u(%)
U(%)
p(%)
THETA(deg.)
(JD - 2,440,000)
6700
7000
7300
7600
7900
8200

Figure 3.12 (cont.)

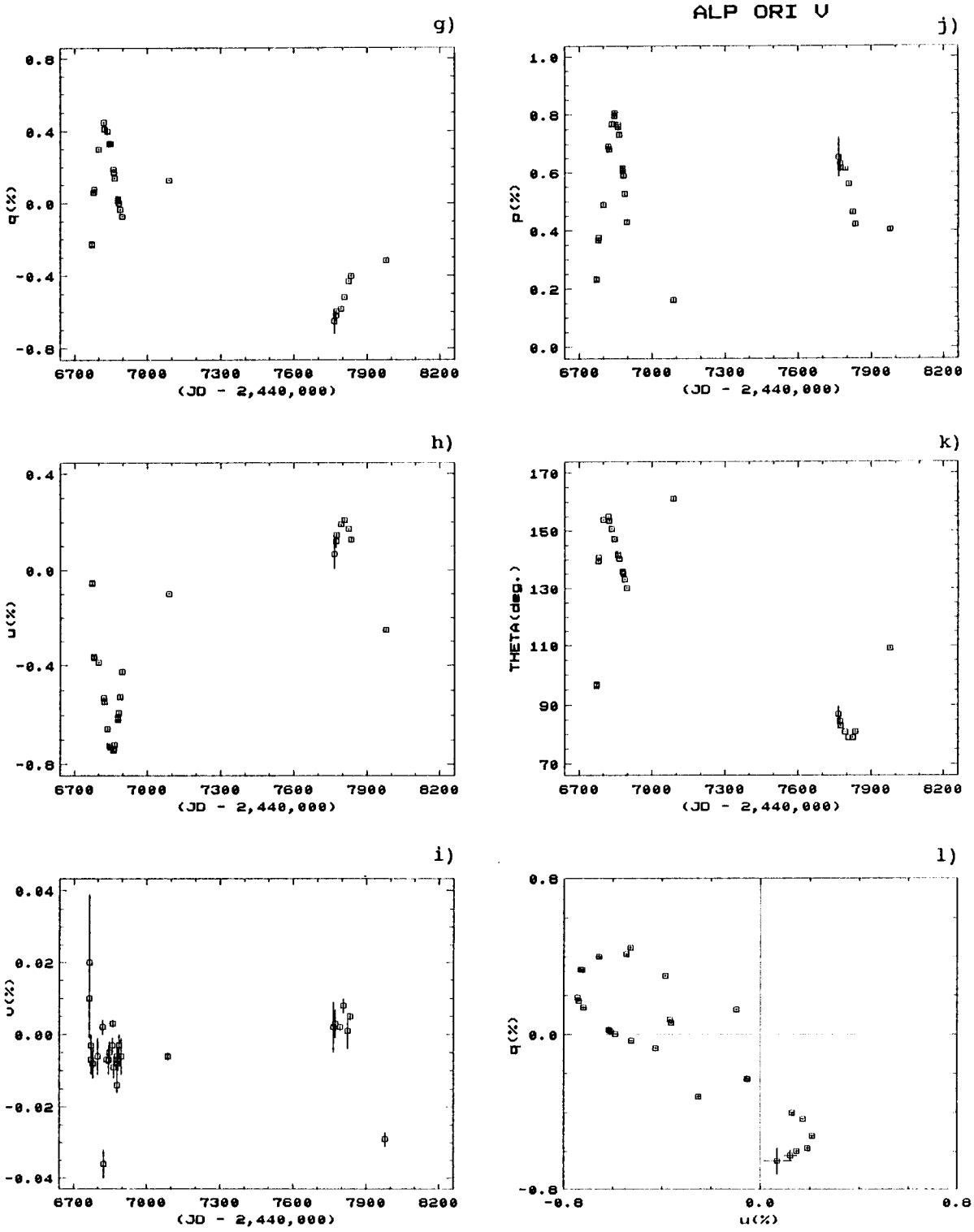

Figure 3.12 (cont.)

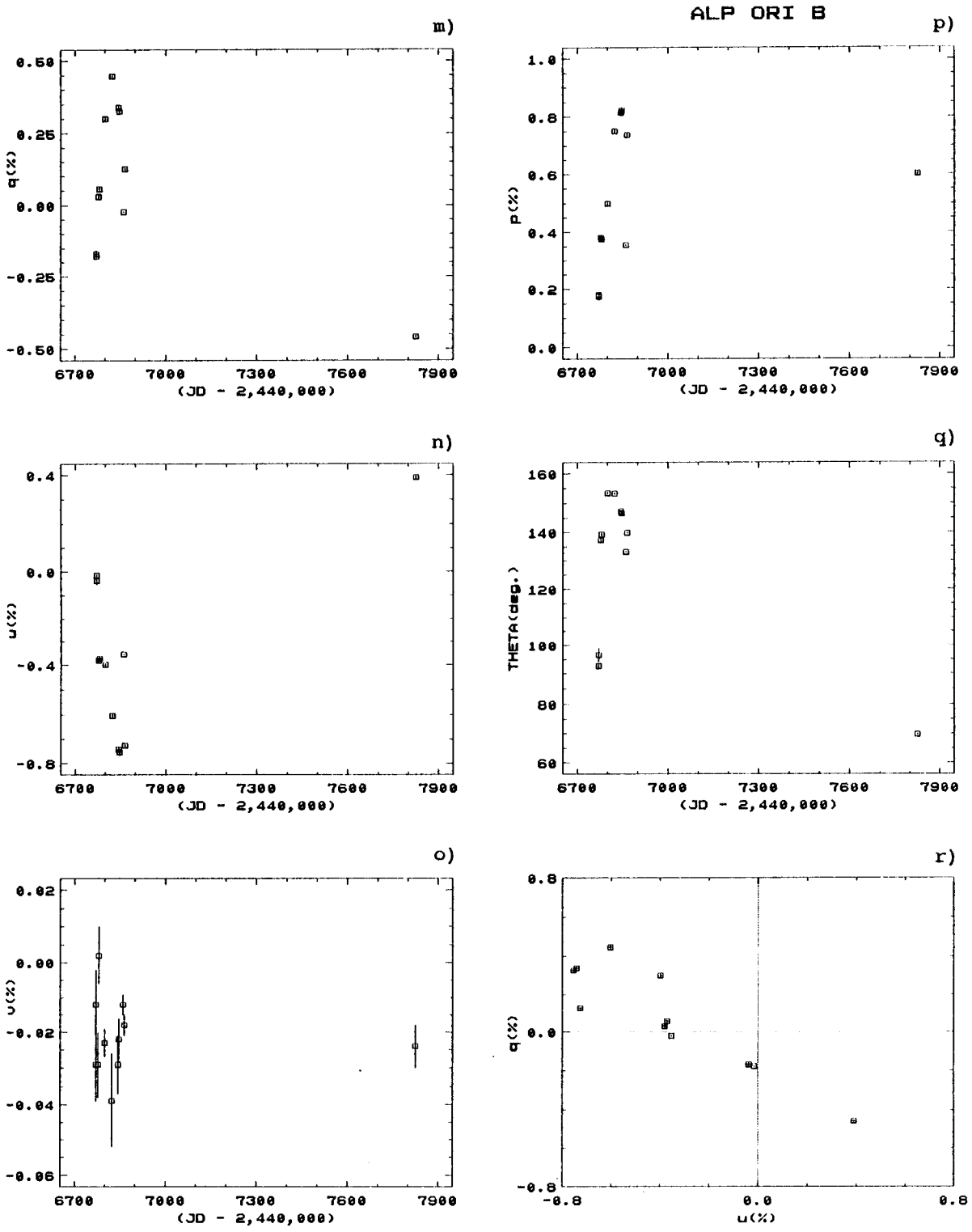

Figure 3.12 (cont.)

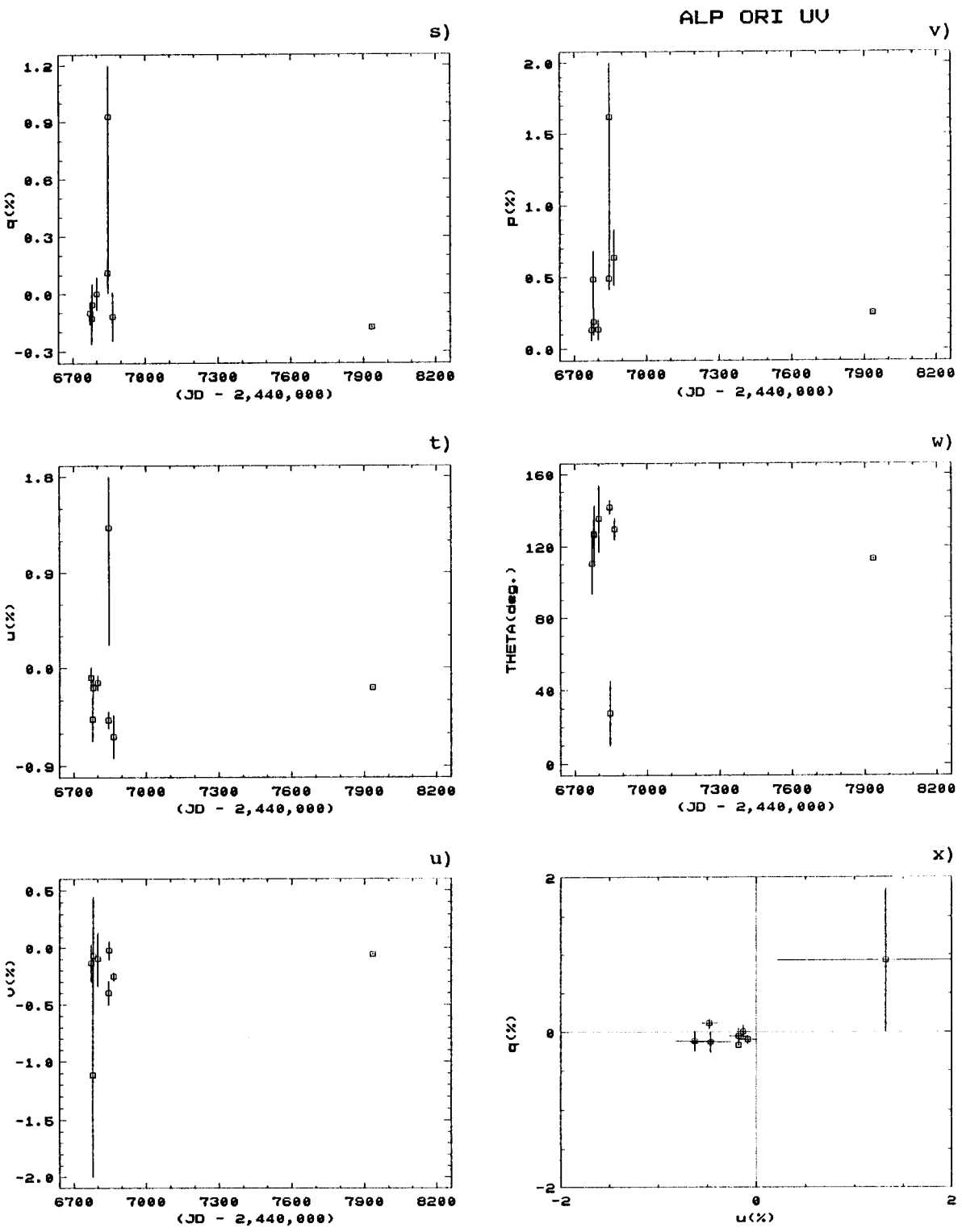

Figure 3.13

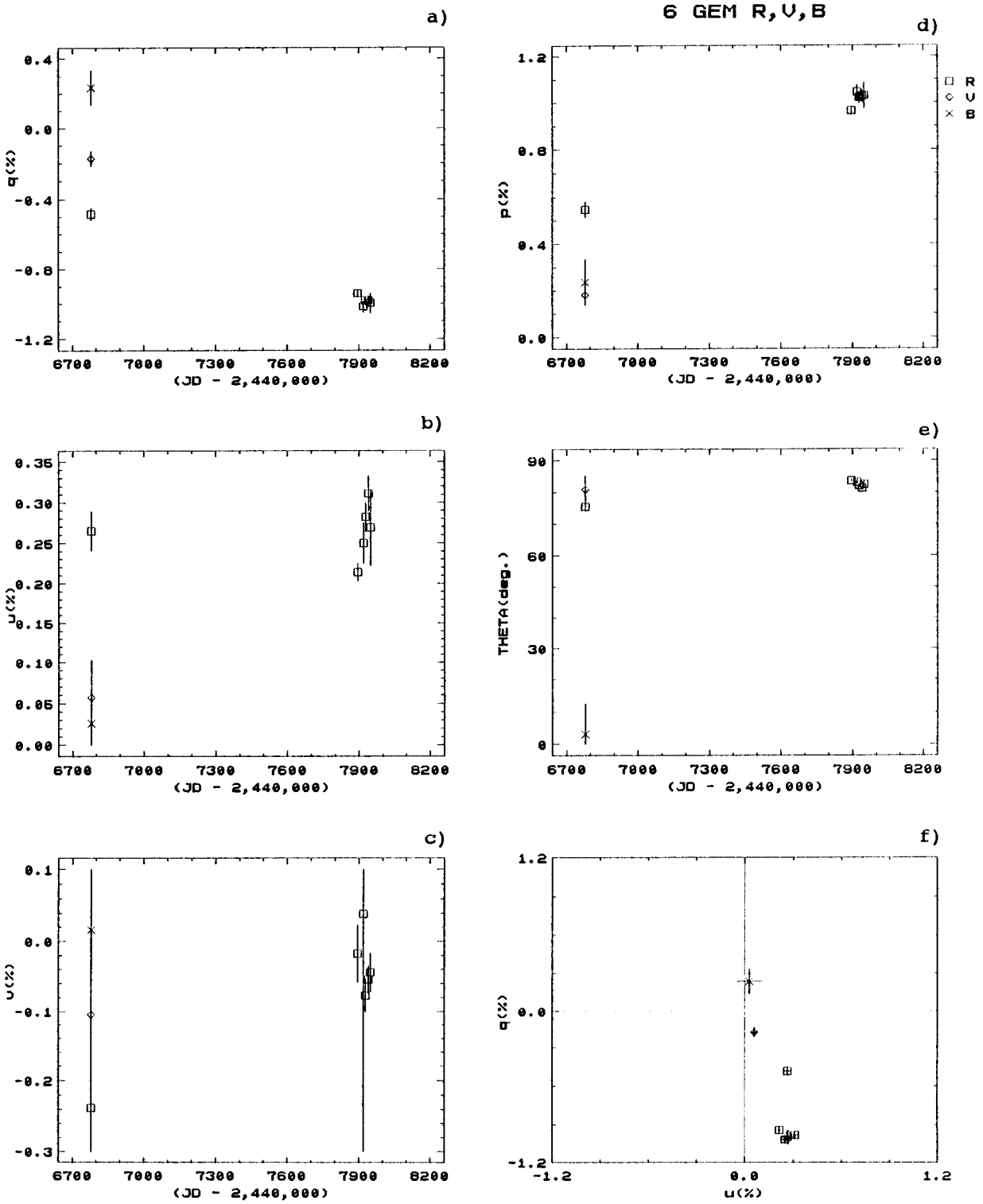

Figure 3.14

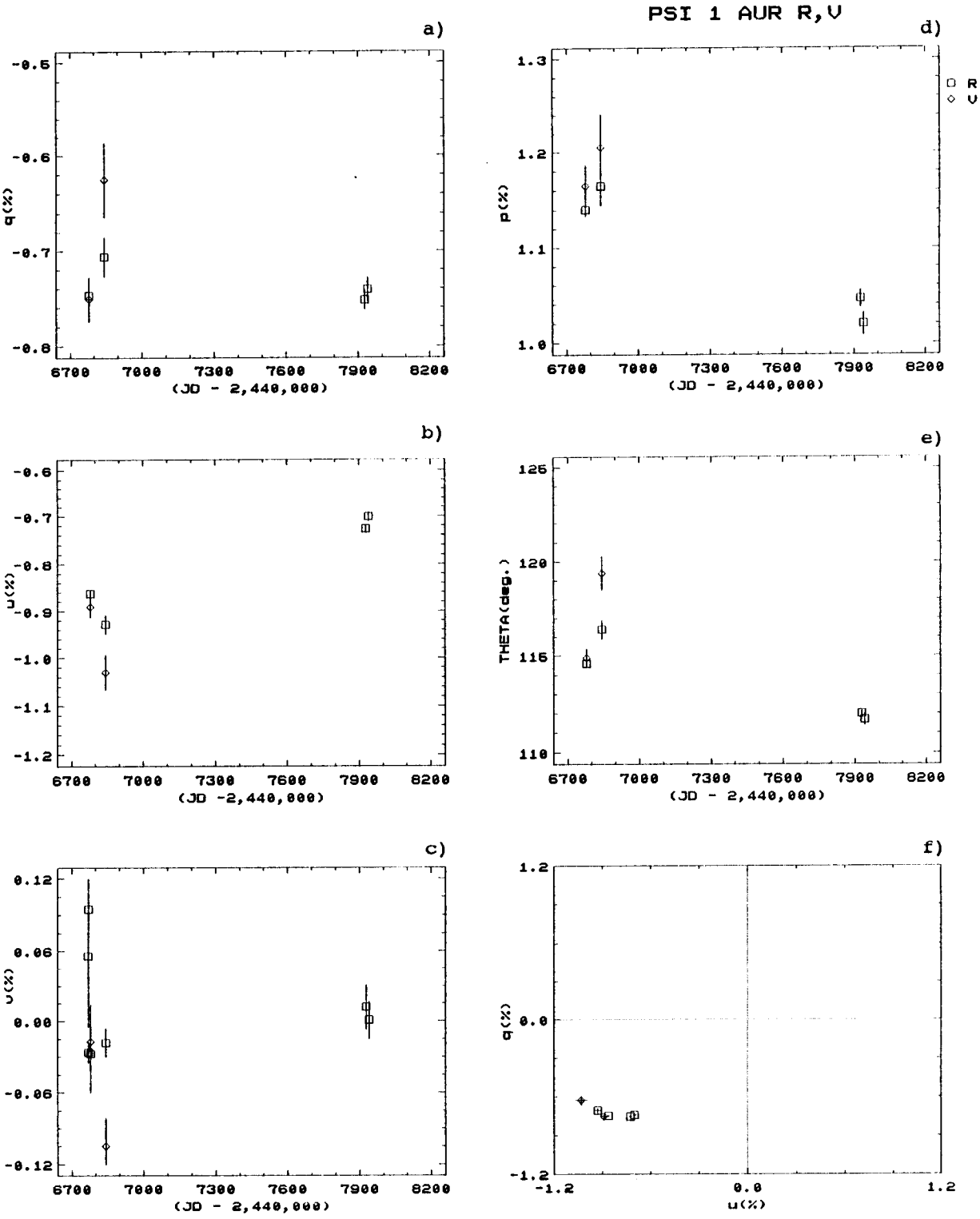

Figure 3.15

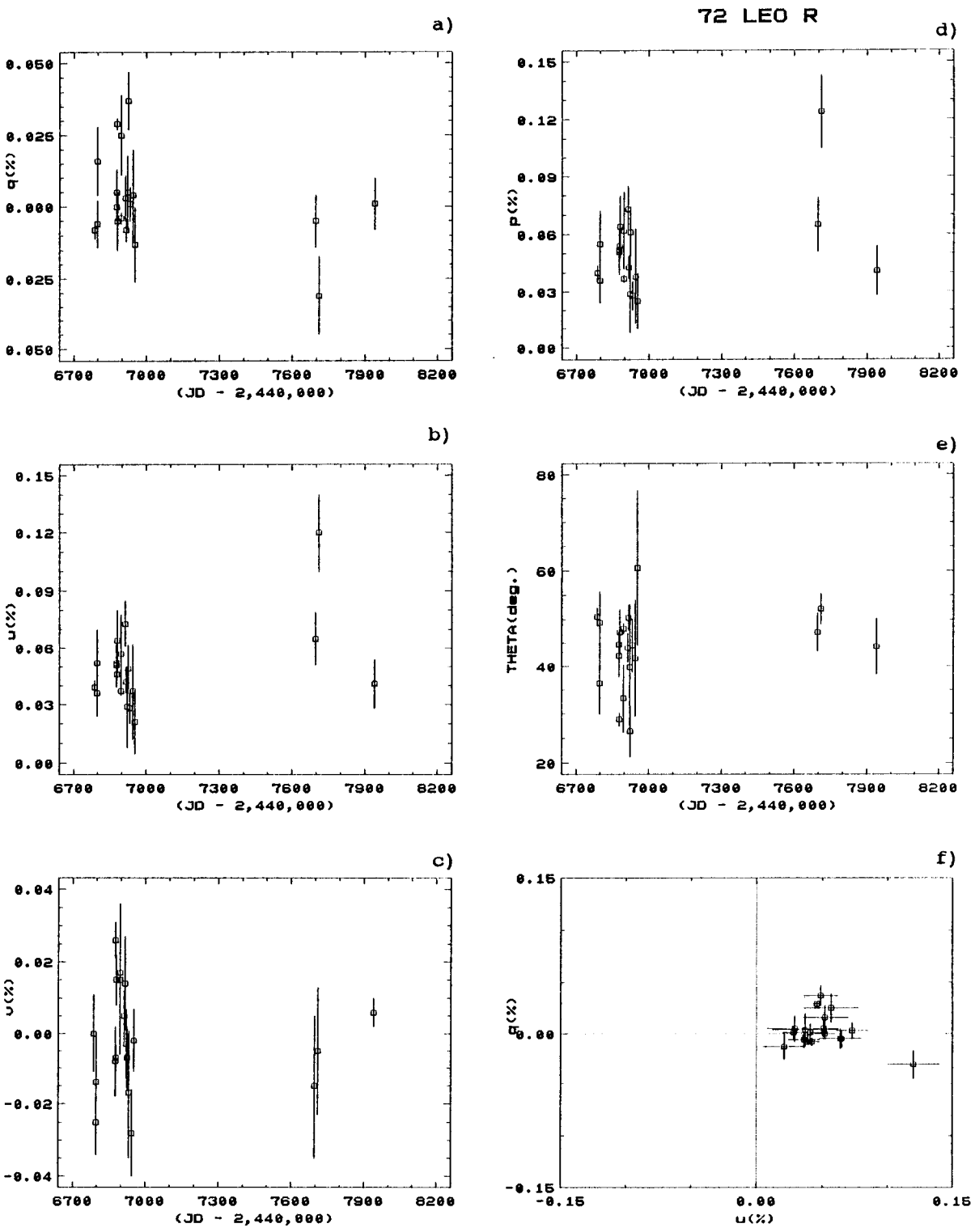
72 LEO R
a)
b)
c)
d)
e)
f)
q(%)
u(%)
v(%)
p(%)
THETA(deg.)
(JD - 2,440,000)
6700
7000
7300
7600
7900
8200
0.050
0.025
0.000
0.025
0.050
0.15
0.12
0.09
0.06
0.03
0.00
-0.04
-0.02
0.02
0.04
80
60
40
20
-0.15
0.00
0.15

Figure 3.15 (cont.)

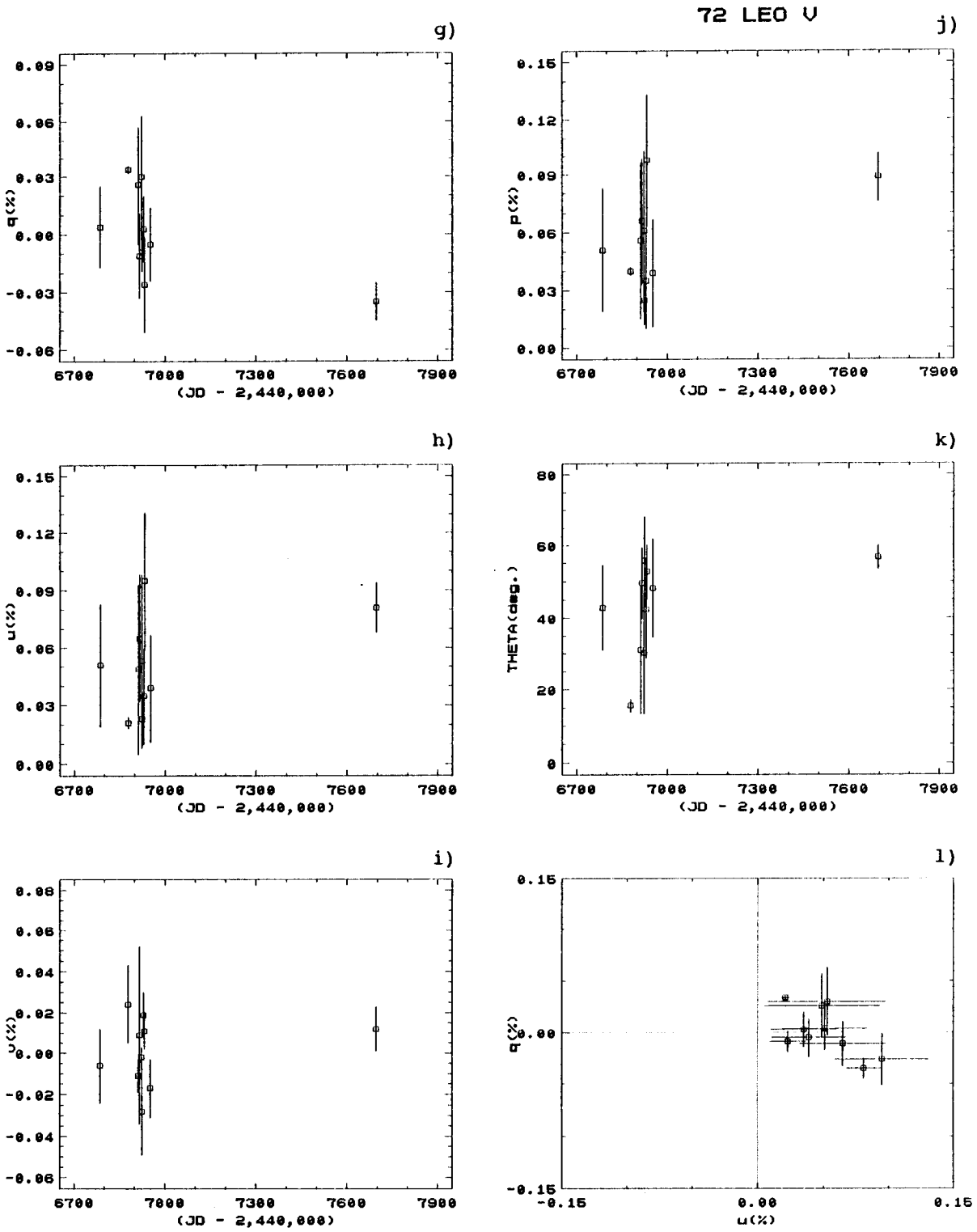

Figure 3.15 (cont.)

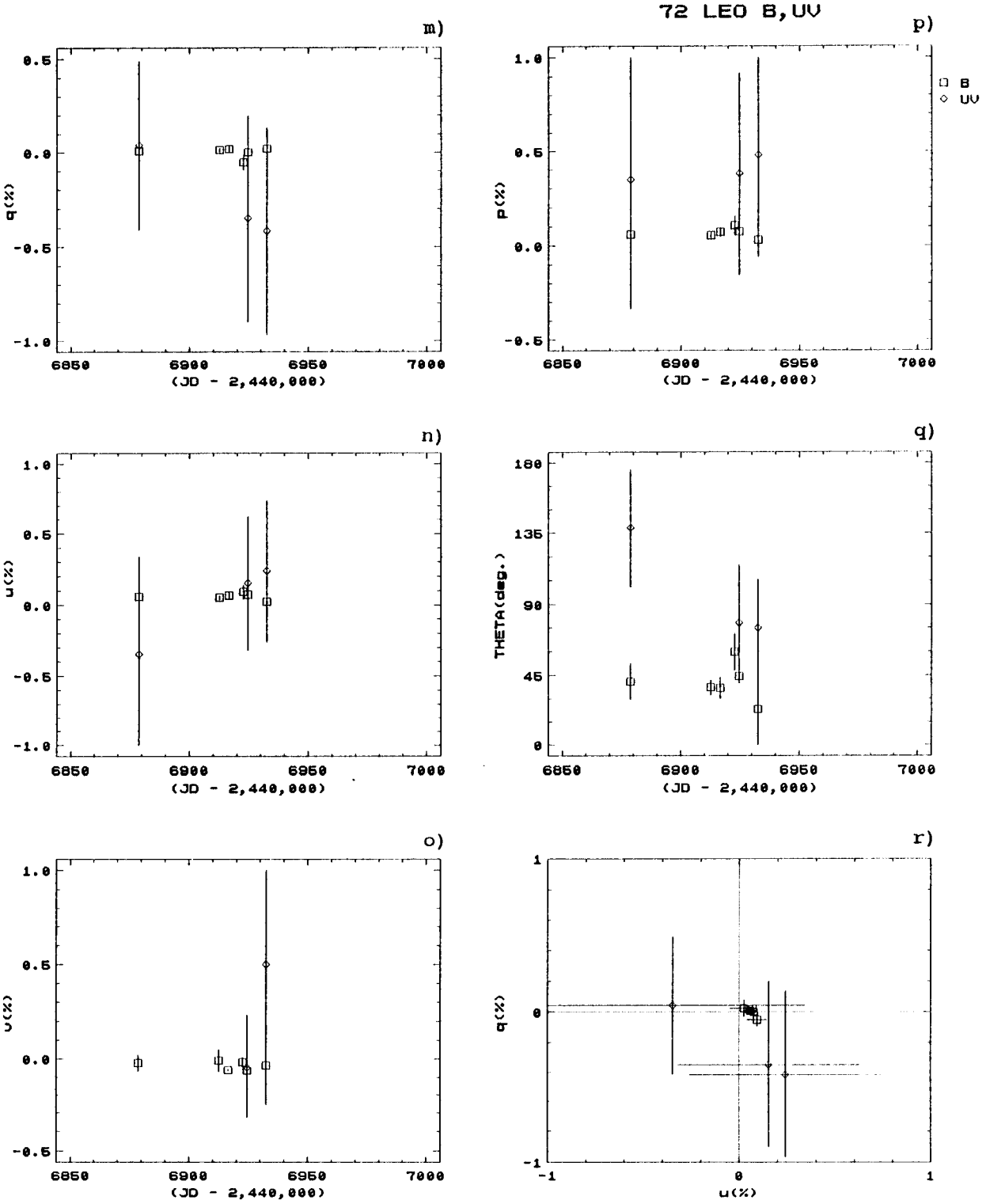

Figure 3.16

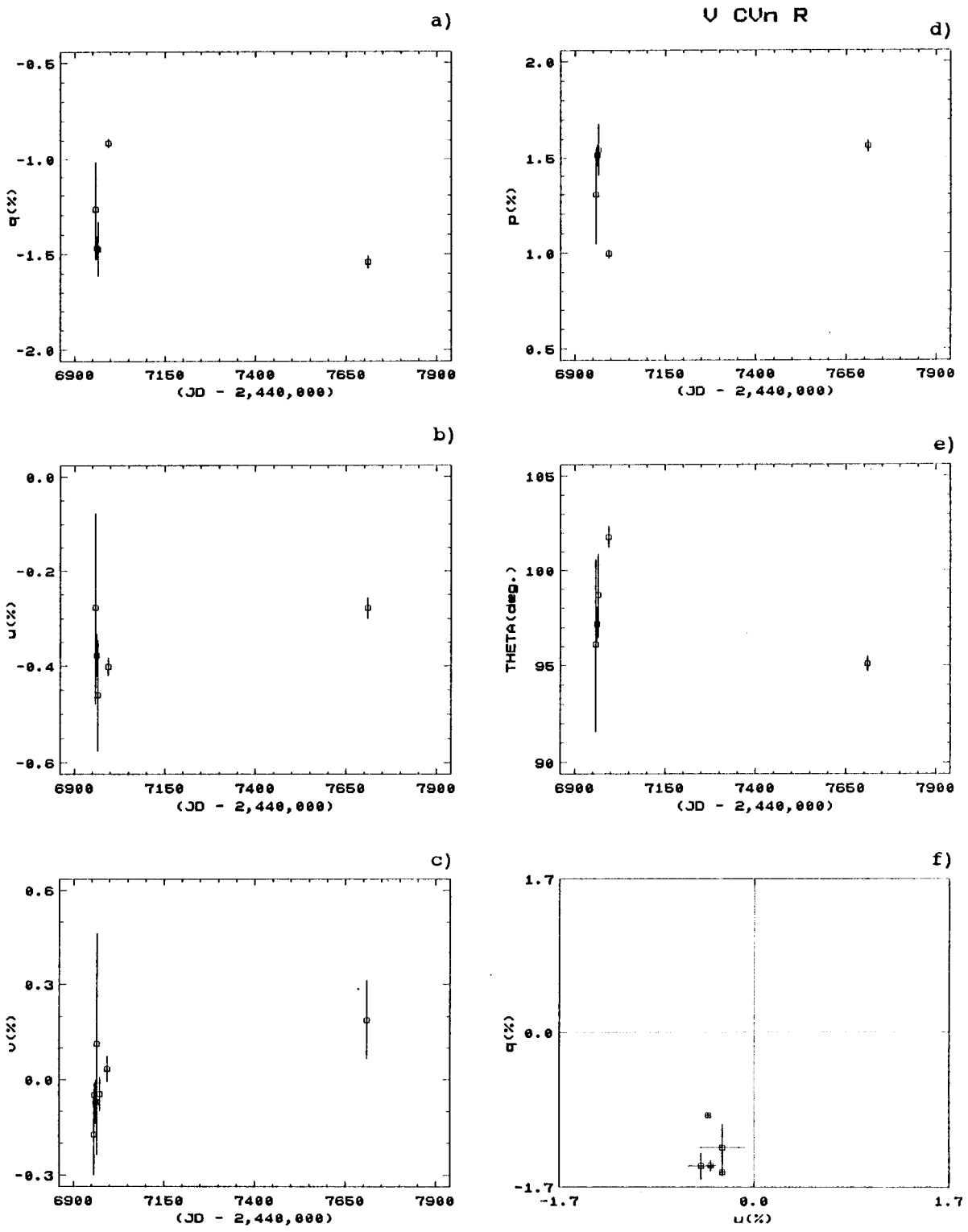
V CVn R
a)
b)
c)
d)
e)
f)
q(%)
u(%)
v(%)
p(%)
THETA(deg.)
(JD - 2,440,000)
6900
7150
7400
7650
7900
-0.5
-1.0
-1.5
-2.0
0.0
-0.2
-0.4
-0.6
0.6
0.3
-0.3
2.0
1.5
1.0
0.5
105
100
95
90
1.7
-1.7

Figure 3.16 (cont.)

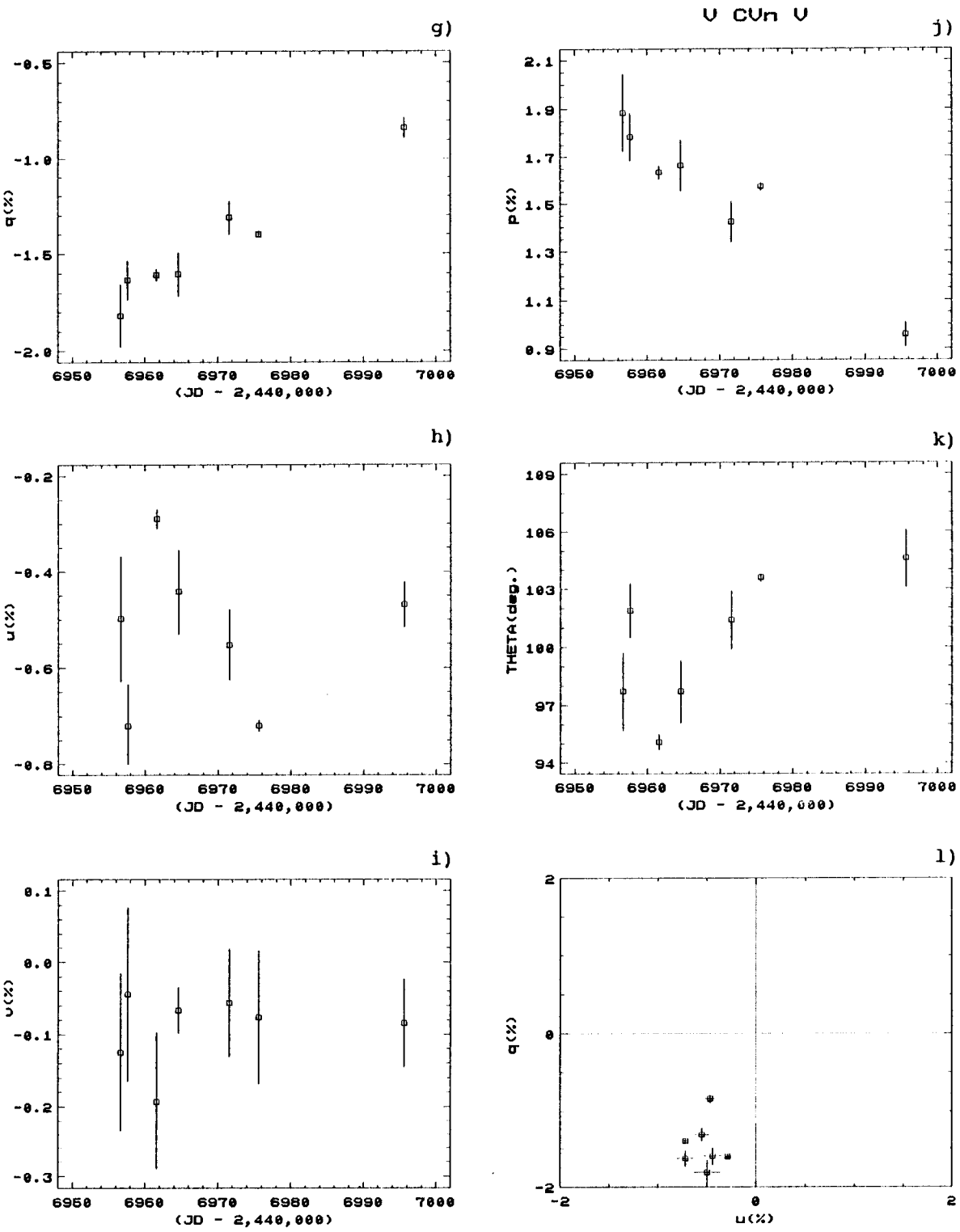

Figure 3.16 (cont.)

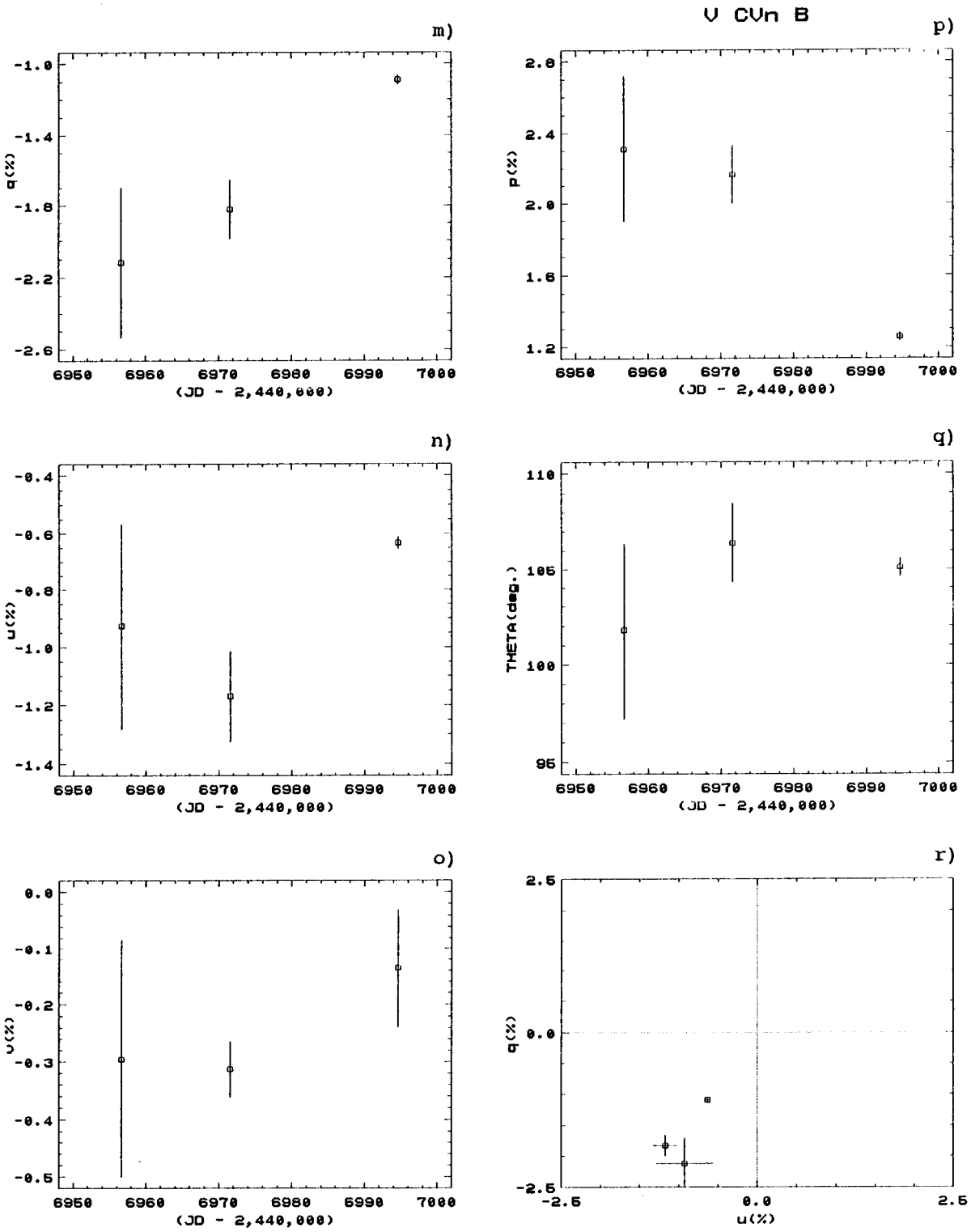

Figure 3.17

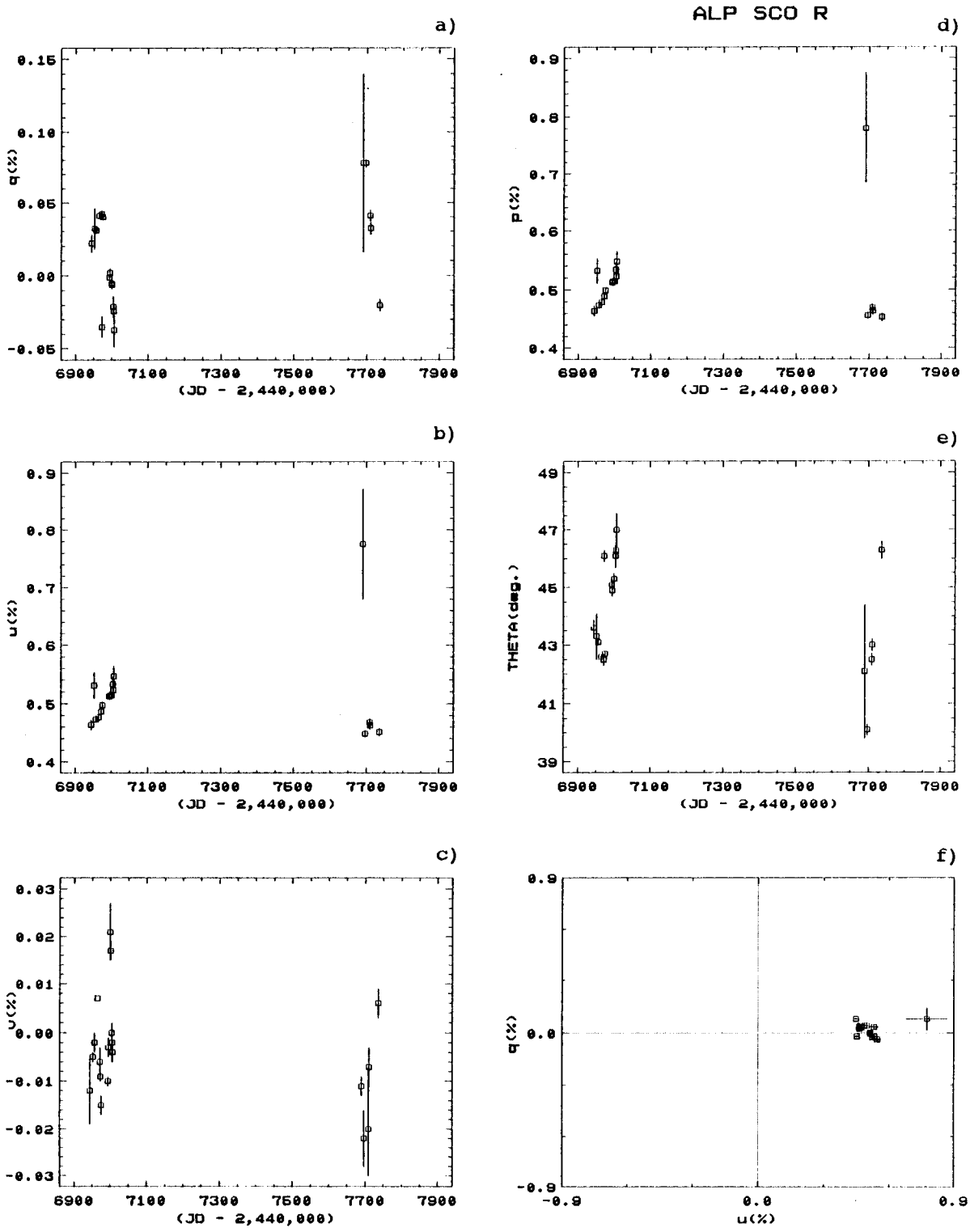
ALP SCO R
a)
b)
c)
d)
e)
f)
q(%)
u(%)
U(%)
p(%)
THETA(deg.)
(JD - 2,440,000)
6900
7100
7300
7500
7700
7900

Figure 3.17 (cont.)

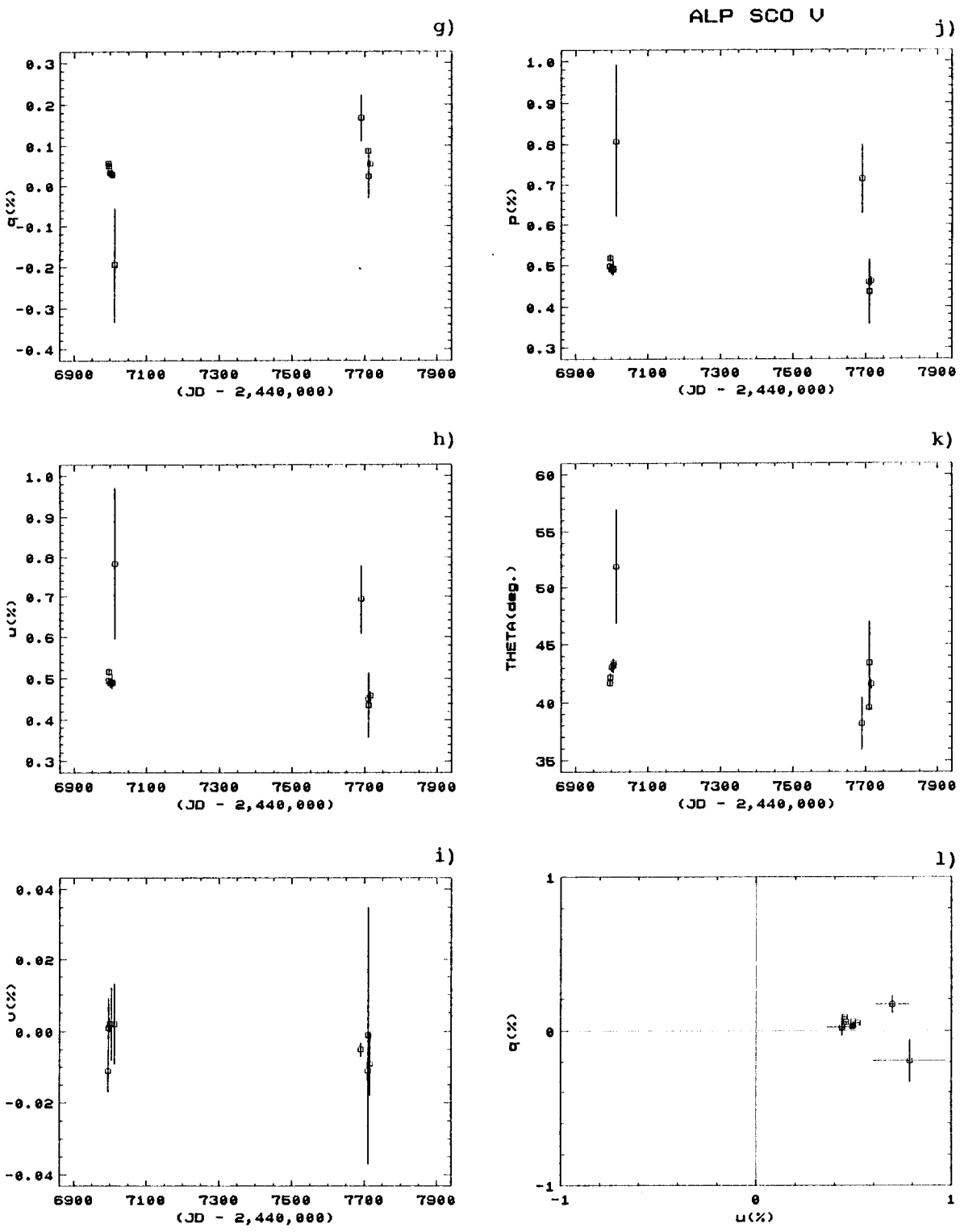

Figure 3.17 (cont.)

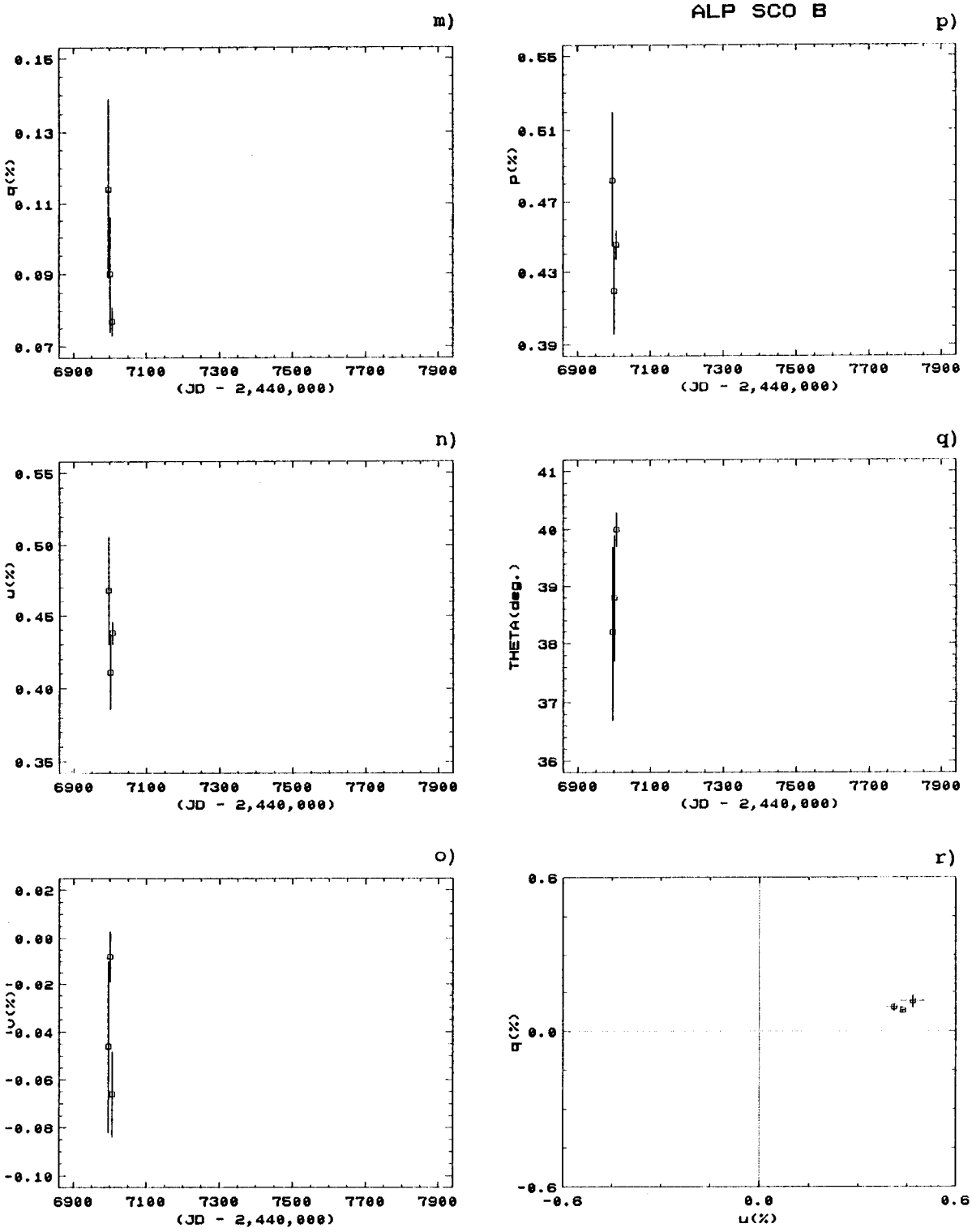

Figure 3.18

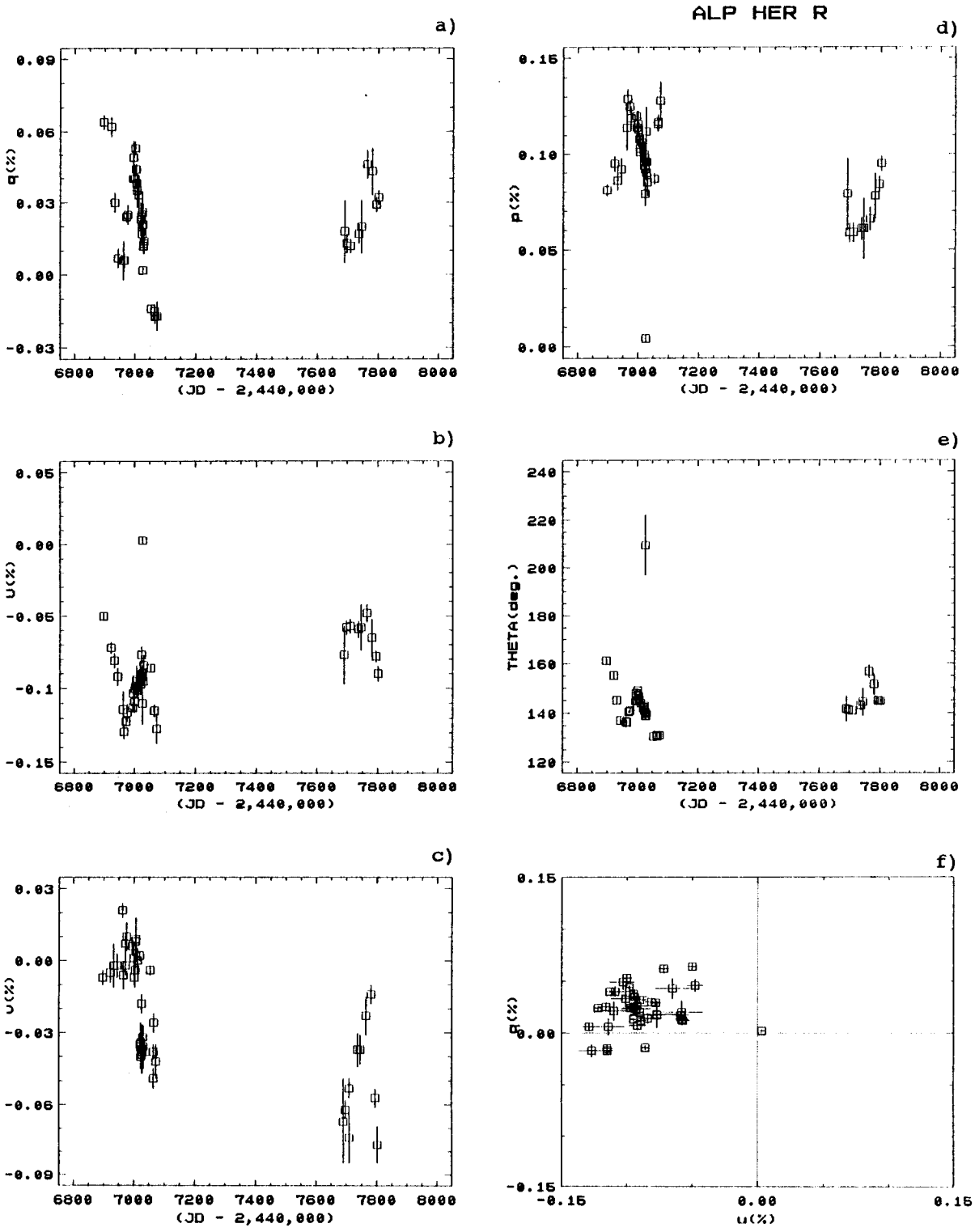
ALP HER R
a)
b)
c)
d)
e)
f)
q(%)
u(%)
v(%)
p(%)
THETA(deg.)
(JD - 2,440,000)
6800
7000
7200
7400
7600
7800
8000
0.09
0.06
0.03
0.00
-0.03
0.05
-0.05
-0.1
-0.15
-0.06
-0.09
0.15
0.10
240
220
200
180
160
140
120
q(%)
u(%)

Figure 3.18 (cont.)

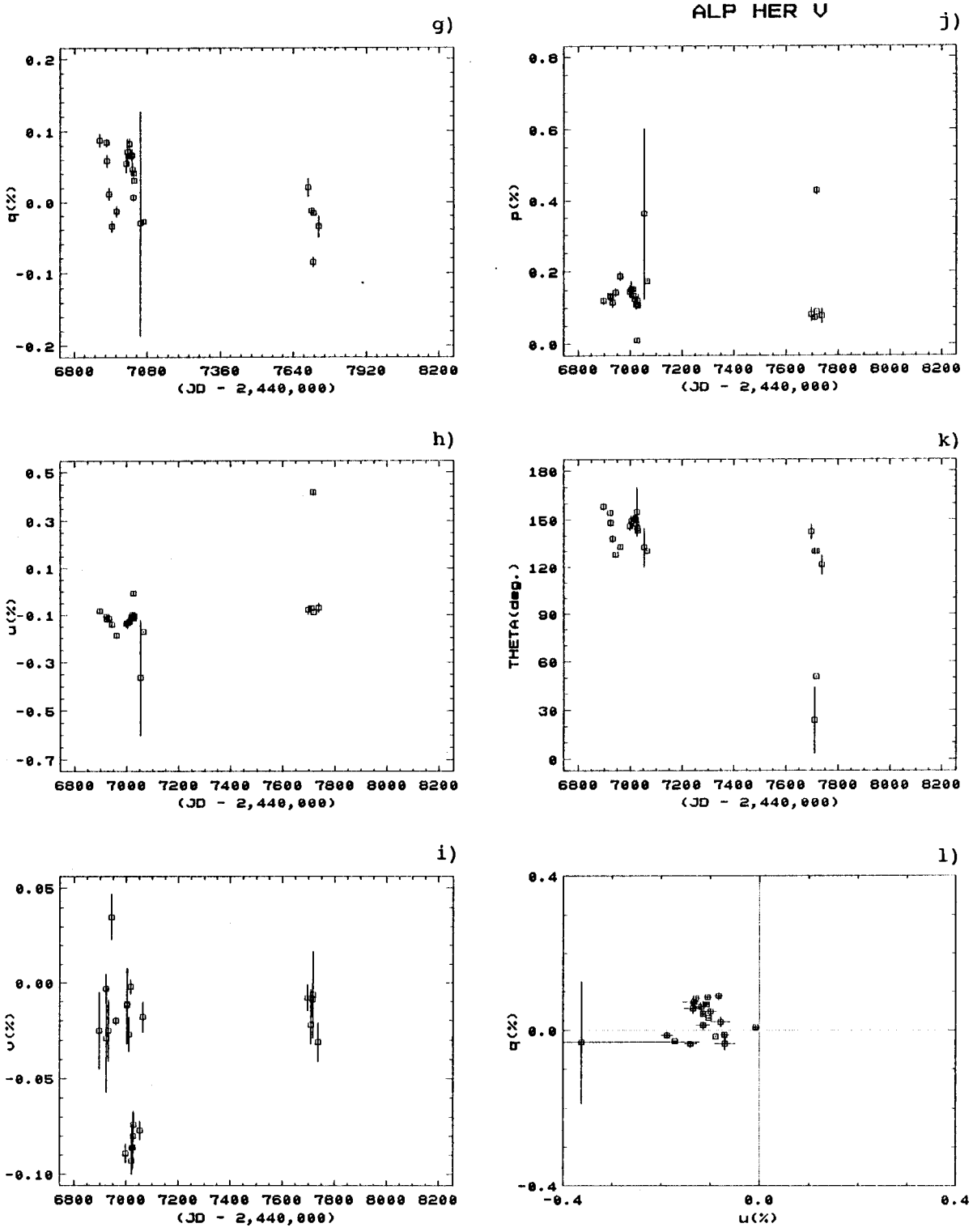

Figure 3.18 (cont.)

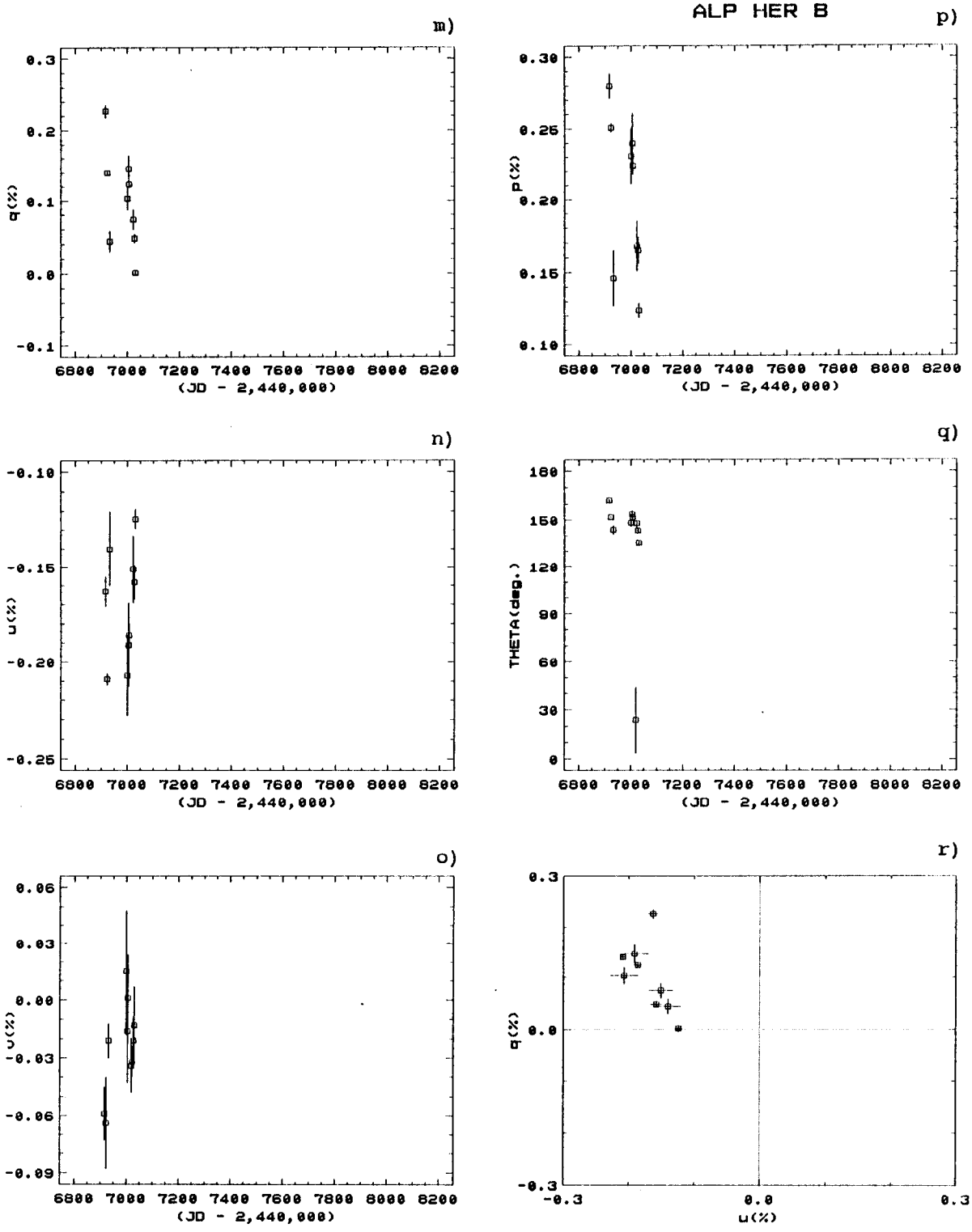

Figure 3.18 (cont.)

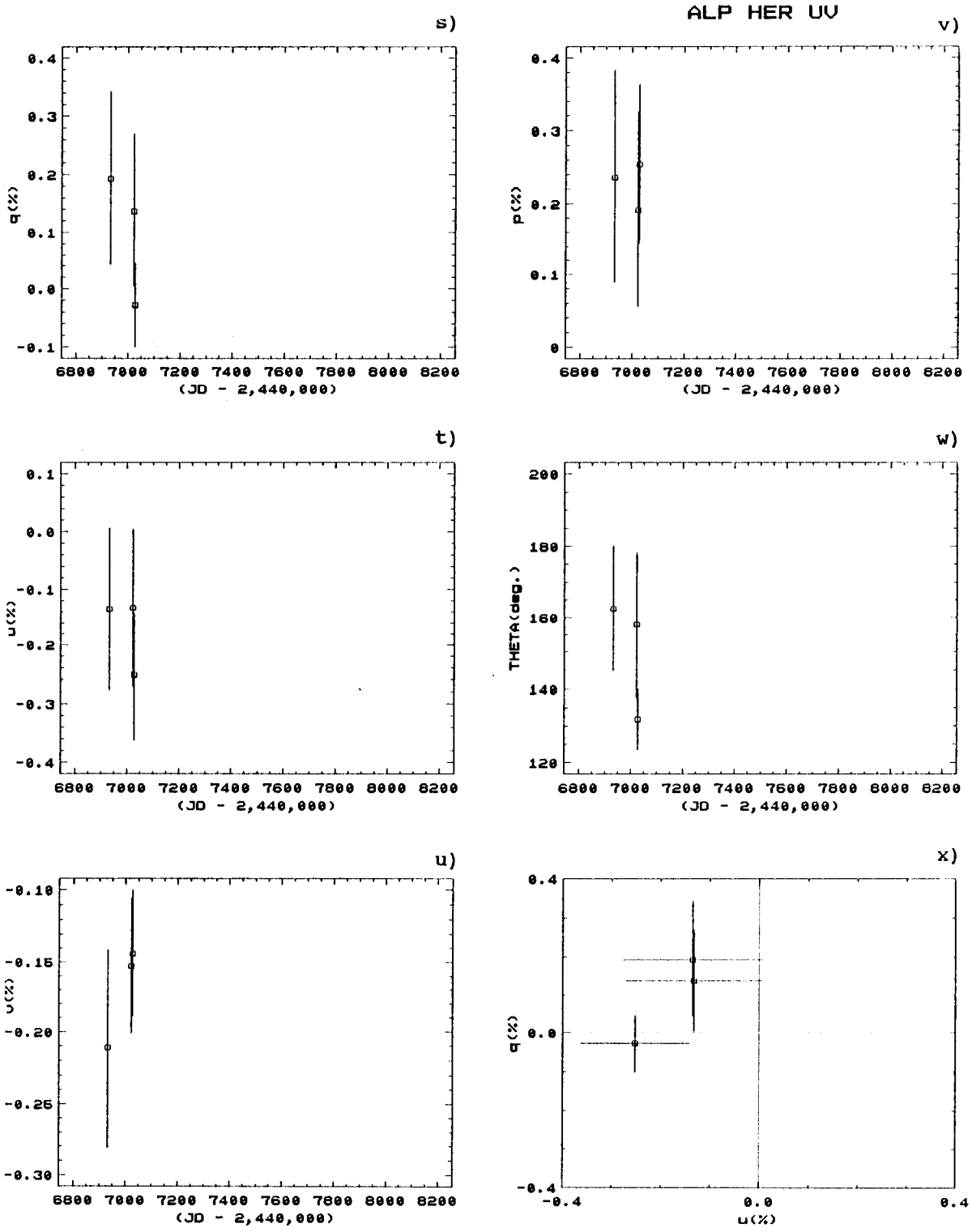

Figure 3.19

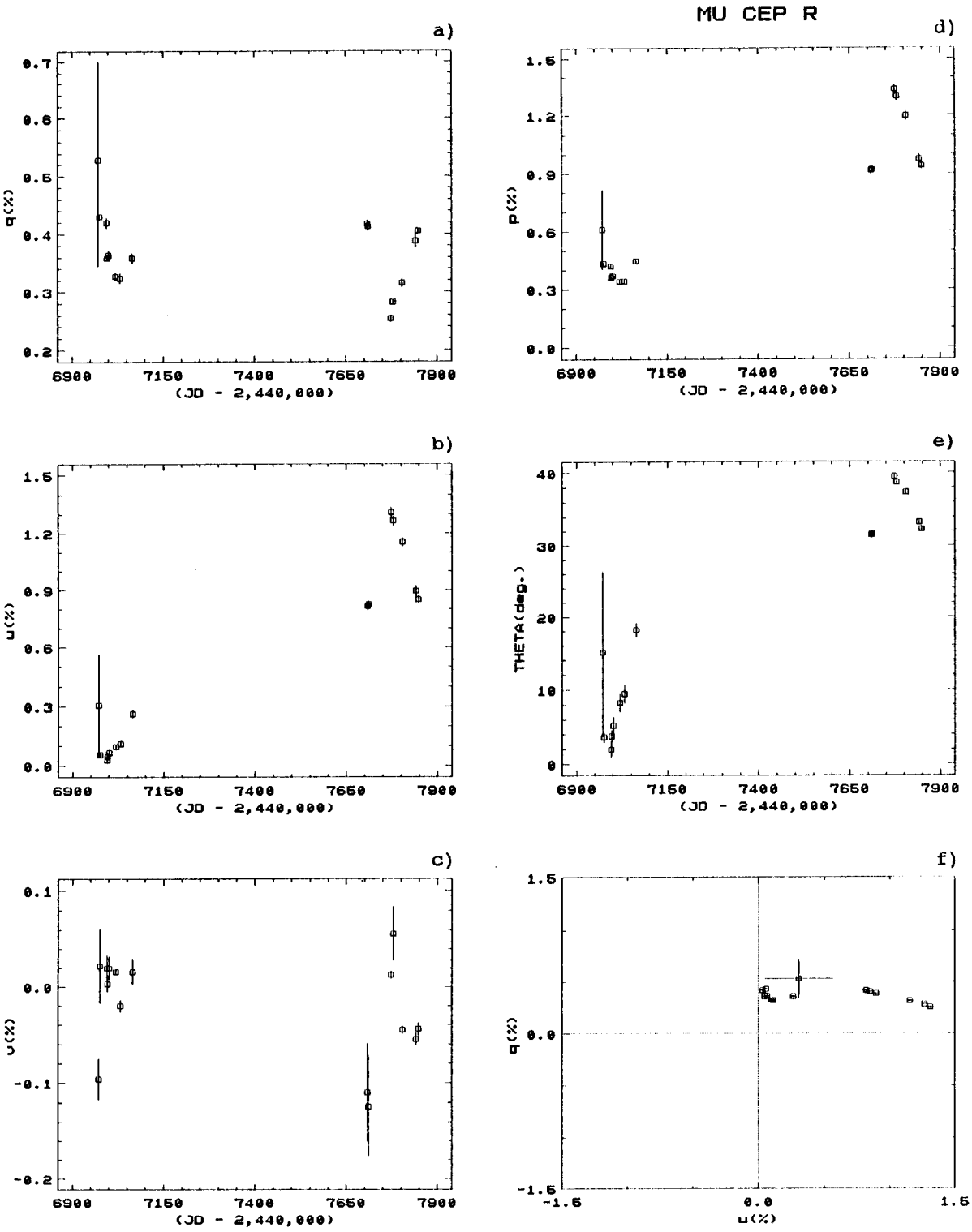
MU CEP R
a)
q(%)
0.7
0.6
0.5
0.4
0.3
0.2
6900
7150
7400
7650
7900
(JD - 2,440,000)
d)
p(%)
1.5
1.2
0.9
0.6
0.3
0.0
6900
7150
7400
7650
7900
(JD - 2,440,000)
b)
u(%)
1.5
1.2
0.9
0.6
0.3
0.0
6900
7150
7400
7650
7900
(JD - 2,440,000)
e)
THETA(deg.)
40
30
20
10
0
6900
7150
7400
7650
7900
(JD - 2,440,000)
c)
v(%)
0.1
0.0
-0.1
-0.2
6900
7150
7400
7650
7900
(JD - 2,440,000)
f)
q(%)
1.5
0.0
-1.5
-1.5
0.0
1.5
u(%)

Figure 3.19 (cont.)

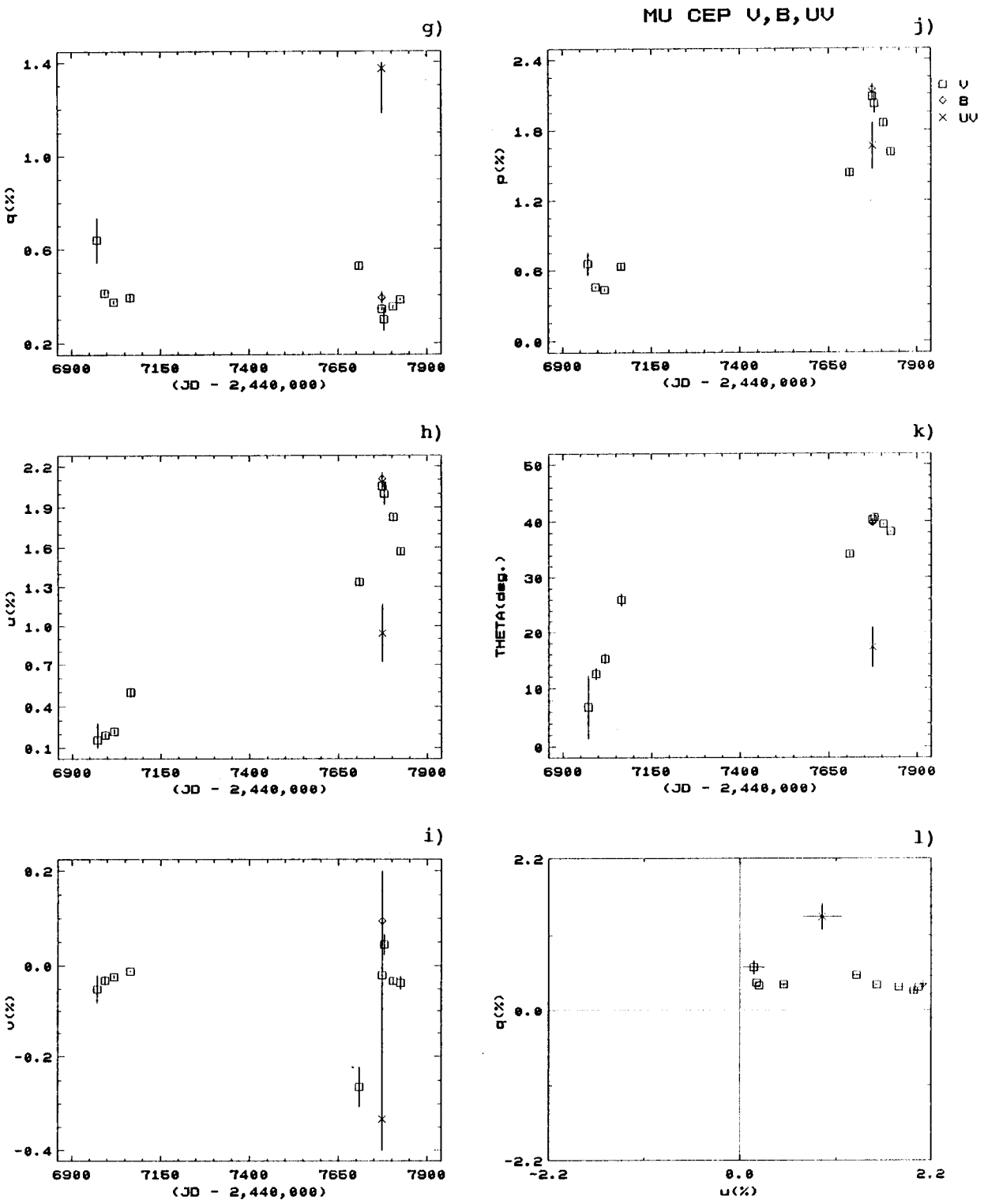

Figure 3.20

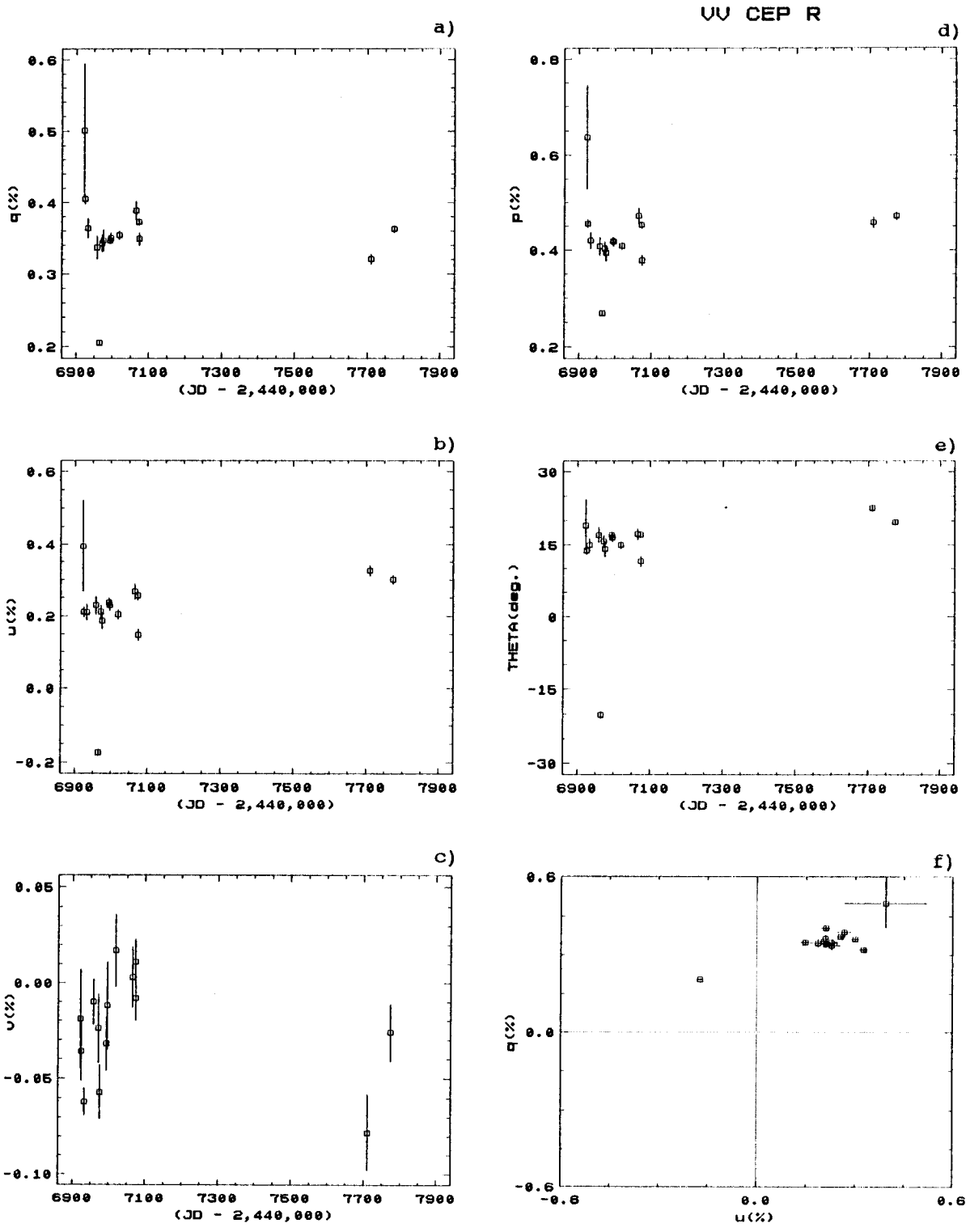
VV CEP R
a)
b)
c)
d)
e)
f)
q(%)
u(%)
v(%)
p(%)
THETA(deg.)
(JD - 2,440,000)
6900
7100
7300
7500
7700
7900
0.6
0.5
0.4
0.3
0.2
0.0
-0.2
0.05
0.00
-0.05
-0.10
0.8
30
15
0
-15
-30
-0.6

Figure 3.20 (cont.)

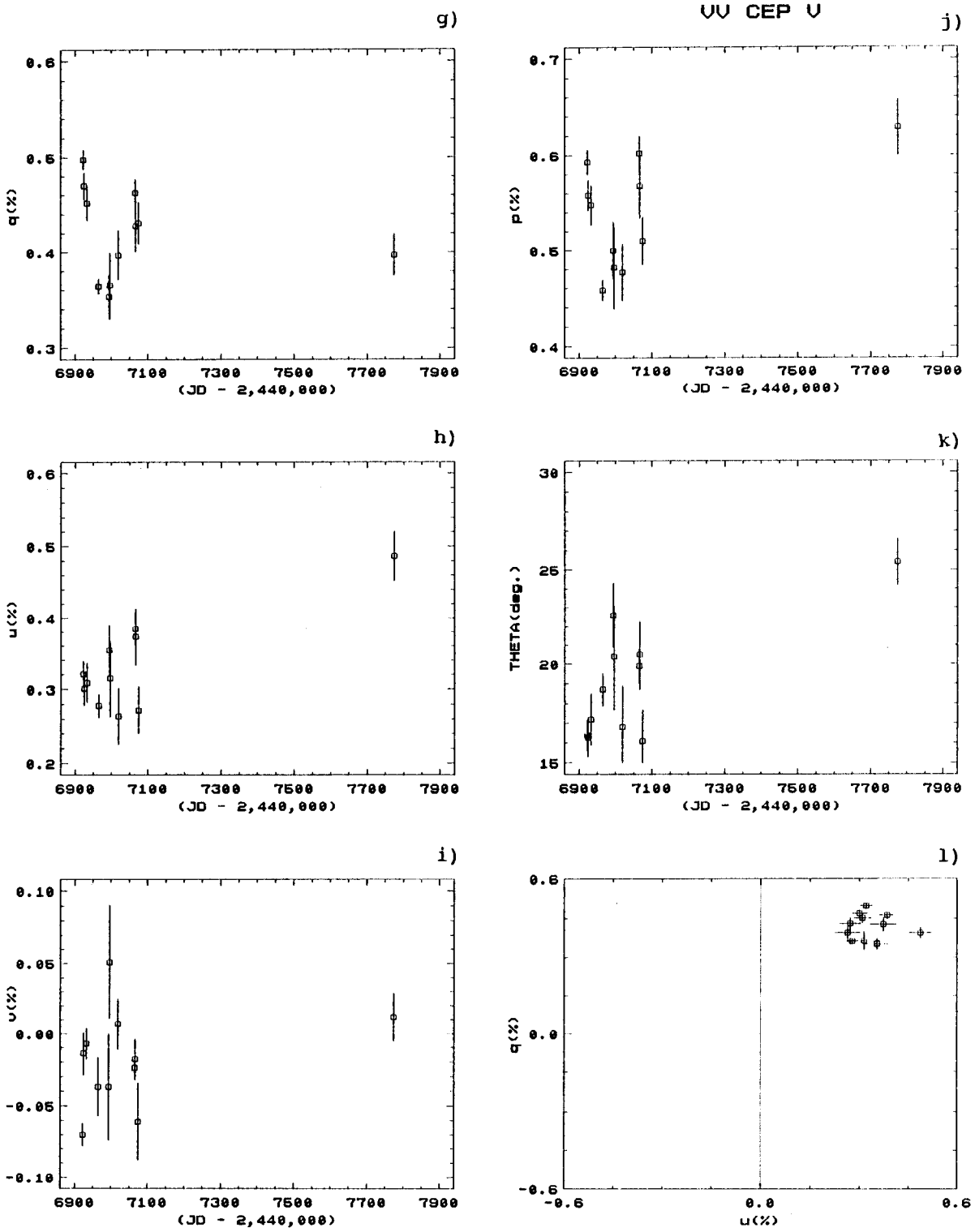

Figure 3.20 (cont.)

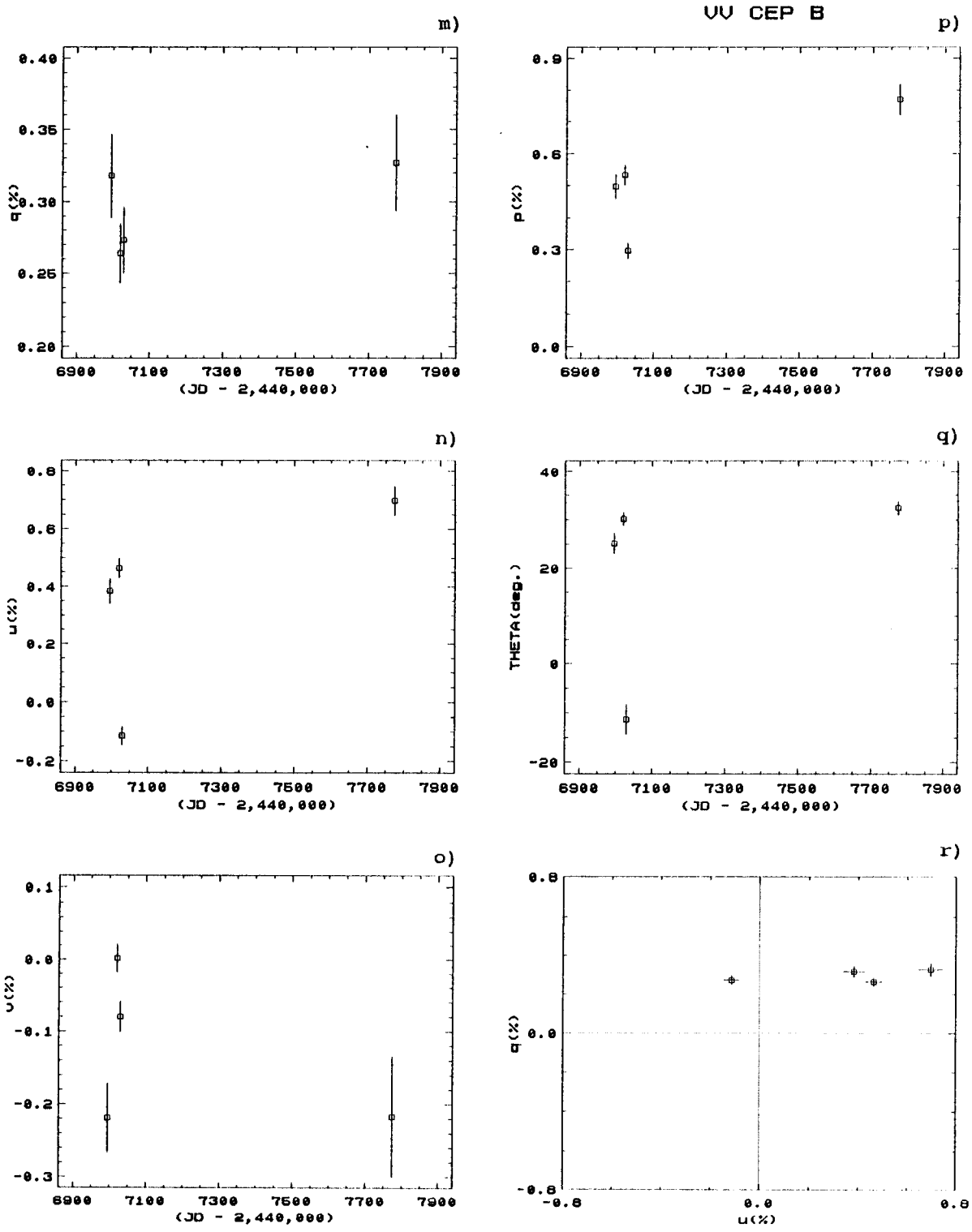

Figure 3.20 (cont.)

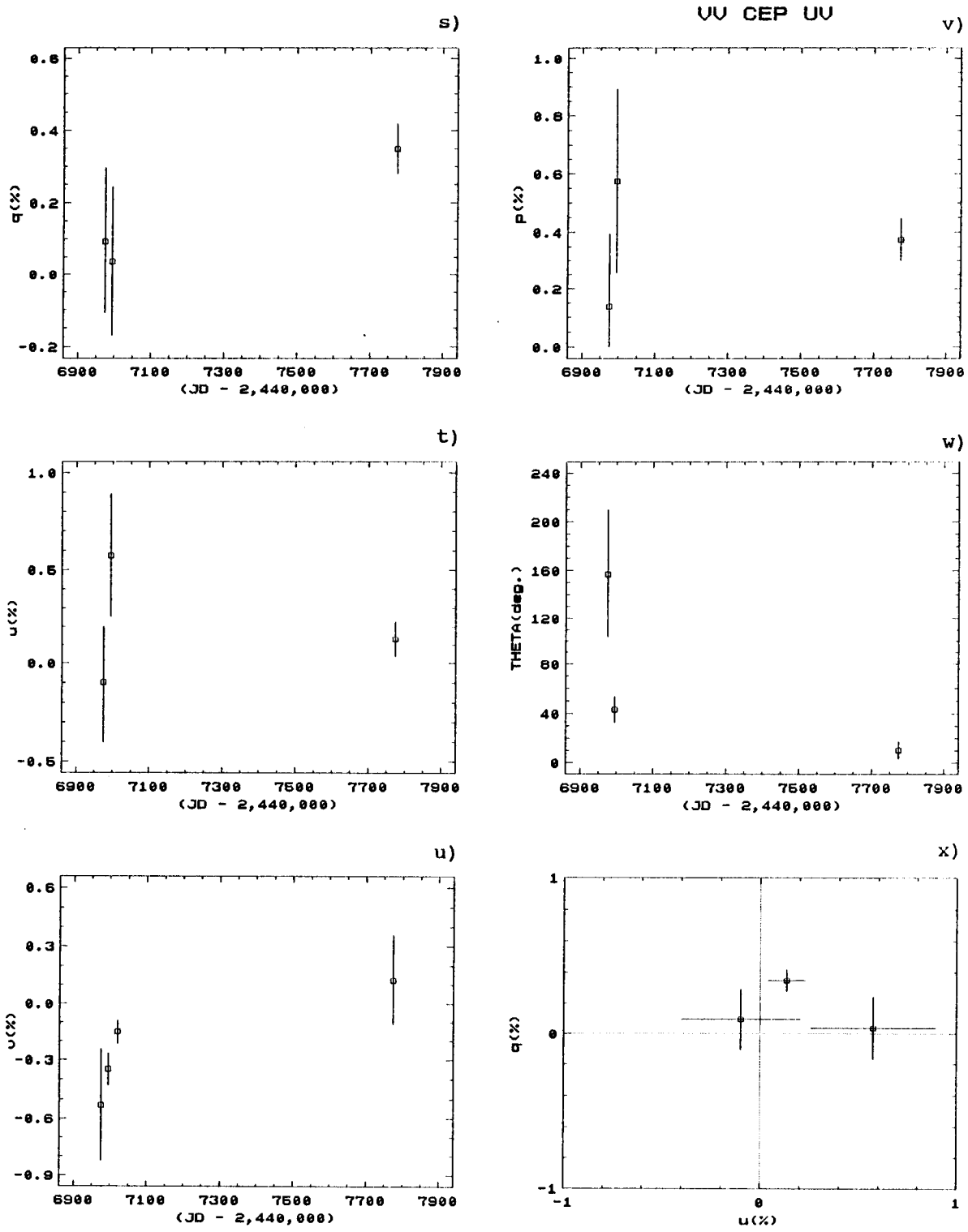

Figure 3.21

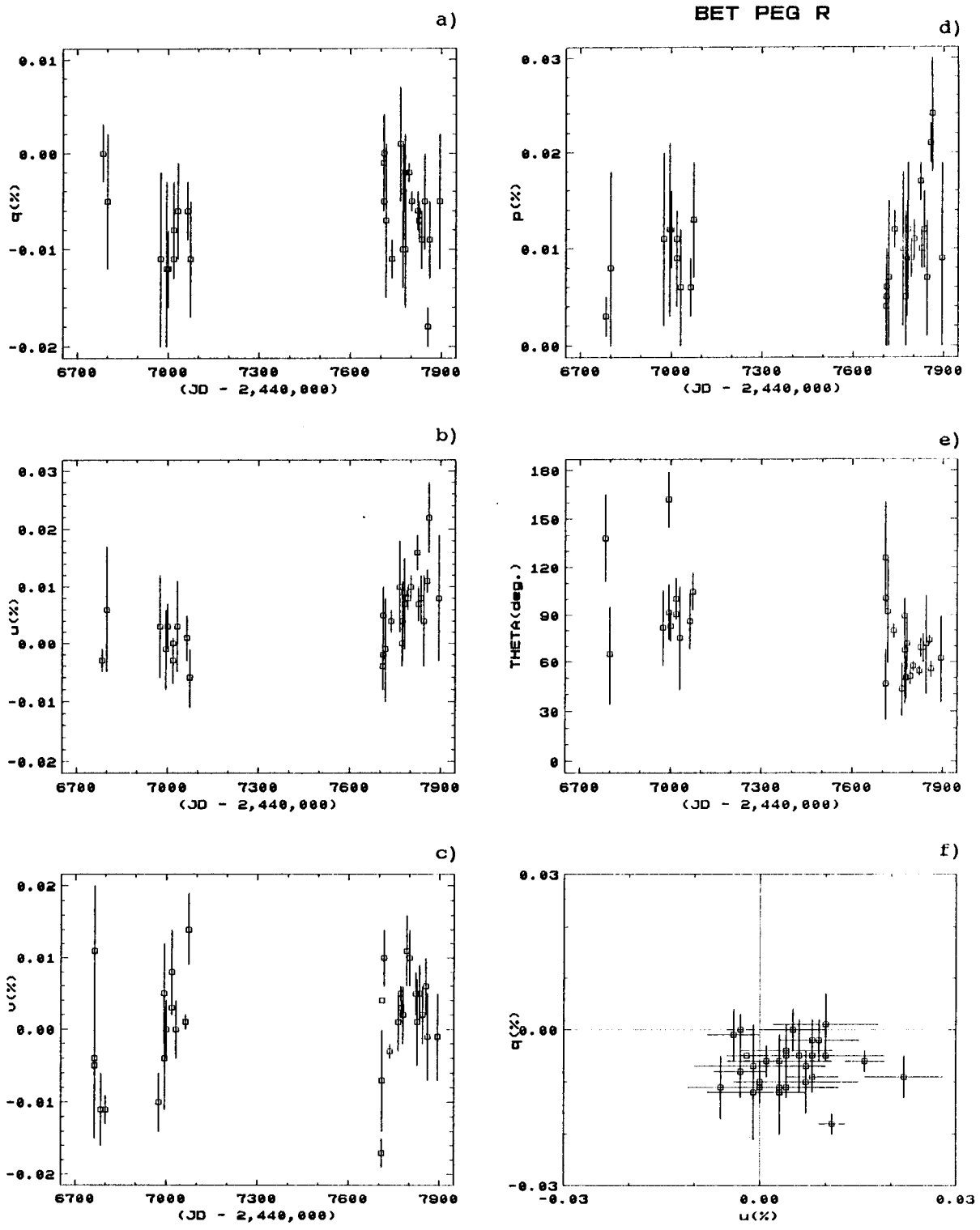
BET PEG R
a)
b)
c)
d)
e)
f)
q(%)
u(%)
v(%)
p(%)
THETA(deg.)
(JD - 2,440,000)
6700
7000
7300
7600
7900
0.01
0.00
-0.01
-0.02
0.03
0.02
180
150
120
90
60
30
0
-0.03

Figure 3.21 (cont.)

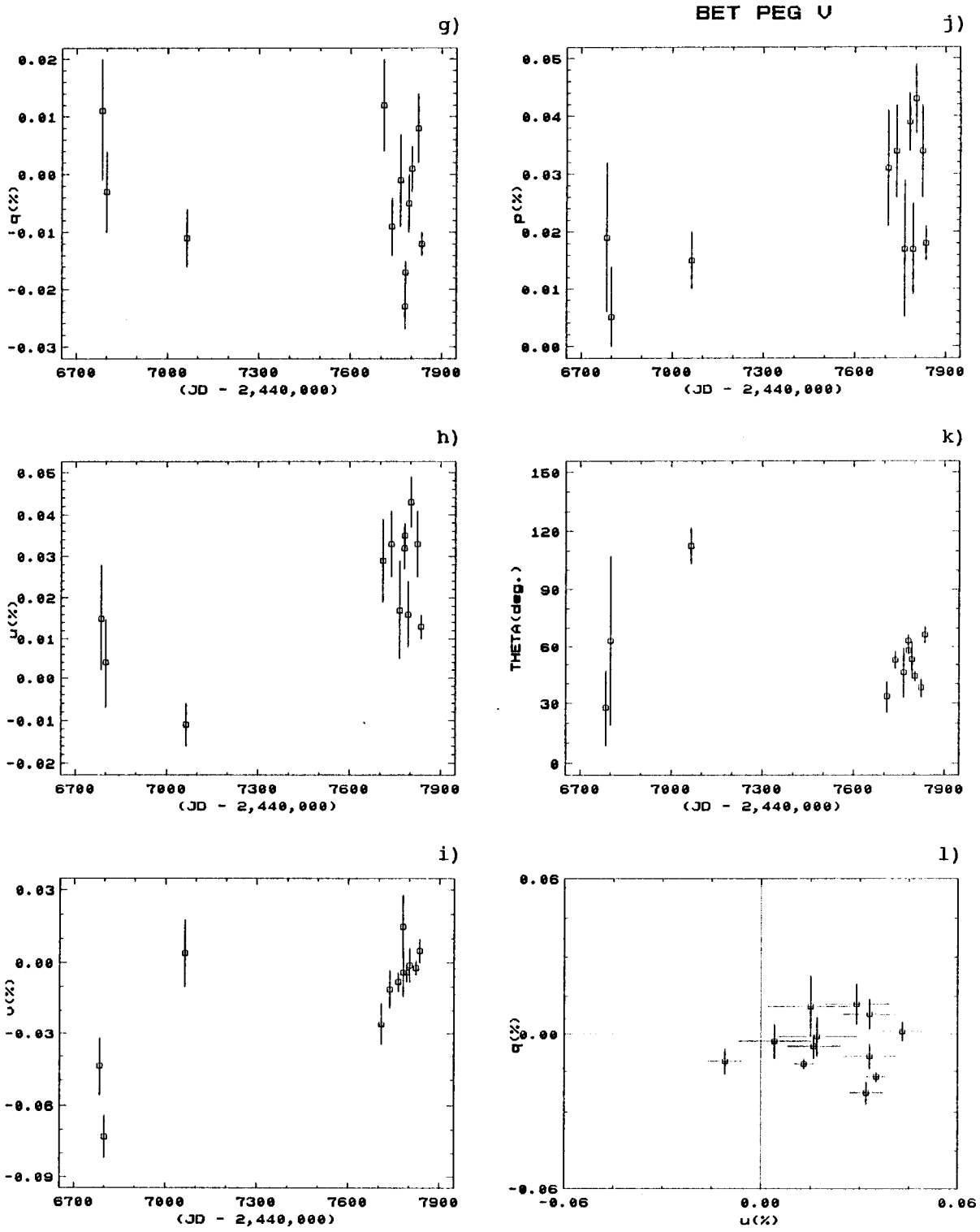

Figure 3.21 (cont.)

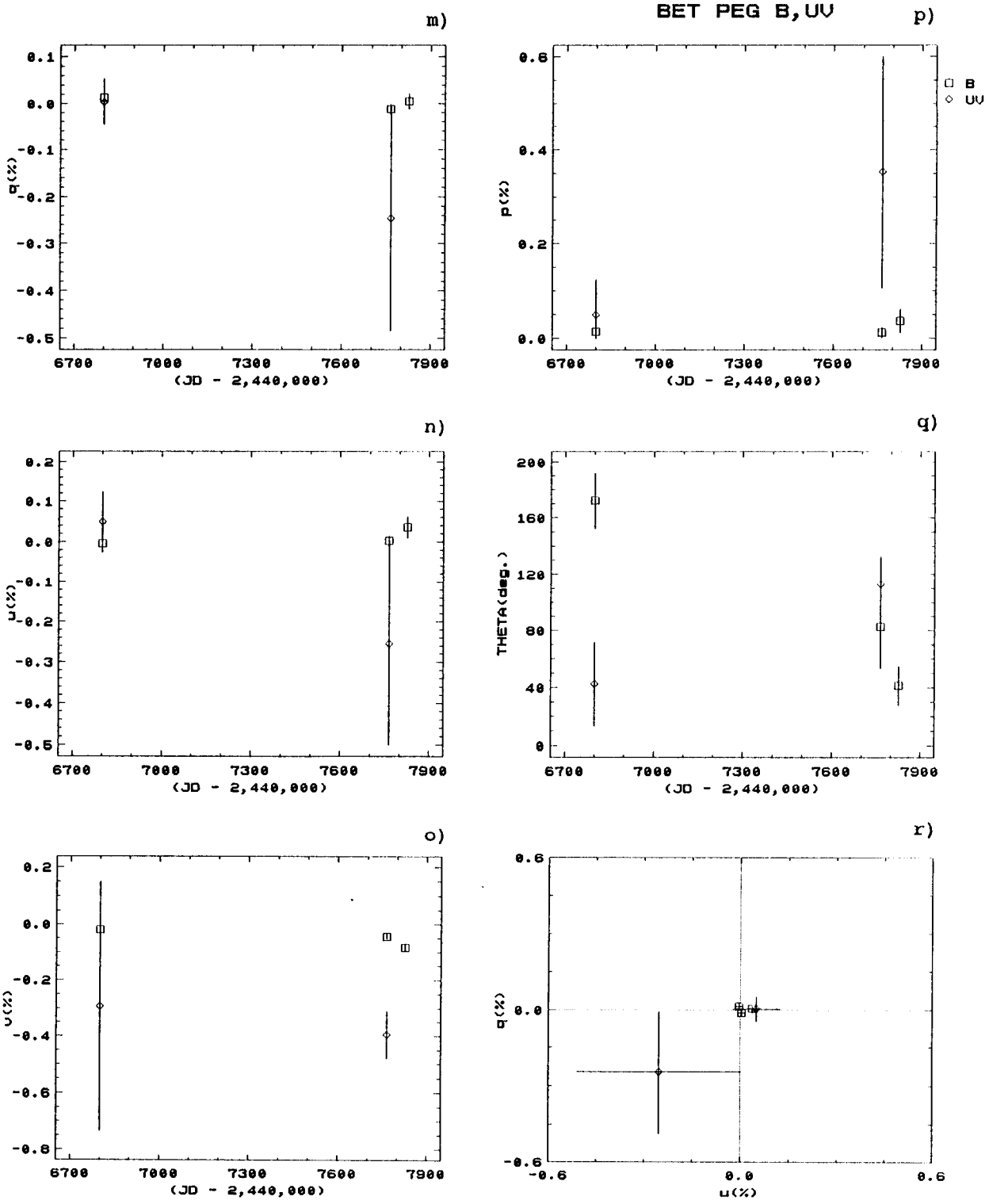

Figure 3.22

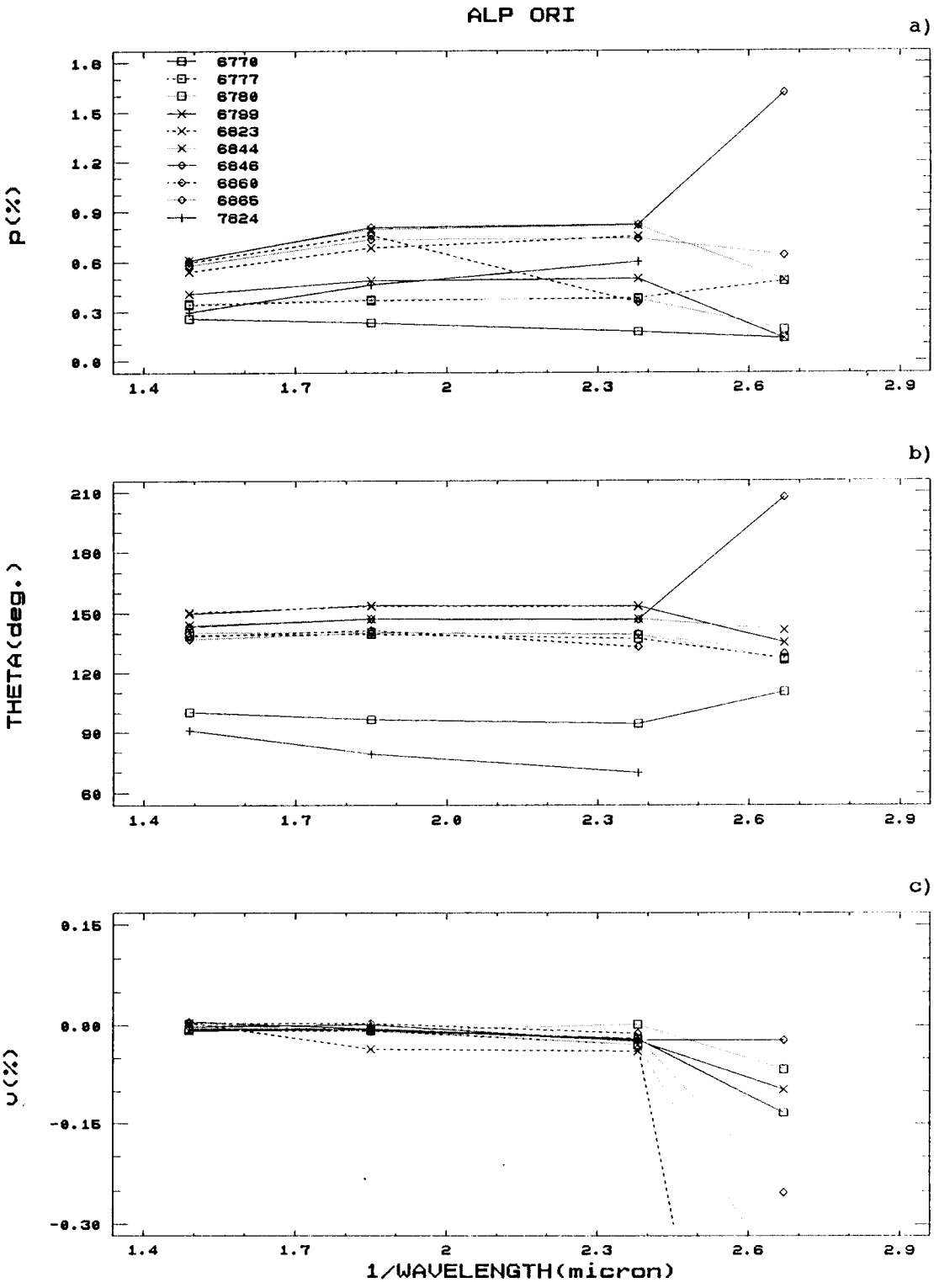
ALP ORI
a)
6770
6777
6780
6799
6823
6844
6846
6860
6865
7824
p(%)
1.8
1.5
1.2
0.9
0.6
0.3
0.0
1.4
1.7
2
2.3
2.6
2.9
b)
THETA(deg.)
210
180
150
120
90
60
1.4
1.7
2.0
2.3
2.6
2.9
c)
U(%)
0.15
0.00
-0.15
-0.30
1.4
1.7
2
2.3
2.6
2.9
1/WAVELENGTH(micron)

Figure 3.23

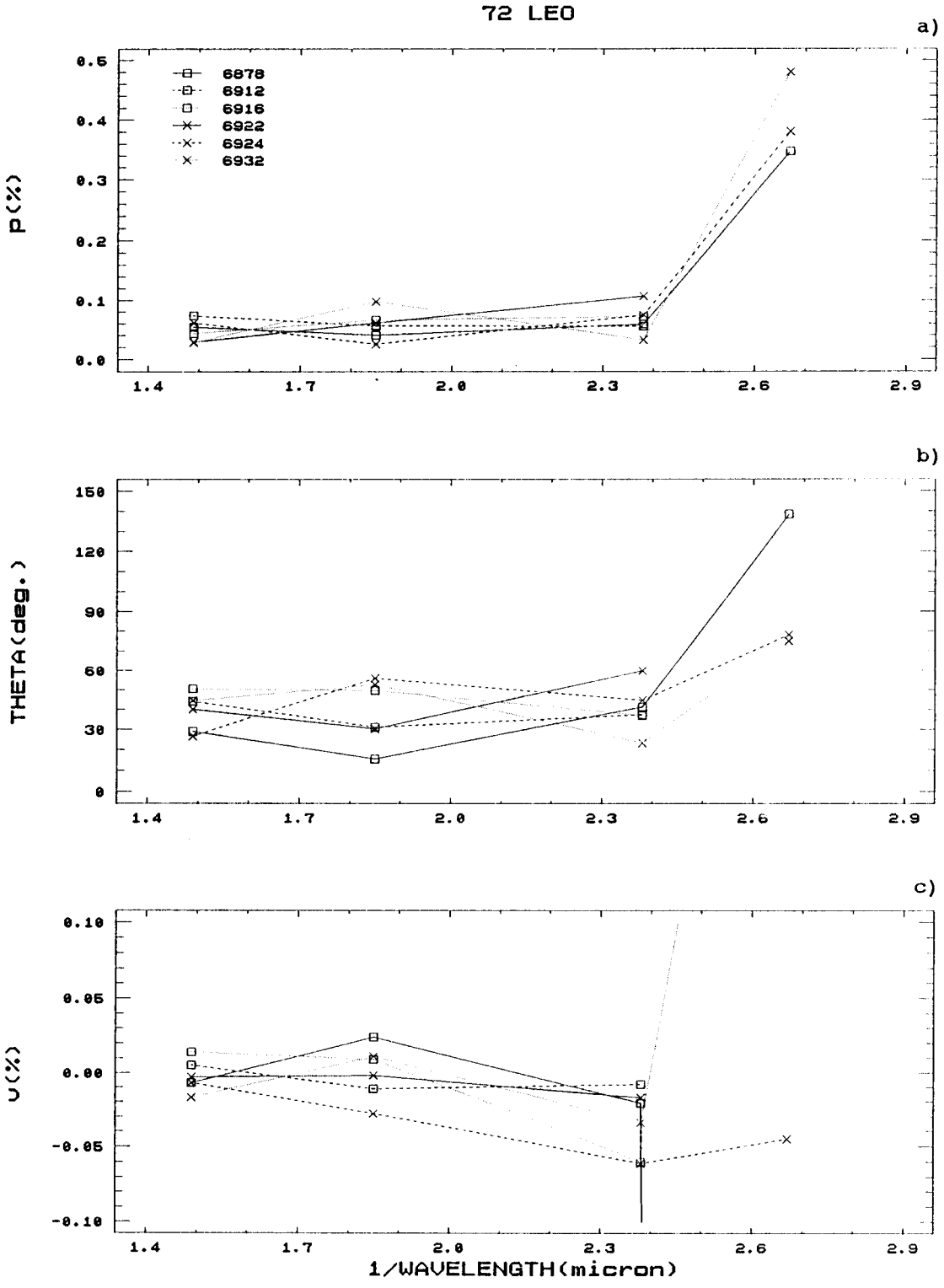
72 LEO
a)
b)
c)
6878
6912
6916
6922
6924
6932
P(%)
THETA(deg.)
U(%)
1/WAVELENGTH(micron)
0.5
0.4
0.3
0.2
0.1
0.0
150
120
90
60
30
0
0.10
0.05
0.00
-0.05
-0.10
1.4
1.7
2.0
2.3
2.6
2.9

Figure 3.24

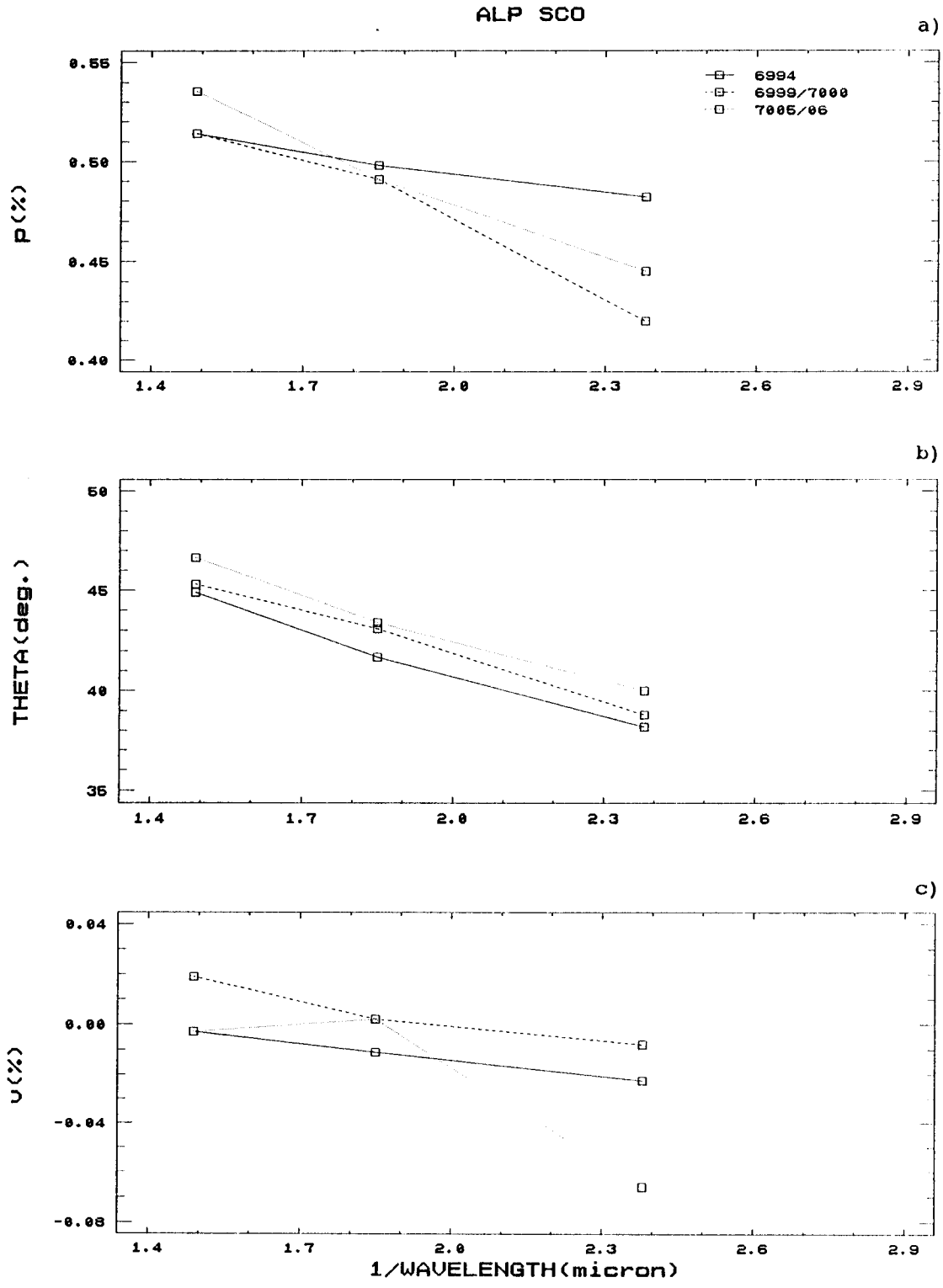
ALP SCO
a)
6994
6999/7000
7005/06
p(%)
0.55
0.50
0.45
0.40
1.4
1.7
2.0
2.3
2.6
2.9
b)
THETA(deg.)
50
45
40
35
c)
U(%)
0.04
0.00
-0.04
-0.08
1/WAVELENGTH(micron)

Figure 3.25

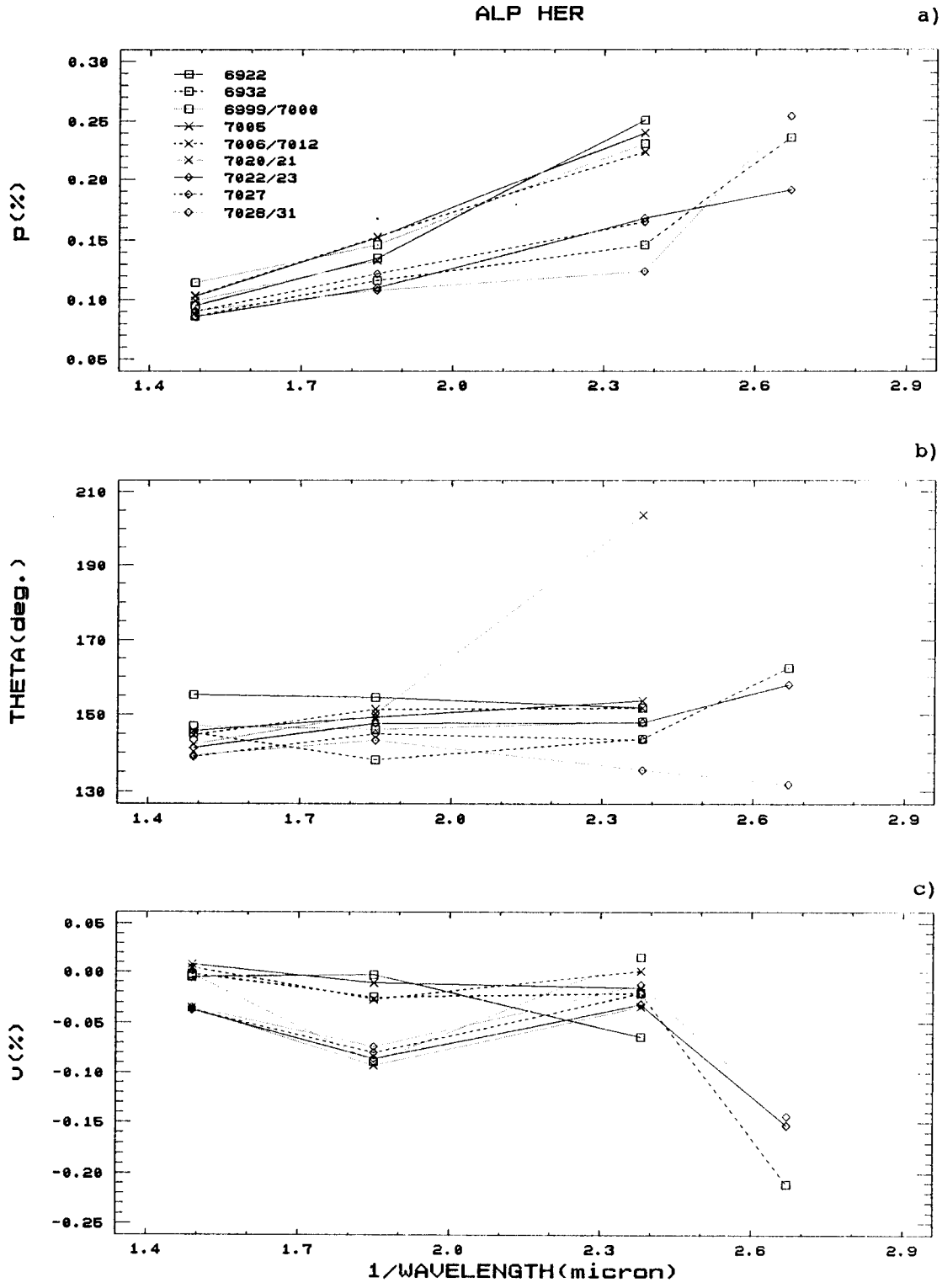
ALP HER
a)
p(%)
0.30
0.25
0.20
0.15
0.10
0.05
6922
6932
6999/7000
7005
7006/7012
7020/21
7022/23
7027
7028/31
1.4
1.7
2.0
2.3
2.6
2.9
b)
THETA(deg.)
210
190
170
150
130
c)
U(%)
0.05
0.00
-0.05
-0.10
-0.15
-0.20
-0.25
1/WAVELENGTH(micron)

Figure 3.26

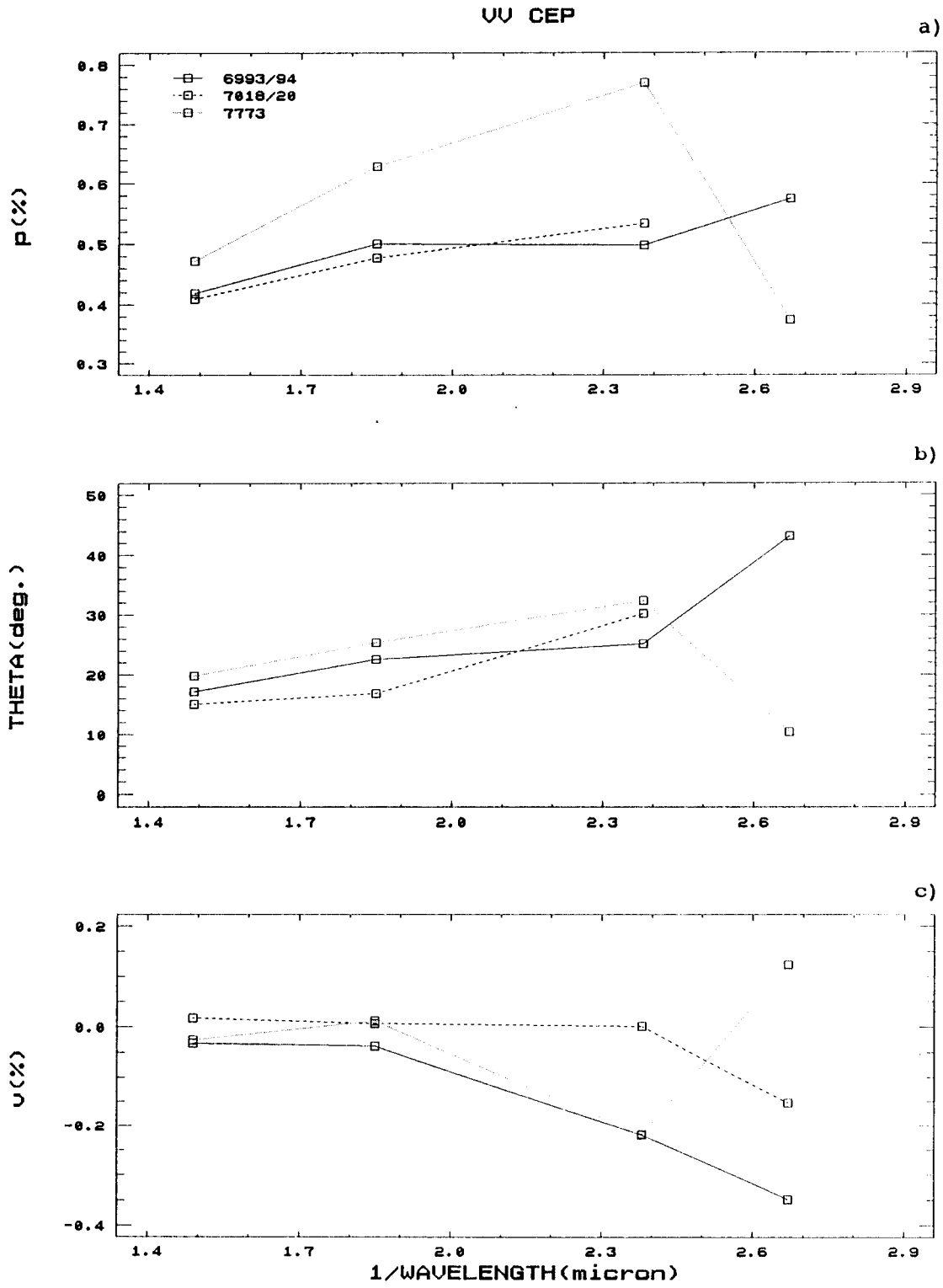
VV CEP
a)
6993/94
7018/20
7773
p(%)
0.8
0.7
0.6
0.5
0.4
0.3
1.4
1.7
2.0
2.3
2.6
2.9
b)
THETA(deg.)
50
40
30
20
10
0
c)
v(%)
0.2
0.0
-0.2
-0.4
1/WAVELENGTH(micron)

Figure 3.27

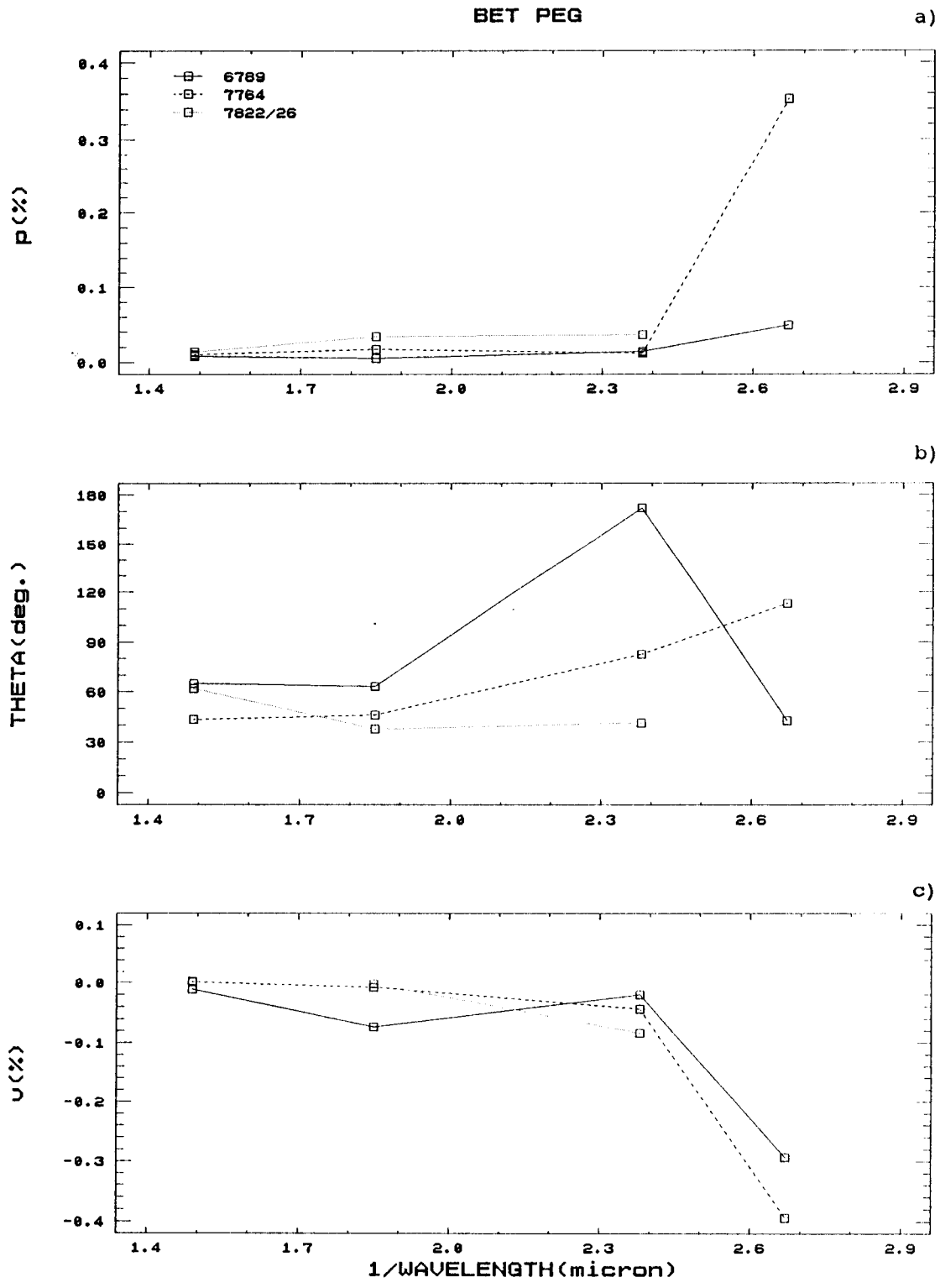
BET PEG
a)
6789
7764
7822/26
p(%)
0.4
0.3
0.2
0.1
0.0
1.4
1.7
2.0
2.3
2.6
2.9
b)
THETA(deg.)
180
150
120
90
60
30
0
c)
U(%)
0.1
0.0
-0.1
-0.2
-0.3
-0.4
1/WAVELENGTH(micron)

Figure 3.28

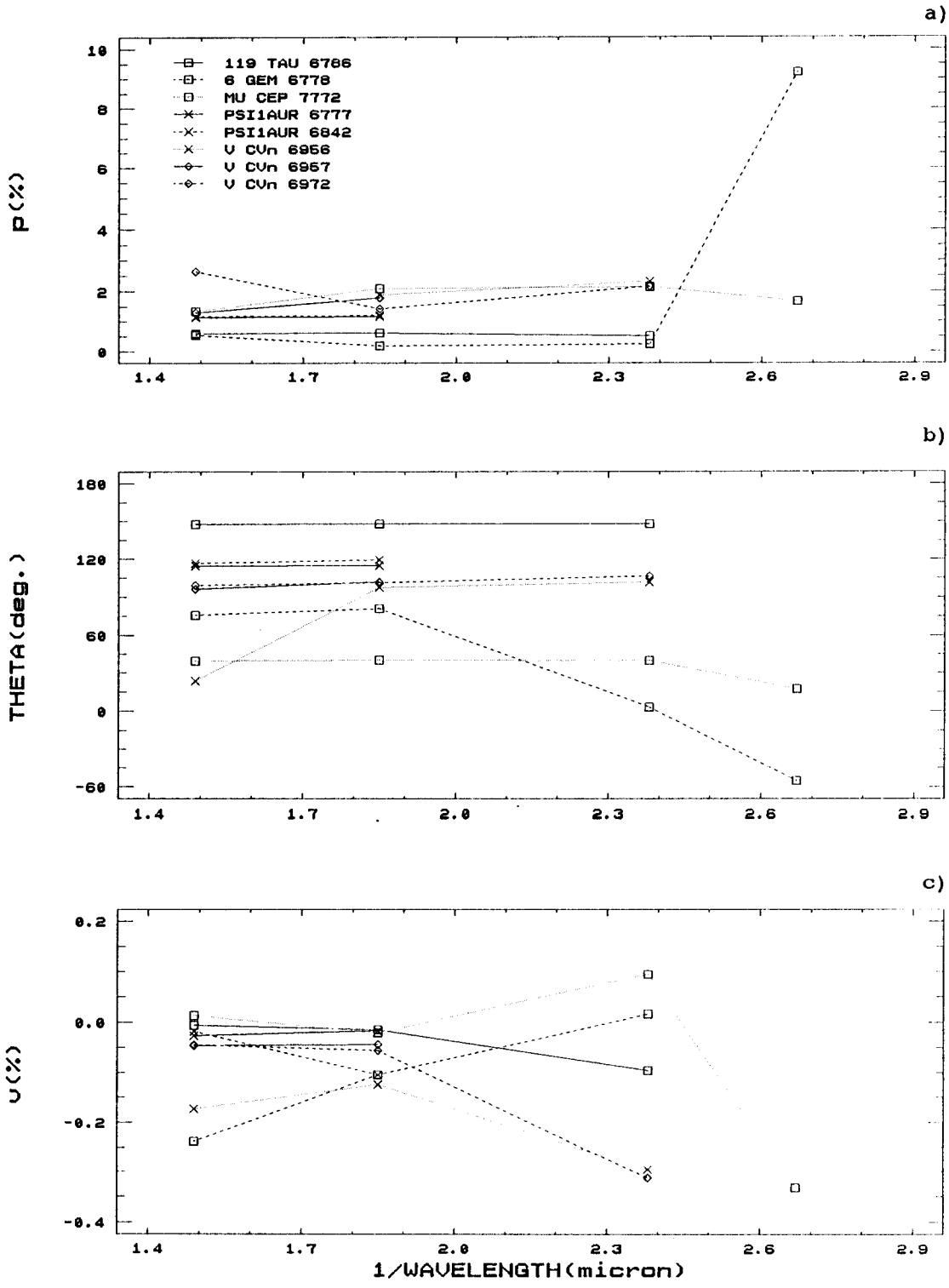
a)
p(%)
10
8
6
4
2
0
119 TAU 6786
6 GEM 6778
MU CEP 7772
PSI1AUR 6777
PSI1AUR 6842
V CVn 6956
V CVn 6957
V CVn 6972
1.4
1.7
2.0
2.3
2.6
2.9
b)
THETA(deg.)
180
120
60
0
-60
1.4
1.7
2.0
2.3
2.6
2.9
c)
U(%)
0.2
0.0
-0.2
-0.4
1.4
1.7
2.0
2.3
2.6
2.9
1/WAVELENGTH(micron)

Figure 3.29

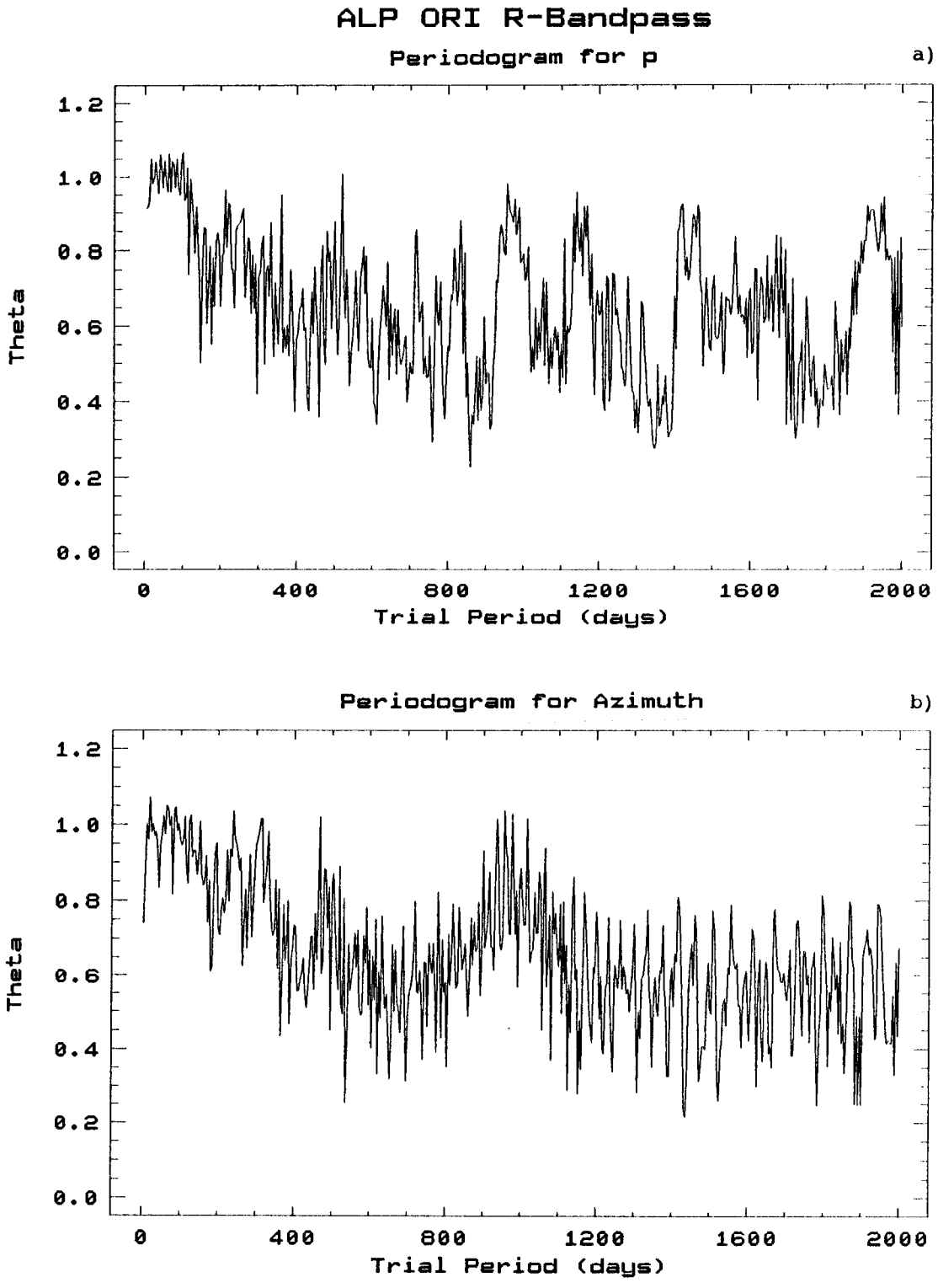
ALP ORI R-Bandpass
Periodogram for p
a)
Theta
1.2
1.0
0.8
0.6
0.4
0.2
0.0
0
400
800
1200
1600
2000
Trial Period (days)
Periodogram for Azimuth
b)
Theta
1.2
1.0
0.8
0.6
0.4
0.2
0.0
0
400
800
1200
1600
2000
Trial Period (days)

Figure 3.29 (cont.)

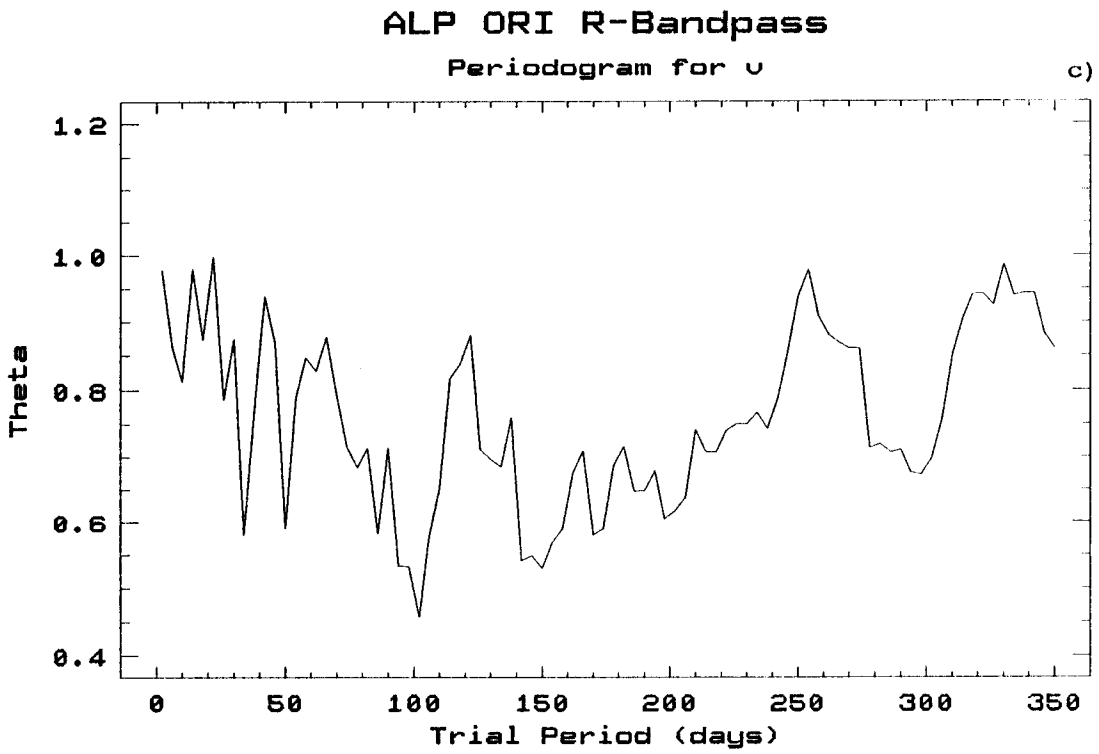

Figure 3.29 (cont.)

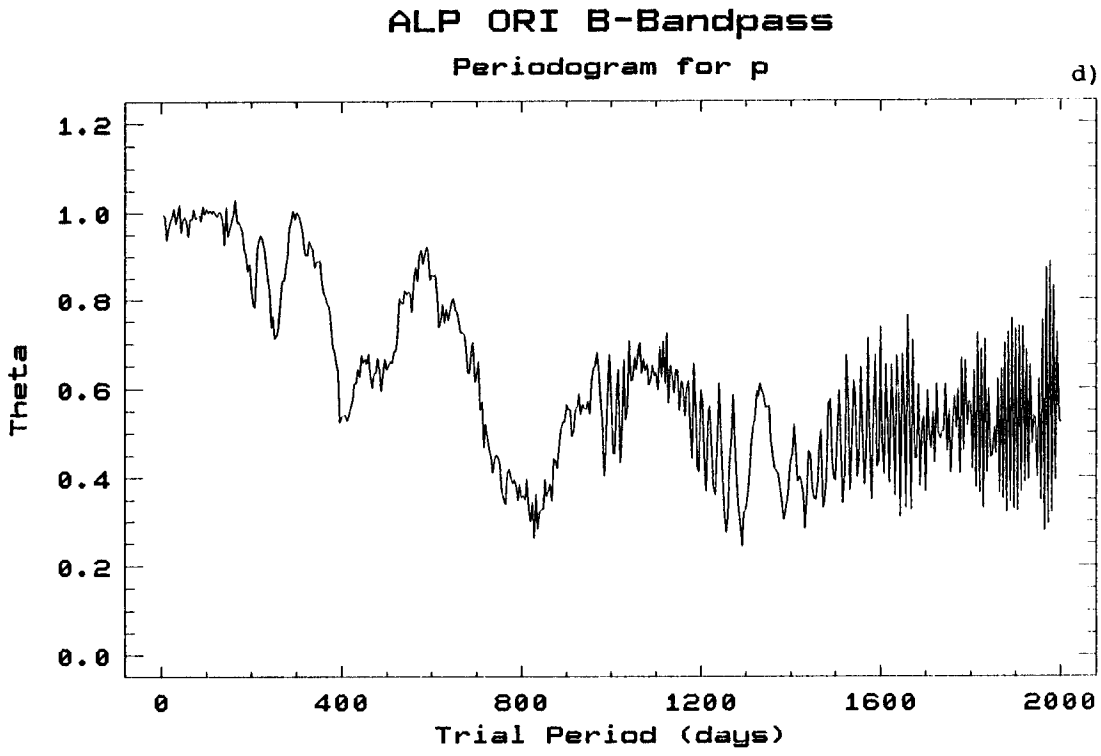

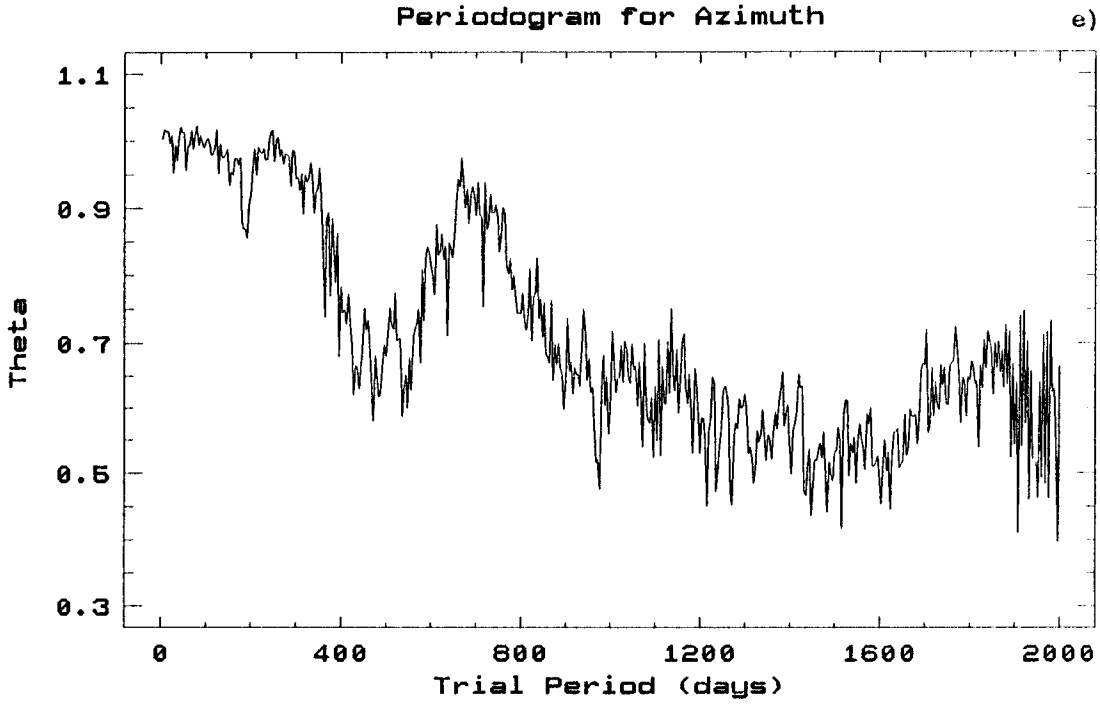

Figure 3.30

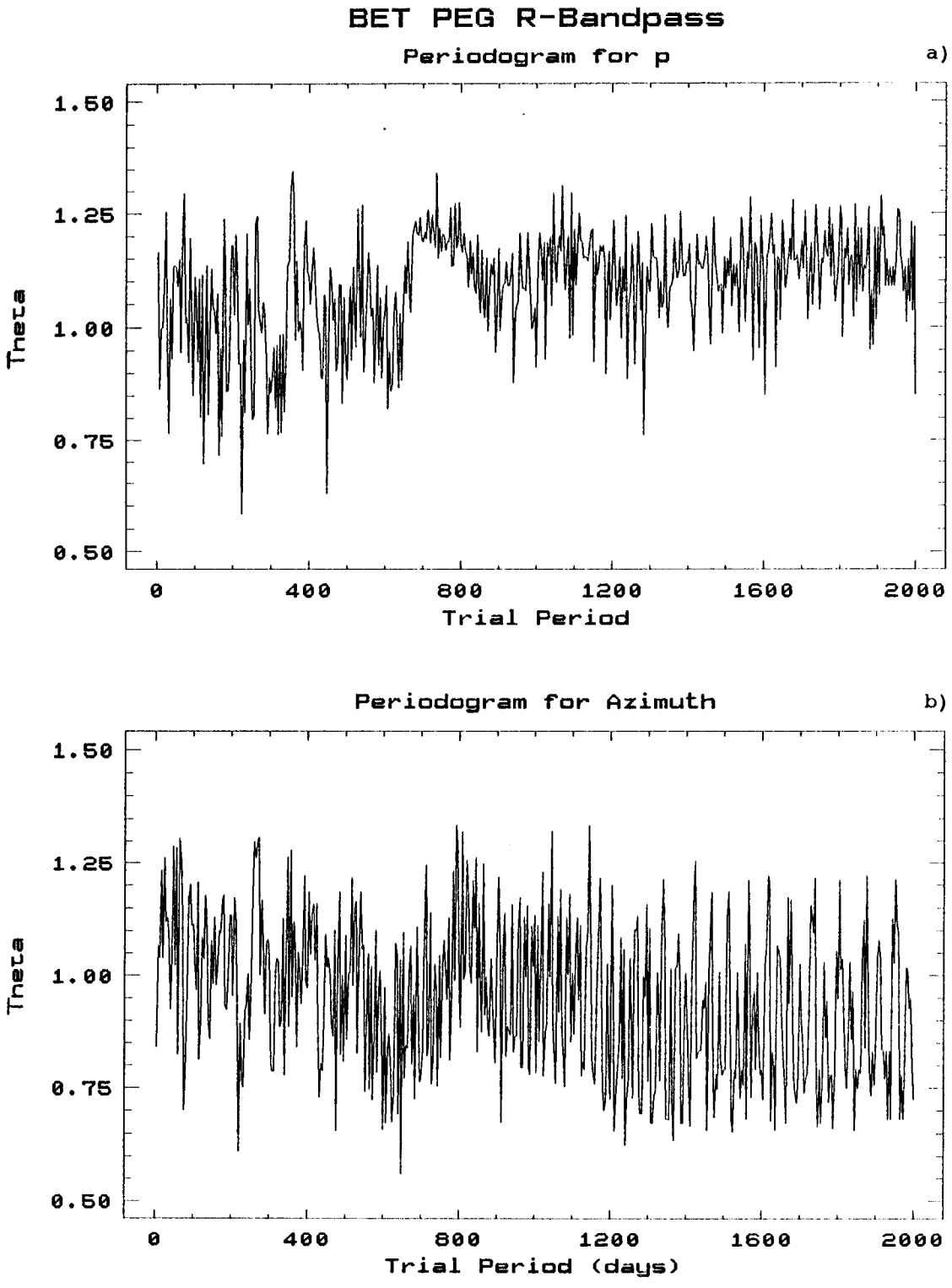
BET PEG R-Bandpass
Periodogram for p
a)
1.50
1.25
1.00
0.75
0.50
Theta
0
400
800
1200
1600
2000
Trial Period
Periodogram for Azimuth
b)
1.50
1.25
1.00
0.75
0.50
Theta
0
400
800
1200
1600
2000
Trial Period (days)

Figure 3.31

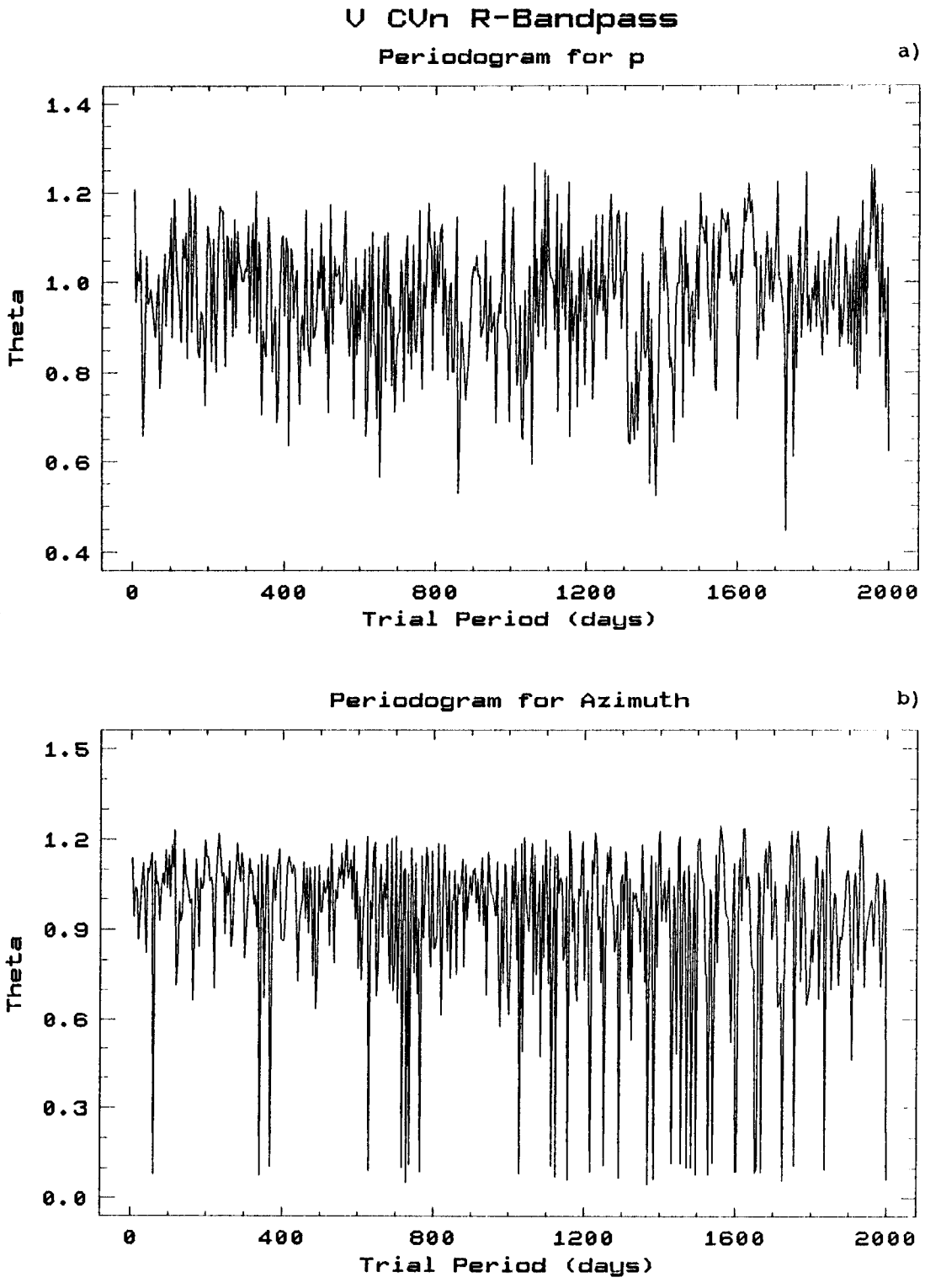
V CVn R-Bandpass
Periodogram for p
a)
Theta
1.4
1.2
1.0
0.8
0.6
0.4
0
400
800
1200
1600
2000
Trial Period (days)
Periodogram for Azimuth
b)
Theta
1.5
1.2
0.9
0.6
0.3
0.0
0
400
800
1200
1600
2000
Trial Period (days)

Figure 3.31 (cont.)

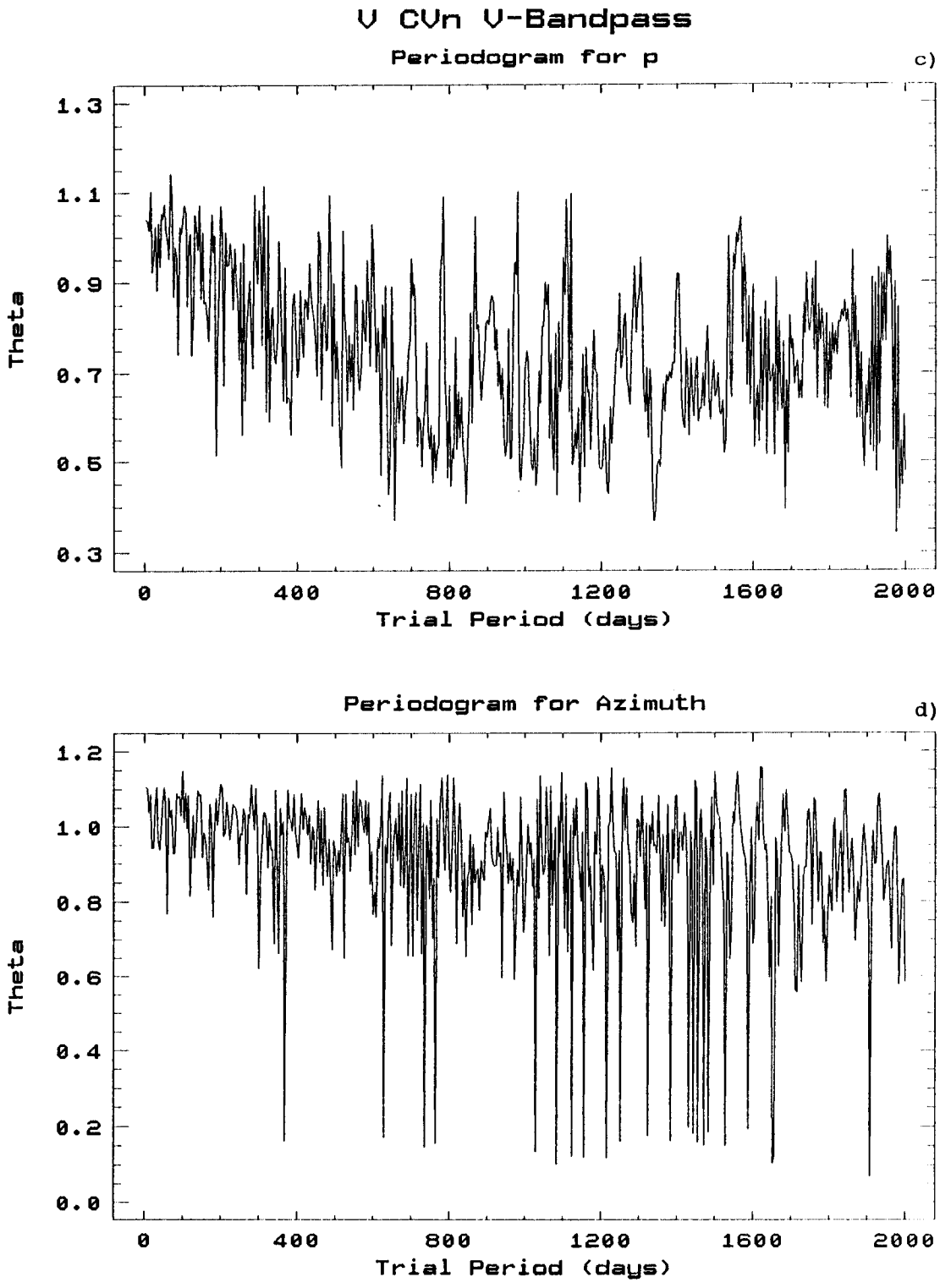

Figure 3.31 (cont.)

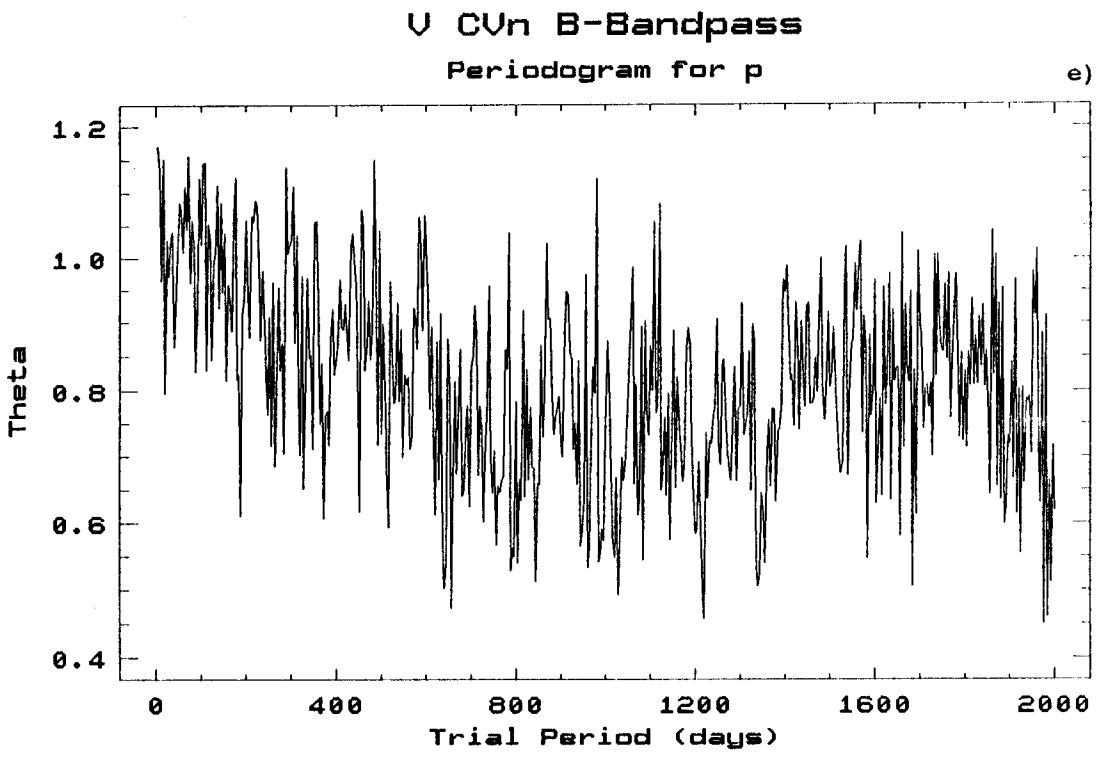

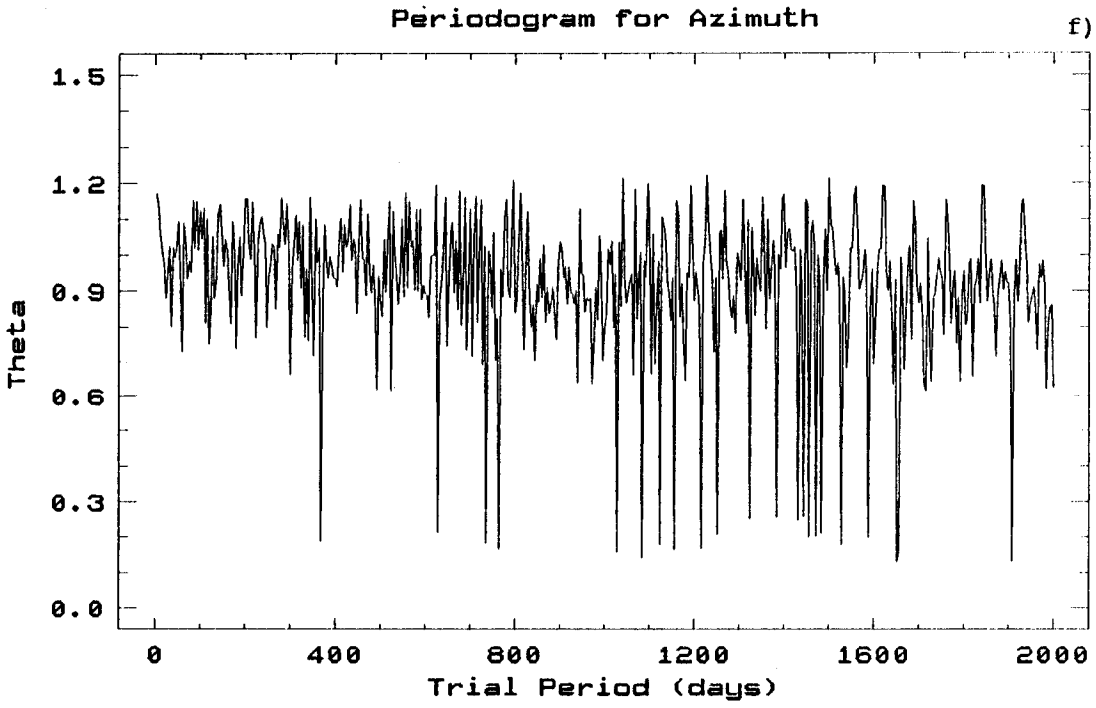

Figure 3.32

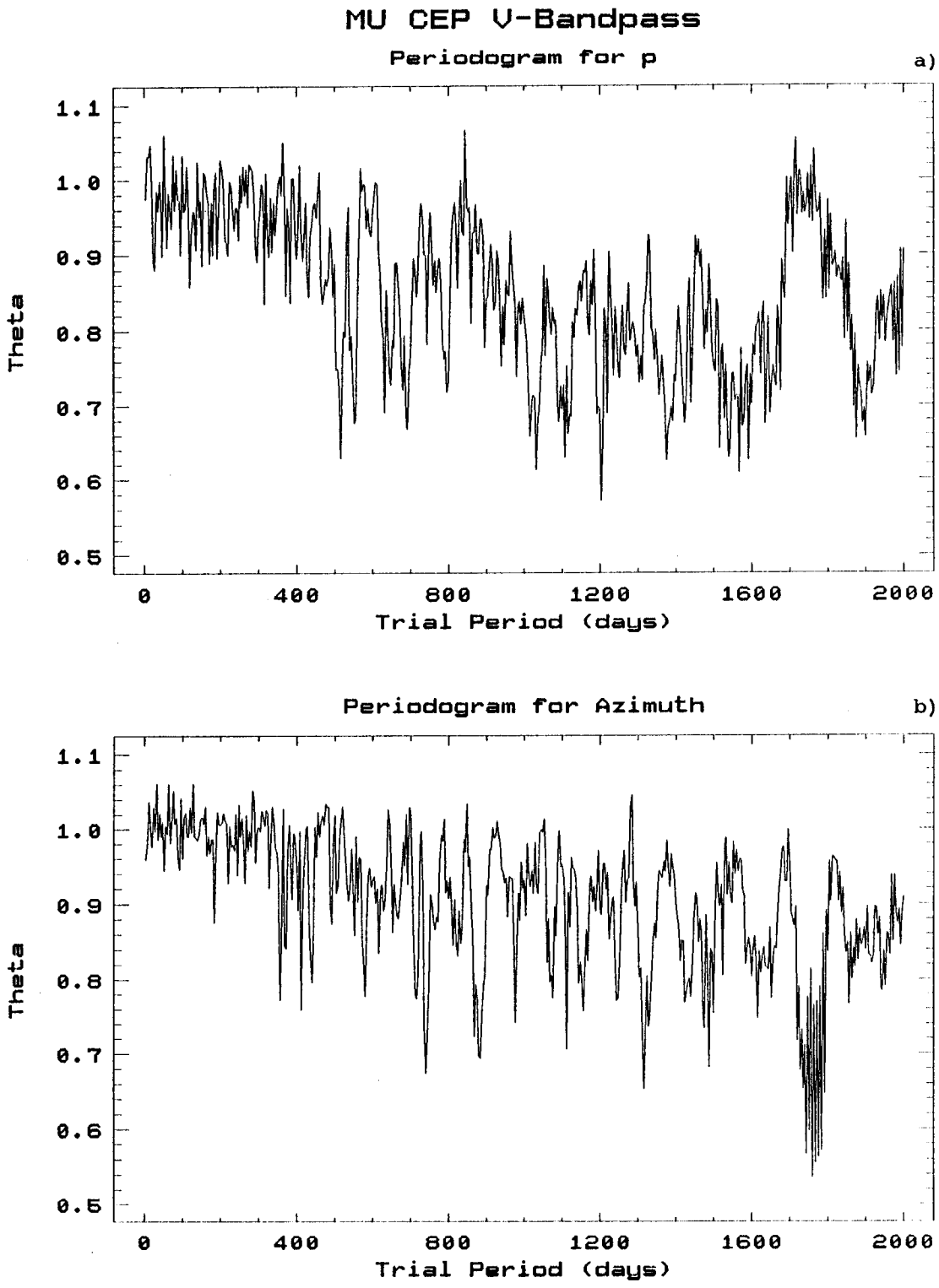
MU CEP V-Bandpass
Periodogram for p
a)
Theta
1.1
1.0
0.9
0.8
0.7
0.6
0.5
0
400
800
1200
1600
2000
Trial Period (days)
Periodogram for Azimuth
b)
Theta
1.1
1.0
0.9
0.8
0.7
0.6
0.5
0
400
800
1200
1600
2000
Trial Period (days)

Figure 3.32 (cont.)

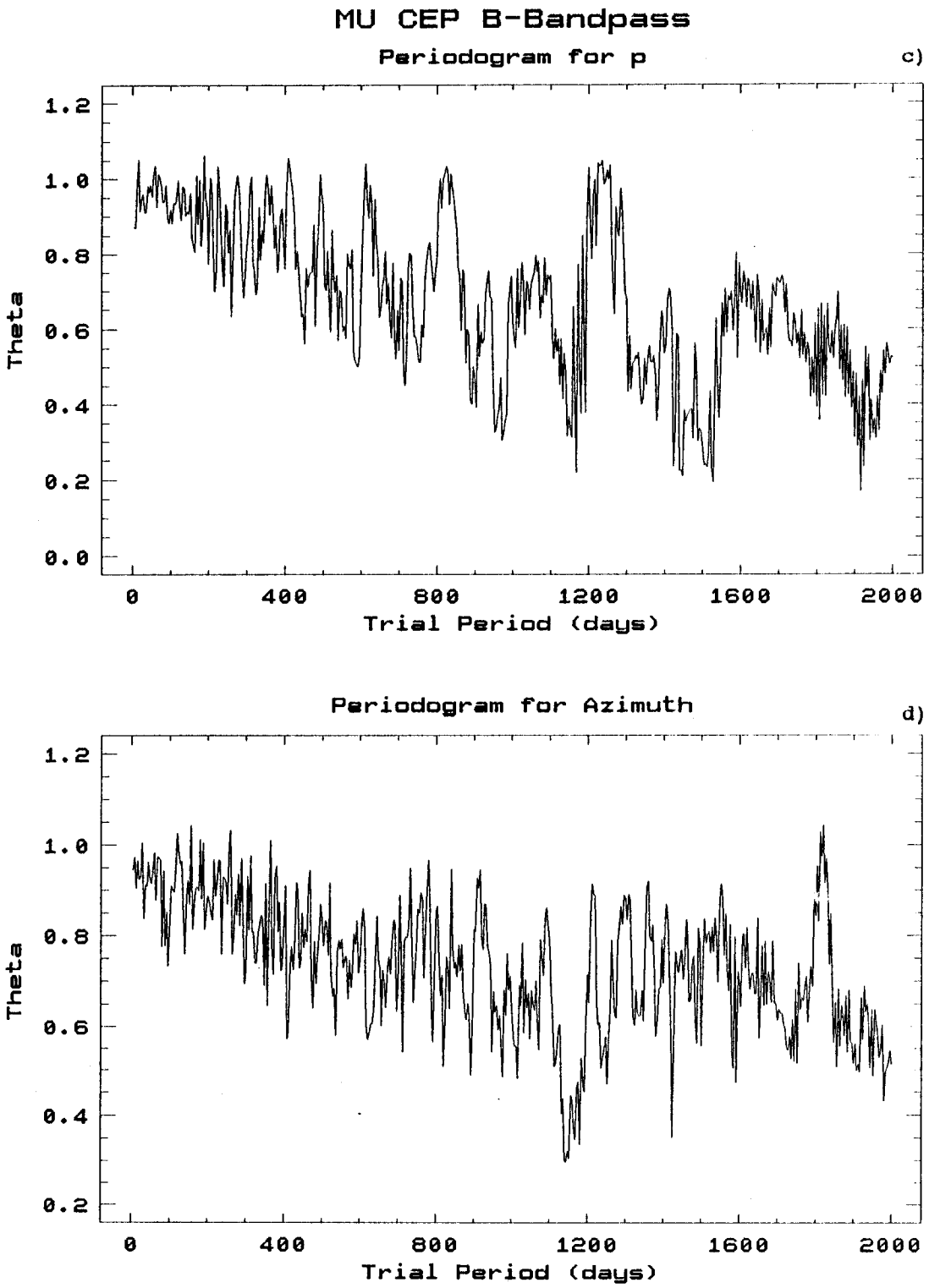

Figure 3.33

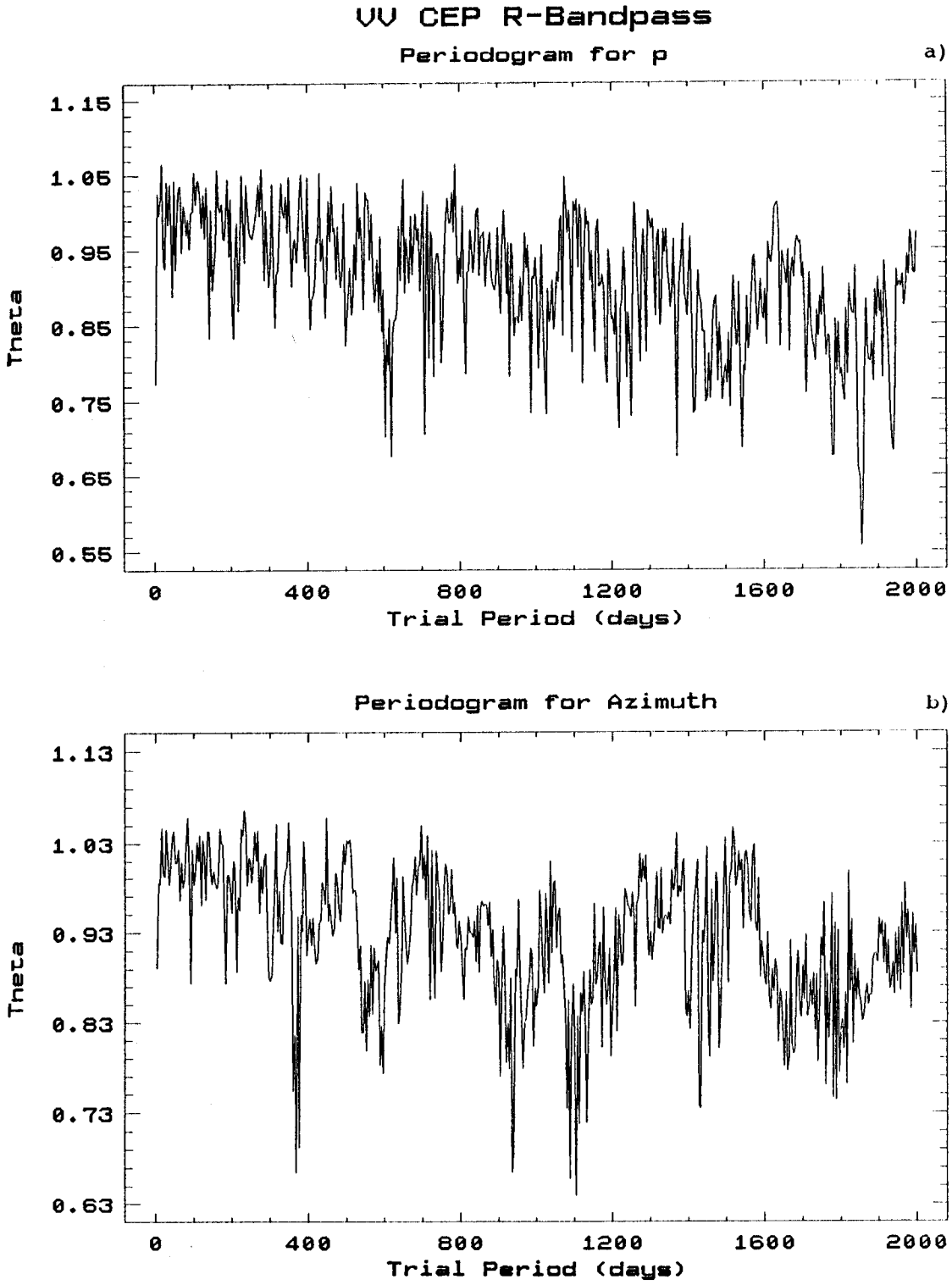
VV CEP R-Bandpass
Periodogram for p
a)
Theta
1.15
1.05
0.95
0.85
0.75
0.65
0.55
0
400
800
1200
1600
2000
Trial Period (days)
Periodogram for Azimuth
b)
Theta
1.13
1.03
0.93
0.83
0.73
0.63
0
400
800
1200
1600
2000
Trial Period (days)

Figure 3.33 (cont.)

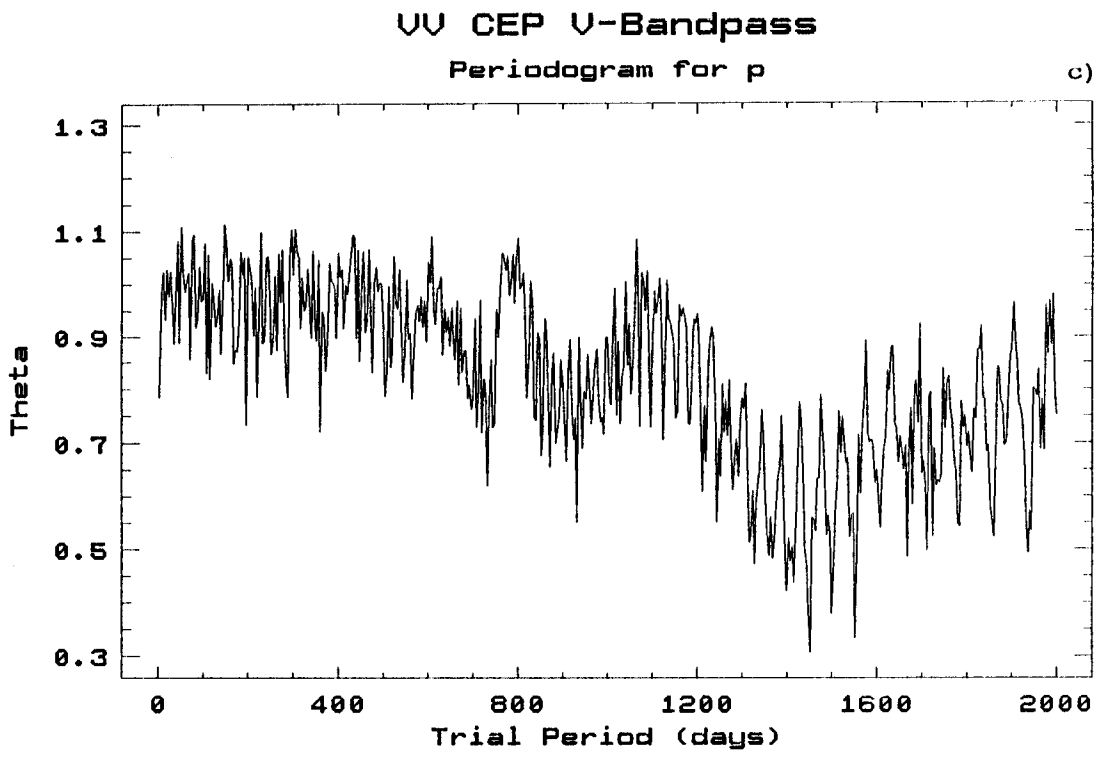

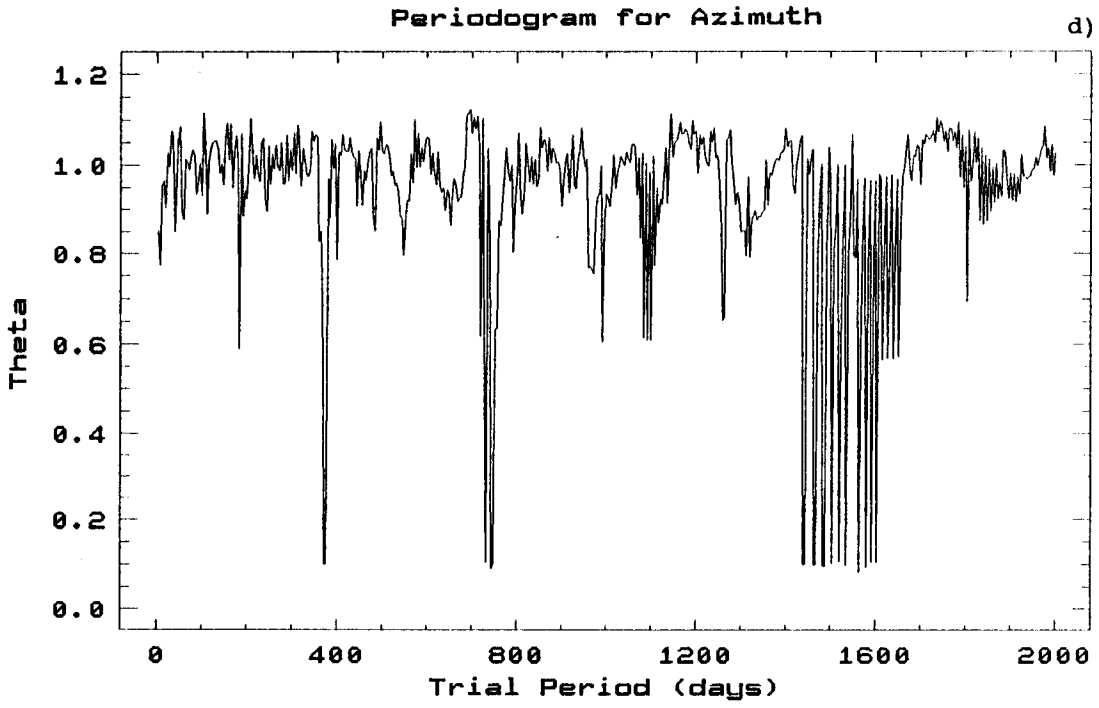

Figure 3.33 (cont.)

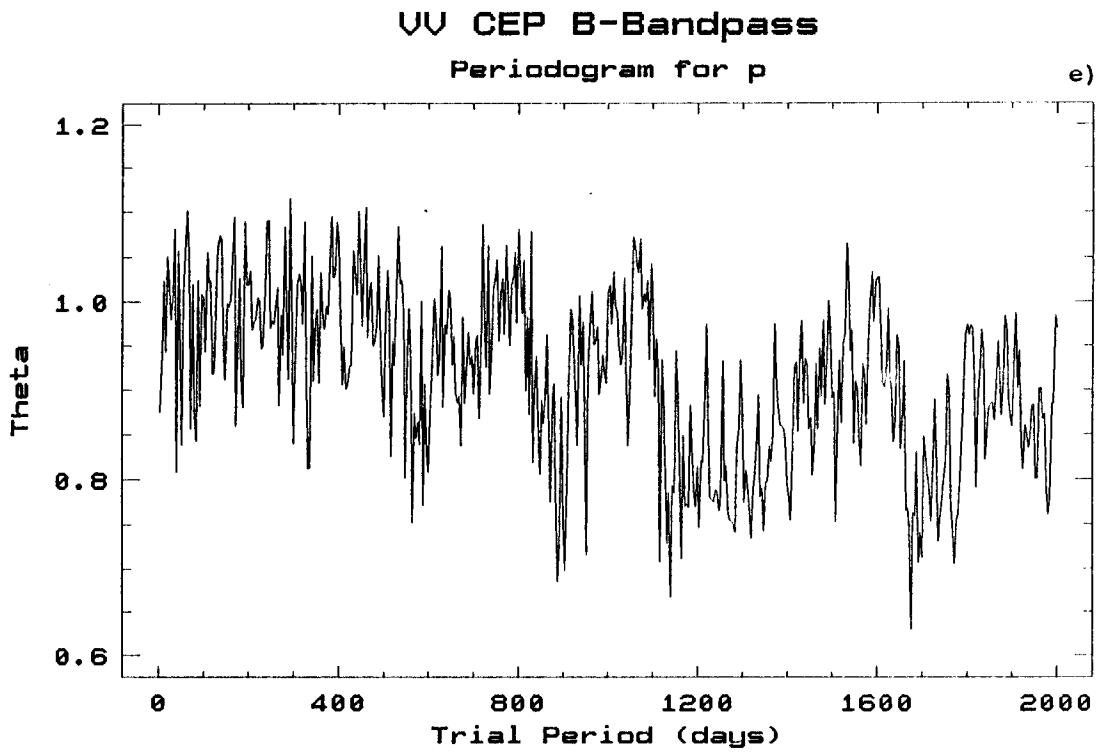

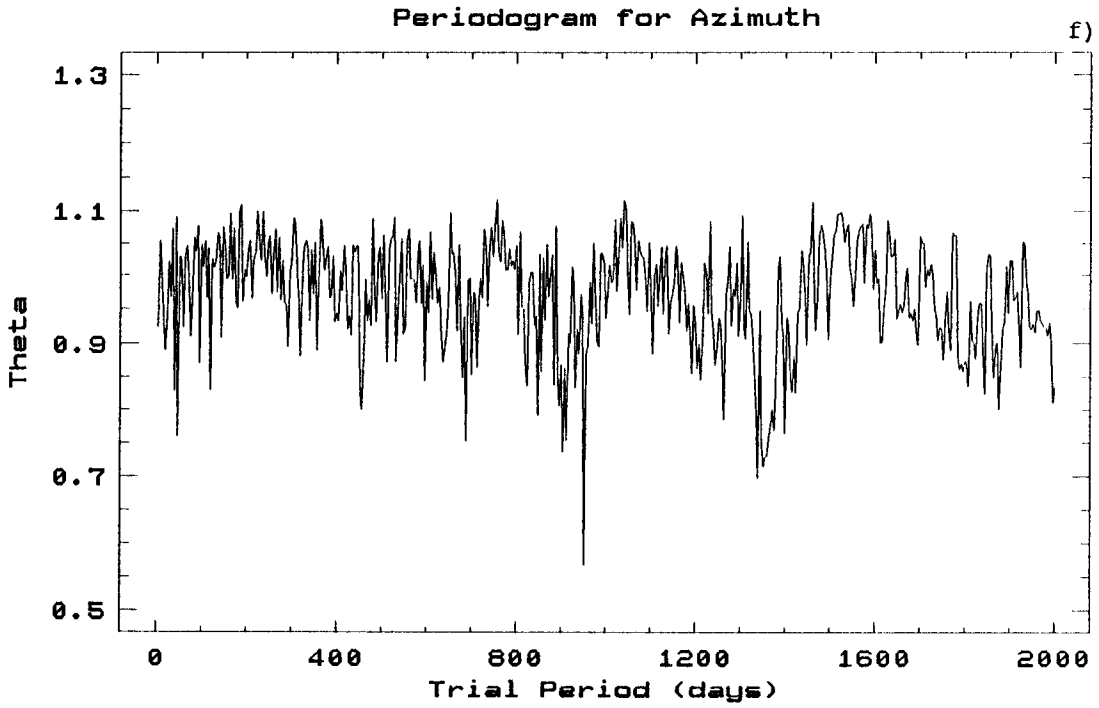

Figure 3.34

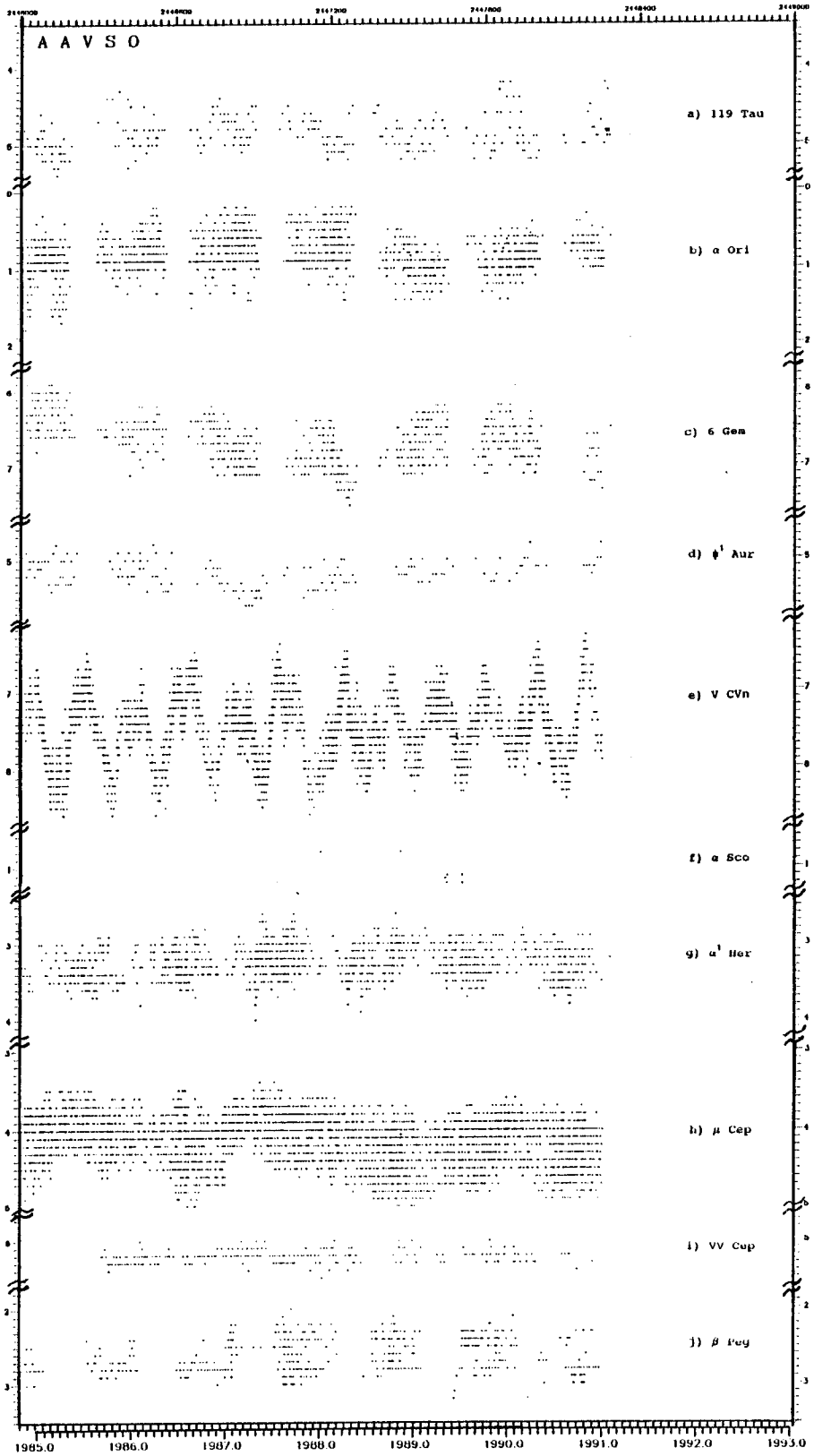
A A V S O
a) 119 Tau
b) α Ori
c) δ Gem
d) φ¹ Aur
e) V CVn
f) α Sco
g) α¹ Her
h) μ Cep
i) VV Cep
j) β Peg
1985.0
1986.0
1987.0
1988.0
1989.0
1990.0
1991.0
1992.0
1993.0

Figure 3.35

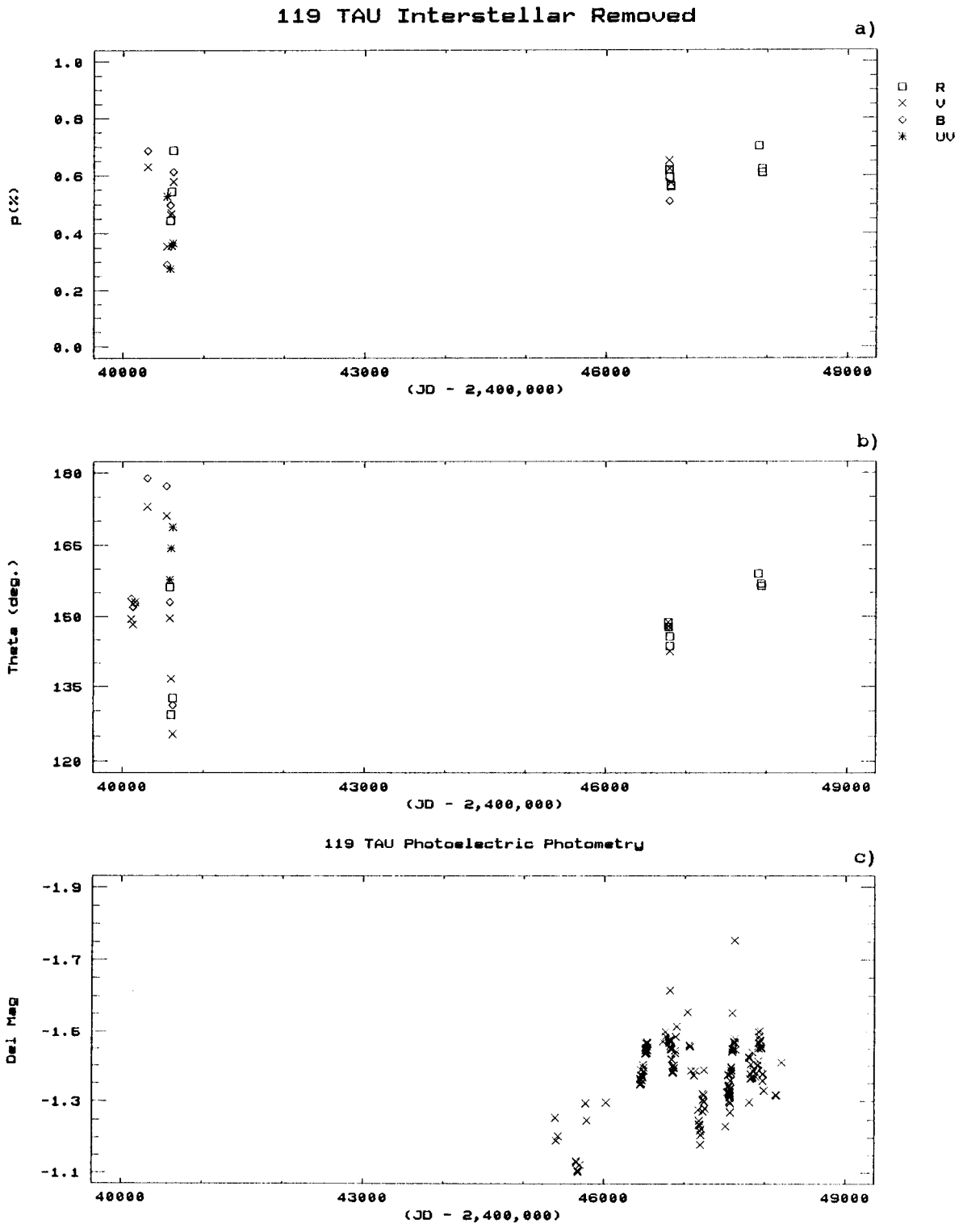
119 TAU Interstellar Removed
a)
p(%)
1.0
0.8
0.6
0.4
0.2
0.0
40000
43000
46000
49000
(JD - 2,400,000)
R
V
B
UV
b)
Theta (deg.)
180
165
150
135
120
40000
43000
46000
49000
(JD - 2,400,000)
119 TAU Photoelectric Photometry
c)
Del Mag
-1.9
-1.7
-1.5
-1.3
-1.1
40000
43000
46000
49000
(JD - 2,400,000)

Figure 3.36

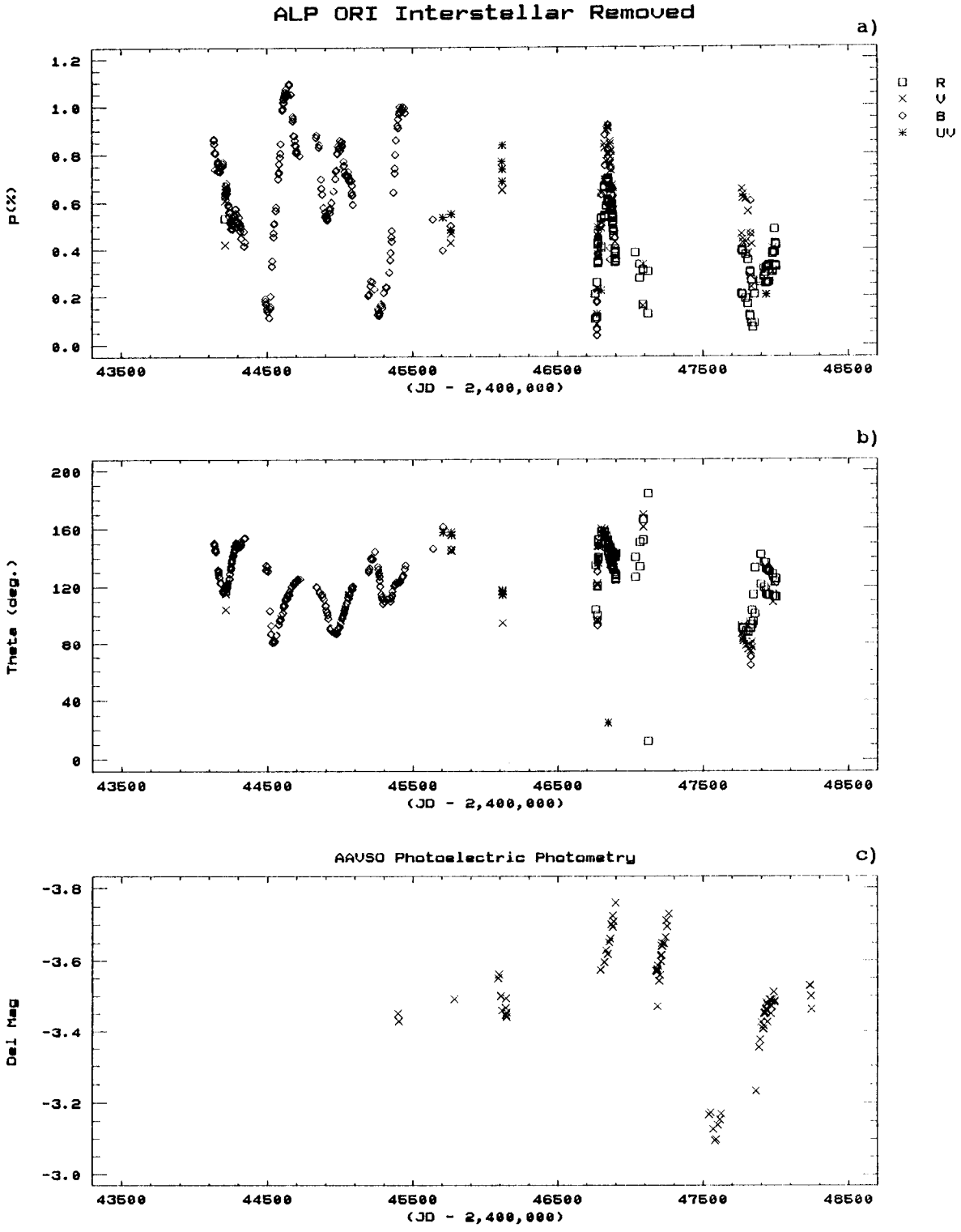
ALP ORI Interstellar Removed
a)
P(%)
1.2
1.0
0.8
0.6
0.4
0.2
0.0
R
V
B
UV
43500
44500
45500
46500
47500
48500
(JD - 2,400,000)
b)
Theta (deg.)
200
160
120
80
40
0
43500
44500
45500
46500
47500
48500
(JD - 2,400,000)
AAVSO Photoelectric Photometry
c)
Del Mag
-3.8
-3.6
-3.4
-3.2
-3.0
43500
44500
45500
46500
47500
48500
(JD - 2,400,000)

Figure 3.37

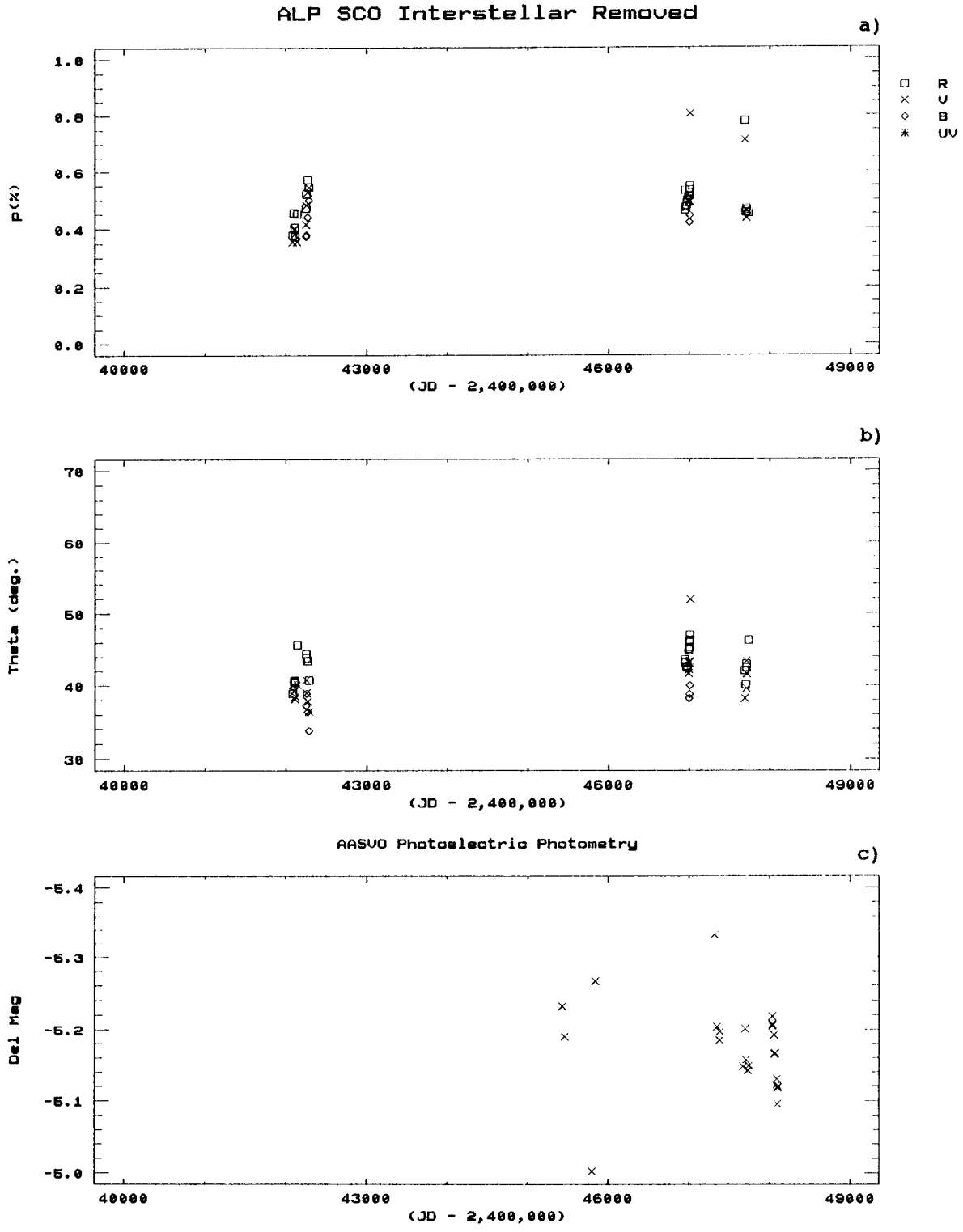
ALP SCO Interstellar Removed
a)
p(%)
1.0
0.8
0.6
0.4
0.2
0.0
R
V
B
UV
40000
43000
46000
49000
(JD - 2,400,000)
b)
Theta (deg.)
70
60
50
40
30
40000
43000
46000
49000
(JD - 2,400,000)
AASVO Photoelectric Photometry
c)
Del Mag
-5.4
-5.3
-5.2
-5.1
-5.0
40000
43000
46000
49000
(JD - 2,400,000)

Figure 3.38

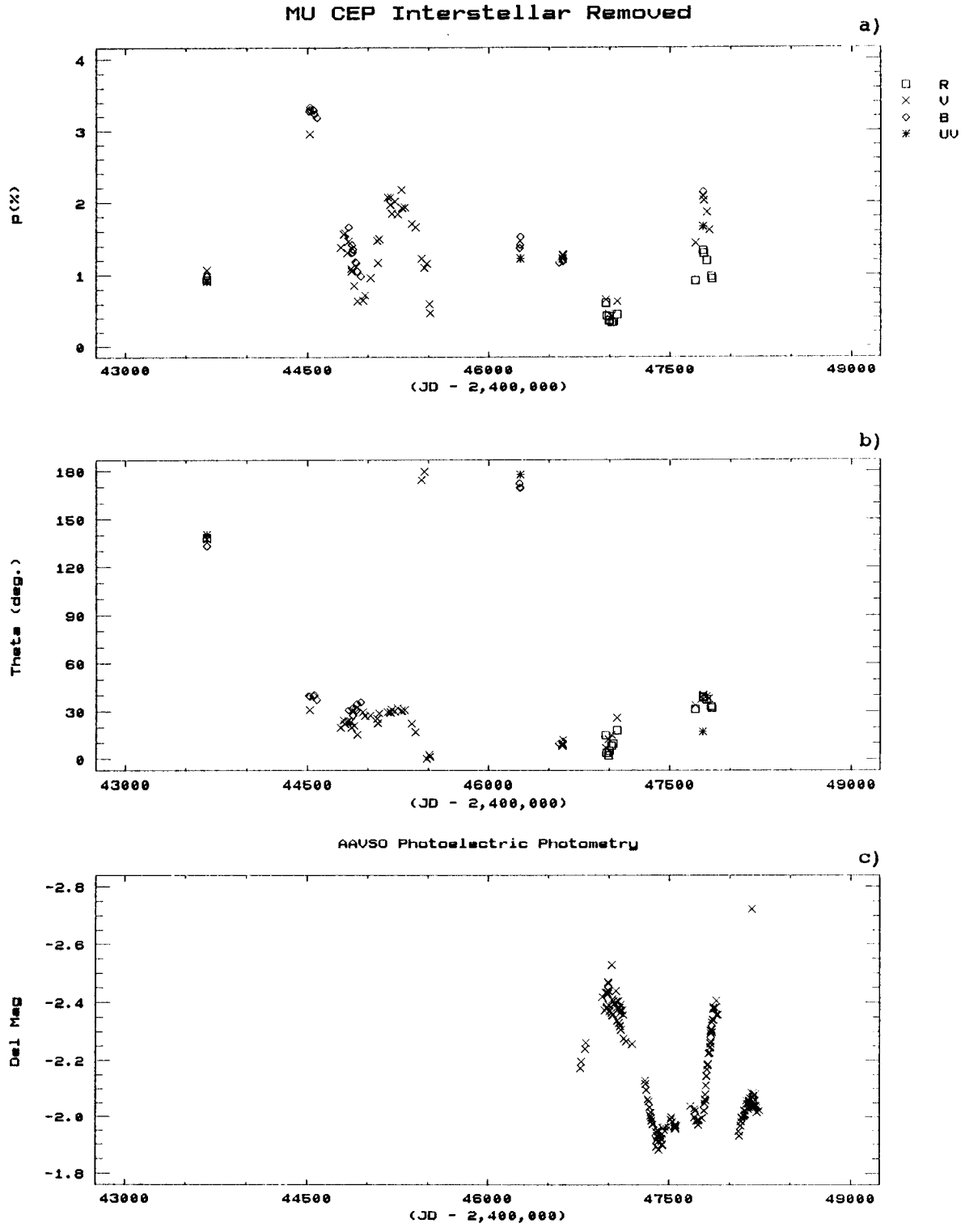
MU CEP Interstellar Removed
a)
p(%)
R
V
B
UV
(JD - 2,400,000)
b)
Theta (deg.)
(JD - 2,400,000)
AAVSO Photoelectric Photometry
c)
Del Mag
(JD - 2,400,000)

CHAPTER 4. Elliptical Polarization Sources

4.1 Massive Dust Shells

The extensive dust shells around most of the program objects should be strong scattering sources. Limiting number densities of the dust in local thermodynamic equilibrium (LTE) with respect to the thermal radiation field may be found from the large infrared excesses by assuming an optically thin shell (Busso *et al.* 1990). The flux density from an object is modelled by two blackbody components:

$$F_{obs,v} = F_{*,v} + F_{dust,v}$$

$$= \frac{2\pi h\nu^3 10^{-A_v/2.5}}{c^2 D_*^2}\left[\frac{R_*^2}{e^{h\nu/kT_e}-1} + \frac{\langle Q_{abs} N a_d^2\rangle}{e^{h\nu/kT_d}-1}\right], \qquad (4.1)$$

where T_e is the effective temperature of the photosphere, T_d is the effective dust temperature, D_* is the distance to the star, R_* is the radius of the star, N is the total number of grains, A_v is the interstellar extinction, a_d is the effective grain radius, and Q_{abs} is the ratio of the absorption cross-section to the geometric cross-section for a dust particle. The maximum dust temperature is less than 1200K (Collison and Fix 1991). Therefore, the photospheric temperature is a factor of three larger than the maximum dust temperature. As a result, dust produces little relative flux in the visible wavelength region. An estimate of the stellar angular radius is then given by:

$$\frac{R_*}{D_*} = \left[\frac{c^2 F_{obs,v} 10^{A_v/2.5}\,(e^{h\nu/kT_e}-1)}{2\pi h\nu^3}\right]^{1/2}, \qquad (4.2)$$

where $F_{obs,v}$ is the flux density measured in the V-bandpass, and A_v is the

corresponding extinction. Once we know the stellar angular radius, the total effective grain cross-section may be calculated from the flux density at long wavelengths:

$$\langle Q_{abs} N a_d^2 \rangle = \left[\frac{F_{obs} C^2 D_*^2 10^{A_\lambda/2.5}}{2\pi h\nu^3} - \frac{R_*^2}{e^{h\nu/kT_*}-1} \right] (e^{h\nu/kT_d}-1) . \qquad (4.3)$$

The total mass of the dust shell, M_d, may be calculated by:

$$M_d = \frac{4}{3}\pi a_d^3 N\rho = \frac{4}{3}\pi \frac{\langle Q N a_d^2 \rangle}{Q} a_d \rho , \qquad (4.4)$$

where ρ is the mean grain density. Mie theory gives (van de Hulst 1957) Q_{abs} for spherical particles:

$$Q_{abs} = -4x\, \Im \left[\frac{m^2-1}{m^2+2} \right], \qquad (4.5)$$

where $m = m' - im''$ is the complex index of refraction of the grain material, $\Im$ represents the imaginary part of the function following, and $x = 2\pi a_d/\lambda$ is the ratio of grain circumference to wavelength. Equation 4.5 gives Q_{abs}=0.1 for 0.05μm particles after assuming m = 1.65 - 0.1i at λ=0.54μm due to a dirty silicate mixture (Zellner 1971). Table 4.1 is a compilation of the dust shell masses for spherical particles for the program objects. The dust temperature used is 1000K, consistent with the work of Collison and Fix (1991). It should be pointed out that line-blanketing from molecules such as TiO reduces the stellar flux thus making the dust mass calculation a lower bound. Figure 4.1a through k shows the stellar flux densities from Table 3.4 dereddened using the extinction law

given by Rieke and Lebofsky (1985). Also shown on these figures are blackbody curves which are normalized to the V-bandpass.

It is immediately apparent that each of the program objects shows an infrared excess. V CVn and μ Cep show tremendous extra flux beyond 12 μm. In contrast, 119 Tau shows only a small excess. The V-bandpass black-body fitting is not good for α^1 Her since it has a close G companion and the visual flux is also affected by the common envelope. As a result, the fitting was performed for this star in the R-bandpass to correct, at least to some extent, for the extra absorption at shorter wavelengths.

4.2 Multi-Parameter Polarization Model

The general prerequisite for the net production of any type of polarization is asymmetry. For example, in LLTV studies, asymmetry can take the form of stellar spots, aligned irregularly-shaped grains, non-spherical scattering clouds, or binary companions. There is a limited set of mechanisms acting on this asymmetry which can produce linear and circular polarization in LLTVs.

Candidate mechanisms for the production of significant linear polarization in LLTVs are Rayleigh and Thompson scattering in the stellar atmosphere from the photosphere up to the dusty grain-forming region, and Mie and Rayleigh scattering in the dust envelope.

Possible mechanisms for circular polarization production include continuum magneto-opacity (also called grey Zeeman splitting), magneto-emission by oriented atoms, and linear birefringence from Mie scattering by circumstellar or interstellar dust on a systemic linear polarization.

A) Continuum Magneto-Opacity

Continuum magneto-opacity is a form of circular dichroism. This mechanism produces circular polarization from Zeeman splitting in a thermal field (Kemp 1970). The amplitude of the effect is characterized by the following relationship:

$$\frac{V}{I} \approx \frac{-eH\lambda}{4\pi m_e c^2}, \qquad (4.6)$$

where e is the electron charge, H is the magnetic field strength, λ is the wavelength of the observation, m_e is the electron mass. When H is expressed in gauss and λ is expressed in m, $V/I \approx 0.0047H\lambda$. Circular polarizations of 0.01% thus require a net stellar field of 40,000 gauss. Only the following three program stars were listed in Didelon's (1983) compilation of stellar magnetic field measurements: α Ori, α Sco, and VV Cep. All had fields less than 500 gauss. It is therefore apparent that this mechanism will be useful only if a star has a compact companion.

B) Magneto-Emission

Sunspots show a net circular polarization of the order of 0.1% as first discovered by Illing, Landman, and Mickey (1975). This is roughly two orders of magnitude larger than that expected from magneto-opacity. A plausible explanation is magneto-emission by atoms oriented in a magnetic field (Kemp and Henson 1983). The representative equation for a sunspot geometry is:

$$\frac{V}{I} \approx \frac{\beta eH\lambda}{8m_e c^2} \frac{\kappa}{\kappa+\kappa_\nu}, \qquad (4.7)$$

where κ is the Rosseland mean opacity, κ_ν is the spectral opacity, and β is a parameter of the model. H^- free-free absorption is the dominant opacity source at long wavelengths. Kemp and Henson concluded that β is about 8 for sunspots. Thus, for short wavelengths $V/I \propto \lambda$ and for long wavelengths $V/I \propto \lambda^{-1}$.

C) Scattering of Various Types

In general, scattering may be characterized by the following relationship (van de Hulst 1957):

$$\begin{bmatrix} E_l \\ E_r \end{bmatrix} = \begin{bmatrix} S_2 & S_3 \\ S_4 & S_1 \end{bmatrix} \frac{e^{-ikR+ikz}}{ikR} \begin{bmatrix} E_{lo} \\ E_{ro} \end{bmatrix}, \tag{4.8}$$

where the parallel wavefront travels along the $+z$ axis before being scattered at $z = 0$, and travels a distance R in the direction given by the cylindrical coordinates (θ,ϕ) after being scattered towards the observer. The subscripts l and r stand, respectively, for the components of the electric vector parallel and perpendicular to the scattering plane. The parameter k is the wave number. The elements of the scattering phase matrix, $\mathbf{S}(\theta,\phi)$, are usually complex numbers and depend upon the index of refraction of the scatterer and the wavelength of the incident light. However, for common particle types and materials, only form-dichroism and form-birefringence are important, thus $S_3 = S_4 = 0$ (van de Hulst 1957). These cross terms can be important in the interstellar medium where the optical depth is large (Serkowski 1962, Chlewicki and Greenberg 1990) or for special particle shapes (Bandermann and Kemp 1973, Schmidt 1972).

The plane parallel wavefronts for the incident and scattered electric vectors may be expressed in the general form:

$$\begin{aligned} E_{lo,ro} &= a_{lo,ro} e^{-i\epsilon_{lo,ro}-ikz+i\omega t}, \\ E_{l,r} &= a_{l,r} e^{-i\epsilon_{l,r}-ikR+i\omega t}, \end{aligned} \tag{4.9}$$

where the a coefficients are the positive real amplitudes, and the ϵ coefficients are the respective phases. The components of the Jones vector may be used to calculate the Stokes vectors as follows:

$$
\begin{aligned}
I &= E_l E_l^* + E_r E_r^* = a_l^2 + a_r^2, \\
Q &= E_l E_l^* - E_r E_r^* = a_l^2 - a_r^2, \\
U &= E_l E_r^* + E_r E_l^* = 2a_l a_r \cos(\epsilon_l - \epsilon_r), \\
V &= i(E_l E_r^* - E_r E_l^*) = 2a_l a_r \sin(\epsilon_l - \epsilon_r),
\end{aligned}
\tag{4.10}
$$

where * stands for the complex conjugate operation.

Substituting Equations 4.8 and 4.9 into the preceding V equation yields the general condition:

$$
a_{lo} a_{ro} \left[\Im(S_2 S_1^*) \cos(\epsilon_{ro} - \epsilon_{lo}) + \Re(S_2 S_1^*) \sin(\epsilon_{ro} - \epsilon_{lo}) \right] \neq 0, \tag{4.11}
$$

in order to scatter circular polarization. Three important conclusions may be made by using this equation. 1). If either a_{lo} or a_{ro} vanish, due to the incident electric vector being either parallel or perpendicular to the scattering plane, the circular polarization is zero regardless of the type of scatterer. 2). This equation must be averaged for incoherent light. Random incident phases yield: $\langle \sin(\epsilon_{ro} - \epsilon_{lo}) \rangle = \langle \cos(\epsilon_{ro} - \epsilon_{lo}) \rangle = 0$. Thus, the incident light must be polarized to produce circular polarization. 3). Linear polarization produces circular polarization from the imaginary term of the scattering phase term product. This means that the S matrix terms must not be all real or all imaginary.

For Rayleigh and Thomson scattering (van de Hulst):

$$
\begin{aligned}
S_1(\theta) &= ik^3\alpha + \frac{2k^6\alpha^2}{3}, \\
S_2(\theta) &= \left(ik^3\alpha + \frac{2k^6\alpha^2}{3} \right) \cos\theta,
\end{aligned}
\tag{4.12}
$$

where:

$$\alpha_{Rayleigh} = \frac{m^2 - 1}{3} a_d^3,$$
$$\alpha_{Thomson} = -\frac{e^2}{m_e \omega^2}, \tag{4.13}$$

where m_e is the electron mass, and $\omega = kc$. The imaginary term of Equation 4.9 is zero and thus Rayleigh and Thomson scattering can transfer but not produce circularly polarized light. A complex index of refraction in Equation 4.13 does not change this result. Use of Equations 4.12 and 4.13 in Equation 4.10 shows the familiar results that the scattered intensity does not depend upon k for Thomson scattering and is proportional to k^4 for Rayleigh scattering.

The coefficients for scattering from a sphere of arbitrary size are (van de Hulst; Lang 1980):

$$S_1(\theta) = \sum_{n=1}^{\infty} \frac{2n+1}{n(n+1)} [a_n \pi_n(\cos\theta) + b_n \tau_n(\cos\theta)],$$
$$S_2(\theta) = \sum_{n=1}^{\infty} \frac{2n+1}{n(n+1)} [b_n \pi_n(\cos\theta) + a_n \tau_n(\cos\theta)], \tag{4.14}$$

where:

$$\pi_n(\cos\theta) = \frac{1}{\sin\theta} P_n^1(\cos\theta),$$
$$\tau_n(\cos\theta) = \frac{d}{d\theta} P_n^1(\cos\theta), \tag{4.15}$$

and a_n and b_n are the usual Mie coefficients for a sphere (and are dependent

upon m), and P^1_n is the first associated Legendre function of order n. Equations 4.14 and 4.15 may be used along with the properties of the associated Legendre function back in Equation 4.11. The phase difference between S_1 and S_2 depends upon the Mie coefficients, a_n and b_n, which, in general, are functions of mx. It emerges that metallic particles are more likely than dielectric particles of the same size to produce detectable circular polarizations since the metallic indices of refraction are generally larger. However, if mx is $<<1$, then the Rayleigh domain is entered and no circular polarization can be produced.

A coordinate renaming is needed to express conveniently the phase coefficients for scattering from a long ($L_c >> \lambda$) circular cylinder. Let the light be moving in the $+z$ direction, and the long axis of the cylinder be along the x axis. The scattering plane is defined to be perpendicular to the cylinder. The scattering phase terms are (van de Hulst):

$$S_{1,2}(\theta,\phi) = \frac{2}{\pi\phi} \sin\left(\frac{kL_c\phi}{2}\right) T_{1,2}(\theta), \tag{4.16}$$

where θ is the longitude of the scattered light and ϕ is the latitude measured with $+x$ being the polar axis, and:

$$\begin{aligned} T_1(\theta) &= c_o + 2\sum_{n=1}^{\infty} c_n \cos n\theta, \\ T_2(\theta) &= d_o + 2\sum_{n=1}^{\infty} d_n \cos n\theta. \end{aligned} \tag{4.17}$$

Here, c_n and d_n are the Mie coefficients for a circular cross-section cylinder. These coefficients are also functions of m. Equation 4.11 is usually satisfied for most orientations.

Realistic components of a multi-parameter model for the polarization

from the program objects are therefore:

1. Thomson and Rayleigh scattering in the atmosphere of the LLTV (produces linear polarization). Candidate light sources are stellar spots and radiation from nearby companions.
2. Magneto-emission from stellar spots (produces circular polarization).
3. Mie scattering from spherical and irregularly shaped grains in the circumstellar dust environment (produces linear and circular polarization). A constraint exists in that the number of scatterers may be restricted by the IR excess (Section 4.1).
4. Interstellar birefringence (produces circular polarization). Note that the interstellar linear polarization was removed from the observations in Chapter 3.

The multi-parameter model does not explicitly include Mie scattering in an extended asymmetric dust envelope (Zellner 1971, Shawl 1975a) since the time scales for the variability of the linear and circular polarizations of the program objects are typically less than one hundred days. This implies that the source of the light and/or scatterers is probably close to the star. An asymmetric dust envelope results in certain latitudes and longitudes producing more scattering. This type of enhanced scattering is a natural result of an asymetric light source. The asymmetric dust shell hypothesis is further discussed along with the program objects in Section 4.4.

A Jones vector transfer equation for the multi-parameter model is then:

$$\begin{bmatrix} E_l \\ E_r \end{bmatrix} = R(-\phi_i) \begin{bmatrix} e^{-i\delta/2} & 0 \\ 0 & e^{+i\delta/2} \end{bmatrix} R(\phi_i) \begin{bmatrix} M_2(\theta) & M_3(\theta) \\ M_4(\theta) & M_1(\theta) \end{bmatrix}_C \begin{bmatrix} E_{lo} \\ E_{ro} \end{bmatrix}, \qquad (4.18)$$

where δ is the interstellar linear birefringence, the C-subscripted matrix is explained below, and the rotator matrix, $R(\phi)$, is given by:

$$R(\phi) = \begin{bmatrix} \cos\phi & \sin\phi \\ -\sin\phi & \cos\phi \end{bmatrix}. \tag{4.19}$$

Choices for ϕ_i include configurations both parallel and perpendicular to the interstellar electric vector. Figure 4.2 is a diagram of the scattering geometry. The $M(\theta)$-scattering phase matrix (C) for multiply-scattered light is the following product of the dust (D) and the Rayleigh and Thomson (RT) scattering phase matrices:

$$\begin{bmatrix} M_2(\theta) & M_3(\theta) \\ M_4(\theta) & M_1(\theta) \end{bmatrix}_C = \frac{-1}{k^2} R(\phi_{D'}) \begin{bmatrix} S_2(\theta_D) & 0 \\ 0 & S_1(\theta_D) \end{bmatrix}_D R(\phi_D) R(\phi_{RT'}) \begin{bmatrix} S_2(\theta_{RT'}) & 0 \\ 0 & S_1(\theta_{RT}) \end{bmatrix}_{RT} R(\phi_{RT}) , \tag{4.20}$$

where the angles, ϕ, are measured clockwise as seen by the observer with respect to the local North on the viewing sphere (the sphere centered on the object with a radius equal to the distance to the object). An additional rotation of the dust component of Equation 4.20 is needed for scattering off aligned cylinders. Note that the inverse dependence upon distance depicted in Equation 4.8 drops out if Equation 4.18 is used for flux determinations which are made per unit solid angle.

The incident electric vector in Equation 4.18 is represented by the following:

$$\begin{bmatrix} E_{lo} \\ E_{ro} \end{bmatrix} = a_{v,rms} \begin{bmatrix} \zeta_1 e^{i\epsilon_1} + \gamma e^{-i\eta/2} \\ \zeta_2 e^{i\epsilon_2} + \gamma e^{+i\eta/2} \end{bmatrix}, \tag{4.21}$$

where $a_{\nu,\mathrm{rms}}$ is the root-mean-square amplitude of the electric vector found from Planck's blackbody function, $\epsilon_{1,2}$ are uniformly distributed random numbers on the interval $[0,2\pi]$, $\zeta_1 = \sin(\iota)$ and $\zeta_2 = \cos(\iota)$ where ι is a uniformly distributed random number on the interval $[0,2\pi]$ in order to preserve the overall amplitude, η equals $+\pi/2$ for right circular polarization and $-\pi/2$ for left circular polarization, and γ parameterizes the degree of magneto-emission and is assumed to be about 0.03 in the vicinity of an LLTV stellar spot.

Equation 4.18 was integrated over a model LLTV environment using a Monte Carlo technique. The integration was accomplished over all scattering directions simultaneously. The output is a polarization map showing what an observer would see when looking at the system from any direction. A schematic diagram of the multi-parameter model over which the integration was accomplished is illustrated in Figure 4.3. There are essentially four layers in this model. The first layer contains the spherical photosphere and any circular bright or dark spots desired. The next layer is the Rayleigh and Thomson scattering layer. This assumed spherical layer is considered to be thin in comparison to the radius of the star. Flux may be lost back into the star after scattering in this layer. The third layer contains either spherical or cylindrical dust scatterers. The orientation of the cylinders is a free parameter. This assumed spherical dust layer is considered to be large with respect to the radius of the star. The outer layer contains the interstellar medium. Here, birefringent dust grains act upon the intrinsic stellar polarization.

The optical depth at any one layer was calculated from the product of the scatterer cross-section, number density, and path length. The scatterer cross-section was calculated from the fundamental extinction formula (van de Hulst; Jackson 1975):

$$C_{ext} = \frac{4\pi}{k^2}\,\Re(S(0)). \qquad (4.22)$$

An alternate constraint for the dust layer was calculated in Section 4.1. The ratio of the quantity $\langle QNa^2 \rangle$ found in Table 4.1 to the square of the dust shell radius gives an approximate optical depth.

A free parameter of the photosphere containing layer is the limb darkening. A linear limb darkening law of the form $1-\mu(1-\cos\theta)$ was used.

The software and implementation notes are included in Appendix H. Section 4.3 contains representative polarization maps relevant to the program objects.

A form-created index of refraction is represented as follows (van de Hulst):

$$m_{1,2} = m'_{1,2} + im''_{1,2} = 1 - i2\pi Nk^{-3}S_{1,2}(0), \qquad (4.23)$$

where N is the particle number density. A further constraint on the model is that the difference in the components of the complex indices of refraction for the grain material must satisfy the Kramers-Kronig dispersion relationships (Shapiro 1975, Chlewicki and Greenberg 1990):

$$\Delta m'(\omega) = \frac{2}{\pi}\int_0^\infty \frac{\omega'\Delta m''(\omega')}{\omega'^2 - \omega^2}\,d\omega' , \qquad (4.24)$$

and

$$\Delta m''(\omega) = \frac{-2\omega}{\pi}\int_0^\infty \frac{\Delta m'(\omega')}{\omega'^2 - \omega^2}\,d\omega' . \qquad (4.25)$$

where the delta corresponds to the difference between the index components 1 and 2. These constraints put a strong wavelength constraint on the

optical material when there exists an isolated linear polarization maximum. Specifically, the wavelength of maximum linear polarization must occur near the zero crossing of the circular polarization.

4.3 Representative Model Output

The error of a determined quantity from a Monte Carlo integration decreases as the square root of the number of test points. Daniel (1978) found that 20,000 test points (photons) were needed for determination of a polarization parameter with an error of 8%. In the present case, the viewing sphere has been broken down into 15 divisions in longitude (0° to 360°) and 7 divisions in latitude (-90° to +90°). It was found that as many as 10,000,000 random test points (flux vectors) are needed to produce a useful map. On the present Motorola 80386-based computer with a 80387 coprocessor, each map must be integrated for ten hours. A critical requirement for Monte Carlo integration is a uniform random number generator. The Microsoft C version 6.1 rand() function was used in an arrangement that does not degenerate unless more than 2.4×10^9 flux vectors are used. It was found for 10,000,000 flux vectors, in the absence of scattering and magneto-emission, that there was produced 0.n% polarization in all Stokes vectors, where n is on the order of one or two. However, at high latitudes the noise is a factor of three larger due to the map projection. An additional check of randomness may be made by examining polarization maps for symmetry when required by the underlying physical processes. A reasonable degree of symmetry was found to exist in the produced maps.

The specific quantities that can be varied in the present multi-parameter polarization model are:

λ	Wavelength of light,
N_m	Number of Monte Carlo flux vectors,
μ	Limb darkening coefficient,

F_r	Ratio of stellar spot emittance (radiant exitance) to average photospheric emittance,
Lat,Long	Latitude and longitude of stellar spot,
θ_{sp}	Angular radius of spot,
γ	Spot magneto-emission from Equation 4.21,
αk^2	Rayleigh/Thomson factor from Equation 4.12,
L_{RT}	Thickness of Rayleigh/Thomson layer around photosphere,
N_{RT}	Number density of Rayleigh/Thomson scatterers,
MieType	Type of dust: cylinders or spheres,
$<QNa_d^2>$.	Dust quantity defined in Section 4.1,
R_*	Radius of star from Table 4.1,
R_r	Ratio of dust shell radius to stellar radius,
ϕ_c	Cylinder orientation with respect to local North discussed with Equation 4.20,
L_c	Length of cylinders from Equation 4.16,
δ	Interstellar phase retardence from Equation 4.18,
ϕ_i	Interstellar orientation with respect to North from Equation 4.18,
<Mie coeff>	The Mie coefficients data file.

The software requires that all quantities be specified in cgs units, except L_c and λ which are expressed in μm and angles which are expressed in radians. A number of trial cases follow. Not all parameters are equally unconstrained. The specific parameter values used are included below. However, N_m values are specified in the figure captions. Common parameters for all of the cases are: $\lambda = 0.54\mu m$, $\mu = 0.8$, and $R_* = 5.55 \times 10^{13} cm$. Locations on the maps are referenced by latitude and longitude in the form: (*Lat*, *Long*).

CASE 1: Figure 4.4a through d represents test maps of a small (θ_{sp} = 0.5 radian), bright spot (F_r = 1.8) on the equator of the model star (0°,180°) with no Mie scattering or magneto-emission. A relatively high

scatterer (electrons) density was used ($\alpha k^2 = 2.8\text{x}10^{-13}$cm, $L_{RT} = 5.0\text{x}10^{+12}$cm, $N_{RT} = 1.0\text{x}10^{+11}$) resulting in $\tau = 0.81$. The maps show a geometrically circular linear polarization ridge circling the spot. There are $+q$ Stokes vector ridges centered at longitudes 90° and 270°. At high latitudes near 180° longitude there are strong $-q$ zones. There are $+u$ Stokes vector regions centered at (+60°,135°) and (-60°,215°), and there are $-u$ Stokes vector regions centered at (-60°,135°) and (+60°,215°). The only circular polarization seen is noise at high latitudes. These maps are more realistic than produced by Clarke and Schwartz (1984) since their spots had square corners. The present model incorporates limb darkening and is thus more relevant to LLTVs than are the numerical simulations by Lefèvre and Daniel (1988).

CASE 2: Figure 4.5a through d shows test maps of a small, bright spot on the equator of the star (same parameters as for Case 1) with no Mie, Rayleigh or Thomson scattering, but with much magneto-emission ($\gamma = 0.1$). The maps show that no linear polarization is generated, but that circular polarization generation is maximum over the spot. Note that the circular polarization is of a single sign.

CASE 3: Figure 4.6a through d shows test maps which are the reverse of Case 1. Here, there is a large ($\theta_{sp} = 1.0$ radian), dark spot ($F_r = 0.7$) on the equator (0°,180°). The other parameters are the same. The model integrations indicate that little net polarization accumulates. This result is consistent with the observations by Elias and Dorren (1990) of the spotted, young, solar-like star HD 129333.

CASE 4: Figure 4.7a through d shows test maps of a small, bright spot on the equator of the star (same parameters as for Case 1) with no Rayleigh and Thomson scattering, or magneto-emission, but with high levels of Mie scattering from newly formed, small ($a_d = 0.05\mu$m), spherical, clean silicate grains ($m = 1.5$). The other parameters are $\langle QNa_d^2 \rangle = 5.0\text{x}10^{28}$ cm^2 and $R_r = 10.0$ which result in $\tau = 0.45$. The maps show that the linear polarization generated is similar to the one generated in Case 1. Since

the dust shell radius is large, linear polarization is now seen on the far side of the star in a pattern which is similar to that seen on the front of the star. No net circular polarization is generated.

CASE 5: Figure 4.8a through d depicts test maps for a situation identical to Case 4, except that the spherical grains are larger (a_d = 0.1μm) and have a dirty-metallic character (m = 3.4 - 1.9i). The maps show that very little linear and circular polarizations are generated since the scattering efficiency for the particles is small.

CASE 6: Figure 4.9a through d was generated the same way as for Case 4, except that there is Mie scattering from metallic cylinders (m = 1.4 - 1.4i, L_c = 1.0μm), not spheres. The long axes are perfectly aligned with meridians of longitude (ϕ_c = 0.0). The cylinders have radii of a_d = 0.034μm. The maps are not unlike those seen for Case 1. However, the sign of the linear stokes vectors is inverted since the extinction is greater along the meridians of longitude. Also, the regions of -q are more extensive than the regions of +q seen in Case 1.

CASE 7: Figure 4.10a through d depicts test maps for a situation identical to Case 6, except that the cylinders are larger (a_d = 0.11μm). The maps show that very little linear and circular polarizations are generated since the particles are near the polarization reversal size of a_d = 0.10μm.

CASE 8: Figure 4.11a through d shows test maps of a medium sized (θ_{sp} = 0.8 radian), bright spot (F_r = 3.0) on the equator of the model star (0°,180°) with no magneto-emission. A relatively high Rayleigh/Thomson scatterer density was used (as in Case 1 except that N_{RT} = 2.0x10^{+11}) resulting in τ_{RT} = 1.37. There is also Mie scattering from cylinders which are not aligned with meridians of longitude (the same parameters as for Case 6 except that ϕ_c = +π/3, $\langle QNa_d^2 \rangle$ = 5.0x10^{29} cm^2 and τ_{Mie} = 1.35). The maps show that the linear polarization produced by the two scattering components produce lots of linear polarization in a pattern which is similar to the pattern seen for Case 1. Some circular polarization is

generated at ±45° orientations to the polar axis, as is predicted by Equation 4.11.

CASE 9: The maps presented in Figure 4.12a through d represent a situation which is similar to Case 1. However, somewhat more extensive linear polarization is generated, but the amplitude is smaller, because the spot is brighter (F_r = 3.0), and the Rayleigh/Thomson number density is larger ($N_{RT} = 2.0 \times 10^{+11}$, τ = 1.37). Also, there is a large interstellar birefringence (δ = 0.6) which is not aligned with respect to North ($\phi_i = +\pi/4$). The maps show circular polarization conversion where the q Stokes vector is large. An important recognition of this type of polarization conversion is that the circular polarization must return to the same value when the underlying linear polarization returns to the same value. Also, a similar conversion to circular polarization would occur if the underlying linear polarization mechanism is Mie scattering. Interstellar birefringence can also act upon the interstellar instead of the intrinsic linear polarization. This has the effect of adding a constant v Stokes vector offset to the observed polarization. This effect is removed by the use of Equation 3.2.

The maps may be interpreted in three important ways. First, the maps were constructed such that the stellar rotation axis is parallel to the North-South axis on the viewing sphere at zero latitude on the maps. Thus, a parallel of latitude (a horizontal, East-West line) represents what should be observed polarimetrically as the star rotates if the rotation axis is tipped towards or away from the observer by an angle given by the latitude on the map. Second, the meridians of longitude represent the inverse situation where the star rotates with its axis parallel to the East-West direction on the viewing sphere. Tracing the meridian of zero (and 180°) longitude (a vertical, North-South movement) represents the star rotating with its axis perpendicular to the line of sight. Tracing a different meridian of longitude represents what one observes if the surface features such as spots are rotated (not the rotation axis) on the surface

by the indicated longitude. Third, since the rotation axes of the program objects are probably inclined with respect to the North-South and East-West orientations on the viewing sphere, one must consider chords which not only follow meridians of longitude or parallels of latitude, but are also small or great circles (arcs) on the maps. For example, if the stellar spot is actually at the pole of the star and the spot is indicated as being at (90°,180°) on the maps, then the maps need to be rotated about the spot center. In other words, the observed polarization behavior seen for the star as it rotates will actually be represented on the map by a small circle which has its center coincident with the spot center.

Maps which are more complicated than those generated for the nine cases described above may be made in certain circumstances without additional integration. This can be done by horizontally offsetting the maps made for a particular case and then adding the Stokes vectors. For instance, in Case 1, a two-spot group with a certain latitude or longitude difference may be simulated by duplicating the maps for Case 1, overlaying them offset by the spot separation, and then adding the Stokes vectors. Adding maps for different cases is usually not possible. However, in certain cases when multiple scattering is small, maps for different cases may be added.

The trial cases represent the richness of the polarimetric behavior a systemic environment. Most of these maps are invoked in more detail in the next Section with regard to the observed polarizations from the program objects.

4.4 Discussion on the Program Objects

None of the program objects produces polarimetric behavior which is identically matched by any single Case from Section 4.3. However, a measure of understanding of the stellar systems may be realized by consideration of the program objects in light of the physical predictions for the Cases expressed by the maps.

Rotational *V*sin*i* velocities are not available for the program objects and are not well known in the upper right-hand corner of the HR diagram. However, Kraft (1960) suggests that the equatorial rotational velocities for M giants through supergiants should be on the order of 5 km/sec. This represents a period of 600 days for the smallest star (72 Leo) and 11,000 days for the largest star (μ Cep). This also implies, for most program objects, that less than one full rotation has been covered by the interval of new observations. It is likely that the spread in rotational velocities for the program objects is between 2 km/sec to 10km/sec. The resulting error in the periods is probably +100% and -50%.

Schwarzschild (1975) obtained a value of 200 days for the time-scale of variation due to convection in the outer layers of giants and supergiants and reasoned that about a dozen convection cells occupy the surface of a giant at any given epoch. He concluded that fewer than 90 cells occupy the surface of a supergiant at one time.

(a) 119 CE Tau

The R-bandpass polarization observations on this star extend 1,157 days for the new elliptical polarization data, and about 7,400 days for the bulk of the total (archival plus new) linear polarization data. The new and total data sets correspond, respectively, to about 90° and 660° (1.8 times around, but with a 6000 day, 540° gap) on the polarization maps since the period of rotation is ~4,000 days. Detail from the polarization maps for Cases 1, 4, 6, 8, and 9 around 90° and 270° longitude and mid-latitudes have variations sufficient to match the observations. The Table 3.2 polarization spectral-index entries for this star are zero within their errors thus giving an indication that Thomson scattering is the likely polarization mechanism. This scattering source is consistent with the calculations found in Table 4.1 and shown in Figure 4.1d since the relatively tiny mass of the dust shell indicates that extensive Mie scattering is not likely. Thus, the maps from Cases 4 and 6 may be

excluded. The fast time scales of large-amplitude polarization variability (about 60° of rotation on Figure 1.3) are further evidence for a localized, atmospheric cause, although longer time-scales (≈ 1,000 days) of variability are also apparent in Figure 3.11. The Case 1 and 8 polarization maps are thus clearly applicable here. The *v* Stokes vector data are noisy but are seen to be close to zero thus possibly indicating that the polarization arises from an asymmetric electron cloud distribution or from a bright photospheric region and not from a stellar dark spot. The small amount of circular polarization could be produced in the feeble dust shell, but this is only possible with Case 8 since circular polarization produced by interstellar birefringence (Case 9) requires the circular polarization to return to the same value if the linear polarization repeats. Between the first and second data sets of Figure 3.11 the distribution concentration or photospheric brightening apparently changed location since the *q* Stokes vector is much larger in the second group of data. The atmospheric identification is consistent with the archival data shown in Figure 1.3a and b for which a steep polarization spectra is not present.

(b) α Ori

α Ori has been observed over an interval spanning 1,246 days in the R-bandpass for the present study, and about 7,800 days in the V-, and B-bandpasses for the majority of the total (archival plus new) linear polarization data. The new data and total data sets correspond, respectively, to about 45° and 360° (once around) on the polarization maps since the period of rotation is ~8,000 days. None of the maps shows linear polarization variations with a high enough frequency to match the observations shown in Figures 1.4 and 3.12 due to stellar rotation alone. Therefore, the variation must result at least in part from non-radial pulsation or multiple bright regions or from fast formation and decay of single bright regions. The maps for Cases 1, 4, 6, 8, and 9 have

sufficient high-frequency detail near 90° and 270° longitude and mid-latitudes to have a degree of variability which matches the observations over 45° of rotation if there exist at least two or more asymmetry sources. Further, the multiple extrema seen on Figure 3.12a, b and c indicate that the maps for Case 2 may be excluded unless there are multiple magneto-emission sources operating simultaneously.

The linear polarization spectral indices for this star are small and are typically between zero and minus one. This evidence alone tends to implicate Thomson scattering in the stellar atmosphere and some Mie scattering in the envelope, and thus excludes Cases 4 and 6. The evidence given in Table 4.1 indicates that the dust shell is massive. The time-scale of variability seen in the new data tends to indicate a light source and/or polarization mechanism that is near the stellar atmosphere. Tinbergen, Greenberg and de Jager (1981) observed a much more negative spectral index which they ascribed to Rayleigh scattering. The spectral indices for their data seen in Table 3.2 (JD 2,442,282 - 2,444,213) were recalculated with the interstellar polarization vector determined in Section 3.2 removed. Their Rayleigh scattering conclusion is untenable in light of the new indices. Magalhães *et al.* (1990) measured bands caused by TiO absorption in their single, high-resolution polarization spectrum of α Ori. These bands were interpreted as an indication that the polarization was generated from light from a small stellar spot or from ejecta near the photosphere. Schwarz and Clarke (1984) interpreted TiO lines from the Tinbergen, Greenberg and de Jager data as arising from a layer of Rayleigh scatterers above the photosphere.

The periodograms shown in Figure 3.30a and d show weak, but broad, dips near 400 and 800 days for the linear polarization parameter. However, the periodogram for the azimuth parameter seems to show only the 400 day dip. Smith, Patten, and Goldberg (1989) and Smith (1990) reported a 420 day pulsation from radial velocity observations of metallic lines plus Hα. Also, Dupree, *et al.* (1987 and 1990) favor a 420 day pulsational period as

the explanation for the MgII emission line flux variations. It is therefore felt that the 800 day period is an artifact of the 400 day period in the polarization data and that the linear polarization arises from asymmetry due to non-radial pulsation. This conclusion is not inconsistent with the hot region model presented by Doherty (1986) since the hot regions could be caused by non-radial pulsation. The conclusion is inconsistent with the convection cell identification made by Hayes (1984) since convection cells presumably would not produce a regular period. The 2.08-year (759 day) period found by Karovska, Nisenson, and Noyes (1986) in the B-bandpass data of Hayes must be an artifact. The Karovska, Nisenson, and Noyes binary companion hypothesis must be false since a companion with a 400 day period, instead of 759 days, would have to be 35 percent closer at periastron and would be within the photosphere of the supergiant. Figure 4.13a and b shows all of the B-bandpass data (new plus archival) phased with a 400 day period. Figure 4.14a and b shows the same data phased with an 800 period. It is apparent from Figure 4.14b that the 800 day period is twice the actual period. The relationship between the linear polarization and light seen in Figure 3.36 is not inconsistent with the non-radial pulsation interpretation since neither maximum nor minimum light coincide with linear polarization extrema on the polarization maps.

The v Stokes vector signal is about fifty times smaller than the linear polarization signal. The linear and circular polarizations are seen to vary on a similar time-scale, but they are not in phase. The first group of data (around JD 2,446,800) seen in Figure 3.12c are explainable by the Case 2 maps if a two-spot group (North and South polarity) were the cause of the asymmetry. The second group of data (centered about JD 2,447,900) could be explained by a larger single spot. The spot-related identification is foiled, however, by the wavelength dependence of the circular polarimetry. It is seen in Figure 3.12c, i, and o that the data are antisymmetric with wavelength, whereas the circular polarization should, for Case 2, be of a single polarity. Therefore, the situation for

the circular polarization is consistent with the linear polarization since the light asymmetry probably arises near the photosphere due to a non-radial pulsation and the bulk of the circular polarization probably arises due to Mie scattering in the dust envelope from linearly polarized light (consistent with Case 8). Le Borgne, Mauron, and Leroy (1986) found no departure at the 10% level from spherical symmetry in the dust shell at 10" in the U-bandpass. A small (0.01%) interstellar circular polarization offset would eliminate the circular polarization spectral objection to magneto-emission (Case 2). However, interstellar birefringence would have to operate on the intrinsic linear polarization as well as on the interstellar linear polarization. Interstellar birefringence fails to explain the observations because the observed circular polarization does not return to the same value when the linear polarization returns to the same point (Case 9). Since the massive dust shell of α Ori does not produce much net polarization, it is likely that the average dust grain may be metallic or its size may be near the point where polarization reversal takes place (Cases 5 and 7). The Shafter and Jura (1980) prediction about the circular conversion efficiency in the circumstellar shell under ideal conditions is confirmed. However, their prediction of 0.005% at 15" is about half the value observed from direct stellar light.

(c) 6 BU Gem

The new R-bandpass elliptical polarization observations of this star extend over an interval of 1,170 days, and the majority of the total (archival plus new) linear polarization data extends about 7,600 days in the V-, and B-bandpasses. The new data and total data sets correspond, respectively, to about 90° and 340° (almost once around, but with a 6,100 day, 270° gap) on the polarization maps since the star is about the same size as α Ori and has a rotation period of ~8,000 days. The shifts in polarization over the intervals of observations seen in Figures 1.5 and 3.13d are matched by detail on the maps for Cases 1, 4, 6, 8, and 9 around

140° and 220° longitude and mid-latitudes. The position angle seen in Figure 3.13e is nearly constant. The linear polarization observations are best matched by the scatterer concentration having increased or by a movement on the maps which is along either the q or u Stokes vector. The Table 3.2 polarization spectral-index entries for this star indicate that a mix of Thomson scattering in the atmosphere and Mie scattering in the large dust shell are likely linear polarization mechanisms. Since the circular polarization observations are zero within their errors (which are large), multiple scattering (Case 8) and interstellar birefringence (Case 9) are not likely. It is most likely that photospheric light as opposed to dust shell geometry is causing the scattering asymmetry.

(d) ψ^1 Aur

ψ^1 Aur has a radius of 1.7 AU and is slightly smaller than 119 Tau. The observations extend over an interval of 1,172 days for the new R-bandpass elliptical polarization data, and about 11,500 days in the R-bandpass for the total (archival plus new) linear polarization data. The new data and total data sets correspond, respectively, to about 120° and 1000° (three times around, but with a 6,100 day, 600° gap) on the polarization maps since the period of rotation is ~3,600 days. The polarization amplitude shift and constant sign of the intrinsic linear Stokes vectors over the period of observations are matched by detail on the maps for Cases 1, 4, 6, 8, and 9 around 140° and 220° longitude near the equator and along parallels (going East-West) or at mid-latitudes near 180° longitude and along meridians (going North-South). Cases 4, 6, and 8 are discredited since the linear polarization spectral indices for this star suggest that Thomson scattering is the likely polarizing mechanism. The fast drop in circular polarization from +0.08% to near 0.00% seen in Figure 3.14c is likely to be noise although flaring cannot be ruled out. The drop is certainly too fast for a spot to dissipate or disappear over the limb of the star (Case 2). Interstellar birefringence (Case 9) is not likely since

there is no connection with the linear polarization. It appears that the linear polarization observations are best fitted by bright regions near the limb of the star, and the circular polarization observations are best fitted by the waxing and waning of stellar active regions. Multiple scattering (Case 8) is further ruled out on the grounds that the circular signal is about 10% of the linear polarization amplitude. Conversion rates this large would arise only under ideal scattering geometries.

(e) 72 Leo

The new R-bandpass elliptical polarization observations extend over an interval of 1,154 days, and the total (archival plus new) linear polarization data extend over an interval of about 7,400 days in the V-bandpass. The relatively small size of this star leads to a ~600 day rotation period. Thus, the new observations extend ~700° on the maps (1.9 times around). The total data set has too many lengthy gaps to be useful for the identification of trends on the maps. The interval of observations of the first group of data seen in Figure 3.15, centered around JD 2,446,900, corresponds to about 100° of rotation. The observed variation is matched by a combination of Case 2 maps along with maps from Cases 1, 4, 6, 8, or 9; however, the match is appropriate only along parallels near 90° and 270° longitude. 72 Leo shows a combination of Thomson and Mie scattering in the R/V/B polarization spectral indices thus preventing a distinction between the maps based purely upon scatterer type. The R/V/B/U spectral indices have large errors, but may indicate a hot atmospheric region. The circular polarization behaves in a fashion which is similar to the q Stokes vector seen in Figure 3.15a. The circular polarization has nearly the same amplitude as the linear polarization and varies on a faster time-scale thus ruling out multiple scattering (Case 8) and interstellar birefringence (Case 9). By comparison between Figure 1.7a and b, it is apparent that the star was most recently observed at a quiet epoch. This is surprising since the dust shell size calculated in Section 4.1 is large.

It is conceivable that the dust shell dissipated somewhat since the *IRAS* data were taken in 1984. The circular polarimetry in the R- and V-bandpasses does not always have the same sign at a given epoch. Either there is an appreciable interstellar circular polarization offset (~ ±0.03%) and one large spot or there are North and South polarity spot groups simultaneously present.

(f) V CVn

V CVn's radius of 0.39AU is slightly larger than the radius of 72 Leo. The new R-bandpass elliptical polarization observations extend over an interval of 753 days, and the bulk of the total (archival plus new) linear polarization data extend about 7,800 days in all bandpasses. The ~780 day rotation period means the new observations correspond to about ~360° (once around) and the total data set corresponds to about 3600° (ten times around) on the polarization maps. The shift in polarization amplitude and constant negative sign of the intrinsic linear Stokes vectors over the interval of observations (Figures 1.8 and 3.16) is matched by detail on the maps for Cases 1, 4, 6, 8, and 9 around 120° and 240° longitude along meridians only. Figures 1.8 and 3.16j show large polarization swings. The linear polarization spectral indices indicate that Mie scattering probably dominates. Coyne and Magalhães (1979) and Magalhães, Coyne, and Benedetti (1986), in contrast, found variation across the 4955Å TiO band and concluded that the linear polarization arises from photospheric origins. Cases 1, 8, and 9 are not likely since the v Stokes vector shown in Figure 3.16i, while noisy, is not zero and is not related to the amplitude of the linear polarization. The peak in the linear polarization of V CVn has been known to occur at minimum light (Serkowski 1966b). Daniel (1980, 1982) and Shawl (1975a) concluded that the responsible mechanism is multiple scattering in an asymmetric dust shell. This conclusion is contradicted by the present observations. The large excursions in light and polarization are due to grain formation in the

Daniel and Shawl interpretations. However, Figure 3.16i shows, for the V-bandpass, that the circular polarization is constant within large errors. It is impossible to have grain formation and a constant circular polarization since multiple scattering is highly sensitive to particle number densities. The circular polarization amplitude is also larger than the square of the linear polarization amplitude. The circular polarization must be generated near the stellar surface perhaps by many stellar spots or a large spot at a high latitude. It seems likely that the light asymmetry is located there as a result and produces the 4955Å TiO band, and the polarizers are in the massive dust shell. Instead of grain formation, the variations in the linear polarization are due to waxing and waning of surface phenomena.

(g) α Sco

The new elliptical polarization observations on this star extend over an interval of 792 days in the R-bandpass, and the total (archival plus new) linear polarization data extend about 9,500 days (also in the R-bandpass). The new data and total data sets correspond, respectively, to about 70° and 860° (2.4 times around, but with a 4,600 day, 410° gap) on the polarization maps since the period of rotation is ~4,000 days. Detail from the polarization maps for Cases 1, 4, 6, 8, and 9 around 90° and 270° longitude and mid-latitudes have variations sufficient to match the observations. α Sco sits next to 119 Tau on the HR-diagram and yet is calculated to have a dust shell mass over one hundred times larger. The polarization spectral indices are all positive. Three possible explanations exist for this type of situation. First, the Mie scattering grains may be highly metallic (Case 5). Metals show a strong rise in their indices of refraction towards the infrared. Therefore, the parameter *mx* defined in Section 4.2 increases, instead of decreases, towards the IR. Also, the flux from the B-star companion would tend to destroy silicate dust near 1200K but would not sublimate the more refractory particles. The

scattering efficiency for these particles is, however, likely to be low (Case 5). The second explanation is that Thomson scattering dominates, but significant Hydrogen self-absorption exists towards the shorter wavelengths. The B-star companion may be the source for this gas component in the circumstellar shell. The decrease in the linear polarization is monotonic and therefore presents a challenge to this explanation. The third explanation is that Thomson scattering dominates, but two or more bright regions exist on the stellar surface and each has a different temperature. Thus, the observations in the R-bandpass would be dominated by a larger, warm region and the observations in the B-bandpass would be dominated by a smaller, hot region. The regions would have to be at different photospheric locations and, therefore, the position angle would be different as is seen in Figure 3.24b (Cases 1, 4, 6, 8, and 9). The observed gradient in position angles is very smooth and this is not expected if there are two different regions. The first two explanations also have trouble dealing with the rotation of the position angle. The third explanation is supported by Clarke and Brooks (1985) who found a polarization dip at the CaII K line thus possibly indicating an atmospheric source of polarization.

The v Stokes vector shows both signs in the B- and R-bandpasses at the same epoch. α Sco is the only star for which a reliable interstellar circular polarization offset is believed to have been found (Case 9 and Section 3.2). The inconsistency with Case 2 is resolved if the interstellar circular polarization determination for α Sco is used with Figure 3.24c. It is then seen that the intrinsic polarization spectra are all of a single sign at the same epoch. Also, it can be seen that the spot polarity switched over the six day interval between JD 2,446,994 and JD 2,447,000. The waxing and waning of two spots may be responsible.

(h) α^1 Her

α^1 Her has been observed in the present study over an interval

spanning 905 days in the R-bandpass. This corresponds to about 70° on the polarization maps since the period of rotation is ~4,700 days. The archival data set has too few data for specifying any areas on the maps. The coverage of α^1 Her is extensive enough to see cyclical polarization swings not unlike those seen for α Ori and β Peg. α^1 Her also does not show phase locking between the linear and circular Stokes vectors. However, the p parameter may be in step to a small degree with the v Stokes vector. None of the maps shows linear polarization variability with a high enough frequency to match the observations shown in Figure 3.18 due to stellar rotation alone. Therefore, the variation must additionally result from non-radial pulsation or multiple bright regions (similar to α Ori). The maps for Cases 1, 4, 6, 8, and 9 have sufficient high-frequency detail near 90° and 270° longitude and mid-latitudes to have a degree of variability which matches the observations over 70° of rotation if there exist at least two or more asymmetry sources. The polarization spectral indices for this star strongly indicate Mie scattering. The star is also known to have a large dust shell despite its relative lack of linear polarization (Cases 5 and 7). α^1 Her must, therefore, have a nearly spherical dust shell which produces little linear polarization (Cases 5 and 7) and the circular polarization may be produced by magneto-emission (Case 2), since multiple scattering between scattering layers (Case 8) cannot explain a situation wherein the amplitude of the v Stokes vector is sometimes larger than the amplitude of the linear Stokes vectors. The wavelength dependence of the v Stokes vector seems to rule out the spot hypothesis since the circular data at individual epochs are of both signs; however, an interstellar circular polarization offset of +0.02% would resolve this problem. α^1 Her thus provides some evidence for large convective cells (Schwarzschild 1975) causing the light asymmetry.

(i) μ Cep

μ Cep's radius of 5.0AU indicates that its rotation period is of the

order of ~11,000 days. The new R-bandpass elliptical polarization observations extend over an interval of 876 days. The archival plus new linear polarization data extends nearly continuously over an interval of about 14,000 days in the V-bandpass. The new data and total data sets correspond, respectively, to about 30° and 450° (1.3 times around). The shift in the polarization amplitude and mix of signs for the intrinsic linear Stokes vectors over the interval of observations as seen in Figures 1.10 and 3.19 are matched by detail on the maps for Cases 1, 4, 6, 8, and 9 around 120° and 240° longitude and near the equator or at mid-latitudes near 180° longitude. The linear polarization amplitude peaks for μ Cep at epochs which occur at minimum light (Polyakova 1984). The linear polarization spectra are nearly flat within the errors thus implying Thomson scattering in the atmosphere to be the responsible mechanism, but a Mie scattering component cannot be ruled out completely. This interpretation is consistent with Hayes (1982) who argued for this conclusion on the basis of polarization variability. However, the star is calculated to have a large dust shell. The *v* Stokes vector is relatively quiet within its error although, in the second group of data (near JD 2,447,800), considerable variability is seen. The *v* Stokes vector in the first group of data (near JD 2,447,000) is seen to show different signs in the R-bandpass compared to the V-bandpass. This seems to rule out magneto-emission (Case 2), but an interstellar circular polarization offset of about +0.03% would remove this problem. It is important to note that the Avery *et al.* (1975) circular polarization data are negative in all bandpasses and of a similar amplitude to the present data. This indicates that the scatterer concentrations are apparently constant over many years and seems to rule out Polyakova's polarization mechanism whereby successive ejections of dust particles would be invoked. The combination of effects present in the multiple-scattering model of Case 8 covers the observations best although interstellar birefringence is still a possible cause of the circular polarization (Case 9). The circular polarization prediction for μ

Cep by Shafter and Jura (1980) of 0.01% at 15" from the star is confirmed, but their amplitude is somewhat low as was seen to be the case also for their prediction for α Ori.

(j) VV Cep

Some program objects have relatively nearby companions (α Sco, α^1 Her). However, the relevance of the multi-parameter polarization model faces a big challenge with this star since this star is an eclipsing binary and the polarization is already well explained (Koch and Pfeiffer 1978, Pfeiffer and Koch 1987) in terms of the scattering of the B star light by the supergiant and contributions from the accretion disk.

The rotation period of a single star of the size of the M supergiant component of VV Cep is on the order of ~8,600 days and the period of revolution is 7,430.5 days. The new R-bandpass elliptical polarization observations extend over an interval of 851 days, and the majority of the total (archival plus new) linear polarization data extend over an interval of about 4,800 days in all bandpasses. The new and total data sets correspond, respectively, to about 35° and 200° on the polarization maps. The shift in polarization amplitude with nearly constant sign for the intrinsic linear Stokes vectors over the interval of observations as seen in Figures 1.11 and 3.20 is matched by detail on the maps for Cases 1, 4, 6, 8, and 9 around 90° and 270° longitude and mid-latitudes along parallels or at high latitudes near 180° longitude along meridians. VV Cep is next to μ Cep on the HR-diagram and has a dust shell that is similar in size. Also, the linear polarization amplitudes during the interval of observations are similar; however, μ Cep shows large excursions in the azimuth of the electric vector. The polarization spectra are also similar and indicate mostly Thomson scattering with some Mie scattering present for VV Cep. It must be noted that contributions from the hot companion of VV Cep have not been removed from the polarization spectra. The linear polarization shown in Figure 3.20 is consistent with that reported by

Pfeiffer and Koch (1987) and shown in Figure 1.11. The star was between phases 0.48 and 0.59 (calculated from primary mid-eclipse) during the observing interval. The noisy data for the *v* Stokes vector are predominantly of one sign and are consistent with a magneto-emission or multiple scattering origin (Cases 2 and 8). Either the M supergiant atmosphere or the accretion disk could be the source of the linear polarization which multiply scatters in the dust shell.

(k) β Peg

β Peg shows polarimetric behavior in all Stokes vectors which is similar to those of α Ori and α^1 Her. β Peg has been observed in the present study over an interval spanning 1,130 days in the R-bandpass. In contrast, the few archival data cover an interval of less than 100 days. The interval for the new data corresponds to about 500° (1.4 times around) on the polarization maps since the period of rotation is ~830 days. The maps for Cases 1, 4, 6, 8, and 9 have sufficient high-frequency detail at mid-latitudes to have a degree of variability which matches the observations over 500° of rotation without the need for multiple asymmetry sources. β Peg has a relatively small dust shell, but Mie scattering predominates in its polarization spectral indices and rules out Case 1. The small dust shell probably results in the small overall linear polarization amplitude (Cases 4 and 6) for β Peg. The circular polarization is of a similar amplitude to the linear polarization thus ruling out multiple scattering (Case 8). The temporal variation of the circular polarization is different from that seen for the linear polarization. This seems to rule out interstellar birefringence (Case 9). The wavelength dependence of the circular polarization is, however, consistent with magneto-emission (Case 2) if there exists an interstellar circular polarization offset of +0.01%. This interpretation implies that the circular polarization features near JD 2,446,750 and JD 2,447,800 result from the spot being on the near side of the star. Possibly these

features are a result of the same spot and the rotation period of β Peg is actually 1050 days. The conclusion is that the linear polarization arises from Mie scattering in the circumstellar shell (Case 4 and 6) and that the circular polarization arises from magneto-emission (Case 2).

The dust shell dimensions for the program objects do not show a preference for HR-diagram position. Also, the linear and circular polarization phenomena also do not show such a preference. The periodograms for the program objects do not show discernible periods. The only exception is α Ori which is shown to have a weak 400 day periodicity in the B-bandpass linear polarization data due to pulsation.

The v Stokes data for all program objects are generally of both signs. However, there appears to be a negative trend in the v Stokes data in the u-bandpass for most stars. One possible explanation is that the interstellar dust grains or dust shell particles satisfy the Kramers-Kronig dispersion relationships (Equations 4.24 and 4.25). An isolated linear polarization maximum, as from the Serkowski, Mathewson, and Ford (1975) relation given in Equation 3.3 or from the index of refraction of the Mie scattering grains, produces a positive maximum to the left side of the maximum (resonance) and a negative minimum on the right (Shapiro 1975, Martin 1974, Martin 1975, Chlewicki and Greenberg 1990). Since the circular polarization is not seen to pass through zero for all stars, other nearby polarization peaks may exist in the polarization spectrum. The net negative circular polarization then arises due to the galactic field changing direction with respect to distance in a consistent fashion for the program objects. This hypothesis is not unreasonable since the interstellar polarization vector of most stars (including the program stars) lies in the plane of the galaxy.

4.5 Conclusions and Remaining Questions

The following general conclusions are made about the observing

program and the elliptical polarization of the program objects. A summary of the conclusions about the program objects is presented in Table 4.2.

1). Simultaneous high-precision circular polarimetry can be made in the Pennsylvania polarimeter configuration. The configuration developed includes a hybrid calibration scheme using a rotation of the Poincaré sphere for the circular calibration, and variable sky vs. background integration lengths to maximize the signal-to-noise ratio.

2). The infrared excesses of LLTVs place useful limits on the dust shell particle numbers and masses. The calculations were accomplished by using the stellar flux at visible wavelengths to estimate and remove the stellar flux at infrared wavelengths.

3). Polarization maps produced by the newly developed multi-parameter modelling software are a useful tool for interpreting the intrinsic linear and observed circular polarization of the program objects. The software model includes contributions from limb darkening, stellar spots, Rayleigh/Thomson scattering in the stellar atmosphere, Mie scattering from multiple particle types in the dust shell, and interstellar birefringence. The maps produced display the Stokes vectors and relative flux expected when looking at the modelled object from any direction. A number of canonical cases were run that illustrate the various model components. It was verified that large dark spots do not produce much net polarization when limb darkening is large.

4). The linear polarization for the program objects arises from

Rayleigh and Thomson scattering in the atmospheres of the objects 119 Tau, ψ^1 Aur, and α Sco and from single scattering off small silicate grains in the dust shells around V CVn, α^1 Her, and β Peg. For α Ori, 6 BU Gem, 72 Leo, μ Cep, and VV Cep the observations are best explained as a composite of both atmospheric and dust shell scattering.

5). Previous to this study, few high-precision circular polarimetric observations of LLTVs had been completed. The new data show that the circular polarimetry of LLTVs is as rich and as complex as it is for the linear polarimetry. It is concluded that the bulk of the circular polarization arises from three mechanisms: 1) single scattering of light that was linearly polarized in the atmosphere of 119 Tau and subsequently Mie scattered off spherical or irregularly-shaped aligned particles; 2) magneto-emission arising from spots on α Sco, V CVn, 72 Leo, ψ^1 Aur, and β Peg and possibly on α Ori, α^1 Her, μ Cep, and VV Cep as well; and 3) interstellar birefringence acting on the intrinsic linear stellar polarization of α Sco and possibly of α Ori, 72 Leo, α^1 Her, μ Cep, and β Peg also. Mechanism 1) also applies to a portion of the circular polarization for α Ori, μ Cep, and VV Cep.

The following work remains:

1). The interstellar circular polarization for all objects is still largely uncertain. It would be beneficial to sustain a program to map the interstellar circular polarization in a similar manner to the way it was done for linear polarization (Hiltner 1951, Hall 1958).

2). The multi-parameter computer code could easily be ported to

a Reduced Instruction Set Computer (RISC) system. More complicated models could be run, thus resulting in much more detail in the polarization maps. This would allow a further refinement in the processes at work in the program objects. Particle size and type distributions could be added. Longer integrations will require that the software be modified to use a random number generator such as the r250 method (Maier 1991).

3). There is value in constructing an instrument to measure linear and circular polarization spectra simultaneously. Polarization changes within a wide bandpass that might otherwise not be seen could thus be monitored.

4). Long-term monitoring of the polarization of the program objects will further define the nature of the polarization present in these objects.

Table 4.1.

Analysis of Radiometry for Program Objects

Name	Te (K)	E(B-V)	----Rs/Ds---- (rad) (Note 1)	(")	Rs (AU)	Fd (Jy)	<QNa²> (cm²) (Note 2)	<QNa²>/Rs²	Rd (AU) (Note 3)	Md (g) (Note 4)	Md (⊙)
119 CE Tau	3500	0.55	2.9E-8	0.0060	1.9	1.6	5.2E25	0.063	0.48	6.4E22	3.2E-11
58 α Ori	3590	0.35	1.2E-7	0.025	3.7	2100	1.5E28	4.8	8.2	1.9E25	9.4E-9
6 BU Gem	3590	0.74	1.3E-8	0.0027	3.7	49.	3.2E28	10.	12.	4.0E25	2.0E-8
46 ψ1 Aur	4165	0.57	1.3E-8	0.0028	1.7	6.8	7.9E26	1.3	1.9	1.0E24	5.0E-10
72 Leo	3360	0.11	1.6E-8	0.0032	0.29	70.	1.2E26	6.3	0.73	1.5E23	7.6E-11
V CVn	3120	0.02	4.9E-9	0.0010	0.38	130	5.7E27	173.	5.0	7.2E24	3.6E-9
21 α Sco	3590	0.33	9.3E-8	0.019	1.9	1700	5.3E27	6.4	4.9	6.7E24	3.3E-9
64 α1 Her	3120	0.00	5.1E-8	0.010	2.2	1100	1.5E28	14.	8.2	1.9E25	9.6E-9
μ Cep	3500	0.83	4.6E-8	0.0096	5.0	940	8.4E28	15.	19.	1.1E26	5.3E-8
VV Cep	3500	0.23	1.2E-8	0.0026	3.9	43	3.1E28	9.1	12.	3.8E25	1.9E-8
53 β Peg	3430	0.14	4.0E-8	0.0083	0.40	110.	7.8E25	2.2	0.59	9.9E22	4.9E-11

Notes:

1. The V-bandpass flux was used in Equation 4.2. The 12μm flux was used in Equation 4.3. However, α^1 Her data were computed from R-bandpass and 12μm data (see text). Also, V- and L-bandpass data were used for 72 Leo.

2. The dust temperature used is 1000K.

3. R_d is the effective radius of the absorption parameter: $\langle QNa_d^2 \rangle$.

4. M_d is for Q = 0.1, a = 0.05μm, ρ = 3g/cm³.

Table 4.2.

Program Object Summary

Name	MK Class	Rs (AU)	$\langle QNa^2 \rangle / Rs^2$	Md (⊙)	Polarization Spectral Indice Range (R/V/B) Min	Max	Linear Polarization Source(s) (Note 1)	Circular Polarization Source(s) (Note 2)
119 CE Tau	M2 Iab-Ib	1.9	0.063	3.2E-11	-0.25(2)	+0.31(30)	Atmospheric Rayleigh/Thomson	Multiple scattering
58 α Ori	M1-2 Ia-Iab	3.7	4.8	9.4E-9	-1.4(3)	+1.4(19)	R/T and dust shell: 400 day non-radial pulsation	Some multiple scattering; possibly some interstellar birefringence and magneto-emission
6 BU Gem	M1-2 Ia-Iab	3.7	10.	2.0E-8	-2.5(13)	+2.34(49)	R/T and dust shell	...
46 ψ1 Aur	K5-M0 Iab-Ib	1.7	1.3	5.0E-10	-0.23(8)	+0.64(13)	Atmospheric R/T	Magneto-emission
72 Leo	M3 IIb	0.29	6.3	7.6E-11	-2.55(31)	+0.65(33)	R/T and dust shell	Magneto-emission
V CVn	M4-6 IIIe	0.38	173.	3.6E-9	-1.9(16)	-1.14(11)	Dust shell	Magneto-emission
21 α Sco	M1.5 Iab-Ib + B4 Ve	1.9	6.4	3.3E-9	+0.14(5)	+1.43(83)	Atmospheric R/T	Magneto-emission plus interstellar birefringence
64 α1 Her	M5 Ib-II +?	2.2	14.	9.6E-9	-2.8(24)	-0.66(8)	Dust shell	Magneto-emission plus interstellar birefringence
μ Cep	M2 Iae	5.0	15.	5.3E-8	-1.05(33)	+1.22(45)	R/T and dust shell	Multiple scattering; possibly some magneto-emission
VV Cep	M2 Iape + O8 V	3.9	9.1	1.9E-8	-1.21(89)	-0.29(55)	R/T and dust shell	Multiple scattering; possibly some magneto-emission
53 β Peg	M2.5 II-III	0.40	2.2	4.9E-11	-1.9(16)	-0.2(12)	Dust shell	Magneto-emission

Note 1. "R/T" means atmospheric Rayleigh/Thomson scattering. "Dust Shell" means Mie scattering in the dust shell.

Note 2. "Multiple scattering" means the second scattering event is due to Mie scattering. "Magneto-emission" means the circularly polarized light is from a stellar spot or other magnetically active surface region. "Interstellar birefringence" means the interstellar dust grains retard the intrinsic or interstellar linear polarization.

Figure 4.1. The dereddened multi-bandpass radiometry (solid lines) of the program objects from Table 3.4. The dotted line corresponds to a black-body at the effective stellar temperature. (*a*) VV Cep. (*b*) ψ^1 Aur. (*c*) V CVn. (*d*) β Peg. (*e*) 119 Tau. (*f*) α^1 Her. (*g*) α Ori. (*h*) μ Cep. (*i*) 6 Gem. (*j*) α Sco. (*k*) 72 Leo.

Figure 4.2. Diagram for the scattering geometry. The observer is positioned on the viewing sphere looking towards the centrally-located stellar system. The scattering angle is θ_s. The components of the electric vector must be rotated an amount ϕ before scattering and an amount ϕ' back to the new local North on the viewing sphere.

Figure 4.3. Diagram of the layers in the multi-parameter polarization model. The figure is not to scale. The inner-most layer (grey ball) includes the photosphere along with bright patches (faculae) or dark stellar spots. The next layer (fine dots, labeled R/T) indicate the Rayleigh/Thomson scattering envelope. The chromosphere of the star is included in this layer. The third layer is the dust shell (dark dots, labeled Dust). Both spherical or cylindrical dust grains are modelled in this shell. The final component (not shown) encompasses the interstellar medium. It contains birefringent dust particles aligned with respect to the interstellar linear polarization vector.

Figure 4.4. Contour maps for Case 1 representing Rayleigh/Thomson scattering in the atmosphere of a model star with a small (θ_{sp} = 0.5 radian), bright spot (F_r = 1.8) on the stellar equator (Latitude = 0°, Longitude = 180°). Mie scattering and magneto-emission are absent. N_m = 10,000,000 flux vectors. (*a*) *q* Stokes vector map. (*b*) *u* Stokes vector map. (*c*) *v* Stokes vector map. Note the noise at high latitudes. (*d*) Relative

flux, F/F(0°,360°) (normalized to the flux at 0° and 360° longitude). Note that the lack of perfect symmetry expected from a circular spot at the indicated location is due to the randomness of the Monte Carlo integration technique.

Figure 4.5. Contour maps for Case 2 representing a star with a small (θ_{sp} = 0.5 radian), bright spot (F_r = 1.8) on the equator of the star (0°,180°). Scattering is absent, but there is a high level of magneto-emission. N_m = 4,000,000 flux vectors. (*a*) *q* Stokes vector map. (*b*) *u* Stokes vector map. (*c*) *v* Stokes vector map. (*d*) Relative flux, F/F(0°,360°) (normalized to the flux at 0° and 360° longitude).

Figure 4.6. Contour maps for Case 3 representing Rayleigh/Thomson scattering in the atmosphere of the star with a large (θ_{sp} = 1.0 radian), dark spot (F_r = 0.7) on the equator of the star (0°,180°). Mie scattering and magneto-emission are absent. Very little net polarization is generated. N_m = 10,000,000 flux vectors. (*a*) *q* Stokes vector map. (*b*) *u* Stokes vector map. (*c*) *v* Stokes vector map. (*d*) Relative flux, F/F(0°,360°) (normalized to the flux at 0° and 360° longitude).

Figure 4.7. Contour maps for Case 4 representing Mie scattering from newly formed, small (a_d = 0.05μm), spherical, clean silicate grains (m = 1.5) in the dust shell. There is a small (θ_{sp} = 0.5 radian), bright spot (F_r = 1.8) on the equator of the star (0°,180°). No Rayleigh/Thomson scattering or magneto-emission is present. The maps are similiar to those for Case 1; however, the polarization of points 180° in longitude away from each other match in sign and amplitude. N_m = 10,000,000 flux vectors. (*a*) *q* Stokes vector map. (*b*) *u* Stokes vector map. (*c*) *v* Stokes vector map. (*d*) Relative flux, F/F(0°,360°) (normalized to the flux at 0° and 360° longitude).

Figure 4.8. Contour maps for Case 5 representing a situation similar to Case 4. Here, however, the Mie scattering is from larger (a_d = 0.1μm), spherical, dirty-metallic (m = 3.4 - 1.9i) grains in the dust shell. No Rayleigh/Thomson scattering or magneto-emission is present. Little polarization is generated since the scattering efficiency is small. N_m = 10,000,000 flux vectors. (*a*) q Stokes vector map. (*b*) u Stokes vector map. (*c*) v Stokes vector map. (*d*) Relative flux, F/F(0°,360°) (normalized to the flux at 0° and 360° longitude).

Figure 4.9. Contour maps for Case 6 representing the same situation as for Case 5. However, the Mie scattering is from metallic cylinders (m = 1.4 - 1.4i, L_c = 1.0μm) not spheres. The long axes are perfectly aligned with lines of longitude (ϕ_c = 0.0). The cylinders have radii of a = 0.034μm. The maps are not unlike those seen for Case 1. However, the sign of the linear stokes vectors is inverted since the extinction is greater along the meridians of longitude. N_m = 10,000,000 flux vectors. (*a*) q Stokes vector map. (*b*) u Stokes vector map. (*c*) v Stokes vector map. (*d*) Relative flux, F/F(0°,360°) (normalized to the flux at 0° and 360° longitude).

Figure 4.10. Contour maps for Case 7 representing the same situation as for Case 6 with, however, the Mie scattering from larger metallic cylinders (a_d = 0.11μm). The maps show that very little linear and circular polarizations are generated since the particles are near the polarization reversal size of a_d = 0.10μm. N_m = 10,000,000 flux vectors. (*a*) q Stokes vector map. (*b*) u Stokes vector map. (*c*) v Stokes vector map. (*d*) Relative flux, F/F(0°,360°) (normalized to the flux at 0° and 360° longitude).

Figure 4.11. Contour maps for Case 8 representing the same situation as for Case 6, except that there is much Rayleigh/Thomson scattering (more

than in Case 1) and Mie scattering from cylinders which are not aligned with meridians (more dust than for Case 6, $\phi_c = +\pi/3$). The linear polarization maps show a larger amplitude and a similar form when compared to Case 1 maps. Some circular polarization production is present from multiple scattering. N_m = 50,000,000 flux vectors. (*a*) *q* Stokes vector map. (*b*) *u* Stokes vector map. (*c*) *v* Stokes vector map. (*d*) Relative flux, F/F(0°,360°) (normalized to the flux at 0° and 360° longitude).

Figure 4.12. Contour maps for Case 9 representing a situation similar to that for Case 1. However, somewhat more extensive linear polarization is generated since the spot is brighter (F_r = 3.0), and the Rayleigh/Thomson number density is larger ($N_e = 2.0\text{x}10^{+11}$). There is a large interstellar birefringence (δ = 0.6) which is not aligned with respect to North ($\phi_i = +\pi/4$). The maps show circular polarization conversion where the *q* Stokes vector is large. Note that the circular polarization returns to the same value when the underlying linear polarization returns to the same value. N_m = 10,000,000 flux vectors. (*a*) *q* Stokes vector map. (*b*) *u* Stokes vector map. (*c*) *v* Stokes vector map. (*d*) Relative flux, F/F(0°,360°) (normalized to the flux at 0° and 360° longitude).

Figure 4.13. α Ori archival plus new B-bandpass linear polarization data phased with a 400.0 day period using JD 2,439,783.9 as the epoch. (*a*) linear polarization vs. phase. (*b*) θ vs. phase.

Figure 4.14. α Ori archival plus new B-bandpass linear polarization data phased with an 800.0 day period using JD 2,439,783.9 as the epoch. (*a*) linear polarization vs. phase. (*b*) θ vs. phase.

Figure 4.1

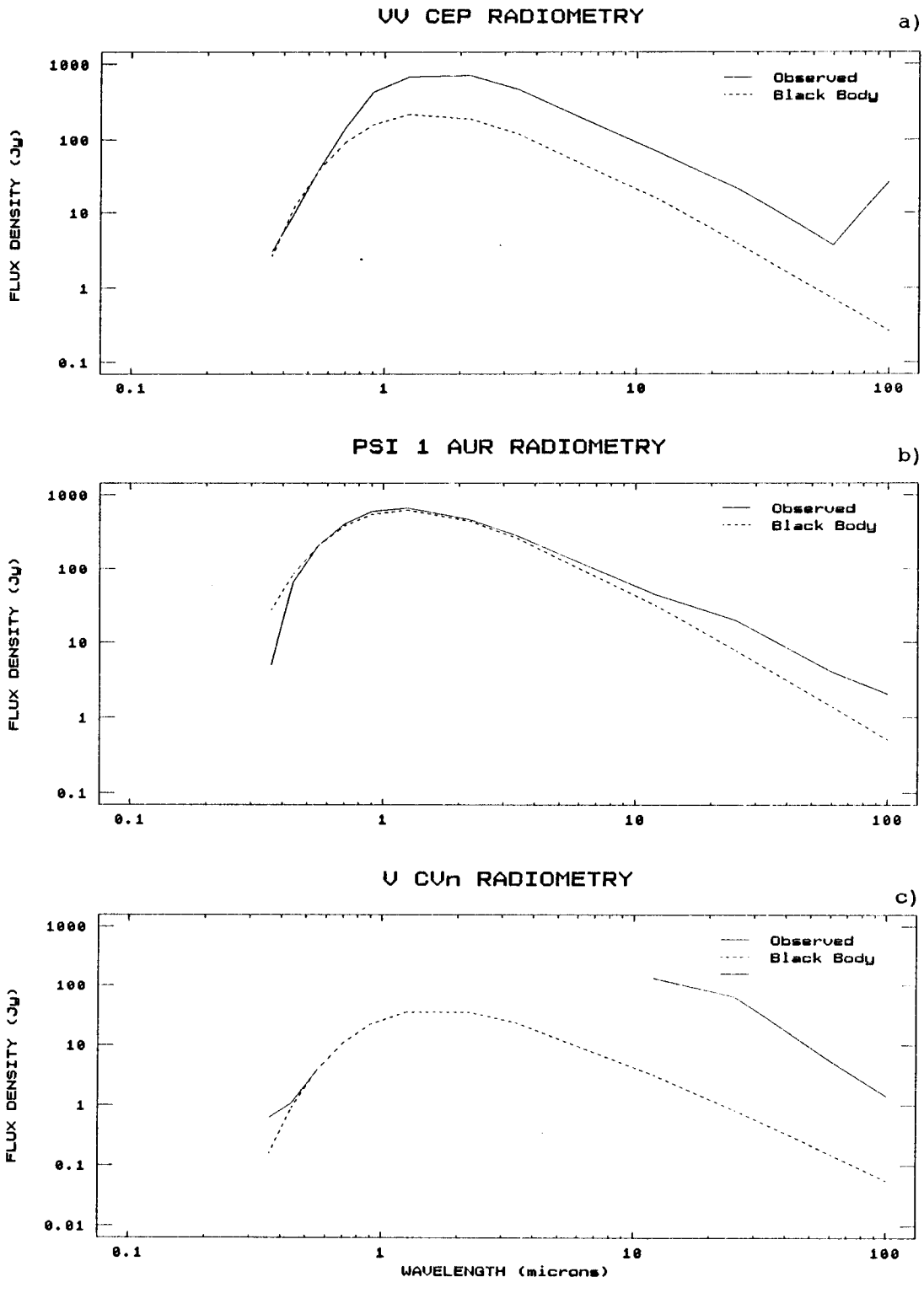
VV CEP RADIOMETRY
a)
Observed
Black Body
FLUX DENSITY (Jy)
1000
100
10
1
0.1
0.1
1
10
100
PSI 1 AUR RADIOMETRY
b)
Observed
Black Body
FLUX DENSITY (Jy)
1000
100
10
1
0.1
0.1
1
10
100
V CVn RADIOMETRY
c)
Observed
Black Body
FLUX DENSITY (Jy)
1000
100
10
1
0.1
0.01
0.1
1
10
100
WAVELENGTH (microns)

Figure 4.1 (cont.)

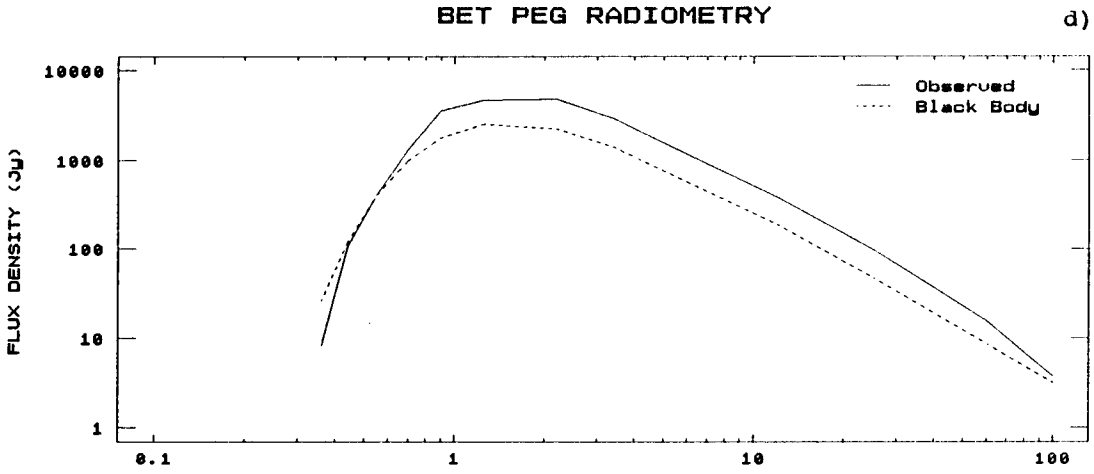

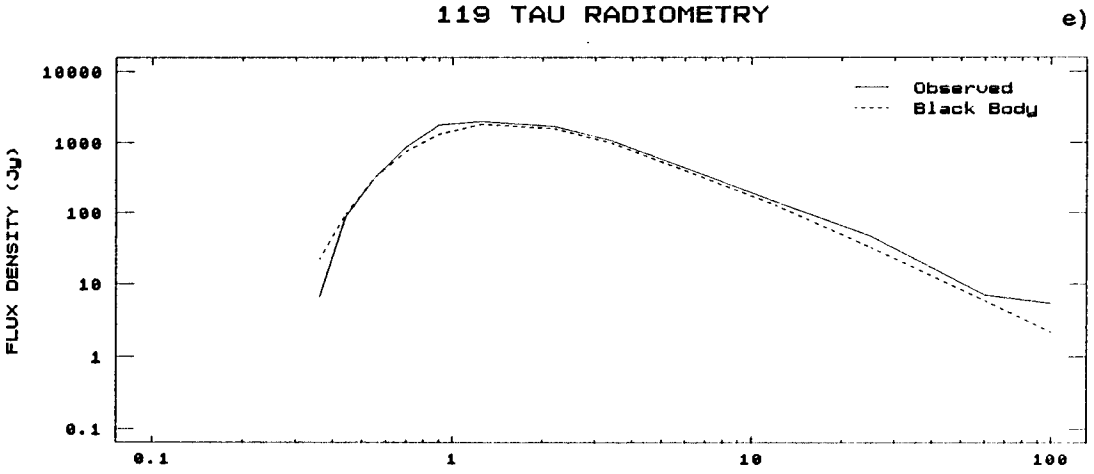

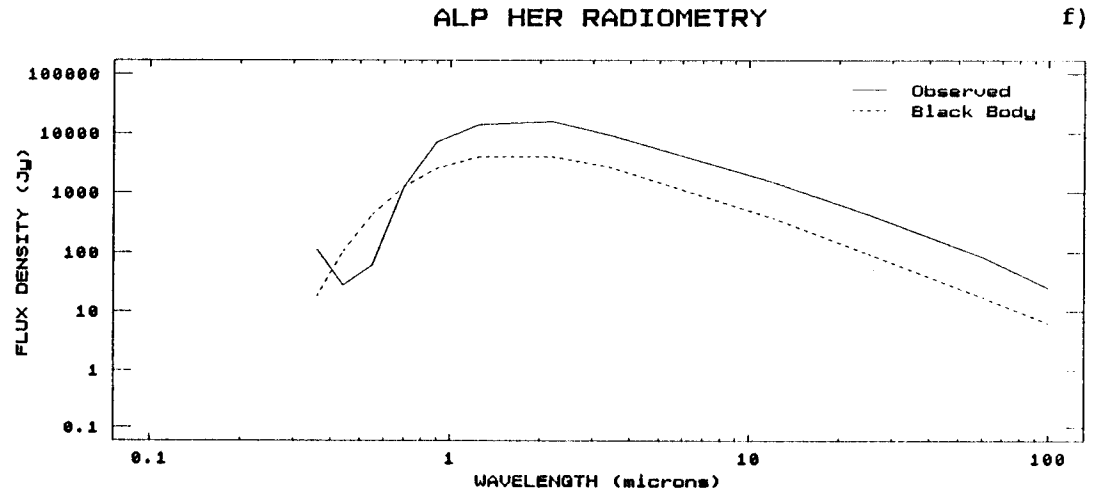

Figure 4.1 (cont.)

g)

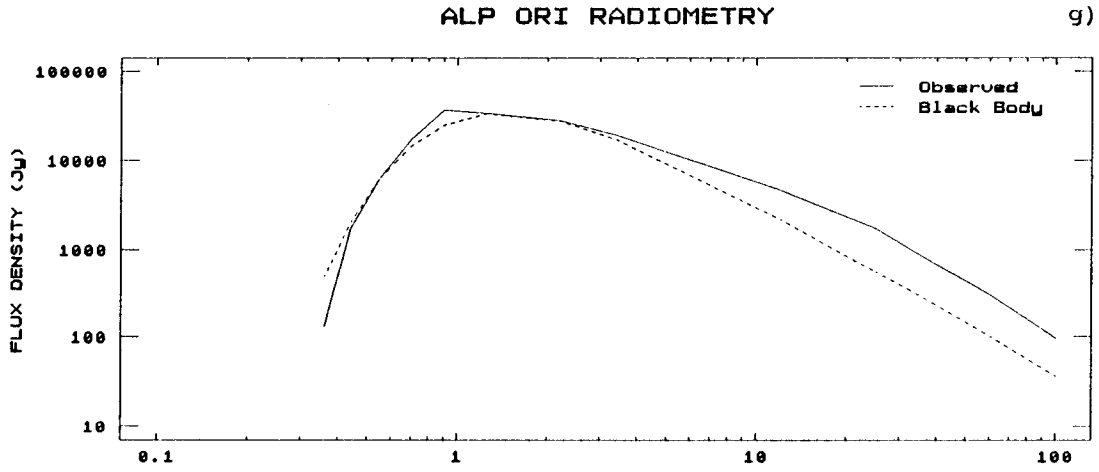

h)

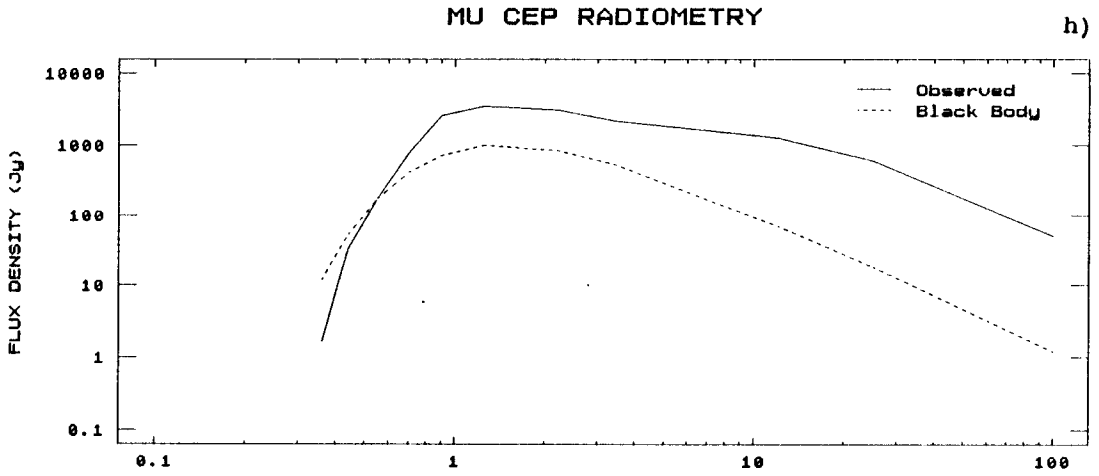

i)

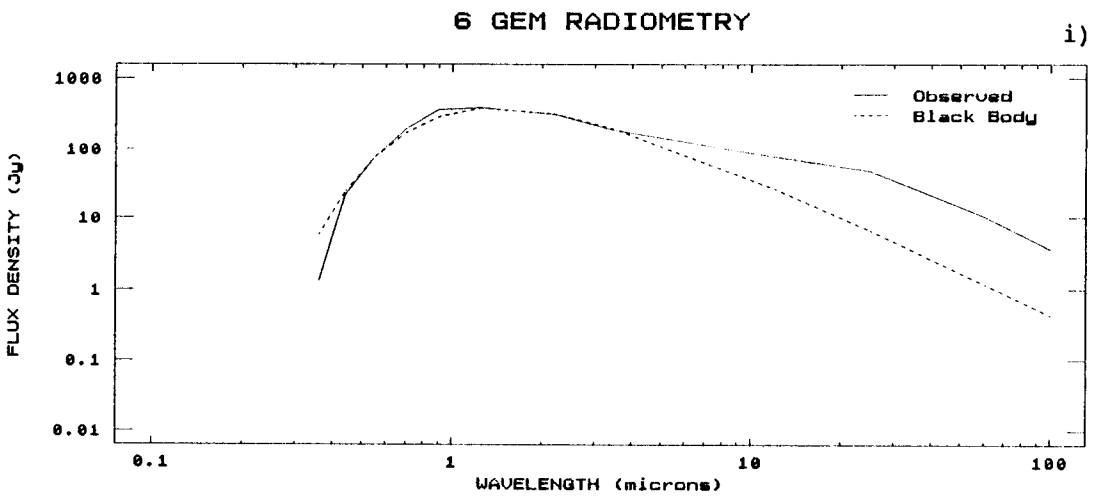

Figure 4.1 (cont.)

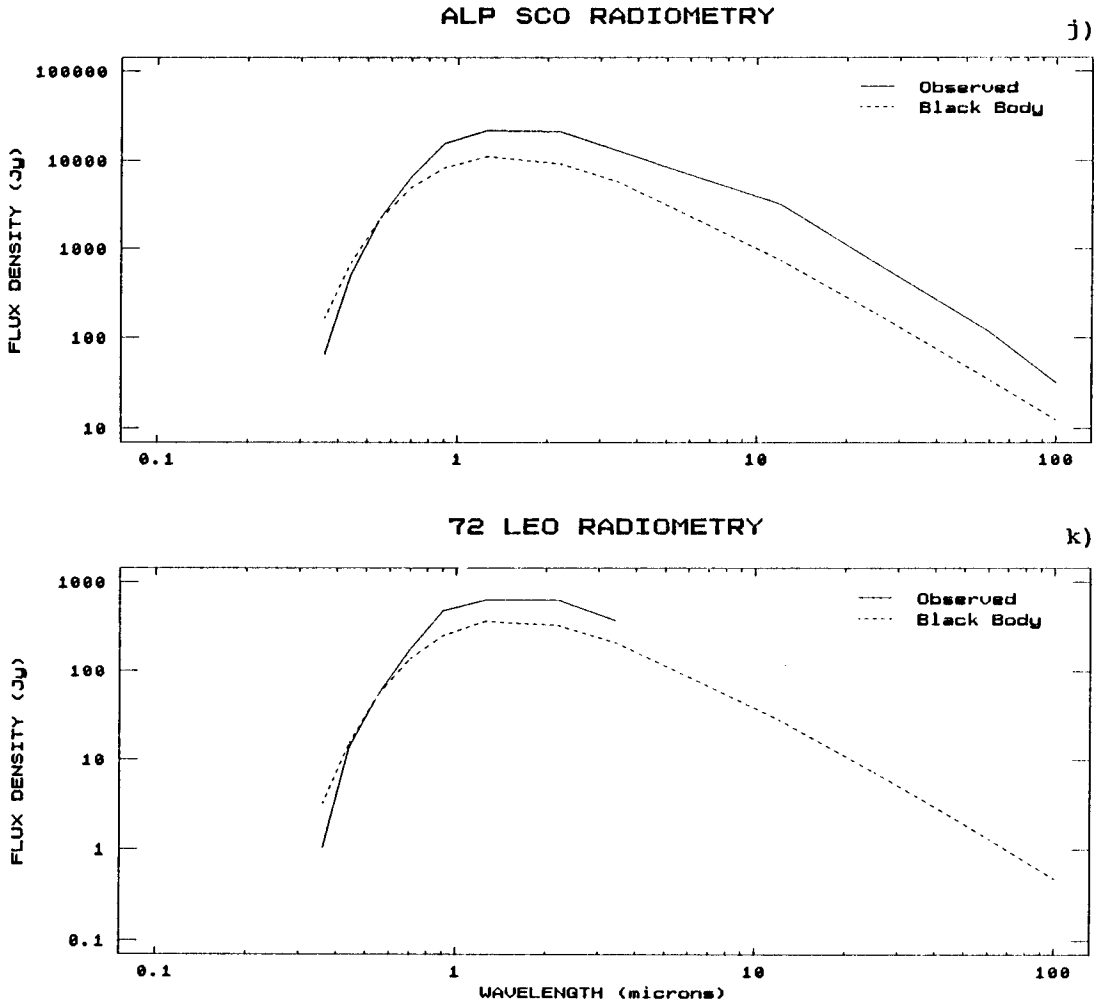

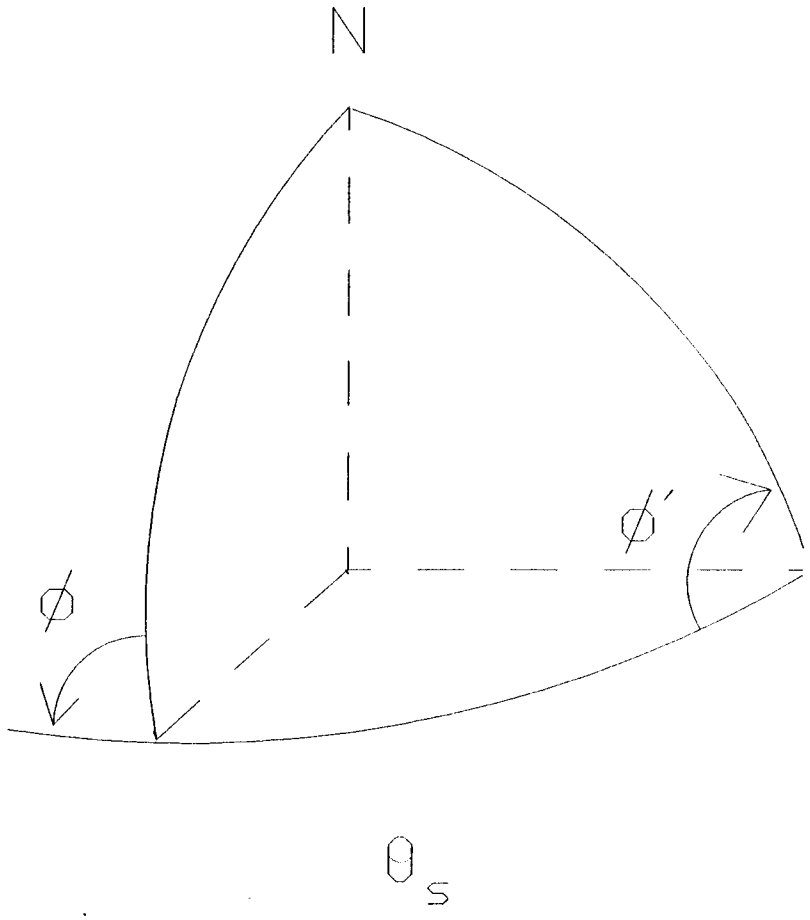

Figure 4.2

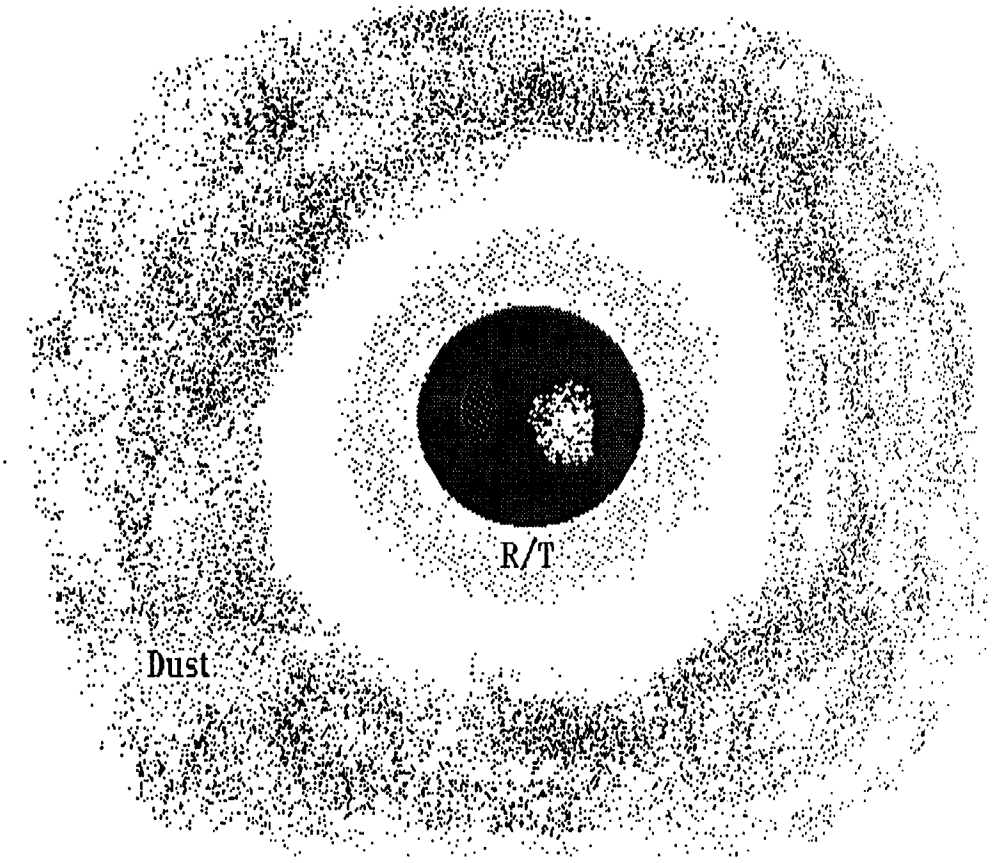

Figure 4.3

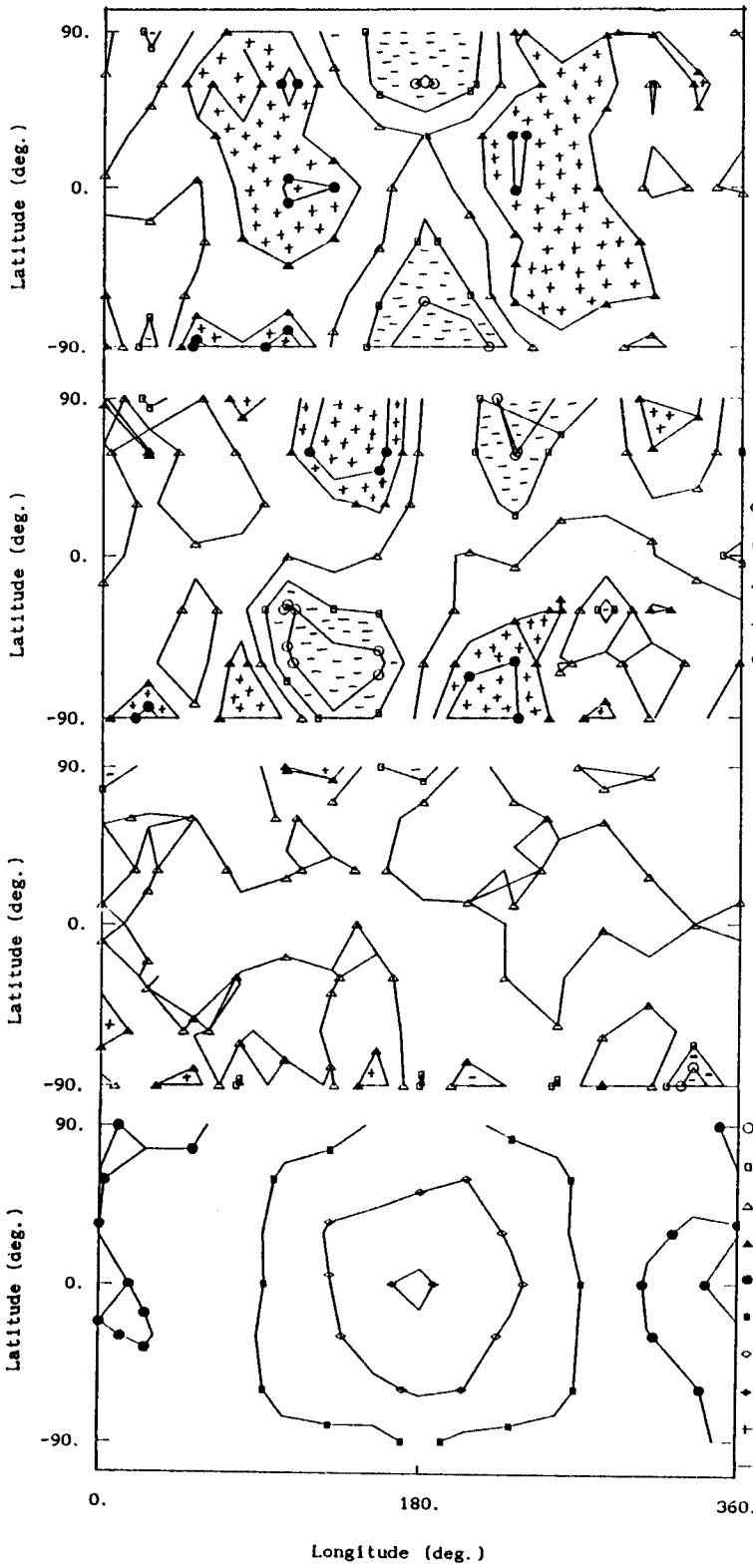

a) Stokes Q

b) Stokes U

c) Stokes V

d) Flux

Figure 4.4

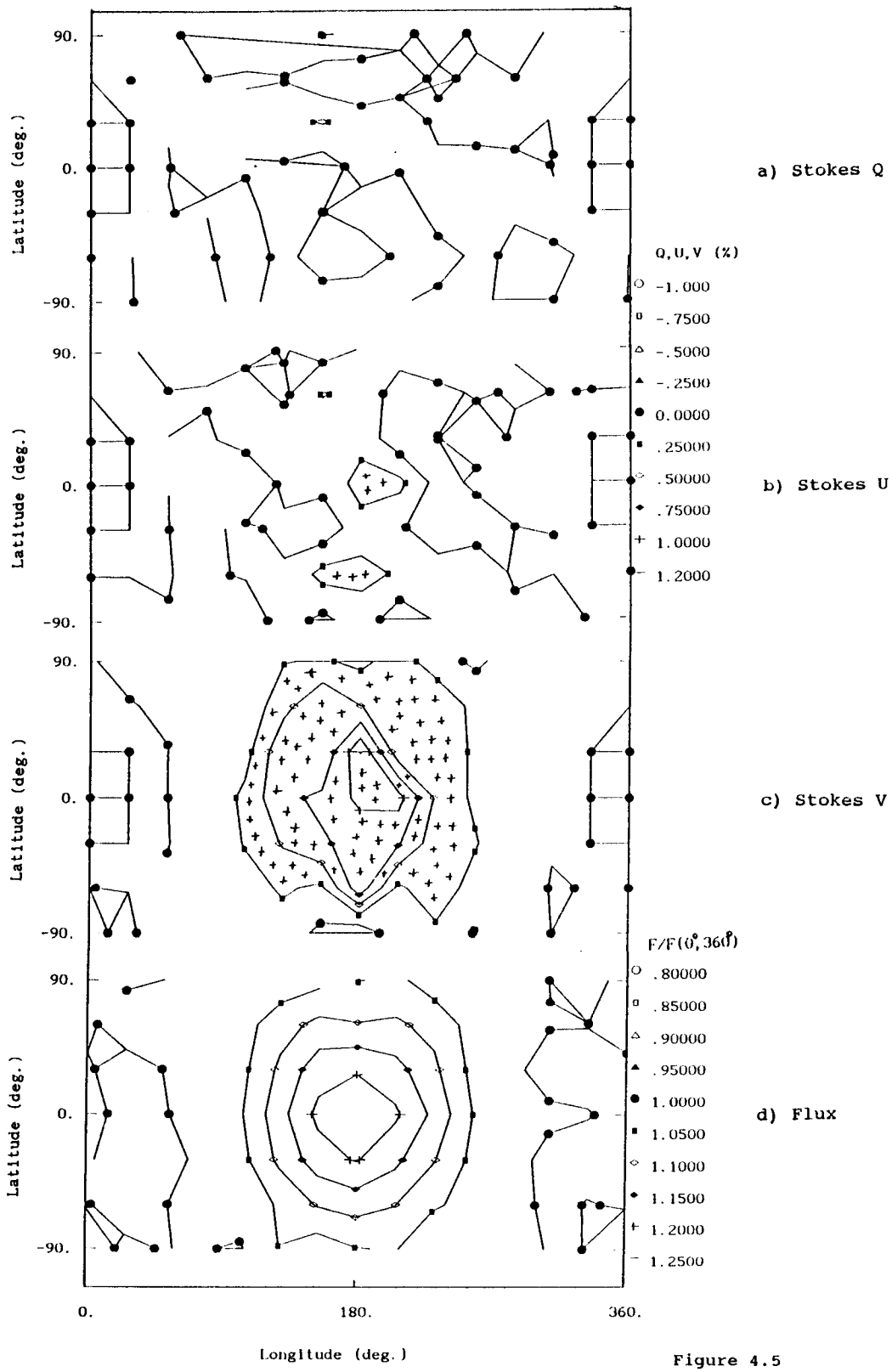
90.
0.
-90.
Latitude (deg.)
Q,U,V (%)
-1.000
-.7500
-.5000
-.2500
0.0000
.25000
.50000
.75000
1.0000
1.2000
a) Stokes Q
b) Stokes U
c) Stokes V
F/F(0°,36(°)
.80000
.85000
.90000
.95000
1.0000
1.0500
1.1000
1.1500
1.2000
1.2500
d) Flux
0.
180.
360.
Longitude (deg.)

Figure 4.5

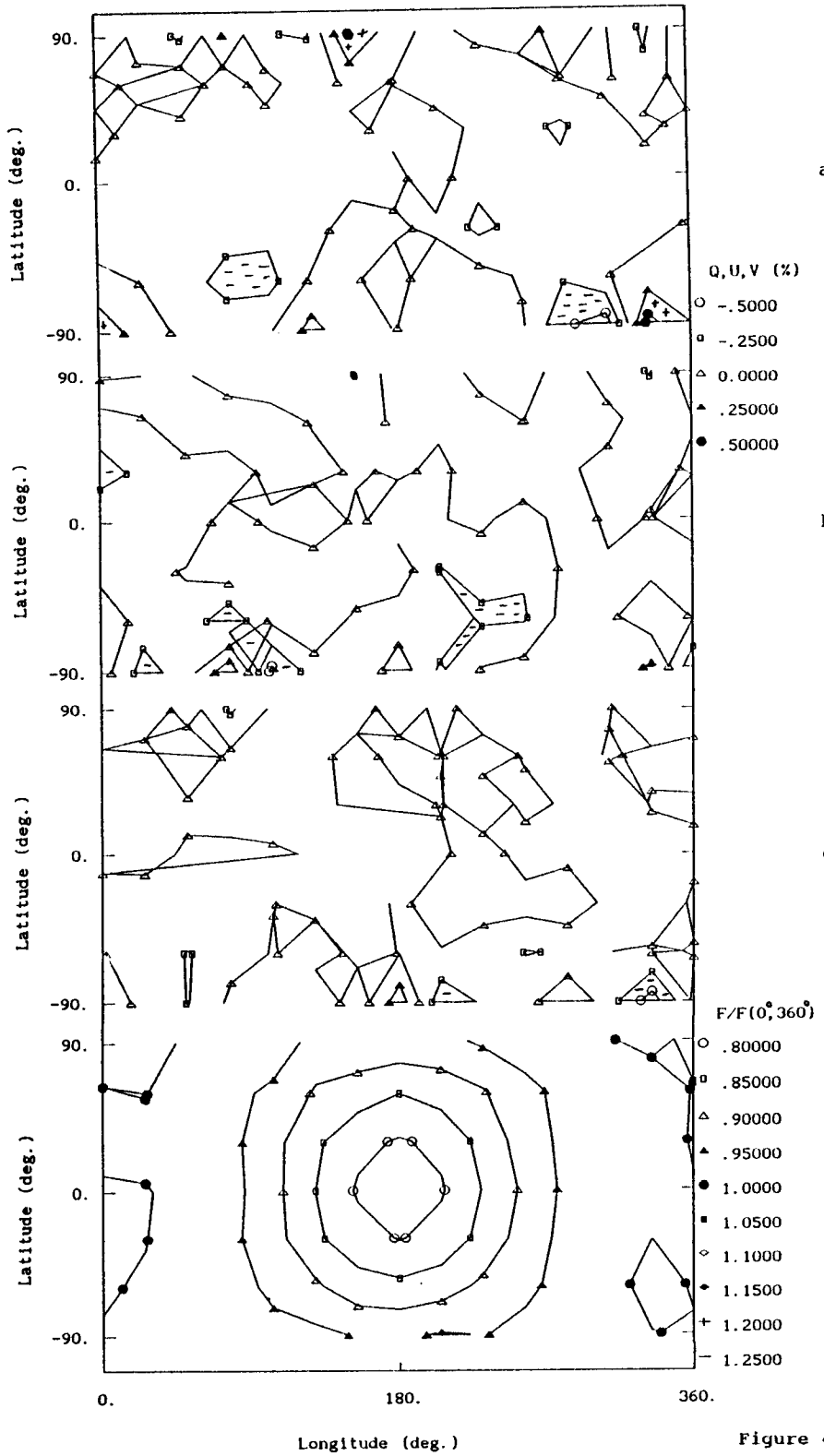
90.
0.
-90.
Latitude (deg.)
a) Stokes Q
Q,U,V (%)
-.5000
-.2500
0.0000
.25000
.50000
b) Stokes U
c) Stokes V
F/F(0°,360°)
.80000
.85000
.90000
.95000
1.0000
1.0500
1.1000
1.1500
1.2000
1.2500
d) Flux
0.
180.
360.
Longitude (deg.)

Figure 4.6

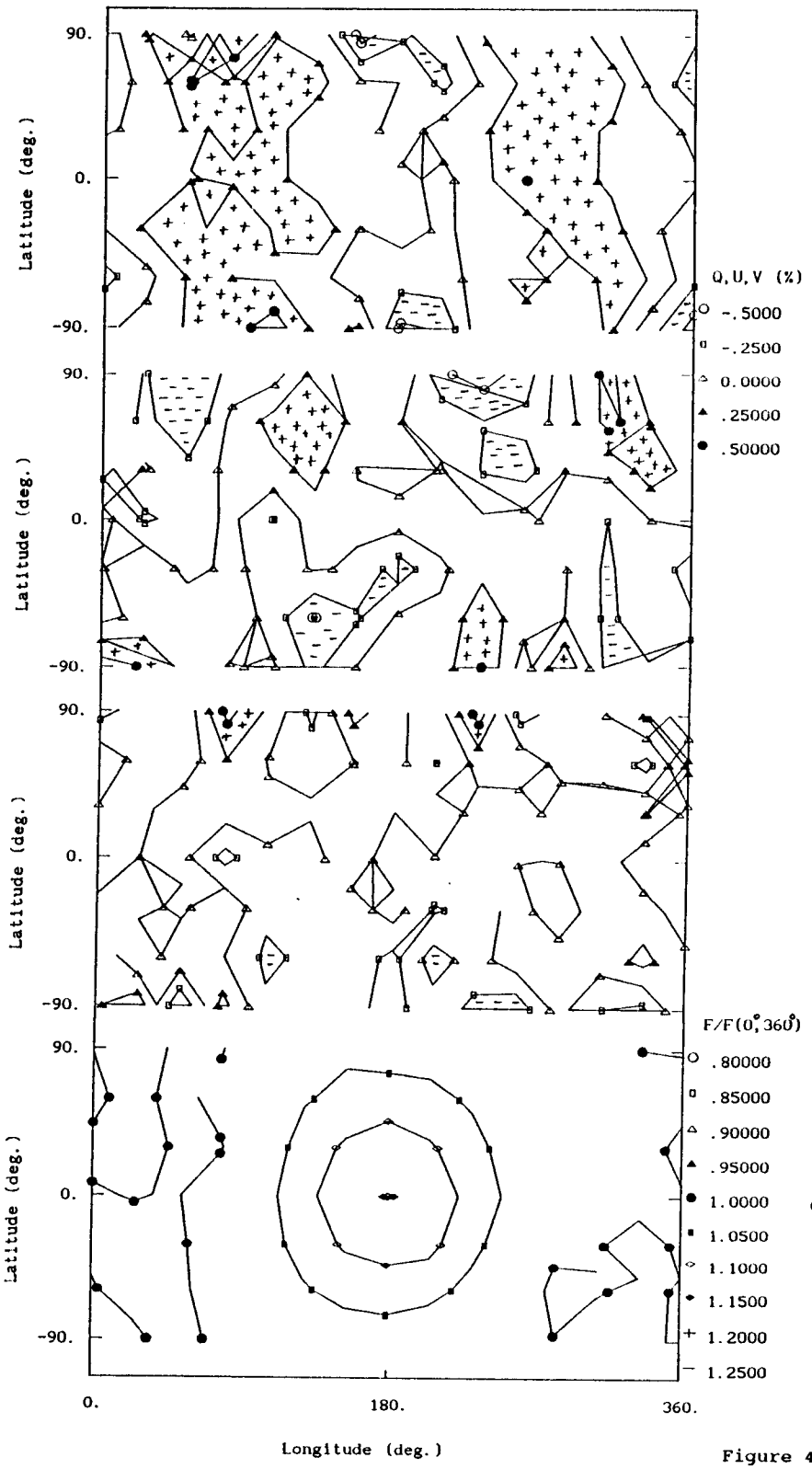
90.
0.
-90.
Latitude (deg.)
Q,U,V (%)
-.5000
-.2500
0.0000
.25000
.50000
a) Stokes Q
b) Stokes U
c) Stokes V
F/F(0°,360°)
.80000
.85000
.90000
.95000
1.0000
1.0500
1.1000
1.1500
1.2000
1.2500
d) Flux
0.
180.
360.
Longitude (deg.)

Figure 4.7

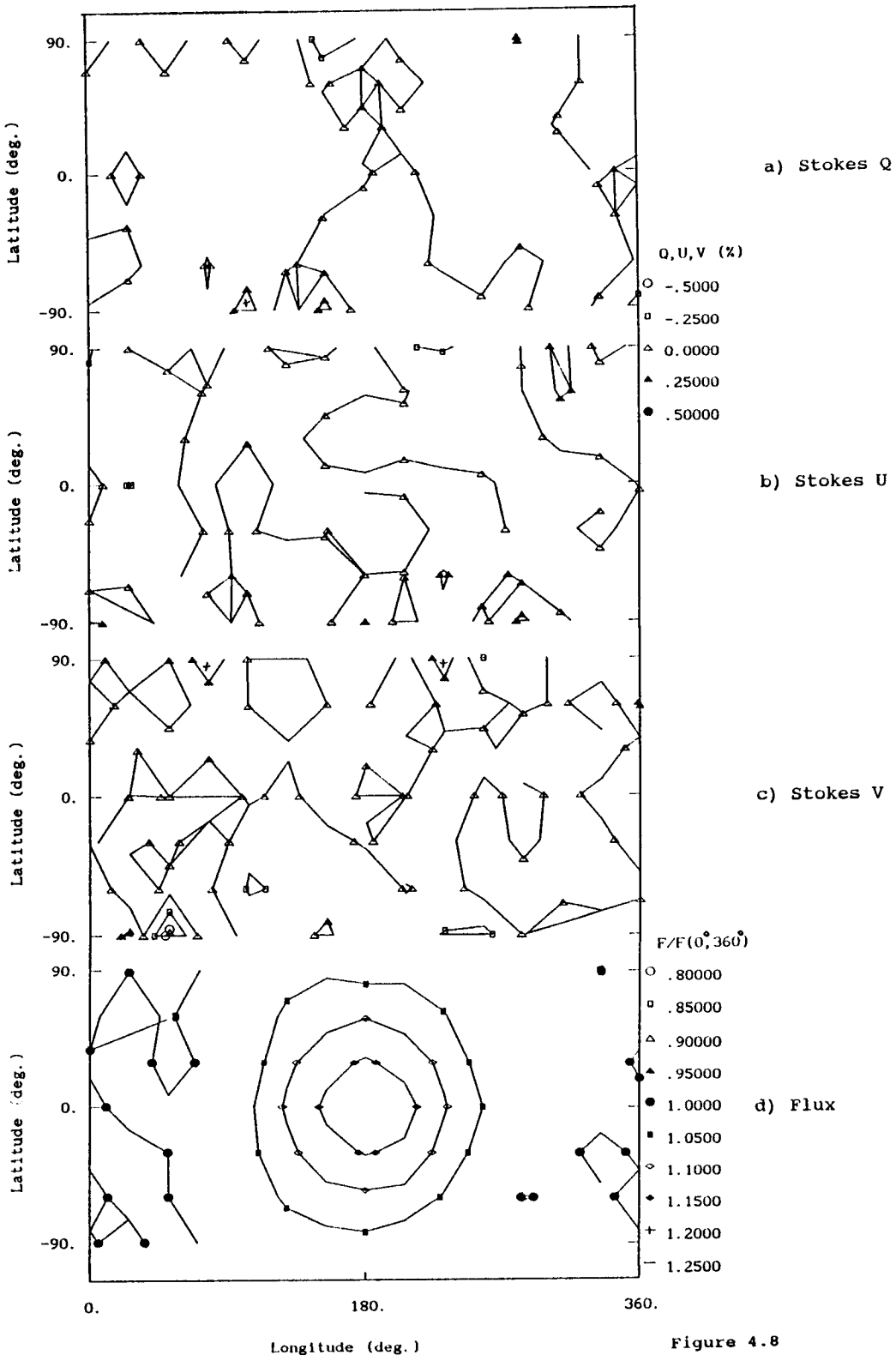
90.
0.
-90.
Latitude (deg.)
a) Stokes Q
Q,U,V (%)
-.5000
-.2500
0.0000
.25000
.50000
b) Stokes U
c) Stokes V
F/F(0°,360°)
.80000
.85000
.90000
.95000
1.0000
d) Flux
1.0500
1.1000
1.1500
1.2000
1.2500
0.
180.
360.
Longitude (deg.)

Figure 4.8

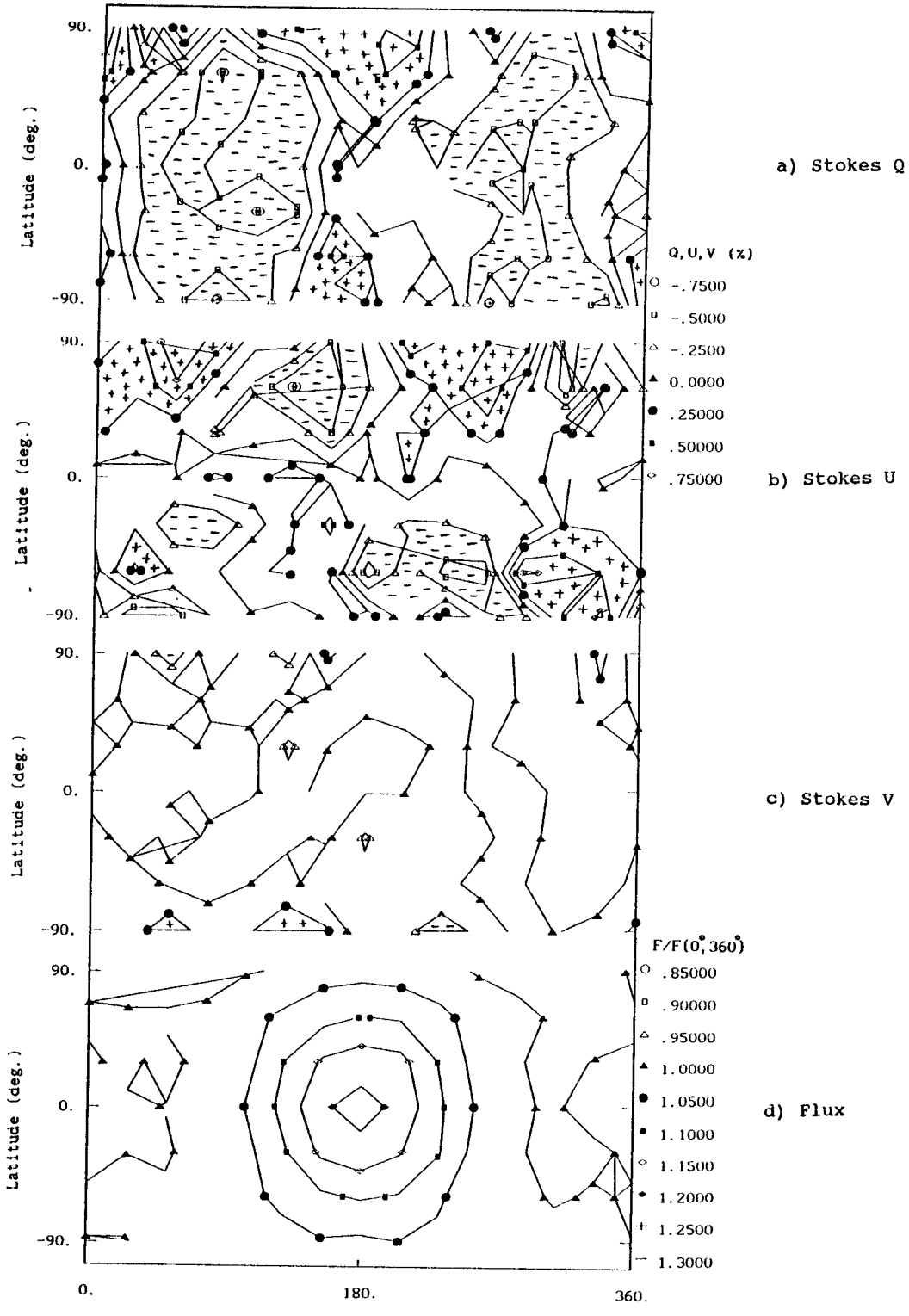
90.
0.
-90.
Latitude (deg.)
Q,U,V (%)
-.7500
-.5000
-.2500
0.0000
.25000
.50000
.75000
a) Stokes Q
b) Stokes U
c) Stokes V
F/F(0°,360°)
.85000
.90000
.95000
1.0000
1.0500
1.1000
1.1500
1.2000
1.2500
1.3000
d) Flux
0.
180.
360.
Longitude (deg.)

Figure 4.9

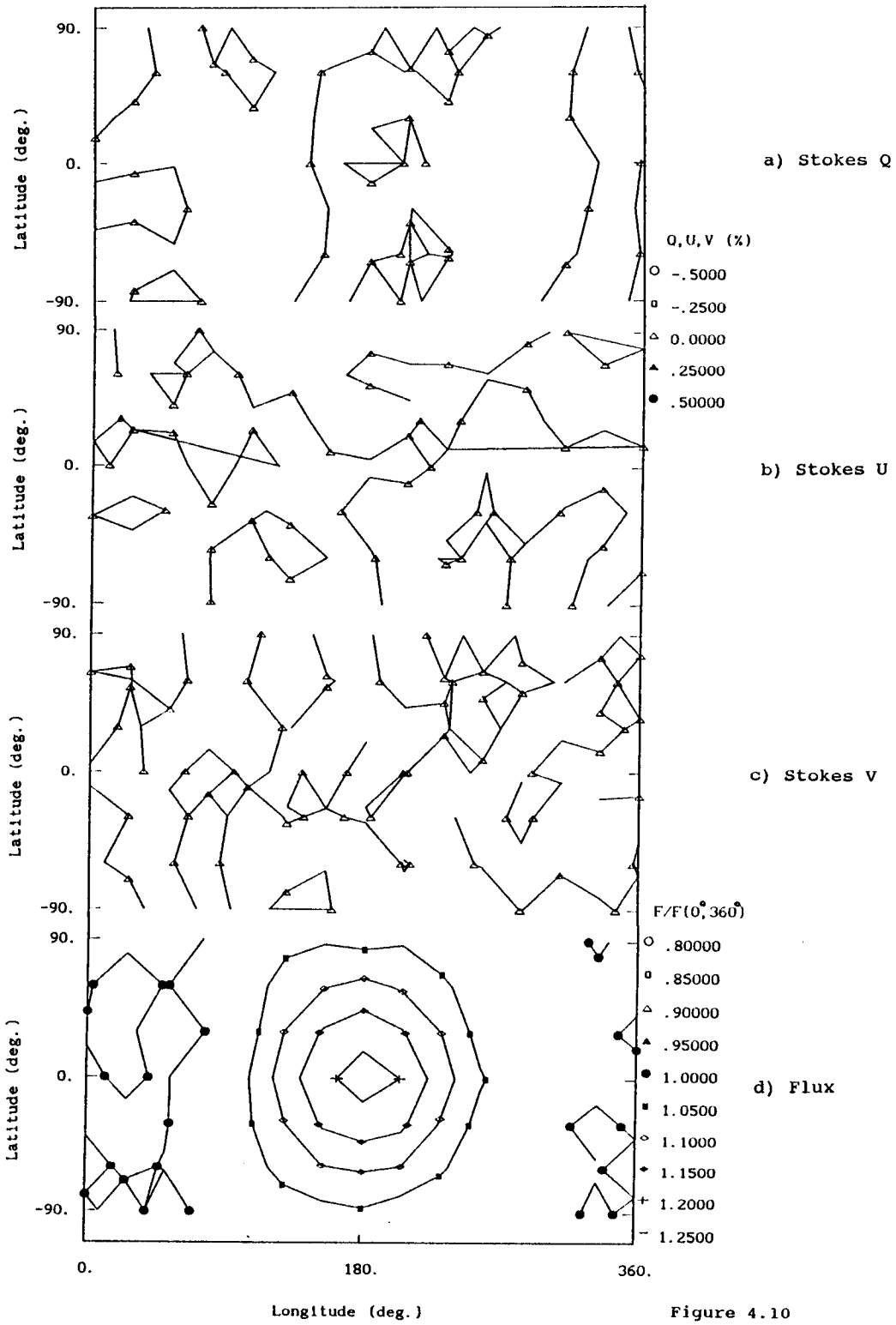
90.
0.
-90.
Latitude (deg.)
Q,U,V (%)
-.5000
-.2500
0.0000
.25000
.50000
a) Stokes Q
b) Stokes U
c) Stokes V
F/F(0°,360°)
.80000
.85000
.90000
.95000
1.0000
1.0500
1.1000
1.1500
1.2000
1.2500
d) Flux
0.
180.
360.
Longitude (deg.)

Figure 4.10

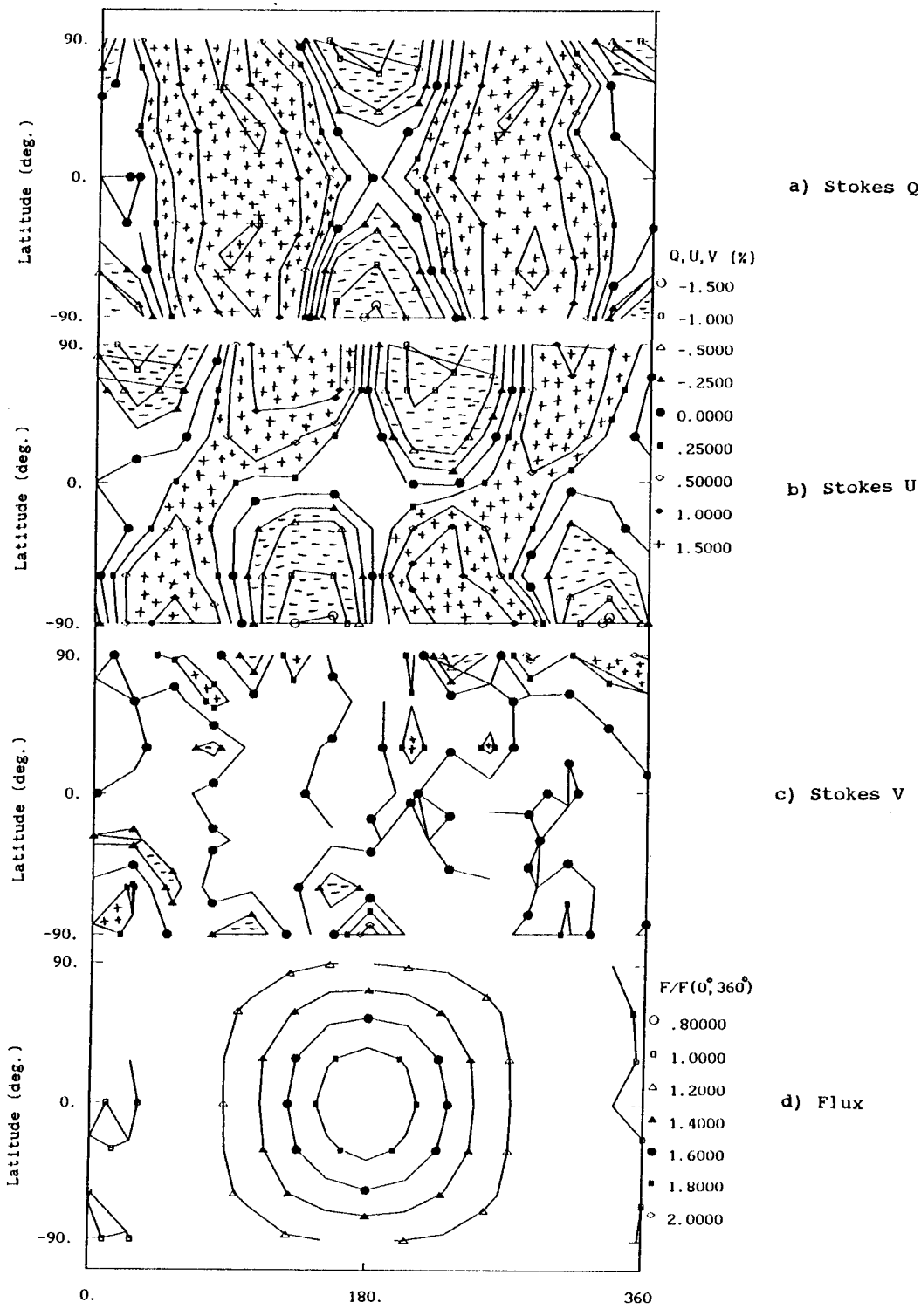
90.
0.
-90.
Latitude (deg.)
Q,U,V (%)
-1.500
-1.000
-.5000
-.2500
0.0000
.25000
.50000
1.0000
1.5000
a) Stokes Q
b) Stokes U
c) Stokes V
F/F(0°,360°)
.80000
1.0000
1.2000
1.4000
1.6000
1.8000
2.0000
d) Flux
0.
180.
360
Longitude (deg.)

Figure 4.11

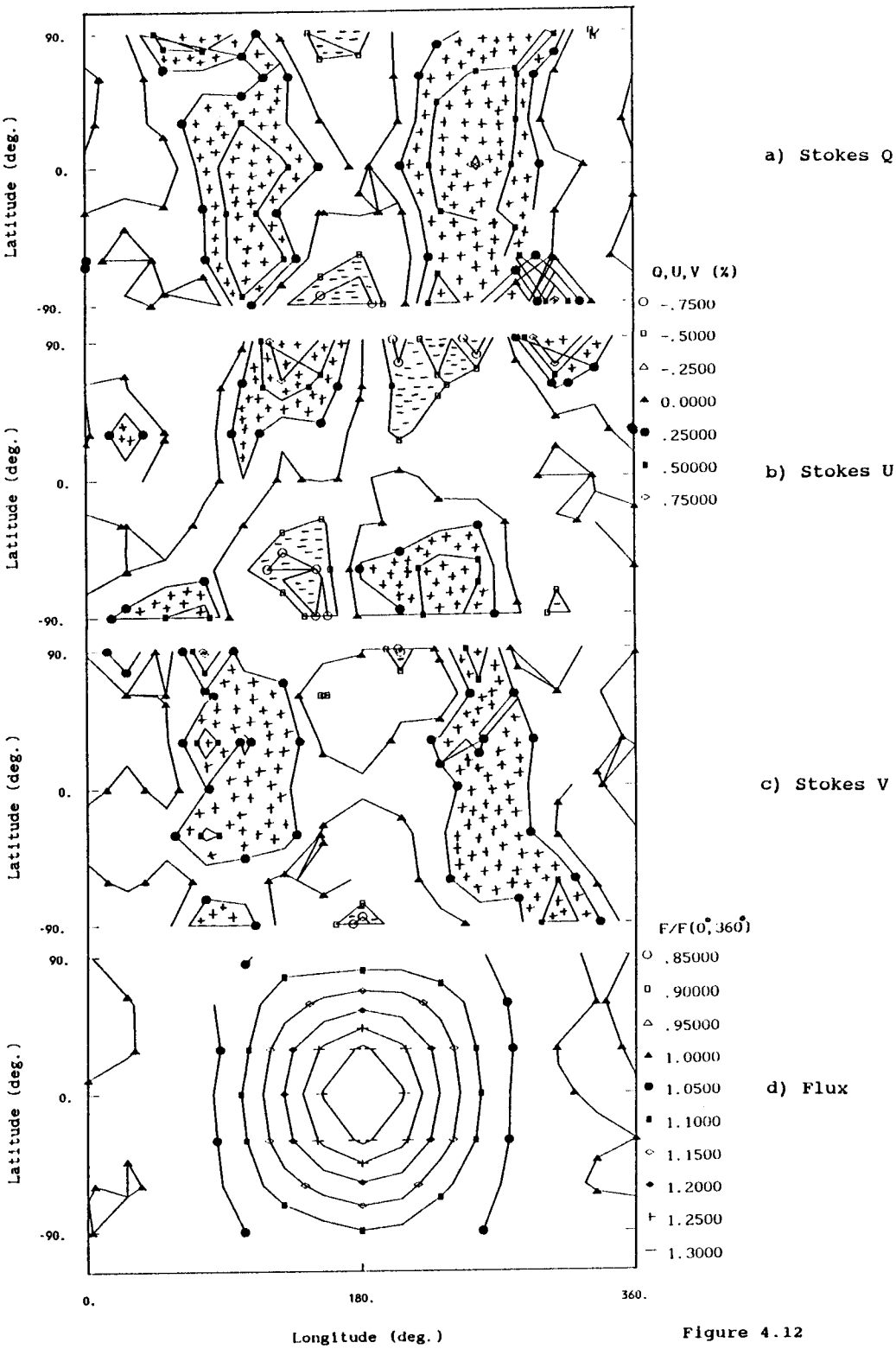
90.
0.
-90.
Latitude (deg.)
Q,U,V (%)
-.7500
-.5000
-.2500
0.0000
.25000
.50000
.75000
a) Stokes Q
b) Stokes U
c) Stokes V
F/F(0°,360°)
.85000
.90000
.95000
1.0000
1.0500
1.1000
1.1500
1.2000
1.2500
1.3000
d) Flux
0.
180.
360.
Longitude (deg.)

Figure 4.12

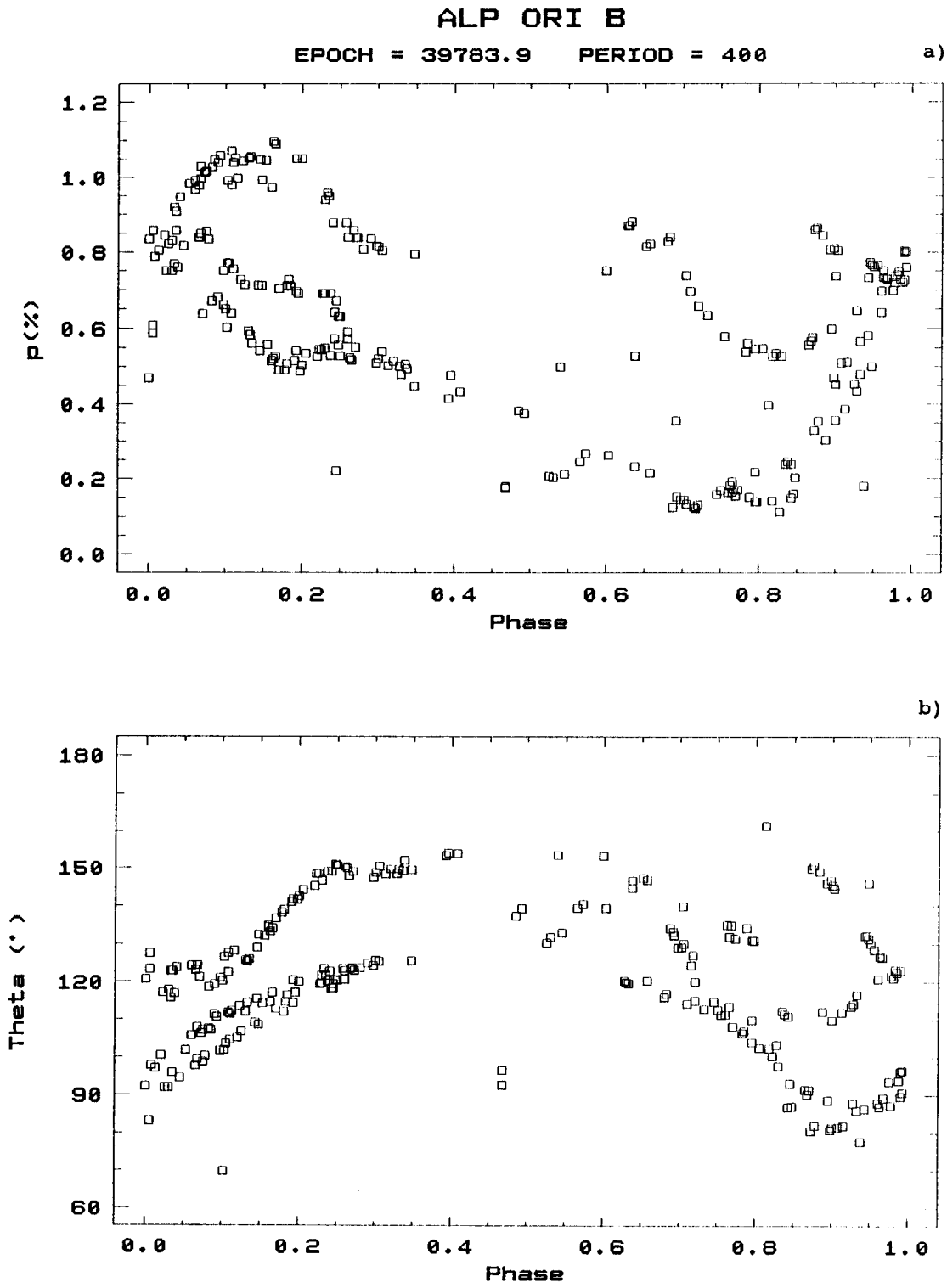
ALP ORI B
EPOCH = 39783.9 PERIOD = 400
a)
p(%)
1.2
1.0
0.8
0.6
0.4
0.2
0.0
0.0
0.2
0.4
0.6
0.8
1.0
Phase
b)
Theta (°)
180
150
120
90
60
0.0
0.2
0.4
0.6
0.8
1.0
Phase

Figure 4.13

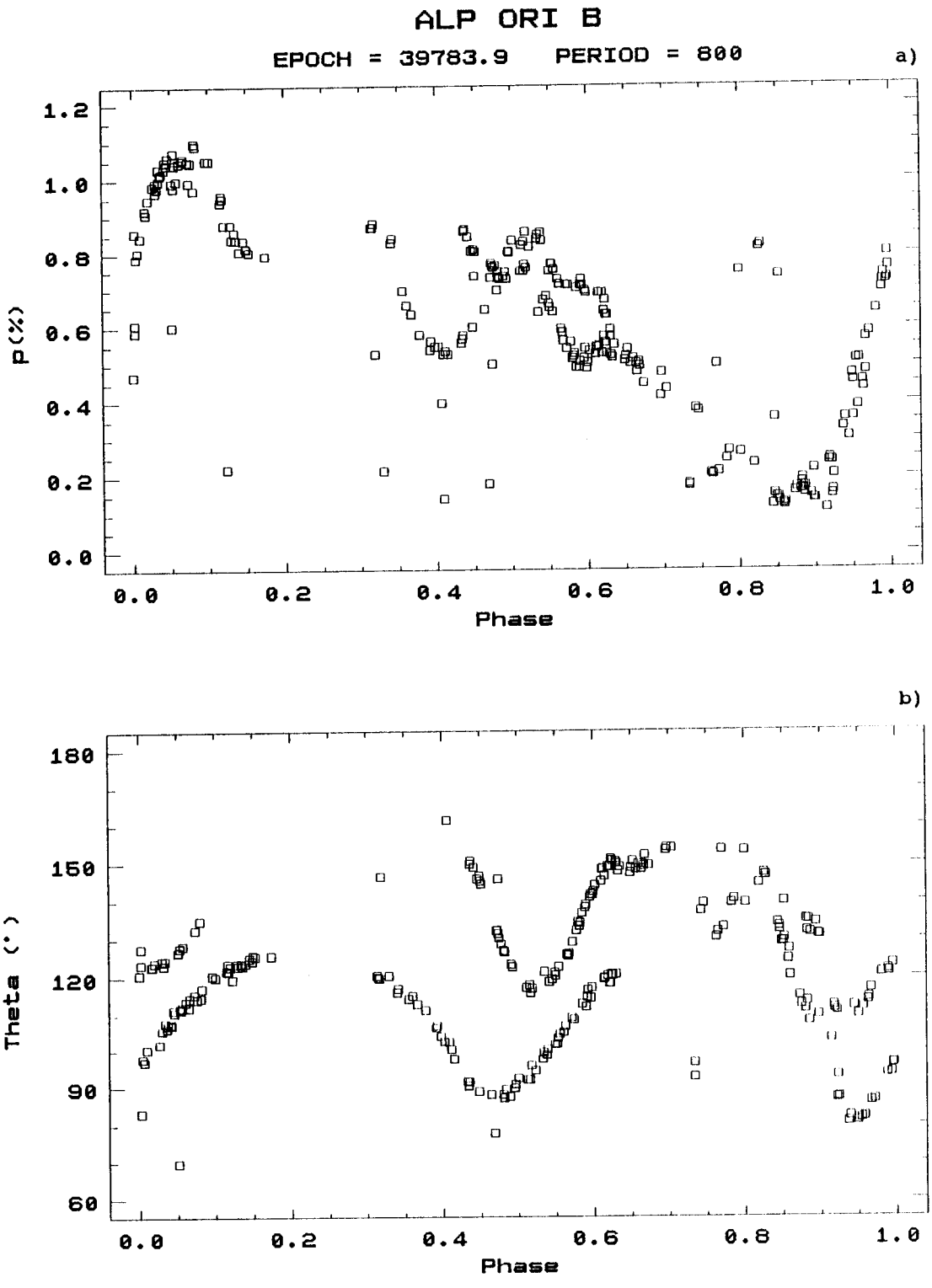
ALP ORI B
EPOCH = 39783.9 PERIOD = 800
a)
p(%)
1.2
1.0
0.8
0.6
0.4
0.2
0.0
0.0
0.2
0.4
0.6
0.8
1.0
Phase
b)
Theta (°)
180
150
120
90
60
0.0
0.2
0.4
0.6
0.8
1.0
Phase

Figure 4.14

APPENDIX A. PEMP Observing Procedure

This section records all steps which must be taken in order to make polarization measures with the PEMP system.

A.1 SETUP

A.1.1 The following electrical equipment is turned on:

IBM AT used for Channels 1 and 2.

The telescope drive power and polarimeter switches.

Dome circuit breakers #1 and #6.

Stanford Lock-in Amplifier.

Ithaco Lock-in (should never be turned off).

Telescope power switches.

A.1.2 The following are turned off:

Humidistat lamp

Main and auxiliary building lighting

A.1.3 Initialization of Channel 1 is accomplished by the following steps. All superfluous lighting is turned off. The Electric Vector is turned on with the green filter in place. The PEM unit driver is set to 5.400. The polarimeter is rotated to 43.5 degrees on the rotating circle. The Ithaco 391A Lock-in is phased by switching the system 90 degrees out of phase (left switch down) and then nulling the output by adjusting the analog phase dial. The switch is then toggled back to 0 degrees. Note that the Electric Vector must be removed after step A.1.4.

A.1.4 The CIRCPOL floppy disk is inserted into the top floppy disk drive on the Channel 3 XT. This computer and its monitor are turned on. Instructions displayed on the monitor are followed in order to initialize

this channel. These instructions are also evident from the source code presented in Appendix C.

A.1.5 At the Channels 1 and 2 IBM-AT the "PEMP" command is entered. The clock drive should start operating at this point.

A.1.6 The dome is opened and the optics uncovered. The telescope is rotated to an azimuth of either zero or 12 hours. The telescope is then set to read Local Sidereal Time directly.

A.2 OBSERVING

A.2.1 The telescope and dome are moved to the object to be observed.

A.2.2 Parameter variables are entered into the IBM-AT for the star to be observed. These parameters include Object name, Channel 1 gain, Channel 2 gain, Star integration length, Background integration length, and comments.

A.2.3 The star name, integration length counts and gain are entered into Channel 3. The integration length count is directly proportional to the duration of integration. Suggested integration length counts used with the Stanford lock-in amplifier are:

90 sec	2100,
60 sec	1400,
30 sec	700,
10 sec	250.

Any other value for the integration length count may also be used.

A.2.4. The proper instrumental settings for the object to be observed are set on the polarimeter and the high voltage supply. The proper filter (R,G,B,u) is set on axis. The PEM is set to 6.700 for Red, 5.400 for

Green, 4.200 for Blue, and 3.750 for u. The focal plane aperture is set (1.5, 2.5, or 5.0 mm). The high voltage used should be between 1200 and 2000 volts. Generally, the voltage setting should be the highest voltage usable without causing overloading in any Channel.

A.2.5 The Polarimeter is rotated to 0.0 degrees (plus or minus 0.5 degrees).

A.2.6 All superfluous lights are turned off.

A.2.7 The object is centered first in the wide angle eyepiece and then in the narrow eyepiece. If necessary, the telescope is focused. The Channel 2 output is checked on the analog meter mounted on the polarimeter.

A.2.8 Integration is started for all Channels.

A.2.9 Once integration ends, the telescope is rotated for 4 to 12 seconds of time in declination so as to measure background data. Integration is restarted.

A.2.10 After integration ends, the Polarimeter is rotated to 40.0 degrees. Steps 2.8 and 2.9 are repeated for this angle except that the slewing recenters the star in the narrow eyepiece.

A.2.11 The process continues for the angles 80, 120, 160, 200, 240, 280, 320 degrees.

A.3 DATA REDUCTION

Data reduction occurs automatically after the last measure if desired, but measurements may be retaken for any angle(s) if required (e.g. due to a

passing cloud). The $\langle\langle NET_2 \rangle\rangle$ average count and the calibration coefficients must be entered into the Channel 3 system at this point.

A.4 A NEW OBJECT

Repeat A.2 OBSERVING and A.3 DATA REDUCTION. All channels query the observer whether or not to go to another object.

A.5 SHUTDOWN

The telescope is moved to the stowed position. The telescope optics and polarimeter are covered. The dome is rotated to its stowed position. Steps A.1.1 and A.1.2 are reversed.

APPENDIX B.

Derivation of Stationary Errors

Equation 5, from Section 7.04 of Smart (1958), is equivalent to:

$$\sigma_k^2 = \frac{(j - 1)\,\sigma_{obs}^2 - \frac{j}{2}\sum_{i=1}^{k}(A_i^2 + B_i^2)}{j - (2k + 1)}, \qquad \text{(B.1)}$$

where σ_k is the standard deviation in the Fourier fit with k harmonics (the DC term is not included in the count), σ_{obs} is the standard deviation of the observations, j is the number of observations, and A and B are the amplitudes of the sine and cosine harmonics respectively.

Suppose there is only noise and no signal. Then by equipartition:

$$\langle A_i^2 \rangle = \langle B_i^2 \rangle = C^2 \geq 0, \qquad \text{(B.2)}$$

where C represents a steady-state value. Substitution of Equation B.2 into Equation B.1 generates the steady-state standard deviation in the Fourier fit:

$$\langle \sigma_k^2 \rangle = \frac{(j - 1)\langle \sigma_{obs}^2 \rangle - jkC^2}{j - (2k + 1)}. \qquad \text{(B.3)}$$

Due to the sampling theorem and the Nyquist critical frequency limit,

$$\langle \sigma^2_{obs} \rangle = \frac{j}{2} C^2, \qquad \text{(B.4)}$$

since aliasing will occur.

Substituting Equation B.4 into Equation B.3 and taking the difference formed by a variation in the number of harmonics in the Fourier fit produces:

$$\langle \sigma^2_k \rangle - \langle \sigma^2_{k+1} \rangle = 0, \qquad \text{(B.5)}$$

which shows that the reported errors are stationary under variation in the number of harmonics up to the Nyquist limit. Adding or subtracting harmonics does not change the reported error on average, although more degrees-of-freedom for the calculation produce less scatter. With the Pennsylvania polarimeter, nine observations are made and seven Fourier terms are calculated. This leaves two degrees-of-freedom for the characterization of the error.

If the assumption made above (i.e. that there is no signal) is false, Equation B.5 does not hold. This illustrates the problem of leaving out harmonics since *a priori* one often does not know when a signal exists or does not exist. Elias (1990) reports an experimental verification of Equation B.5 using polarimeter data. Blitzstein (1991) presents an analysis of different reductions of four runs taken under the same conditions. The third and fourth harmonics derived from the least-squares solution are the consequence of noise fluctuations only.

APPENDIX C.

Data Acquisition and Reduction Software

Listings for the Circular Subsystem

The circular polarimetry software was written over the five year period from 1986 to 1990 in the computer language BASIC as implemented by Microsoft Corporation. The choice of BASIC was made because the language is relatively easy to debug, has continuity with previously implemented systems, and most importantly, is easy to maintain by other workers at the Flower and Cook Observatory. The performance disadvantage of BASIC compared to other languages is not felt since the real-time operations are handled by the embedded system inside the Stanford SR530.

The data acquisition software is called CIRCPOL. It runs on the XT-compatible in the telescope dome and requires an RS232 card connected to a properly configured SR530. A sample elliptical polarization run report follows the program listings; page two is produced by CIRCPOL.

The data reduction software is called REDUCE. It runs on any PC-compatible microcomputer. REDUCE reads a file called STARS which contains an ASCII list of the stars for which data are to be reduced. REDUCE assumes the input data files for the star names have the ".DAT" file extender. The input data must be comma delimited. Missing data must be coded with a star (*).

The format for the input file is:

NAME, FILTER, JD, LINEAR D TERM, LINEAR D PROBABLE ERROR, LINEAR E TERM, LINEAR E PROBABLE ERROR, C1, C2, NET2 AVERAGE, STAR INTEGRATION LENGTH, CIRCULAR A TERM, CIRCULAR A PROBABLE ERROR <cr,lf>.

The format for the output data is compatible with the Statgraphics statistical analysis program. Line one contains Statgraphics variable names, and line 2 to end of file has the following format (in sorted order):

NAME,FILTER,JD,Q(%),STANDARD ERROR IN Q(%),U(%),STANDARD ERROR IN

U(%),LINEAR POLARIZATION Amplitude(%), LINEAR POL STANDARD ERROR, AZIMUTH OF ELECTRIC VECTOR (degrees),STANDARD ERROR IN AZIMUTH,V(%),STANDARD ERROR IN V <cr,lf>.

Samples of an input file and the associated output file follow the elliptical polarization sample report.

```
10  CLEAR,,5000
20 '#########################################################################
30 '#
40 '#                          C I R C P O L
50 '#    Data Acquisition Program For Circular Polarization Measurement
60 '#
70 '#
80 '#     Version 1:  Nov  18, 1986    by Bruce D. Holenstein
90 '#     Version 4:  Nov  29, 1986    by BDH
100 '#    Version 5:  Dec  29, 1986    by BDH
110 '#    Version 6:  Jan  18, 1987    by BDH
120 '#    Version 7:  Jan  25, 1987    by BDH
130 '#    Version 8:  May  11, 1987    by BDH
140 '#    Version 9:  Jul  20, 1987    by BDH
150 '#    Version 10: Aug  10, 1987    by BDH
160 '#    Version 10b:Oct  18, 1988    by RJM
170 '#    Version 11: Oct  16, 1989    by BDH
180 '#    Version 12: Mar   3, 1990    by BDH
190 '#
200  VERS = 12 'version variable
210 '#########################################################################
220 CLS
230 PRINT "                   CIRCPOL             Version: ";VERS
240 PRINT
250 PRINT "SR530  CIRCULAR POLARIZATION MEASUREMENT AND REDUCTION SYSTEM"
260 PRINT
270 PRINT
280 PRINT
290 WIDTH "LPT1:",132
300 DIM OBS(9,2,3) 'observations   (angle, type, value)
310 DIM A(7,9),TH(9),W(7),X(7),BB(7,7,7),PE(7),AEM(7,7),C(7,7),P(9),V(9),VR(9),EM(9),AA(7,7,7),THETA(9)
320 NANGLES = 9 'nine azimuth angles
330 '
340 'INPUT"What is the circular polarization calibration factor";CALFACT
350 '
360 CALFACT=5.8E+07 : ' Hardcoded 10/18/88 by RJM
370 CALFACT=4.14E+07 : ' Changed with version 11
380 '
390 INPUT "Do you want to re-reduce data";RED$
400 IF RED$="n" OR RED$ ="N" THEN 450
410 INPUT "Standard Vectors X,Y? ",SVX,SVY:PRINT:GOTO 910
420 '
430 '
440 '
450 'Configure Stanford Lock-in
460 OPEN"COM2:9600,N,8,2" AS #1
470 'set switch #1 of SW2 down - all others up
480 'turn on lock-in with local switch depressed
490 PRINT #1,"       "
500 PRINT #1,"Z"
510 FOR I = 1 TO 5000:NEXT I
520 PRINT #1,"I 1" 'front panel lock-out: press local key to bypass
530 PRINT #1,"W 0" 'wait amount
540 PRINT #1,"L1,1":PRINT #1,"L2,1"   'line notch filters in
550 PRINT #1,"B 0"  'bandpass filter out
560 PRINT #1,"S 0"  'x - y operation
570 PRINT #1,"G 14" 'set temporary gain
580 PRINT #1,"D 1"  'normal dynamic reserve
590 PRINT #1,"M 0"  'f reference mode
600 PRINT #1,"P 0"  'set phase to zero
610 PRINT #1,"R 1"  'symmetric reference
620 PRINT #1,"T 1,6" '300ms pre time constant
630 PRINT #1,"T 2,1" '100ms post time constant
640 PRINT #1,"E1,0" 'X expand off
650 PRINT #1,"E2,0" 'Y expand off
660 PRINT #1,"X6,10.00" 'set x6 to 10 volts for paddle
670 PRINT #1,"OX 1,80.0E-6" 'ver 11, 80,40,20 microV offset on 200,100,50 sens.
680 PRINT #1,"OY 1,80.0E-6" 'ver 11, 80,40,20 microV offset on 200,100,50 sens.
690 '
700 '############## Determine Standard Vectors ##############################
710 PRINT
720 PRINT "*** STANDARD VECTOR DETERMINATION ***"
730 INPUT "Have you measured them already today";ARED$
740 IF ARED$="n" OR ARED$ ="N" THEN 760
750 INPUT "Standard Vectors X,Y? ",SVX,SVY:PRINT:GOTO 910
760 PRINT "Insert Polaroid Circular Polarizer. Rotate PEM to 43.5 degrees."
770 PRINT "Turn on Electric Vector. Dim ambient lighting."
780 INPUT "Turn Hi-voltage to 1200V. Turn to 1.5 aperture. Next hit ENTER.",JUNK$
790 TS=750:TB=750
800 GOSUB 1340
810 SVX=Q1V:SVY=Q2V
820 INPUT "Turn OFF Electric Vector. Next hit ENTER.",JUNK$
830 TT=750
840 GOSUB 1340
850 SVX=SVX-Q1V:SVY=SVY-Q2V
860  PRINT "Standard Vectors = ";
870  PRINT USING "+#.###^^^^     ";SVX;SVY
880 PRINT "Set all system variables to program star."
890 '
```

```
900 '
910 '########  Get initial information
920 PRINT"CIRCPOL initial information"
930 INPUT"What object";OBJ$
940 IF RED$="y" OR RED$ ="Y" THEN 1220
950 INPUT"Star integration count";TS
960 INPUT"Background integration count";TB
970 PRINT"Gain (Sensitivity) Integer: 12 =  50 micro V  "
980 PRINT"                            13 = 100 micro V  "
990 PRINT"                            14 = 200 micro V  "
1000 INPUT"(Use other integers for different gains: 1 to 24)";GS$
1010 PRINT #1,"G"+GS$
1020 INPUT"Are values correct";Y$
1030 IF Y$<>"y" AND Y$<>"Y" THEN  910
1040 CLS
1050 '
1060 '#########################################################################
1070 'INPUT #1,JUNK$  'empty out anything pending
1080 '**** MAIN LOOP
1090 STYPE=0
1100 TYPE = 0'star
1110  FOR LOOP=0 TO NANGLES-1  'azimuth angles
1120 '
1130 GOSUB 1730 'measure angle
1140 GOSUB 1730 'star and background
1150 GOSUB 1860
1160 '
1170 NEXT LOOP
1180 '
1190 '
1200 INPUT"Do you want to remeasure any azimuth";Y$
1210 IF Y$="y" OR Y$ ="Y" THEN GOTO 1610
1220 GOSUB 4060
1230 GOSUB 2130
1240 GOSUB 3270
1250 INPUT"Start another run";Y$
1260 IF Y$="n" OR Y$ ="N" THEN END
1270 GOTO 910
1280 '
1290 '
1300 '
1310 '#########################################################################
1320  IF TYPE=1 THEN PRINT"BACKGROUND"
1330  IF TYPE=0 THEN PRINT"STAR"
1340 '*** integrate for TT iterations ***
1350 PRINT
1360 PRINT"Press button to integrate                          "
1370 PRINT #1,"X1"
1380 INPUT #1,X1PAD 'paddle voltage
1390 IF X1PAD < 5! THEN 1370  'paddle not pressed
1400 SOUND 200,5
1410 CLS
1420 FOR XX=0 TO 10000:NEXT XX 'pause several time constants
1430 PRINT "int"
1440 Q1V = 0!
1450 Q2V = 0!
1460 IF TYPE=1 THEN TT=TB:GOTO 1480
1470 TT=TS   'star
1480 FOR TL = 1 TO TT
1490 PRINT #1,"QX"  'ver 11 change from q1 to qx
1500 INPUT #1,Q1
1510 PRINT #1,"QY"  'ver 11 change from q2 to qy
1520 INPUT #1,Q2
1530 Q1V = Q1V + Q1  'x
1540 Q2V = Q2V + Q2  'y
1550 NEXT TL
1560 Q1V =  Q1V/TT   'avg value wanted
1570 Q2V =  Q2V/TT   'avg value wanted
1580 RETURN
1590 '
1600 '
1610 '#########################################################################
1620 INPUT"Which angle - 0,40,80,120,160,200,240,280,320";ANGLE
1630 LOOP=ANGLE/40
1640 TYPE=1
1650 STYPE = 2
1660 GOSUB 1730 'star and background
1670 GOSUB 1730
1680 LOOP=8'for printing
1690 GOSUB 1860
1700 GOTO 1200
1710 '
1720 '
1730 '#########################################################################
1740 GOSUB 1310 'integrate
1750 PRINT #1,"F"
1760 INPUT #1,FREQ$
1770 OBS(LOOP,TYPE,1) = Q1V 'x
1780 OBS(LOOP,TYPE,2) = Q2V 'y
```

```
1790 OBS(LOOP,TYPE,3) = VAL(FREQ$)'frequency
1800 SOUND 40,10
1810 STYPE=STYPE+1:IF STYPE>3 THEN STYPE =0
1820 IF STYPE>0 AND STYPE<3 THEN TYPE =1 ELSE TYPE = 0
1830 RETURN
1840 '
1850 '
1860 '#####################################################################
1870 PRINT
1880 PRINT "CIRCPOL - SR530 based system"
1890 PRINT
1900 OPEN "O",#3,"STARDATA"
1910 PRINT DATE$, TIME$
1920 PRINT #3,DATE$, TIME$
1930 PRINT "Gain setting= ";GS$
1940 PRINT #3, "Gain setting= ";GS$
1950 PRINT "Star loop count=   ";TS
1960 PRINT #3, "Star loop count=   ";TS
1970 PRINT "Background loop count=   ";TB
1980 PRINT #3, "Background loop count=   ";TB
1990 PRINT "Standard Vectors = ";
2000 PRINT #3, "Standard Vectors = ";
2009 PRINT USING "+#.###^^^^    ";SVX;SVY
2010 PRINT #3, USING "+#.###^^^^    ";SVX;SVY
2020 PRINT
2030 PRINT "      STAR     (volts)        BACKGROUND              NET"
2040 PRINT "CH X        CH Y           CH X        CH Y          RX,RY"
2050 FOR LD=0 TO LOOP
2056 PRINT USING "+#.###^^^^  ";OBS(LD,0,1);OBS(LD,0,2);
2057 PRINT "|  ";
2058 PRINT USING "+#.###^^^^  ";OBS(LD,1,1);OBS(LD,1,2);
2059 PRINT "|  ";
2060 PRINT #3, USING "+#.###^^^^  ";OBS(LD,0,1);OBS(LD,0,2);OBS(LD,1,1);OBS(LD,1,2);
2069 PRINT USING "+#.###^^^^  ";(OBS(LD,0,1)-OBS(LD,1,1));(OBS(LD,0,2)-OBS(LD,1,2))
2070 PRINT #3, USING "+#.###^^^^  ";(OBS(LD,0,1)-OBS(LD,1,1));(OBS(LD,0,2)-OBS(LD,1,2))
2080 NEXT LD
2090 CLOSE #3
2100 PRINT:PRINT
2110 RETURN
2120 '#####################################################################
2130 REM  ***   Least Squares Routine: PEMP implementation ***
2140 REM
2150 REM N = # of variables to be solved for
2160 N = 7
2170 NPTS=9
2180 REM NPTS = # of Data pairs - from main program
2190 REM Assume Theta(I) already in radians from main program
2200 FOR J=1 TO NPTS
2210  A(1,J)=1
2220  A(2,J)=SIN(TH(J))
2230  A(3,J)=COS(TH(J))
2240  A(4,J)=SIN(2*TH(J))
2250  A(5,J)=COS(2*TH(J))
2260  A(6,J)=SIN(3*TH(J))
2270  A(7,J)=COS(3*TH(J))
2280 NEXT J
2290 FOR I=1 TO N
2300 W(I)=0
2310 X(I)=0
2320 PE(I)=0
2330 FOR J=1 TO N
2340 AEM(I,J)=0
2350 C(I,J)=0
2360 FOR K=1 TO N
2370 AA(I,J,K)=0
2380 BB(I,J,K)=0
2390 NEXT K
2400 NEXT J
2410 NEXT I
2420 FOR I=1 TO NPTS
2430 P(I)=1!
2440 V(I)=0
2450 VR(I)=0
2460 NEXT I
2470 FOR J=1 TO N
2480 AEM(J,1)=0
2490 FOR K=1 TO N
2500 IF (J-1) = 0 THEN 2610
2510 IF (J-1) > 0 THEN 2520
2520 IF (K-J) < 0 THEN 2540
2530 IF (K-J) >= 0 THEN 2610
2540 AA(J,K,1)=AA(K,J,1)
2550 IF (K-1) = 0 THEN 2570
2560 IF (K-1) > 0 THEN 2680
2570 FOR I=1 TO NPTS
2580 AEM(J,1)=AEM(J,1)+A(J,I)*EM(I)*P(I)
2590 NEXT I
2600 GOTO 2680
2610 AA(J,K,1)=0
```

```
2620 FOR II=1 TO NPTS
2630 AA(J,K,1)=AA(J,K,1)+(A(J,II)*A(K,II)*P(II))
2640 IF (K-1) = 0 THEN 2660
2650 IF (K-1) > 0 THEN 2670
2660 AEM(J,1)=AEM(J,1)+A(J,1)*EM(II)*P(II)
2670 NEXT II
2680 NEXT K
2690 NEXT J
2700 FOR I=1 TO N
2710 FOR J=1 TO N
2720 IF (I-J) <> 0 THEN 2740
2730 IF (I-J) = 0 THEN 2760
2740 BB(I,J,1)=0
2750 GOTO 2770
2760 BB(I,J,1)=1!
2770 NEXT J
2780 NEXT I
2790 FOR L=2 TO N
2800 LM=L-1
2810 FOR J=1 TO N
2820 IF (J-L) < 0 THEN 2840
2830 AEM(J,L)=AEM(J,LM)-AEM(LM,LM)*AA(LM,J,LM)/AA(LM,LM,LM)
2840 FOR K=1 TO N
2850 BB(J,K,L)=BB(J,K,LM)-BB(LM,K,LM)*AA(LM,J,LM)/AA(LM,LM,LM)
2860 AA(J,K,L)=AA(J,K,LM)-AA(LM,J,LM)*AA(LM,K,LM)/AA(LM,LM,LM)
2870 NEXT K
2880 NEXT J
2890 NEXT L
2900 FOR ML=1 TO N
2910 L=N-ML+1
2920 LP=L+1
2930 X(L)=AEM(L,L)/AA(L,L,L)
2940 FOR K=1 TO N
2950 IF (L-K) < 0 THEN 3050
2960 C(K,L)=BB(L,K,L)/AA(L,L,L)
2970 IF (L-N) < 0 THEN 2990
2980 IF (L-N) = 0 THEN 3050
2990 FOR J=LP TO N
3000 C(K,L)=C(K,L)-AA(L,J,L)/AA(L,L,L)*C(K,J)
3010 IF (K-1) = 0 THEN 3030
3020 IF (K-1) > 0 THEN 3040
3030 X(L)=X(L)-AA(L,J,L)/AA(L,L,L)*X(J)
3040 NEXT J
3050 NEXT K
3060 W(L)=1!/C(L,L)
3070 NEXT ML
3080 SV=0
3090 VV=0
3100 GME=0
3110 FOR J=1 TO NPTS
3120 V(J)=-EM(J)
3130 FOR I=1 TO N
3140 V(J)=V(J)+A(I,J)*X(I)
3150 NEXT I
3160 VR(J)=V(J)*SQR(P(J))
3170 SV=SV+VR(J)
3180 GME=GME+ABS(VR(J))
3190 VV=VV+VR(J)^2
3200 NEXT J
3210 GME=GME/NPTS
3220 R=.6745*SQR(VV/(NPTS-N))
3230 FOR I=1 TO N
3240 PE(I)=R*SQR(ABS(C(I,I)))
3250 NEXT I
3260 RETURN
3270 '#########################################################################
3280 '   print out solutions
3290 INPUT "Is printer on line (hit return)";JUNK$
3300 LPRINT CHR$(15)
3310 LPRINT
3320 LPRINT CHR$(27);"E"
3330 LPRINT "CIRCPOL - SR530 based system"
3340 LPRINT "Version:  ";VERS
3350 LPRINT CHR$(27);"F"
3360 LPRINT
3370 LPRINT DATE$, TIME$
3380 LPRINT "Object=       ";OBJ$
3390 LPRINT "Gain setting= ";GS$
3400 LPRINT "Star loop count=   ";TS
3410 LPRINT "Background loop count=   ";TB
3420 LPRINT
3430 LPRINT "Standard Vectors = ";
3440 LPRINT USING "+#.###^^^^    ";SVX;SVY
3450 LPRINT "Standard vector angle =";:LPRINT USING "###.##  ";ALPHA :LPRINT
3460 LPRINT
3470 LPRINT "AZ            STAR        (volts)         BACKGROUND             NET          RESIDUALS"
3480 LPRINT "DEG     CH X          CH Y          CH X          CH Y          R Stan Vec"
3490 FOR LD=0 TO NANGLES-1
3500 LPRINT USING "###.##  ";THETA(LD);
```

```
3510 LPRINT USING "+#.###^^^^     ";OBS(LD,0,1);OBS(LD,0,2);OBS(LD,1,1);OBS(LD,1,2);
3520 LPRINT USING "+#.###^^^^     ";EM(LD+1);
3530 LPRINT USING "+#.###^^^^";V(LD+1)   'residuals
3540 NEXT LD
3550 LPRINT
3560 LPRINT "Sum of residuals squared";
3570 LPRINT USING "   +#.###^^^^ ";VV
3580 LPRINT
3590 LPRINT "A";
3600 LPRINT USING "   +#.###^^^^   ";X(1);
3610 LPRINT "+/-";
3620 LPRINT USING "   +#.###^^^^   ";PE(1)
3630 LPRINT "B";
3640 LPRINT USING "   +#.###^^^^   ";X(2);
3650 LPRINT "+/-";
3660 LPRINT USING "   +#.###^^^^   ";PE(2)
3670 LPRINT "C";
3680 LPRINT USING "   +#.###^^^^   ";X(3);
3690 LPRINT "+/-";
3700 LPRINT USING "   +#.###^^^^   ";PE(3)
3710 LPRINT "D";
3720 LPRINT USING "   +#.###^^^^   ";X(4);
3730 LPRINT "+/-";
3740 LPRINT USING "   +#.###^^^^   ";PE(4)
3750 LPRINT "E";
3760 LPRINT USING "   +#.###^^^^   ";X(5);
3770 LPRINT "+/-";
3780 LPRINT USING "   +#.###^^^^   ";PE(5)
3790 LPRINT "F";
3800 LPRINT USING "   +#.###^^^^   ";X(6);
3810 LPRINT "+/-";
3820 LPRINT USING "   +#.###^^^^   ";PE(6)
3830 LPRINT "G";
3840 LPRINT USING "   +#.###^^^^   ";X(7);
3850 LPRINT "+/-";
3860 LPRINT USING "   +#.###^^^^   ";PE(7)
3870 LPRINT
3880 PRINT
3890 INPUT"What is the PEMP average NET2 for this run? ",NET2AVG
3900 INPUT"What is the PEMP C2 coefficient for this run? ",C2PEMP
3910 INPUT"What is the PEMP STAR integration length(sec)? ",TSPEMP
3920 PRINT
3930 LPRINT "Circpol calibration factor: ";CALFACT;"   Star integration length: ";TSPEMP 'ver 11 change
for integration length
3940 LPRINT "Net 2 average: ";NET2AVG;"   C2 coefficient: ";C2PEMP
3950 LPRINT
3960 LPRINT "Stokes V in percent  ";
3970 PRINT "Stokes V in percent  ";
3980 LPRINT USING "   +#.###^^^^   ";(TSPEMP/60)*CALFACT*X(1)/(NET2AVG*C2PEMP);
3990 PRINT USING "   +#.###^^^^   ";(TSPEMP/60)*CALFACT*X(1)/(NET2AVG*C2PEMP);
4000 LPRINT "+/-";
4010 PRINT "+/-";
4020 LPRINT USING "   +#.###^^^^   ";(TSPEMP/60)*CALFACT*PE(1)/(NET2AVG*C2PEMP)
4030 PRINT USING "   +#.###^^^^   ";(TSPEMP/60)*CALFACT*PE(1)/(NET2AVG*C2PEMP)
4040 LPRINT CHR$(12)
4050 RETURN
4060 '#########################################################################
4070 'prompt for angles
4080 PRINT
4090 PRINT
4100 INPUT "Are the azimuth angles OK?  ",AZANS$
4110 IF AZANS$="Y" OR AZANS$="y" THEN 4150
4120 PRINT "Enter the exact angles (degrees) for the 0,40,80,120,160,200,240,280,320"
4130 PRINT "measures";
4140 IF RED$="y" OR RED$ ="Y" THEN PRINT " and the NET Rx Ry." ELSE PRINT". "
4150 FOR QQ=0 TO NANGLES-1
4160 IF AZANS$="Y" OR AZANS$="y" THEN THETA(QQ) = QQ*40:GOTO 4190
4170 PRINT "angle ";QQ*40;"  ";
4180 INPUT THETA(QQ)
4190 TH(QQ+1)=THETA(QQ)*2*3.1416/360!  'convert to radians for lst sqr
4200 RX = (OBS(QQ,0,1)-OBS(QQ,1,1)):RY=(OBS(QQ,0,2)-OBS(QQ,1,2)) ' move data for lst sqr
4210 IF RED$="y" OR RED$ ="Y" THEN INPUT "RX,RY ? ",RX,RY:PRINT
4220  ALPHA=ATN(SVY/SVX)
4230 IF SGN(SVX) = -1 THEN  ALPHA=ALPHA +3.14159
4240  GAMMA=ATN(RY/RX)
4250 IF SGN(RX) = -1 THEN  GAMMA=GAMMA +3.14159
4260  BETA=GAMMA-ALPHA
4270  MAGNITUDE=(RY^2+RX^2)^.5
4280  EM(QQ+1)=MAGNITUDE*COS(BETA)
4290 NEXT QQ
4300 RETURN
```

```
10 CLS
20 DIM F$(15)
30 DIM R$(15)
40 DIM XX!(3)
50 DIM YY!(3)
60 DIM FILB(150,3,2)
70 DIM STAN(4,3,2) 'standardization coefficients: fil,stokes,m&b
80 DIM INTERS(4,3) 'interstellar stokes vectors: fil,stokes
90 '
100 '#################################################################
110 '#
120 '#                      R E D U C E
130 '#     Data Reducetion Program for Elliptical Polarimetry
140 '#
150 '#    Version 1: Jan 11, 1990      by Bruce D. Holenstein
160 '#    Version 2: Mar 20, 1990      by BDH
170 '#    Version 3: Mar 31, 1990      by BDH
180 '#    Version 5: April 15, 1990    by BDH
190 '#    Version 6: April 20, 1990    by BDH (errors calc updated)
200 '#    Version 7: May 24, 1990      by BDH (last two columns)
210 '#    Version 8: July 15, 1990     by BDH (printout formatting)
220 '#    Version 9: Aug. 5, 1990      by BDH (>90 deg, printout)
230 '#    Version 10: Aug. 10, 1990    by BDH (error calculations)
240 '#    Version 11: Aug. 12, 1990    by BDH (statgraphics output)
250 '#    Version 12: Aug. 24, 1990    by BDH (standardization)
260 '#    Version 13: Nov. 20, 1990    by BDH (summary p,theta)
270 '#    Version 14: Nov. 20, 1990    by BDH (interstellar)
280 '#
290 VER$=".V14" 'version variable
300 '#################################################################
310 PRINT "                R E D U C E "
320 PRINT "ELLIPTICAL POLARIZATION DATA REDUCTION: VERSION:"+VER$
330 PRINT "NOTE: This program requires data from CIRCPOL version 10 and up."
340 PRINT "The standard vector angle must be small (and usually negative)"
350 '
360 PRINT
370 INPUT "Do you want the output to load into Statgraphics (Y/N)?",STATG$
380 INPUT "Do you want the output to be standardized (Y/N)?",STAND$
390 INTERS$="N"
400 IF STAND$ = "Y" OR STAND$ = "y" THEN INPUT "Do you want the interstellar polarization removed
(Y/N)?",INTERS$
410 '
420 'Reads list of stars from STARS file
430 '
440 'Initialize calibration variables
450 CIRCGAIN!=414000! 'SR530 system gain (DEGREE)
460 SIGCGAIN!=22000!   'Error in gain
470 CIRCOFF!=0!        'Circular system polarization offset
480 SIGCOFF!=0!        'Error in offset
490 OLDCGAIN!=-3.55    'Ithaco system circular gain (DEGREE)
500 SIGOLDCGAIN!=9.000001E-02 'Error in gain
510 LINQGAIN!=1!       'Linear Q Stokes system gain
520 LINUGAIN!=1!       'Linear U Stokes system gain
530 LINQOFF!=0!        'Linear Q Stokes offset
540 LINUOFF!=0!        'Linear U Stokes offset
550 LINGAIN!=1.031     'Linear total gain
560 L!= 1.139          'Hybrid polarization values L=1.139(.009)
570 M!=-.0845         'Hybrid polarization values M=-0.0845(.02)
580 SIGL! = 8.999999E-03       'Error in L
590 SIGM! = .02        'Error in M
600 C1ERROR! = .005    'Error in C1 is 0.5%
610 C2ERROR! = .005    'Error in C2 is 0.5%
620 '
630 '###### Standardization coefficients (Table 2.3)
640 STAN(1,1,1) = .977          'Red
650 STAN(1,1,2) = -0!
660 STAN(1,2,1) = 1.066
670 STAN(1,2,2) = -.0001
680 STAN(1,3,1) = .992
690 STAN(1,3,2) = -.0057
700 STAN(2,1,1) = .977          'Green
710 STAN(2,1,2) = -.0002
720 STAN(2,2,1) = 1.066
730 STAN(2,2,2) = .0002
740 STAN(2,3,1) = .992
750 STAN(2,3,2) = .0004
760 STAN(3,1,1) = .977          'Blue
770 STAN(3,1,2) = -.002
780 STAN(3,2,1) = 1.066
790 STAN(3,2,2) = .0055
800 STAN(3,3,1) = .992
810 STAN(3,3,2) = .0062
820 STAN(4,1,1) = .977          'UV
830 STAN(4,1,2) = -.0005
840 STAN(4,2,1) = 1.066
850 STAN(4,2,2) = .0037
860 STAN(4,3,1) = .992
870 STAN(4,3,2) = .0005
880 '
```

```
890 OPEN "I",3,"stars"
900 INPUT #3,NI$
910 TEMP$="sort <"+NI$+".dat"+" >TEMP"  'sort data by filter,date
920 PRINT
930 PRINT "PROCESSING:";TEMP$
940 SHELL TEMP$
950 OPEN "I",1,"TEMP" 'process sorted data
960 NO$=NI$+VER$      'create output file with version extension
970 OPEN "O",2,NO$
980 PRINT #2,"STAR,FILTER,JD,Q,SIGQ,U,SIGU,LIN,SIGLIN,AZI,SIGAZI,V,SIGV,C2NET260,veratio"
990 PRINT #2,"Statgraphics: ";STATG$,"Standardized: ";STAND$,"Interstellar corrected: ";INTERS$
1000 LASTFIL$=""
1010 FILTOT=0
1020 '
1030 '################################################################
1040 FOR FIL = 1 TO 4
1050 FOR STOKE = 1 TO 3
1060 INTERS(FIL,STOKE) = 0!
1070 NEXT STOKE
1080 NEXT FIL
1090 IF INTERS$ = "n" OR INTERS$ = "N" THEN 1190
1100 PRINT "Input the interstellar polarization vectors Q,U,V in percent."
1110 FOR FIL = 1 TO 4
1120 IF FIL = 1 THEN PRINT "Red:    ";
1130 IF FIL = 2 THEN PRINT "Visual: ";
1140 IF FIL = 3 THEN PRINT "Blue:   ";
1150 IF FIL = 4 THEN PRINT "UV:     ";
1160 INPUT INTERS(FIL,1),INTERS(FIL,2),INTERS(FIL,3)
1170 NEXT FIL
1180 '
1190 '################################################################
1200 'Read data from sorted temporary data file
1210 FOR X=0 TO 12:INPUT #1,F$(X):NEXT X  'get star data rec
1220 'FOR X=0 TO 12: PRINT F$(X);" ";: NEXT X 'move variables over to output
1230 FOR X=0 TO 12: R$(X) = F$(X): NEXT X 'move variables over to output
1240 PRINT R$(2);" ";
1250 'Missing data will be coded as 9's
1260 R3!=999999!:R4!=999999!:R5!=999999!:R6!=999999!:R11!=999999!:R12!=999999!
1270 POL!=999999!:POLSIG!=999999!:ANGLE!=999999!:ANGLESIG!=999999!
1280 C1!=999999!:C2!=999999!:NET2!=999999!:INTSTAR!=999999!
1290 '
1300 'REDUCE DATA - missing data is coded with a asterik
1310 IF R$(7) <> "*" THEN C1!=VAL(R$(7))          'C1 coeff.
1320 IF R$(8) <> "*" THEN C2!=VAL(R$(8))          'C2 coeff.
1330 IF R$(9) <> "*" THEN NET2!=VAL(R$(9))        'NET2 value
1340 IF R$(10) <> "*" THEN INTSTAR!=VAL(R$(10))   'Star integration length
1350 R2!=VAL(R$(2))                               '(Julian Date-2440000)
1360 SIGC1! = C1ERROR! * C1!                      'Error in C1 (IF IT EXISTS)
1370 SIGC2! = C2ERROR! * C2!                      'Error in C2 (IF IT EXISTS)
1380 IF R$(3) = "*" THEN 1400 'There is no linear data
1390 GOSUB 2020 'Linear reduction
1400 IF R$(11) = "*" THEN 1420 'There is no circular data
1410 GOSUB 2350 'Circular reduction
1420 '
1430 IF STAND$="Y" OR STAND$="y" THEN GOSUB 3040
1440 '
1450 '################################################################
1460 'Produce summary statistics
1470 IF R$(1) <> LASTFIL$ THEN GOSUB 2620
1480 FILTOT=FILTOT+1 'number of datum for filter
1490 FILB(FILTOT,1,1)=R3! 'store data for weighted averages
1500 FILB(FILTOT,1,2)=R4!
1510 FILB(FILTOT,2,1)=R5!
1520 FILB(FILTOT,2,2)=R6!
1530 FILB(FILTOT,3,1)=R11!
1540 FILB(FILTOT,3,2)=R12!
1550 '
1560 'Write reduced data to output file
1570 IF STATG$="Y" OR STATG$="y" THEN GOTO 1720
1580 PRINT#2,"       ";R$(0);" ";
1590 PRINT#2,"       ";R$(1);" ";
1600 PRINT#2,USING "    ####.### ";R2!;
1610 IF R3!<1000 THEN PRINT#2,USING "      +##.### ";R3!; ELSE PRINT#2,"          ...  ";
1620 IF R4!<1000 THEN PRINT#2,USING "  ##.### ";R4!; ELSE PRINT#2,"      ...  ";
1630 IF R5!<1000 THEN PRINT#2,USING "    +##.### ";R5!; ELSE PRINT#2,"       ...  ";
1640 IF R6!<1000 THEN PRINT#2,USING "  ##.### ";R6!; ELSE PRINT#2,"     ...  ";
1650 IF POL!<1000 THEN PRINT#2,USING "     ##.### ";POL!; ELSE PRINT#2,"         ...  ";
1660 IF POLSIG!<1000 THEN PRINT#2,USING "  ##.### ";POLSIG!; ELSE PRINT#2,"     ...  ";
1670 IF R3!<1000 THEN PRINT#2,USING "      ###.# ";ANGLE!; ELSE PRINT#2,"       ...  ";
1680 IF R3!<1000 THEN PRINT#2,USING "  ###.# ";ANGLESIG!; ELSE PRINT#2,"    ...  ";
1690 IF R11!<1000 THEN PRINT#2,USING "    +##.### ";R11!; ELSE PRINT#2,"       ...  ";
1700 IF R12!<1000 THEN PRINT#2,USING "  ##.### ";R12 ELSE PRINT#2,"     ...  "
1710 GOTO 1840
1720 FOR X=0 TO 1:PRINT#2,R$(X);",";:NEXT X
1730 PRINT#2,USING "####.###,";R2!;
1740 PRINT#2,USING "+##.###,";R3!;
1750 PRINT#2,USING " ##.###,";R4!;
1760 PRINT#2,USING "+##.###,";R5!;
1770 PRINT#2,USING " ##.###,";R6!;
```

```
1780 PRINT#2,USING " ##.###,";POL!;
1790 PRINT#2,USING " ##.###,";POLSIG!;
1800 PRINT#2,USING " ###.#,";ANGLE!;
1810 PRINT#2,USING " ###.#,";ANGLESIG!;
1820 PRINT#2,USING "+##.###,";R11!;
1830 PRINT#2,USING " ##.###";R12!
1840 'IF (C2! =999999!) OR (NET2!=999999!) OR (INTSTAR!=999999!) THEN TEMP!=999999! : GOTO 900
1850 'TEMP! = (C2!*NET2!*60!)/INTSTAR!   'Print the avg C2 voltage
1860 'IF TEMP! > 999999! THEN TEMP!=999999!
1870 'PRINT#2,USING "+#.###^^^^, ";TEMP!;
1880 'TEMP! = R11!/R12!                  'Print the ratio of signal to error
1890 'IF R11! = 999999! THEN TEMP!=999999!
1900 'PRINT#2,USING "+#.###^^^^";TEMP!
1910 '
1920 'Check to see if we have processed all data for star
1930 IF EOF(1) = -1 THEN 1960
1940 GOTO 1190
1950 '
1960 GOSUB 2620 'end summary statistics
1970 CLOSE 1
1980 CLOSE 2
1990 'Check to see if we have processed all stars
2000 IF EOF(3) = -1 THEN END
2010 GOTO 900
2020 '#################################################################
2030 'Linear reduction              Reference: Blitzstein (1987)
2040 D!=VAL(R$(3))                 'Linear D term
2050 SD!=1.483*VAL(R$(4))          'Linear SE D term  (sigma errors)
2060 E!=VAL(R$(5))                 'Linear E term
2070 SE!=1.483*VAL(R$(6))          'Linear SE E term
2080 '
2090 N!=(D!^2 + E!^2)^.5
2100 WP!=LINGAIN!*(N!* C1!)/C2!       'Linear polarization amplitude
2110 POL!=100!*(L!*WP! + M!*(WP!)^2)  'based upon hybrid polarization cal.
2120 SIGN! = (SD!^2 + SE!^2)^.5       'Error in N
2130 SIGWP!= LINGAIN!*( (N!^2*SIGC1!^2)/C2!^2 + (C1!^2*SIGN!^2)/C2!^2 + (C1!^2*N!^2*SIGC2!^2)/C2!^4 )^.5
2140 POLSIG!=100!*( WP!^2*SIGL!^2 + (L!+2*M!*WP!)^2*SIGWP!^2 + WP!^4*SIGM!^2 )^.5
2150 ANGLE!=.5*ATN(D!/E!) 'Calculate azimuth of first negative peak
2160 IF D! > 0! THEN IF E! > 0! THEN ANGLE! = ANGLE! + 1.570796 '90degrees
2170 IF D! > 0! THEN IF E! < 0! THEN ANGLE! = ANGLE! + 3.14159  '180degrees
2180 IF D! < 0! THEN IF E! > 0! THEN ANGLE! = ANGLE! + 1.570796 '90degrees
2190 ANGLE!=.80983 + ANGLE! '90-43.6degrees=0.80983rad (43.6=AZI of El vector)
2200 ANGLESIG!=((SD!^2 * E!^2 + SE!^2 * D!^2)/(4!*(E!^2+D!^2)^2))^.5
2210 '
2220 'PRINT "n,wp,pol,sign,sigwp,polsig",N!,WP!,POL!,SIGN!,SIGWP!,POLSIG!
2230 'PRINT
2240 R3!= LINQGAIN!* POL!*COS(2*ANGLE!)+LINQOFF! 'Linear Q term
2250 R4!= LINQGAIN!* (POLSIG!^2 * (COS(2*ANGLE!))^2 + 4 * POL!^2 * (SIN(2*ANGLE!))^2 * ANGLESIG!^2)^.5
'Linear SIG Q term
2260 R5!= LINUGAIN!* POL!*SIN(2*ANGLE!)+LINUOFF! 'Linear U term
2270 R6!= LINUGAIN!* (POLSIG!^2 * (SIN(2*ANGLE!))^2 + 4 * POL!^2 * (COS(2*ANGLE!))^2 * ANGLESIG!^2)^.5
'Linear SIG U term
2280 ANGLE! = ANGLE!* 57.296 'Convert to degrees
2290 IF ANGLE! > 180! THEN ANGLE!=ANGLE!-180!
2300 IF ANGLE! < 0! THEN ANGLE!=ANGLE!+180!
2310 ANGLESIG! = ANGLESIG!* 57.296
2320 IF ANGLESIG!>90! THEN ANGLESIG!=90! 'all error
2330 RETURN
2340 '
2350 '#################################################################
2360 'Circular reduction
2370 IF LEFT$(R$(0),1)="*" THEN 2510  'Star indicates Ithaco circ data
2380 'SR530 reduction (lam/2 pem amplitude)
2390 CIRAMP! = VAL(R$(11))
2400 CIR!= CIRCGAIN!*CIRAMP!*INTSTAR!/(C2!*NET2*60)+CIRCOFF!'CIRCULAR A term
2410 R11!=100*CIR!
2420 SIGAMP! = 1.483*VAL(R$(12))
2430 SIGNET2! = (NET2!)^.5
2440 SIGCIR! = ( SIGCOFF!^2 + (INTSTAR!/60!)^2*( (CIRAMP!/(C2!*NET2!))^2*SIGCGAIN!^2 +
(CIRCGAIN!/(C2!*NET2!))^2*SIGAMP!^2 + (CIRCGAIN!*CIRAMP!/(C2!^2*NET2!))^2*SIGC2!^2 +
(CIRCGAIN!*CIRAMP!/(C2!*NET2!^2))^2*SIGNET2!^2) )^.5
2450 R12!= 100*SIGCIR!
2460 'PRINT "ciramp,cir,sigamp,signet2,sigcir",CIRAMP!,CIR!,SIGAMP!,SIGNET2!,SIGCIR!
2470 'PRINT
2480 RETURN
2490 '
2500 '###############################
2510 'ITHACO reduction  (lam/4 pem amplitude)
2520 CIRAMP! = VAL(R$(11))
2530 SIGAMP! = 1.483*VAL(R$(12))
2540 CIR!= OLDCGAIN!*CIRAMP!*C1!/C2!+CIRCOFF!
2550 R11!=100*CIR! 'Percent
2560 SIGCIR! = ( SIGCOFF!^2 + (CIRAMP!*C1!/C2!)^2*SIGOLDCGAIN!^2 + (OLDCGAIN!*C1!/C2!)^2*SIGAMP!^2 +
(OLDCGAIN!*CIRAMP!/C2!)^2*SIGC1!^2 + (OLDCGAIN!*CIRAMP!*C1!/C2!^2)^2*SIGC2!^2 )^.5
2570 R12!= 100*SIGCIR! 'Percent
2580 'PRINT "ciramp,cir,sigamp,signet2,sigcir",CIRAMP!,CIR!,SIGAMP!,SIGNET2!,SIGCIR!
2590 'PRINT
2600 RETURN
2610 '
```

```
2620 '##############################
2630 'Reduction for summary statistics
2640 IF STATG$ = "y" OR STATG$ = "Y" THEN RETURN
2650 IF FILTOT < 2 OR LASTFIL$="" THEN FILTOT=0: LASTFIL$=R$(1):RETURN
2660 MM = 1
2670 T1!=0: T2!=0: T3! =0
2680 FOR NN = 1 TO FILTOT
2690 IF FILB(NN,MM,2) <= .00001 THEN FILB(NN,MM,2) = .0005  'define a min error
2700 IF FILB(NN,MM,1) > 100 THEN GOTO 2730
2710 T1! = T1! + FILB(NN,MM,1)/FILB(NN,MM,2)^2
2720 T2! = T2! + 1/FILB(NN,MM,2)^2
2730 NEXT NN
2740 IF T2! = 0 THEN T2!=1 'prevent divide by zero
2750 XX!(MM)= T1!/T2!
2760 MISSING =1 ' always down one degree of freedom
2770 FOR NN = 1 TO FILTOT
2780 IF FILB(NN,MM,1) > 100 THEN MISSING = MISSING +1:GOTO 2800
2790 T3! = T3! + (FILB(NN,MM,1) - XX!(MM))^2 / FILB(NN,MM,2)^2
2800 NEXT NN
2810 IF FILTOT<=MISSING THEN MISSING = FILTOT-1 'no divide by zero error
2820 YY!(MM)= (T3!/((FILTOT-MISSING)*T2!))^.5
2830 MM = MM + 1
2840 IF MM < 4 THEN GOTO 2670
2850 '
2860 PRINT #2,"       Weighted average: ";
2870 PRINT#2,SPACE$(19);
2880 PRINT #2, USING "+##.###  ";XX!(1);
2890 PRINT #2, USING " ##.###     ";YY!(1);
2900 PRINT #2, USING "+##.###  ";XX!(2);
2910 PRINT #2, USING " ##.###  ";YY!(2);
2920 S3!=XX!(1):S5!=XX!(2):S4!=YY!(1):S6!=YY!(2)
2930 GOSUB 3250
2940 PRINT #2, USING "    ##.###  ";SPOL!;
2950 PRINT #2, USING " ##.###  ";SPOLSIG!;
2960 PRINT #2, USING "     ###.#   ";SANGLE!;
2970 PRINT #2, USING " ##.#     ";SANGLESIG!;
2980 PRINT #2, USING "+##.###  ";XX!(3);
2990 PRINT #2, USING " ##.###  ";YY!(3)
3000 LASTFIL$=R$(1)
3010 FILTOT=0
3020 RETURN
3030 '
3040 '#############################################################
3050 'Standardization procedure
3060 FIL=0
3070 IF R$(1) = "R" THEN FIL=1
3080 IF R$(1) = "V" THEN FIL=2
3090 IF R$(1) = "B" THEN FIL=3
3100 IF R$(1) = "NUV" THEN FIL=4
3110 IF R$(1) = "WUV" THEN FIL=4
3120 IF FIL=0 THEN R$(0)=R$(0)+"*not stan*":RETURN
3130 '
3140 R3!=STAN(FIL,1,1)*R3! - STAN(FIL,1,2) - INTERS(FIL,1)
3150 R4!=STAN(FIL,1,1)*R4!
3160 R5!=STAN(FIL,2,1)*R5! - STAN(FIL,2,2) - INTERS(FIL,2)
3170 R6!=STAN(FIL,2,1)*R6!
3180 R11!=STAN(FIL,3,1)*R11! - STAN(FIL,3,2) - INTERS(FIL,3)
3190 R12!=STAN(FIL,3,1)*R12!
3200 S3!=R3!:S5!=R5!:S4!=R4!:S6!=R6!
3210 GOSUB 3250
3220 ANGLE!=SANGLE!:ANGLESIG!=SANGLESIG!:POL!=SPOL!:POLSIG!=SPOLSIG!
3230 RETURN
3240 '
3250 '#############################################################
3260 'Calculate p, theta from q,u in percent.
3270 SPOL!=(S3!^2 + S5!^2)^.5 'pol amplitude
3280 IF S3!=0 THEN GOTO 3400 'divide by zero
3290 SPOLSIG!=( (S3!*S4!)^2 + (S5!*S6!)^2 )^.5 /SPOL!
3300 SANGLE!=.5*ATN(S5!/S3!)  'angle
3310 IF S5! > 0! THEN IF S3! < 0! THEN SANGLE! = SANGLE! + 1.570796 '90degrees
3320 IF S5! < 0! THEN IF S3! > 0! THEN SANGLE! = SANGLE! + 3.14159  '180degrees
3330 IF S5! < 0! THEN IF S3! < 0! THEN SANGLE! = SANGLE! + 1.570796 '90degrees
3340 SANGLE! = SANGLE!* 57.296 'Convert to degrees
3350 IF SANGLE! > 180! THEN SANGLE!=SANGLE!-180!
3360 IF SANGLE! < 0! THEN SANGLE!=SANGLE!+180!
3370 SANGLESIG!=((S6!^2 * S3!^2 + S4!^2 * S5!^2)/(4!*(S3!^2+S5!^2)^2))^.5
3380 SANGLESIG!=SANGLESIG!*57.296
3390 IF SANGLESIG!>90! THEN SANGLESIG!=90! 'all error
3400 RETURN
```

PEM POLARIMETER REDUCTION

ALP ORI FS 27 28 JANUARY 1990

Julian Day Number: 2447918.723
Phase : 0.5341
Airmass : -8.721551402
Hour Angle : -634.3909436

JD (Primary) : 55555+666E
Right Ascension: 666h66m66s
Declination : 666°66'66"

Filter: RED

CH1 Gain : 0.3 MV
C1 : 1.928003594E-4
Temp Lock-in/cnts: 60.4/173779.3333
Integration time Star : 90 sec

Ch 2 Gain : -6 A
C2 : 0.161468
Temp Polar/cnts: 31.4/171998
Integration time Background : 30 sec

Remarks: CLR, V CLD, 1300V

AZI	C1	B1	Net1	C2	B2	Net2	Net1/Net2	Res.	Net1/Net2	Res.
0.09	510485	467595	42890	142428	92265	50163	0.855013	5.730E-003	0.849	1.45E-006
40.25	474929	467571	7358	142406	92268	50138	0.146755	-2.637E-003	0.149	-7.89E-007
80.06	467003	467679	-676	143024	92268	50756	-0.013319	-7.059E-004	-0.012	4.89E-008
120.75	495241	467670	27571	143211	92268	50943	0.541213	4.010E-003	0.537	7.05E-007
160.51	512894	467616	45278	142603	92289	50314	0.899909	-6.868E-003	0.907	-1.38E-006
200.45	486205	463392	22813	141491	92307	49184	0.463830	8.855E-003	0.455	1.88E-006
240.57	457452	466038	-8586	141171	92271	48900	-0.175583	-9.825E-003	-0.166	-2.17E-006
280.47	474164	465915	8249	140958	92271	48687	0.169429	9.662E-003	0.160	2.21E-006
320.10	510224	465768	44456	140736	92271	48465	0.917281	-8.221E-003	0.925	-1.95E-006

Ave net2 counts 49727.77778

Sum of Residuals Squared 4.39E-004 2.21E-011

A	4.22E-001	+/-	3.33E-003	4.22E-001	+/- 7.47E-007
B	2.01E-002	+/-	4.71E-003	2.02E-002	+/- 1.06E-006
C	5.12E-002	+/-	4.71E-003	5.12E-002	+/- 1.06E-006
D	-3.77E-001	+/-	4.71E-003	-3.77E-001	+/- 1.05E-006
E	3.95E-001	+/-	4.72E-003	3.95E-001	+/- 1.06E-006
F	-3.16E-002	+/-	4.73E-003	-3.16E-002	+/- 1.06E-006
G	-1.75E-002	+/-	4.70E-003	-1.75E-002	+/- 1.05E-006
J	8.20E-003	+/-	3.76E-005		
H	5.66E-003	+/-	3.76E-005		

Peak Modulation : 0.5458 +/- 1.1E-006
Azimuth of first negative peak : 68.163997 +/- 3.83E-005
Natural position angle of electric vector: 114.5640 DEG +/- 3.83E-005 DEG
Natural Polarization : 0.0765 % +/- 0.0004 %
Natural Q: -0.0501 % Natural U: -0.0579 %

CIRCPOL - SR530 based system
Version: 11

01-03-1988 01:17:10
Object= alp cri r
Gain setting= 14
Star loop count= 2100
Background loop count= 700

Standard Vectors = +3.615E-05 -5.620E-06
Standard vector angle = -0.16

AZ	STAR (volts)		BACKGROUND		NET	RESIDUALS
DEG	CH X	CH Y	CH X	CH Y	R Stan Vec	
0.00	+8.265E-05	+1.004E-04	+8.675E-05	+1.021E-04	-3.779E-06	-9.613E-08
40.00	+8.113E-05	+9.847E-05	+8.677E-05	+1.010E-04	-5.165E-06	+4.936E-07
80.00	+8.298E-05	+9.965E-05	+8.647E-05	+1.012E-04	-3.199E-06	-8.315E-07
120.00	+8.205E-05	+9.791E-05	+8.627E-05	+1.014E-04	-3.614E-06	+1.069E-06
160.00	+8.058E-05	+8.965E-05	+8.031E-05	+8.816E-05	+3.391E-08	-1.178E-06
200.00	+7.745E-05	+8.395E-05	+8.027E-05	+8.706E-05	-2.287E-06	+1.144E-06
240.00	+7.936E-05	+8.118E-05	+7.823E-05	+7.928E-05	+8.157E-07	-9.731E-07
280.00	+7.909E-05	+8.211E-05	+7.852E-05	+8.262E-05	+6.462E-07	+6.343E-07
320.00	+7.807E-05	+8.236E-05	+7.836E-05	+8.238E-05	-3.247E-07	-3.129E-07

Sum of residuals squared +6.298E-12

A	-1.875E-06	+/-	+3.990E-07
B	-2.209E-06	+/-	+5.642E-07
C	-1.091E-06	+/-	+5.642E-07
D	-8.303E-07	+/-	+5.642E-07
E	-5.911E-07	+/-	+5.642E-07
F	+2.551E-07	+/-	+5.642E-07
G	-3.178E-07	+/-	+5.642E-07

Circpol calibration factor: 4.14E+07 Star integration length: 90
Net 2 average: 49727.78 C2 coefficient: .16147

Stokes V in percent -1.450E-02 +/- +3.086E-03

Sample ASCII input file for REDUCE program.

```
HD21389,R,  6784.518,-3.98E0,  8.90E-2,  6.40E0,   8.98E-2,  6.047E-5,  .01576,   17613, 60,   4.57E-7,   1.99E-7
HD21389,V,  6784.547,-4.30E0,  6.75E-2,  6.54E0,   6.71E-2,  6.058E-5,  .01575,   14966, 60,   6.70E-8,   1.64E-7
HD21389,B,  6784.572,-4.09E0,  5.08E-2,  6.17E0,   5.09E-2,  6.065E-5,  .01574,    9077, 60,   9.02E-8,   9.01E-8
HD21389,R,  6801.541,-3.79E0,  1.52E-2,  6.21E0,   1.52E-2,  6.103E-5,  .01566,   17262, 60,   3.567E-7,  5.682E-8
HD21389,V,  6801.634,-3.82E0,  1.55E-2,  6.56E0,   1.55E-2,  6.121E-5,  .01563,   15900, 60,  -1.17E-8,   1.24E-7
HD21389,B,  6801.662,-3.62E0,  6.61E-3,  6.16E0,   6.59E-3,  6.124E-5,  .01562,   11155, 60,   7.41E-9,   1.34E-7
HD21389,NUV,6801.698,-9.84E-2, 5.54E-3,  1.80E-1,  5.57E-3,  1.988E-5, 1.74E-4,  76738, 60,   1.73E-7,   5.84E-8
HD21389,R,  6759.613,-3.87E0,  8.02E-3,  6.18E0,   7.96E-3,  6.008E-5,  .015818,      *,  *,         *,        *
HD21389,R,  6769.666,-3.69E0,  1.85E-2,  6.21E0,   1.84E-2,  6.076E-5,  .015716,      *,  *,         *,        *
HD21389,R,  6769.716,-3.68E0,  1.78E-2,  6.22E0,   1.75E-2,  6.117E-5,  .01571,       *,  *,         *,        *
HD21389,R,  6769.743,-3.64E0,  4.57E-2,  6.18E0,   4.57E-2,  6.103E-5,  .01571,       *,  *,         *,        *
```

Sample ASCII output file from REDUCE program (Statgraphics output format).

```
STAR,FILTER,JD,Q,SIGQ,U,SIGU,LIN,SIGLIN,AZI,SIGAZI,V,SIGV,C2NET260,veratio
Statgraphics: Y              Standardized: N              Interstellar corrected: N
HD21389,B,6784.572, -1.708,  0.042, -2.873,  0.054,  3.342,  0.060, 119.6,   0.3, +0.026,  0.039
HD21389,B,6801.662, -1.523,  0.017, -2.908,  0.031,  3.282,  0.035, 121.2,   0.0, +0.002,  0.047
HD21389,NUV,6801.698, -1.199,  0.121, -2.472,  0.150,  2.747,  0.158, 122.1,   1.1, +0.536,  0.270
HD21389,R,6759.613, -1.586,  0.018, -2.831,  0.031,  3.245,  0.035, 120.4,   0.0,%+999999.000, %999999.000
HD21389,R,6769.666, -1.532,  0.021, -2.892,  0.035,  3.273,  0.039, 121.0,   0.1,%+999999.000, %999999.000
HD21389,R,6769.716, -1.538,  0.021, -2.917,  0.035,  3.297,  0.039, 121.1,   0.1,%+999999.000, %999999.000
HD21389,R,6769.743, -1.518,  0.038, -2.891,  0.051,  3.265,  0.056, 121.2,   0.3,%+999999.000, %999999.000
HD21389,R,6784.518, -1.647,  0.068, -2.961,  0.085,  3.388,  0.091, 120.5,   0.5, +0.068,  0.044
HD21389,R,6801.541, -1.590,  0.020, -2.917,  0.034,  3.322,  0.038, 120.7,   0.1, +0.055,  0.013
HD21389,V,6784.547, -1.791,  0.054, -3.038,  0.067,  3.527,  0.074, 119.7,   0.4, +0.012,  0.043
HD21389,V,6801.634, -1.604,  0.021, -3.092,  0.036,  3.483,  0.040, 121.3,   0.1, -0.002,  0.031
```

APPENDIX D

Journal of Observations for Standard Polarization Sources (Unstandardized Values)

Name	Filter (Note 1)	(JD-2440000)	q (%)	σq (%)	u (%)	σu (%)	p (%)	σp (%)	θ (o)	σθ (o)	v (%)	σv (%)
EV+LAM	V	6887.632	+8.107	0.766	-7.143	0.734	10.805	0.867	159.3	1.6	+74.380	4.128
EV+LAM000	V	7793.263	-14.159	1.791	-37.623	2.304	40.199	2.378	124.7	1.2	-68.203	3.711
EV+LAM040	V	7793.276	-43.830	4.632	+42.122	4.576	60.789	5.264	68.1	1.8	-50.349	2.765
EV+LAM080	V	7793.288	-42.055	4.400	-42.650	4.419	59.896	5.044	112.7	1.8	+50.866	2.769
EV+LAM120	V	7793.300	-14.778	1.738	+37.648	2.224	40.444	2.302	55.7	1.2	+67.729	3.703
EV+LAM120	V	7815.690	-15.369	1.833	+37.702	2.330	40.715	2.417	56.1	1.2	+68.011	3.812
EV+LAM160	V	7793.314	-66.721	7.268	-29.540	5.940	72.968	7.556	101.9	2.2	-28.737	1.570
EV+LAM200	V	7793.326	+4.409	0.339	+15.928	0.479	16.527	0.489	37.3	0.6	-76.982	4.231
EV+LAM240	V	7793.340	-78.867	8.876	+0.028	6.579	78.867	8.876	90.0	2.4	-0.317	0.067
EV+LAM280	V	7793.352	+5.479	0.254	-14.112	0.351	15.138	0.366	145.6	0.4	+77.312	4.212
EV+LAM280	V	7815.673	+5.032	0.279	-14.596	0.389	15.439	0.402	144.5	0.5	+77.938	4.362
EV+LAM320	V	7793.365	-68.483	7.647	+27.997	6.177	73.985	7.909	78.9	2.3	+27.182	1.511
IOT PER	R	7502.809	+0.001	0.018	+0.013	0.025	0.013	0.025	41.7	39.4	+0.003	0.003
IOT PER	R	7508.756	+0.018	0.006	+0.016	0.006	0.024	0.007	20.2	6.0	+0.012	0.024
IOT PER	R	7531.639	-0.011	0.012	-0.013	0.013	0.017	0.014	114.7	16.9	+0.001	0.013
IOT PER	R	7540.622	+0.004	0.003	-0.014	0.004	0.014	0.004	142.8	6.1	-0.034	0.004
IOT PER	R	7543.649	-0.001	0.014	-0.015	0.020	0.015	0.020	133.7	27.6	+0.003	0.024
IOT PER	R	7546.658	+0.018	0.006	+0.001	0.004	0.018	0.006	1.9	6.6	-0.029	0.014
IOT PER	R	7548.664	-0.002	0.021	+0.009	0.028	0.009	0.029	50.7	66.0	+0.028	0.005
IOT PER	R	7570.600	-0.005	0.016	-0.004	0.014	0.007	0.017	108.0	52.1	-0.023	0.005
IOT PER	R	7596.505	+0.003	0.008	+0.005	0.010	0.006	0.010	30.8	33.8	-0.046	0.032

APPENDIX D (cont.)

Journal of Observations for Standard Polarization Sources (Unstandardized Values)

Name	Filter (Note 1)	(JD-2440000)	q (%)	σq (%)	u (%)	σu (%)	p (%)	σp (%)	θ (o)	σθ (o)	v (%)	σv (%)
IOT PER	R	7824.748	+0.003	0.015	+0.010	0.019	0.011	0.020	36.3	36.5	+0.001	0.014
Weighted average:			+0.007	0.003	-0.002	0.004	0.007	0.003	173.5	14.3	-0.006	0.007
IOT PER	V	7479.787	-0.013	0.015	+0.035	0.019	0.037	0.020	55.4	10.7	+0.005	0.013
IOT PER	V	7483.778	-0.016	0.017	-0.024	0.019	0.029	0.021	118.0	14.9	+0.005	0.005
IOT PER	V	7502.786	+0.013	0.009	+0.007	0.008	0.015	0.010	14.0	13.8	...	...
IOT PER	V	7507.777	+0.010	0.002	-0.006	0.002	0.012	0.002	163.2	4.2	+0.011	0.016
IOT PER	V	7508.729	+0.017	0.019	-0.016	0.019	0.023	0.022	159.1	19.3	+0.001	0.001
IOT PER	V	7531.614	+0.000	0.009	-0.027	0.013	0.027	0.013	135.2	9.5	+0.006	0.005
IOT PER	V	7540.598	+0.005	0.008	+0.016	0.011	0.017	0.011	36.5	13.9	+0.015	0.006
IOT PER	V	7543.625	+0.006	0.018	+0.015	0.023	0.016	0.024	34.0	29.8	+0.007	0.015
IOT PER	V	7544.581	+0.002	0.010	+0.030	0.013	0.030	0.014	43.3	9.1	-0.112	0.042
IOT PER	V	7546.633	+0.008	0.013	+0.009	0.014	0.012	0.016	24.8	26.3	-0.011	0.010
IOT PER	V	7548.639	+0.033	0.010	+0.009	0.007	0.035	0.010	7.3	5.9	-0.002	0.002
IOT PER	V	7558.625	+0.018	0.019	+0.006	0.014	0.019	0.019	8.6	20.5	-0.034	0.018
IOT PER	V	7569.606	+0.002	0.012	-0.002	0.013	0.003	0.014	153.8	90.0	-0.025	0.007
IOT PER	V	7570.571	-0.010	0.003	+0.004	0.002	0.011	0.003	79.2	6.0	-0.004	0.005
IOT PER	V	7595.521	+0.013	0.004	+0.011	0.004	0.017	0.004	19.2	5.3	+0.009	0.025
Weighted average:			+0.005	0.003	+0.000	0.002	0.005	0.003	2.5	12.5	-0.000	0.002
IOT PER	B	7507.748	-0.019	0.011	+0.002	0.008	0.019	0.011	86.4	11.4	+0.052	0.014
IOT PER	B	7531.586	-0.005	0.018	-0.008	0.020	0.010	0.022	118.8	45.0	+0.041	0.010
IOT PER	B	7540.573	-0.001	0.007	+0.005	0.009	0.005	0.009	50.5	37.3	-0.003	0.020

APPENDIX D (cont.)

Journal of Observations for Standard Polarization Sources (Unstandardized Values)

Name	Filter (Note 1)	(JD-2440000)	q (%)	σq (%)	u (%)	σu (%)	p (%)	σp (%)	θ (o)	σθ (o)	v (%)	σv (%)
IOT PER	B	7543.603	+0.003	0.007	+0.013	0.010	0.014	0.010	37.7	14.3	+0.005	0.017
IOT PER	B	7546.608	+0.001	0.024	+0.013	0.034	0.013	0.034	41.9	54.0	+0.002	0.013
IOT PER	B	7548.614	+0.024	0.004	-0.020	0.004	0.031	0.004	160.0	2.8	+0.020	0.011
IOT PER	B	7558.600	-0.012	0.013	-0.022	0.016	0.025	0.017	120.6	13.6	-0.011	0.004
IOT PER	B	7569.580	-0.026	0.007	+0.016	0.006	0.031	0.008	73.9	5.4	-0.017	0.018
IOT PER	B	7587.517	+0.029	0.020	+0.010	0.016	0.031	0.021	9.9	13.8	-0.014	0.026
IOT PER	B	7834.703	+0.022	0.005	-0.011	0.004	0.025	0.005	166.5	4.0	-0.006	0.013
Weighted average:			+0.011	0.006	-0.008	0.004	0.013	0.005	161.6	10.6	+0.000	0.007
HD17378	R	6786.694	-2.569	0.089	-5.754	0.122	6.302	0.129	123.0	0.4	+0.053	0.042
HD17378	V	6786.718	-2.756	0.035	-5.830	0.066	6.448	0.073	122.3	0.1	+0.016	0.053
2H CAM	B	7407.833	-1.804	0.021	-2.557	0.028	3.129	0.034	117.4	0.1	...	...
HD21389	R	6759.613	-1.586	0.018	-2.831	0.031	3.245	0.035	120.4	0.0	...	...
HD21389	R	6769.666	-1.532	0.021	-2.892	0.035	3.273	0.039	121.0	0.1	...	...
HD21389	R	6769.716	-1.538	0.021	-2.917	0.035	3.297	0.039	121.1	0.1	...	...
HD21389	R	6769.743	-1.518	0.038	-2.891	0.051	3.265	0.056	121.2	0.3	...	...
HD21389	R	6784.518	-1.647	0.068	-2.961	0.085	3.388	0.091	120.5	0.5	+0.068	0.044
HD21389	R	6801.541	-1.590	0.020	-2.917	0.034	3.322	0.038	120.7	0.1	+0.055	0.013
Weighted average:			-1.563	0.013	-2.889	0.016	3.285	0.016	120.8	0.1	+0.056	0.004
HD21389	V	6784.547	-1.791	0.054	-3.038	0.067	3.527	0.074	119.7	0.4	+0.012	0.043

APPENDIX D (cont.)

Journal of Observations for Standard Polarization Sources (Unstandardized Values)

Name	Filter (Note 1)	(JD-2440000)	q (%)	σq (%)	u (%)	σu (%)	p (%)	σp (%)	θ (o)	σθ (o)	v (%)	σv (%)
HD21389	V	6801.634	-1.604	0.021	-3.092	0.036	3.483	0.040	121.3	0.1	-0.002	0.031
Weighted average:			-1.628	0.063	-3.080	0.022	3.484	0.035	121.1	0.5	+0.003	0.006
HD21389	B	6784.572	-1.708	0.042	-2.873	0.054	3.342	0.060	119.6	0.3	+0.026	0.039
HD21389	B	6801.662	-1.523	0.017	-2.908	0.031	3.282	0.035	121.2	0.0	+0.002	0.047
Weighted average:			-1.548	0.064	-2.899	0.015	3.287	0.033	120.9	0.5	+0.016	0.012
HD21389	NUV	6801.698	-1.199	0.121	-2.472	0.150	2.747	0.158	122.1	1.1	+0.536	0.270
9 GEM	R	7502.938	+2.678	0.031	-0.805	0.013	2.796	0.032	171.6	0.1	-0.054	0.082
9 GEM	V	7502.916	+2.810	0.052	-0.772	0.032	2.914	0.053	172.3	0.3	+0.136	0.027
ALP CMI	LOW	7928.754	-0.104	0.127	+0.040	0.099	0.111	0.132	79.4	24.0	-0.081	0.103
ALP CMI	R	6871.666	-0.004	0.002	-0.003	0.001	0.005	0.002	109.0	7.1	-0.021	0.002
ALP CMI	R	6872.636	-0.004	0.006	+0.002	0.005	0.005	0.006	74.6	26.4	-0.004	0.004
ALP CMI	R	6874.638	+0.002	0.001	+0.000	0.000	0.002	0.001	7.4	6.6	-0.006	0.001
ALP CMI	R	6874.663	+0.000	0.001	+0.003	0.002	0.003	0.002	40.9	12.9	-0.007	0.002
ALP CMI	R	6877.612	-0.001	0.003	+0.006	0.004	0.006	0.004	51.4	12.4	-0.002	0.002
ALP CMI	R	6877.639	-0.002	0.002	+0.009	0.003	0.009	0.003	52.1	6.9	-0.003	0.003
ALP CMI	R	6878.632	-0.003	0.003	+0.004	0.003	0.006	0.004	63.8	13.3	-0.005	0.001
ALP CMI	R	6879.653	+0.001	0.000	+0.007	0.000	0.008	0.000	39.2	1.2	-0.004	0.003
ALP CMI	R	6887.578	+0.000	0.004	+0.006	0.005	0.006	0.005	45.0	18.3	-0.006	0.001

APPENDIX D (cont.)

Journal of Observations for Standard Polarization Sources (Unstandardized Values)

Name	Filter (Note 1)	(JD-2440000)	q (%)	σq (%)	u (%)	σu (%)	p (%)	σp (%)	θ (o)	σθ (o)	v (%)	σv (%)
ALP CMI	R	6895.576	-0.003	0.001	+0.006	0.002	0.006	0.002	59.1	5.4	-0.007	0.002
ALP CMI	R	6896.558	-0.004	0.001	+0.001	0.001	0.004	0.001	86.3	6.2	-0.005	0.005
ALP CMI	R	6896.589	-0.002	0.002	+0.003	0.002	0.003	0.002	59.9	14.1	-0.006	0.001
ALP CMI	R	6899.554	-0.000	0.001	+0.010	0.002	0.010	0.002	45.4	3.5	-0.005	0.003
ALP CMI	R	6912.543	-0.006	0.004	+0.005	0.004	0.008	0.005	70.3	11.9	-0.009	0.004
ALP CMI	R	7923.634	-0.039	0.026	-0.040	0.026	0.056	0.030	112.7	10.9	-0.010	0.009
ALP CMI	R	7923.710	-0.001	0.003	+0.008	0.004	0.008	0.004	49.3	10.3	-0.021	0.010
ALP CMI	R	7940.607	-0.002	0.001	+0.005	0.001	0.006	0.001	55.6	3.4	-0.005	0.002
ALP CMI	R	7948.606	-0.001	0.003	+0.000	0.002	0.001	0.003	82.7	66.6	+0.001	0.003
ALP CMI	R	7976.558	+0.000	0.002	+0.006	0.003	0.006	0.003	44.5	9.8	-0.002	0.003
ALP CMI	R	7998.548	-0.001	0.001	+0.003	0.001	0.004	0.001	55.4	7.4	-0.014	0.003
ALP CMI	R	8007.540	-0.001	0.002	+0.001	0.002	0.001	0.002	66.8	34.6	-0.010	0.002
Weighted average:			+0.000	0.000	+0.003	0.001	0.003	0.001	41.9	3.4	-0.007	0.001
ALP CMI	V	6844.740	-0.000	0.002	-0.002	0.003	0.002	0.003	129.3	30.0	-0.004	0.003
ALP CMI	V	6844.769	-0.003	0.002	+0.001	0.001	0.003	0.002	84.5	9.5	-0.003	0.007
ALP CMI	V	6846.746	-0.006	0.006	-0.002	0.005	0.007	0.006	99.0	18.6	-0.008	0.004
ALP CMI	V	6865.648	+0.001	0.001	+0.006	0.001	0.006	0.001	42.0	4.6	-0.006	0.003
ALP CMI	V	6871.640	+0.005	0.001	+0.011	0.002	0.012	0.002	33.0	3.4	-0.007	0.003
ALP CMI	V	6878.656	+0.006	0.002	-0.000	0.001	0.006	0.002	178.1	5.2	-0.010	0.002
ALP CMI	V	6879.629	-0.002	0.004	-0.003	0.004	0.004	0.004	115.8	22.9	-0.006	0.001
ALP CMI	V	6887.601	+0.004	0.003	-0.001	0.002	0.004	0.003	172.5	15.7	-0.001	0.004
ALP CMI	V	6895.554	-0.004	0.004	+0.001	0.003	0.004	0.004	84.9	19.4	-0.005	0.002

APPENDIX D (cont.)

Journal of Observations for Standard Polarization Sources (Unstandardized Values)

Name	Filter (Note 1)	(JD-2440000)	q (%)	σq (%)	u (%)	σu (%)	p (%)	σp (%)	θ (o)	σθ (o)	v (%)	σv (%)
ALP CMI	V	6916.552	-0.003	0.004	-0.007	0.005	0.007	0.005	124.7	13.2	-0.004	0.002
ALP CMI	V	6922.532	-0.024	0.014	+0.076	0.018	0.079	0.019	53.9	4.8	+0.001	0.003
ALP CMI	V	7918.747	+0.024	0.007	-0.009	0.005	0.026	0.007	170.3	5.6	-0.027	0.006
ALP CMI	V	7930.721	+0.002	0.004	-0.002	0.004	0.002	0.005	157.2	39.2	+0.008	0.002
ALP CMI	V	7943.614	+0.002	0.002	-0.000	0.001	0.002	0.002	176.	31.	-0.000	0.002
ALP CMI	V	7948.630	+0.001	0.001	+0.001	0.001	0.002	0.001	9.9	12.3	+0.002	0.002
ALP CMI	V	7976.579	+0.004	0.001	-0.001	0.001	0.004	0.001	171.4	3.3	+0.001	0.005
ALP CMI	V	7978.549	+0.004	0.002	+0.003	0.002	0.005	0.003	17.3	10.5	+0.001	0.001
ALP CMI	V	8000.561	+0.003	0.001	-0.003	0.001	0.005	0.002	157.2	6.6	-0.002	0.005
ALP CMI	V	8009.541	+0.001	0.005	-0.005	0.007	0.005	0.007	142.9	25.9	-0.003	0.003
Weighted average:			+0.002	0.001	+0.000	0.001	0.002	0.001	0.3	8.8	-0.002	0.001
ALP CMI	B	6860.671	-0.003	0.004	-0.001	0.003	0.003	0.004	95.3	23.4	-0.010	0.003
ALP CMI	B	6860.695	+0.007	0.004	-0.003	0.003	0.008	0.004	170.2	10.6	-0.001	0.001
ALP CMI	B	7923.690	+0.006	0.010	+0.005	0.009	0.008	0.011	18.3	28.1	-0.029	0.004
ALP CMI	B	7935.587	-0.006	0.004	+0.005	0.004	0.008	0.004	71.6	11.8	+0.006	0.003
ALP CMI	B	7972.618	+0.000	0.001	+0.004	0.002	0.004	0.002	41.2	9.8	...	...
ALP CMI	B	7990.561	+0.000	0.004	+0.013	0.005	0.013	0.005	44.9	8.2	-0.004	0.004
ALP CMI	B	8004.536	+0.003	0.002	+0.010	0.002	0.010	0.002	36.9	4.3	-0.002	0.004
Weighted average:			+0.001	0.001	+0.004	0.002	0.004	0.002	37.9	7.4	-0.005	0.004
ALP CMI	WUV	7918.770	-0.003	0.004	+0.003	0.004	0.004	0.005	70.8	23.6	-0.034	0.002
ALP CMI	WUV	7919.753	-0.008	0.003	+0.003	0.002	0.008	0.003	79.4	6.7	-0.040	0.005

APPENDIX D (cont.)

Journal of Observations for Standard Polarization Sources (Unstandardized Values)

Name	Filter (Note 1)	(JD-2440000)	q (%)	σq (%)	u (%)	σu (%)	p (%)	σp (%)	θ (o)	σθ (o)	v (%)	σv (%)
ALP CMI	WUV	7928.731	-0.003	0.003	+0.007	0.003	0.008	0.003	56.4	9.0	+0.008	0.006
ALP CMI	WUV	7995.554	+0.002	0.002	+0.004	0.002	0.004	0.002	33.6	11.8	+0.007	0.008
ALP CMI	WUV	8005.545	-0.001	0.006	-0.000	0.004	0.002	0.006	95.3	75.3	+0.007	0.006
Weighted average:			-0.002	0.002	+0.003	0.001	0.004	0.001	58.6	12.3	-0.026	0.009
BET VIR	R	7569.827	+0.008	0.004	+0.013	0.004	0.015	0.005	29.8	6.4	-0.002	0.024
BET VIR	R	7587.757	+0.006	0.007	+0.021	0.010	0.022	0.010	36.5	9.4	...	...
BET VIR	R	7595.750	+0.002	0.005	-0.003	0.006	0.004	0.006	150.3	36.2	-0.015	0.012
BET VIR	R	7628.680	-0.008	0.012	+0.001	0.008	0.008	0.012	86.4	28.6	...	...
BET VIR	R	7636.648	-0.008	0.008	+0.005	0.007	0.009	0.009	74.7	18.9	...	...
BET VIR	R	7640.614	-0.015	0.008	+0.008	0.006	0.017	0.008	75.9	9.6	...	...
Weighted average:			+0.002	0.003	+0.007	0.003	0.007	0.003	38.6	12.9	-0.012	0.005
BET VIR	V	7569.804	+0.008	0.018	-0.024	0.024	0.025	0.024	144.8	19.6	+0.008	0.018
BET VIR	V	7587.729	-0.002	0.002	+0.012	0.003	0.012	0.003	50.9	4.7	...	...
BET VIR	V	7596.762	-0.001	0.006	+0.011	0.008	0.011	0.008	48.7	14.9	+0.006	0.023
BET VIR	V	7628.658	+0.010	0.012	+0.003	0.009	0.010	0.013	8.2	25.1	...	...
BET VIR	V	7636.628	-0.006	0.007	-0.007	0.007	0.009	0.008	116.3	17.9	...	...
BET VIR	V	7637.628	-0.016	0.011	+0.010	0.010	0.019	0.012	73.3	12.8	...	...
BET VIR	V	7639.644	-0.012	0.011	+0.007	0.010	0.014	0.012	74.2	17.8	...	...
BET VIR	V	7675.613	-0.003	0.009	+0.011	0.012	0.012	0.012	51.3	20.8	...	...
Weighted average:			-0.003	0.001	+0.009	0.002	0.009	0.002	53.6	4.3	+0.007	0.001

APPENDIX D (cont.)

Journal of Observations for Standard Polarization Sources (Unstandardized Values)

Name	Filter (Note 1)	(JD-2440000)	q (%)	σq (%)	u (%)	σu (%)	p (%)	σp (%)	θ (o)	σθ (o)	v (%)	σv (%)
BET VIR	B	7595.727	+0.008	0.009	-0.012	0.011	0.014	0.012	150.8	16.5	+0.054	0.041
BET VIR	B	7596.740	+0.004	0.024	-0.002	0.020	0.005	0.025	164.8	90.0	+0.044	0.008
BET VIR	B	7628.639	-0.028	0.003	+0.007	0.002	0.029	0.003	82.9	2.4	...	...
BET VIR	B	7637.608	+0.014	0.023	+0.003	0.017	0.014	0.023	6.7	33.5	...	...
BET VIR	B	7639.624	-0.012	0.026	+0.010	0.025	0.016	0.030	69.9	37.9	...	...
BET VIR	B	7640.590	-0.007	0.004	-0.002	0.003	0.008	0.005	97.4	11.9	...	...
BET VIR	B	7668.641	-0.011	0.017	+0.001	0.012	0.011	0.017	87.8	30.5	...	...
Weighted average:			-0.018	0.005	+0.003	0.002	0.018	0.005	84.7	3.6	+0.045	0.002
BET VIR	NUV	7668.622	-0.128	0.081	-0.088	0.072	0.155	0.089	107.3	11.6	...	...
BET VIR	NUV	7675.594	+0.050	0.028	+0.052	0.029	0.072	0.033	23.0	9.2	...	...
BET VIR	NUV	7682.632	+0.033	0.101	-0.004	0.072	0.033	0.101	176.7	61.4	-0.058	0.209
Weighted average:			+0.031	0.037	+0.029	0.033	0.042	0.035	21.3	23.8	-0.058	0.209
25 BOO	V	7262.780	-0.009	0.007	+0.015	0.008	0.017	0.008	60.5	9.6	...	...
16 SER	V	7262.713	-0.018	0.045	+0.023	0.049	0.029	0.054	63.5	37.6	...	...
25 SER	V	7262.752	-0.937	0.043	+0.113	0.030	0.944	0.043	86.6	0.9	...	...
25 SER	V	7277.726	-0.933	0.024	+0.097	0.016	0.938	0.024	87.0	0.5	...	...
25 SER	V	7290.772	-0.887	0.091	+0.012	0.064	0.887	0.091	89.6	2.1	+0.039	0.012
25 SER	V	7336.609	-0.904	0.019	+0.073	0.012	0.907	0.019	87.7	0.4	-0.024	0.022
25 SER	V	7337.587	-0.877	0.025	+0.038	0.017	0.878	0.025	88.7	0.5	+0.047	0.027

APPENDIX D (cont.)

Journal of Observations for Standard Polarization Sources (Unstandardized Values)

Name	Filter (Note 1)	(JD-2440000)	q (%)	σq (%)	u (%)	σu (%)	p (%)	σp (%)	θ (o)	σθ (o)	v (%)	σv (%)
25 SER	V	7340.586	-0.920	0.024	+0.065	0.016	0.923	0.024	88.0	0.5	+0.034	0.037
25 SER	V	7343.592	-0.925	0.023	+0.077	0.015	0.928	0.023	87.6	0.5	+0.017	0.014
25 SER	V	7358.637	-0.893	0.034	+0.054	0.024	0.895	0.034	88.3	0.8	+0.031	0.041
Weighted average:			-0.911	0.007	+0.071	0.007	0.914	0.007	87.8	0.2	+0.024	0.009
86 HER	R	7682.759	+0.003	0.010	-0.011	0.013	0.011	0.013	142.3	23.5	-0.045	0.013
86 HER	B	7688.740	+0.004	0.008	+0.004	0.007	0.005	0.009	21.2	33.1	+0.003	0.011
86 HER	B	7732.673	-0.018	0.001	+0.009	0.001	0.020	0.002	75.9	1.5	-0.022	0.015
Weighted average:			-0.017	0.004	+0.009	0.001	0.019	0.003	75.5	3.1	-0.006	0.012
86 HER	NUV	7688.721	+0.053	0.053	+0.081	0.061	0.097	0.066	28.5	13.9	-0.004	0.040
86 HER	NUV	7689.745	+0.016	0.028	-0.061	0.037	0.063	0.038	142.4	12.1	+0.278	0.282
86 HER	NUV	7707.685	-0.007	0.009	+0.078	0.013	0.078	0.013	47.5	3.5	+0.032	0.022
Weighted average:			-0.003	0.008	+0.062	0.031	0.062	0.031	46.3	3.8	+0.025	0.016
ALP LYR	R	6993.685	-0.001	0.001	+0.002	0.002	0.002	0.002	56.5	18.3	+0.002	0.001
ALP LYR	R	6994.627	+0.001	0.004	+0.007	0.006	0.007	0.006	41.8	16.4	-0.009	0.003
ALP LYR	R	6995.649	-0.002	0.000	-0.000	0.000	0.002	0.000	90.2	5.1	-0.005	0.001
ALP LYR	R	6999.650	-0.001	0.004	+0.004	0.005	0.004	0.005	53.5	23.2	-0.002	0.003
ALP LYR	R	7005.772	-0.004	0.000	+0.005	0.000	0.006	0.000	64.2	1.3	-0.005	0.001
ALP LYR	R	7018.631	+0.001	0.001	+0.006	0.002	0.006	0.002	42.0	7.2	-0.010	0.002
ALP LYR	R	7021.649	-0.003	0.002	+0.004	0.002	0.005	0.002	62.2	9.0	-0.004	0.002

APPENDIX D (cont.)

Journal of Observations for Standard Polarization Sources (Unstandardized Values)

Name	Filter (Note 1)	(JD-2440000)	q (%)	σq (%)	u (%)	σu (%)	p (%)	σp (%)	θ (o)	σθ (o)	v (%)	σv (%)
ALP LYR	R	7025.604	-0.001	0.001	+0.005	0.001	0.005	0.002	53.0	5.8	-0.001	0.001
ALP LYR	R	7026.635	-0.001	0.001	-0.002	0.002	0.002	0.002	114.1	16.7	-0.006	0.002
ALP LYR	R	7027.612	-0.002	0.001	+0.004	0.001	0.004	0.002	56.5	7.1	+0.000	0.001
ALP LYR	R	7029.606	-0.004	0.003	+0.004	0.003	0.006	0.004	65.1	13.4	-0.009	0.001
ALP LYR	R	7031.621	...	...	...	...	...	...	...	...	-0.005	0.001
ALP LYR	R	7031.656	+0.002	0.003	-0.002	0.003	0.003	0.003	163.4	24.9	-0.004	0.002
ALP LYR	R	7053.598	+0.002	0.000	+0.005	0.000	0.006	0.000	32.4	1.0	-0.007	0.001
ALP LYR	R	7064.598	+0.002	0.004	+0.005	0.006	0.005	0.006	33.2	23.5	-0.004	0.001
ALP LYR	R	7065.562	-0.000	0.000	+0.006	0.001	0.006	0.001	46.9	2.4	-0.009	0.002
ALP LYR	R	7696.739	+0.001	0.003	+0.007	0.004	0.007	0.004	39.0	12.9	-0.001	0.002
ALP LYR	R	7708.739	-0.003	0.002	+0.004	0.002	0.004	0.003	62.0	11.5	-0.009	0.002
ALP LYR	R	7710.624	+0.004	0.000	+0.005	0.000	0.006	0.000	24.0	1.0	-0.004	0.004
ALP LYR	R	7716.831	-0.002	0.002	+0.001	0.002	0.002	0.002	73.0	22.2	-0.004	0.001
ALP LYR	R	7764.694	+0.000	0.002	+0.005	0.003	0.005	0.003	43.3	10.1	-0.000	0.003
ALP LYR	R	7773.524	+0.005	0.013	+0.002	0.006	0.006	0.014	12.	13.	+0.002	0.003
ALP LYR	R	7794.591	+0.001	0.001	+0.007	0.001	0.007	0.001	41.5	4.2	+0.003	0.001
ALP LYR	R	7801.615	+0.002	0.001	+0.002	0.001	0.003	0.001	16.6	5.1	-0.012	0.003
ALP LYR	R	7809.549	-0.002	0.001	+0.007	0.001	0.007	0.001	53.6	2.5	-0.003	0.003
Weighted average:			+0.001	0.001	+0.004	0.000	0.004	0.000	37.8	4.3	-0.003	0.001
ALP LYR	V	6995.669	-0.004	0.004	+0.002	0.003	0.004	0.004	76.3	21.1	-0.002	0.002
ALP LYR	V	7018.654	-0.001	0.003	+0.001	0.003	0.002	0.004	61.1	50.1	-0.002	0.001
ALP LYR	V	7020.614	+0.003	0.002	+0.007	0.002	0.008	0.002	33.1	5.7	-0.005	0.002

APPENDIX D (cont.)

Journal of Observations for Standard Polarization Sources (Unstandardized Values)

Name	Filter (Note 1)	(JD-2440000)	q (%)	σq (%)	u (%)	σu (%)	p (%)	σp (%)	θ (o)	σθ (o)	v (%)	σv (%)
ALP LYR	V	7021.585	+0.001	0.002	+0.002	0.003	0.002	0.003	33.4	27.7	+0.000	0.004
ALP LYR	V	7026.608	+0.001	0.001	-0.004	0.001	0.004	0.001	144.5	5.8	+0.003	0.001
ALP LYR	V	7028.624	-0.006	0.001	+0.004	0.001	0.007	0.001	72.6	3.2	-0.003	0.001
ALP LYR	V	7064.575	+0.007	0.002	+0.006	0.002	0.009	0.002	19.6	4.9	-0.006	0.002
ALP LYR	V	7065.592	+0.006	0.003	+0.003	0.002	0.007	0.003	13.9	9.6	-0.005	0.002
ALP LYR	V	7073.572	+0.005	0.004	-0.003	0.003	0.006	0.004	166.1	12.9	-0.008	0.001
ALP LYR	V	7709.742	-0.005	0.003	+0.023	0.004	0.023	0.004	51.6	3.1	-0.000	0.001
ALP LYR	V	7736.697	+0.000	0.001	+0.018	0.001	0.018	0.001	44.9	1.4	-0.001	0.002
ALP LYR	V	7772.533	-0.002	0.001	+0.017	0.002	0.017	0.002	48.	3.	-0.004	0.003
ALP LYR	V	7780.636	-0.004	0.002	+0.018	0.003	0.018	0.003	51.4	3.2	+0.004	0.001
ALP LYR	V	7807.558	+0.008	0.003	+0.019	0.003	0.021	0.003	34.2	3.3	+0.001	0.003
ALP LYR	V	7822.572	+0.011	0.001	+0.014	0.001	0.018	0.001	26.6	1.3	+0.002	0.002
ALP LYR	V	8043.805	-0.004	0.002	+0.016	0.003	0.017	0.003	51.1	3.3	-0.005	0.002
Weighted average:			+0.002	0.001	+0.008	0.002	0.008	0.002	38.8	5.3	-0.001	0.001
ALP LYR	B	7006.696	-0.001	0.004	+0.005	0.006	0.005	0.006	53.3	22.7	+0.001	0.003
ALP LYR	B	7020.594	-0.007	0.003	+0.006	0.003	0.009	0.003	69.0	7.0	-0.005	0.003
ALP LYR	B	7022.618	-0.002	0.001	+0.005	0.001	0.006	0.001	56.5	4.3	-0.004	0.002
ALP LYR	B	7029.584	-0.004	0.002	-0.001	0.002	0.004	0.002	97.2	11.3	-0.004	0.002
ALP LYR	B	7770.553	-0.006	0.002	+0.002	0.001	0.006	0.002	79.	10.	-0.006	0.002
ALP LYR	B	7778.525	-0.007	0.003	+0.005	0.003	0.008	0.003	70.7	8.5	+0.001	0.003
ALP LYR	B	7794.617	-0.008	0.002	+0.005	0.002	0.010	0.003	73.1	5.4	-0.002	0.001

APPENDIX D (cont.)

Journal of Observations for Standard Polarization Sources (Unstandardized Values)

Name	Filter (Note 1)	(JD-2440000)	q (%)	σq (%)	u (%)	σu (%)	p (%)	σp (%)	θ (o)	σθ (o)	v (%)	σv (%)
ALP LYR	B	8068.605	-0.005	0.002	+0.009	0.003	0.011	0.003	59.3	6.0	-0.003	0.001
Weighted average:			-0.004	0.001	+0.004	0.001	0.006	0.001	64.7	4.9	-0.002	0.001
ALP LYR	NUV	7028.597	-0.009	0.010	+0.001	0.007	0.009	0.010	87.5	20.2	-0.041	0.003
ALP LYR	NUV	7028.648	-0.009	0.006	+0.001	0.004	0.009	0.006	88.3	13.2	+0.003	0.004
ALP LYR	NUV	7028.683	-0.011	0.004	+0.006	0.003	0.012	0.004	75.7	6.9	-0.035	0.009
ALP LYR	NUV	7031.601	-0.002	0.008	-0.007	0.010	0.007	0.011	126.1	30.5	+0.006	0.006
ALP LYR	NUV	7031.679	-0.012	0.009	+0.006	0.007	0.013	0.010	77.6	14.5	-0.006	0.010
ALP LYR	NUV	7031.704	+0.007	0.003	+0.010	0.003	0.012	0.003	27.8	5.3	-0.043	0.003
ALP LYR	NUV	7769.629	-0.012	0.005	+0.012	0.005	0.017	0.006	68.	10.	-0.002	0.005
ALP LYR	NUV	7774.526	+0.004	0.002	+0.000	0.001	0.004	0.002	1.	15.	-0.013	0.005
Weighted average:			-0.001	0.004	+0.006	0.002	0.006	0.002	48.8	18.4	-0.030	0.009
ALP LYR	LAM	7716.854	-0.081	0.072	+0.016	0.023	0.082	0.073	84.5	6.5	+0.026	0.007
ALP LYR	POL	7027.641	+3.216	0.867	-22.901	1.217	23.125	1.223	139.0	1.1	+56.184	3.719
SIG SGR	R	6975.728	+0.011	0.013	-0.021	0.015	0.024	0.016	148.2	13.8	...	...
SIG SGR	R	6993.662	-0.001	0.004	-0.007	0.006	0.007	0.006	131.2	18.8	-0.013	0.012
SIG SGR	R	6994.681	-0.001	0.001	-0.028	0.001	0.028	0.001	133.9	0.9	-0.001	0.016
SIG SGR	R	6999.679	-0.006	0.012	-0.011	0.015	0.013	0.016	121.6	24.7	-0.027	0.018
SIG SGR	R	7005.644	-0.003	0.008	-0.009	0.011	0.009	0.011	127.0	24.2	+0.007	0.007
SIG SGR	R	7006.644	+0.039	0.058	-0.060	0.066	0.071	0.071	151.7	20.5	-0.015	0.019
SIG SGR	R	7012.620	-0.003	0.012	-0.019	0.017	0.019	0.017	130.8	18.2	+0.030	0.007

APPENDIX D (cont.)

Journal of Observations for Standard Polarization Sources (Unstandardized Values)

Name	Filter (Note 1)	(JD-2440000)	q (%)	σq (%)	u (%)	σu (%)	p (%)	σp (%)	θ (o)	σθ (o)	v (%)	σv (%)
SIG SGR	R	7012.644	-0.006	0.019	-0.011	0.023	0.013	0.024	121.9	38.7	+0.055	0.043
Weighted average:			-0.001	0.000	-0.027	0.002	0.027	0.002	133.8	0.4	+0.010	0.008
SIG SGR	V	6995.691	-0.022	0.015	-0.013	0.012	0.026	0.016	105.3	12.1	+0.006	0.013
SIG SGR	V	7005.665	+0.004	0.007	-0.018	0.010	0.018	0.010	140.9	11.3	-0.011	0.007
Weighted average:			-0.002	0.011	-0.016	0.002	0.016	0.003	132.2	18.7	-0.007	0.007
SIG SGR	B	6971.751	+0.011	0.008	-0.013	0.009	0.018	0.010	154.9	11.0	-0.007	0.005
ALP AQL	R	6993.724	-0.001	0.003	-0.002	0.003	0.002	0.003	113.4	31.0	-0.004	0.003
ALP AQL	R	6994.651	-0.003	0.005	-0.003	0.004	0.004	0.005	110.3	24.5	-0.009	0.003
ALP AQL	R	7000.642	+0.005	0.003	+0.001	0.002	0.005	0.003	7.8	13.4	-0.036	0.003
ALP AQL	R	7005.700	+0.000	0.002	-0.001	0.003	0.001	0.003	142.3	43.1	-0.015	0.004
ALP AQL	R	7018.688	+0.019	0.005	-0.002	0.004	0.019	0.005	177.1	5.2	-0.010	0.001
ALP AQL	R	7026.665	+0.001	0.001	-0.003	0.001	0.003	0.001	149.0	6.1	+0.002	0.003
ALP AQL	R	7809.580	+0.000	0.002	+0.007	0.003	0.007	0.003	43.8	10.1	+0.002	0.003
Weighted average:			+0.001	0.001	-0.002	0.001	0.002	0.001	155.1	12.5	-0.009	0.004
ALP AQL	V	7020.641	-0.000	0.002	-0.001	0.003	0.001	0.003	132.7	90.0	-0.010	0.002
ALP AQL	V	8043.831	-0.005	0.002	+0.008	0.003	0.010	0.003	60.2	6.0	-0.006	0.003
Weighted average:			-0.002	0.002	+0.004	0.004	0.004	0.004	58.8	20.2	-0.009	0.002
ALP AQL	WUV	8043.853	+0.006	0.004	+0.004	0.003	0.007	0.004	18.2	11.5	+0.003	0.002

APPENDIX D (cont.)

Journal of Observations for Standard Polarization Sources (Unstandardized Values)

Name	Filter (Note 1)	(JD-2440000)	q (%)	σq (%)	u (%)	σu (%)	p (%)	σp (%)	θ (o)	σθ (o)	v (%)	σv (%)
EPS CYG	R	6995.716	-0.006	0.014	-0.002	0.011	0.006	0.015	100.0	49.3	-0.020	0.004
55 CYG	V	7392.593	+2.704	0.030	+0.364	0.006	2.728	0.030	3.8	0.1	-0.043	0.020
55 CYG	V	7395.587	+2.681	0.034	+0.247	0.014	2.692	0.034	2.6	0.1	-0.049	0.031
55 CYG	V	7396.562	+2.697	0.033	+0.189	0.012	2.703	0.033	2.0	0.1	-0.054	0.014
Weighted average:			+2.695	0.007	+0.315	0.051	2.713	0.009	3.3	0.5	-0.050	0.003
61 CYGB	R	7029.629	+0.011	0.017	-0.027	0.021	0.029	0.022	146.3	15.5	-0.003	0.020
HD204827	R	6771.533	-2.481	0.027	+4.059	0.044	4.757	0.051	60.7	0.0	-0.464	0.140
HD204827	R	6779.504	-2.490	0.027	+3.915	0.042	4.639	0.049	61.2	0.0	+0.314	0.285
Weighted average:			-2.486	0.005	+3.983	0.072	4.695	0.061	61.0	0.2	-0.313	0.308
HD204827	V	6771.559	-2.883	0.076	+4.518	0.094	5.360	0.104	61.3	0.3	+0.030	0.167
HD204827	V	6779.577	-2.503	0.381	+4.944	0.466	5.541	0.492	58.4	1.8	-0.071	0.093
HD204827	V	7807.734	-2.537	0.148	+4.677	0.181	5.321	0.193	59.2	0.7	-0.162	0.377
HD204827	V	7843.645	-2.655	0.161	+4.433	0.191	5.167	0.207	60.5	0.8	-0.071	0.106
Weighted average:			-2.779	0.085	+4.543	0.056	5.326	0.065	60.7	0.4	-0.059	0.023
HD204827	B	6771.588	-2.505	0.138	+4.721	0.171	5.344	0.182	59.0	0.7	+0.201	0.171
HD204827	B	6779.606	-2.787	0.151	+4.683	0.181	5.450	0.195	60.4	0.7	+0.227	0.271
Weighted average:			-2.633	0.140	+4.703	0.019	5.390	0.070	59.6	0.7	+0.208	0.012

APPENDIX D (cont.)

Journal of Observations for Standard Polarization Sources (Unstandardized Values)

Name	Filter (Note 1)	(JD-2440000)	q (%)	σq (%)	u (%)	σu (%)	p (%)	σp (%)	θ (o)	σθ (o)	v (%)	σv (%)
HD204827	NUV	6771.612	-3.295	0.868	+7.330	1.085	8.036	1.133	57.1	2.9	+1.103	3.655
HD204827	LAM	7807.756	-3.607	0.143	+1.139	0.105	3.783	0.146	81.2	0.8	-2.726	0.351
12 PEG	V	7405.578	+0.082	0.013	+0.548	0.019	0.554	0.019	40.8	0.7	...	...

Note 1. Filter (Column 2):

R Red bandpass

V Visual bandpass

B Blue bandpass

NUV Narrow UV bandpass

WUV Wide UV bandpass

LOW Far red bandpass

LAMxxx Visual bandpass with quarter-wave plate inserted at a xxx angle measured in degrees and referenced to side of slide.

POL Circular polaroid sheet inserted into slide for testing.

See the main text for more information on the filters.

APPENDIX E

Journal of Standardized Observations for Program Objects

Name	Filter (Note 1)	(JD-2440000)	q (%)	σq (%)	u (%)	σu (%)	p (%)	σp (%)	θ (o)	σθ (o)	v (%)	σv (%)
119 TAU	R	6778.826	+0.737	0.010	+0.061	0.005	0.739	0.010	2.4	0.2	-0.046	0.007
119 TAU	R	6786.747	+0.706	0.009	+0.073	0.004	0.710	0.009	2.9	0.2	-0.006	0.008
119 TAU	R	6798.660	+0.657	0.009	+0.083	0.004	0.662	0.009	3.6	0.2	-0.014	0.013
119 TAU	R	6798.688	+0.618	0.008	+0.074	0.004	0.623	0.008	3.4	0.2	+0.003	0.010
119 TAU	R	7894.725	+0.971	0.015	+0.140	0.009	0.981	0.015	4.1	0.3	+0.002	0.012
119 TAU	R	7928.643	+0.881	0.020	+0.160	0.014	0.895	0.020	5.1	0.5	+0.001	0.010
119 TAU	R	7935.692	+0.866	0.013	+0.162	0.008	0.881	0.013	5.3	0.3	-0.011	0.011
Weighted average:			+0.722	0.043	+0.085	0.012	0.727	0.042	3.4	0.5	-0.015	0.008
119 TAU	V	6778.861	+0.751	0.019	+0.042	0.013	0.753	0.019	1.6	0.5	-0.039	0.037
119 TAU	V	6786.798	+0.722	0.012	+0.060	0.007	0.724	0.012	2.4	0.3	-0.015	0.023
119 TAU	V	6799.753	+0.598	0.009	+0.065	0.005	0.602	0.009	3.1	0.3	-0.029	0.012
Weighted average:			+0.659	0.047	+0.061	0.004	0.662	0.047	2.6	0.3	-0.027	0.004
119 TAU	B	6786.821	+0.632	0.053	+0.100	0.041	0.640	0.053	4.5	1.9	-0.096	0.025
119 TAU*	LAM	6799.725	+0.050	0.029	+0.150	0.038	0.158	0.039	35.8	5.0	+0.680	0.052
119 TAU	NUV	6786.845	+0.731	1.301	+1.480	1.707	1.651	1.635	31.8	24.1	-0.190	1.601
ALP ORI*	FR	6872.611	-0.041	0.012	-0.148	0.016	0.154	0.016	127.3	2.1	-0.024	0.014
ALP ORI	R	6754.674	...	...	...	...	...	...	...	...	+0.012	0.002
ALP ORI	R	6756.670	...	...	...	...	...	...	...	...	+0.012	0.005
ALP ORI	R	6757.640	...	...	...	...	...	...	...	...	+0.009	0.006

APPENDIX E (cont.)

Journal of Standardized Observations for Program Objects

Name	Filter (Note 1)	(JD-2440000)	q (%)	σq (%)	u (%)	σu (%)	p (%)	σp (%)	θ (o)	σθ (o)	v (%)	σv (%)
ALP ORI	R	6757.654	...	...	...	...	...	...	...	...	+0.016	0.005
ALP ORI	R	6764.619	...	...	...	...	...	...	...	...	+0.006	0.004
ALP ORI	R	6764.748	...	...	...	...	...	...	...	...	-0.002	0.008
ALP ORI	R	6764.766	...	...	...	...	...	...	...	...	+0.007	0.007
ALP ORI	R	6764.854	...	...	...	...	...	...	...	...	+0.007	0.004
ALP ORI	R	6764.872	...	...	...	...	...	...	...	...	+0.004	0.002
ALP ORI	R	6764.890	...	...	...	...	...	...	...	...	+0.008	0.002
ALP ORI	R	6764.908	...	...	...	...	...	...	...	...	-0.010	0.003
ALP ORI	R	6768.804	...	...	...	...	...	...	...	...	+0.000	0.003
ALP ORI	R	6768.820	...	...	...	...	...	...	...	...	-0.002	0.004
ALP ORI	R	6768.838	...	...	...	...	...	...	...	...	+0.002	0.009
ALP ORI	R	6768.856	...	...	...	...	...	...	...	...	-0.007	0.004
ALP ORI	R	6768.873	...	...	...	...	...	...	...	...	+0.004	0.006
Weighted average:			...	...	...	...	...	...	...	...	+0.004	0.002
ALP ORI	R	6759.643	-0.066	0.001	+0.112	0.002	0.130	0.001	60.3	0.3	...	...
ALP ORI	R	6770.711	-0.123	0.003	+0.120	0.003	0.172	0.003	67.9	0.4	-0.009	0.003
ALP ORI	R	6770.728	-0.121	0.002	+0.119	0.003	0.170	0.003	67.7	0.4	-0.002	0.003
ALP ORI	R	6777.711	+0.175	0.002	-0.133	0.002	0.219	0.002	161.4	0.2	-0.011	0.004
ALP ORI	R	6777.851	+0.171	0.002	-0.127	0.002	0.213	0.002	161.6	0.3	-0.007	0.002
ALP ORI	R	6780.685	+0.187	0.003	-0.134	0.003	0.230	0.003	162.2	0.4	...	...
ALP ORI	R	6799.579	+0.321	0.005	-0.143	0.003	0.351	0.005	168.0	0.3	-0.010	0.012
ALP ORI	R	6799.706	+0.324	0.005	-0.148	0.003	0.356	0.005	167.7	0.3	-0.006	0.006

APPENDIX E (cont.)

Journal of Standardized Observations for Program Objects

Name	Filter (Note 1)	(JD-2440000)	q (%)	σq (%)	u (%)	σu (%)	p (%)	σp (%)	θ (o)	σθ (o)	v (%)	σv (%)
ALP ORI	R	6820.570	+0.412	0.007	-0.240	0.005	0.476	0.006	164.9	0.3	+0.005	0.001
ALP ORI	R	6820.595	+0.403	0.005	-0.245	0.003	0.472	0.004	164.3	0.2	+0.001	0.002
ALP ORI	R	6820.616	+0.405	0.007	-0.246	0.006	0.474	0.007	164.4	0.4	+0.003	0.004
ALP ORI	R	6820.637	+0.407	0.006	-0.247	0.005	0.476	0.006	164.4	0.3	+0.010	0.003
ALP ORI	R	6823.604	+0.401	0.005	-0.258	0.004	0.477	0.005	163.6	0.3	+0.006	0.003
ALP ORI	R	6823.626	+0.402	0.005	-0.255	0.004	0.476	0.005	163.8	0.3	+0.002	0.002
ALP ORI	R	6823.648	+0.400	0.008	-0.258	0.007	0.476	0.007	163.6	0.4	+0.004	0.005
ALP ORI	R	6834.606	+0.368	0.004	-0.319	0.004	0.487	0.004	159.5	0.2	+0.002	0.002
ALP ORI	R	6834.630	+0.364	0.004	-0.320	0.004	0.484	0.004	159.3	0.2	+0.000	0.001
ALP ORI	R	6834.658	+0.365	0.004	-0.322	0.004	0.487	0.004	159.3	0.3	+0.003	0.001
ALP ORI	R	6842.686	+0.327	0.004	-0.357	0.004	0.484	0.004	156.2	0.2	+0.012	0.001
ALP ORI	R	6844.617	+0.311	0.004	-0.371	0.005	0.484	0.004	155.0	0.2	+0.002	0.002
ALP ORI	R	6846.709	+0.297	0.003	-0.373	0.004	0.477	0.004	154.3	0.2	+0.006	0.003
ALP ORI	R	6851.616	+0.259	0.003	-0.380	0.005	0.460	0.004	152.2	0.2	+0.003	0.001
ALP ORI	R	6851.640	+0.260	0.004	-0.380	0.005	0.460	0.005	152.2	0.3	+0.006	0.002
ALP ORI	R	6852.602	+0.254	0.003	-0.384	0.004	0.461	0.004	151.7	0.2	+0.003	0.003
ALP ORI	R	6852.626	+0.251	0.003	-0.385	0.004	0.460	0.004	151.6	0.2	+0.004	0.004
ALP ORI	R	6852.650	+0.257	0.007	-0.383	0.009	0.462	0.008	151.9	0.5	+0.005	0.000
ALP ORI	R	6857.621	+0.214	0.003	-0.383	0.005	0.439	0.004	149.6	0.2	+0.006	0.003
ALP ORI	R	6857.645	+0.213	0.003	-0.383	0.005	0.438	0.004	149.5	0.2	+0.009	0.001
ALP ORI	R	6859.625	+0.209	0.004	-0.379	0.006	0.433	0.005	149.4	0.3	+0.005	0.003
ALP ORI	R	6860.597	+0.193	0.003	-0.383	0.005	0.429	0.004	148.4	0.2	+0.003	0.001
ALP ORI	R	6865.517	+0.162	0.002	-0.370	0.004	0.404	0.004	146.9	0.2	+0.003	0.003

APPENDIX E (cont.)

Journal of Standardized Observations for Program Objects

Name	Filter (Note 1)	(JD-2440000)	q (%)	σq (%)	u (%)	σu (%)	p (%)	σp (%)	θ (o)	σθ (o)	v (%)	σv (%)
ALP ORI	R	6865.542	+0.160	0.003	-0.369	0.005	0.402	0.004	146.7	0.2	+0.006	0.003
ALP ORI	R	6871.590	+0.125	0.003	-0.343	0.005	0.365	0.005	145.0	0.2	+0.002	0.000
ALP ORI	R	6871.613	+0.126	0.002	-0.341	0.004	0.364	0.004	145.1	0.2	+0.004	0.002
ALP ORI	R	6872.580	+0.127	0.002	-0.342	0.004	0.365	0.004	145.2	0.2	-0.000	0.001
ALP ORI	R	6874.585	+0.109	0.001	-0.322	0.003	0.340	0.003	144.4	0.1	-0.004	0.001
ALP ORI	R	6874.612	+0.111	0.002	-0.323	0.004	0.342	0.004	144.5	0.2	-0.001	0.002
ALP ORI	R	6877.586	+0.098	0.001	-0.302	0.003	0.318	0.003	144.0	0.1	-0.010	0.002
ALP ORI	R	6878.556	+0.091	0.002	-0.298	0.004	0.312	0.004	143.5	0.2	-0.009	0.001
ALP ORI	R	6879.525	+0.085	0.002	-0.295	0.004	0.307	0.004	143.0	0.2	-0.008	0.001
ALP ORI	R	6879.570	+0.086	0.002	-0.291	0.004	0.304	0.004	143.2	0.2	-0.008	0.001
ALP ORI	R	6881.520	+0.074	0.001	-0.277	0.003	0.287	0.003	142.5	0.1	-0.006	0.001
ALP ORI	R	6881.565	+0.075	0.001	-0.276	0.003	0.286	0.003	142.6	0.1	-0.007	0.001
ALP ORI	R	6887.525	+0.061	0.001	-0.240	0.003	0.248	0.003	142.1	0.2	-0.005	0.001
ALP ORI	R	6894.510	+0.026	0.006	-0.162	0.010	0.164	0.010	139.6	1.1	-0.005	0.003
ALP ORI	R	6895.508	+0.000	0.018	-0.120	0.028	0.120	0.028	135.0	4.4	-0.001	0.003
ALP ORI	R	6896.510	+0.011	0.012	-0.134	0.018	0.135	0.018	137.4	2.5	-0.007	0.003
ALP ORI	R	6896.534	+0.038	0.003	-0.168	0.004	0.172	0.004	141.4	0.4	-0.003	0.002
ALP ORI	R	6899.529	+0.037	0.001	-0.128	0.002	0.133	0.002	143.1	0.2	-0.001	0.002
ALP ORI	R	6912.514	...	...	...	...	...	...	...	...	-0.003	0.002
ALP ORI	R	7031.887	+0.008	0.001	-0.161	0.003	0.161	0.003	136.4	0.2	-0.005	0.001
ALP ORI	R	7064.815	+0.110	0.002	-0.067	0.001	0.129	0.002	164.3	0.3	-0.004	0.001
ALP ORI	R	7087.865	+0.213	0.003	+0.074	0.002	0.226	0.003	9.6	0.3	-0.011	0.002
ALP ORI	R	7122.644	+0.236	0.003	+0.263	0.003	0.353	0.003	24.1	0.3	-0.003	0.002

APPENDIX E (cont.)

Journal of Standardized Observations for Program Objects

Name	Filter (Note 1)	(JD-2440000)	q (%)	σq (%)	u (%)	σu (%)	p (%)	σp (%)	θ (o)	σθ (o)	v (%)	σv (%)
ALP ORI	R	7764.870	-0.277	0.006	+0.199	0.006	0.341	0.006	72.2	0.5	+0.009	0.001
ALP ORI	R	7772.870	-0.272	0.004	+0.207	0.003	0.342	0.004	71.3	0.3	+0.004	0.002
ALP ORI	R	7773.861	-0.271	0.004	+0.209	0.004	0.343	0.004	71.2	0.3	+0.010	0.002
ALP ORI	R	7794.818	-0.256	0.003	+0.226	0.003	0.341	0.003	69.3	0.3	+0.011	0.001
ALP ORI	R	7807.791	-0.233	0.002	+0.232	0.002	0.329	0.002	67.6	0.2	+0.005	0.003
ALP ORI	R	7822.818	-0.185	0.002	+0.205	0.002	0.276	0.002	66.0	0.2	+0.002	0.002
ALP ORI	R	7824.795	-0.178	0.002	+0.198	0.003	0.266	0.003	65.9	0.3	-0.002	0.001
ALP ORI	R	7834.785	-0.145	0.002	+0.180	0.002	0.231	0.002	64.4	0.2	+0.003	0.000
ALP ORI	R	7843.805	-0.112	0.001	+0.167	0.002	0.201	0.002	62.0	0.2	-0.002	0.003
ALP ORI	R	7855.759	-0.072	0.001	+0.132	0.002	0.150	0.002	59.3	0.3	+0.004	0.001
ALP ORI	R	7894.695	-0.002	0.002	-0.031	0.002	0.031	0.002	133.5	1.4	+0.002	0.002
ALP ORI	R	7918.723	-0.049	0.001	-0.062	0.001	0.079	0.001	115.8	0.5	-0.009	0.005
ALP ORI	R	7928.590	-0.052	0.033	-0.033	0.030	0.062	0.032	106.2	14.2	+0.012	0.009
ALP ORI	R	7930.669	-0.083	0.003	-0.040	0.003	0.092	0.003	102.8	0.9	+0.009	0.001
ALP ORI	R	7935.610	-0.092	0.002	-0.037	0.002	0.100	0.002	101.0	0.5	+0.005	0.003
ALP ORI	R	7940.560	-0.095	0.001	-0.036	0.001	0.102	0.001	100.5	0.3	+0.009	0.001
ALP ORI	R	7942.609	-0.095	0.004	-0.038	0.003	0.103	0.003	100.8	0.8	+0.006	0.001
ALP ORI	R	7942.636	-0.097	0.002	-0.037	0.001	0.104	0.002	100.4	0.4	+0.005	0.003
ALP ORI	R	7943.589	-0.093	0.006	-0.035	0.005	0.099	0.006	100.4	1.5	+0.004	0.001
ALP ORI	R	7948.574	-0.102	0.002	-0.039	0.001	0.109	0.001	100.5	0.3	+0.010	0.002
ALP ORI	R	7955.608	-0.106	0.003	-0.038	0.002	0.113	0.003	99.8	0.6	+0.006	0.001
ALP ORI	R	7976.528	-0.130	0.003	-0.076	0.003	0.150	0.003	105.2	0.5	+0.013	0.001
ALP ORI	R	7977.590	-0.136	0.002	-0.082	0.001	0.158	0.001	105.6	0.2	+0.009	0.002

APPENDIX E (cont.)

Journal of Standardized Observations for Program Objects

Name	Filter (Note 1)	(JD-2440000)	q (%)	σq (%)	u (%)	σu (%)	p (%)	σp (%)	θ (o)	σθ (o)	v (%)	σv (%)
ALP ORI	R	7990.527	-0.219	0.003	-0.136	0.002	0.258	0.003	105.9	0.2	-0.028	0.003
ALP ORI	R	7995.530	-0.173	0.003	-0.097	0.003	0.198	0.003	104.6	0.4	+0.011	0.001
ALP ORI	R	7998.527	-0.170	0.004	-0.093	0.004	0.194	0.004	104.4	0.6	+0.009	0.004
ALP ORI	R	8000.528	-0.174	0.002	-0.087	0.002	0.195	0.002	103.3	0.3	+0.004	0.003
Weighted average:			+0.024	0.015	-0.065	0.017	0.069	0.017	145.3	6.4	+0.004	0.001
ALP ORI	V	6764.788	...	...	...	...	...	...	...	...	+0.010	0.005
ALP ORI	V	6764.808	...	...	...	...	...	...	...	...	+0.020	0.019
ALP ORI	V	6764.831	...	...	...	...	...	...	...	...	+0.010	0.011
Weighted average:			...	...	...	...	...	...	...	...	+0.011	0.002
ALP ORI	V	6770.753	-0.104	0.005	+0.145	0.006	0.179	0.006	62.9	0.9	-0.007	0.004
ALP ORI	V	6770.772	-0.108	0.003	+0.148	0.003	0.183	0.003	63.1	0.5	-0.003	0.003
ALP ORI	V	6777.731	+0.179	0.004	-0.163	0.004	0.242	0.004	158.9	0.4	-0.008	0.003
ALP ORI	V	6780.712	+0.196	0.003	-0.168	0.003	0.258	0.003	159.7	0.3	-0.008	0.004
ALP ORI	V	6799.729	+0.421	0.005	-0.187	0.003	0.461	0.005	168.0	0.2	-0.006	0.005
ALP ORI	V	6820.662	+0.568	0.006	-0.329	0.004	0.656	0.006	165.0	0.2	+0.002	0.002
ALP ORI	V	6823.674	+0.532	0.008	-0.345	0.006	0.634	0.008	163.5	0.3	-0.036	0.004
ALP ORI	V	6834.689	+0.521	0.007	-0.456	0.006	0.693	0.006	159.4	0.3	-0.007	0.001
ALP ORI	V	6844.644	+0.452	0.005	-0.524	0.006	0.692	0.005	155.4	0.2	-0.007	0.004
ALP ORI	V	6846.686	+0.454	0.005	-0.532	0.006	0.699	0.006	155.2	0.2	-0.005	0.003
ALP ORI	V	6859.651	+0.308	0.003	-0.544	0.006	0.625	0.005	149.7	0.2	-0.003	0.002
ALP ORI	V	6860.620	+0.293	0.004	-0.538	0.007	0.613	0.006	149.3	0.2	+0.003	0.001
ALP ORI	V	6865.568	+0.257	0.005	-0.520	0.008	0.580	0.007	148.1	0.3	-0.009	0.003

APPENDIX E (cont.)

Journal of Standardized Observations for Program Objects

Name	Filter (Note 1)	(JD-2440000)	q (%)	σq (%)	u (%)	σu (%)	p (%)	σp (%)	θ (o)	σθ (o)	v (%)	σv (%)
ALP ORI	V	6878.581	+0.144	0.004	-0.417	0.007	0.441	0.006	144.5	0.3	-0.014	0.002
ALP ORI	V	6878.604	+0.140	0.003	-0.414	0.006	0.437	0.006	144.4	0.2	-0.006	0.002
ALP ORI	V	6879.549	+0.134	0.002	-0.407	0.005	0.428	0.005	144.1	0.2	-0.008	0.006
ALP ORI	V	6881.542	+0.121	0.002	-0.390	0.005	0.408	0.005	143.6	0.2	-0.007	0.003
ALP ORI	V	6887.548	+0.086	0.004	-0.325	0.006	0.337	0.006	142.4	0.3	-0.003	0.003
ALP ORI	V	6895.528	+0.049	0.003	-0.225	0.005	0.230	0.005	141.1	0.4	-0.006	0.005
ALP ORI	V	7087.888	+0.247	0.004	+0.102	0.003	0.268	0.004	11.2	0.4	-0.006	0.001
ALP ORI	V	7764.894	-0.530	0.069	+0.267	0.061	0.593	0.068	76.6	3.0	+0.002	0.007
ALP ORI	V	7772.898	-0.501	0.029	+0.321	0.026	0.594	0.028	73.7	1.3	+0.003	0.004
ALP ORI	V	7773.885	-0.478	0.007	+0.347	0.006	0.590	0.007	72.0	0.3	+0.003	0.002
ALP ORI	V	7793.842	-0.463	0.005	+0.391	0.005	0.606	0.005	69.9	0.2	+0.002	0.001
ALP ORI	V	7807.816	-0.400	0.005	+0.409	0.005	0.572	0.005	67.2	0.2	+0.008	0.002
ALP ORI	V	7824.815	-0.311	0.004	+0.372	0.005	0.485	0.005	64.9	0.3	+0.001	0.005
ALP ORI	V	7834.811	-0.281	0.005	+0.328	0.006	0.432	0.006	65.3	0.4	+0.005	0.001
ALP ORI	V	7978.526	-0.197	0.007	-0.051	0.005	0.203	0.007	97.3	0.7	-0.029	0.002
Weighted average:			+0.103	0.044	-0.117	0.056	0.156	0.051	155.7	9.1	-0.004	0.002
ALP ORI	B	6770.798	-0.059	0.011	+0.141	0.015	0.152	0.014	56.4	2.2	-0.029	0.010
ALP ORI	B	6770.817	-0.068	0.002	+0.164	0.003	0.177	0.003	56.3	0.4	-0.012	0.010
ALP ORI	B	6777.749	+0.140	0.007	-0.201	0.009	0.245	0.008	152.5	0.9	-0.029	0.009
ALP ORI	B	6780.731	+0.166	0.006	-0.191	0.006	0.253	0.006	155.4	0.7	+0.002	0.008
ALP ORI	B	6799.751	+0.410	0.006	-0.218	0.004	0.464	0.006	166.0	0.3	-0.023	0.004
ALP ORI	B	6823.729	+0.558	0.007	-0.423	0.006	0.700	0.007	161.4	0.3	-0.039	0.013

APPENDIX E (cont.)

Journal of Standardized Observations for Program Objects

Name	Filter (Note 1)	(JD-2440000)	q (%)	σq (%)	u (%)	σu (%)	p (%)	σp (%)	θ (o)	σθ (o)	v (%)	σv (%)
ALP ORI	B	6844.676	+0.449	0.008	-0.561	0.009	0.719	0.009	154.3	0.3	-0.029	0.008
ALP ORI	B	6846.659	+0.437	0.010	-0.574	0.012	0.721	0.012	153.6	0.4	-0.022	0.006
ALP ORI	B	6860.644	+0.088	0.001	-0.174	0.002	0.195	0.002	148.4	0.2	-0.012	0.003
ALP ORI	B	6865.594	+0.236	0.003	-0.547	0.006	0.596	0.006	146.7	0.2	-0.018	0.003
ALP ORI	B	7824.836	-0.348	0.004	+0.571	0.007	0.668	0.006	60.7	0.2	-0.024	0.006
Weighted average:			+0.074	0.046	-0.124	0.076	0.145	0.069	150.3	11.0	-0.019	0.002
ALP ORI	NUV	6770.852	+0.000	0.059	+0.073	0.091	0.073	0.091	44.8	23.3	-0.133	0.165
ALP ORI	NUV	6777.772	-0.028	0.133	-0.308	0.204	0.309	0.203	132.4	12.4	-1.115	0.961
ALP ORI	NUV	6780.753	+0.044	0.109	-0.021	0.092	0.049	0.106	167.0	55.8	-0.066	0.512
ALP ORI	NUV	6799.774	+0.102	0.087	+0.025	0.071	0.105	0.086	6.9	19.6	-0.097	0.240
ALP ORI	NUV	6844.704	+0.213	0.065	-0.318	0.078	0.383	0.074	151.9	5.2	-0.396	0.108
ALP ORI	NUV	6846.633	+1.029	0.925	+1.483	1.106	1.805	1.051	27.6	15.7	-0.022	0.084
ALP ORI	NUV	6865.619	-0.018	0.128	-0.468	0.198	0.468	0.198	133.9	7.9	-0.252	0.037
Weighted average:			+0.077	0.041	-0.090	0.074	0.119	0.062	155.3	13.8	-0.225	0.042
ALP ORI	WUV	7935.639	-0.074	0.005	-0.021	0.004	0.076	0.005	97.9	1.4	-0.055	0.004
ALP ORI*	LAM	6823.700	+0.015	0.005	-0.199	0.007	0.200	0.007	137.1	0.7	-0.509	0.029
ALP ORI*	LAM	6881.590	+0.047	0.002	-0.222	0.003	0.227	0.003	141.0	0.2	+0.104	0.006
Weighted average:			+0.044	0.011	-0.218	0.009	0.223	0.009	140.6	1.4	+0.080	0.117
6 GEM	R	6778.705	+2.024	0.036	-0.559	0.024	2.100	0.035	172.3	0.3	-0.238	0.071

APPENDIX E (cont.)

Journal of Standardized Observations for Program Objects

Name	Filter (Note 1)	(JD-2440000)	q (%)	σq (%)	u (%)	σu (%)	p (%)	σp (%)	θ (o)	σθ (o)	v (%)	σv (%)
6 GEM	R	7894.792	+1.566	0.020	-0.610	0.011	1.680	0.019	169.4	0.2	-0.017	0.041
6 GEM	R	7918.804	+1.491	0.033	-0.574	0.025	1.598	0.032	169.5	0.5	+0.039	0.339
6 GEM	R	7928.676	+1.525	0.026	-0.542	0.018	1.618	0.025	170.2	0.3	-0.077	0.024
6 GEM	R	7940.647	+1.525	0.030	-0.513	0.022	1.609	0.030	170.7	0.4	-0.054	0.020
6 GEM	R	7948.663	+1.511	0.058	-0.555	0.047	1.610	0.057	169.9	0.9	-0.044	0.028
Weighted average:			+1.589	0.069	-0.576	0.016	1.691	0.065	170.0	0.5	-0.061	0.016
6 GEM	V	6778.733	+2.442	0.041	-0.803	0.027	2.571	0.039	170.9	0.3	-0.105	0.530
6 GEM	B	6778.761	+2.704	0.099	-0.786	0.077	2.816	0.098	171.9	0.8	+0.016	0.238
6 GEM	NUV	6778.788	-0.951	3.815	-9.379	5.774	9.427	5.757	132.1	11.7	-20.891	24.100
PSI1AUR	R	6768.903	...	...	...	...	...	...	...	...	+0.056	0.020
PSI1AUR	R	6768.926	...	...	...	...	...	...	...	...	-0.026	0.009
PSI1AUR	R	6769.821	...	...	...	...	...	...	...	...	+0.095	0.100
PSI1AUR	R	6777.881	+0.512	0.007	-0.355	0.006	0.623	0.007	162.6	0.3	-0.027	0.033
PSI1AUR	R	6842.728	+0.553	0.021	-0.421	0.020	0.695	0.020	161.4	0.8	-0.018	0.012
PSI1AUR	R	7928.704	+0.507	0.010	-0.220	0.007	0.553	0.009	168.3	0.4	+0.012	0.019
PSI1AUR	R	7940.672	+0.518	0.013	-0.194	0.010	0.553	0.013	169.7	0.5	+0.001	0.016
Weighted average:			+0.514	0.006	-0.289	0.044	0.590	0.022	165.3	1.9	-0.009	0.010
PSI1AUR	V	6777.910	+0.586	0.023	-0.352	0.021	0.684	0.022	164.5	0.9	-0.017	0.031
PSI1AUR	V	6842.771	+0.712	0.039	-0.491	0.036	0.865	0.038	162.7	1.2	-0.105	0.024
Weighted average:			+0.619	0.055	-0.386	0.060	0.729	0.057	164.0	2.3	-0.072	0.043

APPENDIX E (cont.)

Journal of Standardized Observations for Program Objects

Name	Filter (Note 1)	(JD-2440000)	q (%)	σq (%)	u (%)	σu (%)	p (%)	σp (%)	θ (o)	σθ (o)	v (%)	σv (%)
72 LEO	R	6786.887	-0.013	0.003	+0.046	0.004	0.048	0.004	52.7	1.6	-0.000	0.011
72 LEO	R	6797.922	-0.011	0.008	+0.043	0.012	0.044	0.011	51.9	5.3	-0.014	0.013
72 LEO	R	6797.947	+0.011	0.012	+0.059	0.018	0.060	0.018	39.6	5.8	-0.025	0.009
72 LEO	R	6877.676	-0.000	0.008	+0.058	0.012	0.058	0.012	45.1	3.9	+0.026	0.005
72 LEO	R	6877.701	-0.005	0.005	+0.059	0.008	0.059	0.008	47.2	2.5	-0.008	0.010
72 LEO	R	6878.685	+0.024	0.002	+0.053	0.003	0.058	0.003	32.9	1.3	-0.007	0.004
72 LEO	R	6879.682	-0.010	0.010	+0.071	0.016	0.072	0.016	49.0	4.2	+0.015	0.007
72 LEO	R	6895.608	-0.009	0.002	+0.044	0.002	0.045	0.002	50.8	1.0	+0.015	0.021
72 LEO	R	6896.628	+0.020	0.014	+0.064	0.021	0.067	0.020	36.5	6.4	+0.017	0.012
72 LEO	R	6912.573	-0.002	0.008	+0.080	0.012	0.080	0.012	45.9	2.9	+0.005	0.007
72 LEO	R	6916.668	-0.013	0.004	+0.049	0.006	0.051	0.006	52.4	2.3	+0.014	0.013
72 LEO	R	6922.593	+0.000	0.013	+0.036	0.021	0.036	0.021	44.9	10.6	-0.003	0.010
72 LEO	R	6924.573	+0.032	0.010	+0.056	0.013	0.064	0.012	30.2	4.8	-0.007	0.009
72 LEO	R	6932.621	-0.004	0.006	+0.035	0.008	0.035	0.008	48.7	4.5	-0.017	0.018
72 LEO	R	6944.607	-0.001	0.016	+0.044	0.025	0.044	0.025	45.5	10.3	-0.028	0.012
72 LEO	R	6952.601	-0.018	0.013	+0.028	0.016	0.034	0.015	61.2	12.0	-0.002	0.009
72 LEO	R	7696.564	-0.010	0.009	+0.072	0.014	0.072	0.014	49.0	3.7	-0.015	0.020
72 LEO	R	7709.562	-0.036	0.014	+0.127	0.020	0.132	0.019	52.9	3.1	-0.005	0.018
72 LEO	R	7940.699	-0.004	0.009	+0.048	0.013	0.048	0.013	47.4	5.2	+0.006	0.004
Weighted average:			-0.003	0.003	+0.049	0.002	0.049	0.002	46.7	1.9	+0.002	0.003
72 LEO	V	6786.914	-0.001	0.021	+0.058	0.032	0.058	0.032	45.6	10.4	-0.006	0.018
72 LEO	V	6878.710	+0.029	0.002	+0.028	0.003	0.040	0.003	21.8	1.8	+0.024	0.019
72 LEO	V	6912.598	+0.021	0.031	+0.056	0.044	0.060	0.043	34.8	15.8	-0.011	0.008

APPENDIX E (cont.)

Journal of Standardized Observations for Program Objects

Name	Filter (Note 1)	(JD-2440000)	q (%)	σq (%)	u (%)	σu (%)	p (%)	σp (%)	θ (o)	σθ (o)	v (%)	σv (%)
72 LEO	V	6916.643	-0.016	0.022	+0.072	0.033	0.074	0.033	51.1	8.9	+0.009	0.043
72 LEO	V	6922.565	+0.025	0.033	+0.060	0.045	0.065	0.043	33.8	15.4	-0.002	0.005
72 LEO	V	6924.630	-0.014	0.010	+0.030	0.014	0.033	0.013	57.6	9.4	-0.028	0.021
72 LEO	V	6929.579	-0.002	0.017	+0.042	0.025	0.042	0.025	46.2	11.3	+0.019	0.011
72 LEO	V	6932.548	-0.031	0.025	+0.102	0.036	0.106	0.035	53.5	7.1	+0.011	0.009
72 LEO	V	6952.622	-0.010	0.019	+0.046	0.028	0.047	0.027	50.9	11.6	-0.017	0.014
72 LEO	V	7696.586	-0.040	0.010	+0.088	0.013	0.097	0.013	57.2	3.1	+0.012	0.011
Weighted average:			+0.021	0.006	+0.031	0.004	0.037	0.005	27.9	4.4	+0.000	0.004
72 LEO	B	6878.735	+0.003	0.023	+0.064	0.036	0.064	0.036	43.7	10.4	-0.021	0.043
72 LEO	B	6912.625	+0.009	0.009	+0.059	0.013	0.060	0.013	40.5	4.2	-0.008	0.058
72 LEO	B	6916.696	+0.015	0.016	+0.075	0.025	0.076	0.024	39.4	6.2	-0.060	0.004
72 LEO	B	6922.618	-0.058	0.040	+0.099	0.051	0.115	0.049	60.1	10.8	-0.017	0.026
72 LEO	B	6924.652	-0.004	0.012	+0.081	0.018	0.081	0.018	46.4	4.2	-0.061	0.036
72 LEO	B	6932.596	+0.017	0.053	+0.030	0.072	0.034	0.068	29.9	49.3	-0.034	0.041
Weighted average:			+0.005	0.005	+0.068	0.005	0.068	0.005	43.0	2.2	-0.058	0.004
72 LEO	NUV	6878.761	+0.037	0.449	-0.340	0.686	0.342	0.683	138.1	37.9	-7.547	2.696
72 LEO	NUV	6924.605	-0.353	0.547	+0.159	0.472	0.387	0.535	77.9	35.9	-0.045	0.279
72 LEO	NUV	6932.571	-0.419	0.550	+0.246	0.500	0.486	0.538	74.8	30.2	+0.499	0.753
Weighted average:			-0.205	0.149	+0.092	0.155	0.225	0.150	77.9	19.7	-0.050	0.529
V CVN	R	6956.604	...	...	...	...	...	...	...	...	-0.173	0.128
V CVN	R	6957.593	-1.270	0.255	-0.266	0.201	1.298	0.253	95.9	4.5	-0.047	0.037

APPENDIX E (cont.)

Journal of Standardized Observations for Program Objects

Name	Filter (Note 1)	(JD-2440000)	q (%)	σq (%)	u (%)	σu (%)	p (%)	σp (%)	θ (o)	σθ (o)	v (%)	σv (%)
V CVN	R	6961.639	-1.467	0.058	-0.366	0.045	1.512	0.057	97.0	0.9	-0.070	0.070
V CVN	R	6964.585	-1.473	0.140	-0.459	0.115	1.543	0.138	98.7	2.2	+0.113	0.350
V CVN	R#	6972.592	-1.256	0.065	-0.417	0.050	1.323	0.064	99.2	0.6	-0.045	0.053
V CVN	R	6993.618	-0.914	0.024	-0.390	0.019	0.993	0.023	101.5	0.6	+0.034	0.040
V CVN	R	7709.640	-1.540	0.033	-0.267	0.022	1.563	0.032	94.9	0.4	+0.189	0.124
Weighted average:			-1.269	0.216	-0.376	0.066	1.323	0.208	98.3	1.9	-0.020	0.025
V CVN	V	6956.624	-1.817	0.162	-0.487	0.130	1.881	0.160	97.5	2.0	-0.125	0.110
V CVN	V	6957.617	-1.633	0.102	-0.709	0.086	1.780	0.100	101.7	1.4	-0.044	0.121
V CVN	V	6961.618	-1.608	0.030	-0.278	0.020	1.632	0.030	94.9	0.4	-0.193	0.096
V CVN	V	6964.611	-1.604	0.111	-0.431	0.088	1.661	0.109	97.5	1.6	-0.066	0.032
V CVN	V	6971.575	-1.312	0.087	-0.541	0.073	1.419	0.085	101.2	1.5	-0.056	0.075
V CVN	V	6975.590	-1.399	0.017	-0.708	0.011	1.568	0.016	103.4	0.2	-0.076	0.092
V CVN	V	6995.601	-0.837	0.053	-0.457	0.047	0.954	0.052	104.3	1.5	-0.084	0.061
Weighted average:			-1.413	0.075	-0.603	0.072	1.536	0.075	101.6	1.3	-0.078	0.013
V CVN	B	6956.645	-2.116	0.420	-0.916	0.358	2.306	0.411	101.7	4.6	-0.296	0.213
V CVN	B	6971.595	-1.821	0.169	-1.160	0.156	2.159	0.166	106.3	2.1	-0.313	0.049
V CVN	B	6994.603	-1.088	0.025	-0.622	0.021	1.253	0.024	104.9	0.5	-0.135	0.104
Weighted average:			-1.107	0.086	-0.633	0.052	1.275	0.079	104.9	1.4	-0.282	0.048
ALP SCO	R	6944.738	-0.108	0.006	+0.424	0.009	0.437	0.009	52.1	0.4	-0.012	0.007
ALP SCO	R	6952.689	-0.098	0.014	+0.491	0.022	0.501	0.021	50.6	0.8	-0.005	0.001

APPENDIX E (cont.)

Journal of Standardized Observations for Program Objects

Name	Filter (Note 1)	(JD-2440000)	q (%)	σq (%)	u (%)	σu (%)	p (%)	σp (%)	θ (o)	σθ (o)	v (%)	σv (%)
ALP SCO	R	6956.673	-0.099	0.002	+0.433	0.005	0.444	0.005	51.4	0.1	-0.002	0.002
ALP SCO	R	6964.653	-0.089	0.002	+0.437	0.005	0.446	0.005	50.8	0.1	+0.007	0.000
ALP SCO	R	6971.637	-0.088	0.003	+0.447	0.006	0.456	0.006	50.5	0.2	-0.006	0.003
ALP SCO	R#	6972.634	-0.082	0.007	+0.434	0.014	0.442	0.014	50.4	0.2	-0.009	0.001
ALP SCO	R	6975.632	-0.090	0.002	+0.458	0.006	0.466	0.006	50.6	0.2	-0.015	0.002
ALP SCO	R	6993.569	-0.131	0.001	+0.473	0.005	0.491	0.005	52.8	0.1	-0.010	0.001
ALP SCO	R	6994.560	-0.128	0.003	+0.474	0.007	0.491	0.007	52.6	0.2	-0.003	0.002
ALP SCO	R	6999.561	-0.135	0.003	+0.474	0.006	0.492	0.006	53.0	0.2	+0.021	0.006
ALP SCO	R	7000.556	-0.136	0.003	+0.474	0.006	0.493	0.006	53.0	0.2	+0.017	0.002
ALP SCO	R	7004.546	-0.151	0.007	+0.493	0.012	0.516	0.011	53.5	0.4	+0.000	0.001
ALP SCO	R	7005.545	-0.154	0.005	+0.483	0.009	0.507	0.009	53.9	0.3	-0.002	0.004
ALP SCO	R	7006.540	-0.167	0.012	+0.507	0.017	0.534	0.017	54.1	0.7	-0.004	0.002
ALP SCO	R	7689.656	-0.052	0.062	+0.736	0.096	0.738	0.096	47.0	2.4	-0.011	0.002
ALP SCO	R	7696.675	-0.052	0.003	+0.409	0.006	0.412	0.006	48.6	0.2	-0.022	0.006
ALP SCO	R	7709.588	-0.089	0.004	+0.428	0.007	0.437	0.007	50.9	0.2	-0.020	0.013
ALP SCO	R	7710.566	-0.098	0.004	+0.423	0.007	0.434	0.007	51.5	0.3	-0.007	0.004
ALP SCO	R	7736.563	-0.150	0.004	+0.412	0.007	0.439	0.007	55.0	0.3	+0.006	0.003
Weighted average:			-0.109	0.006	+0.454	0.013	0.467	0.013	51.7	0.4	+0.004	0.001
ALP SCO	V	6994.580	-0.083	0.004	+0.455	0.008	0.462	0.008	50.2	0.3	-0.011	0.006
ALP SCO	V	6995.560	-0.090	0.005	+0.477	0.009	0.485	0.008	50.3	0.3	+0.001	0.008
ALP SCO	V	6999.581	-0.107	0.007	+0.450	0.011	0.462	0.010	51.7	0.4	+0.002	0.002
ALP SCO	V	7004.569	-0.109	0.011	+0.453	0.017	0.466	0.016	51.8	0.7	+0.002	0.010
ALP SCO	V	7005.564	-0.112	0.006	+0.450	0.009	0.464	0.009	52.0	0.4	+0.002	0.000

APPENDIX E (cont.)

Journal of Standardized Observations for Program Objects

Name	Filter (Note 1)	(JD-2440000)	q (%)	σq (%)	u (%)	σu (%)	p (%)	σp (%)	θ (o)	σθ (o)	v (%)	σv (%)
ALP SCO	V	7012.536	-0.334	0.140	+0.744	0.188	0.815	0.181	57.1	5.2	+0.002	0.011
ALP SCO	V	7689.685	+0.027	0.056	+0.654	0.086	0.654	0.086	43.8	2.4	-0.005	0.002
ALP SCO	V	7709.610	-0.053	0.005	+0.412	0.008	0.415	0.008	48.7	0.3	-0.011	0.003
ALP SCO	V	7710.593	-0.116	0.054	+0.396	0.079	0.412	0.077	53.2	3.9	-0.001	0.036
ALP SCO	V	7715.574	-0.085	0.007	+0.419	0.011	0.428	0.011	50.7	0.5	-0.009	0.009
Weighted average:			-0.086	0.007	+0.446	0.008	0.454	0.008	50.5	0.4	+0.001	0.001
ALP SCO	B	6995.579	-0.006	0.025	+0.428	0.038	0.428	0.038	45.4	1.7	-0.046	0.036
ALP SCO	B	7000.576	-0.030	0.016	+0.371	0.025	0.372	0.025	47.3	1.2	-0.008	0.011
ALP SCO	B	7006.561	-0.043	0.004	+0.398	0.008	0.401	0.008	48.1	0.3	-0.066	0.018
Weighted average:			-0.041	0.005	+0.397	0.007	0.399	0.007	48.0	0.3	-0.026	0.019
ALP SCO*	LAM	7715.596	+0.045	0.010	+0.164	0.013	0.170	0.013	37.3	1.6	+0.475	0.039
ALP HER	R	6896.719	+0.064	0.003	-0.050	0.003	0.081	0.003	161.2	1.1	-0.007	0.003
ALP HER	R	6922.718	+0.062	0.004	-0.072	0.004	0.095	0.004	155.2	1.1	-0.005	0.004
ALP HER	R	6932.650	+0.030	0.004	-0.081	0.005	0.086	0.005	145.2	1.3	-0.002	0.009
ALP HER	R	6944.641	+0.007	0.004	-0.092	0.006	0.092	0.006	137.1	1.2	-0.002	0.005
ALP HER	R	6961.668	+0.006	0.008	-0.114	0.012	0.114	0.012	136.5	2.0	+0.021	0.003
ALP HER	R	6964.685	+0.006	0.003	-0.129	0.005	0.129	0.005	136.3	0.7	-0.006	0.006
ALP HER	R	6971.662	+0.024	0.002	-0.122	0.003	0.125	0.003	140.5	0.4	-0.002	0.004
ALP HER	R#	6972.657	+0.022	0.001	-0.123	0.003	0.125	0.003	140.0	0.1	+0.007	0.005
ALP HER	R	6975.653	+0.025	0.004	-0.116	0.006	0.119	0.006	141.1	0.9	+0.010	0.006

APPENDIX E (cont.)

Journal of Standardized Observations for Program Objects

Name	Filter (Note 1)	(JD-2440000)	q (%)	σq (%)	u (%)	σu (%)	p (%)	σp (%)	θ (o)	σθ (o)	v (%)	σv (%)
ALP HER	R	6993.640	+0.040	0.001	-0.113	0.002	0.120	0.001	144.9	0.2	+0.006	0.004
ALP HER	R	6995.623	+0.049	0.007	-0.103	0.010	0.114	0.009	147.9	2.0	+0.006	0.003
ALP HER	R	6999.601	+0.040	0.005	-0.109	0.007	0.116	0.007	145.1	1.3	+0.001	0.007
ALP HER	R	7000.619	+0.053	0.003	-0.100	0.004	0.113	0.004	148.9	0.8	-0.007	0.003
ALP HER	R	7003.593	+0.044	0.002	-0.098	0.003	0.108	0.003	147.1	0.6	-0.004	0.007
ALP HER	R	7005.623	+0.038	0.002	-0.095	0.003	0.103	0.003	145.8	0.6	+0.008	0.002
ALP HER	R	7006.613	+0.035	0.007	-0.094	0.010	0.101	0.009	145.3	2.1	+0.009	0.009
ALP HER	R	7012.566	+0.033	0.008	-0.101	0.011	0.106	0.011	144.0	2.2	+0.000	0.005
ALP HER	R	7018.546	+0.023	0.007	-0.093	0.011	0.096	0.011	142.1	2.2	+0.002	0.002
ALP HER	R	7020.553	+0.024	0.004	-0.097	0.006	0.100	0.006	142.0	1.2	-0.035	0.003
ALP HER	R	7021.538	+0.025	0.004	-0.095	0.005	0.098	0.005	142.4	1.1	-0.036	0.002
ALP HER	R	7022.534	+0.020	0.002	-0.090	0.003	0.092	0.003	141.3	0.6	-0.040	0.005
ALP HER	R	7023.535	+0.017	0.004	-0.077	0.006	0.079	0.006	141.3	1.4	-0.034	0.008
ALP HER	R	7024.559	+0.026	0.006	-0.092	0.008	0.096	0.008	142.9	1.8	-0.037	0.005
ALP HER	R	7025.580	+0.021	0.009	-0.110	0.014	0.112	0.013	140.5	2.4	-0.018	0.004
ALP HER	R	7026.535	+0.002	0.001	+0.003	0.002	0.004	0.002	29.5	12.7	-0.039	0.004
ALP HER	R	7027.528	+0.012	0.003	-0.089	0.004	0.090	0.004	138.9	0.9	-0.037	0.010
ALP HER	R	7028.535	+0.013	0.001	-0.095	0.002	0.096	0.002	138.9	0.3	-0.038	0.006
ALP HER	R	7029.524	+0.014	0.005	-0.084	0.007	0.085	0.007	139.8	1.6	-0.032	0.004
ALP HER	R	7031.500	...	...	...	...	...	...	...	...	-0.036	0.009
ALP HER	R	7038.547	-0.157	0.147	-0.128	0.146	0.202	0.147	109.6	20.7	-0.038	0.003
ALP HER	R	7053.515	-0.014	0.002	-0.086	0.003	0.087	0.003	130.5	0.6	-0.004	0.002
ALP HER	R	7064.500	-0.015	0.003	-0.115	0.004	0.116	0.004	131.2	0.7	-0.049	0.004

Journal of Standardized Observations for Program Objects

Name	Filter (Note 1)	(JD-2440000)	q (%)	σq (%)	u (%)	σu (%)	p (%)	σp (%)	θ (o)	σθ (o)	v (%)	σv (%)
ALP HER	R	7064.510	...	...	...	...	...	...	...	...	-0.038	0.003
ALP HER	R	7066.517	-0.017	0.003	-0.115	0.004	0.117	0.004	130.7	0.7	-0.026	0.004
ALP HER	R	7073.517	-0.017	0.006	-0.127	0.010	0.128	0.010	131.1	1.4	-0.042	0.007
ALP HER	R	7689.716	+0.018	0.013	-0.077	0.020	0.079	0.019	141.7	5.0	-0.067	0.018
ALP HER	R	7696.697	+0.013	0.004	-0.058	0.005	0.059	0.005	141.4	1.8	-0.062	0.004
ALP HER	R	7708.684	...	...	...	...	...	...	...	...	-0.053	0.004
ALP HER	R	7709.694	+0.012	0.003	-0.057	0.005	0.059	0.005	141.1	1.6	-0.074	0.011
ALP HER	R	7736.590	+0.017	0.004	-0.059	0.006	0.061	0.006	143.2	2.0	-0.037	0.007
ALP HER	R	7744.550	+0.020	0.011	-0.058	0.016	0.061	0.016	144.5	5.6	-0.037	0.006
ALP HER	R	7764.667	+0.046	0.006	-0.048	0.006	0.066	0.006	156.7	2.6	-0.023	0.008
ALP HER	R	7780.604	+0.043	0.010	-0.065	0.013	0.078	0.012	151.6	4.1	-0.014	0.004
ALP HER	R	7794.563	+0.029	0.003	-0.078	0.004	0.084	0.004	145.0	1.1	-0.057	0.004
ALP HER	R	7801.577	+0.032	0.003	-0.090	0.005	0.095	0.004	144.9	1.0	-0.077	0.008
Weighted average:			+0.025	0.003	-0.090	0.008	0.093	0.007	142.7	1.1	-0.017	0.003
ALP HER	V	6896.744	+0.088	0.009	-0.083	0.009	0.121	0.009	158.3	2.1	-0.025	0.020
ALP HER	V	6922.684	+0.085	0.006	-0.105	0.007	0.135	0.006	154.5	1.3	-0.003	0.008
ALP HER	V	6924.737	+0.059	0.009	-0.118	0.012	0.131	0.011	148.3	2.1	-0.029	0.028
ALP HER	V	6932.673	+0.012	0.009	-0.115	0.014	0.116	0.014	138.1	2.3	-0.025	0.016
ALP HER	V	6944.714	-0.035	0.008	-0.140	0.012	0.144	0.012	128.0	1.7	+0.035	0.012
ALP HER	V	6961.694	-0.013	0.008	-0.188	0.012	0.188	0.012	133.0	1.1	-0.020	0.002
ALP HER	V	6999.623	+0.055	0.013	-0.135	0.018	0.146	0.017	146.1	2.8	-0.089	0.005
ALP HER	V	7004.597	+0.072	0.018	-0.134	0.023	0.152	0.022	149.2	3.6	-0.012	0.020

Journal of Standardized Observations for Program Objects

Name	Filter (Note 1)	(JD-2440000)	q (%)	σq (%)	u (%)	σu (%)	p (%)	σp (%)	θ (o)	σθ (o)	v (%)	σv (%)
ALP HER	V	7005.583	+0.072	0.003	-0.133	0.004	0.152	0.004	149.3	0.7	-0.011	0.019
ALP HER	V	7012.591	+0.083	0.007	-0.129	0.009	0.153	0.008	151.4	1.5	-0.027	0.009
ALP HER	V	7018.578	+0.066	0.004	-0.107	0.005	0.125	0.005	150.8	1.1	-0.002	0.004
ALP HER	V	7021.560	+0.067	0.009	-0.115	0.011	0.133	0.010	150.2	2.0	-0.093	0.014
ALP HER	V	7022.554	+0.047	0.009	-0.099	0.012	0.110	0.012	147.7	2.5	-0.086	0.012
ALP HER	V	7026.558	+0.007	0.005	-0.008	0.006	0.010	0.006	154.9	15.1	-0.086	0.011
ALP HER	V	7027.548	+0.041	0.004	-0.115	0.005	0.122	0.005	144.9	1.0	-0.080	0.013
ALP HER	V	7029.544	+0.031	0.002	-0.104	0.003	0.108	0.003	143.2	0.6	-0.074	0.007
ALP HER	V	7053.542	-0.030	0.157	-0.362	0.240	0.363	0.239	132.6	12.5	-0.077	0.005
ALP HER	V	7064.523	-0.028	0.002	-0.172	0.003	0.175	0.003	130.3	0.3	-0.018	0.008
ALP HER	V	7696.717	+0.021	0.013	-0.079	0.019	0.082	0.019	142.4	4.7	-0.008	0.007
ALP HER	V	7708.708	...	...	...	...	...	...	...	...	-0.008	0.005
ALP HER	V	7709.718	-0.012	0.005	-0.071	0.008	0.073	0.008	130.1	2.2	-0.022	0.010
ALP HER	V	7715.574	-0.085	0.007	+0.419	0.011	0.428	0.011	50.7	0.5	-0.009	0.009
ALP HER	V	7716.705	-0.016	0.001	-0.089	0.001	0.090	0.001	130.0	0.2	-0.006	0.023
ALP HER	V	7736.613	-0.035	0.016	-0.070	0.021	0.078	0.021	121.5	6.5	-0.031	0.010
Weighted average:			-0.006	0.006	-0.098	0.012	0.098	0.012	133.3	1.7	-0.030	0.006
ALP HER	B	6916.732	+0.227	0.009	-0.163	0.008	0.280	0.009	162.2	0.9	-0.059	0.014
ALP HER	B	6922.656	+0.140	0.002	-0.209	0.003	0.251	0.003	151.9	0.3	-0.064	0.024
ALP HER	B	6932.700	+0.044	0.014	-0.140	0.020	0.146	0.019	143.7	2.8	-0.021	0.009
ALP HER	B	7000.599	+0.103	0.016	-0.207	0.021	0.231	0.020	148.2	2.2	+0.015	0.033
ALP HER	B	7005.603	+0.146	0.019	-0.191	0.022	0.240	0.021	153.7	2.4	-0.016	0.027

APPENDIX E (cont.)

Journal of Standardized Observations for Program Objects

Name	Filter (Note 1)	(JD-2440000)	q (%)	σq (%)	u (%)	σu (%)	p (%)	σp (%)	θ (o)	σθ (o)	v (%)	σv (%)
ALP HER	B	7006.589	+0.124	0.005	-0.186	0.006	0.224	0.006	151.8	0.7	+0.001	0.023
ALP HER	B	7020.531	...	...	...	...	...	...	...	...	-0.034	0.014
ALP HER	B	7022.573	+0.074	0.014	-0.151	0.018	0.168	0.017	148.0	2.5	-0.032	0.008
ALP HER	B	7027.567	+0.048	0.006	-0.158	0.009	0.165	0.009	143.4	1.1	-0.021	0.013
ALP HER	B	7031.559	+0.002	0.003	-0.124	0.005	0.124	0.005	135.5	0.8	-0.013	0.020
Weighted average:			+0.103	0.021	-0.185	0.011	0.212	0.014	149.5	2.6	-0.029	0.005
ALP HER	NUV	6932.725	+0.193	0.150	-0.135	0.142	0.236	0.147	162.5	17.6	-0.211	0.070
ALP HER	NUV	7023.555	+0.137	0.133	-0.133	0.138	0.191	0.135	158.0	20.3	-0.153	0.048
ALP HER	NUV	7028.555	-0.028	0.073	-0.252	0.110	0.254	0.109	131.8	8.3	-0.144	0.045
Weighted average:			+0.038	0.065	-0.187	0.042	0.191	0.043	140.7	9.7	-0.160	0.017
ALP HER*	LAM	7716.733	-0.096	0.006	-0.055	0.005	0.110	0.007	104.9	1.2	-0.042	0.008
MU CEP	R	6971.782	+0.457	0.184	+1.235	0.257	1.316	0.250	34.9	4.2	-0.096	0.021
MU CEP	R	6975.818	+0.358	0.004	+0.983	0.011	1.046	0.010	35.0	0.2	+0.022	0.039
MU CEP	R	6994.870	+0.348	0.009	+0.958	0.015	1.019	0.015	35.0	0.3	+0.020	0.013
MU CEP	R	6995.779	+0.287	0.004	+0.975	0.011	1.017	0.010	36.8	0.1	+0.003	0.008
MU CEP	R	7000.783	+0.292	0.008	+0.994	0.015	1.036	0.014	36.8	0.2	+0.020	0.012
MU CEP	R	7018.829	+0.255	0.007	+1.025	0.014	1.056	0.014	38.0	0.2	+0.016	0.003
MU CEP	R	7031.791	+0.252	0.008	+1.039	0.015	1.069	0.015	38.2	0.2	-0.020	0.006
MU CEP	R	7064.631	+0.287	0.009	+1.192	0.018	1.227	0.018	38.2	0.2	+0.016	0.013
MU CEP	R	7708.765	+0.345	0.007	+1.745	0.021	1.779	0.020	39.4	0.1	-0.110	0.051

APPENDIX E (cont.)

Journal of Standardized Observations for Program Objects

Name	Filter (Note 1)	(JD-2440000)	q (%)	σq (%)	u (%)	σu (%)	p (%)	σp (%)	θ (o)	σθ (o)	v (%)	σv (%)
MU CEP	R	7710.768	+0.341	0.007	+1.752	0.020	1.785	0.020	39.5	0.1	-0.124	0.052
MU CEP	R	7772.761	+0.182	0.006	+2.238	0.025	2.245	0.025	42.7	0.1	+0.013	0.004
MU CEP	R	7778.794	+0.210	0.003	+2.195	0.023	2.205	0.023	42.3	0.0	+0.056	0.028
MU CEP	R	7804.519	+0.243	0.007	+2.083	0.024	2.097	0.024	41.7	0.1	-0.045	0.004
MU CEP	R	7840.546	+0.316	0.012	+1.823	0.026	1.850	0.026	40.1	0.2	-0.055	0.006
MU CEP	R	7847.564	+0.333	0.004	+1.779	0.019	1.810	0.019	39.7	0.1	-0.044	0.007
Weighted average:			+0.273	0.016	+1.251	0.112	1.281	0.109	38.8	0.6	-0.011	0.008
MU CEP	V	6971.813	+0.565	0.096	+1.118	0.125	1.252	0.120	31.6	2.3	-0.051	0.030
MU CEP	V	6993.845	+0.336	0.008	+1.154	0.016	1.202	0.016	36.9	0.2	-0.032	0.010
MU CEP	V	7018.807	+0.297	0.007	+1.181	0.015	1.218	0.015	37.9	0.2	-0.024	0.003
MU CEP	V	7064.674	+0.316	0.019	+1.462	0.031	1.496	0.031	38.9	0.4	-0.012	0.001
MU CEP	V	7708.789	+0.453	0.015	+2.299	0.032	2.343	0.031	39.4	0.2	-0.264	0.042
MU CEP	V	7772.787	+0.267	0.006	+3.015	0.033	3.027	0.033	42.5	0.1	-0.021	0.021
MU CEP	V	7778.770	+0.224	0.047	+2.961	0.079	2.970	0.079	42.8	0.5	+0.045	0.022
MU CEP	V	7804.495	+0.276	0.007	+2.787	0.031	2.801	0.031	42.2	0.1	-0.033	0.007
MU CEP	V	7824.661	+0.307	0.005	+2.531	0.027	2.550	0.027	41.5	0.1	-0.037	0.014
Weighted average:			+0.301	0.013	+1.679	0.249	1.705	0.245	39.9	0.8	-0.014	0.003
MU CEP	B	7772.812	+0.320	0.025	+3.007	0.050	3.024	0.050	42.0	0.2	+0.095	0.034
MU CEP	NUV	7772.838	+1.307	0.190	+1.785	0.223	2.212	0.212	26.9	2.6	-0.333	1.656
VV CEP	R	6922.787	+0.561	0.094	+1.294	0.127	1.410	0.123	33.3	2.0	-0.019	0.026

APPENDIX E (cont.)

Journal of Standardized Observations for Program Objects

Name	Filter (Note 1)	(JD-2440000)	q (%)	σq (%)	u (%)	σu (%)	p (%)	σp (%)	θ (o)	σθ (o)	v (%)	σv (%)
VV CEP	R	6924.818	+0.465	0.007	+1.111	0.014	1.204	0.013	33.7	0.2	-0.036	0.015
VV CEP	R	6932.756	+0.424	0.014	+1.110	0.022	1.188	0.021	34.6	0.4	-0.062	0.007
VV CEP	R	6957.687	+0.397	0.016	+1.129	0.025	1.197	0.024	35.3	0.4	-0.010	0.012
VV CEP	R	6964.774	+0.265	0.003	+0.726	0.008	0.772	0.007	35.0	0.1	...	...
VV CEP	R	6971.845	+0.403	0.012	+1.111	0.020	1.182	0.019	35.0	0.3	-0.024	0.018
VV CEP	R	6975.770	+0.407	0.015	+1.087	0.023	1.160	0.023	34.7	0.4	-0.057	0.014
VV CEP	R	6993.752	+0.407	0.005	+1.136	0.013	1.207	0.012	35.2	0.2	-0.032	0.014
VV CEP	R	6995.739	+0.410	0.008	+1.129	0.015	1.201	0.014	35.0	0.2	-0.012	0.023
VV CEP	R	7018.742	+0.414	0.006	+1.104	0.013	1.180	0.012	34.7	0.2	+0.017	0.019
VV CEP	R	7064.730	+0.449	0.013	+1.167	0.021	1.251	0.020	34.5	0.3	+0.003	0.016
VV CEP	R	7073.629	+0.433	0.005	+1.156	0.013	1.235	0.012	34.7	0.1	+0.011	0.012
VV CEP	R	7074.652	+0.409	0.009	+1.048	0.016	1.125	0.015	34.3	0.3	-0.008	0.012
VV CEP	R	7710.793	+0.381	0.007	+1.226	0.015	1.284	0.015	36.4	0.2	-0.078	0.020
VV CEP	R	7773.731	+0.423	0.005	+1.201	0.013	1.274	0.012	35.3	0.1	-0.026	0.015
Weighted average:			+0.367	0.020	+1.038	0.048	1.101	0.046	35.3	0.6	-0.030	0.008
VV CEP	V	6922.823	+0.558	0.010	+1.281	0.018	1.398	0.017	33.2	0.2	-0.070	0.008
VV CEP	V	6924.792	+0.530	0.014	+1.261	0.022	1.368	0.021	33.6	0.3	-0.014	0.015
VV CEP	V	6932.782	+0.512	0.018	+1.269	0.027	1.368	0.026	34.0	0.4	-0.007	0.011
VV CEP	V	6964.807	+0.424	0.008	+1.238	0.016	1.309	0.015	35.5	0.2	-0.037	0.020
VV CEP	V	6993.776	+0.413	0.023	+1.314	0.036	1.377	0.035	36.3	0.5	-0.037	0.037
VV CEP	V	6995.758	+0.425	0.035	+1.275	0.052	1.344	0.050	35.8	0.8	+0.051	0.040
VV CEP	V	7018.718	+0.457	0.026	+1.224	0.038	1.307	0.036	34.8	0.6	+0.007	0.018

APPENDIX E (cont.)

Journal of Standardized Observations for Program Objects

Name	Filter (Note 1)	(JD-2440000)	q (%)	σq (%)	u (%)	σu (%)	p (%)	σp (%)	θ (o)	σθ (o)	v (%)	σv (%)
VV CEP	V	7064.707	+0.523	0.014	+1.345	0.023	1.443	0.022	34.4	0.3	-0.024	0.004
VV CEP	V	7066.583	+0.488	0.027	+1.333	0.040	1.419	0.039	34.9	0.6	-0.018	0.014
VV CEP	V	7074.626	+0.491	0.022	+1.232	0.032	1.326	0.030	34.1	0.5	-0.061	0.027
VV CEP	V	7773.755	+0.457	0.022	+1.447	0.034	1.518	0.033	36.2	0.4	+0.012	0.017
Weighted average:			+0.483	0.017	+1.281	0.017	1.369	0.017	34.7	0.4	-0.026	0.006
VV CEP	B	6994.794	+0.378	0.029	+1.314	0.044	1.367	0.043	37.0	0.6	-0.219	0.047
VV CEP	B	7020.673	+0.324	0.021	+1.394	0.034	1.431	0.034	38.5	0.4	+0.002	0.020
VV CEP	B	7029.654	+0.333	0.023	+0.816	0.032	0.881	0.031	33.9	0.8	-0.080	0.021
VV CEP	B	7773.785	+0.387	0.033	+1.627	0.051	1.672	0.051	38.3	0.6	-0.217	0.083
Weighted average:			+0.346	0.015	+1.204	0.175	1.253	0.168	37.0	1.2	-0.057	0.040
VV CEP	NUV	6975.793	+0.154	0.202	+0.791	0.301	0.806	0.298	39.5	7.3	-0.532	0.291
VV CEP	NUV	6994.816	+0.097	0.206	+1.464	0.319	1.467	0.318	43.1	4.0	-0.348	0.082
VV CEP	NUV	7020.696	...	...	...	...	...	...	...	...	-0.152	0.063
VV CEP	NUV	7773.809	+0.409	0.069	+1.023	0.095	1.102	0.092	34.1	1.9	+0.124	0.234
Weighted average:			+0.357	0.078	+1.037	0.097	1.096	0.095	35.5	2.1	-0.219	0.073
BET PEG	R	6764.461	...	...	...	...	...	...	...	...	-0.005	0.007
BET PEG	R	6764.477	...	...	...	...	...	...	...	...	-0.004	0.004
BET PEG	R	6764.495	...	...	...	...	...	...	...	...	+0.011	0.026
Weighted average:			...	...	...	...	...	...	...	...	-0.004	0.001

APPENDIX E (cont.)

Journal of Standardized Observations for Program Objects

Name	Filter (Note 1)	(JD-2440000)	q (%)	σq (%)	u (%)	σu (%)	p (%)	σp (%)	θ (o)	σθ (o)	v (%)	σv (%)
BET PEG	R	6784.474	+0.005	0.003	-0.000	0.002	0.005	0.003	179.3	12.4	-0.011	0.005
BET PEG	R	6799.475	-0.000	0.007	+0.009	0.011	0.009	0.011	46.2	21.7	-0.011	0.002
BET PEG	R	6975.845	-0.006	0.009	+0.006	0.009	0.008	0.009	66.7	30.9	-0.010	0.004
BET PEG	R	6993.873	+0.043	0.030	-0.025	0.027	0.050	0.029	165.1	16.1	+0.005	0.007
BET PEG	R	6995.804	-0.007	0.009	+0.002	0.007	0.007	0.009	80.7	30.0	-0.004	0.007
BET PEG	R	7000.812	-0.007	0.004	+0.006	0.004	0.009	0.004	69.5	13.0	+0.000	0.004
BET PEG	R	7018.856	-0.006	0.001	+0.003	0.001	0.006	0.001	76.1	3.8	+0.008	0.006
BET PEG	R	7018.877	-0.003	0.005	-0.000	0.004	0.003	0.005	90.3	34.5	+0.003	0.001
BET PEG	R	7031.820	-0.001	0.005	+0.006	0.008	0.006	0.008	47.9	24.0	+0.000	0.004
BET PEG	R	7064.756	-0.001	0.003	+0.004	0.004	0.004	0.004	53.2	19.9	+0.001	0.001
BET PEG	R	7073.676	-0.006	0.006	-0.003	0.005	0.007	0.006	104.1	21.8	+0.014	0.005
BET PEG	R	7708.818	+0.004	0.005	-0.001	0.004	0.004	0.005	172.5	31.8	-0.017	0.002
BET PEG	R	7709.849	+0.005	0.004	+0.008	0.005	0.009	0.004	29.7	12.3	-0.007	0.007
BET PEG	R	7710.825	-0.000	0.000	+0.001	0.001	0.001	0.001	53.3	11.5	+0.004	0.000
BET PEG	R	7716.804	-0.002	0.008	+0.002	0.009	0.003	0.008	67.8	70.9	+0.010	0.004
BET PEG	R	7736.748	-0.006	0.002	+0.007	0.002	0.010	0.002	66.0	5.5	-0.003	0.001
BET PEG	R	7764.720	+0.006	0.006	+0.013	0.008	0.014	0.007	33.4	12.1	+0.001	0.004
BET PEG	R	7772.733	-0.005	0.004	+0.003	0.004	0.006	0.004	74.3	19.0	+0.005	0.001
BET PEG	R	7773.701	+0.001	0.005	+0.007	0.007	0.007	0.007	39.9	20.5	+0.003	0.001
BET PEG	R	7778.714	+0.003	0.004	+0.012	0.006	0.012	0.006	37.2	9.7	+0.002	0.004
BET PEG	R	7780.695	-0.005	0.006	+0.010	0.008	0.011	0.007	57.7	15.7	+0.002	0.002
BET PEG	R	7791.709	+0.003	0.001	+0.011	0.002	0.012	0.002	37.2	3.5	+0.011	0.005
BET PEG	R	7801.824	+0.000	0.001	+0.013	0.002	0.013	0.002	44.3	2.4	+0.010	0.004

APPENDIX E (cont.)

Journal of Standardized Observations for Program Objects

Name	Filter (Note 1)	(JD-2440000)	q (%)	σq (%)	u (%)	σu (%)	p (%)	σp (%)	θ (o)	σθ (o)	v (%)	σv (%)
BET PEG	R	7822.665	-0.001	0.002	+0.019	0.003	0.019	0.003	45.9	2.5	+0.005	0.003
BET PEG	R	7826.530	-0.002	0.002	+0.010	0.003	0.010	0.002	52.2	5.1	+0.001	0.006
BET PEG	R	7834.601	-0.004	0.003	+0.011	0.004	0.012	0.004	54.7	8.1	+0.005	0.004
BET PEG	R	7843.674	-0.000	0.005	+0.007	0.008	0.007	0.008	46.3	21.5	+0.002	0.004
BET PEG	R	7855.573	-0.013	0.002	+0.014	0.002	0.019	0.002	66.5	3.2	+0.006	0.004
BET PEG	R	7860.595	-0.004	0.004	+0.025	0.006	0.025	0.006	49.0	4.4	-0.001	0.006
BET PEG	R	7894.512	-0.000	0.007	+0.011	0.011	0.011	0.011	46.1	19.7	-0.001	0.006
Weighted average:			-0.001	0.001	+0.004	0.001	0.004	0.001	53.3	4.1	+0.002	0.001
BET PEG	V	6784.492	+0.016	0.012	+0.018	0.013	0.024	0.013	24.9	15.0	-0.044	0.012
BET PEG	V	6799.495	+0.002	0.007	+0.007	0.011	0.008	0.010	38.3	27.4	-0.073	0.009
BET PEG	V	7064.783	-0.006	0.005	-0.008	0.005	0.010	0.005	116.9	14.3	+0.004	0.014
BET PEG	V	7708.842	+0.017	0.008	+0.032	0.010	0.036	0.010	30.7	6.9	-0.026	0.009
BET PEG	V	7736.723	-0.004	0.005	+0.036	0.008	0.036	0.008	48.2	4.2	-0.011	0.008
BET PEG	V	7764.743	+0.004	0.008	+0.020	0.012	0.020	0.011	38.7	11.4	-0.008	0.004
BET PEG	V	7778.743	-0.018	0.004	+0.035	0.005	0.039	0.005	59.1	3.0	+0.015	0.013
BET PEG	V	7780.666	-0.012	0.002	+0.038	0.003	0.040	0.003	53.7	1.8	-0.004	0.010
BET PEG	V	7791.737	+0.000	0.005	+0.019	0.008	0.019	0.008	44.4	8.1	-0.004	0.004
BET PEG	V	7801.802	+0.006	0.004	+0.046	0.006	0.046	0.006	41.0	2.6	-0.001	0.007
BET PEG	V	7822.638	+0.013	0.006	+0.036	0.008	0.039	0.007	34.8	4.3	-0.002	0.003
BET PEG	V	7834.622	-0.007	0.002	+0.016	0.003	0.018	0.003	57.2	4.1	+0.005	0.005
Weighted average:			-0.006	0.003	+0.025	0.005	0.026	0.005	51.1	3.1	-0.007	0.004

APPENDIX E (cont.)

Journal of Standardized Observations for Program Objects

Name	Filter (Note 1)	(JD-2440000)	q (%)	σq (%)	u (%)	σu (%)	p (%)	σp (%)	θ (o)	σθ (o)	v (%)	σv (%)
BET PEG	B	6799.519	+0.018	0.012	-0.001	0.010	0.018	0.012	178.8	14.9	-0.020	0.020
BET PEG	B	7764.772	-0.007	0.011	+0.006	0.013	0.009	0.012	69.5	37.0	-0.044	0.008
BET PEG	B	7826.550	+0.010	0.017	+0.039	0.026	0.040	0.025	38.0	12.6	-0.083	0.014
Weighted average:			+0.006	0.008	+0.005	0.008	0.008	0.008	19.8	30.0	-0.050	0.014
BET PEG	NUV	6799.546	+0.009	0.050	+0.052	0.075	0.053	0.074	40.1	27.5	-0.293	0.443
BET PEG	NUV	7764.797	-0.241	0.239	-0.251	0.256	0.348	0.248	113.1	20.4	-0.394	0.085
Weighted average:			-0.001	0.050	+0.028	0.082	0.028	0.082	46.4	50.9	-0.390	0.019

Note 1. Filter (Column 2):

See the notes after Appendix D. The data for filters marked POL, LAM, FR, and LOW have not been standardized. These data are marked with a star (*).

Filters marked with a pound sign (#) indicate a night (JD 24446972) where the Channel 1 lock-in amplifier had a functional problem. This problem did not affect the Channel 3 (circular polarization) data.

APPENDIX F

Linear Polarization Observations of Field Stars

Name (Note 1)	---GALACTIC--- LONG. (o)	LAT. (o)	Program Object (Note 2)	Polarization Reference(s) (Note 3)	p (%)	Theta (o)	Spectral Type	<V>	<B-V>	<M>	Distance (Note 4) (pc)
34251	185.29	-11.23	06	3,4	0.64	67	B3.5 III	+7.18	+0.10	-1.6	390s
35147	187.41	-10.70	03	7	0.4	70	F8 V	8.0	+0.5	4.0	62s
35395	184.58	-8.39	06	3	1.6	150	B0.5 III	6.77	+0.23	-5.5	1400s
35671	187.06	-9.42	06	4	0.18	20	B5 V	5.42	-0.10	-1.1	200s
35708	183.75	-7.17	06	4	0.37	6	B3 V	4.88	-0.15	-1.7	210s
36113	185.26	-7.41	06	4	0.64	29	B5.5 V	7.08	-0.05	-1.0	360s
36280	173.40	+0.79	06	4,6	1.20	158	B0.5 IV	8.85	+0.10	-4.3	2500s
36337	190.24	-10.14	06	4	0.78	35	B5.5 V	6.6	+0.0	-1.0	310s
36547	182.95	-5.88	06	3,4,6	1.61	146	B1 III	8.81	+0.34	-4.4	1900s
36576	187.39	-7.83	06	2,4	0.11	75	B p	5.69	+0.01	...	...
36653	191.04	-10.06	06	4	0.74	32	B3 V	5.64	-0.14	-1.7	290s
36819	182.95	-4.52	06	4	...	...	B3 V	5.38	-0.09	-1.7	240s
36822†	195.40	-12.29	03	4	...	...	B0 IV	4.41	-0.16	-4.6	570s
36824	198.79	-14.24	03	4	0.37	4	B3 V	6.69	-0.15	-1.7	480s
36861	195.05	-11.99	03	4	0.51	112	O8	3.39	-0.18	-1.7	...
36879	185.22	-5.89	06	4,5,6	2.16	153	O6	7.57	+0.19	...	...
37202	185.69	-5.63	06	3,4	1.37	24	B2 IV p	3.00	-0.19	-3.0	150s
37232	196.19	-12.03	03	4	...	...	B1.5 V	6.12	-0.17	-3.0	630s
38191	186.30	-4.03	06	5,6	1.82	152	B1 V	8.73	+0.13	-3.5	56s
38309	201.57	-12.81	03	1	0.07	27	F0 IV	6.09	+0.31	1.7	75s
38527	196.90	-9.70	03	1	0.05	32	G8 III	5.79	+0.88	0.3	130s
38672	194.50	-8.01	03	4	0.37	169	B5.5 V	6.68	-0.10	-1.0	320s
38710	199.75	-10.98	03	1	0.09	54	dA5 n	5.27	+0.23	2.1	43s

APPENDIX F (cont.)

Linear Polarization Observations of Field Stars

Name (Note 1)	---GALACTIC--- LONG. (o)	LAT. (o)	Program Object (Note 2)	Polarization Reference(s) (Note 3)	p (%)	Theta (o)	Spectral Type	<V>	<B-V>	<M>	Distance (Note 4) (pc)
39007	196.98	-8.85	03	1	0.17	30	G7 III	+5.80	+0.87	0.3	130s
39051	201.83	-11.48	03	1	0.22	75	K3 III	+5.97	+1.36	-0.2	150s
39587	188.46	-2.73	06	2	0.03	112	G0 V	4.41	+0.59	4.4	9.9t
39680	194.07	-5.87	06	5	0.6	143	O6 pe	7.85	+0.06	...	...
39698†	188.98	-2.88	06,11	3	0.6	164	B2 V	5.92	-0.17	-2.5	480s
39970	185.32	-0.22	06,11	3,5	1.75	166	A0 Ia	6.02	+0.39	-7.1	2700s
40003	186.06	-0.58	06	5,6	2.8	167	B3 Ib	8.60	+0.82	-5.7	1700s
40160	166.03	+11.16	04	4	1.06	8	B5.5 V	7.48	-0.07	-1.0	490s
40183	167.46	+10.41	04	2	0.09	151	A2 IV	1.90	+0.03	0.6	22ts
40239	166.60	+10.94	04	2	0.26	6	M3 II	4.26	+1.72	-2.4	200s
40932†	198.68	-6.31	03	1	0.05	159	A m	4.12	+0.15	...	37t
40978	166.40	+11.96	04	4	1.06	6	B2.5 e	7.21	-0.05	...	...
41117	189.69	-0.86	11	2,3,4	3.00	177	B2 Ia	4.63	+0.28	-6.8	1100s
41161	164.97	+12.90	04	4	2.58	169	O9 n	6.79	-0.10	...	...
41253	204.89	-9.21	03	1,4	1.00	107	B5.5 V	7.31	-0.02	-1.0	420s
41361	202.73	-7.78	03	1	0.19	168	G8 III	5.67	+1.04	0.3	100s
41380	203.85	-8.38	03	1	0.18	179	G7 II	5.63	+1.04	-2.1	350s
41690	188.60	+0.75	11	3,4,5,6	2.90	176	B1 V	7.71	+0.21	-3.5	1000s
42087	187.75	+1.77	11	2,3,4,5,6	1.99	170	B2.5 Ib	5.75	+0.21	-5.7	1200s
42088	190.04	+0.49	11	4,5,6	2.53	178	O6	7.55	+0.06	...	...
42379	189.28	+1.34	11	3,4,5,6	3.41	176	B1 V	7.39	+0.35	-5.1	1500s
42400	189.87	+1.04	11	4,5,6	2.21	169	B5 II	6.83	+0.18	-3.7	920s
42475	189.08	+1.60	11	4,5	2.99	172	M1 Iab	6.60	+1.6	-5.7	2200s

APPENDIX F (cont.)

Linear Polarization Observations of Field Stars

Name (Note 1)	---GALACTIC--- LONG. (o)	LAT. (o)	Program Object (Note 2)	Polarization Reference(s) (Note 3)	p (%)	Theta (o)	Spectral Type	<V>	<B-V>	<M>	Distance (Note 4) (pc)
42597	201.82	-5.31	03	4	0.78	160	B2.5 IV	7.05	-0.09	-2.6	760s
42618	202.36	-5.59	03	1	0.005	147	G4 V	+6.87	+0.63	5.0	26ts
42655	199.25	-3.85	03	4	0.74	170	B5.5 V	+7.50	-0.05	-1.0	470s
42896	190.81	+1.26	11	4,5,6	0.83	7	B1 V	8.59	-0.07	-5.1	4200s
43078	189.07	+2.50	11	3,4,5,6	3.36	165	B0 IV	8.78	+0.35	-4.6	1900s
43384	187.99	+3.53	11	3,4,5,6	2.81	170	B3 Iab	6.25	+0.45	-6.3	1400s
43582	189.07	+3.21	11	4,5,6	1.29	8	B0 III	9.12	+0.81	-6.0	2300s
43703	188.47	+2.92	11	3,4,5,6	1.75	142	B1 IV	8.62	+0.42	-3.9	1200s
43753	188.87	+3.59	11	3,4,5,6	2.53	161	B0.5 III	7.90	+0.30	-5.5	2100s
43818	188.49	+3.88	11	3,4,5,6	2.16	176	B0 II	6.92	+0.29	-5.6	1600s
43836	188.67	+3.80	11	3,4,5	0.69	157	B9 II	6.95	+0.48	-3.1	550s
43837	191.04	+2.50	11	4,5	2.49	150	...	8.4	...	...	...
43907	189.73	+3.32	11	4,5	1.43	16	...	8.8	...	...	...
44139	189.83	+3.64	11	4,5,6	2.12	2	B0.5 V	8.78	+0.28	-3.9	1600s
44597	191.65	+3.29	11	4,5,6	2.16	170	O9 V	9.02	+0.26	-4.8	2600s
44811	192.42	+3.22	11	4,5,6	1.61	172	O7.5 V	8.42	+0.13	-5.1	2800s
47914	171.18	+17.26	04	2	0.06	33	K5 III	5.02	+1.48	-0.3	120s
48781	167.25	+19.47	04	2	0.097	63	K1 III	5.28	+0.9	0.0	100t
50658	170.30	+20.07	04	2	0.62	16	B8 IV	5.80	-0.06	-0.6	190s
94601	211.60	+63.91	07	2	0.01	9	A1 V	4.32	+0.02	1.2	42s
97603	224.23	+66.83	07	2	0.005	143	A4 V	2.56	+0.12	1.9	16ts
100600	239.18	+69.47	07	3	<0.4	...	B3 V	5.95	-0.16	-1.7	340s
101484	228.85	+72.91	07	2	0.01	40	K0 III	5.26	+0.98	0.2	100s

APPENDIX F (cont.)

Linear Polarization Observations of Field Stars

Name (Note 1)	---GALACTIC--- LONG. (o)	LAT. (o)	Program Object (Note 2)	Polarization Reference(s) (Note 3)	p (%)	Theta (o)	Spectral Type	<V>	<B-V>	<M>	Distance (Note 4) (pc)
110897	128.83	+77.78	05	2	0.04	158	G0 V	5.95	+0.55	4.4	17t
112413	118.29	+78.77	05	2	0.02	3	A0p	2.90	-0.12	...	20mn
114376	105.54	+77.97	05	2	0.06	27	B7 III	+6.28	-0.12	-1.6	380s
114447	105.18	+77.98	05	2	0.12	41	A9 III-IV	+5.91	+0.29	+1.1	91s
115004	104.83	+76.18	05	2	0.08	48	K0 III	4.92	+1.06	+0.2	79s
115604	102.73	+75.52	05	2	0.06	32	F0 II-III	4.73	+0.30	-0.7	52mx
120315	100.70	+65.32	05	4,2	0.06	130	B3 V	1.86	-0.19	-1.7	33mx
147165†	351.31	+17.00	02	4,2	1.46	177	B1 III	2.89	+0.13	-4.4	180s
147888	353.64	+17.71	02	3,4,5	2.95	52	B3 V	6.74	+0.31	-1.7	230s
147889	352.85	+17.04	02	3,4,5,6	3.22	178	B2 V	7.90	+0.84	-2.5	320s
147932	353.72	+17.71	02	3,4	2.39	57	B5 V	7.27	+0.32	-1.1	230s
147933	353.68	+17.69	02	2,3,4	2.28	47	B2 V	4.59	+0.24	-2.5	230s
148605	353.10	+15.80	02	2,4	0.37	89	B2 V	4.79	-0.11	-2.5	260s
149438	351.53	+12.81	02	4	0.28	108	B0 V	2.82	-0.25	-4.1	240s
149881	31.37	+36.23	01	3	<0.4	...	B0.5 III	7.05	-0.18	-5.5	2800s
152516	359.39	+13.47	02	5	3.0	52	B5.5 V	8.04	+0.08	-1.0	520s
152614	28.73	+30.66	01	2	0.05	44	B8 IV	4.38	-0.08	-0.6	99s
158148	42.71	+27.27	01	4	0.37	61	B6 V	5.54	-0.13	-0.9	190s
204116	96.38	+3.55	09	3	3.0	22	B1 V pe	7.94	+0.49	-3.5	1300s
204827	99.17	+5.55	09	3,4,5,6	5.43	59	B0 V	7.95	+0.80	-4.1	610s
204932	98.16	+4.36	09	3	<0.3	...	F2	8.3	...	...	...
205139	100.54	+6.62	09,10	3,4	1.24	34	B1 II	5.53	+0.12	-5.1	870s
205196	98.57	+4.41	09	3,4,5,6	2.81	79	B0 Ib	7.43	+0.58	-5.8	1500s

APPENDIX F (cont.)

Linear Polarization Observations of Field Stars

Name (Note 1)	---GALACTIC--- LONG. (o)	LAT. (o)	Program Object (Note 2)	Polarization Reference(s) (Note 3)	p (%)	Theta (o)	Spectral Type	<V>	<B-V>	<M>	Distance (Note 4) (pc)
205794	98.64	+3.99	09	3,4	1.98	15	B3	8.7	...	...	...
206165	102.27	+7.25	10	3,4	0.51	18	B2 Ib	4.73	+0.30	-5.7	640s
206183	98.89	+3.40	09	4,5,6	0.69	42	B0 V	+7.41	+0.14	-4.1	1200s
206267†	99.29	+3.74	09	3,4	1.34	38	O6	+5.62	+0.21	...	...
206327	102.02	+6.76	09,10	4	1.06	40	...	8.7	...	...	...
206773	99.50	+3.59	09	3,4,5,6	2.03	169	B0 V	6.91	+0.21	-4.1	790s
207198	103.14	+6.99	10	3,4	1.15	26	O9 II	5.95	+0.31	-5.8	950s
207260	102.31	+5.93	09,10	3,4,5,6	1.70	42	A2 Ia	4.29	+0.52	-7.5	1200s
207308	103.11	+6.82	10	3,4	0.87	162	B0.5 V	7.49	+0.25	-3.9	910s
207538	101.60	+4.67	09	3,4,5,6	2.16	61	B0 V	7.31	+0.33	-4.1	910s
207872	102.15	+4.84	09,10	3,4	0.78	66	B5.5 V	7.98	+0.43	-1.0	330s
207951	103.23	+6.05	09,10	4	0.74	49	...	8.3	...	...	...
208095†	99.57	+1.29	09	3	<0.3	...	B7 V	5.34	-0.11	-0.6	150s
208218	103.98	+6.62	10	3,4	1.15	44	B1 III	6.80	+0.24	-4.4	920s
208392	104.03	+6.46	10	3,4	1.34	44	B1 IV	7.02	+0.28	-3.9	770s
208501	100.39	+1.68	09	4,5,6	1.70	42	B8 Ib	5.80	+0.73	-5.6	710s
208682	105.89	+8.45	10	4	1.52	140	B2 IVe	5.86	-0.06	-3.0	500s
208905	103.53	+5.17	09,10	3,4,5,6	0.78	38	B1 V p	6.98	+0.09	-3.5	930s
208947†	106.55	+9.00	10	4	0.51	124	B2 V	6.43	-0.05	-2.5	520s
209145	103.11	+4.23	09	5,6	<0.18	...	B1 V	7.61	+0.32	-3.5	810s
209162	104.91	+6.59	10	4	1.24	23	...	8.7	...	...	...
209296	100.74	+1.23	09	3,4,5,6	0.92	22	B6 V	8.28	+0.2	-0.9	390s
209339	104.58	+5.87	10	3,4	1.66	64	B0 IV	6.66	+0.06	-4.6	1200s

APPENDIX F (cont.)

Linear Polarization Observations of Field Stars

Name (Note 1)	---GALACTIC--- LONG. (o)	LAT. (o)	Program Object (Note 2)	Polarization Reference(s) (Note 3)	p (%)	Theta (o)	Spectral Type	<V>	<B-V>	<M>	Distance (Note 4) (pc)
209481†	102.00	+2.18	09	3,4,5	1.79	69	O9 V	5.56	+0.06	-4.8	890s
209744	103.28	+3.50	09	3,4	0.64	55	B1 V	6.71	+0.23	-3.5	620s
209975	104.88	+5.39	10	4,5,6	1.01	70	O9.5 Ib	5.10	+0.08	-6.0	970s
210072	100.84	-0.38	09	6	0.69	47	B2 V	+7.65	+0.30	-2.5	550s
210352	104.46	+4.26	10	4	0.97	48	...	8.6	...	...	...
210478	104.48	+4.12	10	4,5	0.83	49	B1 V	7.32	0.08	-3.5	990s
211880	106.67	+5.29	10	4,5,6	0.46	52	B0.5 V	7.34	0.32	-3.9	770s
213087	108.50	+6.39	10	5	0.8	33	B0.5 Ib	5.46	0.37	-5.8	730s
214930	88.30	-30.14	08	4	0.18	175	B3 V	7.40	-0.13	-1.7	650s
214994	91.71	-25.59	08	2	0.05	107	A1 V	4.79	-0.01	+1.2	52s
215182	92.50	-24.95	08	2	0.03	6	G2 II-III	2.94	0.86	-0.9	53s
216131	90.68	-30.56	08	2	0.01	176	K0 III	3.48	0.93	+0.2	45s
220222	101.57	-27.32	08	4	0.37	104	B3 V	5.32	-0.11	-1.7	230s
220657	98.56	-35.36	08	2	0.04	32	F8 IV	4.40	0.61	+2.4	22s
245310	185.48	-5.86	06	6	3.91	146	B1 V	8.87	0.28	-3.5	1400s
248587	189.20	-3.71	06	6	2.49	146	A0 Iab	7.94	0.65	-6.5	3100s
E239758	100.91	+4.41	09	4,5,6	2.12	51	B2 III	9.50	0.26	-3.9	2300s
E245310	185.48	-5.86	06	4,6	3.91	146	B1 V	8.87	0.28	-3.5	1400s
E248587	189.19	-3.71	06	5,6	2.49	2.5	A0 Iab	7.94	0.65	-6.6	3500s
E248753	183.64	-0.14	11	3	1.9	140	B0	8.5	...	...	...
E248893	186.82	-1.87	06	5,6	3.4	155	B0II-III	9.69	0.44	-6.0	4900s
E248894	187.89	-2.51	06	5,6	2.2	146	O8 V	9.29	0.24	-5.0	3400s
E250028	184.92	+0.80	11	4,5,6	4.28	164	B2 V	9.09	0.23	-2.5	1100s

APPENDIX F (cont.)

Linear Polarization Observations of Field Stars

Name (Note 1)	---GALACTIC--- LONG. (o)	LAT. (o)	Program Object (Note 2)	Polarization Reference(s) (Note 3)	p (%)	Theta (o)	Spectral Type	<V>	<B-V>	<M>	Distance (Note 4) (pc)
E250163	190.10	-2.07	06	5,6	1.7	136	B1.5 V	9.62	0.58	-3.0	1000s
E250289	186.58	+0.15	11	4,5,6	2.95	162	B2 III	8.27	0.56	-3.9	870s
E250290	186.62	+0.14	11	4,5,6	3.36	163	B3 Ib	7.38	0.61	-5.7	1400s
E251204	186.99	+0.98	11	4,6	4.65	155	B0 IV	10.28	0.48	-4.6	3200s
E251311	187.36	+0.86	11	4,5,6	2.21	0	B1.5 IV	8.81	0.34	-3.5	1200s
E252325	189.85	+0.44	11	4,6	4.79	163	B1 V	10.79	0.57	-3.5	2300s
E253049	190.58	+0.75	11	4,5,6	1.84	176	B2 IV	9.56	0.14	-3.0	1900s
E253214	183.69	+4.75	11	3,4,5,6	2.58	176	B1.5 V	9.47	0.24	-3.0	1500s
E254042	187.59	+3.47	11	4,5,6	3.91	173	B0.5 IV	8.93	0.35	-4.3	1900s
E254699	188.30	+3.73	11	4,5,6	3.41	176	B1 V	9.04	0.40	-3.5	1300s
E254755	189.10	+3.35	11	4,5,6	1.80	8	O9 V	8.84	0.60	-4.8	1500s
E255055	188.68	+3.87	11	4,5,6	0.87	163	O9 V	9.38	0.26	-4.8	3100s
E256276	189.91	+4.28	11	4,5,6	1.52	9	B1.5 V	9.24	0.16	-3.0	1500s
E256413	192.15	+3.18	11	4,5,6	2.49	168	B5 III	8.93	0.35	-2.0	710s
56+2626	99.04	+2.91	09	4,6	2.21	20	B0.5 III	10.47	0.65	-5.5	4300s
56+2640	99.67	+2.65	09	4,6	1.57	23	B0.5 V	9.25	0.70	-3.9	1100s
58+2373	102.83	+3.44	09	4,6	3.45	41	B5 Ia	9.34	0.92	-6.8	3500s
60+2380	105.36	+3.21	10	4,6	0.37	168	B2 III	9.04	0.39	-3.9	1600s
Hi 1100	105.14	+3.74	10	4,6	0.28	100	B2 V	10.68	0.60	-2.5	1300s
Hi 510	189.41	-1.23	11	4,6	2.03	170	B1 V	11.50	0.61	-3.5	3000s

Notes:

1. Name (Column 1) is predominantly the HD or HDE designation. Names containing a "+" are BD designations and those which start with "Hi" are from Hiltner's catalogs. The symbol † following some names indicates that the star is shown for reference only and was not included in the interstellar determination. Most of these stars are known spectroscopic binaries.

2. The Program Object codes are as follows:

01 ALP HER
02 ALP SCO
03 ALP ORI
04 PSI1 AUR
05 V CVN
06 119 TAU
07 72 LEO
08 BET PEG
09 MU CEP
10 VV CEP
11 6 GEM

3. The Polarization References are:

1 = Appenzeller (1966)
2 = Behr (1959)
3 = Hall and Mikesell (1950)
4 = Hall (1958)
5 = Hiltner (1951)
6 = Hiltner (1956)
7 = Smith (1956)

4. Distances labeled with "s" are determined from spectroscopic parallax. All other distances are determined by trigonometric parallax: "mn" and "mx" refer, respectively, to the minimum and maximum values allowable by trigonometric parallax.

APPENDIX G

Circular Polarization Observations of Field Stars

Name (Note 1)	---GALACTIC--- LONG. (o)	LAT. (o)	Program Object (Note 2)	Polarization Reference(s) (Note 3)	Filter	v (%)	Spectral Type	<V>	<B-V>	<M>	Distance (Note 2) (pc)
37202†	185.69	-5.63	06	6	R	-0.02(10)	B2 IV p	+3.00	-0.19	-3.0	150s
				6	V	-0.01(3)					
				6	B	-0.13(3)					
39970	185.32	-0.22	06,11	6	R	+0.24(19)	A0 Ia	6.02	+0.39	-7.1	2700s
				6	V	+0.24(28)					
				6	B	+0.02(28)					
40589	182.89	+2.23	11	6	R	+0.01(28)	B9 Iab	6.05	+0.25	-6.5	2400s
				6	V	+0.02(26)					
				6	B	+0.18(13)					
41117	189.69	-0.86	06,11	6	R	+0.05(9)	B2 Ia	4.63	+0.28	-6.8	1100s
				6	V	-0.05(22)					
				5,6	B	+0.0021(19)					
42087	187.75	+1.77	11	5	B	-0.0059(72)	B2.5 Ib	5.75	+0.21	-5.7	1200s
43384	187.99	+3.53	11	5,6	R	-0.083(44)	B3 Iab	6.25	+0.45	-6.3	1400s
				5,6	V	+0.143(83)					
				5,6	B	+0.0054(54)					
45910†	205.33	-1.95	03	6	R	+0.10(22)	B2 III	6.77	+0.33	-3.6	1100s
				6	V	-0.00(15)					
				6	B	-0.06(11)					
46150	206.30	-2.07	03	6	R	+0.04(18)	O6	+6.76	+0.13	...	...
				6	V	+0.05(13)					
				6	B	+0.06(6)					

APPENDIX G (cont.)

Circular Polarization Observations of Field Stars

Name (Note 1)	---GALACTIC--- LONG. (o)	LAT. (o)	Program Object (Note 2)	Polarization Reference(s) (Note 3)	Filter	v (%)	Spectral Type	<V>	<B-V>	<M>	Distance (Note 2) (pc)
112413	118.29	+78.77	05	5,6	R	-0.032(28)	A0 p	+2.90	-0.12	...	20mn
				6	V	+0.05(10)					
				5,6	B	+0.054(56)					
143275	350.10	+22.49	02	2	B	+0.0030(20)	B0 V	2.32	-0.12	-4.1	170s
145502†	354.61	+22.70	02	4	R	-0.004(5)	B2 IV-V	4.00	+0.05	-2.8	170s
147084	352.33	+18.05	02	2,4	R	+0.013(3)	A5 II	4.55	+0.84	-2.1	92s
				2	B	-0.0290(20)					
147165†	351.31	+17.00	02	2	R	+0.0040(10)	B1 III	2.89	+0.13	-4.4	180s
				2	B	-0.0160(30)					
147700	356.17	+20.18	02	2	B	-0.0020(10)	K0 III	4.50	+1.01	+0.2	72s
147889	352.85	+17.04	02	1,4	R	-0.009(10)	B2 V	7.90	+0.84	-2.5	320s
				4	B	+0.022(6)					
147933	353.68	+17.69	02	2	R	-0.0040(15)	B2 V	4.59	+0.24	-2.5	230s
				2	B	+0.0240(30)					
204827	99.17	+5.55	09,10	1,4	R	-0.054(2)	B0 V	7.95	+0.80	-4.1	610s
				4	B	-0.008(9)					
				4	U	+0.034(12)					
206165	102.27	+7.25	09,10	5	B	-0.0010(59)	B2 Ib	4.73	+0.30	-5.7	640s
206267†	99.29	+3.74	09,10	1	B	+0.0103(27)	O6	5.62	+0.21	...	...
207260	102.31	+5.93	09,10	1,3	R	-0.0058(28)	A2 Ia	+4.29	+0.52	-7.5	1200s
				1	V	+0.0023(23)					
				1,3	B	+0.0036(18)					

APPENDIX G (cont.)

Circular Polarization Observations of Field Stars

Name (Note 1)	---GALACTIC--- LONG. (o)	LAT. (o)	Program Object (Note 2)	Polarization Reference(s) (Note 3)	Filter	v (%)	Spectral Type	<V>	<B-V>	<M>	Distance (Note 2) (pc)
209481†	102.00	+2.18	09,10	6	R	-0.10(19)	O9 V	+5.56	+0.06	-4.8	890s
				6	V	+0.01(4)					
				5,6	B	+0.032(28)					
209975	104.88	+5.39	09,10	5	B	-0.0036(56)	O9.5 Ib	5.10	+0.08	-6.0	970s
210745	103.06	+1.67	09,10	5	R	-0.0011(10)	K1 Ib	3.35	+1.57	-4.4	220s
				5	B	+0.0030(16)					
210839	103.83	+2.61	09,10	5	V	+0.0034(35)	O6.8	+5.04	+0.25	...	42mn

Notes:

1. The name is the HD designation. See the notes for Appendix F on the † designation.
2. See the notes for Appendix F for the Program Object codes and Distance designation information.
3. The Polarization References are:
   - 1 = Avery et al. (1975)
   - 2 = Kemp and Wolstencroft (1972)
   - 3 = Michalsky et al. (1974)
   - 4 = Serkowski, Mathewson, and Ford (1975)
   - 5 = Stokes et al. (1974)
   - 6 = Wolf (1972) Note: sign of circular data had to be inverted.

APPENDIX H

Multi-Parameter Polarization Model

Software Listings

The polarization model software was written in the computer language C (version 6.1) as implemented by Microsoft Corporation. Microsoft C was chosen because it is fast, portable and has a rich software tool library.

The polarization model software is called SCATTER. Once compiled, it runs on the PC-compatible (preferably those with Motorola 80386 and 80387 chips). SCATTER output is discussed in Sections 4.2 and 4.3. The usage statement is:

SCATTER <initialization file> <Mie coefficients file>.

Sample initialization and Mie coefficients files follow the software listing. The output data file is called "scatter.dat". It is compatible with the Statgraphics or Digraph statistical analysis programs. The first lines of this file contains startup information. The rest of the lines of the file have the following format:

LATITUDE, LONGITUDE, Q(%), U(%), V(%), P(%), FLUX.

Here FLUX corresponds to the sum of the photon amplitudes squared. The flux values have been normalized by the average of the flux at 0° and 360° longitude. An abbreviated output file follows the sample Mie coefficient file.

```
/*************************************************************************
*
*    Copyright 1991 (C) B D H
*
* Program: SCATTER.C
* Author:
*          Bruce D. Holenstein
*          (215) 430-6830
*
* Version History:
*
* Version   Date        Who        Reason
* -------  ----------  ---------  --------------
* 1.00     02/04/91    bdh        initial version
* 2.00     03/04/91    bdh        rt scattering added
* 3.00     03/10/91    bdh        mie scattering added
*
*  This program calculates the scattering diagram of the multi-parameter
*  polarization model.  Please note that the format of the code follows the
*  thesis text.  The result is that the execution speed may not be optimum.
*  Many speed improvements may be made.  However, some are not necessary
*  since the Microsoft compiler completes many optimizations.
*/
/*-----------------------------------------------------------------------*/

#include <fcntl.h>
#include <sys\types.h>
#include <sys\stat.h>
#include <io.h>
#include <stdio.h>
#include <math.h>
#include <string.h>
#include <stdlib.h>

#define NUM_MIE_COEFF 10          /* Number of complex Mie Coeff. */
#define HORIZONTAL 15             /* Number of longitude bins */
#define VERTICAL 7                /* Number of latitude bins */
#define SPHERES 1
#define CYLINDERS 2
#define TRUE 1
#define FALSE 0
#define PI        3.141592654
#define PI_H      1.570796327
#define PI_MH    -1.570796327
#define PI_3      4.712388980
#define PI_M3    -4.712388980
#define PI2       6.283185307
#define MAX_INT        32768.0
#define MAX_DOUBLE_INT 65536.0
#define DEGRAD    57.29578
#define SMALL     0.0000000001
#define NEARONE   0.9999999999
#define E         2.718281828
#define INTOSTAR 999
#define NP        17L             /* used in get_flux_vector calculation */
#define N1        1000L           /* used in get_sphere_position */
#define N2        100000L         /* 100*N1*/
#define N2F       100000.0        /* floating N2 */
#define N2_HF     50000.0         /* half of N2F */
#define N3        10000000L       /* 100*N2 */

typedef struct   /* Mie coefficients */
        {
      double a_r;         /*a(n) real*/
      double a_i;         /*a(n) imag*/
      double b_r;
      double b_i;
        } mie_coeff_def;

typedef struct   /* Flux_vector form */
        {
      double pl_r;         /*amplitude parallel to scattering plane*/
      double pl_i;         /*imag part*/
      double pr_r;         /*amplitude perpendicular*/
      double pr_i;         /*imag part*/
      double theta;        /*flux_vector direction*/
      double phi;
      int spot;            /*flux_vector from a spot*/
      int scattered;       /*flux_vector was scattered*/
        } flux_vector_def;

typedef struct   /* Scattering matrix form */
      {
      double s1_r;
      double s1_i;
      double s2_r;
      double s2_i;
      double s3_r;
      double s3_i;
```

```
      double s4_r;
      double s4_i;
      } scatter_def;

typedef struct   /* Rotation matrix form */
      {
      double r1_r;
      double r2_r;
      double r3_r;
      double r4_r;
      } rotate_def;

typedef struct   /* Initial conditions structure */
      {
      int graphics;
      double wavelength;
      long num_flux_vectors;

      /*Spots*/
      int spot;
      double flux_spot;
      double spot_theta;
      double spot_phi;
      double spot_radius;
      double spot_gamma;
      double limb_darkening_coeff;

      /*Rayleigh/Thomson*/
      int rayleigh;
      double alpha_k_k; /*used with rayleigh scattering*/
      double rayleigh_thick;
      double Ne;        /*number density of scatterers*/

      /*Mie*/
      int mie_type;           /*1=spheres,2=cylinders*/
      double QNa2;            /*calculated from IR excess*/
      double dust_ratio;      /*ratio of dust shell radius to star radius */
      double dust_orientation;
      double star_radius;
      double dust_length;     /*length of dust cylinders*/
      /*Interstellar*/
      double interstellar_phase;
      double interstellar_orientation;

      } initial_def;

mie_coeff_def  mie_coeff[NUM_MIE_COEFF];
flux_vector_def     flux_vector;
initial_def    initial_conditions;
scatter_def    sr; /*rayleigh scattering matrix*/
scatter_def    sm; /*Mie scattering matrix*/
scatter_def    si; /*Interstellar birefringence*/

FILE *handle;          /* Mie data handle */
FILE *c_handle;        /* Initial conditions data handle */
int out_hand;          /* output data handle */
char temp_str[120];
int   bytes;
double theta_sp; /* the direction in which the flux_vector leaves*/
double phi_sp;
double k1;                      /*wavenumber*/
double mie_transmission;        /*percentage of flux transmitted*/
double mie_normalizing;
double rayleigh_cross_section;
long  single_rt_scatters;
long  single_mie_scatters;
long  double_scatters;
long  no_scatters;

double sum_i[HORIZONTAL][VERTICAL];
double sum_q[HORIZONTAL][VERTICAL];
double sum_u[HORIZONTAL][VERTICAL];
double sum_v[HORIZONTAL][VERTICAL];

/*-------------------------------------------------------------------------*/

main(argc, argv)

int  argc;
char *argv[];

    {
    if (argc < 2)
       {
       printf("\nArguments not right...\n");
       printf(" Usage is: SCATTER <conditions file> <coeff file>\n\n");
       exit(0);
       }
```

```
    sc_initialization(argv);

    scatter_light();

    termination();

    }   /* end main */

/*-------------------------------------------------------------------------*/

sc_initialization(argv)

char *argv[];

   {
   long  pos;
   int   i, j, bytes;
   char  c;
   double phase;

   initial_conditions.graphics = FALSE;
   printf("\nSelect Option:\n");
   printf("Graphics format output?\n");
   c = toupper(getche());

   if (c == 'Y')
      initial_conditions.graphics = TRUE;

   c_handle = fopen(argv[1], "rb");
   if (c_handle == 0)
      {
      printf("error opening data file %s\n",argv[1]);
      exit(0);
      }

   read_initial_conditions();

   if (initial_conditions.mie_type != FALSE)
      {
      handle = fopen(argv[2], "rb");
      if (handle == 0)
         {
         printf("error opening data file %s\n",argv[2]);
         exit(0);
         }
      read_mie_coeff();
      }

   out_hand = open("scatter.dat",O_CREAT | O_TRUNC | O_TEXT | O_WRONLY, S_IWRITE);
   if (out_hand == -1)
      {
      printf("error opening output file\n");
      exit(0);
      }

   for (i = 0; i < 100; i++)
      temp_str[i] = ' ';

   bytes = sprintf(temp_str,"\nSCATTERING DIAGRAM - CONDITIONS FILE: %s\n", argv[1]);
   printf("%s",temp_str);
   bytes = write(out_hand, temp_str, bytes);

   if (initial_conditions.mie_type != FALSE)
      {
      bytes = sprintf(temp_str,"\nSCATTERING DIAGRAM - COEFFICIENT FILE: %s\n", argv[2]);
      printf("%s",temp_str);
      bytes = write(out_hand, temp_str, bytes);
      }

   for (i = 0; i < 100; i++)
      temp_str[i] = ' ';

   /* Change the seed value for different runs, or keep constant*/
   /* for testing. */
   srand(99);   /* initialize the random number generator */

   /*kl = wave number in 1/microns*/
   kl = PI2/initial_conditions.wavelength;

   /* initialize the elements of the arrays */
   for (i = 0; i < HORIZONTAL; i++)
      {
      for (j = 0; j < VERTICAL; j++)
         {
         sum_i[i][j] = 0.0F;
         sum_q[i][j] = 0.0F;
         sum_u[i][j] = 0.0F;
         sum_v[i][j] = 0.0F;
         }
```

```
      }

   /*Generate the interstellar birefringence phase matrix*/
   phase = initial_conditions.interstellar_phase/2.0;

   si.s2_r = cos(phase);
   si.s2_i = sin(phase);

   si.s1_r = si.s2_r;
   si.s1_i = -1.0*si.s2_i;

   si.s3_r = 0.0;
   si.s3_i = 0.0;

   si.s4_r = 0.0;
   si.s4_i = 0.0;

   if (initial_conditions.mie_type != FALSE)
      {
      /* we need to normalize the mie_coefficients.  This will be applied */
      /* in procedure mie_coefficients */
      mie_normalizing = 1.0;
      mie_coefficients(0.0);  /* S(0)*/
      mie_normalizing = sqrt((sm.s1_r + sm.s2_r)/2.0);

      /* calculate the Mie transmission % from the dust optical depth: ratio of*/
      /* the dust area to the area of the shell.  We could also use the mie_normalizing*/
      /* factor above in conjunction with the fundamental extinction thm. */
      if (initial_conditions.mie_type != FALSE)
         {  /* implicit Q(abs) and Q(ext) about the same */
         mie_transmission = initial_conditions.QNa2 /
            (  4.0*pow( (initial_conditions.dust_ratio *
                        initial_conditions.star_radius),2.0) );
         mie_transmission = pow(E,(-1.0*mie_transmission));
         }
      }

   /*keeps track of number of flux_vectors*/
   single_rt_scatters = 0L;
   single_mie_scatters = 0L;
   double_scatters = 0L;
   no_scatters = 0L;

   /*calculate the rayleigh/thomson cross-section*/
   rayleigh_cross_section = (8.0*PI/3.0)*pow(initial_conditions.alpha_k_k,2.0)
         * initial_conditions.Ne;
   }  /* end procedure initialization */

/*-------------------------------------------------------------------------*/
/*
    This procedure scatters the light inside the star envelope.
*/

scatter_light()

   {
   int i, j;
   int bytes;
   long flux_vector_num;   /*the number of the flux_vector being processed*/
   double x1,x2,x3,x4,x5;
   double max_light[VERTICAL];
   double latitude, longitude;

   /* Calculate the scattering diagram */
   for (flux_vector_num = 0L;
      flux_vector_num < initial_conditions.num_flux_vectors; flux_vector_num++)
   {
   get_sphere_position(flux_vector_num);

   get_flux_vector_amplitude(flux_vector_num);

   scatter_rayleigh();

   if (flux_vector.scattered != INTOSTAR)  /*scattered back into star?*/
      {
      scatter_mie();

      interstellar_birefringence();

      sum_scattering_diagram();  /*add flux_vector into scattering diagram*/
      }
   }
   /* End scattering calculation */

   bytes = sprintf(temp_str,"Scatters:  none %ld  rt only %ld  mie only %ld  double %ld\n",
         no_scatters,single_rt_scatters,single_mie_scatters,double_scatters);
   printf("%s",temp_str);
   bytes = write(out_hand, temp_str, bytes);
```

```
   for (j = 0; j < VERTICAL; j++)
      {
      /* Normalize the longitude flux values */
      max_light[j] = 0.5*(sum_i[0][j] +
           sum_i[HORIZONTAL-1][j]);
      if (max_light[j] == 0.0)
         max_light[j] = 1.0;  /*prevent divide by zero*/

      }

   /* print out the tables with the scatter data */
   for (i = (HORIZONTAL-1); i >= 0; i--)
      {
      longitude = DEGRAD*(double)i/(double)(HORIZONTAL - 1) * PI2;

      for (j = 0; j < VERTICAL; j++)
         {
         if (sum_i[i][j] > 0.0)
            {  /* Normalize the Stokes vectors */
            x1 = 100.0 * sum_q[i][j]/sum_i[i][j];
            x2 = 100.0 * sum_u[i][j]/sum_i[i][j];
            x3 = 100.0 * sum_v[i][j]/sum_i[i][j];
            x4 = sqrt(x1*x1 + x2*x2);     /* linear pol in % */
            x5 = sum_i[i][j]/max_light[j];
            }
         else
            {  /* Set to zero */
            x1 = 0.0F;
            x2 = 0.0F;
            x3 = 0.0F;
            x4 = 0.0F;
            x5 = 0.0F;
            }

         latitude = DEGRAD*(0.5 - (double)j/(double)(VERTICAL - 1)) * PI;

         if (initial_conditions.graphics == TRUE)   /*comma delimit */
            bytes = sprintf(temp_str,"%.1f, %.1f, %.4f, %.4f, %.4f, %.4f, %.4f \n",
                  longitude,latitude,x1,x2,x3,x4,x5);
         else
            bytes = sprintf(temp_str,"%.1f %.1f %.4f %.4f %.4f %.4f %.4f \n",
                  longitude,latitude,x1,x2,x3,x4,x5);
         printf("%s",temp_str);
         bytes = write(out_hand, temp_str, bytes);
         }
      }
   }  /* end procedure scatter_light */

/*-------------------------------------------------------------------------*/
/* This procedure gets the Mie coefficients from the specified file */

read_mie_coeff()

   {
   register int  i;         /* Used as index into loops                    */
   int   numbytes;          /* Number of bytes read per record             */
   int   line_length = 90;  /* Mie coeff: Raaa,Iaaa,Rbbb,Ibbb (R=real,I=Im.) */
   char  temp_data[90], *result, *a, *b;

   for (i = 0; i < NUM_MIE_COEFF; i++)
      {
      mie_coeff[i].a_r = 0.0F;
      mie_coeff[i].a_i = 0.0F;
      mie_coeff[i].b_r = 0.0F;
      mie_coeff[i].b_i = 0.0F;
      }  /* end i-loop */

   for (i = 0; i < NUM_MIE_COEFF; i++)
      {
      result = fgets( temp_data, line_length, handle);
      if (result == 0)
         {
         printf("\nTotal number of lines read #%d...\n", i);
         i = NUM_MIE_COEFF;  /* exit loop */
         }
      else if (strlen(temp_data) > 8)  /* minimum line length */
         {
         a = strchr(temp_data,',');
         *a = 0; /* null terminate */
         a++;
         mie_coeff[i].a_r = atof( temp_data );

         b = strchr(a,',');
         *b = 0; /* null terminate */
         b++;
         mie_coeff[i].a_i = atof( a );

         a = strchr(b,',');
         *a = 0; /* null terminate */
```

```
         a++;
         mie_coeff[i].b_r = atof( b );

         b = strchr(a,'!');   /*looking for comment */
         *b = 0; /* null terminate */
         mie_coeff[i].b_i = atof( a );

         printf("Mie coefficients for n= %d are  ar= %.2f ai= %.2f br= %.2f bi=%.2f\n",
                         i,mie_coeff[i].a_r,mie_coeff[i].a_i,
                         mie_coeff[i].b_r,mie_coeff[i].b_i);
         }

      }  /* end i-loop */

   }  /* end procedure read_mie_coeff */

/*-------------------------------------------------------------------------------*/

read_initial_conditions()
   {
   register int  i;          /* Used as index into loops              */
   int   numbytes;           /* Number of bytes read per record       */
   int   line_length = 90;   /* Conditions: label, value !description */
   char  temp_data[90], *result, *a, *b;
   int   key;

   initial_conditions.rayleigh = FALSE;
   initial_conditions.mie_type = FALSE;

   for (i = 0; i < 100; i++)    /* 100 max initial conditions */
      {
      result = fgets( temp_data, line_length, c_handle);
      if (result == 0)
         {
         printf("\nTotal number of condition lines read #%d...\n", i);
         i = 100;  /* exit loop */
         }
      else if (strlen(temp_data) > 8)  /* minimum line length */
         {
         a = strchr(temp_data,',');
         *a = 0; /* null terminate */
         a++;
         key = atoi( temp_data );

         b = strchr(a,'!');
         *b = 0; /* null terminate */

         switch (key)
            {
            case 1:  /* Wavelength of light */
               initial_conditions.wavelength = atof( a );
               break;

            case 2:  /* Number of Monte Carlo flux_vectors */
               initial_conditions.num_flux_vectors = atol( a );
               break;

            case 3:  /* limb darkening coefficient */
               initial_conditions.limb_darkening_coeff = atof( a );
               break;

            case 4:  /* photosphere spots */
               initial_conditions.spot = atoi( a );
               break;

            case 5:  /* flux(spot)/average flux */
               initial_conditions.flux_spot = atof( a );
               break;

            case 6:  /* spot theta */
               initial_conditions.spot_theta = atof( a );
               break;

            case 7:  /* spot phi */
               initial_conditions.spot_phi = atof( a );
               break;

            case 8:  /* spot radius */
               initial_conditions.spot_radius = atof( a );
               break;

            case 9:  /* spot gamma */
               initial_conditions.spot_gamma = atof( a );
               break;

            case 10:  /* series 10 are for rayleigh/thomson */
               initial_conditions.rayleigh = atoi( a );
               break;
```

```
            case 12:  /* Rayleigh alpha times k squared parameter */
               initial_conditions.alpha_k_k = atof( a );
               break;

            case 13:  /* thickness */
               initial_conditions.rayleigh_thick = atof( a );
               break;

            case 14:  /* Ne */
               initial_conditions.Ne = atof( a );
               break;

            case 20:  /* series 20 are for Mie scattering */
               initial_conditions.mie_type = atoi( a );
               break;

            case 21:
               initial_conditions.QNa2 = atof( a );
               break;

            case 22:
               initial_conditions.dust_ratio = atof( a );
               break;

            case 23:
               initial_conditions.dust_orientation = atof( a );
               break;

            case 24:
               initial_conditions.star_radius = atof( a );
               break;

            case 25:
               initial_conditions.dust_length = atof( a );
               break;

            case 30:  /* series 30 are for interstellar birefringence */
               initial_conditions.interstellar_phase = atof( a );
               break;

            case 31:  /* orientation of interstellar birefringence */
               initial_conditions.interstellar_orientation = atof( a );
               break;

            default:
               printf("\nWE HAVE AN INVALID CONDITION: %d \n",key);

            } /* end case */
         }

      }  /* end i-loop */

   }  /* end procedure read_initial_conditions */

/*---------------------------------------------------------------------------*/
/* This procedure gets a position on the photosphere */

get_sphere_position(number)

long number;

   {
   double area;
   double spangle;   /* angle to spot */
   double a,b,c,d,e,f;

   flux_vector.spot = FALSE;       /* not yet in a spot region */
   flux_vector.scattered = FALSE;  /* not yet been scattered */

   /*int area; */
   /*flux_vector.phi = PI2 * (double)rand() / MAX_INT;*/
   /*area = (double)rand()/MAX_INT; */ /*we get a random area then find theta */

   /*The following gets an ordered position on the sphere since the computer is */
   /* not fast enough for convergence with random positions. */
   flux_vector.phi = PI2 * (double)(N1 * (number/N1))/N2F;

   area = ((double)(N2*(number/N2)) + N2_HF)
       /initial_conditions.num_flux_vectors;

   flux_vector.theta = acos( 1.0 - 2.0 * area );  /* pi is max */

   /*************************************/
   /**** Test restriction to equator *****/
   /*half way around
   flux_vector.phi = PI;
   */
   /*equator
   flux_vector.theta = PI_H;
```

```
   */

   /* figure out if we are in a spot region */
   if (initial_conditions.spot == TRUE)
      {
      a = initial_conditions.spot_theta;
      b = flux_vector.theta;
      c = initial_conditions.spot_phi;
      d = flux_vector.phi;

      /* fine determination: optimize calculation of spot tig fcns */
      e = cos(a)*cos(b) + sin(a)*sin(b)*cos(c-d);
      if ( (e > 1.0) || (e < -1.0) )
         e = modf(e, &f);
      spangle = acos( e );

      if (spangle <= initial_conditions.spot_radius)
         flux_vector.spot = TRUE;
      } /* spot == true*/

   }  /* end procedure get_sphere_position */

/*-------------------------------------------------------------------------*/
/* This procedure gets the flux_vector amplitude, phase and direction. */
/* Also, if there is a spot it adds in a circular signal.    */

get_flux_vector_amplitude(number)

long number;

   {
   int area;
   double phase, r_amplitude, l_amplitude;
   double argument;
   double limb_dark;
   double circular = 0.0;

   /* temporary local flux_vector direction variables */
   phi_sp = PI2 * (double)rand() / MAX_INT;

   /* we get a random area then find theta */
   /*2 PI ster*/
   argument = 1.0 - (double)rand()/ MAX_INT;

   theta_sp = acos( argument );

   /************************************************/
   /**** Test restriction for flux direction *******/
   /*
   phi_sp = 0.0;
   theta_sp = 0.0;
   argument = 1.0;
   theta_sp = .8;
   argument = 0.6967;
   */

   /*Limb darkening*/
   limb_dark = 1.0 - initial_conditions.limb_darkening_coeff * (1.0-argument);
   /*Lambert's cosine*/
   limb_dark = limb_dark * argument;

   if (flux_vector.spot == TRUE)
      {
      limb_dark = sqrt(limb_dark * initial_conditions.flux_spot);  /*flux depression*/
      /*we add in the magneto-emission*/
      circular = 0.707*initial_conditions.spot_gamma;
      /*
      printf("One in the spot\n"); */
      }
   else
      limb_dark = sqrt(limb_dark); /* since we are dealing with amplitudes */

   /* Here we generate the amplitude components of the flux_vector. */
   /* Note that the initial amplitude of the flux_vector must equal one. */
   if (circular != 0.0) /*we must add flux amplitudes incoherently*/
      {
      phase = PI2 * (double)rand() / MAX_INT;
      l_amplitude = cos(phase);
      r_amplitude = sin(phase);

      phase = PI2 * (double)rand() / MAX_INT;
      flux_vector.pl_r = (l_amplitude * cos(phase) + circular) * limb_dark;
      flux_vector.pl_i = (l_amplitude * sin(phase) - circular) * limb_dark; /*subtract*/

      phase = PI2 * (double)rand() / MAX_INT;
      }
   else
      {
      /* The following improves convergence when there is no magneto-emission.*/
```

```
      /* The flux is fixed so that there is no initial net polarization. */
      l_amplitude = 0.707;
      r_amplitude = 0.707;

      /* the following corresponds to phase = 0.0; */
      flux_vector.pl_r = l_amplitude * limb_dark;
      flux_vector.pl_i = 0.0;

      /* The following uniformly covers the possible phases */
      phase = PI2 * (double)number / NP;    /*parallel part*/
      }

   /*parallel part*/
   flux_vector.pr_r = (r_amplitude * cos(phase) + circular) * limb_dark;
   flux_vector.pr_i = (r_amplitude * sin(phase) + circular) * limb_dark;

   /*
   printf("flux_vector %.4f %.4f %.4f %.4f %.4f\n",limb_dark,
          flux_vector.pl_r,flux_vector.pl_i,flux_vector.pr_r,flux_vector.pr_i);
   */
   }  /* end procedure get_flux_vector_amplitude */

/*-------------------------------------------------------------------------*/
/* This procedure Rayleigh/Thomson scatters the flux_vector */

scatter_rayleigh()

   {
   double scatter_theta;  /* local scattering angle */
   double scatter_phi;
   double path;  /* path length in rayleigh layer */
   double rayleigh_transmission;
   int area;
   double argument;
   double temp;
   rotate_def rot;  /*a rotation matrix */
   double rotate_phi;
   double original_theta;
   double spangle;   /* angle to flux */
   double a,b,c,d,e,f;

   /* calculate the thickness of the rayleigh layer */

   temp = cos(theta_sp);
   if (temp < SMALL)
      temp = SMALL;

   path = initial_conditions.rayleigh_thick / temp;

   /* we can now add the local flux_vector direction to the flux_vector position */
   a = flux_vector.theta;  /*save original photosphere exit direction*/
   c = flux_vector.phi;
   add_angles(&flux_vector,theta_sp,phi_sp);

   rayleigh_transmission = path * rayleigh_cross_section;
   rayleigh_transmission = pow(E,(-1.0*rayleigh_transmission));

   /* Do we follow the scatter vector? we randomize */
   if ( (initial_conditions.rayleigh == TRUE) &&
        ( ((double)rand()/MAX_INT) > rayleigh_transmission ) )
      {
      /* we are scattering the flux_vector: all of the flux is going*/
      /* into a random scattering direction */
      /*printf("This one RT scattered       *RT* \n");*/
      flux_vector.scattered = 1;

      /* get random scattering direction*/
      scatter_phi = PI2 * (double)rand() / MAX_INT;

      area = rand();    /* we get a random area then find phi */
      /* the flux_vector scatters into 4 pi ster */
      argument = 1.0 - 2.0*(double)area/ MAX_INT;
      scatter_theta = acos( argument );

      /************************************/
      /*test restrictions
         scatter_theta = PI_H -0.2;
         argument = cos(scatter_theta);
         scatter_phi = 0.7852;
         scatter_phi = initial_conditions.interstellar_phase;
      */
      /*Note that we already factored in the cross-section when deciding */
      /*this flux_vector will be scattered */
      sr.s1_r = 1.2247;         /*normalized by sqrt(3/2) */
      sr.s1_i = 0.0;

      sr.s2_r = 1.2247*argument;    /* cos(scatter_theta); */
      sr.s2_i = 0.0;
```

```
      sr.s3_r = 0.0;
      sr.s3_i = 0.0;

      sr.s4_r = 0.0;
      sr.s4_i = 0.0;

      /*rotate electric vectors to the scatter plane*/
      rotate_phi = 0.0 - scatter_phi;  /* rotate in the reverse direction */
      gen_rotate(rotate_phi,&rot);
      rotate_mul(&flux_vector,&rot);

      /* now scatter the electric vector */
      multiply22x21(&flux_vector,&sr); /*complex multiply of flux vector 2x1 by sr 2x2 */
      /*rotate electric vectors back. NOTE: new local north is different */
      /*since the flux_vector direction has changed. */

      original_theta = flux_vector.theta;  /*this is theta before scattering */
      /* add the flux_vector scatter direction to the original direction.      */
      add_angles(&flux_vector,scatter_theta,scatter_phi);

      temp = sin(flux_vector.theta)*sin(scatter_theta);
      if ( (temp < SMALL) && (temp > -SMALL) )
         temp = SMALL;
      temp = ( cos(original_theta) -
         cos(flux_vector.theta)*cos(scatter_theta) )/temp;
      if (temp > NEARONE)
         temp = NEARONE;
      else if (temp < -NEARONE)
         temp = -NEARONE;

      /* rotate in the proper direction */
      if (scatter_phi <= PI)
         rotate_phi = PI - acos(temp);
      else
         rotate_phi = PI + acos(temp);

      gen_rotate(rotate_phi,&rot);
      rotate_mul(&flux_vector,&rot);    /*rotate electric vector to local north*/

      /* figure out if the flux hits the star after RT scattering */
      b = flux_vector.theta;  /*new positions*/
      d = flux_vector.phi;

      /* fine determination: optimize calculation of spot tig fcns */
      e = cos(a)*cos(b) + sin(a)*sin(b)*cos(c-d);
      if ( (e > 1.0) || (e < -1.0) )
         e = modf(e, &f);
      spangle = acos( e );

      if (spangle > PI_H)
         { /*unfortunately this flux vector heads back into the star*/
         flux_vector.scattered = INTOSTAR;
         }
      }

   }  /* end procedure scatter_rayleigh */

/*-------------------------------------------------------------------------*/
/* This procedure Mie scatters the flux_vector via spheres or cylinders */

scatter_mie()

   {
   double scatter_theta;  /* local scattering angle */
   double scatter_phi;
   int area;
   double argument;
   double temp;
   rotate_def rot;  /*a rotation matrix */
   double rotate_phi;
   double original_theta;

   /* Do we follow a scatter vector? we randomize */
   if ( (initial_conditions.mie_type != FALSE) &&
       ( ((double)rand()/MAX_INT) > mie_transmission ) )
      {
      /* we are scattering the flux_vector */
      /*printf("This one Mie scattered        **     *Mie* \n");  */
      flux_vector.scattered = flux_vector.scattered + 2;

      /* get random scattering direction*/
      scatter_phi = PI2 * (double)rand() / MAX_INT;
      area = rand();     /* we get a random area then find phi */
      /* the flux_vector scatters into 4 pi ster */
      argument = 1.0 - 2.0*(double)area/ MAX_INT;
      scatter_theta = acos( argument );

      /* fills the mie coefficient structure */
      mie_coefficients(scatter_theta);
```

```
      /*rotate electric vectors to the scatter plane*/
      rotate_phi = -1.0 *(initial_conditions.dust_orientation + scatter_phi);
      gen_rotate(rotate_phi,&rot);
      rotate_mul(&flux_vector,&rot);

      /* now scatter the electric vector */
      multiply22x21(&flux_vector,&sm); /*complex multiply of flux_vector 2x1 by sr 2x2 */
      /*rotate electric vectors back. NOTE: new local north is different */
      /*since the flux_vector direction has changed. */

      original_theta = flux_vector.theta;  /*this is theta before scattering */
      /* add the flux_vector scatter direction to the original direction.      */
      add_angles(&flux_vector,scatter_theta,scatter_phi);

      temp = sin(flux_vector.theta)*sin(scatter_theta);
      if ( (temp < SMALL) && (temp > -SMALL) )
         temp = SMALL;
      temp = ( cos(original_theta) -
         cos(flux_vector.theta)*cos(scatter_theta) )/temp;
      if (temp > NEARONE)
         temp = NEARONE;
      else if (temp < -NEARONE)
         temp = -NEARONE;

      /* rotate in the proper direction */
      if (scatter_phi <= PI)
         rotate_phi = PI - acos(temp);
      else
         rotate_phi = PI + acos(temp);

      /*return to the local North*/
      rotate_phi = rotate_phi + initial_conditions.dust_orientation;

      gen_rotate(rotate_phi,&rot);
      rotate_mul(&flux_vector,&rot);    /*rotate electric vector to local north*/

      }

   }  /* end procedure scatter_mie */

/*---------------------------------------------------------------------------*/
/* This procedure builds the scattering phase matrix from the Mie coefficients */

mie_coefficients(scatter_theta)

double scatter_theta;

   {
   double ori, phi, ssm, cs;
   double T1_r = 0.0, T1_i = 0.0, T2_r = 0.0, T2_i = 0.0;
   int m;

   sm.s1_r = 0.0;
   sm.s1_i = 0.0;

   sm.s2_r = 0.0;
   sm.s2_i = 0.0;

   sm.s3_r = 0.0;
   sm.s3_i = 0.0;

   sm.s4_r = 0.0;
   sm.s4_i = 0.0;

   /*Setup the scattering phase function */
   if (initial_conditions.mie_type == SPHERES)
      {   /*valid for mx < 1.0 */
      cs = cos(scatter_theta);
      sm.s1_r = 1.5*(mie_coeff[1].a_r + mie_coeff[1].b_r*cs)
           + 2.5*(mie_coeff[2].a_r*cs
           + mie_coeff[2].b_r*cos(2.0*scatter_theta));

      sm.s1_i = 1.5*(mie_coeff[1].a_i + mie_coeff[1].b_i*cs)
           + 2.5*(mie_coeff[2].a_i*cs
           + mie_coeff[2].b_i*cos(2.0*scatter_theta));

      sm.s2_r = 1.5*(mie_coeff[1].a_r*cs + mie_coeff[1].b_r)
           + 2.5*(mie_coeff[2].a_r*cos(2.0*scatter_theta)
           + mie_coeff[2].b_r*cs);

      sm.s2_i = 1.5*(mie_coeff[1].a_i*cs + mie_coeff[1].b_i)
           + 2.5*(mie_coeff[2].a_i*cos(2.0*scatter_theta)
           + mie_coeff[2].b_i*cs);
      }
   else if (initial_conditions.mie_type == CYLINDERS)
      {
      ori = initial_conditions.dust_orientation;
      phi = PI_H;  /* at right angles */
      ssm = (2.0/(PI*phi)) * sin(kl*initial_conditions.dust_length*phi/2.0);
```

```
      for (m = 1; m < NUM_MIE_COEFF; m++)
         {
         cs = cos( ((double)m * scatter_theta) );

         T1_r = T1_r + mie_coeff[m].a_r * cs;
         T1_i = T1_i + mie_coeff[m].a_i * cs;
         T2_r = T2_r + mie_coeff[m].b_r * cs;
         T2_i = T2_i + mie_coeff[m].b_i * cs;
         }

      T1_r = mie_coeff[0].a_r + 2.0*T1_r;
      T1_i = mie_coeff[0].a_i + 2.0*T1_i;
      T2_r = mie_coeff[0].b_r + 2.0*T2_r;
      T2_i = mie_coeff[0].b_i + 2.0*T2_i;

      sm.s1_r = ssm * T1_r;
      sm.s1_i = ssm * T1_i;
      sm.s2_r = ssm * T2_r;
      sm.s2_i = ssm * T2_i;
      }

   sm.s1_r = sm.s1_r/mie_normalizing;
   sm.s1_i = sm.s1_i/mie_normalizing;
   sm.s2_r = sm.s2_r/mie_normalizing;
   sm.s2_i = sm.s2_i/mie_normalizing;

   }  /* end procedure mie_coefficients */

/*-------------------------------------------------------------------------*/
/* This procedure applies the interstellar birefringence */

interstellar_birefringence()

   {
   double rotate_phi;
   rotate_def rot;  /*a rotation matrix */

   /*Note that the S matrix is filled in the setup area*/

   /*rotate electric vectors to the scatter plane*/
   rotate_phi = initial_conditions.interstellar_orientation;
   gen_rotate(rotate_phi,&rot);
   rotate_mul(&flux_vector,&rot);

   /* now scatter the electric vector */
   multiply22x21(&flux_vector,&si); /*complex multiply of flux_vector 2x1 by sr 2x2 */

   /*rotate electric vectors back.*/
   gen_rotate((-1.0*rotate_phi),&rot);
   rotate_mul(&flux_vector,&rot);

   }  /* end procedure interstellar_birefringence */

/*-------------------------------------------------------------------------*/
/* This procedure adds the flux_vector into the Stokes arrays */

sum_scattering_diagram()  /* add flux_vector into scattering diagram */

   {
   int i,j;
   double a, b, c, d;

   i = (int)((flux_vector.phi/PI2)*HORIZONTAL);

   /* invert so zero theta is at the top */
   j = (int)((1.0 - flux_vector.theta/PI)*VERTICAL);

   if ((i<0) || (i>=HORIZONTAL) || (j<0) || (j>=VERTICAL))
      {
      printf("\nSUM SCATTERING PROBLEM: %d %d",i,j);
      if (i >= HORIZONTAL)
         i = HORIZONTAL-1;
      if (j >= VERTICAL)
         j = VERTICAL-1;
      }

   a = flux_vector.pl_r;
   b = flux_vector.pl_i;

   c = flux_vector.pr_r;
   d = flux_vector.pr_i;

   sum_i[i][j] = sum_i[i][j] + a*a + b*b + c*c + d*d;  /*intensity*/

   /*keeps track of number of flux_vectors*/
   if (flux_vector.scattered == 1)
      single_rt_scatters = single_rt_scatters + 1;
   else if (flux_vector.scattered == 2)
      single_mie_scatters = single_mie_scatters + 1;
```

```
   else if (flux_vector.scattered == 3)
      double_scatters = double_scatters + 1;
   else
      no_scatters = no_scatters + 1;

   /* add only if interesting */
   if ( (flux_vector.scattered != FALSE) ||
      ( (flux_vector.spot == TRUE) &&
        (initial_conditions.spot_gamma != 0.0) ) )
      {
      sum_q[i][j] = sum_q[i][j] + a*a + b*b - c*c - d*d;

      sum_u[i][j] = sum_u[i][j] + 2.0*(a*c+b*d);

      sum_v[i][j] = sum_v[i][j] + 2.0*(a*d-b*c);
      }
   }  /* end procedure sum_scattering_diagram */

/*-------------------------------------------------------------------------*/
/* complex multiply of 2x1 flux_vector matrix by 2x2 scatter matrix */
multiply22x21(a,b)

flux_vector_def *a;
scatter_def *b;

   {
   flux_vector_def c;

   c.pl_r =   a->pl_r*b->s2_r - a->pl_i*b->s2_i
            + a->pr_r*b->s3_r - a->pr_i*b->s3_i;

   c.pl_i =   a->pl_i*b->s2_r + a->pl_r*b->s2_i
            + a->pr_i*b->s3_r + a->pr_r*b->s3_i;

   c.pr_r =   a->pl_r*b->s4_r - a->pl_i*b->s4_i
            + a->pr_r*b->s1_r - a->pr_i*b->s1_i;

   c.pr_i =   a->pl_i*b->s4_r + a->pl_r*b->s4_i
            + a->pr_i*b->s1_r + a->pr_r*b->s1_i;

   a->pl_r = c.pl_r;
   a->pl_i = c.pl_i;
   a->pr_r = c.pr_r;
   a->pr_i = c.pr_i;

   }  /* end procedure multiply22x21 */

/*-------------------------------------------------------------------------*/
/* Generate the rotation matrix */
gen_rotate(angle,b)

double angle;
rotate_def *b;

   {
   /*R matrix is of the form [R1,R2#R3,R4] */

   b->r1_r = cos(angle);

   b->r4_r = b->r1_r;

   b->r2_r = sin(angle);

   b->r3_r = -1.0*b->r2_r;

   }  /* end procedure gen_rotate */

/*-------------------------------------------------------------------------*/
/* multiply of 2x1 flux_vector matrix by 2x2 rotation matrix */
rotate_mul(a,b)

flux_vector_def *a;
rotate_def *b;

   {
   flux_vector_def c;

   c.pl_r =   a->pl_r*b->r1_r + a->pr_r*b->r2_r;

   c.pl_i =   a->pl_i*b->r1_r + a->pr_i*b->r2_r;

   c.pr_r =   a->pl_r*b->r3_r + a->pr_r*b->r4_r;

   c.pr_i =   a->pl_i*b->r3_r + a->pr_i*b->r4_r;

   a->pl_r = c.pl_r;
   a->pl_i = c.pl_i;
   a->pr_r = c.pr_r;
   a->pr_i = c.pr_i;
```

```
   }  /* end procedure rotate_mul */

/*-------------------------------------------------------------------------*/
/* addition of scattered direction to original flux_vector direction. */
/* angles are added on the inside of the viewing sphere.              */
add_angles(a,t,p)

flux_vector_def *a;
double  t, p;    /* theta, phi */

   {
   flux_vector_def c;
   double  ss, st, cs, ct, cp, temp, temp2, junk;

   ss = sin(a->theta);
   cs = cos(a->theta);   /*sqrt(1-ss*ss);*/
   ct = cos(t);
   st = sin(t);          /*sqrt(1-ct*ct);*/
   cp = cos(p);

   /*See page 149 of the CRC Standard Math Tables 28th Ed. */
   /* North is zero azimuth (phi) on the inside of the sphere */
   temp = cp*st*ss + cs*ct;

   if ( (temp < -1.0) || (temp > 1.0) )
      temp = modf(temp, &junk);
   c.theta = acos( temp );

   temp2 = sin(c.theta)*ss;   /*sqrt(1-temp*temp)*ss;*/
   if ( (temp2 < SMALL) && (temp2 > -SMALL) )
      temp2 = SMALL;
   temp = (ct - temp*cs)/temp2;
   if ( (temp < -1.0) || (temp > 1.0) )
      temp = modf(temp, &junk);

   if ( (p >= 0.0) && (p <= PI) )  /* go in right direction */
      c.phi = a->phi + acos( temp );
   else
      c.phi = a->phi - acos( temp );

   /* keeps the angle positive - just in case */
   if (c.phi > PI2)
      c.phi = PI2 * modf((c.phi/PI2), &junk);

   if (c.phi < 0.0)
      c.phi = PI2 *  (1.0 + modf((c.phi/PI2), &junk) );

   if (c.theta > PI)
      c.theta = PI * (1.0 - modf((c.theta/PI), &junk) );

   if (c.theta < 0.0)
      c.theta = -1.0 * PI * modf((c.theta/PI), &junk);

   a->theta = c.theta;
   a->phi = c.phi;

   }  /* end procedure add_angles */

/*-------------------------------------------------------------------------*/

termination()

    {

    fclose(handle);
    fclose(c_handle);
    close(out_hand);

    }   /* end procedure termination */
```

The following is an example initialization file. The first element is the parameter lable number. The second is the element value. The text following the exclamation mark is commentary.

```
1,  0.54       !Wavelength of light  (microns)
2,  70000000   !Number of flux vectors
3,  0.7        !Limb darkening coeff
4,  1          !Is there a spot? 1=TRUE,0=FALSE
5,  0.8        !Flux(spot)/flux(avg)    0.8 is about 200K different at 3500K
6,  1.57080    !Spot theta  (radians)    1.5708 is on the equator
7,  3.14159    !Spot phi (radians)  2 PI around
8,  1.0        !Spot angular radius (radians)   0.087=5degrees
9,  0.00       !Spot gamma for circular polarization
10, 1          !Rayleigh layer  1=TRUE,0=FALSE
12, 2.8E-13    !Rayleigh/Thomson alpha_k_k    (cm)   classical radius
13, 0.5E+13    !Rayleigh/Thomson layer thickness (cm)   1.5E+13cm = 1AU.
14, 1.0E+11    !Ne: number density of Rayleigh/Thomson particles (1/cm)^3
20, 2          !Mie scattering:  spheres =1, cylinders =2, none =0
21, 1.5E+28    !QNa2  product of the efficiency, number and size^2  (cm^2)
22, 3.0        !Ratio of dust shell radius to stellar radius
23, 0.3        !Cylinder orientation with respect to North
24, 5.55E+13   !Star radius (cm)
25, 1.0        !Length of cylinders in microns
30, 0.6        !Interstellar phase retardance
31, 0.9        !Interstellar orientation with respect to North
```

This is a sample Mie coefficient file. Four elements are on each line. They correspond to the a and b coefficients for spheres or to the c and d coefficients for cylinders in the format:

```
      a(real), a(imaginary), b(real), b(imaginary)  !comment
or    c(real), c(imaginary), d(real), d(imaginary)  !comment.
```

The first row starts with n = 0. Files for spheres should have zeros for the first row.

```
0.3322,  -0.2502,  0.7361,   0.0809   !Page 320 of van de Hulst (1957)
0.3834,   0.2406,  0.3321,  -0.2502   !m=1.41-1.41i  cylinders
0.1780,   0.1300,  0.0600,  -0.0490   !x=1.4, note that van de Hulst
0.0160,   0.0230,  0.0030,  -0.0020   !has a misprint for case I n=3.
0.0010,   0.0020,  0.0,      0.0      !
```

This is an abbreviated sample output file. The format is described in the introduction to this appendix.

```
SCATTERING DIAGRAM - CONDITIONS FILE: alpori.ini
Scatters:  none 1528346  rt only 3471654  mie only 0  double 0
60.0, 90.0, 0.2387, -0.4823, -0.2989, 0.5381,1.4524
60.0, 64.3, -0.3539, 0.0423, 0.2633, 0.3564, 1.1753
60.0, 38.6, 0.5422, -0.3085, -0.3625, 0.6238, 1.4490
60.0, 12.9, -0.0496, 0.0992, 0.2804, 0.1109, 1.6917
60.0, -12.9, 0.1654, 0.3675, -0.2779, 0.4030, 1.4342
60.0, -38.6, -0.2715, 0.3073, -0.0706, 0.4100, 1.1706
60.0, -64.3, -0.1561, 0.4313, 0.2521, 0.4587, 1.2886
60.0, -90.0, -0.1043, -0.2729, -0.2272, 0.2921, 1.6910
80.0, 90.0, -0.3674, 0.1954, 0.4306, 0.4162, 1.2335
80.0, 64.3, -0.0269, 0.2704, 0.1544, 0.2717, 1.8277
80.0, 38.6, -0.1991, 0.1192, -0.0657, 0.2321, 1.5932
80.0, 12.9, -0.1567, 0.3918, -0.1363, 0.4220, 1.9095
80.0, -12.9, -0.0823, -0.1047, 0.1879, 0.1332, 1.6115
80.0, -38.6, 0.0026, -0.1141, -0.0155, 0.1141, 1.5852
80.0, -64.3, 0.4094, 0.3209, 0.1414, 0.5202, 1.4392
80.0, -90.0, -0.0802, -0.5013, 0.0838, 0.5077,1.7633
```

REFERENCES

Appenzeller, I. 1966, *Zeit. Ap.*, **64**, 269.

Arsenijevic, J., Kubicela, A., and Vince, I. 1980, *I.B.V.S. No. 1859.*

Avery, R.W., Stokes, R.A., Michalsky, J.J., and Ekstrom, P.A. 1975, *Astron. J.*, **80**, 1026.

Bandermann, L.W., and Kemp, J.C. 1973, *M.N.R.A.S.*, **162**, 367.

Bastien, P., Drissen, L., Menard, F., Moffat, A.F.J., Robert, C., and St. Louis, N. 1988, *Astron. J.*, **95**, 900.

Behr, A. 1959, *Veröff. Univ. Sternw. Göttingen,* No. 126.

Blitzstein, W.B. 1987a, *PEMP System Hardware Technical Manual: Electronics, Optics, Electro-Optics.*

Blitzstein, W.B. 1987b, *PEMP Systems Analysis Technical Manual.*

Blitzstein, W.B. 1991, private communication.

Boyle, R.P., Aspin, C., Coyne, G.V., and McLean, I.S. 1986, *A. Ap.*, **164**, 310.

Busso, M., Scaltriti, F., Ferrari-Toniolo, M., Origlia, L., Persi, P., Robberto, M., and Silvestro, G. 1990, *Mem. S. A. It.*, **61**, 77.

Chlewicki, G., and Greenberg, J.M. 1990, *Ap. J.*, **365**, 230.

Clarke, D., and Brooks, A. 1985, *M.N.R.A.S.*, **212**, 211.

Clarke, D., and Schwartz, H.E. 1984, *A. and Ap.*, **132**, 375.

Collison, A.J., and Fix, J.D. 1991, *Ap. J.*, **368**, 545.

Corcoran, M.F. 1988, *Ph. D. thesis, University of Pennsylvania.* (Published: 1991, *Ap. J.*, **366**, 308).

Cowley, A.P. 1969, *P.A.S.P.*, **81**, 297.

Coyne, G.V. 1988, *Polarized Radiation of Circumstellar Origin,* G.V. Coyne, S.J., A.M. Magalhães, A.F.J. Moffat, R.E. Schulte-Ladbeck, S. Tapia, and D.T. Wickramasinghe, eds. (Tucson: University of Arizona Press), p. 511.

Coyne, G.V., and Gehrels, T. 1966, *Astron. J.*, **71**, 355.

Coyne, G.V., and Kruszewski, A. 1968, *Astron. J.*, **73**, 20.

Coyne, G.V., and Magalhães, A.M. 1979, *Astron. J.*, **84**, 1200.

Coyne, G.V., and Wickramasinghe, N.C. 1969, *Astron. J.*, **74**, 1179.

Daniel, J.-Y. 1978, *A. Ap.*, **67**, 345.

Daniel, J.-Y. 1980, *A. Ap.*, **87**, 204.

Daniel, J.-Y. 1982, *A. Ap.*, **111**, 58.

Deutsch, A.J. 1955, *Ap. J.*, **123**, 210.

Didelon, P. 1983, *A. Ap. Supp.*, **53**, 119.

Doherty, L.R. 1986, *Ap J.*, **307**, 261.

Dupree, A.K., Baliunas, S.L., Guinan, E.F., Hartman, L., Nassiopoulos, G.E., and Sonneborn, G. 1987, *Ap. J.*, **317**, L85.

Dupree, A.K., Baliunas, S.L., Guinan, E.F., Hartman, L., and Sonneborn, G. 1990, *Alpha Ori: Evidence for Pulsation*, presented at *Confrontation between Stellar Evolution and Pulsation*, Bologna, Italy.

Dyck, H.M. 1968, *Astron. J.*, **73**, 688.

Dyck, H.M., Forbes, F.F., and Shawl, S.J. 1971, *Astron. J.*, **76**, 901.

Dyck, H.M., Forrest, W.J., Gillett, F.C., Stein, W.A., Gehrz, R.D., Woolf, N.J., and Shawl, S.J. 1971, *Ap. J.*, **165**, 57.

Dyck, H.M., and Jennings, M.C. 1971, *Astron. J.*, **76**, 431.

Dyck, H.M., and Simon, T. 1975, *Ap. J.*, **195**, 689.

Egret, D., Wenger, M., and Dubois, P. 1991, *The Simbad astronomical database,* in *Databases and On-Line Data in Astronomy,* D. Egret and M. Albrecht, eds. (Dordrecht, Netherlands: Kluwer Academic Publishers).

Elias, N.M. 1990, *Ph. D. thesis, University of Pennsylvania.*

Elias, N.M., and Dorren, J.D. 1990, *Astron. J.*, **100**, 818.

Grigorian, K.A. 1958, *Soob. Byurakan Obs.*, **25**, 45.

Hall, J.S. 1958, *Pub. U.S. Naval Obs.*, **17**, 275.

Hall, J.S., and Mikesell, A.H. 1950, *Pub. U.S. Naval Obs.*, **17**, 7.

Hayes, D.P. 1981, *I.B.V.S., No. 1984.*

Hayes, D.P. 1982, *I.B.V.S., No. 2064.*

Hayes, D.P. 1984, *Ap. J. Suppl.*, **55**, 179.

Hebden, J.C., Christou, J.C., Cheng, A.Y.S., Hege, E.K., Strittmatter, P.A., Beckers, J.M., and Murphy, H.P. 1986, *Ap. J.*, **309**, 745.

Hiltner, W.A. 1951, *Ap. J.*, **114**, 241.

Hiltner, W.A. 1956, *Ap. J. Supp.*, **2**, 389.

Hirshfield, A., and Sinnot, R.W. (eds.) 1982, *Sky Catalog 2000.0: Stars to Magnitude 8.0,* (Cambridge, Mass.: Sky Publishing Corp.).

Holenstein, B.D. 1987, *B.A.A.S.*, **19**, 754.

Holenstein, B.D. 1991, *B.A.A.S.*, **23**, 830.

Holenstein, B.D., Koch, R.H., and Pfeiffer, R.J. 1988, *Lect. Notes Phys.* **305**, 181. (Proc. IAU Coll. No. 108 *Atmospheric Diagnostics of Stellar Evolution, Chemical Pecularity, Mass Loss and Explosion* (ed. K. Nomoto)).

Hsu, J.C., and Breger, M. 1982, *Ap. J.*, **262**, 732.

Illing, R.M.E., Landman D.A., and Mickey, D.L. 1975, *A. Ap.*, **41**, 183.

Jackson, J.D. 1975, *Classical Electrodynamics*, (2nd. ed., New York: Wiley).

Jennings, M.C., and Dyck, H.M. 1971, *Ap J.* **177**, 427.

Johnson, H.L., 1965, *Comm. Ariz. Univ. Lunar and Planetary Lab,* 3 (No. 53), 73.

Johnson, H.L., Iriate, B., Mitchell, R.I., and Wisniewskj, W.Z., 1966, *Comm. Ariz. Univ. Lunar and Planetary Lab,* 4 (No. 63), 99.

Karovska, M., Nisenson, P., and Noyes, R. 1986, *Ap. J.*, **308**, 260.

Karovska, M., Nisenson, P., Noyes, R.W., Stachnik, R., Loeser, J.G., Baliunas, S.L., Guinan, E.F., Mattei, J.A., and Wacker, S. 1985, *Proceedings of Fourth Cambridge Workshop on Cool Stars, Stellar Systems, and the Sun.*

Kemp, J.C. 1969, *J. Opt. Soc. Am.*, **59**, 950.

Kemp, J.C. 1970, *Ap. J.*, **162**, 169.

Kemp, J.C., and Henson, G.D. 1983, *Ap. J.*, **266**, L69.

Kemp, J.C., Henson, G.D., Kraus, D.J., and Dunaway, M.H. 1987, *B.A.A.S.*, **19**, 752.

Kemp, J.C., and Wolstencroft, R.D. 1972, *Ap. J.*, **176**, L115.

Koch, R.H. 1975, *Pennsylvania Polarization Standards*.

Koch, R.H. 1987, private communication.

Koch, R.H. 1992, *Polarized Radiation from Close Binaries*, in *Realm of Interacting Binary Stars*, J. Sahade , Y. Kondo, and G.E. McClusky eds. (in press).

Koch, R.H., Elias, N.M., Corcoran, M.F., and Holenstein, B.D. 1989, *Space Sci. Rev.* **50**, 63. (Proc. IAU Coll. No. 107 Algols (ed. A.H. Batten)).

Koch, R.H., Hrivnak, B.J., Bradstreet, D.H., Blitzstein, W.B., Pfeiffer, R.J., and Perry, P.M. 1985, *Ap. J.*, **288**, 731.

Koch, R.H., and Pfeiffer, R.J. 1978, *Astron. J.*, **83**, 183.

Koch, R.H., Scaltriti, F., Piirola, V., Elias, N.M., Holenstein, B.D., and Coyne, G.V. 1992, *A.Ap.* (submitted).

Kraft, R.P. 1960, *Stellar Atmospheres*, Vol. 6 of *Stars and Stellar Systems*, J.L. Greenstein, ed. (Chicago: Univ. Chicago Press), p 370.

Kruszewski, A., Gehrels, T., and Serkowski, K. 1968, *Astron. J.*, **73**, 677.

Lang, K.R. 1980, *Astrophysical Formulae* (2nd ed; New York: Springer-Verlag).

Le Borgne, J.F., and Mauron, N. 1989, *A. Ap.*, **210**, 198.

Le Borgne, J.F., Mauron, N., and Leroy, J.L. 1986, *A. Ap.*, **168**, 211.

Lee, T.A. 1970, *Astron. J.*, **162**, 217.

Lefèvre, J., and Daniel, J.-Y. 1988, *Polarized Radiation of Circumstellar Origin*, G.V. Coyne, S.J., A.M. Magalhães, A.F.J. Moffat, R.E. Schulte-Ladbeck, S. Tapia, and D.T. Wickramasinghe, eds. (Tucson: University of Arizona Press), p. 523.

Loeser, J.G., Baliunas, S.L., Guinan, E.F., Mattei, J.A., and Wacker, S. 1985, *Proceedings of the Fourth Cambridge Workshop on Cool Stars, Stellar Systems, and the Sun.*

Magalhães, A.M. 1988, *Polarized Radiation of Circumstellar Origin*, G.V. Coyne, S.J., A.M. Magalhães, A.F.J. Moffat, R.E. Schulte-Ladbeck, S. Tapia, and D.T. Wickramasinghe, eds. (Tucson: University of Arizona Press), p. 461.

Magalhães, A.M., Coyne, G.V., and Benedetti, E.K. 1986, *Astron. J.*, **91**, 919.

Magalhães, A.M., Nordsieck, K.H., Nook, M.A., Knoop, G.P., Anderson, C.M., Babler, B., Bjorkman, K.S., Diamond, S.M., Macdonald, A.J., Meade, M.R., Roberts, T.P., Schulte-Ladbeck, R.E., Taylor, M.J., and Wolf, M.J. 1990, *B.A.A.S.*, **22**, 1209.

Maier, W.L. 1991, *A Fast Pseudo Random Number Generator*, in the May, 1991 issue of *Dr. Dobb's Journal*, p. 152.

Martin, P.G. 1974, *Ap. J.*, **187**, 461.

Martin, P.G. 1975, *Ap. J.*, **202**, 389.

Mattei, J.A. 1991, *AAVSO* observations, private communication.

Michalsky, J.J., Swedlund, J.B., Stokes, R.A., and Avery, R.W. 1974, *Ap. J.*, **187**, L13.

Polyakova, T.A. 1984, *Astrofizika*, **21**, 125.

Pfeiffer, R.J. 1975, *Ph. D. thesis, University of Pennsylvania.*

Pfeiffer, R.J., and Koch, R.H. 1977, *P.A.S.P.*, **89**, 147.

Pfeiffer, R.J., and Koch, R.H. 1987, *Astron. J.*, **94**, 484.

Rieke, G.H., and Lebofsky, M.J. 1985, *Ap. J.*, **288**, 618.

Schmidt, T. 1972, *Elliptical Polarization by Light Scattering from Sub-Micron Spheroids*, presented at the IAU Symposium No. 52, at Albany, New York.

Schwarz, H.E., and Clarke, D. 1984, *A. Ap.*, **132**, 370.

Schwarzchild, M. 1975, *Ap. J.*, **195**, 131.

Serkowski, K. 1962, *Adv. Astr. and Ap.*, **1**, 289.

Serkowski, K. 1966a, *Ap. J.*, **144**, L857.

Serkowski, K. 1966b, *I.B.V.S. No. 141.*

Serkowski, K., and Chojnacki, W. 1969, *A. Ap.*, **1**, 442.

Serkowski, K., Mathewson, D.S., and Ford, V.L. 1975, *Ap. J.*, **196**, 261.

Shafter, A., and Jura, M. 1980, *Astron. J.*, **85**, 1513.

Shakhovskoi, N.M. 1964, *Soviet Astronomy-A.J.*, **7**, 806.

Shapiro, P.R. 1975, *Ap. J.*, **201**, 151.

Shawl, S.J. 1975a, *Astron. J.*, **80**, 595.

Shawl, S.J. 1975b, *Astron. J.*, **80**, 602.

Shurcliff, W.A. 1966, *Polarized Light: Production and Use* (Cambridge: Harvard University Press).

Smart, W.M. 1958, *Combination of Observations*, (Cambridge: Cambridge University Press).

Smith, E. van P. 1956, *Ap. J.*, **124**, 43.

Smith, M.A. 1990, *B.A.A.S.*, **22**, 1208.

Smith, M.A., Patten, B.M., and Goldberg, L. 1989, *Astron. J.*, **98**, 2233.

Stellingwerf, R.F. 1978, *Ap. J.*, **224**, 953.

Stencel, R.E., Pesce, J., and Bauer, W.H. 1988, *Astron. J.*, **95**, 141.

Stokes, R.A., Ekstrom, P.A., and Swedlund, J.B. 1976, *Optical Eng.*, **15**, 1.

Stokes, R.A., Swedlund, J.B., Avery, R.W., and Michalsky, J.J. 1974, *Astron. J.*, **79**, 678.

Tinbergen, J., Greenberg, J.M., and de Jager, C. 1981, *A. Ap.*, **95**, 215.

Treanor, P.J. 1963, *Astron. J.*, **68**, 185.

Tsuji, T. 1978, *P.A.S.J.*, **30**, 435.

van de Hulst, H.C. 1957, *Light Scattering by Small Particles* (New York: Wiley, reprinted 1981. New York: Dover).

Wilking, B.A., Lebofsky, M.J., and Rieke, G.H. 1982, *Astron. J.*, **87**, 695.

Wolf, G.W. 1970, *Ph. D. thesis, University of Pennsylvania.*

Wolf, G.W. 1972, *Astron. J.*, **77**, 576.

Zellner, B. 1971, *Astron. J.*, **76**, 651.

INDEX

α Ori v, x, xi, xii, xiii, 3, 5, 11-13, 43, 57, 58, 62, 64, 66, 68, 69, 70, 71, 76-79, 81-83, 154, 170, 171, 173, 179, 180, 182, 183-185, 187-189, 192
α Sco v, x, xi, xii, xiii, 3, 7, 11, 12, 14, 43, 59, 61, 64, 66, 69, 70, 73, 76-78, 80, 81, 83, 154, 177, 178, 181, 184, 185, 187, 188, 189
α1 Her v, xii, 3, 8, 11, 12, 64, 66, 70, 73, 76, 77, 80, 81, 83, 153, 178, 179, 181, 182, 184, 185, 187-189
β Peg v, x, xi, xii, 3, 9, 11, 12, 14, 60, 65, 66, 70, 75-77, 79, 81, 82, 83, 179, 182, 184, 185, 187-189
μ Cep v, x, xi, xii, xiii, 3, 8, 11, 12, 14, 56, 60, 64, 68-70, 74, 76, 77, 79, 80, 82, 83, 153, 169, 179-181, 184, 185, 187, 188, 189
ψ1 Aur v, x, xi, xii, 3, 6, 11-13, 58, 63, 70, 72, 76-79, 82, 83, 174, 184, 185, 187-189
119 CE Tau v, x-xiii, 3, 4, 11-12, 43, 57, 62, 69, 70, 71, 76, 77, 78, 79, 82, 83, 153, 169, 174, 177, 184, 185, 187, 188, 189, 245, 276
6 BU Gem v, x-xii, 3, 5, 11, 12, 13, 58, 63, 66, 70, 71, 72, 76, 77, 78, 79, 82, 83, 173, 184, 187, 188, 189, 252, 253, 276
72 Leo v, x, xi, xii, 3, 6, 14, 58, 63, 66, 69, 78, 80, 81, 169, 175, 176, 184, 185, 187, 189, 254, 255, 276
AAVSO iv, 68-69, 83
Absolute magnitude x, 4, 13
AC amplifier 26-30, 26, 27
Angular radius of spot 157, 164
Background limiting aperture 26
Bessel function 28
Betelgeuse 5
Binaries 1, 9, 276, 300
Binary companions 153
Birefringence v, vi, 1, 59, 153, 155, 159, 167, 170, 173-175, 180, 182, 184, 185, 188, 192, 282, 284, 287, 292
Birefringence of interstellar grains 59
Carbon monoxide 7
CASE 1 xiii, 164-168, 170, 182, 189-192, 286
CASE 2 xiii, 165, 171-175, 178-180, 182, 190, 286
CASE 3 xiii, 165, 190, 286
CASE 4 xiii, 165, 166, 182, 190, 191, 286
CASE 5 xiii, 166, 177, 179, 191, 286
CASE 6 xiii, 166, 191, 192, 286
CASE 7 xiii, 166, 191, 286
CASE 8 xiii, 166, 170, 173-175, 179, 180, 182, 191, 286
CASE 9 xiii, 166, 170, 173-175, 178, 180, 182, 192, 286
Cassegrain reflector 1, 26
Celestial sphere 27
Circular cylinder 158
Circular dichroism 153
Circumstellar shell 5, 173, 178, 182
Complex index of refraction 152, 157
Continuum magneto-opacity 153
Convection 169, 172
Cross-calibration multiplicative factor 37
Curly braces 10, 164, 295
Data acquisition and reduction software 33, 35, 216
DC amplifier 26, 27, 29, 26
Degenerate companions 10
Dust v, vi, vii, 5, 8, 9, 55, 60, 61, 151-153, 159-162, 164, 165, 169, 170, 171, 173-177, 179-185, 187-192, 282, 284, 287, 291, 295

Dust grains 8, 9, 161, 173, 183, 188, 189
Dust shell v-vii, 151, 152, 159, 162, 164, 165, 169-171, 173-177, 179-185, 188-191, 282, 295
Dusty atmospheres 2
Effective temperature 4, 13, 151
Electric vector 30, 36, 37, 57, 59, 60, 66, 155, 156, 160, 181, 189, 210, 217, 218, 290-292
Elliptical polarimeter vii, 26, 27
Equatorial rotational velocities 168
Fabry lens 26
Field stars viii, 55-60, 78, 79, 269-275, 277-279
Flower and Cook Observatory 1, 3, 26, 33, 36, 216
Flux vectors 163, 189-192, 295
Fourier coefficients 33
Fundamental extinction formula 161
Galactic neighborhood 55
Galactic position 4, 56
Giants 3, 169
Glan-Thompson prism 26
Grey Zeeman splitting 153
H- free-free absorption 154
Harmonics 30, 34, 35, 214, 215
Hertzsprung-Russell diagram 4, 10
IAU Colloquium 23 37
IBM-AT 27, 31, 211
IBM-XT 27
Index of refraction 152, 155, 157, 162, 183
Infrared Astronomical Satellite 69 (see IRAS)
Integration length 30, 211, 216, 222, 224
Integration time 28-30
International Ultraviolet Explorer 68 (see IUE)
Interstellar birefringence v, vi, 159, 167, 170, 173-175, 180, 182, 184, 185, 188, 192, 282, 284, 287, 292
Interstellar circular polarization 58, 60, 61, 173, 176, 178-180, 182, 185
Interstellar phase retardence 164
Interstellar polarization vectors 55, 224
Intrinsic polarization vectors 61, 55
Intrinsic polarizations vii, 61
IRAS vii, 68, 69, 77, 175
IRAS Point Source Catalog 69
Ithaco lock-in amplifier 27
IUE vii, ix, 68, 76
IUE Spectral Image Processing System 68
Janskys 69
Jones vector 155, 159
Kitt Peak National Observatory 3
Kramers-Kronig dispersion relationships 162, 183
Limb darkening v, 162, 163, 165, 184, 286, 288, 295
Linear birefringence 153, 159
Linear polarization spectra 56, 180
LLTVs v, 2, 3, 153, 158, 161, 165, 184, 185
Local thermodynamic equilibrium 151
LTE 151
Luminous late-type variables v, 1, 2 (see LLTV)
M supergiants 5
Magnetic fields 1, 9, 10
Magneto-emission vi, 153, 154, 159, 161, 163-166, 171, 173, 179-182, 185, 188-191, 288
Mean-squared error 34

Methods for calibration 36
Microsoft 163, 216, 280, 281
Mie coefficients 157, 158, 164, 280, 281, 285, 286, 291
Mie scattering v, 66, 153, 159, 164-167, 169, 171, 173-177, 179-184, 188-192, 281, 282, 287, 295
Milky Way 57-60
Monte Carlo v, 7, 161, 163, 190, 286
Morvue PEM-FS3 26
Mueller calculus 37
Multi-parameter model 158, 159, 161
Multi-Parameter Polarization Model vii, viii, 153, 163, 181, 189, 280
Nebulae 58, 59
Number density 1, 151, 161, 162, 164, 167, 177, 192, 282, 295
Nyquist criterion 68
Observing procedure viii, 30, 210
Observing program v, vii, 2, 4, 183
Orion-Cygnus arm 57, 58, 59, 60, 56
Overtones 34
PDM 66, 67
PEM 26-28, 30, 34, 210, 211, 218, 225
PEMP viii, x, 1, 2, 4, 26, 45, 210, 211, 220, 222, 297
Pennsylvania polarimeter 1, 27, 34, 38, 183, 215
Phase Dispersion Minimization 66 (see PDM)
Photoelastic modulator polarimeter 1 (see PEMP)
Photomultiplier tube 26, 27, 26
Photomultiplier voltage 28, 29
Photosphere 5, 151, 153, 161, 162, 164, 171, 172, 189, 286, 287, 289
Planck's blackbody function 160
Pockels cells 28
Poincaré sphere v, 36, 38, 184
Polarimetric data vii, 54
Polarization row vectors 10
Polarization spectra vii, xii, 56, 65, 81, 82, 170, 178, 180, 181, 186
Polarization standards v, ix, 37, 39-41, 300
Polaroid 7, 30, 218, 244
Positive circular polarization 37
Program Object Parameters ix, 11
Program stars vii, 3, 33, 54, 57, 60, 61, 78, 154, 183
Pulsation 7, 170-172, 179, 183, 188, 298
Pulsational period 4, 5, 171
Quarter wave plate 36, 37
Ramsden disk 34
Random number generator 163, 186, 283, 301
Rayleigh scattering 5, 66, 153, 157, 158, 171, 282, 5, 158, 160, 161
Reduced Instruction Set Computer 185
Reflection nebulosity 7, 59
Retarder 26-28, 34, 36, 37, 43
RISC 185
Rosseland mean opacity 154
Sagittarius arm 56
Scatterer cross-section 161
Scattering v, vi, xiii, 1, 5, 7-9, 66, 151, 153, 155-161, 163-169, 171, 173-185, 188-192, 281, 282, 284, 287, 289, 290, 291-293, 295, 296, 301, 302
Scattering phase matrix 155, 160, 291
Scattering plane 155, 156, 158, 281
Scintillation noise 32
Shot-noise 32

SIMBAD iii, 3, 298
Sky Catalog 2000.0 3, 299
Speckle interferometry 5
Spectral indices ix, 65, 66, 71-75, 171, 174-177, 179, 182
Spots v, vi, 2, 9, 10, 153, 159, 161, 165, 167, 177, 178, 184, 185, 189, 282, 286
Standard deviation 10, 68, 214
Standardization coefficients ix, 38, 44, 54, 223
Standardized polarimetric data 54
Stanford Research Systems lock-in amplifier 27
Stellar angular radius 151, 152
Stokes vectors v, x, xi, 2, 13, 14, 36, 38, 45, 54, 55, 63, 64, 155, 163, 166, 168, 174, 176, 179-182, 184, 191, 223, 285
Sunspots 154
Supergiants 3, 5, 169
Thomson scattering v, vi, 66, 156, 157, 161, 165, 169, 171, 174, 177, 178, 180, 181, 184, 188-191, 158, 160
TiO 152, 171, 176, 177
Types of scatterers 1, 9
Uncertainty 10, 58, 10
V CVn v, x, xi, xii, 3, 6, 7, 11, 12, 14, 57, 58, 63, 70, 72, 73, 76, 77, 78, 80, 82, 83, 153, 176, 184, 185, 187-189, 255, 256, 276
Variability state ix, 3, 12
Variable integration lengths vii, 30, 31, 33
Viewing sphere 160, 163, 167, 189, 294
Voltage controlled oscillator 27
VV Cep v, x, xi, xii, 3, 9, 11, 12, 14, 56, 60, 65, 66, 70, 74, 76, 77, 79-83, 154, 181, 184, 185, 187-189, 263-265, 276
Weighted average 38, 54, 226, 231-243, 245, 246, 250-258, 260-265, 267, 268
Weighted error 54
Zeeman splitting 153